frontiers | Research Topics

Molecular advances and applications of machine learning in understanding autism and comorbid psychiatric disorders

Edited by
Salam Salloum-Asfar, Javier Corral, Jesualdo Tomás Fernández-Breis and Nasser H. Zawia

Published in
Frontiers in Molecular Neuroscience

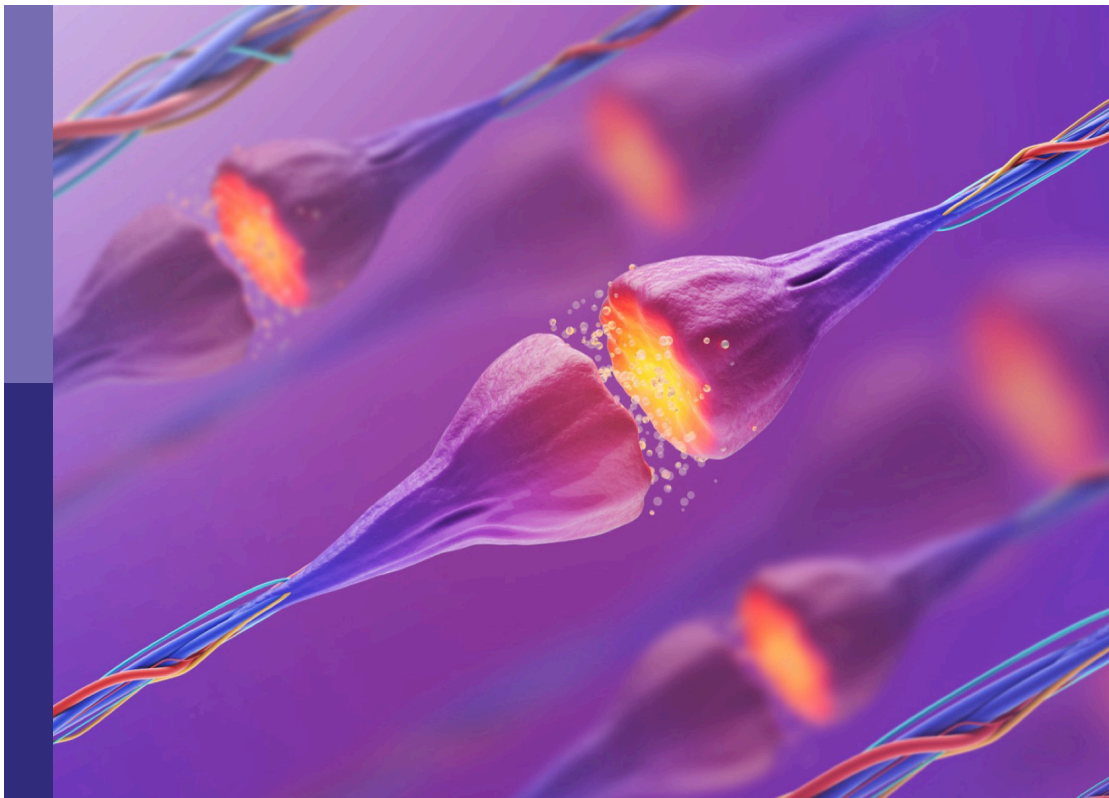

FRONTIERS EBOOK COPYRIGHT STATEMENT

The copyright in the text of individual articles in this ebook is the property of their respective authors or their respective institutions or funders. The copyright in graphics and images within each article may be subject to copyright of other parties. In both cases this is subject to a license granted to Frontiers.

The compilation of articles constituting this ebook is the property of Frontiers.

Each article within this ebook, and the ebook itself, are published under the most recent version of the Creative Commons CC-BY licence. The version current at the date of publication of this ebook is CC-BY 4.0. If the CC-BY licence is updated, the licence granted by Frontiers is automatically updated to the new version.

When exercising any right under the CC-BY licence, Frontiers must be attributed as the original publisher of the article or ebook, as applicable.

Authors have the responsibility of ensuring that any graphics or other materials which are the property of others may be included in the CC-BY licence, but this should be checked before relying on the CC-BY licence to reproduce those materials. Any copyright notices relating to those materials must be complied with.

Copyright and source acknowledgement notices may not be removed and must be displayed in any copy, derivative work or partial copy which includes the elements in question.

All copyright, and all rights therein, are protected by national and international copyright laws. The above represents a summary only. For further information please read Frontiers' Conditions for Website Use and Copyright Statement, and the applicable CC-BY licence.

ISSN 1664-8714
ISBN 978-2-8325-2994-2
DOI 10.3389/978-2-8325-2994-2

About Frontiers

Frontiers is more than just an open access publisher of scholarly articles: it is a pioneering approach to the world of academia, radically improving the way scholarly research is managed. The grand vision of Frontiers is a world where all people have an equal opportunity to seek, share and generate knowledge. Frontiers provides immediate and permanent online open access to all its publications, but this alone is not enough to realize our grand goals.

Frontiers journal series

The Frontiers journal series is a multi-tier and interdisciplinary set of open-access, online journals, promising a paradigm shift from the current review, selection and dissemination processes in academic publishing. All Frontiers journals are driven by researchers for researchers; therefore, they constitute a service to the scholarly community. At the same time, the *Frontiers journal series* operates on a revolutionary invention, the tiered publishing system, initially addressing specific communities of scholars, and gradually climbing up to broader public understanding, thus serving the interests of the lay society, too.

Dedication to quality

Each Frontiers article is a landmark of the highest quality, thanks to genuinely collaborative interactions between authors and review editors, who include some of the world's best academicians. Research must be certified by peers before entering a stream of knowledge that may eventually reach the public - and shape society; therefore, Frontiers only applies the most rigorous and unbiased reviews. Frontiers revolutionizes research publishing by freely delivering the most outstanding research, evaluated with no bias from both the academic and social point of view. By applying the most advanced information technologies, Frontiers is catapulting scholarly publishing into a new generation.

What are Frontiers Research Topics?

Frontiers Research Topics are very popular trademarks of the *Frontiers journals series*: they are collections of at least ten articles, all centered on a particular subject. With their unique mix of varied contributions from Original Research to Review Articles, Frontiers Research Topics unify the most influential researchers, the latest key findings and historical advances in a hot research area.

Find out more on how to host your own Frontiers Research Topic or contribute to one as an author by contacting the Frontiers editorial office: frontiersin.org/about/contact

Molecular advances and applications of machine learning in understanding autism and comorbid psychiatric disorders

Topic editors

Salam Salloum-Asfar — Hamad bin Khalifa University, Qatar
Javier Corral — University of Murcia, Spain
Jesualdo Tomás Fernández-Breis — University of Murcia, Spain
Nasser H. Zawia — Hamad bin Khalifa University, Qatar

Citation

Salloum-Asfar, S., Corral, J., Fernández-Breis, J. T., Zawia, N. H., eds. (2023). *Molecular advances and applications of machine learning in understanding autism and comorbid psychiatric disorders*. Lausanne: Frontiers Media SA. doi: 10.3389/978-2-8325-2994-2

Table of contents

frontiers | Frontiers in Molecular Neuroscience

TYPE Editorial
PUBLISHED 31 August 2023
DOI 10.3389/fnmol.2023.1277814

Check for updates

OPEN ACCESS

EDITED AND REVIEWED BY
Clive R. Bramham,
University of Bergen, Norway

*CORRESPONDENCE
Salam Salloum-Asfar
ssalloumasfar@hbku.edu.qa

RECEIVED 15 August 2023
ACCEPTED 17 August 2023
PUBLISHED 31 August 2023

CITATION
Salloum-Asfar S (2023) Editorial: Molecular advances and applications of machine learning in understanding autism and comorbid psychiatric disorders.
Front. Mol. Neurosci. 16:1277814.
doi: 10.3389/fnmol.2023.1277814

COPYRIGHT
© 2023 Salloum-Asfar. This is an open-access article distributed under the terms of the Creative Commons Attribution License (CC BY). The use, distribution or reproduction in other forums is permitted, provided the original author(s) and the copyright owner(s) are credited and that the original publication in this journal is cited, in accordance with accepted academic practice. No use, distribution or reproduction is permitted which does not comply with these terms.

Editorial: Molecular advances and applications of machine learning in understanding autism and comorbid psychiatric disorders

Salam Salloum-Asfar*

Neurological Disorders Research Center, Qatar Biomedical Research Institute, Hamad Bin Khalifa University, Qatar Foundation, Doha, Qatar

KEYWORDS

autism, neurodevelopmental disorders, molecular factors, genomic, transcriptome, artificial intelligence, modeling

Editorial on the Research Topic
Molecular advances and applications of machine learning in understanding autism and comorbid psychiatric disorders

Welcome to this Research Topic titled "*Molecular Advances and Applications of Machine Learning in Understanding Autism and Comorbid Psychiatric Disorders*." In assembling this Research Topic, I express my gratitude to the dedicated reviewers who thoughtfully evaluated submissions, and to the authors who entrusted us with their valuable research, allowing us to enhance and refine their work.

This editorial encapsulates 15 meticulously curated articles, contributing to the profound exploration of neurodevelopmental disorders (NDDs), with a distinct focus on autism spectrum disorder (ASD) and its intricate interplay with comorbid psychiatric conditions. The contributions cast light on the intricate etiology and molecular mechanisms underlying these complex disorders. This Research Topic examines myriad dimensions, encompassing various facets, such as genetic predisposition, dynamic gene expression, signal transduction pathways, compensatory mechanisms, and neural network organization. A summary of the 15 accepted articles is provided below in eight categories:

1. Gut microbiota, depression, and neurodevelopmental dysfunction

The study from Liu et al. uncovers the impact of gut microbiota-dysbiosis on hippocampal gene regulation, elucidating the significant role of molecular dysregulation in neurodevelopmental dysfunction.

2. Cerebellar dysfunction and autism

Yang et al. meticulously examine the implications of SCN8A gene knockout in cerebellar Purkinje cells. The research unveils compromised social interaction, motor learning, reversal learning, and cerebellar degeneration, with mutations in the SCN8A gene linked to epilepsy, intellectual disability, and ASD.

3. Sensory processing and behavior problems in ASD

The study by Alateyat et al. employs machine learning models to predict behavior outcomes based on sensory profile scores, shedding light on the intricate interplay between sensory processing abilities and behavioral patterns in ASD.

4. Brain laterality, AI, and MRI neuroimaging in ASD detection

Keeratitanont et al. investigate brain laterality by F-18 fluorodeoxyglucose positron emission computed tomography (PET/CT) among high-functioning ASD individuals. The study uncovers altered glucose metabolism and lateralization indices, hinting at potential left laterality aberrations as contributory factors to ASD. Moreover, Moridian et al. review artificial intelligence (AI) and MRI neuroimaging for automatic ASD detection. Various AI methods, including machine learning (ML) and deep learning (DL), are assessed for their potential in accurate and efficient ASD diagnosis.

5. Genomic, transcriptomic factors in ASD, and genetic similarities between ASD and comorbid brain disorders

Multiple studies provide valuable insights into genomic and transcriptomic factors in ASD and their shared genetic traits with comorbid brain disorders. Chen et al. investigated the role of the NECAB2 gene, uncovering its impact on psychomotor and social behavior via mGluR1 signaling modulation. Krgovic et al. employed whole exome sequencing to spotlight ultrarare variants in ASD-associated genes, revealing their interconnectedness with various NDDs. Vilela et al. genetic similarity disease network study unveiled shared genetics between ASD and comorbid brain disorders, revealing novel insights into shared biological pathways and underlying mechanisms.

Mahmoud et al. comprehensively explored the genomic landscape of 1p13.3, identifying autosomal dominant candidate genes and emphasizing the role of small CNVs in shaping clinical outcomes. Yoo Y. E. et al. studied transcriptomic changes in Shank2-mutant mice, revealing distinct patterns across brain regions, gene dosages, and ages, shedding light on the dynamic interplay between Shank2 mutations and brain region-specific transcriptomic alterations. George-Hyslop et al. reviewed CNTNAP2's multifaceted role in neurodevelopmental disorders and human cerebral cortex evolution, highlighting its association with conditions like ASD and SLI. Shen et al. provided an overview of Gadd45b's preclinical and clinical effects, hypothesized mechanisms of action, and its role in various neurological disorders. Yoo T. et al. investigated transcriptomic variations in Shank3-mutant mice, revealing opposing and similar profiles to ASD across different ages, brain regions, and gene dosages. This study highlighted the intricate interplay of age, brain region, and gene dosage in shaping transcriptomic changes.

6. Homocysteine metabolism and ASD

An investigation by Li et al. into the interplay between serum homocysteine, folate, and vitamin B12 levels, assessing their correlation with ASD clinical manifestations and severity, underscoring the pertinence of homocysteine metabolism dysregulation in the context of ASD.

7. The role of MAP2 in neurodevelopmental disorders

A hypothesis and theory article by DeGiosio et al. postulates the potential pathogenic functions of the microtubule-associated protein 2 (MAP2) in NDDs. While traditionally recognized as a somatodendritic marker, its intricate influence on microtubule dynamics and neurite outgrowth is discussed, highlighting its relevance in various neurodegenerative and neuropsychiatric conditions.

Overall, this compendium of research articles synthesizes a rich tapestry of insights into the intricate molecular fabric of ASD and comorbid psychiatric disorders. By comprehending these underlying mechanisms, the prospects for early intervention and improved outcomes for affected individuals are significantly augmented. It is my sincere hope that this compilation serves as a pivotal steppingstone toward more precise diagnostics, individualized treatments, and enhanced therapeutic interventions in the realm of neurodevelopmental disorders.

Author contributions

SS-A: Investigation, Supervision, Writing—original draft, Writing—review and editing.

Conflict of interest

The author declares that the research was conducted in the absence of any commercial or financial relationships that could be construed as a potential conflict of interest.

Publisher's note

All claims expressed in this article are solely those of the authors and do not necessarily represent those of their affiliated organizations, or those of the publisher, the editors and the reviewers. Any product that may be evaluated in this article, or claim that may be made by its manufacturer, is not guaranteed or endorsed by the publisher.

frontiers in Molecular Neuroscience

ORIGINAL RESEARCH
published: 11 January 2022
doi: 10.3389/fnmol.2021.745437

Integrative Analysis of Long Non-coding RNAs, Messenger RNAs, and MicroRNAs Indicates the Neurodevelopmental Dysfunction in the Hippocampus of Gut Microbiota-Dysbiosis Mice

*Lanxiang Liu[1,2,3], Haiyang Wang[2,4], Xueyi Chen[2], Yangdong Zhang[2], Wenxia Li[2], Xuechen Rao[2,5], Yiyun Liu[2], Libo Zhao[1], Juncai Pu[2,3], Siwen Gui[2], Deyu Yang[1], Liang Fang[1] and Peng Xie[1,2,3,4]**

[1] Department of Neurology, Yongchuan Hospital of Chongqing Medical University, Chongqing, China, [2] NHC Key Laboratory of Diagnosis and Treatment on Brain Functional Diseases, The First Affiliated Hospital of Chongqing Medical University, Chongqing, China, [3] Department of Neurology, The First Affiliated Hospital of Chongqing Medical University, Chongqing, China, [4] College of Stomatology and Affiliated Stomatological Hospital of Chongqing Medical University, Chongqing, China, [5] College of Biomedical Engineering, Chongqing Medical University, Chongqing, China

OPEN ACCESS

Edited by:
Ildikó Rácz,
University Hospital Bonn, Germany

Reviewed by:
Kai K. Kummer,
Medical University of Innsbruck, Austria
Simin Li,
Southern Medical University, China

***Correspondence:**
Peng Xie
xiepeng@cqmu.edu.cn

Specialty section:
This article was submitted to Molecular Signalling and Pathways, a section of the journal Frontiers in Molecular Neuroscience

Received: 22 July 2021
Accepted: 08 December 2021
Published: 11 January 2022

Citation:
Liu L, Wang H, Chen X, Zhang Y, Li W, Rao X, Liu Y, Zhao L, Pu J, Gui S, Yang D, Fang L and Xie P (2022) Integrative Analysis of Long Non-coding RNAs, Messenger RNAs, and MicroRNAs Indicates the Neurodevelopmental Dysfunction in the Hippocampus of Gut Microbiota-Dysbiosis Mice. Front. Mol. Neurosci. 14:745437. doi: 10.3389/fnmol.2021.745437

Major depressive disorder is caused by gene–environment interactions and the gut microbiota plays a pivotal role in the development of depression. However, the underlying mechanisms remain elusive. Herein, the differentially expressed hippocampal long non-coding RNAs (lncRNAs), messenger RNAs (mRNAs), and microRNAs (miRNAs) between mice inoculated with gut microbiota from major depressive disorder patients or healthy controls were detected, to identify the effects of gut microbiota-dysbiosis on gene regulation patterns at the transcriptome level, and in further to explore the microbial-regulated pathological mechanisms of depression. As a result, 200 mRNAs, 358 lncRNAs, and 4 miRNAs were differentially expressed between the two groups. Functional analysis of these differential mRNAs indicated dysregulated inflammatory response to be the primary pathological change. Intersecting these differential mRNAs with targets of differentially expressed miRNAs identified 47 intersected mRNAs, which were mainly related to neurodevelopment. Additionally, a microbial-regulated lncRNA–miRNA–mRNA network based on RNA–RNA interactions was constructed. Subsequently, according to the competitive endogenous RNAs (ceRNA) hypothesis and the biological functions of these intersected genes, two neurodevelopmental ceRNA sub-networks implicating in depression were identified, one including two lncRNAs (4930417H01Rik and AI480526), one miRNA (mmu-miR-883b-3p) and two mRNAs (*Adcy1* and *Nr4a2*), and the other including six lncRNAs (5930412G12Rik, 6430628N08Rik, A530013C23Rik, A930007I19Rik, Gm15489, and Gm16251), one miRNA (mmu-miR-377-3p) and three mRNAs (*Six4*, *Stx16,* and

Ube3a), and these molecules could be recognized as potential genetic and epigenetic biomarkers in microbial-associated depression. This study provides new understanding of the pathogenesis of depression induced by gut microbiota-dysbiosis and may act as a theoretical basis for the development of gut microbiota-based antidepressants.

Keywords: depression, gut microbiota, lncRNAs, mRNAs, miRNAs

INTRODUCTION

Major depressive disorder (MDD) is a heterogeneous and multifactorial psychiatric disorder. Globally, more than 350 million people suffer from depression and the lifetime prevalence of MDD is 6.8% (GBD 2017 Disease and Injury Incidence and Prevalence Collaborators, 2018). Gene–environment interaction plays a crucial role in the etiology of MDD (Assary et al., 2018). The gut microbiota, a community of microorganisms in the gastrointestinal tract, is a pivotal environmental factor that is recognized to play an important role in regulating human health and disease through microbiota–host bidirectional communication (Lynch and Pedersen, 2016). In genetically susceptible individuals, the gut microbiota may interact with genetic factors to co-regulate the host's disease symptoms. Alternatively, a "pathogenic" microbiota may be sufficient to trigger a psychiatric condition, such as depression, even without a genetic risk.

Abundant preclinical and clinical evidence indicates moderating effects of the gut microbiota on the onset of depression. Significantly, disturbances in the gut microbiota, characterized by alterations in the relative abundances of the phyla *Actinobacteria*, *Bacteroidetes*, *Firmicutes,* and *Proteobacteria*, were identified in patients with MDD (Jiang et al., 2015; Zheng et al., 2016; Simpson et al., 2021). Moreover, transplant of fecal microbiota from patients with MDD into microbiota-deficient rodents promoted depressive-like behaviors indicating a causal role of gut microbiota dysbiosis in depression (Kelly et al., 2016; Zheng et al., 2016). A key question is, therefore, how do these "pathogenic" microbiota trigger the development of depression? Gut microbiota can regulate depression via the microbiota-gut-brain axis (Foster and McVey Neufeld, 2013). Previously, disruption to mitochondria-mediated biological processes, the MAPK pathway and the CAMKII-CREB pathway, and the hypothalamic-pituitary-adrenal (HPA) axis were identified in gut microbiota-dysbiosis depressed mice (Li et al., 2018; Liu et al., 2020a; Wang et al., 2020). Many pathways in the gut-brain axis, from intricate neuronal pathways to subtle small molecule messaging systems, are involved in the mechanisms by which gut microbiota dysbiosis causes depression-related brain dysfunction and behavioral changes (Cryan et al., 2019). However, the exact mechanisms are complex and remain incompletely understood.

Psychiatric disorders are characterized by transcriptional dysregulation (Gandal et al., 2018; Egervari et al., 2019), and transcriptional signatures of depression have been described (Li et al., 2021; Seney et al., 2021). MicroRNAs (miRNAs) are small non-coding RNAs of 18–25 nucleotides that can suppress gene expression by degrading and/or repressing translation of target mRNAs after binding to complementary sequences in the 3′-untranslated region (UTR) (De Martinis et al., 2020). Long non-coding RNAs (lncRNAs) are more than 200 nucleotides in length and outnumber mRNAs by 3–100 times. However, the function of most lncRNAs is still not clear. lncRNAs can regulate protein-coding genes at various levels, e.g., at epigenetic, transcriptional and post-transcriptional levels (Yao et al., 2019). lncRNAs can act as competitive endogenous RNAs (ceRNAs) that sponge miRNAs through microRNA response elements (Salmena et al., 2011), thereby regulating gene expression of target mRNAs. The absence of gut microbiota can cause changes to the expression of hippocampal mRNAs, miRNAs and lncRNAs (Moloney et al., 2017; Liu et al., 2020b), indicating a regulatory role of gut microbiota in transcriptional activity. However, the microbial-regulated lncRNA–miRNA–mRNA ceRNA network has not been investigated with respect to gut microbiota-dysbiosis-induced depression.

To comprehensively understand microbiota-regulated transcriptional networks in depression, the expression profiling of lncRNA, mRNA, and miRNA in the hippocampus of mice that had been inoculated with "depression microbiota" (microbiota from fecal samples of MDD patients) or "healthy microbiota" (microbiota from fecal samples of healthy controls) were analyzed, and the disturbed biological functions was explored to uncover the pathological mechanisms of gut microbiota-dysbiosis-regulated depression. Finally, a lncRNA–miRNA–mRNA ceRNA network was constructed based on the RNA-RNA interactions.

MATERIALS AND METHODS

Animals

Eighteen male germ-free Kunming mice (8-week-old, 30–40 g) were used in this study. During the experiment, all mice were kept under standard environmental conditions with a 12 h light/dark cycle, a temperature of 22–24°C and humidity of 45–55%. The germ-free status of mice was verified to meet the Chinese Laboratory Animal Microbiological Standards and Monitoring (GB 14922.2-2011) via testing the feces and skin. This experiment was performed in accordance with NIH Guidelines (No. 8023, revised 1978) and approved by the Ethics Committee of Chongqing Medical University.

Fecal Microbiota Transplantation

As previously described (Liu et al., 2020a), after collecting the fecal samples from MDD patients and healthy controls, 100 milligrams of feces from each sample were suspended in 1.5 ml 0.9% sterile saline, and equal volumes of suspensions

were mixed to generate a "depression microbiota" pool and a "healthy microbiota" pool. Germ-free mice (8-week-old) were randomly inoculated with 200 μl pooled samples by gavage to generate "depression microbiota" and "healthy microbiota" recipient mice. To avoid interplay of gut microbiota, mice in the two groups were kept in a separate gnotobiotic isolator. Two weeks is sufficient for successful colonization after fecal microbiota transplantation and is the benchmark time point for assessing disease phenotypes (Turnbaugh et al., 2006; Koren et al., 2012). Therefore, depression-related changes in mice were evaluated 2 weeks after colonization in present study.

Sample Collection

After anesthesia with 10% chloral hydrate (200 mg/kg, i.p.), mice were killed and the entire hippocampus, a key brain area in the neural circuitry of depression (Mayberg, 2009), was collected, rapidly frozen in liquid nitrogen, and stored at −80°C until microarray analysis. Hippocampal tissues from three randomly chosen experimental mice were mixed as a sample pool, generating three sample pools per group.

Microarray Analysis

Long Non-coding RNAs and Messenger RNAs Profiling

Total RNA was extracted using TRIzol® Reagent (Invitrogen, United States) and quantified using a NanoDrop ND-1000. Purified mRNA was obtained after removing ribosomal RNA using an mRNA-ONLY™ Eukaryotic mRNA Isolation Kit (Epicentre, United States). After labeling with a Quick Amp Labeling Kit, One-Color (Agilent, United States), the prepared RNA sample was amplified and transcribed into fluorescent cRNA using a random priming method. The labeled cRNAs were purified using an RNeasy Mini Kit (Qiagen, Germany) and hybridized onto a Mouse lncRNA Array v2.0 (8 × 60K, Arraystar, United States). Arrays were scanned with the Agilent Scanner G2505C and the acquired images were analyzed using Agilent Feature Extraction software (v 11.0.1.1). The raw data was normalized using the GeneSpring GX v12.0 software package (Agilent, United States). lncRNAs and mRNAs for which at least three out of six samples had Present or Marginal flags ("All Targets Value") were used for further analysis. Differentially expressed lncRNAs (DELs) and differentially expressed mRNAs (DEGs) between "depression microbiota" and "healthy microbiota" recipient mice with an absolute fold-change $\geq$ 1.5 and a false discovery rate (FDR) $<$ 0.05 were selected for further functional analysis. Hierarchical clustering was performed to show distinguishable DEL and DEG expression patterns among samples.

MicroRNAs Profiling

Total RNA was harvested using TRIzol® Reagent (Invitrogen, United States) and an miRNeasy mini kit (Qiagen, Germany) according to manufacturers' instructions. The quality and quantity of RNA was measured using a NanoDrop ND-1000 and RNA integrity was determined by gel electrophoresis. Samples were labeled using the miRCURY™ Hy3™/Hy5™ Power labeling kit (Exiqon, Denmark) and hybridized on a 7th generation miRCURY™ LNA Array (v.18.0) (Exiqon, Denmark). An Axon GenePix 4000B was used to scan the slides and the images were processed using GenePix Pro 6.0 software (Axon). The average was calculated for replicated miRNAs. miRNAs with an intensity $\geq$ 30 were chosen. After Median normalization, differentially expressed miRNAs (DEMs) were identified based on the thresholds of an absolute fold-change $\geq$ 1.5 and a FDR $<$ 0.05.

Prediction of Differentially Expressed MicroRNAs and Differentially Expressed Long Non-coding RNAs Targets

Target mRNAs of DEMs were first predicted using TargetScanMouse 7.2 (Agarwal et al., 2015), miRDB (Chen and Wang, 2020), DIANA-TarBase v8 (Karagkouni et al., 2018), and miRTarBase 8.0 (Chou et al., 2018) online tools, and by microRNA Target Filter analysis based on the Ingenuity Pathway Analysis (IPA) database. In addition, target lncRNAs of DEMs were analyzed using ENCORI-starBase v2.0 (Li et al., 2014) and DIANA-LncBase v2 (Paraskevopoulou et al., 2016) tools. Finally, the target mRNAs of DELs were defined as *cis*-regulated genes located within 300 kb upstream or downstream of the genomic location of the DELs.

Functional Pathway and Network Enrichment Analysis

Gene ontology (GO) analysis was applied to DEGs and the intersected mRNA targets of DEMs to determine biological process, cellular component and molecular function GO terms using OmicsBean online software[1] with default parameters. To reveal potential pathological mechanisms of gut microbiota-dysbiosis induced depression, enrichment analysis to identify functional pathways and networks were performed through uploading the gene lists (gene symbols) with the corresponding fold changes and *p*-values onto the IPA software[2], and the analysis parameters were default. Moreover, gene-gene interactions were analyzed based on the STRING database[3], and an interaction with a confidence score $>$ 0.4 was included in further network analysis. Then, the gene interaction networks were visualized using Cytoscape software (v3.7.2) (Su et al., 2014) on the basis of gene-gene interactions. Highly connected clusters were identified using the MCODE plug-in (Bader and Hogue, 2003) and the hub gene was analyzed using the NetworkAnalyzer plug-in (Doncheva et al., 2012).

Construction of the lncRNA–miRNA–mRNA Competitive Endogenous RNAs Network

To identify the key genes in microbial-associated depression, intersection analysis of the DEGs and the target genes of DEMs was performed, and the intersected mRNAs sets were used to analyze the mRNA–mRNA interactions, as

[1]http://www.omicsbean.cn/

[2]http://www.ingenuity.com

[3]https://string-db.org/

well as miRNA–mRNA regulatory pairs. In addition, the DELs were also intersected with the target lncRNAs of DEMs, and the intersected lncRNAs were selected to generate miRNA–lncRNA pairs. Subsequently, the lncRNA–miRNA–mRNA network was constructed on the basis of mRNA–mRNA interactions, miRNA–mRNA regulatory correlations, and miRNA–lncRNA relationships. According to the ceRNAs hypothesis, the DEMs and their negatively regulated DEGs and DELs were selected to generate the lncRNA–miRNA–mRNA ceRNA sub-networks. The final networks were visualized using Cytoscape software (v3.7.2).

RESULTS

Quality Assessment of RNA Data

Quality of RNA data was assessed after low intensity filtering. Box-plots of the lncRNA and mRNA indicated the distributions of the normalized intensities among all tested samples were nearly the same (**Supplementary Figures 1A,B**). Scatter-plots indicated the variation and reproducibility of the lncRNA and mRNA expression between the two compared groups (**Supplementary Figures 1C,D**). A box-plot of the miRNA is shown in **Supplementary Figure 2** to visualize the distribution of each sample, and a scatter-plot to assess the correlation among replicate experiments is shown in **Supplementary Figure 3**. Microarray-based analysis of hippocampal tissues from gut microbiota-dysbiosis mice identified the levels of lncRNAs, mRNAs, and miRNAs.

Functional Analysis of DEGs in Response to Gut Microbiota-Dysbiosis

In total, 19,775 mRNAs in the hippocampus of gut microbiota-dysbiosis mice were quantified. Based on the aforementioned screening criteria for differentially expressed RNAs, 200 DEGs were identified between the two groups (**Supplementary Table 1**). Of these, 112 were up-regulated and 88 were down-regulated in "depression microbiota" inoculated mice compared with "healthy microbiota" inoculated mice (**Figure 1A**). DEGs ranged in length from 427 to 15,363 nucleotides, with the average being 2922 nucleotides. GO annotations were performed to explore the functions of DEGs and DEGs, and several relevant GO terms were enriched (**Figure 1B**). Single-organism cellular process was the dominant GO term in biological process annotations (**Supplementary Table 2**). For the cellular component category, the DEGs were mainly annotated to extracellular space (**Supplementary Table 3**), and most DEGs under molecular function terms were annotated to binding, especially protein binding (**Supplementary Table 4**).

To explore the biological processes affected by gut microbiota-dysbiosis in mice, functional pathway and network analysis were performed. Significant canonical pathways, displayed in **Figure 1C**, were disrupted in several biological functions related to the inflammatory response, including the role of pattern recognition receptors in the recognition of bacteria and viruses, interferon signaling, and IL-12 signaling and production in macrophages. DEGs were most enriched in axonal guidance signaling function. Network analysis indicated that antimicrobial response, inflammatory response, cellular assembly and organization were the most significantly altered biological functions (**Figure 1D**). Consistently, upstream regulator analysis identified the inhibition of interferons, e.g., interferon gamma (IFNG), IFNA2, IFNL1, IRF3, and IRF7, and the activation of ACKR2, PNPT1, TRIM24, and NKX2-3 (**Figures 2A,B**), indicating perturbations of the inflammatory response in gut microbiota-dysbiosis-induced depression mice. Of the seven DEGs that led to the prediction of IFNG as the highest-ranked upstream regulator, three (*Fos*, *Lgals3bp,* and *Ifitm3*) were down-regulated and four (*Lep*, *Ins*, *Igf1,* and *Clec7a*) were up-regulated (**Figure 2C**).

Identification of gene–gene interactions was performed to further explore the pathological mechanisms of gut microbiota-dysbiosis induced depression. Our DEGs dataset produced a gene–gene network with a highly connected cluster of nodes, including *Ifi27l2a*, *Ifitm3*, *Isg15*, *Lgals3bp*, *Usp18*, *Trim21,* and *Rtp4*. The proteins encoded by these genes have synergistic functions in response to bacteria and viruses (**Figure 2D**). In addition, *Fos*, with the highest degree of interaction, was recognized as a hub gene in this gene-gene network. Interestingly, *Fos* is a transcription factor and its mRNA level can act as an index of neuronal activity. Taken together, the inhibition and activation of upstream cytokines, as well changes in the expression of related genes, indicated that dysregulation in the inflammatory response caused by gut microbiota-dysbiosis may lead to decreased neuronal activity, characterized by the down-regulation of *Fos* mRNA.

Functional Analysis of Differentially Expressed Long Non-coding RNAs in Response to Gut Microbiota-Dysbiosis

Microarray-based analysis identified 26,494 lncRNAs and 358 DELs (195 up-regulated, 163 down-regulated) between "depression microbiota" and "healthy microbiota" inoculated mice (**Figure 3A** and **Supplementary Table 5**). When DELs were compared with DEGs, half of the DELs were less than 1000 bp in length, while more than half of the DEGs were more than 2000 bp in length (**Figure 3B**). The chromosome distribution of DELs and DEGs is displayed in **Figure 3C**. According to the relationship between DELs and their associated protein-coding genes, DELs detected by Arraystar Microarray were classified as intergenic (50%), antisense overlap (26%), sense overlap (12%), and bidirectional (12%) lncRNAs (**Figure 3D**).

lncRNA subgroup analysis was performed to identify putative functional relationships between DELs and their associated protein-coding genes. Intergenic lncRNAs (lincRNAs) were the most abundant subgroup of lncRNAs, so they were used for further functional analysis. To uncover potential functions of these differentially expressed lincRNAs, *cis*-regulated, nearby genes, located within 300 kb, were predicted. After intersecting with DEGs, four target genes were identified for four lincRNAs (**Figure 3E**). *Sh3bp5l* was down-regulated in gut microbiota-dysbiosis-induced depression mice. SH3BP5L is an SH3 domain-binding protein that plays important roles in regulating

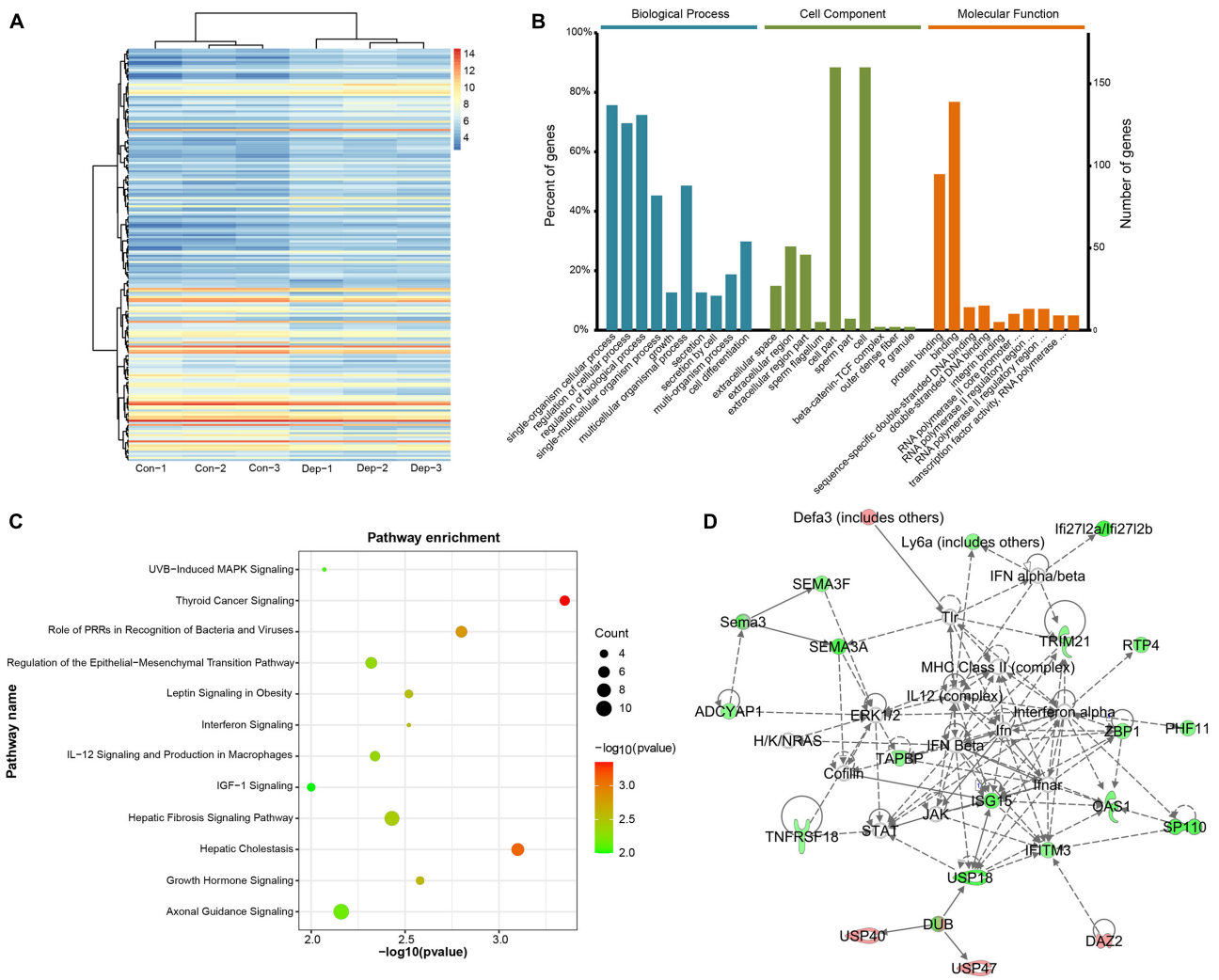

FIGURE 1 | Identification and functional analysis of differentially expressed mRNAs (DEGs) in gut microbiota-dysbiosis mice. **(A)** Hierarchical clustering of DEGs. **(B)** Gene ontology (GO) annotations of DEGs. **(C)** Canonical pathway enrichment for DEGs analyzed by Ingenuity Pathway Analysis (IPA) software. **(D)** Functional network analysis for DEGs revealed by IPA software.

proteins or signaling pathways associated with development (Hu et al., 2008). In addition, *Crabp2* was also down-regulated, and the protein it encodes functions in transporting retinoic acid from the cytosol to the nucleus. However, the functions of *Ccdc137* and *Ccdc122* remain largely unknown.

Functional Analysis of Differentially Expressed MicroRNAs in Response to Gut Microbiota-Dysbiosis

A total of 3552 miRNAs expressed in the hippocampus of gut microbiota-dysbiosis mice were identified. Screening of these miRNAs for differential expression revealed three DEMs, mmu-miR-465c-5p, mmu-miR-200b-3p, and mmu-miR-883b-3p (**Figure 4A**). mmu-miR-377-3p with a *p*-value less than 0.05 has a significant trend of decrease after FDR correction in "depression microbiota" inoculated mice, and was also included for further analysis. miRNAs can regulate gene expression by binding to the complementary sequences of their targets; therefore, putative biological functions of these four DEMs can be proposed by the functions of their target genes. Using online prediction tools, 4632 target mRNAs were identified for these four DEMs. After intersecting the target genes with the DEGs, 47 intersecting mRNAs were obtained and were used for further functional analysis. The miRNA-mRNA interaction pairs are shown in **Table 1**.

The enriched GO terms of these intersected targets are displayed in **Figure 4B**. Significantly, the generation of neurons, ganglion development, and neurogenesis were the primarily enriched biological process annotations (**Supplementary Table 6**). Meanwhile, the somatodendritic compartment and protein binding were the most significant terms in the cellular component and molecular function categories, respectively (**Supplementary Tables 7, 8**). Functional pathway

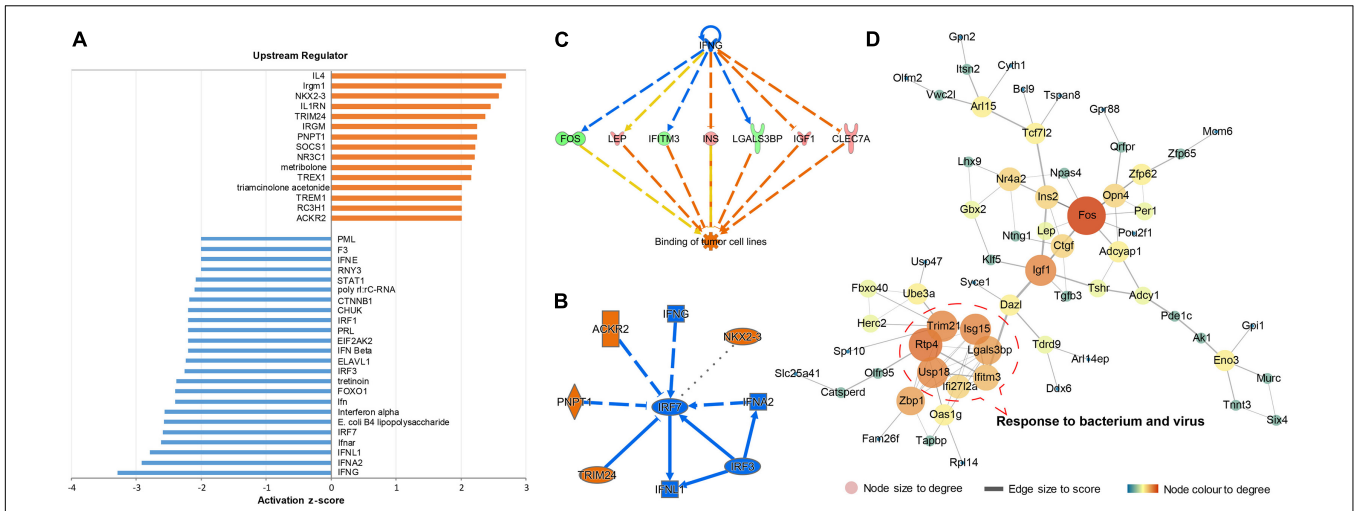

FIGURE 2 | Upstream regulator prediction and protein–protein interaction (PPI) analysis of DEGs in gut microbiota-dysbiosis mice. **(A)** Histogram showing the inhibited and activated upstream regulators of DEGs. **(B)** Graphical summary of the upstream regulators. **(C)** The highest-ranked upstream regulator, IFNG, and its downstream DEGs. **(D)** PPI network analysis of DEGs.

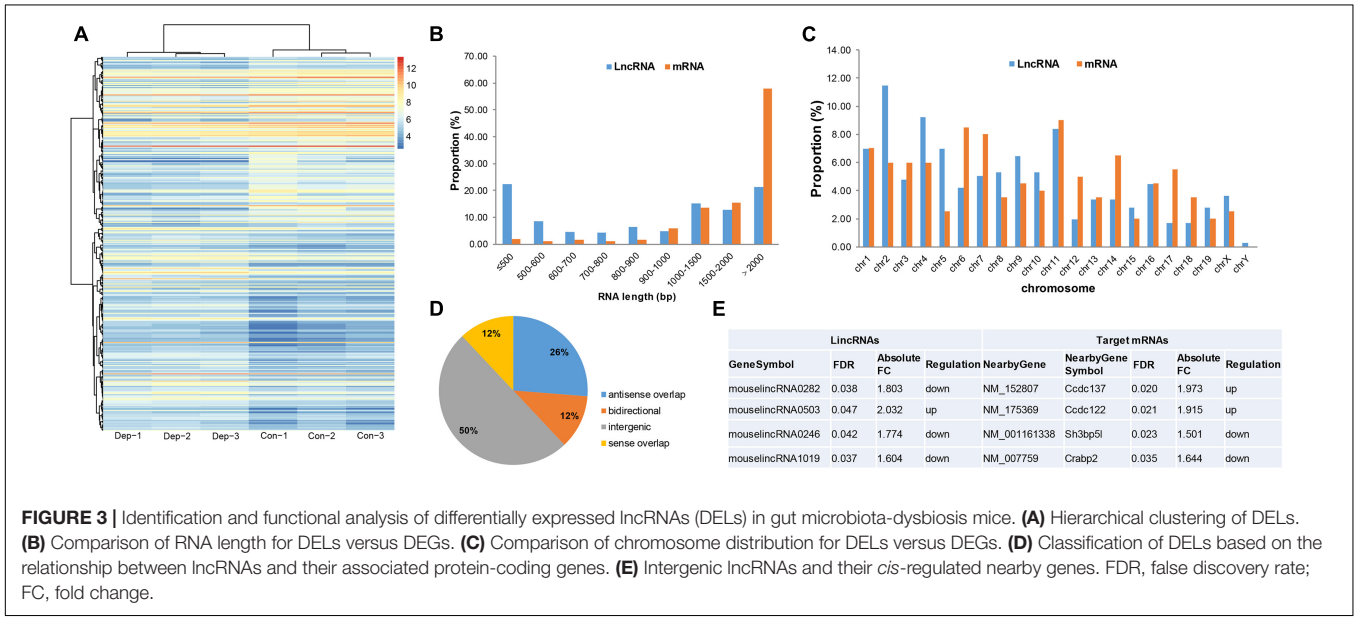

LincRNAs				Target mRNAs				
GeneSymbol	FDR	Absolute FC	Regulation	NearbyGene	NearbyGene Symbol	FDR	Absolute FC	Regulation
mouselincRNA0282	0.038	1.803	down	NM_152807	Ccdc137	0.020	1.973	up
mouselincRNA0503	0.047	2.032	up	NM_175369	Ccdc122	0.021	1.915	up
mouselincRNA0246	0.042	1.774	down	NM_001161338	Sh3bp5l	0.023	1.501	down
mouselincRNA1019	0.037	1.604	down	NM_007759	Crabp2	0.035	1.644	down

FIGURE 3 | Identification and functional analysis of differentially expressed lncRNAs (DELs) in gut microbiota-dysbiosis mice. **(A)** Hierarchical clustering of DELs. **(B)** Comparison of RNA length for DELs versus DEGs. **(C)** Comparison of chromosome distribution for DELs versus DEGs. **(D)** Classification of DELs based on the relationship between lncRNAs and their associated protein-coding genes. **(E)** Intergenic lncRNAs and their *cis*-regulated nearby genes. FDR, false discovery rate; FC, fold change.

analysis found that most target genes were enriched in axonal guidance signaling (*Herc2*, *Ntng1*, *Sema3a,* and *Sema3f*) and synaptogenesis signaling (*Adcy1*, *Itsn2,* and *Stx16*) (**Figure 4C**). Cellular assembly and organization, cellular compromise, nervous system development and function were the top-ranked biological functions (**Figure 4D**). Thus, the biological functions of these DEMs were mainly related to neurodevelopment.

Competitive Endogenous RNAs Regulatory Network in Response to Gut Microbiota-Dysbiosis

The miRNA–lncRNA interactions were analyzed to identify ceRNAs that sponge miRNAs. Total of 2193 target lncRNAs for these four DEMs were predicted, and nine lncRNAs survived after intersecting the target lncRNAs with the DELs. The resulting miRNA-lncRNA interaction pairs are shown in **Table 2**. Combining with the miRNA–mRNA interactions mentioned above, as well as the gene-gene interactions for the 47 intersected mRNAs, a lncRNA–miRNA–mRNA regulatory network was constructed (**Figure 5A**). According to the ceRNA hypothesis and the biological process annotations for these 47 intersecting genes, two sub-transcriptional ceRNA networks were re-constructed, one including two lncRNAs (4930417H01Rik and AI480526), one miRNA (mmu-miR-883b-3p) and two mRNAs (*Adcy1* and *Nr4a2*) (**Figure 5B**), and the other including six lncRNAs (5930412G12Rik, 6430628N08Rik, A530013C23Rik, A930007I19Rik, Gm15489,

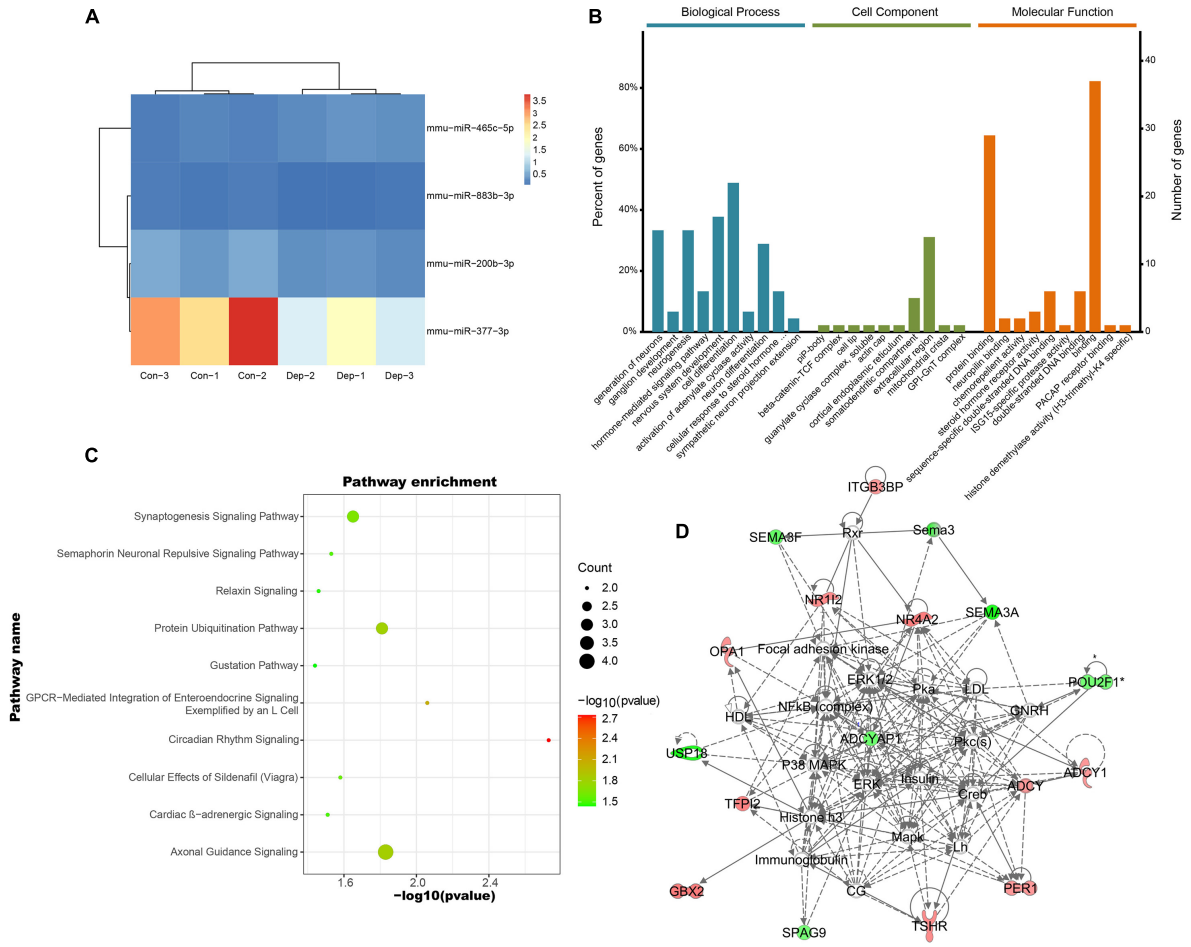

FIGURE 4 | Identification and functional analysis of differentially expressed miRNAs (DEMs) in gut microbiota-dysbiosis mice. **(A)** Hierarchical clustering of DEMs. **(B)** GO annotations of the intersected DEM targets. **(C)** Canonical pathway enrichment for the 47 intersected DEM targets analyzed using IPA software. **(D)** Functional network analysis for the 47 intersected DEM targets revealed by IPA software.

and Gm16251), one miRNA (mmu-miR-377-3p) and three mRNAs (*Six4*, *Stx16*, and *Ube3a*) (**Figure 5C**). These two ceRNA sub-networks are indicated to play important roles in neurodevelopment.

DISCUSSION

The composition of the gut microbiota in MDD is inconsistent across studies; however, higher abundance of *Actinobacteria* and *Eggerthella* and lower abundance of *Bacteroidetes*, *Prevotellaceae*, *Coprococcus*, *Faecalibacterium,* and *Sutterella* are the most consistent findings in patients with MDD compared with healthy controls (Simpson et al., 2021). Previously reports have found that germ-free mice inoculated with fecal microbiota from patients with MDD exhibited typical depressive-like behaviors, characterized by an increase in immobility time in the forced swimming and tail suspension tests compared with germ-free mice inoculated with fecal microbiota from healthy controls (Zheng et al., 2016; Liu et al., 2020a). These behavioral phenotypes may have been caused by mono-colonization or synergism of multiple bacterial species; however, the potential mechanisms by which gut microbiota-dysbiosis regulate depressive-like behaviors were complex and still unclear. In the present study, microarrays were used to profile transcript changes in gut microbiota-dysbiosis mice. Integrated analysis found that dysregulation of the inflammatory response and neurodevelopment were the primary pathological changes. In addition, two neurodevelopmental-associated lncRNA–miRNA–mRNA ceRNA regulatory network were constructed in gut microbiota-dysbiosis-induced depression, one including two lncRNAs (4930417H01Rik and AI480526), one miRNA (mmu-miR-883b-3p) and two mRNAs (*Adcy1* and *Nr4a2*), and the other including six lncRNAs (5930412G12Rik, 6430628N08Rik, A530013C23Rik, A930007I19Rik, Gm15489, and Gm16251), one miRNA (mmu-miR-377-3p) and three mRNAs (*Six4*, *Stx16,* and *Ube3a*), and these molecules could be recognized as potential genetic and epigenetic biomarkers in microbial-associated depression.

TABLE 1 | Differentially expressed miRNAs and their differentially expressed mRNA targets.

miRNAs					Target mRNAs				
ID	**Name**	**FC[a]**	**FDR[b]**	**Regulation**	**Seqname**	**GeneSymbol**	**FC (abs)[c]**	**FDR[b]**	**Regulation**
42519	mmu-miR-465c-5p	1.532561563	0.049692	Up	NM_001033407	Gm815	1.521011	0.04507730	Down
					NM_010738	Ly6a	1.621894	0.03735421	Down
					NM_001163350	Ntng1	1.795526	0.04875637	Down
					NM_001025568	Pde1c	1.544196	0.04748477	Down
					NM_198932	Pou2f1	1.5370071	0.04118802	Down
					NM_009152	Sema3a	2.5020425	0.04096039	Down
					NM_177164	Vwc2l	1.8152527	0.02411733	Down
					NM_145575	Cald1	1.602462	0.04895628	Up
					NM_001037321	Fbxo40	1.5813568	0.02854253	Up
					NM_010262	Gbx2	2.0050368	0.04074322	Up
					NM_010418	Herc2	1.6062031	0.04839108	Up
					NM_026348	Itgb3bp	1.5665871	0.00909908	Up
					NM_001098404	Nr1i2	1.7842534	0.04952551	Up
					NM_133752	Opa1	1.6633599	0.03013054	Up
					NM_001003717	Osbpl8	1.6370533	0.04842034	Up
					NM_028748	Paqr5	1.7612659	0.02971225	Up
					NM_001159367	Per1	1.567625	0.02170788	Up
					NM_011137	Pou2f1	1.5176835	0.02779596	Up
					NM_178227	Scn3b	1.6376927	0.02688412	Up
					NM_001113404	Tshr	1.7740262	0.03473434	Up
147186	mmu-miR-200b-3p	0.658253975	0.041228	down	NM_009649	Akap2	1.522913	0.04842372	Up
					NM_172595	Arl15	1.5095077	0.04860469	Up
					NM_029933	Bcl9	1.5354732	0.02891231	Up
					NM_001081225	Fam178a	1.6083025	0.04959859	Up
					NM_030201	Hspa13	3.1505609	0.01178443	Up
					NM_011365	Itsn2	1.7630032	0.03734254	Up
					NM_178227	Scn3b	1.6376927	0.02688412	Up
					NM_173010	Ube3a	1.6787672	0.01200062	Up
					NM_001109691	Phf21a	1.859211	0.03746215	Down
					NM_011081	Piga	1.6523745	0.04463066	Down
					NM_009152	Sema3a	2.5020425	0.04096039	Down
					NM_011349	Sema3f	1.7213542	0.04393336	Down
					NM_001199205	Spag9	1.517349	0.04762527	Down
					NM_029056	Tdrd9	1.5761601	0.04880729	Down
					NM_001101640	Tmem207	1.8919897	0.04882137	Down
					NM_011909	Usp18	2.5167851	0.02862872	Down
42883	mmu-miR-883b-3p	0.569539569	0.039109	Down	NM_009622	Adcy1	1.580024	0.03985197	Up
					NM_172595	Arl15	1.5095077	0.04860469	Up
					NM_001163333	Cttnbp2nl	1.7116936	0.01972822	Up
					NM_152895	Kdm5b	1.687644	0.04898798	Up
					NM_001139509	Nr4a2	1.9803841	0.04820689	Up
					NM_133752	Opa1	1.6633599	0.03013054	Up
					NM_009364	Tfpi2	1.9140846	0.04680254	Up
					NM_009625	Adcyap1	1.6437125	0.03973875	Down
					NM_009152	Sema3a	2.5020425	0.04096039	Down
					NM_001039967	Zfp869	1.7256061	0.02157675	Down
11091	mmu-miR-377-3p	0.471786427	0.066332*	down	NM_021483	Pex5l	1.618897	0.03024903	Up
					NM_011382	Six4	1.510553	0.04898937	Up
					NM_177829	Spink10	1.535757	0.02555243	Up
					NM_001102425	Stx16	1.6225739	0.04827980	Up
					NM_173010	Ube3a	1.6787672	0.01200062	Up
					NM_019626	Cbln1	2.1865587	0.03002855	Down
					NM_001164518	Iglon5	1.9751669	0.02888774	Down
					NM_001025568	Pde1c	1.544196	0.04748477	Down
					NM_001109691	Phf21a	1.859211	0.03746215	Down

[a] *Fold change = the ratio of normalized intensities between two conditions (use normalized data, ratio scale). Normalized Data = (Foreground–Background)/median.*

[b] *False discovery rate that was calculated by Benjamini–Hochberg method.*

[c] *Absolute fold change = the absolute ratio (no log scale) of normalized intensities between two conditions.*

**This miRNA has a p-value < 0.05.*

TABLE 2 | Differentially expressed miRNAs and their differentially expressed lncRNAs targets.

ID	Name	FC[a]	FDR[b]	Regulation	Seqname	GeneSymbol	FDR[b]	FC(abs)[c]	Regulation
147186	mmu-miR-200b-3p	0.658254	0.041228	Down	ENSMUST00000159119	Gas5	0.04911062	2.3057933	Down
42883	mmu-miR-883b-3p	0.56954	0.039109	Down	ENSMUST00000148977	4930417H01Rik	0.04292526	1.6698261	Up
					ENSMUST00000160227	AI480526	0.03374033	1.9144645	Up
11091	mmu-miR-377-3p	0.471786	0.066332*	Down	ENSMUST00000126472	5930412G12Rik	0.03637584	1.8078425	Up
					ENSMUST00000165938	6430628N08Rik	0.04965351	1.5305915	Up
					NR_015500	A530013C23Rik	0.04294613	2.0565884	Up
					ENSMUST00000155013	A930007I19Rik	0.04227756	1.5199345	Up
					ENSMUST00000132811	Gm15489	0.04533299	2.6704226	Up
					ENSMUST00000162649	Gm16251	0.04966378	1.9383893	Up

[a] *Fold change = the ratio of normalized intensities between two conditions (use normalized data, ratio scale). Normalized Data = (Foreground–Background)/median.*
[b] *False discovery rate that was calculated by Benjamini–Hochberg method.*
[c] *Absolute fold change = the absolute ratio (no log scale) of normalized intensities between two conditions.*
**This miRNA has a p-value < 0.05.*

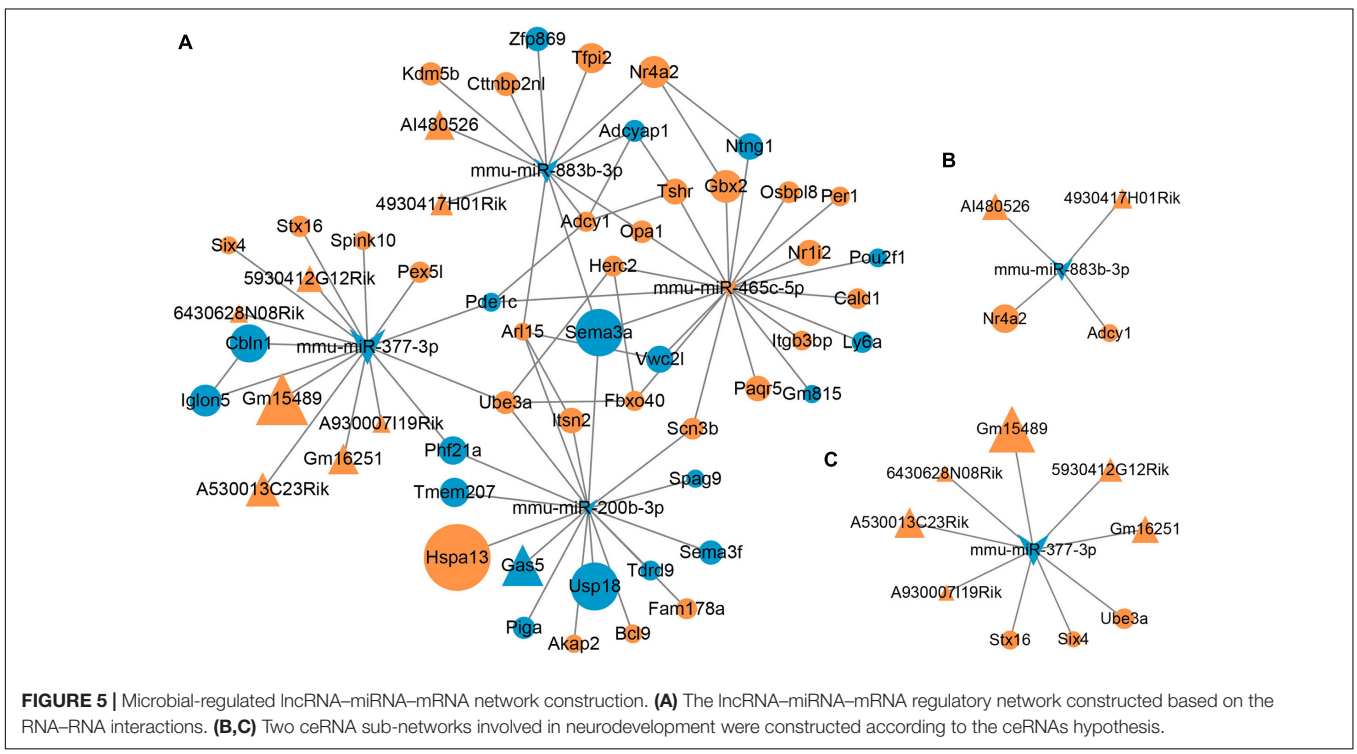

FIGURE 5 | Microbial-regulated lncRNA–miRNA–mRNA network construction. **(A)** The lncRNA–miRNA–mRNA regulatory network constructed based on the RNA–RNA interactions. **(B,C)** Two ceRNA sub-networks involved in neurodevelopment were constructed according to the ceRNAs hypothesis.

According to the hygiene hypothesis, the development and balance of the immune system are closely related to gut microbiota colonization (Bach, 2018). Under conditions of gut microbiota-dysbiosis, toxins and harmful bacteria can trigger an imbalanced inflammatory response that can lead to autoimmune diseases (Pickard et al., 2017). MDD was characterized to have a lower abundance of anti-inflammatory bacteria (e.g., *Coprococcus* and *Faecalibacterium*) and a higher relative abundance of pro-inflammatory species (e.g., *Eggerthella*) (Simpson et al., 2021). In addition to the effects of gut microbiota *per se*, imbalanced inflammatory responses are widely recognized to contribute to the pathogenesis of depression (Gałecki and Talarowska, 2018). In patients with depression, the levels of CRP, IL-6, IL-12, and TNF-α are significantly elevated, indicating a pro-inflammatory state (Osimo et al., 2020). Clinical studies have shown anti-inflammatory agents, in particular cytokine-inhibitors and non-steroidal anti-inflammatory drugs (NSAIDs), to have antidepressant effects either as an add-on strategy or as monotherapy (Kohler et al., 2016), indicating an etiological role of inflammation in depression. In the present study, several biological functions related to the inflammatory response were dysregulated, such as the role of pattern recognition receptors in the recognition of bacteria and viruses, interferon signaling, and IL-12 signaling and production in macrophages. Previous study has indicated that transplanting the fecal microbiota from chronic unpredictable mild stress mice caused depressive-like behaviors in recipient mice via the gut microbiota-inflammation-brain axis (Li et al., 2019). Dysregulation of

the downstream inflammatory response leads to the inhibition or activation of the corresponding upstream regulators, e.g., the inhibition of IFNG, IFNA2, IFNL1, IRF3, and IRF7, and the activation of ACKR2, PNPT1, TRIM24, and NKX2-3. As the highest-ranked upstream regulator, IFNG was predicted to be inhibited, and its downstream target, *Fos*, an index of neuronal activity, was down-regulated in gut microbiota-dysbiosis mice. IFNG has been proved to play a role in the development of depressive-like behaviors and its related hippocampal neurogenesis through regulating the function of microglia (Zhang et al., 2020). Neuroinflammatory-mediated mechanisms can influence neuronal activity as well as synaptic plasticity and have been implicated in the neurobiology of depression (Wohleb et al., 2016). Thus, it is inferred that dysregulation of the inflammatory response caused by gut microbiota-dysbiosis may lead to decreased neuronal activity in depression, characterized by the down-regulation of *Fos* mRNA.

Brain development occurs in parallel with gut microbiota development during early postnatal life (Tognini, 2017; Wang et al., 2018), indicating an essential role of gut microbiota in neurodevelopment, including neurogenesis, myelination, microglia maturation, and formation of the blood-brain barrier (Sharon et al., 2016). Imbalance in the relative abundance of specific "pathogenic" bacteria in the gut microbiota is strongly associated with the onset of psychiatric disorders, e.g., depression, possibly because of altered neurodevelopment (Lima-Ojeda et al., 2017; Settanni et al., 2021). Both germ-free mice and antibiotic-treated specific pathogen free mice show alterations in hippocampal neurogenesis (Möhle et al., 2016), as well as in cortical myelination and myelin plasticity (Hoban et al., 2016). Deficient hippocampal neurogenesis is implicated in the pathogenesis of depression (Snyder et al., 2011), while increasing hippocampal neurogenesis is sufficient to recover depressive-like behaviors in mice (Hill et al., 2015). In this study, GO analysis showed that the intersected DEGs regulated by DEMs were mainly enriched in neurodevelopment, in particular axonal guidance signaling (*Herc2*, *Ntng1*, *Sema3a,* and *Sema3f*) and synaptogenesis (*Adcy1*, *Itsn2,* and *Stx16*), as well as neuron generation, ganglion development and neurogenesis. According to the negative regulatory relationships between mRNAs and miRNAs, it is inferred that the microbial-regulated pairs of mmu-miR-465c-5p-*Ntng1*, mmu-miR-465c-5p-*Sema3a*, mmu-miR-883b-3p-*Adcy1*, mmu-miR-200b-3p-*Itsn2,* and mmu-miR-377-3p-*Stx16* play important roles in neurodevelopment. Interestingly, miR-200 microRNA family has been recently identified as an important regulator of gliogenesis and neurogenesis and of adult neural homeostasis in the central nervous system of rodents (Trümbach and Prakash, 2015), and the expression levels of miR-200 family were elevated in mature and differentiated neurons (Jauhari and Yadav, 2019). The downregulation of mmu-miR-200b-3p in present study suggested the impairment of neurodevelopment in gut microbiota-dysbiosis induced depression mice. However, the exact effects of new genetic biomarkers, i.e., mmu-miR-465c-5p, mmu-miR-883b-3p, and mmu-miR-377-3p, on neurodevelopment needed to be further warranted. Consistently, our previous phosphoproteomics study indicated that axon guidance was the primary functional change shared among gut microbiota-dysbiosis-induced depression mice, stress-induced depression rats and MDD postmortem brains (Wang et al., 2020). Taken together, it is suggested that alterations in neurodevelopment, such as axonal guidance, neurogenesis and myelination, underlie the pathological mechanisms by which gut microbiota-dysbiosis induces depression in mice.

It is speculated that miRNAs regulate approximately one third of human genes. miRNAs can suppress gene expression through mRNA translational repression, degradation, or both. In addition to miRNAs, lncRNAs are also emerging as important regulators of gene expression at epigenetic, transcriptional and post-transcriptional levels (Yao et al., 2019). Based on the ceRNA hypothesis, in which lncRNAs act as ceRNAs that sponge miRNAs via microRNA response elements to regulate mRNA, two microbial-regulated lncRNA–miRNA–mRNA ceRNA networks that play important roles in neurodevelopment in depression were constructed in present study. From these two sub-networks, these eight novel lncRNAs (4930417H01Rik, AI480526, 5930412G12Rik, 6430628N08Rik, A530013C23Rik, A930007I19Rik, Gm15489, and Gm16251), two miRNAs (mmu-miR-883b-3p and mmu-miR-377-3p) and five mRNAs (*Adcy1*, *Nr4a2*, *Six4*, *Stx16,* and *Ube3a*) were speculated as key molecules in gut microbiota-dysbiosis-induced depression, and these molecules could be recognized as potential genetic and epigenetic biomarkers in microbial-associated depression. miR-377-3p functions in regulating the inflammatory response, cell proliferation and apoptosis rate (Sun et al., 2021). Previously, dysregulated expression of *Adcy1* mRNA was identified in the hippocampus and prefrontal cortex of restraint stress induced depression mice, and suggested *Adcy1* as a potential biomarkers in depression, and may act as a target in treatment of depression (Yang et al., 2020). *Nr4a2* gene polymorphisms were found to be associated with several symptoms of MDD, and may be a predictor of antidepressant efficacy (Song et al., 2021). Whereas, further evidences were still required to verify the potential roles of the remaining molecules as genetic and epigenetic biomarkers in depression.

Integrated analysis of lncRNAs, miRNAs, and mRNAs enables us to comprehensively screen the potential genetic and epigenetic biomarkers in depression at the transcriptional level and clarify their regulatory roles in the microbiota-gut-brain axis, which will be essential to explore the diagnostic biomarkers and therapeutic targets for depression, especially in the gut microbiota-dysbiosis caused depression. However, extending the present findings to the diagnosis and treatment of depression in humans is still a substantial challenge, due to the obvious biological differences between animals and humans, and the complexity, individuality, and dynamics of biological features in humans aggravate this challenge. Anyhow, the identification of these genetic and epigenetic biomarkers promotes the progress to develop the diagnosis and treatment strategies for depression.

This study has some limitations. Although the high sensitivity and specificity of the microarrays provide a high level of confidence for the present findings, it can't exclude the false negative rates due to the small sample sizes; thus, these findings

needed to be experimentally verified in future studies. In addition, further studies are required to determine whether dysregulated inflammation is a response of the host to gut microbiota *per se* or a pathological change in depression caused by gut microbiota-dysbiosis.

CONCLUSION

In summary, significant alterations have been identified in the composition of fecal microbiomes of patients with MDD. In the present study, the effects of depression-related gut microbiota on gene transcription in mice were analyzed to explore the pathological mechanisms of depression caused by gut microbiota dysbiosis, and found that dysregulation of the inflammatory response and neurodevelopment were the primary pathological changes. In addition, two microbial-regulated lncRNA–miRNA–mRNA ceRNA regulatory networks involved in depression-related neurodevelopment were constructed, one including two lncRNAs (4930417H01Rik and AI480526), one miRNA (mmu-miR-883b-3p) and two mRNAs (*Adcy1* and *Nr4a2*), and the other including six lncRNAs (5930412G12Rik, 6430628N08Rik, A530013C23Rik, A930007I19Rik, Gm15489 and Gm16251), one miRNA (mmu-miR-377-3p) and three mRNAs (*Six4*, *Stx16*, and *Ube3a*), and these molecules could be recognized as potential genetic and epigenetic biomarkers in microbial-associated depression. This study provides new clues for understanding the pathogenesis of gut microbiota-dysbiosis-induced depression and may act as a theoretical basis for the development of gut microbiota-based antidepressants.

DATA AVAILABILITY STATEMENT

The datasets presented in the present study can be found in GEO DataSets, and the GEO accession is GSE189234.

ETHICS STATEMENT

The animal study was reviewed and approved by Ethics Committee of Chongqing Medical University.

AUTHOR CONTRIBUTIONS

PX and LL designed the work. HW, XC, YZ, and XR performed the experiments. WL and DY bred the germ-free mice. JP, LF, and SG analyzed the data. LL drafted the manuscript. YL, LZ, and PX revised the manuscript. All authors have read and approved the final manuscript.

FUNDING

This study was supported by the National Key R&D Program of China (Grant No. 2017YFA0505700), the Non-Profit Central Research Institute Fund of the Chinese Academy of Medical Sciences (Grant No. 2019PT320002), the Natural Science Foundation Project of China (Grant No. 81820108015), the China Postdoctoral Science Foundation (Nos. 2020TQ0393, 2020M683634XB, and 2021M693926), and the Chongqing Science & Technology Commission (Nos. cstc2021jcyj-bsh0026 and cstc2021jcyj-bsh0034).

SUPPLEMENTARY MATERIAL

The Supplementary Material for this article can be found online at: https://www.frontiersin.org/articles/10.3389/fnmol.2021.745437/full#supplementary-material

REFERENCES

Agarwal, V., Bell, G. W., Nam, J. W., and Bartel, D. P. (2015). Predicting effective microRNA target sites in mammalian mRNAs. *Elife* 4:5. doi: 10.7554/eLife.05005

Assary, E., Vincent, J. P., Keers, R., and Pluess, M. (2018). Gene-environment interaction and psychiatric disorders: review and future directions. *Semin. Cell Dev. Biol.* 77, 133–143. doi: 10.1016/j.semcdb.2017.10.016

Bach, J. F. (2018). The hygiene hypothesis in autoimmunity: the role of pathogens and commensals. *Nat. Rev. Immunol.* 18, 105–120. doi: 10.1038/nri.2017.111

Bader, G. D., and Hogue, C. W. V. (2003). An automated method for finding molecular complexes in large protein interaction networks. *BMC Bioinform.* 4:2. doi: 10.1186/1471-2105-4-2

Chen, Y., and Wang, X. (2020). miRDB: an online database for prediction of functional microRNA targets. *Nucleic Acids Res.* 48, D127–D131. doi: 10.1093/nar/gkz757

Chou, C.-H., Shrestha, S., Yang, C.-D., Chang, N.-W., Lin, Y.-L., Liao, K.-W., et al. (2018). miRTarBase update 2018: a resource for experimentally validated microRNA-target interactions. *Nucleic Acids Res.* 46, D296–D302. doi: 10.1093/nar/gkx1067

Cryan, J. F., O'Riordan, K. J., Cowan, C. S. M., Sandhu, K. V., Bastiaanssen, T. F. S., Boehme, M., et al. (2019). The Microbiota-Gut-Brain Axis. *Physiol. Rev.* 99, 1877–2013. doi: 10.1152/physrev.00018.2018

De Martinis, M., Ginaldi, L., Allegra, A., Sirufo, M. M., Pioggia, G., Tonacci, A., et al. (2020). The osteoporosis/microbiota linkage: the role of miRNA. *Int. J. Mol. Sci.* 21:21238887. doi: 10.3390/ijms21238887

Doncheva, N. T., Assenov, Y., Domingues, F. S., and Albrecht, M. (2012). Topological analysis and interactive visualization of biological networks and protein structures. *Nat. Protoc.* 7, 670–685. doi: 10.1038/nprot.2012.004

Egervari, G., Kozlenkov, A., Dracheva, S., and Hurd, Y. L. (2019). Molecular windows into the human brain for psychiatric disorders. *Mol. Psychiatry.* 24, 653–673. doi: 10.1038/s41380-018-0125-2

Foster, J. A., and McVey Neufeld, K.-A. (2013). Gut-brain axis: how the microbiome influences anxiety and depression. *Trends Neurosci.* 36, 305–312. doi: 10.1016/j.tins.2013.01.005

Gałecki, P., and Talarowska, M. (2018). Inflammatory theory of depression. *Psychiatr. Pol.* 52, 437–447. doi: 10.12740/pp/76863

Gandal, M. J., Zhang, P., Hadjimichael, E., Walker, R. L., Chen, C., Liu, S., et al. (2018). Transcriptome-wide isoform-level dysregulation in ASD, schizophrenia, and bipolar disorder. *Science* 362:8127. doi: 10.1126/science.aat8127

GBD 2017 Disease and Injury Incidence and Prevalence Collaborators (2018). Global, regional, and national incidence, prevalence, and years lived with disability for 354 diseases and injuries for 195 countries and territories, 1990-2017: a systematic analysis for the Global Burden of Disease Study 2017. *Lancet* 392, 1789–1858. doi: 10.1016/S0140-6736(18)32279-7

Hill, A. S., Sahay, A., and Hen, R. (2015). Increasing adult hippocampal neurogenesis is sufficient to reduce anxiety and depression-like behaviors. *Neuropsychopharmacology* 40, 2368–2378. doi: 10.1038/npp.2015.85

Hoban, A. E., Stilling, R. M., Ryan, F. J., Shanahan, F., Dinan, T. G., Claesson, M. J., et al. (2016). Regulation of prefrontal cortex myelination by the microbiota. *Transl. Psychiatry*. 6:e774. doi: 10.1038/tp.2016.42

Hu, Z.-G., Chen, Y., Zhou, Q., Lv, X.-Y., Zhang, Z., Wang, Y.-D., et al. (2008). Characterization of a novel Xenopus SH3 domain binding protein 5 like (xSH3BP5L) gene. *Biochem. Biophys. Res. Commun.* 365, 214–220. doi: 10.1016/j.bbrc.2007.10.146

Jauhari, A., and Yadav, S. (2019). MiR-34 and MiR-200: regulator of cell fate plasticity and neural development. *Neuromol. Med.* 21:9. doi: 10.1007/s12017-019-08535-9

Jiang, H., Ling, Z., Zhang, Y., Mao, H., Ma, Z., Yin, Y., et al. (2015). Altered fecal microbiota composition in patients with major depressive disorder. *Brain Behav. Immun.* 48, 186–194. doi: 10.1016/j.bbi.2015.03.016

Karagkouni, D., Paraskevopoulou, M. D., Chatzopoulos, S., Vlachos, I. S., Tastsoglou, S., Kanellos, I., et al. (2018). DIANA-TarBase v8: a decade-long collection of experimentally supported miRNA-gene interactions. *Nucleic Acids Res.* 46, D239–D245. doi: 10.1093/nar/gkx1141

Kelly, J. R., Borre, Y., O' Brien, C., Patterson, E., El Aidy, S., Deane, J., et al. (2016). Transferring the blues: Depression-associated gut microbiota induces neurobehavioural changes in the rat. *J. Psychiatr. Res.* 82, 109–118. doi: 10.1016/j.jpsychires.2016.07.019

Kohler, O., Krogh, J., Mors, O., and Benros, M. E. (2016). Inflammation in depression and the potential for anti-inflammatory treatment. *Curr. Neuropharmacol.* 14, 732–742. doi: 10.2174/1570159x14666151208113700

Koren, O., Goodrich, J. K., Cullender, T. C., Spor, A., Laitinen, K., Backhed, H. K., et al. (2012). Host remodeling of the gut microbiome and metabolic changes during pregnancy. *Cell* 150, 470–480. doi: 10.1016/j.cell.2012.07.008

Li, B., Guo, K., Zeng, L., Zeng, B., Huo, R., Luo, Y., et al. (2018). Metabolite identification in fecal microbiota transplantation mouse livers and combined proteomics with chronic unpredictive mild stress mouse livers. *Transl. Psychiatry* 8:34. doi: 10.1038/s41398-017-0078-2

Li, J., Seidlitz, J., Suckling, J., Fan, F., Ji, G.-J., Meng, Y., et al. (2021). Cortical structural differences in major depressive disorder correlate with cell type-specific transcriptional signatures. *Nat. Commun.* 12:1647. doi: 10.1038/s41467-021-21943-5

Li, J.-H., Liu, S., Zhou, H., Qu, L.-H., and Yang, J.-H. (2014). starBase v2.0: decoding miRNA-ceRNA, miRNA-ncRNA and protein-RNA interaction networks from large-scale CLIP-Seq data. *Nucleic Acids Res.* 42, D92–D97. doi: 10.1093/nar/gkt1248

Li, N., Wang, Q., Wang, Y., Sun, A., Lin, Y., Jin, Y., et al. (2019). Fecal microbiota transplantation from chronic unpredictable mild stress mice donors affects anxiety-like and depression-like behavior in recipient mice via the gut microbiota-inflammation-brain axis. *Stress* 22, 592–602. doi: 10.1080/10253890.2019.1617267

Lima-Ojeda, J. M., Rupprecht, R., and Baghai, T. C. (2017). "I am i and my bacterial circumstances": linking gut microbiome, neurodevelopment, and depression. *Front. Psychiatry* 8:153. doi: 10.3389/fpsyt.2017.00153

Liu, L., Wang, H., Rao, X., Yu, Y., Li, W., Zheng, P., et al. (2020a). Comprehensive analysis of the lysine acetylome and succinylome in the hippocampus of gut microbiota-dysbiosis mice. *J. Adv. Res.* 2020:2. doi: 10.1016/j.jare.2020.12.002

Liu, L., Wang, H., Yu, Y., Zeng, B., Rao, X., Chen, J., et al. (2020b). Microbial regulation of a lincRNA-miRNA-mRNA network in the mouse hippocampus. *Epigenomics* 12, 1377–1387. doi: 10.2217/epi-2019-0307

Lynch, S. V., and Pedersen, O. (2016). The human intestinal microbiome in health and disease. *N. Engl. J. Med.* 375, 2369–2379. doi: 10.1056/NEJMra1600266

Mayberg, H. S. (2009). Targeted electrode-based modulation of neural circuits for depression. *J. Clin. Invest.* 119, 717–725. doi: 10.1172/JCI38454

Möhle, L., Mattei, D., Heimesaat, M. M., Bereswill, S., Fischer, A., Alutis, M., et al. (2016). Ly6C(hi) monocytes provide a link between antibiotic-induced changes in gut microbiota and adult hippocampal neurogenesis. *Cell Rep.* 15, 1945–1956. doi: 10.1016/j.celrep.2016.04.074

Moloney, G. M., O'Leary, O. F., Salvo-Romero, E., Desbonnet, L., Shanahan, F., Dinan, T. G., et al. (2017). Microbial regulation of hippocampal miRNA expression: Implications for transcription of kynurenine pathway enzymes. *Behav. Brain Res.* 334, 50–54. doi: 10.1016/j.bbr.2017.07.026

Osimo, E. F., Pillinger, T., Rodriguez, I. M., Khandaker, G. M., Pariante, C. M., and Howes, O. D. (2020). Inflammatory markers in depression: A meta-analysis of mean differences and variability in 5,166 patients and 5,083 controls. *Brain Behav. Immun.* 87, 901–909. doi: 10.1016/j.bbi.2020.02.010

Paraskevopoulou, M. D., Vlachos, I. S., Karagkouni, D., Georgakilas, G., Kanellos, I., Vergoulis, T., et al. (2016). DIANA-LncBase v2: indexing microRNA targets on non-coding transcripts. *Nucleic Acids Res.* 44, D231–D238. doi: 10.1093/nar/gkv1270

Pickard, J. M., Zeng, M. Y., Caruso, R., and Núñez, G. (2017). Gut microbiota: Role in pathogen colonization, immune responses, and inflammatory disease. *Immunol. Rev.* 279, 70–89. doi: 10.1111/imr.12567

Salmena, L., Poliseno, L., Tay, Y., Kats, L., and Pandolfi, P. P. (2011). A ceRNA hypothesis: the Rosetta Stone of a hidden RNA language? *Cell* 146, 353–358. doi: 10.1016/j.cell.2011.07.014

Seney, M. L., Glausier, J., and Sibille, E. (2021). Large-Scale transcriptomics studies provide insight into sex differences in depression. *Biol. Psychiatry* 2021:25. doi: 10.1016/j.biopsych.2020.12.025

Settanni, C. R., Ianiro, G., Bibbò, S., Cammarota, G., and Gasbarrini, A. (2021). Gut microbiota alteration and modulation in psychiatric disorders: current evidence on fecal microbiota transplantation. *Prog. Neuropsychopharmacol. Biol. Psychiatry* 109:110258. doi: 10.1016/j.pnpbp.2021.110258

Sharon, G., Sampson, T. R., Geschwind, D. H., and Mazmanian, S. K. (2016). The central nervous system and the gut microbiome. *Cell* 167, 915–932. doi: 10.1016/j.cell.2016.10.027

Simpson, C. A., Diaz-Arteche, C., Eliby, D., Schwartz, O. S., Simmons, J. G., and Cowan, C. S. M. (2021). The gut microbiota in anxiety and depression - a systematic review. *Clin. Psychol. Rev.* 83:101943. doi: 10.1016/j.cpr.2020.101943

Snyder, J. S., Soumier, A., Brewer, M., Pickel, J., and Cameron, H. A. (2011). Adult hippocampal neurogenesis buffers stress responses and depressive behaviour. *Nature* 476, 458–461. doi: 10.1038/nature10287

Song, X., Sun, N., Zhang, A., Lei, L., Li, X., Liu, Z., et al. (2021). Association between NR4A2 Gene polymorphism and depressive symptoms and antidepressant effect. *Neuropsychiatr. Dis. Treat.* 17, 2613–2623. doi: 10.2147/NDT.S319548

Su, G., Morris, J. H., Demchak, B., and Bader, G. D. (2014). Biological network exploration with Cytoscape 3. *Curr. Protoc. Bioinform.* 2014:47. doi: 10.1002/0471250953.bi0813s47

Sun, Q., Shen, X., Ma, J., Lou, H., and Sha, W. (2021). LncRNA NEAT1 participates in inflammatory response in macrophages infected by mycobacterium tuberculosis through targeted regulation of miR-377-3p. *Microb. Pathog.* 150:104674. doi: 10.1016/j.micpath.2020.104674

Tognini, P. (2017). Gut microbiota: a potential regulator of neurodevelopment. *Front. Cell Neurosci.* 11:25. doi: 10.3389/fncel.2017.00025

Trümbach, D., and Prakash, N. (2015). The conserved miR-8/miR-200 microRNA family and their role in invertebrate and vertebrate neurogenesis. *Cell Tissue Res.* 359, 161–177. doi: 10.1007/s00441-014-1911-z

Turnbaugh, P. J., Ley, R. E., Mahowald, M. A., Magrini, V., Mardis, E. R., and Gordon, J. I. (2006). An obesity-associated gut microbiome with increased capacity for energy harvest. *Nature* 444, 1027–1031. doi: 10.1038/nature05414

Wang, H., Liu, L., Rao, X., Zeng, B., Yu, Y., Zhou, C., et al. (2020). Integrated phosphoproteomic and metabolomic profiling reveals perturbed pathways in the hippocampus of gut microbiota dysbiosis mice. *Transl. Psychiatry* 10:346. doi: 10.1038/s41398-020-01024-9

Wang, S., Harvey, L., Martin, R., van der Beek, E. M., Knol, J., Cryan, J. F., et al. (2018). Targeting the gut microbiota to influence brain development and function in early life. *Neurosci. Biobehav. Rev.* 95, 191–201. doi: 10.1016/j.neubiorev.2018.09.002

Wohleb, E. S., Franklin, T., Iwata, M., and Duman, R. S. (2016). Integrating neuroimmune systems in the neurobiology of depression. *Nat. Rev. Neurosci.* 17, 497–511. doi: 10.1038/nrn.2016.69

Yang, M., Ding, Q., Zhang, M., Moon, C., and Wang, H. (2020). Forebrain overexpression of type 1 adenylyl cyclase promotes molecular stability and behavioral resilience to physical stress. *Neurobiol. Stress* 13:100237. doi: 10.1016/j.ynstr.2020.100237

Yao, R. W., Wang, Y., and Chen, L. L. (2019). Cellular functions of long noncoding RNAs. *Nat. Cell Biol.* 21, 542–551. doi: 10.1038/s41556-019-0311-8

Zhang, J., He, H., Qiao, Y., Zhou, T., He, H., Yi, S., et al. (2020). Priming of microglia with IFN-γ impairs adult hippocampal neurogenesis and leads to depression-like behaviors and cognitive defects. *Glia* 68, 2674–2692. doi: 10.1002/glia.23878

Zheng, P., Zeng, B., Zhou, C., Liu, M., Fang, Z., Xu, X., et al. (2016). Gut microbiome remodeling induces depressive-like behaviors through a pathway mediated by the host's metabolism. *Mol. Psychiatry* 21, 786–796. doi: 10.1038/mp.2016.44

Conflict of Interest: The authors declare that the research was conducted in the absence of any commercial or financial relationships that could be construed as a potential conflict of interest.

Publisher's Note: All claims expressed in this article are solely those of the authors and do not necessarily represent those of their affiliated organizations, or those of the publisher, the editors and the reviewers. Any product that may be evaluated in this article, or claim that may be made by its manufacturer, is not guaranteed or endorsed by the publisher.

Copyright © 2022 Liu, Wang, Chen, Zhang, Li, Rao, Liu, Zhao, Pu, Gui, Yang, Fang and Xie. This is an open-access article distributed under the terms of the Creative Commons Attribution License (CC BY). The use, distribution or reproduction in other forums is permitted, provided the original author(s) and the copyright owner(s) are credited and that the original publication in this journal is cited, in accordance with accepted academic practice. No use, distribution or reproduction is permitted which does not comply with these terms.

frontiers | Frontiers in Molecular Neuroscience

ORIGINAL RESEARCH
published: 26 April 2022
doi: 10.3389/fnmol.2022.822129

Social Deficits and Cerebellar Degeneration in Purkinje Cell *Scn8a* Knockout Mice

*Xiaofan Yang[1,2], Hongqiang Yin[3,4], Xiaojing Wang[2], Yueqing Sun[2], Xianli Bian[5], Gaorui Zhang[6], Anning Li[6], Aihua Cao[1], Baomin Li[1], Darius Ebrahimi-Fakhari[7], Zhuo Yang[3], Miriam H. Meisler[8,9] and Qiji Liu[2,10]**

[1] Department of Pediatrics, Qilu Hospital of Shandong University, Jinan, China, [2] Key Laboratory of Experimental Teratology, Ministry of Education, Department of Genetics, School of Basic Medical Sciences, Shandong University, Jinan, China, [3] Medical School, State Key Laboratory of Medicinal Chemical Biology, Key Laboratory of Bioactive Materials for Ministry of Education, Nankai University, Tianjin, China, [4] Department of Operational Medicine, Tianjin Institute of Environmental & Operational Medicine, Tianjin, China, [5] Department of Neurology, Second Hospital of Shandong University, Jinan, China, [6] Department of Radiology, Qilu Hospital of Shandong University, Jinan, China, [7] Department of Neurology, The F.M. Kirby Neurobiology Center, Boston Children's Hospital, Harvard Medical School, Boston, MA, United States, [8] Department of Human Genetics, University of Michigan, Ann Arbor, MI, United States, [9] Department of Neurology, University of Michigan, Ann Arbor, MI, United States, [10] Key Laboratory of Birth Regulation and Control Technology of National Health Commission of China, Maternal and Child Health Care Hospital of Shandong Province, Jinan, China

OPEN ACCESS

Edited by:
Rainer Schwarting, University of Marburg, Germany

Reviewed by:
Yuri Bozzi, University of Trento, Italy
Price E. Dickson, Marshall University, United States

***Correspondence:**
Qiji Liu
liuqiji@sdu.edu.cn

Specialty section:
This article was submitted to Brain Disease Mechanisms, a section of the journal Frontiers in Molecular Neuroscience

Received: *25 November 2021*
Accepted: *18 February 2022*
Published: *26 April 2022*

Citation:
Yang X, Yin H, Wang X, Sun Y, Bian X, Zhang G, Li A, Cao A, Li B, Ebrahimi-Fakhari D, Yang Z, Meisler MH and Liu Q (2022) Social Deficits and Cerebellar Degeneration in Purkinje Cell Scn8a Knockout Mice. Front. Mol. Neurosci. 15:822129. doi: 10.3389/fnmol.2022.822129

Mutations in the *SCN8A* gene encoding the voltage-gated sodium channel α-subunit Nav1. 6 have been reported in individuals with epilepsy, intellectual disability and features of autism spectrum disorder. *SCN8A* is widely expressed in the central nervous system, including the cerebellum. Cerebellar dysfunction has been implicated in autism spectrum disorder. We investigated conditional *Scn8a* knockout mice under C57BL/6J strain background that specifically lack *Scn8a* expression in cerebellar Purkinje cells (*Scn8a*$^{flox/flox}$, *L7Cre*$^{+}$ mice). Cerebellar morphology was analyzed by immunohistochemistry and MR imaging. Mice were subjected to a battery of behavioral tests including the accelerating rotarod, open field, elevated plus maze, light-dark transition box, three chambers, male-female interaction, social olfaction, and water T-maze tests. Patch clamp recordings were used to evaluate evoked action potentials in Purkinje cells. Behavioral phenotyping demonstrated that *Scn8a*$^{flox/flox}$, *L7Cre*$^{+}$ mice have impaired social interaction, motor learning and reversal learning as well as increased repetitive behavior and anxiety-like behaviors. By 5 months of age, *Scn8a*$^{flox/flox}$, *L7Cre*$^{+}$ mice began to exhibit cerebellar Purkinje cell loss and reduced molecular thickness. At 9 months of age, *Scn8a*$^{flox/flox}$, *L7Cre*$^{+}$ mice exhibited decreased cerebellar size and a reduced number of cerebellar Purkinje cells more profoundly, with evidence of additional neurodegeneration in the molecular layer and deep cerebellar nuclei. Purkinje cells in *Scn8a*$^{flox/flox}$, *L7Cre*$^{+}$ mice exhibited reduced repetitive firing. Taken together, our experiments indicated that loss of *Scn8a* expression in cerebellar Purkinje cells leads to cerebellar degeneration and several ASD-related behaviors. Our study demonstrated the specific contribution of loss of Scn8a in cerebellar Purkinje cells to behavioral deficits

characteristic of ASD. However, it should be noted that our observed effects reported here are specific to the C57BL/6 genome type.

Keywords: Purkinje cell, *SCN8A*, mouse, autism, cerebellum, anxiety

INTRODUCTION

Autism spectrum disorder (ASD) is a behaviorally defined pervasive neurodevelopmental disorder, characterized by persistent impairment of social communication, restricted interests and repetitive behaviors (Varghese et al., 2017). In addition to these core symptoms, there may be psychiatric or neurological comorbidities, of which attention-deficit/hyperactivity disorder (ADHD), anxiety, depression and epilepsy are most common (Lord et al., 2020). It is estimated that the prevalence of ASD is 1–2% in the general population (Wisniowiecka-Kowalnik and Nowakowska, 2019). Over the past decade, genomic technologies have enabled rapid progress in the identification of genes linked to ASD (Abrahams and Geschwind, 2008; Arnett et al., 2019). Although much effort has centered on the genetic delineation of syndromic forms of ASD, the underlying molecular mechanisms remain incompletely understood (Hampson and Blatt, 2015).

Several lines of evidence implicate cerebellar dysfunction in the development of ASD. Post-mortem studies have demonstrated a reduced number and density of cerebellar Purkinje cells (PC) in patients with ASD, and isolated cerebellar injury has been associated with a higher incidence of ASD (Wang et al., 2014; Hampson and Blatt, 2015). The cerebellum has been consistently implicated in several monogenetic syndromes associated with ASD (Fatemi and Folsom, 2015; Sundberg and Sahin, 2015; Varghese et al., 2017). Recent studies suggest that PC dysfunction caused by mutations in *Tsc1*, *Tsc2*, *Shank2*, and *PTEN* during a critical developmental period may contribute to behavioral deficits relevant to ASDs (Tsai et al., 2012, 2018; Reith et al., 2013; Cupolillo et al., 2016; Peter et al., 2016).

The *Scn8a* gene encodes the voltage-gated sodium channel α subunit Nav1.6. Nav1.6 is enriched at the neuronal axon initial segment and nodes of Ranvier, where it promotes neuronal excitability by participating in the initiation and propagation of action potentials (O'Brien and Meisler, 2013; Meisler et al., 2016). $Na_v1.6$ is expressed throughout the central nervous system, including high expression in cerebellum, particularly in PCs (Schaller and Caldwell, 2003; Chen et al., 2009). In humans, pathogenic *SCN8A* variants are associated with a wide spectrum of phenotypes, from benign familial infantile seizures to developmental and epileptic encephalopathies (Gardella and Moller, 2019; Gertler and Carvill, 2019; Meisler, 2019). While prior work focused on the role of *SCN8A* in epileptic encephalopathies, there is evidence in humans and mice that variants in *SCN8A* are also associated with intellectual disability and neuropsychiatric abnormalities (Trudeau et al., 2006; McKinney et al., 2008; Blanchard et al., 2015; Butler et al., 2017; Wagnon et al., 2017; Liu et al., 2019; Meisler et al., 2021). Mice with heterozygous loss of *Scn8a* expression display enhanced emotionality in contextual fear conditioning, open field test and the light dark box test (McKinney et al., 2008). Conditional PC-specific *Scn8a* knockout mice were previously found to exhibit ataxia, impaired coordination, and deficits in delay eyeblink conditioning and Morris water maze tests (Levin et al., 2006; Woodruff-Pak et al., 2006) which are frequently observed in animal models with autistic features (Tsai et al., 2012; Reith et al., 2013; Piochon et al., 2014; Kloth et al., 2015; Cupolillo et al., 2016). Similar to findings in PC-specific *Tsc1* and *PTEN* knockout mice, PC-specific *Scn8a* knockout mice had a lower frequency of spontaneous firing of PC indicative of lower excitability (Raman et al., 1997; Khaliq et al., 2003; Levin et al., 2006).

Motivated by these studies implicating the PC of *Scn8a* mutant mice in ASD related traits, we used the Cre-loxP recombination system to generate conditional knockout mice in which *Scn8a* inactivation is restricted to PC. We found that PC-specific *Scn8a* knockout mice of C57BL/6J strain background exhibited late-onset cerebellar degeneration and deficits in motor coordination and social interaction, increased repetitive behavior, anxiety and abnormal activity of PC, demonstrating the specific contribution of PC to these *Scn8a*-dependent phenotypes.

METHODS

Subjects

All animal experimental procedures were performed in accordance with the animal protocol approved by the Institutional Animal Care and Use Committee at the School of Medicine, Shandong University. *Scn8a*$^{flox/flox}$ mice (Levin and Meisler, 2004) have been maintained on a C57BL/6J strain background since 2004 in the Meisler lab at the University of Michigan, and were imported to Shandong University in 2017. *L7/PCP2-Cre* transgenic mice (stock number: J006207) were purchased from the Model Animal Research Center of Nanjing University (Nanjing, China), where they had also been maintained on the C57BL/6J strain background. Mice were housed in a 12-h light/dark cycle (lights on 7:00 AM) with controlled temperature and humidity and ventilated with a dedicated system. All mice had *ad libitum* access to sterile food and water. We crossed *Scn8a*$^{flox/flox}$, *L7Cre*$^{+}$ female mice and *Scn8a*$^{flox/flox}$,*L7Cre*$^{-}$ male mice to generate *Scn8a*$^{flox/flox}$,*L7Cre*$^{-}$ (control) and *Scn8a*$^{flox/flox}$ *L7Cre*$^{+}$ (mutant) mice on the C57BL/6J strain background using the previously described breeding scheme (Levin et al., 2006).

Immunohistochemistry

Mice were intraperitoneally anesthetized with 4% chloral hydrate and transcardially perfused with PBS and then 4% paraformaldehyde (PFA). Brains were extracted, postfixed overnight in 4% PFA, dehydrated, embedded in paraffin, and sectioned at 3 μm. The sections were submerged into EDTA antigenic retrieval buffer (pH 8.0) and microwaved for antigenic

retrieval. Sections were blocked with 10% goat serum and 0.5% Triton X-100 in 1× PBS for 20 min. Slides were incubated in primary antibody solution overnight at 4°C. Sections were washed in 3× PBS and incubated with secondary antibody for 1 h at room temperature, then washed in 3× PBS and incubated with DAPI. Finally, anti-fluorescence quencher was used to seal the sections (Wuhan goodbio technology CO., LTD, Wuhan, China). Fluorescence images were acquired using a Nikon Eclipse Ti-SR Inverted Microscope. Images were then processed and analyzed using CaseViewer software (3D Histech Ltd, Budapest, Hungary).

The following primary antibodies were used: Calbindin (1:100; ab82812, Abcam), $Na_v1.6$ (1:100; ab65166, Abcam), Caspase3 (1:250; GB11532, Wuhan goodbio technology CO., LTD, Wuhan, China). Secondary antibodies were: goat anti-mouse 488 (1:400; GB25301, Wuhan goodbio, Wuhan, China), goat anti-rabbit 488 (1:400; GB25303, Wuhan goodbio, Wuhan, China), goat anti-mouse Cy3-IgG (1:300; GB21301, Wuhan goodbio, Wuhan, China), goat anti-rabbit Cy3-IgG (1:300; GB21303, Wuhan goodbio, Wuhan, China).

MRI Scanning Parameters

MRIs were collected on a 3-tesla MRI scanner (GE Healthcare, USA) using a standard birdcage head coil. Before the functional scans, high-resolution anatomical scans were acquired for each subject [repetition time (TR) = 2,100 ms, echo time (TE) = 111, field of view (FOV) = 10 × 10 cm, 190 slices, slice thickness = 1 mm] for later coregistration with functional maps. PD/T2 (TR = 2,500 ms, TE = 11.1/90, flip angle = 90°, FOV = 5 cm, slice thickness = 1 mm).

Patch Clamp Recording

Six to eight week old mice were anesthetized with urethane (1.2 g/kg, i.p.) and decapitated. Parasagittal cerebellar slices were prepared with vibratome (VT 1000S, Leica, Germany) with a thickness of 300 μm. The slices were incubated in ACSF (saturated with 95% O_2 to 5% CO_2) for at least 1 h before recording.

After incubation, the slices were promptly transferred to the recording chamber placed on the staged of a modified upright Olympus microscope and continuously perfused with ACSF (95% O_2 to 5% CO_2). The patch electrodes (3–7 MΩ) were pulled on a multistage micropipette puller (P-97, Sutter Instrument, USA), and the pipette solution contained (in mM): KCl 140, $MgCl_2$ 2, EGTA 10, HEPES 10, Mg-ATP 2, buffered to pH = 7.4 with KOH. After the whole-cell clamp configuration was formatted, the cells were stabilized for 5 min before recording. Then the PCs were depolarized by current steps to evoke action potential at a holding potential of −70 mV.

TUNEL Staining Assay

Terminal deoxynucleotidyl transferase dUTP nick end labeling (TUNEL) staining was carried out on cerebellar slices according to the manufacturer's instructions (Roche). TUNEL-positive and DAPI-positive nuclei were examined using a fluorescence light inverted microscope (Nikon Eclipse TI-SR). The ratio of TUNEL-positive to total DAPI positive cells was calculated in six visual fields at ×100 magnification.

Behavioral Tests

All behavioral tests were performed during the light cycle between 07:00 and 19:00. Male and female 5–9-week old mice were used. Similar numbers of male and female mice for each genotype were included. It is possible that genotype effects may have been underestimated or overlooked if they were sex dependent or if the baseline differences between female and male mice increased the variance in the data. Therefore, analysis of variance (ANOVA) models was used to test for the sex dependence of the genotype effects. A three-way repeated measures ANOVA with between-subject factors for genotype and sex and a repeated measure for training day was applied to accelerating rotarod and water-T maze data; a three-way ANOVA with factors for genotype, sex and pairing group was used for three-chambered test, and a two-way ANOVA with factors for genotype and sex was utilized for open-field test, light-dark transition box, elevated plus maze, grooming and male-female interaction. These analyses did not show any measures in which there was a significant effect of sex or a sex-genotype interaction. All behavioral assays were performed with the examiner blind to mouse genotypes. All the videos were analyzed by Smart software (Pan Lab, Harvard Apparatus).

Motor Function

Gait Analysis

The gait of $Scn8a^{flox/flox}$ $L7Cre^{+}$ mutant mice was compared with $Scn8a^{flox/flox}$ $L7Cre^{-}$ control mice by footprint analysis as previously described (Carter et al., 1999). Briefly, to obtain footprints the fore and hind paws of the mice were coated with red and black non-toxic, water-soluble paint, respectively. Footprint patterns were analyzed using a runway (50 cm × 9 cm wide) with white paper on the bottom. The average length and width of the steps were measured.

Rotarod Test

Motor coordination and balance were tested with the accelerating rotarod (Panlab, Harvard apparatus) as described previously (Buitrago et al., 2004). Animals were tested over 5 consecutive days, each day consisting of 3–5 trials. The mice were placed on a 3 cm diameter rod which began rotating at 4 rpm and accelerated to 40 rpm over a period of 2 min. Latency to fall was recorded. Animals were tested at 5–6 weeks of age.

Locomotor Activity and Anxiety

Open Field Test

Exploratory locomotor activity was measured in an open field as previously described (Burne et al., 2005). Each mouse was placed in an opaque open field (30 cm × 30 cm × 30 cm), under dim light. Mice were placed in the chamber for a 15 min period. Distance traveled in 1 min time bins was recorded using a centrally placed video camera and automated video tracking software (Smart software, Pan Lab/Harvard Apparatus). To assess anxiety-related behaviors, the number of entries in the center zone and percent of time in the center of the chamber was also recorded (Bailey and Crawley, 2009). Measurements were taken from animals aged 6 weeks.

Elevated Plus-Maze Tests

The elevated plus maze is a plus-shaped apparatus consisted of two open arms 8 × 25 cm and two closed arms (8 × 25 × 25 cm) with 8 × 8 cm central area, elevated 50 cm from the floor. Mice were placed in the central area facing one of the open arms, and allowed to freely explore the maze for 5 min. The number of entries and time spent in open or enclosed arms was measured as a parameter of anxiety-like behavior using an overhead camera and tracking system (SMART®; Panlab, Harvard Apparatus).

Light-Dark Box Test

To further measure anxiety-like responses, the light-dark box test was performed as described previously (Tang et al., 2017). The light/dark box was constructed of plexiglass (45 × 27 × 27 cm) consisting of two chambers, a black chamber (18 × 27 cm) and a light chamber (27 × 27 cm). Mice were placed into the dark box and allowed to freely move between the light box and dark box for 5 min. The amount of time spent in the dark side and the total number of transitions between the light and dark sides were recorded.

Social Behaviors

Social Interaction

The automated three-chambered social approach task is commonly employed as a standard test for assaying sociability in mice (Yang et al., 2011). The apparatus consists of a rectangular, three-chambered box made from clear polycarbonate. Retractable doorways within the two dividing walls allowed access to the side chambers. The number of entries and time spent in the chambers were automatically recorded using an overhead camera and tracking system (Smart software, Pan Lab/Harvard Apparatus). The subject mouse was allowed to habituate in the apparatus for 20 min before the sociability test, first for 10 min in the central chamber, followed by 10 min of free exploration in the entire empty arena with both doors open. In the social interaction testing period, a novel object (an inverted wire mesh cup) was placed in one of the side chambers and a novel mouse (with different genetic background matched to the subject mouse by sex and age) was placed inside an identical inverted wire cup in the other side chamber. In the social novelty testing period, another novel mouse was placed inside the empty wire cup. The apparatus was cleaned with 70% ethanol and water between subjects. Time spent interacting with the novel animal and with the object was recorded by an examiner with a stopwatch (Crawley, 2007). Animals were tested between 7 and 9 weeks of age.

Olfaction

We evaluated the ability of the mouse to detect novel odors and social odors as previously described (Yang et al., 2011; Tsai et al., 2012). Animals were placed in an empty, clean observation cage containing a thin layer of clean bedding and a hole on the flat filter top lid for inserting a cotton-tipped swab. Mice were habituated for 30 min with a clean cotton swab and then presented sequentially with non-social odors and social odors. Odors were presented in three consecutive trials per odorant stimulus (2 min per trial) in the following order: water, almond extract (1:100), banana extract (1:100), social odor 1, social odor 2. Social odors were created by swabbing the cotton tip in a zigzag fashion in previously soiled bedding from cages containing unfamiliar gender and age-matched animals the experimental animal had not interacted with. Time spent sniffing the swab with each presentation for each 2 min trial was measured by an investigator with a stopwatch. Measurements were taken from animals aged 7–8 weeks.

Male-Female Interaction

The procedure was adapted from a previously described protocol (Cupolillo et al., 2016). The test for male-female interaction was performed in a clean testing cage (Plexiglass box, 25 × 40 × 18.5 cm). Each male mouse was habituated to the testing cage for 15 min, after which an unfamiliar female of the same genotype was placed into the testing cage with a single layer of corncob bedding. An experimenter blind to the mouse genotype measured the cumulative time (by means of a stopwatch) that the male mouse spent in close contact with the female. Social interaction behavior included close following at the same speed behind the female, touching, nose-to-nose sniffing, anogenital sniffing and/or mouthing and licking the fur of the female. The cumulative time was measured (using a stopwatch) by the investigator and calculated as total time spent in contact. Animals were tested between 7 and 8 weeks of age.

Repetitive Behavior and Reversal Learning

Grooming

Mice were scored for spontaneous repetitive self-grooming behavior as previously described (Silverman et al., 2010a). Each mouse was placed individually into a standard mouse shoebox observation cage with no bedding and a flat filter top lid. After habituation for 10 min, animals were observed for another 10 min. Two mice were scored simultaneously by a trained observer, who was blind to mouse genotype. Cumulative grooming time in the observation period was recorded using stopwatches. Measurements were taken from animals aged 5–6 weeks.

Water T-Maze

To measure reversal learning, the water T-maze was performed as described (Bednar et al., 2002; Tsai et al., 2018). A transparent platform submerged about 1 cm below the surface of the water at one of the short arms of the T-maze and served as an escape for the animals. After 1 day consisting of a habituation swim trial (60 s) with no platform present, mice were given 15 trials a day for 3 consecutive days to learn the location of the platform. After 15 trials on day 4, the platform was changed to the other short arm of the maze. Mice were then tested for 15 additional trials (reversal day 1). Then for 2 subsequent days (reversal days 2 and 3), mice were given 15 trials per day. The number of correct trials and the number of trials required to achieve five consecutive correct trials were recorded. Measurements were taken from animals aged 8–9 weeks.

Statistical Analysis

Data are expressed as mean ± s.e.m., and statistical analysis was carried out using GraphPad Prism 8 software (GraphPad Software Inc., La Jolla, CA, USA). Statistical analyses included Student's *T*-test (paired or unpaired), one-way ANOVA followed by Tukey's *post-hoc* analysis, two-way repeated measures ANOVA followed by Bonferroni's *post-hoc* analysis. $P < 0.05$ was considered statistically significant.

RESULTS

Abnormal Morphology of *Scn8a* Mutant Cerebellum

We generated Purkinje cell specific *Scn8a* knockout mice of genotype $Scn8a^{flox/flox}$,Cre^{+} (PC *Scn8a* mutant mice) according to the breeding scheme (Levin et al., 2006). As shown in **Supplementary Figure S1**, PC *Scn8a* mutant mice had reduced expression of Nav 1.6 in Purkinje cells compared with control mice, whereas expression remained high in granule cells and neurons (stellate cells and basket cells) of the molecular layer in PC mutant mice.

Consistent with earlier reports (Sprunger et al., 1999; Levin et al., 2006), cerebellar malformations were not detected in both 2 and 4-month-old PC *Scn8a* mutant mice. Calbindin staining indicated that the Purkinje cells in the mutant mice retained the regular orientation of dendrites present in control animals (**Supplementary Figure S2**). However, calbindin staining was noted in the granule cell layer of PC *Scn8a* mutant mice (**Supplementary Figure S2**, arrows). This pattern of labeling has previously been described in $Scn8a^{med-jo}$ (A1071T) mice (Dick et al., 1985) and $Scn8a^{flox/flox}$,$L7Cre^{+}$ mice (Levin et al., 2006) and may reflect axonal swelling. We revealed that PC density, size of soma, and thickness of the molecular layer were normal at both 2 and 4 months of age (**Figure 1**). However, by 5 months of age, there was a reduction in the density of Purkinje cells and the thickness of molecular cell ($P < 0.01$), but the size of Purkinje cells retained normal. At 9 months of age there was a significant reduction in the thicknesses of the molecular layer and both the size and the density of Purkinje cells was significantly reduced ($P < 0.0001$. $n > 3$ per group, two-way ANOVA, Bonferroni's *post-hoc* analysis). Overall brain volume was decreased at 9 months of age, as evident in the whole-mount brain (**Figure 2A**). MRI measurements revealed reduced area of the cerebellum of the mutant mice in both axial and coronal views (**Figures 2B–D**).

Increased Apoptosis in the Cerebellum of *Scn8a* PC Mutant Mice

To determine whether neurodegeneration could account for the observed cerebellar atrophy, we adopted TUNEL staining to quantify apoptosis. The number of TUNEL-positive cells was significantly increased in PC *Scn8a* mutant mice in both the molecular layer (**Figures 2E,F**) and cerebellar deep nuclei (**Figures 2G,H**) ($P < 0.001$; $n = 4$ for mutants and control, unpaired student's *t*-test).

Reduced Excitability in *Scn8a* Mutant PCs

It was previously demonstrated that partial or complete loss of Nav1.6 from cerebellar Purkinje cells reduces excitability and repetitive firing (Raman et al., 1997; Khaliq et al., 2003; Levin et al., 2006). To examine excitability of PCs in our mice, evoked APs were recorded by whole-cell patch clamp. Repetitive firing spikes were evoked by current injection of 200 pA with 500 ms duration. The frequency of repetitive firing was inhibited in *Scn8a* mutant PCs compared with that in control (**Supplementary Figures S3A,B**). The mean frequency of repetitive firing at each current injection from 50 to 400 pA was significantly reduced in *Scn8a* mutant PCs (**Supplementary Figure S3C**). These results confirm the previous evidence that loss of *Scn8a* inhibits the excitability of PCs (Levin et al., 2006).

Impaired Motor Coordination in PC *Scn8a* Mutant Mice

By 6–8 weeks of age, PC *Scn8a* mutant mice developed a mildly ataxic, waddling gait that appeared to be caused by poor hindlimb coordination. However, at 6 weeks of age, mutant and control mice had comparable fore-base width and no difference in stride length and hind-base width (**Figures 3A,B**) ($P > 0.05$, Student's unpaired *t*-test, control 6wk $n = 10$, mutant 6wk $n = 10$). However, at 12 weeks of age, PC *Scn8a* mutant mice displayed a narrower stride length ($P = 0.022$) and a wider hind-base width ($P = 0.007$) (control $n = 6$, mutant $n = 9$), demonstrating a deficit in motor coordination.

Consistent with previous work (Levin et al., 2006), mutant mice demonstrated impaired performance on the rotarod test (**Supplementary Figure S4**). At 5 weeks of age, the latency to fall was significantly different between wildtype and mutant mice [two-way repeated measures ANOVA $F_{(1,18)} = 27.99$, Bonferroni *post-hoc*, $P < 0.0001$, $n = 9$ for control, $n = 11$ for mutant]. While control mice remained on the rod longer during each of 5 daily sessions of training, mutant mice had shorter latency to fall on day 1 ($P < 0.001$) and did not improve with time. These findings further demonstrate impaired motor coordination and poor motor learning in mice with ongoing PC loss.

Increased Anxiety-Like Behavior in PC *Scn8a* Mutant Mice

Patients harboring loss of function variants of *Scn8a* exhibit neuropsychological abnormalities including emotional instability, anxiety and attention deficit hyperactivity disorders (Trudeau et al., 2006; Wagnon et al., 2017). We therefore carried out behavioral testing of 6-week-old PC *Scn8a* mutant mice to assess their anxiety level.

The open field exploration test is a behavioral assay widely used to evaluate locomotor responses to novel environments in rodents. Representative tracks are shown in **Figure 3C**. During a 15-min test, the distance traveled by mutant mice in the open field during a 1 min time bin was similar to controls [**Figure 3D**, two-way ANOVA, Bonferroni's *post-hoc* analysis, $F_{(1,17)} = 0.6760$, $P = 0.4223$]. The total distance traveled

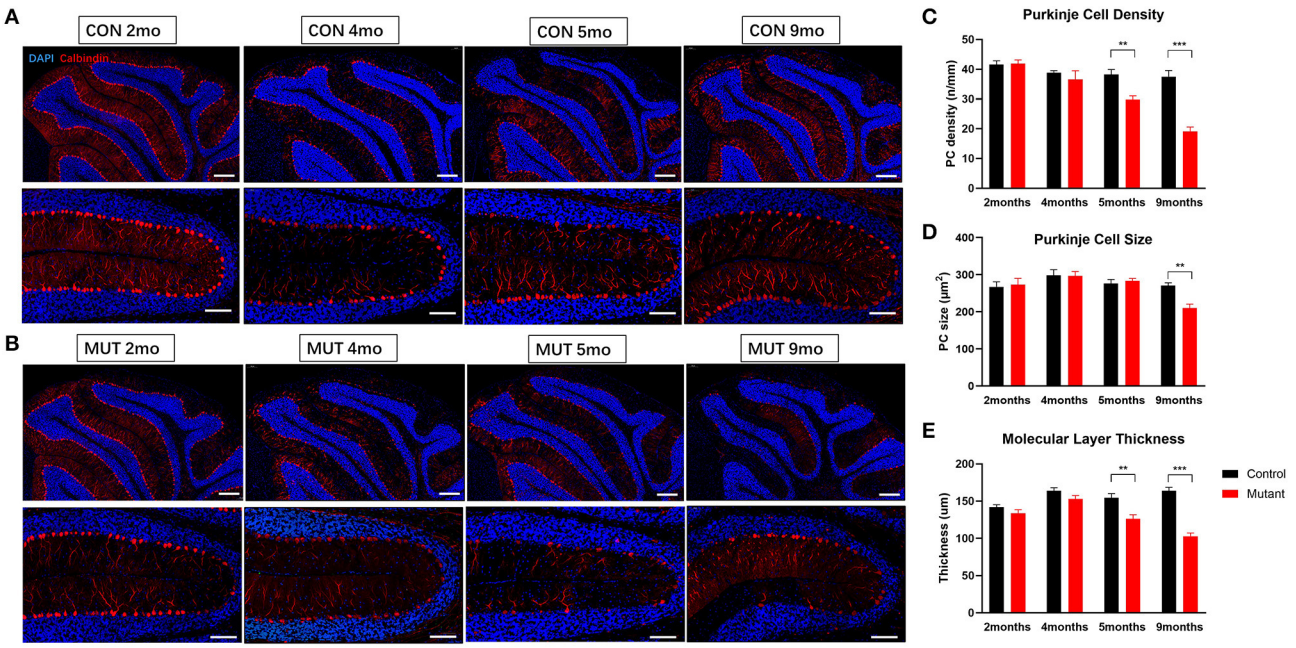

FIGURE 1 | PC *Scn8a* mutant mice exhibit histological changes in cerebellum. **(A,B)** Abnormal PC morphology and gradual reduced PC number and molecular layer thickness in Scn8a mutant cerebellum (Scale bar upper row 200 μm. bottom row 100 μm). **(C,D)** The quantification of PC density and the quantification of PC soma area was performed in the IV–V. PC loss was not apparent until 5 months of age, and showed ongoing loss till 9 months **(C)**. At 9 months, mutant Purkinje cell size decreased significantly **(D)**. **(E)** The thickness of the molecular layer (ML) was normal in mutant cerebellum at 4 months of age, whereas it decreased afterward at 5 months ($n \geq 3$ per group. Data shown are means ± SEM. $^{**}P < 0.01$, $^{***}P < 0.001$, two-way ANOVA, Bonferroni's *post-hoc* analysis).

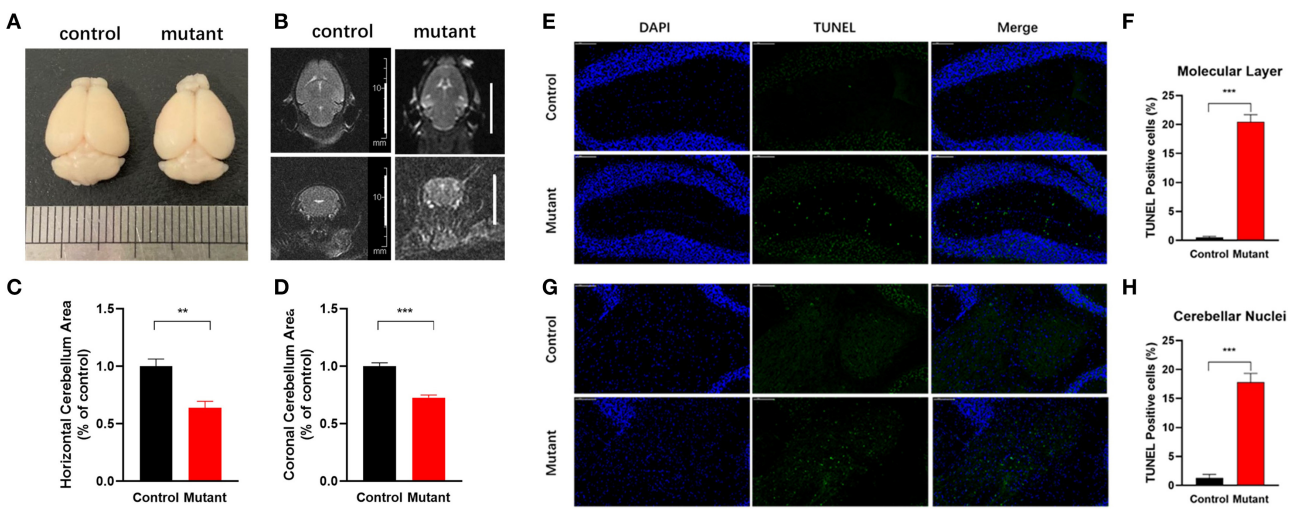

FIGURE 2 | Reduced cerebellar volume and increased apoptosis in *Scn8a* PC mutant cerebellum. **(A)** Representative whole-mount images of control and PC *Scn8a* mutant brains at 9 months of age. The mutant cerebellum appears smaller than control. **(B)** Magnetic resonance imaging T2 axial and coronal images of the brain showing cerebellar volume loss in the mutant mice at 9–10 months of age (scale bar 10 mm). **(C,D)** Measurement of the cerebellar area of *Scn8a* mutant and control mice using T2-weighted 3.0 T MR imaging. Quantitative analysis revealed a significant reduction in cerebellar area in mutant animals in both axial **(C)** and coronal area **(D)** (Mean ± SEM; $n = 5$ per group; $^{**}P < 0.01$, $^{***}P < 0.001$, Student's unpaired *t*-test). **(E,G)** Sections of cerebellum of control and PC *Scn8a* mutant mice at 9–10 months of age labeled with TUNEL showing apoptosis in the molecular cell layer and cerebellar nuclei (Scale bar: 100 μm). **(F,H)** Percentage of TUNEL-positive cells per unit area of cerebellar molecular layer and deep cerebellar nuclei in the PC *Scn8a* mice compared with controls ($n = 4$ for each group, $^{***}P < 0.001$, Student's unpaired *t*-test).

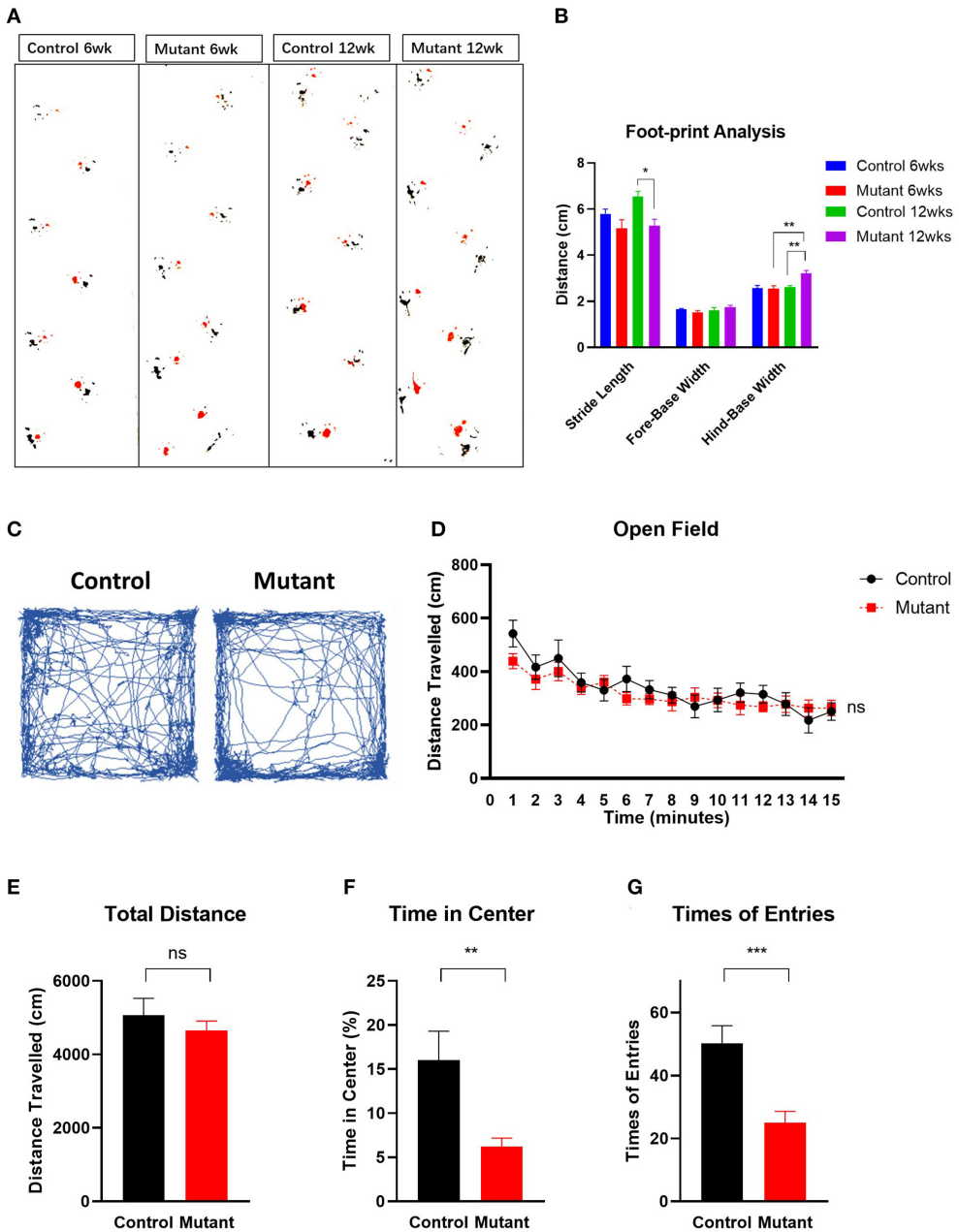

FIGURE 3 | Motor coordination impairment and locomotor activity in PC *Scn8a* mutant mice. **(A)** Representative walking footprint patterns. **(B)** Gait footprint analysis at 6 and 12 weeks was evaluated for stride length, fore-base width and hind-base width. Mutant mice displayed ataxic gait with reduced stride length and increased stride width at 12 weeks of age ($n > 6$ per group. $^{*}P < 0.05$, $^{**}P < 0.01$; $^{***}P < 0.001$, two-way ANOVA, Bonferroni's *post-hoc* analysis). **(C)** Representative traces of mouse activity in an open field during a 15-min recording time. **(D)** Locomotor activity in the open field was comparable between control ($n = 9$) and mutant mice ($n = 11$) in a 15 min time bin ($P = 0.4223$). Time in minutes is shown on the X-axis. **(E)** The total distance moved in the open field test was not significantly different between controls and mutants ($P > 0.05$). **(F,G)** Mutant mice spent less time **(F)** in the center of the open field ($P = 0.0063$), and entered the center of the open field less often **(G)** than the controls ($P < 0.001$). Data shown are means ± SEM. ns, not significant. $^{*}P < 0.05$, $^{**}P < 0.01$, $^{***}P < 0.001$, two-way ANOVA, Bonferroni's *post-hoc* analysis for **(D)**. Student unpaired *t*-test for **(E–G)**.

was also similar in controls and mutants [**Figure 3E**, Student unpaired *t*-test, $t_{(17)} = 0.822$, $P > 0.05$]. However, PC *Scn8a* mutants spent significantly less time in the center of the open field [**Figure 3F**, Student unpaired *t*-test, $t_{(17)} = 3.254$, $P = 0.0047$] and had fewer entries into the center [**Figure 3G**, Student unpaired *t*-test, $t_{(17)} = 3.982$, $P < 0.001$] (control $n = 8$, mutant $n = 11$).

As an independent test of anxiety, we used the light/dark box transition task (Bourin and Hascoet, 2003). The number of entries into the light compartment [$t_{(25)} = 5.297$, $P < 0.0001$]

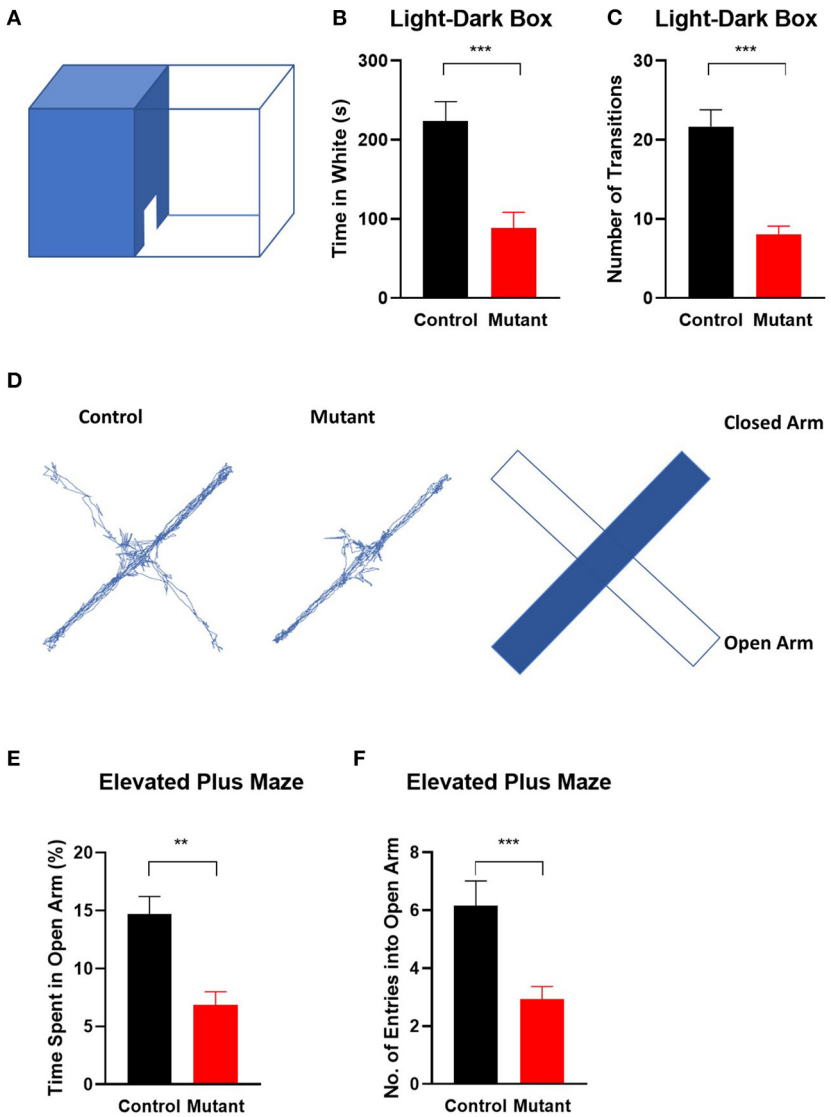

FIGURE 4 | Elevation of anxiety in *Scn8a* PC mutant mice. **(A)** Schematic of light-dark transition box. In the light–dark preference test, PC *Scn8a* mutant mice spent significantly less time in the light room **(B)** and entered it less often than controls **(C)**. ($n = 15$ for control and $n = 13$ for mutant). **(D)** Representative elevated plus maze tracking plots and diagram illustrates locations of open and closed arms of the maze. Mutant mice demonstrated decreased time spent in the open arms **(E)**, and less frequently enter into the open arms **(F)** of the elevated plus maze (Control: $n = 13$ Mutant: $n = 16$). $^{**}P < 0.01$, $^{***}P < 0.001$. All *P*-values by the Student's unpaired *t*-test.

and the time spent in the bright area [$t_{(25)} = 4.129$, $P < 0.001$] were significantly decreased in PC *Scn8a* mutant mice, indicating increased innate anxiety-like behavior (control $n = 15$, mutant $n = 13$ Student's unpaired *t*-test) (**Figures 4A–C**).

To further assess anxiety, we analyzed behavior on an elevated plus maze (Hogg, 1996) (**Figures 4D–F**). As in the open field, mutant mice demonstrated decreased total time spent in the open arms [$t_{(27)} = 4.191$, $P < 0.001$], and a reduced number of entries into the open arms of the elevated plus maze [$t_{(27)} = 3.532$, $P = 0.0015$] (control $n = 13$ and mutant $n = 16$, Student's unpaired *t*-test).

Taken together, these assays indicate that mutant mice display increased anxiety compared with control littermates.

Altered Social and Repetitive Behaviors in PC *Scn8a* Mice

A three-chambered apparatus was used to measure social approach and social novelty (**Figure 5**). Compared with control mice, PC *Scn8a* mutant mice spent less time in the side chamber with the novel mouse and more time with the novel object (**Figure 5B**, $P > 0.05$). Control mice spent significantly more time with the novel mouse than with the novel object [$P < 0.001$,

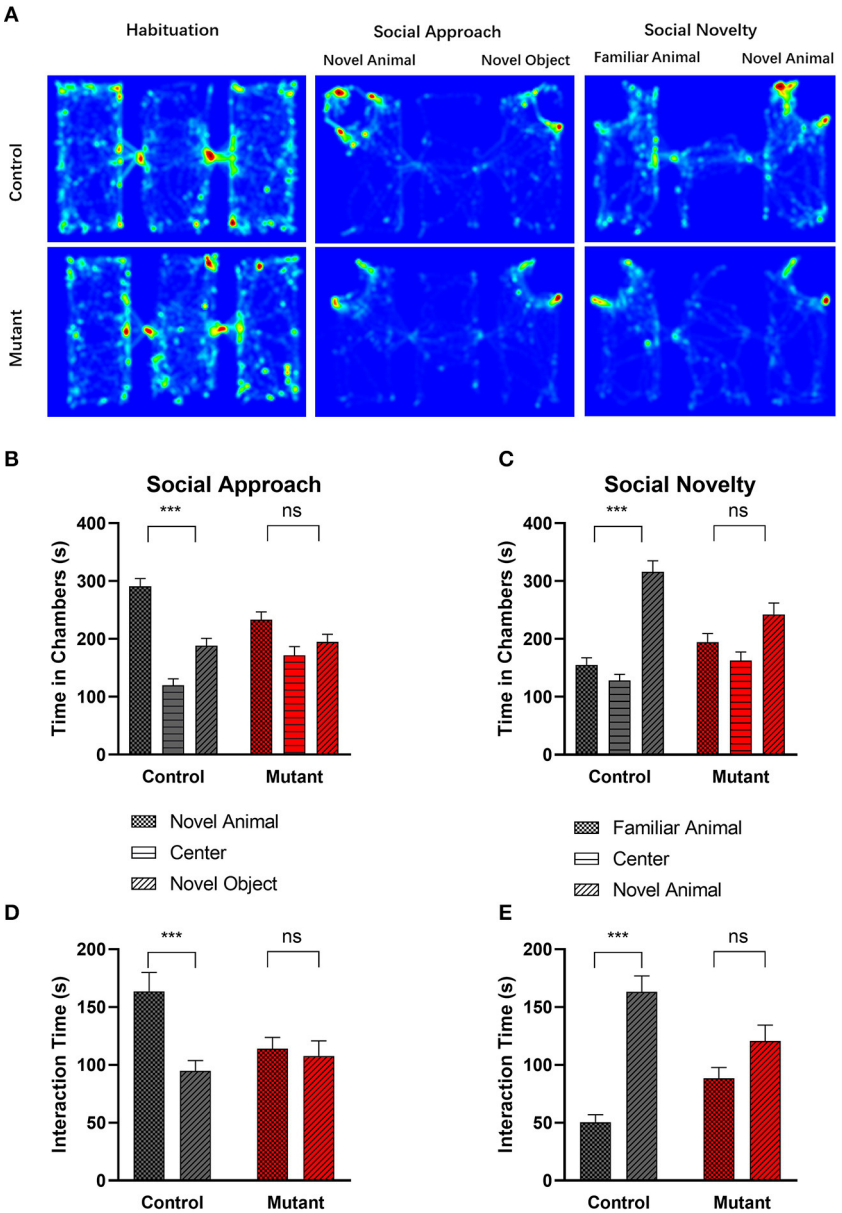

FIGURE 5 | Abnormal social behavior in PC *Scn8a* mutant mice. **(A)** Representative heat maps showing time spent by Control mice (upper panel) and PC *Scn8a* mutant mice (lower panel) at each location of the three-chambered apparatus during the test. **(B,D)** In the social approach test, WT mice spent more time in the chamber with the stranger animal than in the chamber with the inanimate object **(B)**, and spent more time interacting with novel animal **(D)** in comparison with a novel object, whereas PC *Scn8a* mutant mice show no preference. **(C,E)** PC *Scn8a* mutant mice show no preference for the chamber with the novel animal in comparison with that with a familiar animal in an assay of social novelty **(C)**, and spent similar time interacting with both the novel and familiar animals **(E)**. This is in distinct contrast to control mice. Control: $n = 16$; Mutants: $n = 17$, $^{***}P < 0.001$, two-way ANOVA, Bonferroni's *post-hoc* analysis.

chamber×genotype Interaction $F_{(1,31)} = 3.984$, $P = 0.0548$, chamber effect $F_{(1,31)} = 19.10$, $P = 0.0001$, genotype effect $F_{(1,31)} = 7.637$, $P = 0.0095$, $n = 16$ for control, $n = 17$ for mutant, two-way repeated measures ANOVA, Bonferroni's *post-hoc* analysis].

We examined the amount of time each experimental mouse spent interacting with the novel mouse or the object through sniffing [**Figure 5D**, Genotype×chamber interaction, $F_{(1,31)} = 7.420$, $P = 0.010$; Chamber effect $F_{(1,31)} = 11.17$, $P = 0.0022$; Genotype effect $F_{(1,31)} = 1.035$, $P = 0.3168$, two-way repeated measures ANOVA, Bonferroni's *post-hoc* analysis]. While control mice showed more interest in interacting with the novel mouse ($P < 0.001$), mutant mice spent a comparable amount of time sniffing the novel mouse and the novel object ($P > 0.05$).

When the inanimate object was replaced with another novel mouse, control mice spent more time in the chamber containing a novel mouse than in the chamber with the familiar mouse

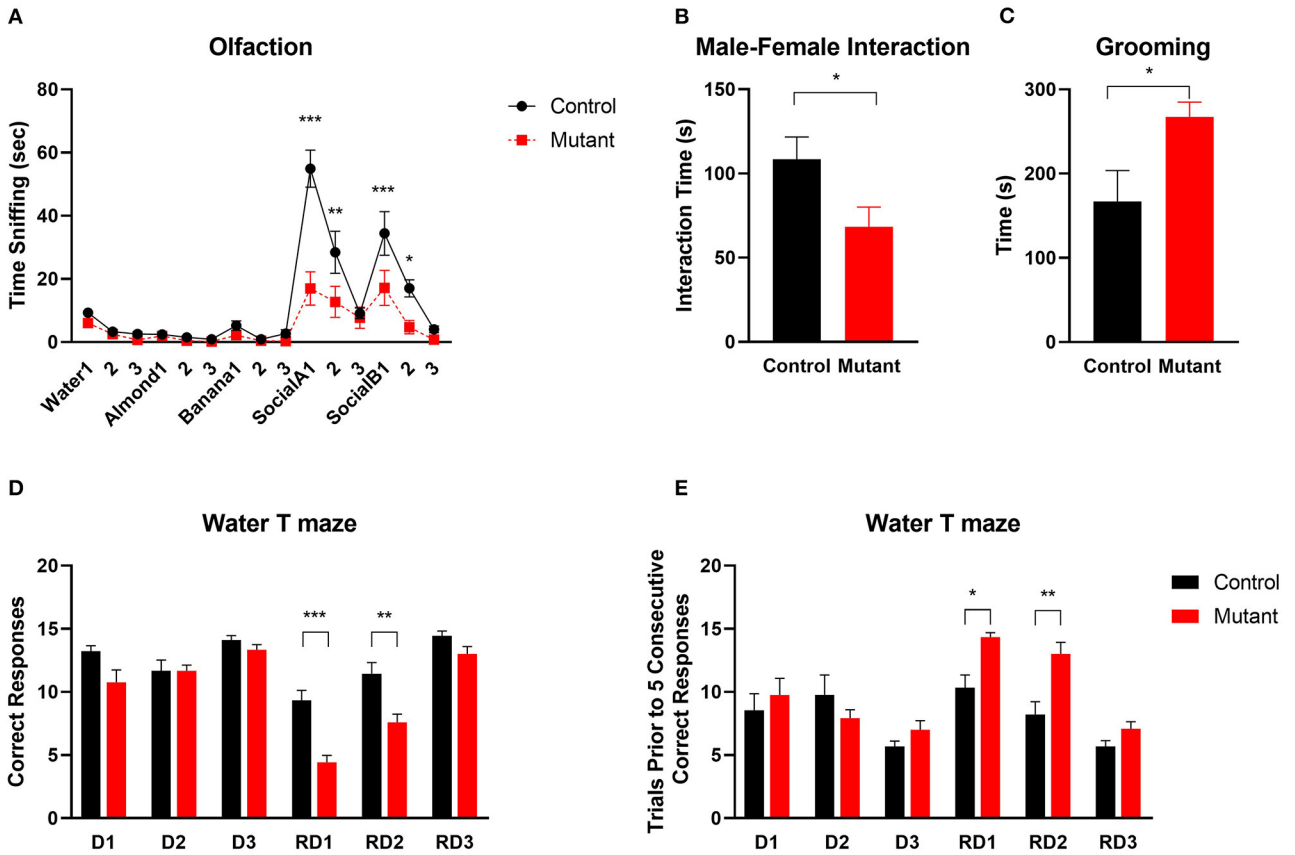

FIGURE 6 | Abnormal social and repetitive behaviors and impaired reversal learning in PC *Scn8a* mutant mice. **(A)** Mutant mice spent comparable time sniffing non-social stimuli whereas less time sniffing social odor cues ($n = 11$ per group). **(B)** Reduced sociability of KO mice is indicated by reduced time interacting with a female conspecific (Control: $n = 8$; Mutant: $n = 10$). **(C)** PC *Scn8a* mutant mice spent more time self-grooming (Control: $n = 10$; Mutant: $n = 11$). **(D,E)** On Day 1 to Day 3, mutants display normal acquisition learning of the escape platform location in the water T maze as indicated by total correct trials **(D)** and trials needed for 5 consecutive correct responses **(E)**. However, on reversal day 1 and day 2, PC *Scn8a* mutant mice have significantly fewer correct trials **(D)**, and take more trials to achieve five consecutive correct responses (Control: $n = 9$, Mutant: $n = 12$). RD, Reversal Day. Data shown are means ± SEM. $^*P < 0.05$, $^{**}P < 0.01$, $^{***}P < 0.001$, Two-way ANOVA, Bonferroni *post-hoc* analysis in **(A)**, Student's unpaired *t*-test in **(B–E)**.

($P < 0.001$), demonstrating normal sociability [genotype × chamber interaction $F_{(1,31)} = 6.596$, $P = 0.0153$, Chamber effect $F_{(1,31)} = 22.62$, $P < 0.0001$, Genotype effect $F_{(1,31)} = 3.479$, $P = 0.0717$, two-way repeated measures ANOVA, Bonferroni's *post-hoc* analysis] (**Figure 5C**). In contrast, the PC *Scn8a* mutants failed to show any preference between the two social chambers ($P > 0.05$). Control mice also spent more time sniffing the novel animal over the familiar animal (**Figure 5E**, $P < 0.001$), while mutant mice failed to show such preference ($P > 0.05$) [genotype × chamber interaction $F_{(1,31)} = 9.777$, $P = 0.0038$, chamber effect $F_{(1,31)} = 33.51$, $P < 0.0001$, genotype effect $F_{(1,31)} = 0.02699$, $P = 0.8706$, two-way repeated measures ANOVA, Bonferroni's *post-hoc* analysis].

It is thought that impaired discrimination of social olfactory cues may contribute to social deficits in mice (Silverman et al., 2010b). We used a social olfaction assay to assess interaction with social olfactory cues (**Figure 6A**). When mice were first presented with three non-social odor cues (water, almond extract and banana extract), there were no significant differences between mutant and wildtype mice ($P > 0.05$, $n = 11$ Control and 11 mutants), demonstrating normal olfactory function. When social odors (social A and social B) were applied, PC *Scn8a* mutant mice spent less time sniffing the cotton tips than control mice, suggesting a lack of interest in social odor stimuli [$n = 11$ per group, two-way repeated measures ANOVA $F_{(1,20)} = 15.25$ Bonferroni *post-hoc*, $P < 0.0001$ for Social A1, $P = 0.001$ for Social A2, $P < 0.0001$ for Social B1, $P = 0.036$ for Social B2].

Social behavior was further tested by assessing social interaction with a female conspecific mouse. Compared with control mice, there was a significant reduction in the time spent sniffing, allogrooming, mounting, or following the female by male PC *Scn8a* mutant mice [Student's *t*-test $t_{(18)} = 2.23$, $P = 0.038$; Control $n = 8$; Mutant $n = 12$] (**Figure 6B**).

One of the diagnostic behavioral symptoms of autism is repetitive behavior. We analyzed grooming as an index for stereotyped, repetitive behaviors. PC *Scn8a* mutant mice engaged in much longer bouts of self-grooming than control mice

(**Figure 6C**) [$n = 14$ per group, Student's t-test $t_{(26)} = 2.48$, $P = 0.019$].

Perseveration (Behavioral Inflexibility) in PC *Scn8a* Mutant Mice

ASD patients often show inflexible and rigid behavior and thinking (Bralten et al., 2018). To evaluate behavioral flexibility, we used the reversal water-T maze assay (**Figures 6D,E**). During the first 3 days of training, while the platform was in the right arm of the maze, both groups of mice performed equally well and learned the location of submerged platform. On the first reversal day with the platform moved to the left arm of the maze, PC *Scn8a* mutant mice incorrectly visited the right arm more frequently than control mice. Mutant mice also needed more trials to achieve 5 consecutive correct responses. Comparable results were observed on Reversal day 2. [Reversal Day 1, number of correct trials: Student's t-test $t_{(19)} = 5.097$, $P < 0.0001$; number of trials prior to five consecutive correct trials: Student's t-test $t_{(19)} = 3.221$, $P = 0.0045$; Reversal Day 2: number of correct trials: Student's t-test $t_{(19)} = 3.48$, $P = 0.0025$; number of trials prior to five consecutive correct trials: Student's t-test $t_{(19)} = 3.467$, $P = 0.0026$]. By the third reversal day, the mutant mice behaved similarly to the control mice in number of correct trials and number of trials prior to 5 consecutive correct responses.

DISCUSSION

The first link between human disease and *SCN8A* mutation was obtained in 2006 in a study of a small pedigree in which heterozygous carriers of a loss-of-function *SCN8A* mutation exhibited a range of phenotypes including ataxia, cognitive deficits, and emotional instability (Trudeau et al., 2006). Since the development of next generation sequencing, many pathogenic variants of *SCN8A* have been identified in patients with a spectrum of neurodevelopmental disorders, and some genotype-phenotype correlations have emerged. *SCN8A* missense variants with gain-of-function channel properties are associated with developmental epileptic encephalopathy with early onset of severe seizures, hypotonia, and paroxysmal dyskinesia. In contrast, loss of function mutations of SCN8A can cause autism or intellectual disability without seizures (Larsen et al., 2015; Gertler and Carvill, 2019; Liu et al., 2019; Meisler et al., 2021). In a recent study by Wong et al. (2021), they generated a novel *Scn8a* mouse model carrying the human R1620L mutation (with both gain- and loss-of-function effects) which exhibited a range of behavioral abnormalities, including hyperactivity, impaired learning and memory and social deficits. These findings suggest that *SCN8A* dysfunction may contribute to other neurological and neuropsychiatric disorders. Neuropsychiatric comorbidities were not previously studied in Purkinje cell specific *Scn8a* knockout model, and the role of reduced Nav1.6 in cerebellar function was incompletely characterized.

In this study, we provide evidence that *SCN8A* in cerebellar PCs has a key role in mechanisms involved in ASDs. We show that mice of C57BL/6J strain background with selective disruption of *Scn8a* in PCs display behavioral traits related to neuropsychiatric abnormalities such as ASDs and anxiety, associated with graded loss of PCs and progressive cerebellar atrophy.

One of the main symptoms of cerebellar dysfunction in humans is ataxia (Schniepp et al., 2017). Our results revealed that PC *Scn8a* mutant mice exhibit deficits in motor coordination and motor learning in the rotarod test. Gait analysis demonstrated wide base and ataxic gait. Similar features are also seen in patients with loss of function mutation of *SCN8A* (Trudeau et al., 2006), and in patients with ASD and other murine models of ASD (Fatemi et al., 2012; Tsai et al., 2012; Reith et al., 2013; Cupolillo et al., 2016).

PC *Scn8a* mutant mice were previously shown to be impaired in delay eyeblink conditioning (Woodruff-Pak et al., 2006), an additional connection to cerebellar dysfunction and autism. Eyeblink conditioning is affected in the general ASD patient population, and is viewed as a biomarker for ASD (Oristaglio et al., 2013; Welsh and Oristaglio, 2016). Eyeblink-conditioning defects appear more often in mouse autism models than in non-autism-like phenotypes (Kloth et al., 2015). Given the similarity of the PC Scn8a mutant mice to other autism models with regards to motor deficit, delay eye-blink conditioning impairment and electrophysiological changes in Purkinje cells, it is not surprising that PC *Scn8a* mutant mice also exhibit ASD-relevant social deficits.

Purkinje cell loss is the most consistent presentation in post mortem studies of ASD patients, with 35–95% fewer cerebellar Purkinje cells in ASD brains than controls (Whitney et al., 2009; Wegiel et al., 2014; Mosconi et al., 2015). Purkinje cells are recognized as key cells mediating autism-like phenotypes in mice (Fatemi et al., 2012; Tsai et al., 2012; Reith et al., 2013; Cupolillo et al., 2016). PC *Scn8a* mutant mice also displayed abnormalities in the composition of the cerebellum. The thickness of molecular layer as well as the density of Purkinje cells were comparable at early age. However, Purkinje cell beginning to lose between 4 and 5 months of age, with an ongoing and significantly decreased in both Purkinje cell density and thickness of molecular layer in PC *Scn8a* mutant mice by 9 months of age (**Figure 1**). Progressive PC loss is accompanied by cerebellar atrophy indicated by both gross anatomy and MR imaging of cerebellum.

Previous studies demonstrated a relationship between cerebellar function and behavior including sociability (novel mouse vs. novel object), social preference (familiar mouse vs. novel mouse), social odor preference (conspecific urine vs. water), and male-female interaction (Tsai et al., 2012; Cupolillo et al., 2016). Our demonstration of social deficits in three-chambered tests were highly consistent with earlier studies in other cerebellar genetic mouse models of autism (Tsai et al., 2012; Reith et al., 2013). PC *Scn8a* mutant mice also displayed reduced responses to female social cues in a male-female reciprocal social interaction context. Mutant mice spent significantly less time sniffing the social odors than control mice in the context of olfaction test.

Autism and anxiety disorders are frequently comorbid with each other (Adams et al., 2020; Baribeau et al., 2020, 2021), and autistic and anxious traits are highly correlated (Ha et al., 2016; Tatsukawa et al., 2019). Likewise, co-existing anxiety-like

behaviors were observed in the *Scn8a* PC mutant mice. Anxiety-like behaviors in the mutant mice included reduced exploration behavior in the center in the open field test and reduced non-social anxiety in the elevated plus maze and light-dark transition test. Similar anxiety-like behaviors also presented in autistic mice with Purkinje cell-specific deficiency of Shank2 (Ha et al., 2016) and Pianp mice (Winkler et al., 2020). McKinney et al. (2008) investigated mice heterozygous for a null mutation of *Scn8a* (*Scn8a*$^{+/-}$) and demonstrated avoidance of well-lit, open environments as well as pronounced stress-induced coping behavior. Impaired Purkinje cell firing was also demonstrated in heterozygous *Scn8a*$^{+/-}$ null mice (Raman et al., 1997; Khaliq et al., 2003). Our data on the PC-specific KO of *Scn8a* suggest that the enhanced anxiety-like behaviors in *Scn8a* heterozygous null mice may be mediated by altered output signaling from the cerebellum.

It has been observed that cognitive inflexibility and cerebellar pathology co-occur in psychiatric disorders (e.g., autism, schizophrenia, addiction). Recent studies using lurcher mutant mouse, which lose 100% of their Purkinje cells postnatally or lurcher mouse chimeras, which lose varying numbers of Purkinje cells, suggested impairment in behavioral flexibility, reversal learning and increased repetitive behaviors, as well as higher level cognitive processes (Dickson et al., 2010, 2017; Martin et al., 2010). Inflexibility to change in routine can be viewed as a form of perseverative behavior, and assessments of reversal learning are used as a behavioral endpoint in studies of rodent models. In water T-maze tests, the initial acquisition of the behavior was normal but PC *Scn8a* mutant mice exhibited impaired reversal learning. Autistic patients often exhibit repetitive behaviors that refuse to change (Hollander et al., 2003). This feature can be recapitulated by rodent grooming behaviors (Crawley, 2004). PC *Scn8a* mutant mice displayed increased repetitive behavior, including self-grooming. All these results, together with previous findings in lurcher mutant mouse and lucher chimeras, indicated that cerebellar pathology may play a causal role in the generation of repetitive behaviors and cognitive inflexibility.

Previous research found the levels of Bcl-2 and P53 protein, two important markers of apoptosis, were increased in cerebellum of autistic subjects compared with controls (Araghi-Niknam and Fatemi, 2003). Dong et al. (2018) demonstrated elevation of ER stress signals, oxidative stress, and apoptosis in the molecular layer of the autistic cerebellum. Deep cerebellar nuclear cells to which Purkinje cells project are abnormal in ASD, showing enlargement during childhood followed by reduction in size and number during adolescence and adulthood (Bauman, 1991). Using the TUNEL assay, we found increased cell apoptosis in molecular layer of PC *Scn8a* mutant mice. Interestingly, we also noted obvious cell apoptosis in neurons of the deep cerebellar nuclei.

In Purkinje cells lacking Nav1.6 channels, both spontaneous firing activity and high frequency discharge are impaired (Raman et al., 1997; Khaliq et al., 2003; Levin et al., 2006). We also confirmed the reduced excitability in *Scn8a* mutant PCs. Since PC provide the only output from the cerebellar cortex, the reduced firing of Purkinje cells observed in many ASD-like mouse models (Tsai et al., 2012; Cupolillo et al., 2016; Yang et al., 2020) may disinhibit the downstream deep cerebellar nuclei, which gate the outgoing information to the thalamus, basal ganglia, and neocortex (Sundberg and Sahin, 2015), potentially influencing integrative networks (Bostan and Strick, 2018). Neurons of the deep cerebellar nuclei receive major basal and driven inhibition from PC, but they are also spontaneously active, producing action potentials even without excitation (Zheng and Raman, 2011). Therefore, we suggest that loss of *Scn8a* in Purkinje cells might disrupt Purkinje-mediated inhibition and increase firing in the deep cerebellar nuclei. The resulting elevated spontaneous activity of cerebellar nuclei could result in oxidative stress and induced apoptosis. Further research is needed to elucidate the mechanism connecting Purkinje cell loss to cerebellar apoptosis.

However, it should be noted that our study was performed on a single inbred strain, C57BL/6J. Therefore, our understanding of these effects is limited to this single genome type. However, recent studies showed that results from studies that utilize diverse genetic backgrounds are a better model of complex disease across individuals and are more likely to generalize across patient populations (Neuner et al., 2019). Therefore, further research is needed to validate the effects of loss of *Scn8a* expression in Purkinje cells on cognitive and autistic behavior changes using different inbred strains.

CONCLUSION

We have demonstrated that mice with loss of *Scn8a* in Purkinje cells provide a new model of features of ASD. Mice of C57BL/6J strain with homozygous loss-of-function of Nav1.6 channels in Purkinje cells exhibit motor deficits and autistic traits such as deficits in social interaction, stereotyped behaviors and anxiety-like behaviors, demonstrating an ASD-like phenotype with strong resemblance to other Purkinje cell-dependent models of ASD (Fatemi et al., 2012; Tsai et al., 2012; Reith et al., 2013; Cupolillo et al., 2016). Together with previously reports of reduced spontaneous and repetitive firing (Raman et al., 1997; Levin et al., 2006), learning deficits in the rotarod test (Levin et al., 2006) and delay eyeblink conditioning impairment (Woodruff-Pak et al., 2006), these studies support PC *Scn8a* mutant mice as a model that reproduces many symptoms of patients with *SCN8A* loss of function mutations.

Our study has demonstrated the specific contribution of loss of *Scn8a* in cerebellar Purkinje cells to behavioral deficits characteristic of ASD. These results provide novel insights into mechanisms contributing to the pathogenesis of ASDs. Future research to unravel the pathogenesis underlying molecular and cellular alterations will improve our understanding of the still enigmatic fields of ASD and anxiety, and open new avenues for molecular diagnosis and therapy.

DATA AVAILABILITY STATEMENT

The original contributions presented in the study are included in the article/**Supplementary Materials**, further inquiries can be directed to the corresponding author/s.

ETHICS STATEMENT

The animal study was reviewed and approved by Ethics Committee of the School of Basic Medical Sciences of Shandong University.

AUTHOR CONTRIBUTIONS

XY and QL designed the experiments and synthesized and analyzed data. HY performed the electrophysiology study and analyzed data. XY, BL, and AC performed behavioral studies. AL and GZ performed and analyzed MRI data. XW, YS, and XB contributed to animal husbandry. XY and XW performed immunohistochemistry experiments and analyzed data. XY and MM organized the manuscript. DE-F, ZY, MM, and QL reviewed and revised the manuscript. All authors contributed to the article and approved the submitted version.

FUNDING

This project was supported by National Natural Science Foundation of China (Grant Nos. 81601195, 81671114, 81741055, and 81873878), Natural Science Foundation of Shandong Province (Grant Nos. ZH2016HB38 and ZR2021MH229), and Open Research Fund of National Health Commission Key Laboratory of Birth Defects Prevention (ZD202101).

ACKNOWLEDGMENTS

The authors are grateful to Dr. Jingwei Liu from Qilu Hospital of Shandong University for helpful discussions and comments on the manuscript. We thank Dr. Young Park of the University of Michigan for breeding, maintenance and shipping of the *Scn8a* floxed mice. We thank the Translational Medicine Core Facility of Shandong University for consultation and instrument availability that supported this work.

SUPPLEMENTARY MATERIAL

The Supplementary Material for this article can be found online at: https://www.frontiersin.org/articles/10.3389/fnmol.2022.822129/full#supplementary-material

Supplementary Figure S1 | Sagittal cryosection of cerebellar Nav1.6 staining (green) and calbindin staining (red) showing the deficiency of Nav1.6 expression in PC of the *Scn8a* mutant mice. Nav1.6 staining in control Purkinje cells are indicated by yellow arrows. Scale bar 50 μm.

Supplementary Figure S2 | Scattered calbindin staining in the granule cell layer along the proximal segment of PC axons of Purkinje Scn8a mutant mice (arrows). Scale bar 100 μm.

Supplementary Figure S3 | Reduced excitability of *Scn8a* mutant PCs. **(A,B)** The evoked action potential in control and *Scn8a* mutant PCs in response to depolarization of 200 pA. **(C)** Comparison of the mean frequency of repetitive firing at command potentials ($n = 10$ for both control and Scn8a mutant groups. All data were presented as mean ± SEM, $^{***}P < 0.001$).

Supplementary Figure S4 | Motor coordination and motor learning assessed on an accelerating rotarod. PC *Scn8a* mutants displayed decreased time on an accelerating rotarod and no improvement with training (Control: $n = 9$, Mutant: $n = 11$. $P < 0.001$, two-way ANOVA, Bonferroni's *post-hoc* analysis).

REFERENCES

Abrahams, B. S., and Geschwind, D. H. (2008). Advances in autism genetics: on the threshold of a new neurobiology. *Nat. Rev. Genet.* 9, 341–355. doi: 10.1038/nrg2346

Adams, D., Clark, M., and Simpson, K. (2020). The relationship between child anxiety and the quality of life of children, and parents of children, on the autism spectrum. *J. Autism Dev. Disord.* 50, 1756–1769. doi: 10.1007/s10803-019-03932-2

Araghi-Niknam, M., and Fatemi, S. H. (2003). Levels of Bcl-2 and P53 are altered in superior frontal and cerebellar cortices of autistic subjects. *Cell. Mol. Neurobiol.* 23, 945–952. doi: 10.1023/B:CEMN.0000005322.27203.73

Arnett, A. B., Trinh, S., and Bernier, R. A. (2019). The state of research on the genetics of autism spectrum disorder: methodological, clinical and conceptual progress. *Curr. Opin. Psychol.* 27, 1–5. doi: 10.1016/j.copsyc.2018.07.004

Bailey, K. R., and Crawley, J. N. (2009). "Chapter 5: Anxiety-related behaviors in mice," in *Methods of Behavior Analysis in Neuroscience*, ed J. J. Buccafusco (Boca Raton, FL: Press/Taylor & Francis).

Baribeau, D. A., Vigod, S., Pullenayegum, E., Kerns, C. M., Mirenda, P., Smith, I. M., et al. (2020). Repetitive behavior severity as an early indicator of risk for elevated anxiety symptoms in autism spectrum disorder. *J. Am. Acad. Child. Adolesc. Psychiatry* 59, 890–899 e893. doi: 10.1016/j.jaac.2019.08.478

Baribeau, D. A., Vigod, S., Pullenayegum, E., Kerns, C. M., Mirenda, P., Smith, I. M., et al. (2021). Co-occurring trajectories of anxiety and insistence on sameness behaviour in autism spectrum disorder. *Br. J. Psychiatry* 218, 20–27. doi: 10.1192/bjp.2020.127

Bauman, M. L. (1991). Microscopic neuroanatomic abnormalities in autism. *Pediatrics* 87, 791–796. doi: 10.1542/peds.87.5.791

Bednar, I., Paterson, D., Marutle, A., Pham, T. M., Svedberg, M., Hellstrom-Lindahl, E., et al. (2002). Selective nicotinic receptor consequences in APP(SWE) transgenic mice. *Mol. Cell. Neurosci.* 20, 354–365. doi: 10.1006/mcne.2002.1112

Blanchard, M. G., Willemsen, M. H., Walker, J. B., Dib-Hajj, S. D., Waxman, S. G., Jongmans, M. C., et al. (2015). De novo gain-of-function and loss-of-function mutations of SCN8A in patients with intellectual disabilities and epilepsy. *J. Med. Genet.* 52, 330–337. doi: 10.1136/jmedgenet-2014-102813

Bostan, A. C., and Strick, P. L. (2018). The basal ganglia and the cerebellum: nodes in an integrated network. *Nat. Rev. Neurosci.* 19, 338–350. doi: 10.1038/s41583-018-0002-7

Bourin, M., and Hascoet, M. (2003). The mouse light/dark box test. *Eur. J. Pharmacol.* 463, 55–65. doi: 10.1016/S0014-2999(03)01274-3

Bralten, J., Van Hulzen, K. J., Martens, M. B., Galesloot, T. E., Arias Vasquez, A., Kiemeney, L. A., et al. (2018). Autism spectrum disorders and autistic traits share genetics and biology. *Mol. Psychiatry* 23, 1205–1212. doi: 10.1038/mp.2017.98

Buitrago, M. M., Schulz, J. B., Dichgans, J., and Luft, A. R. (2004). Short and long-term motor skill learning in an accelerated rotarod training paradigm. *Neurobiol. Learn. Mem.* 81, 211–216. doi: 10.1016/j.nlm.2004.01.001

Burne, T. H., Mcgrath, J. J., Eyles, D. W., and Mackay-Sim, A. (2005). Behavioural characterization of vitamin D receptor knockout mice. *Behav. Brain Res.* 157, 299–308. doi: 10.1016/j.bbr.2004.07.008

Butler, K. M., Da Silva, C., Shafir, Y., Weisfeld-Adams, J. D., Alexander, J. J., Hegde, M., et al. (2017). De novo and inherited SCN8A epilepsy mutations detected by gene panel analysis. *Epilepsy Res.* 129, 17–25. doi: 10.1016/j.eplepsyres.2016.11.002

Carter, R. J., Lione, L. A., Humby, T., Mangiarini, L., Mahal, A., Bates, G. P., et al. (1999). Characterization of progressive motor deficits in mice transgenic for the human Huntington's disease mutation. *J. Neurosci.* 19, 3248–3257. doi: 10.1523/JNEUROSCI.19-08-03248.1999

Chen, K., Godfrey, D. A., Ilyas, O., Xu, J., and Preston, T. W. (2009). Cerebellum-related characteristics of Scn8a-mutant mice. *Cerebellum* 8, 192–201. doi: 10.1007/s12311-009-0110-z

Crawley, J. N. (2004). Designing mouse behavioral tasks relevant to autistic-like behaviors. *Ment. Retard. Dev. Disabil. Res. Rev.* 10, 248–258. doi: 10.1002/mrdd.20039

Crawley, J. N. (2007). Mouse behavioral assays relevant to the symptoms of autism. *Brain Pathol.* 17, 448–459. doi: 10.1111/j.1750-3639.2007.00096.x

Cupolillo, D., Hoxha, E., Faralli, A., De Luca, A., Rossi, F., Tempia, F., et al. (2016). Autistic-like traits and cerebellar dysfunction in purkinje cell pten knock-out mice. *Neuropsychopharmacology* 41, 1457–1466. doi: 10.1038/npp.2015.339

Dick, D. J., Boakes, R. J., and Harris, J. B. (1985). A cerebellar abnormality in the mouse with motor end-plate disease. *Neuropathol. Appl. Neurobiol.* 11, 141–147. doi: 10.1111/j.1365-2990.1985.tb00011.x

Dickson, P. E., Cairns, J., Goldowitz, D., and Mittleman, G. (2017). Cerebellar contribution to higher and lower order rule learning and cognitive flexibility in mice. *Neuroscience* 345, 99–109. doi: 10.1016/j.neuroscience.2016.03.040

Dickson, P. E., Rogers, T. D., Del Mar, N., Martin, L. A., Heck, D., Blaha, C. D., et al. (2010). Behavioral flexibility in a mouse model of developmental cerebellar Purkinje cell loss. *Neurobiol. Learn. Mem.* 94, 220–228. doi: 10.1016/j.nlm.2010.05.010

Dong, D., Zielke, H. R., Yeh, D., and Yang, P. (2018). Cellular stress and apoptosis contribute to the pathogenesis of autism spectrum disorder. *Autism Res.* 11, 1076–1090. doi: 10.1002/aur.1966

Fatemi, S. H., Aldinger, K. A., Ashwood, P., Bauman, M. L., Blaha, C. D., Blatt, G. J., et al. (2012). Consensus paper: pathological role of the cerebellum in autism. *Cerebellum* 11, 777–807. doi: 10.1007/s12311-012-0355-9

Fatemi, S. H., and Folsom, T. D. (2015). GABA receptor subunit distribution and FMRP-mGluR5 signaling abnormalities in the cerebellum of subjects with schizophrenia, mood disorders, and autism. *Schizophr. Res.* 167, 42–56. doi: 10.1016/j.schres.2014.10.010

Gardella, E., and Moller, R. S. (2019). Phenotypic and genetic spectrum of SCN8A-related disorders, treatment options, and outcomes. *Epilepsia* 60(Suppl. 3), S77–S85. doi: 10.1111/epi.16319

Gertler, T. S., and Carvill, G. L. (2019). SCN8A: when neurons are so excited, they just can't hide it. *Epilepsy Curr.* 19, 269–271. doi: 10.1177/1535759719858338

Ha, S., Lee, D., Cho, Y. S., Chung, C., Yoo, Y. E., Kim, J., et al. (2016). Cerebellar Shank2 regulates excitatory synapse density, motor coordination, and specific repetitive and anxiety-like behaviors. *J. Neurosci.* 36, 12129–12143. doi: 10.1523/JNEUROSCI.1849-16.2016

Hampson, D. R., and Blatt, G. J. (2015). Autism spectrum disorders and neuropathology of the cerebellum. *Front. Neurosci.* 9, 420. doi: 10.3389/fnins.2015.00420

Hogg, S. (1996). A review of the validity and variability of the elevated plus-maze as an animal model of anxiety. *Pharmacol. Biochem. Behav.* 54, 21–30. doi: 10.1016/0091-3057(95)02126-4

Hollander, E., King, A., Delaney, K., Smith, C. J., and Silverman, J. M. (2003). Obsessive-compulsive behaviors in parents of multiplex autism families. *Psychiatry Res.* 117, 11–16. doi: 10.1016/S0165-1781(02)00304-9

Khaliq, Z. M., Gouwens, N. W., and Raman, I. M. (2003). The contribution of resurgent sodium current to high-frequency firing in Purkinje neurons: an experimental and modeling study. *J. Neurosci.* 23, 4899–4912. doi: 10.1523/JNEUROSCI.23-12-04899.2003

Kloth, A. D., Badura, A., Li, A., Cherskov, A., Connolly, S. G., Giovannucci, A., et al. (2015). Cerebellar associative sensory learning defects in five mouse autism models. *Elife* 4, e06085. doi: 10.7554/eLife.06085.017

Larsen, J., Carvill, G. L., Gardella, E., Kluger, G., Schmiedel, G., Barisic, N., et al. (2015). The phenotypic spectrum of SCN8A encephalopathy. *Neurology* 84, 480–489. doi: 10.1212/WNL.0000000000001211

Levin, S. I., Khaliq, Z. M., Aman, T. K., Grieco, T. M., Kearney, J. A., Raman, I. M., et al. (2006). Impaired motor function in mice with cell-specific knockout of sodium channel Scn8a (NaV1.6) in cerebellar purkinje neurons and granule cells. *J. Neurophysiol.* 96, 785–793. doi: 10.1152/jn.01193.2005

Levin, S. I., and Meisler, M. H. (2004). Floxed allele for conditional inactivation of the voltage-gated sodium channel Scn8a (NaV1.6). *Genesis* 39, 234–239. doi: 10.1002/gene.20050

Liu, Y., Schubert, J., Sonnenberg, L., Helbig, K. L., Hoei-Hansen, C. E., Koko, M., et al. (2019). Neuronal mechanisms of mutations in SCN8A causing epilepsy or intellectual disability. *Brain* 142, 376–390. doi: 10.1093/brain/awy326

Lord, C., Brugha, T. S., Charman, T., Cusack, J., Dumas, G., Frazier, T., et al. (2020). Autism spectrum disorder. *Nat. Rev. Dis. Primers* 6, 5. doi: 10.1038/s41572-019-0138-4

Martin, L. A., Goldowitz, D., and Mittleman, G. (2010). Repetitive behavior and increased activity in mice with Purkinje cell loss: a model for understanding the role of cerebellar pathology in autism. *Eur. J. Neurosci.* 31, 544–555. doi: 10.1111/j.1460-9568.2009.07073.x

McKinney, B. C., Chow, C. Y., Meisler, M. H., and Murphy, G. G. (2008). Exaggerated emotional behavior in mice heterozygous null for the sodium channel Scn8a (Nav1.6). *Genes Brain Behav.* 7, 629–638. doi: 10.1111/j.1601-183X.2008.00399.x

Meisler, M. H. (2019). SCN8A encephalopathy: mechanisms and models. *Epilepsia* 60(Suppl. 3), S86–S91. doi: 10.1111/epi.14703

Meisler, M. H., Helman, G., Hammer, M. F., Fureman, B. E., Gaillard, W. D., Goldin, A. L., et al. (2016). SCN8A encephalopathy: research progress and prospects. *Epilepsia* 57, 1027–1035. doi: 10.1111/epi.13422

Meisler, M. H., Hill, S. F., and Yu, W. (2021). Sodium channelopathies in neurodevelopmental disorders. *Nat. Rev. Neurosci.* 22, 152–166. doi: 10.1038/s41583-020-00418-4

Mosconi, M. W., Wang, Z., Schmitt, L. M., Tsai, P., and Sweeney, J. A. (2015). The role of cerebellar circuitry alterations in the pathophysiology of autism spectrum disorders. *Front. Neurosci.* 9, 296. doi: 10.3389/fnins.2015.00296

Neuner, S. M., Heuer, S. E., Huentelman, M. J., O'connell, K. M. S., and Kaczorowski, C. C. (2019). Harnessing genetic complexity to enhance translatability of Alzheimer's disease mouse models: a path toward precision medicine. *Neuron* 101, 399–411 e395. doi: 10.1016/j.neuron.2018.11.040

O'Brien, J. E., and Meisler, M. H. (2013). Sodium channel SCN8A (Nav1.6): properties and de novo mutations in epileptic encephalopathy and intellectual disability. *Front. Genet.* 4, 213. doi: 10.3389/fgene.2013.00213

Oristaglio, J., Hyman West, S., Ghaffari, M., Lech, M. S., Verma, B. R., Harvey, J. A., et al. (2013). Children with autism spectrum disorders show abnormal conditioned response timing on delay, but not trace, eyeblink conditioning. *Neuroscience* 248, 708–718. doi: 10.1016/j.neuroscience.2013.06.007

Peter, S., Ten Brinke, M. M., Stedehouder, J., Reinelt, C. M., Wu, B., Zhou, H., et al. (2016). Dysfunctional cerebellar Purkinje cells contribute to autism-like behaviour in Shank2-deficient mice. *Nat. Commun.* 7, 12627. doi: 10.1038/ncomms12627

Piochon, C., Kloth, A. D., Grasselli, G., Titley, H. K., Nakayama, H., Hashimoto, K., et al. (2014). Cerebellar plasticity and motor learning deficits in a copy-number variation mouse model of autism. *Nat. Commun.* 5, 5586. doi: 10.1038/ncomms6586

Raman, I. M., Sprunger, L. K., Meisler, M. H., and Bean, B. P. (1997). Altered subthreshold sodium currents and disrupted firing patterns in Purkinje neurons of Scn8a mutant mice. *Neuron* 19, 881–891. doi: 10.1016/S0896-6273(00)80969-1

Reith, R. M., Mckenna, J., Wu, H., Hashmi, S. S., Cho, S. H., Dash, P. K., et al. (2013). Loss of Tsc2 in Purkinje cells is associated with autistic-like behavior in a mouse model of tuberous sclerosis complex. *Neurobiol. Dis.* 51, 93–103. doi: 10.1016/j.nbd.2012.10.014

Schaller, K. L., and Caldwell, J. H. (2003). Expression and distribution of voltage-gated sodium channels in the cerebellum. *Cerebellum* 2, 2–9. doi: 10.1080/14734220309424

Schniepp, R., Mohwald, K., and Wuehr, M. (2017). Gait ataxia in humans: vestibular and cerebellar control of dynamic stability. *J. Neurol.* 264, 87–92. doi: 10.1007/s00415-017-8482-3

Silverman, J. L., Tolu, S. S., Barkan, C. L., and Crawley, J. N. (2010a). Repetitive self-grooming behavior in the BTBR mouse model of autism is blocked by the mGluR5 antagonist MPEP. *Neuropsychopharmacology* 35, 976–989. doi: 10.1038/npp.2009.201

Silverman, J. L., Yang, M., Lord, C., and Crawley, J. N. (2010b). Behavioural phenotyping assays for mouse models of autism. *Nat. Rev. Neurosci.* 11, 490–502. doi: 10.1038/nrn2851

Sprunger, L. K., Escayg, A., Tallaksen-Greene, S., Albin, R. L., and Meisler, M. H. (1999). Dystonia associated with mutation of the neuronal sodium channel Scn8a and identification of the modifier locus Scnm1 on mouse chromosome 3. *Hum. Mol. Genet.* 8, 471–479. doi: 10.1093/hmg/8.3.471

Sundberg, M., and Sahin, M. (2015). Cerebellar development and autism spectrum disorder in tuberous sclerosis complex. *J. Child Neurol.* 30, 1954–1962. doi: 10.1177/0883073815600870

Tang, G. B., Zeng, Y. Q., Liu, P. P., Mi, T. W., Zhang, S. F., Dai, S. K., et al. (2017). The histone H3K27 demethylase UTX regulates synaptic plasticity and cognitive behaviors in mice. *Front. Mol. Neurosci.* 10, 267. doi: 10.3389/fnmol.2017.00267

Tatsukawa, T., Raveau, M., Ogiwara, I., Hattori, S., Miyamoto, H., Mazaki, E., et al. (2019). Scn2a haploinsufficient mice display a spectrum of phenotypes affecting anxiety, sociability, memory flexibility and ampakine CX516 rescues their hyperactivity. *Mol. Autism* 10, 15. doi: 10.1186/s13229-019-0265-5

Trudeau, M. M., Dalton, J. C., Day, J. W., Ranum, L. P., and Meisler, M. H. (2006). Heterozygosity for a protein truncation mutation of sodium channel SCN8A in a patient with cerebellar atrophy, ataxia, and mental retardation. *J. Med. Genet.* 43, 527–530. doi: 10.1136/jmg.2005.035667

Tsai, P. T., Hull, C., Chu, Y., Greene-Colozzi, E., Sadowski, A. R., Leech, J. M., et al. (2012). Autistic-like behaviour and cerebellar dysfunction in Purkinje cell Tsc1 mutant mice. *Nature* 488, 647–651. doi: 10.1038/nature11310

Tsai, P. T., Rudolph, S., Guo, C., Ellegood, J., Gibson, J. M., Schaeffer, S. M., et al. (2018). Sensitive periods for cerebellar-mediated autistic-like behaviors. *Cell Rep. 25* 357–367 e354. doi: 10.1016/j.celrep.2018.09.039

Varghese, M., Keshav, N., Jacot-Descombes, S., Warda, T., Wicinski, B., Dickstein, D. L., et al. (2017). Autism spectrum disorder: neuropathology and animal models. *Acta Neuropathol.* 134, 537–566. doi: 10.1007/s00401-017-1736-4

Wagnon, J. L., Barker, B. S., Ottolini, M., Park, Y., Volkheimer, A., Valdez, P., et al. (2017). Loss-of-function variants of SCN8A in intellectual disability without seizures. *Neurol Genet.* 3, e170. doi: 10.1212/NXG.0000000000000170

Wang, S. S., Kloth, A. D., and Badura, A. (2014). The cerebellum, sensitive periods, and autism. *Neuron* 83, 518–532. doi: 10.1016/j.neuron.2014.07.016

Wegiel, J., Flory, M., Kuchna, I., Nowicki, K., Ma, S. Y., Imaki, H., et al. (2014). Stereological study of the neuronal number and volume of 38 brain subdivisions of subjects diagnosed with autism reveals significant alterations restricted to the striatum, amygdala and cerebellum. *Acta Neuropathol. Commun.* 2, 141. doi: 10.1186/s40478-014-0141-7

Welsh, J. P., and Oristaglio, J. T. (2016). Autism and classical eyeblink conditioning: performance changes of the conditioned response related to autism spectrum disorder diagnosis. *Front. Psychiatry* 7, 137. doi: 10.3389/fpsyt.2016.00137

Whitney, E. R., Kemper, T. L., Rosene, D. L., Bauman, M. L., and Blatt, G. J. (2009). Density of cerebellar basket and stellate cells in autism: evidence for a late developmental loss of Purkinje cells. *J. Neurosci. Res.* 87, 2245–2254. doi: 10.1002/jnr.22056

Winkler, M., Biswas, S., Berger, S. M., Kuchler, M., Preisendorfer, L., Choo, M., et al. (2020). Pianp deficiency links GABAB receptor signaling and hippocampal and cerebellar neuronal cell composition to autism-like behavior. *Mol. Psychiatry* 25, 2979–2993. doi: 10.1038/s41380-019-0519-9

Wisniowiecka-Kowalnik, B., and Nowakowska, B. A. (2019). Genetics and epigenetics of autism spectrum disorder-current evidence in the field. *J. Appl. Genet.* 60, 37–47. doi: 10.1007/s13353-018-00480-w

Wong, J. C., Grieco, S. F., Dutt, K., Chen, L., Thelin, J. T., Inglis, G., et al. (2021). Autistic-like behavior, spontaneous seizures, and increased neuronal excitability in a Scn8a mouse model. *Neuropsychopharmacology* 46, 2011–2020. doi: 10.1038/s41386-021-00985-9

Woodruff-Pak, D. S., Green, J. T., Levin, S. I., and Meisler, M. H. (2006). Inactivation of sodium channel Scn8A (Na-sub(v)1.6) in Purkinje neurons impairs learning in Morris water maze and delay but not trace eyeblink classical conditioning. *Behav. Neurosci.* 120, 229–240. doi: 10.1037/0735-7044.120.2.229

Yang, M., Silverman, J. L., and Crawley, J. N. (2011). Automated three-chambered social approach task for mice. *Curr. Protoc. Neurosci.* Chapter 8, Unit 8.26. doi: 10.1002/0471142301.ns0826s56

Yang, Y. M., Arsenault, J., Bah, A., Krzeminski, M., Fekete, A., Chao, O. Y., et al. (2020). Identification of a molecular locus for normalizing dysregulated GABA release from interneurons in the Fragile X brain. *Mol. Psychiatry* 25, 2017–2035. doi: 10.1038/s41380-018-0240-0

Zheng, N., and Raman, I. M. (2011). Prolonged postinhibitory rebound firing in the cerebellar nuclei mediated by group I metabotropic glutamate receptor potentiation of L-type calcium currents. *J. Neurosci.* 31, 10283–10292. doi: 10.1523/JNEUROSCI.1834-11.2011

Conflict of Interest: The authors declare that the research was conducted in the absence of any commercial or financial relationships that could be construed as a potential conflict of interest.

Publisher's Note: All claims expressed in this article are solely those of the authors and do not necessarily represent those of their affiliated organizations, or those of the publisher, the editors and the reviewers. Any product that may be evaluated in this article, or claim that may be made by its manufacturer, is not guaranteed or endorsed by the publisher.

Copyright © 2022 Yang, Yin, Wang, Sun, Bian, Zhang, Li, Cao, Li, Ebrahimi-Fakhari, Yang, Meisler and Liu. This is an open-access article distributed under the terms of the Creative Commons Attribution License (CC BY). The use, distribution or reproduction in other forums is permitted, provided the original author(s) and the copyright owner(s) are credited and that the original publication in this journal is cited, in accordance with accepted academic practice. No use, distribution or reproduction is permitted which does not comply with these terms.

frontiers | Frontiers in Molecular Neuroscience

BRIEF RESEARCH REPORT
published: 09 May 2022
doi: 10.3389/fnmol.2022.889641

A Machine Learning Approach in Autism Spectrum Disorders: From Sensory Processing to Behavior Problems

Heba Alateyat[1†], Sara Cruz[2†], Eva Cernadas[1], María Tubío-Fungueiriño[3,4,5], Adriana Sampaio[6], Alberto González-Villar[6], Angel Carracedo[3,7,8,9], Manuel Fernández-Delgado[1] and Montse Fernández-Prieto[3,5,8,9]*

[1] Centro Singular de Investigación en Tecnoloxías Intelixentes da USC (CiTIUS), Universidade de Santiago de Compostela (USC), Santiago de Compostela, Spain, [2] The Psychology for Positive Development Research Center, Lusíada University—North, Porto, Portugal, [3] Genomics and Bioinformatics Group, Centre for Research in Molecular Medicine and Chronic Diseases (CiMUS), Universidade de Santiago de Compostela (USC), Santiago de Compostela, Spain, [4] Grupo de Medicina Xenómica, Universidade de Santiago de Compostela (USC), Santiago de Compostela, Spain, [5] Fundación Instituto de Investigación Sanitaria de Santiago de Compostela (FIDIS), Santiago de Compostela, Spain, [6] Psychological Neuroscience Lab, Centro de Investigação em Psicologia, School of Psychology, University of Minho, Campus de Gualtar, Braga, Portugal, [7] Fundación Pública Galega de Medicina Xenómica, Servicio Galego de Saúde (SERGAS), Santiago de Compostela, Spain, [8] Grupo de Medicina Xenómica, U-711, Centro de Investigación en Red de Enfermedades Raras (CIBERER), Universidade de Santiago de Compostela (USC), Santiago de Compostela, Spain, [9] Grupo de Genética, Instituto de Investigación Sanitaria de Santiago (IDIS), Santiago de Compostela, Spain

OPEN ACCESS

Edited by:
Salam Salloum-Asfar, Qatar Biomedical Research Institute, Qatar

Reviewed by:
Sara Cibralic, The Ingham Institute, Australia
Sara A. Abdulla, Qatar Biomedical Research Institute, Qatar

***Correspondence:**
Manuel Fernández-Delgado
manuel.fernandez.delgado@usc.es

[†] These authors have contributed equally to this work and share first authorship

Specialty section:
This article was submitted to Neuroplasticity and Development, a section of the journal Frontiers in Molecular Neuroscience

Received: *04 March 2022*
Accepted: *06 April 2022*
Published: *09 May 2022*

Citation:
Alateyat H, Cruz S, Cernadas E, Tubío-Fungueiriño M, Sampaio A, González-Villar A, Carracedo A, Fernández-Delgado M and Fernández-Prieto M (2022) A Machine Learning Approach in Autism Spectrum Disorders: From Sensory Processing to Behavior Problems. Front. Mol. Neurosci. 15:889641. doi: 10.3389/fnmol.2022.889641

Atypical sensory processing described in autism spectrum disorders (ASDs) frequently cascade into behavioral alterations: isolation, aggression, indifference, anxious/depressed states, or attention problems. Predictive machine learning models might refine the statistical explorations of the associations between them by finding out how these dimensions are related. This study investigates whether behavior problems can be predicted using sensory processing abilities. Participants were 72 children and adolescents (21 females) diagnosed with ASD, aged between 6 and 14 years (M = 7.83 years; SD = 2.80 years). Parents of the participants were invited to answer the Sensory Profile 2 (SP2) and the Child Behavior Checklist (CBCL) questionnaires. A collection of 26 supervised machine learning regression models of different families was developed to predict the CBCL outcomes using the SP2 scores. The most reliable predictions were for the following outcomes: total problems (using the items in the SP2 touch scale as inputs), anxiety/depression (using avoiding quadrant), social problems (registration), and externalizing scales, revealing interesting relations between CBCL outcomes and SP2 scales. The prediction reliability on the remaining outcomes was "moderate to good" except somatic complaints and rule-breaking, where it was "bad to moderate." Linear and ridge regression achieved the best prediction for a single outcome and globally, respectively, and gradient boosting machine achieved the best prediction in three outcomes. Results highlight the utility of several machine learning models in studying the predictive value of sensory processing impairments (with an early onset) on specific behavior alterations, providing evidences of relationship between sensory processing impairments and behavior problems in ASD.

Keywords: machine learning, autism spectrum disorders, sensory processing, behavior problems, regression

INTRODUCTION

Autism spectrum disorder (ASD) is a neurodevelopmental condition with a consistently high prevalence worldwide (Chiarotti and Venerosi, 2020) that poses a serious burden to the society and affected families. An early diagnosis of ASD is crucial for implementing interventional approaches on individuals with this disorder (Cidav et al., 2017). Multiple risk factors contribute to the ASD phenotype, including genetic, biological, psychosocial, and environmental contributors (Parenti et al., 2021; Deb and Bateup, 2022). This disorder is characterized by impairments in different areas of development, including deficits in social interactions and communication, by restricted/repetitive behaviors, and by sensory-perceptual alterations, which were added as an ASD diagnostic criterion (American Psychiatric Association, 2013). Impairments in sensory processing are described as unusual interests in sensory aspects of the environment (e.g., visual, auditory, or tactile stimuli) to which individuals with ASD frequently display atypical responses (Tseng et al., 2011; American Psychiatric Association, 2013). These responses can be organized and classified as hyper-reactivity (tendency to respond at lower intensity thresholds quicker and more intensely or longer) or hypo-reactivity (tendency to respond with "indifference," unawareness, or slowly) to sensory input (Tavassoli et al., 2016) that seems to be underpinned by specific neurophysiological markers (see Marco et al., 2011 for a detailed review). Atypical processing patterns have been observed in ASD across all sensory modalities, including visual, auditory, olfactory, proprioceptive, somatosensory, or interoceptive stimulation, and multisensory integration, regardless of age and symptoms severity in children and adolescent (Ben-Sasson et al., 2009). Sensory alterations have an early onset and are one of the first signs of ASD, as early as observed in the first months of life (Iarocci and McDonald, 2006). In consequence, these alterations can impact behavior and social functioning of children and adolescents and may be at the root of social deficits during development (Thye et al., 2018).

Indeed, altered sensory responsivity in ASD cascades into social and behavioral impairments (Thye et al., 2018). The relationship between hypo-responsiveness and hyper-responsiveness to sensory stimuli and maladaptive behavior has been documented, with atypical processing of stimuli being correlated with social, cognitive, and communicative impairments (Kojovic et al., 2019), and the presence of repetitive and restricted interests and behaviors (Foss-Feig et al., 2012). Sensory abnormalities were also linked to isolation, reactivity to change, disinterest and indifference, self-aggression, irritability, or emotional lability (Gonthier et al., 2016). Additionally, altered sensory processing has been related to anxiety (Uljarević et al., 2016) and depressive (Bitsika et al., 2016) states in children and adolescents with ASD, with a great impact on their adaptive behaviors (Tomcheck and Dunn, 2007; Lane et al., 2010; Zachor and Curatolo, 2014). One of the earliest and most common sensory alterations described in ASD is related to abnormalities in tactile processing, for example, food texture (Mikkelsen et al., 2018).

Tactile contact is considered a precursor for the development of social and communication abilities, and impaired touch processing has been linked to emotional and social distress early in life, as it imposes limits on environmental learning opportunities (Mikkelsen et al., 2018). Moreover, evidence suggests that increased difficulties in touch processing are associated with behavioral impairments (e.g., difficulties in inhibitory control) in children and adolescents with ASD (Puts et al., 2014; Piccardi et al., 2021). In addition, altered touch processing was related to increased social and communication deficits (Foss-Feig et al., 2012; Miguel et al., 2017), to non-verbal communication impairments and repetitive behaviors (Foss-Feig et al., 2012), as well as anxious/depressed states and repetitive/obsessive behavior (Fernández-Prieto et al., 2021). Therefore, it is important to further clarify the relationship between sensory processing and behavior in children and adolescents with ASD, by exploring to what extent sensory processing is predictive of behavioral outcomes in this population. The Sensory Profile 2—SP2 (Dunn, 2014)—and the Child Behavior Checklist—CBCL (Achenbach and Rescorla, 2001)—are two widely used tools to measure sensory and behavioral competencies, respectively. These questionnaires provide standardized measures of child's development and offer guidance for future clinical interventions. In addition, the scores of SP2 and CBCL subscales are correlated (Miguel et al., 2017). New tools—like machine learning (ML) techniques—can offer novel insights into how sensory processing and behavior—measured by these questionnaires—are associated. Some works in the literature showed the interest of using ML in the study of ASD to analyze continuous/dimensional or categorical/qualitative variation between and within individuals (Lombardo et al., 2019). In addition, ML can offer improved diagnostic timing, precision, and quality, allowing clinicians to provide more robust diagnosis and intervention programs (Thabtah, 2019), as well as providing evidence on possible altered processes (e.g., reactivity to sensorial stimuli) for implementing early personalized care therapies and/or strategies. The ML models provide satisfactory solutions to medical and non-medical applications due to its ability to extract information and make predictions (Briscoe and Marín, 2020).

This study aims to use a wide collection of supervised ML algorithms (multiple linear regression, support vector machines, gradient boosting machine, and regression tree-based ensembles such as cubist and random forest, among others) to investigate how sensory processing predicts behavioral problems in ASD. With these algorithms, we sought to examine how SP2 quadrant scores (seeking, avoiding, sensitivity, and registration) and touch processing (given the evidence suggesting that tactile impairments are related to the onset of ASD, and being the most common sensory alteration in this population) are predictive of CBCL subscales: anxious/depressed, withdrawn/depressed, somatic complaints, social problems, thought problems, attention problems, rule-breaking behavior, aggressive behavior, and the two empirically derived internalizing and externalizing broadband scales. It is expected that hyper-responsive and hypo-responsive sensory experiences assessed using the SP2, i.e., items corresponding to seeking and avoiding

TABLE 1 | List of the six item sets used as inputs by the machine learning regressors (touch, total, and the four quadrants from the SP2 questionnaire), with the number of items and the items included in each set.

Item set	No. items	Items in SP2 questionnaire
Touch	11	16–26
Seeking	19	14, 21, 22, 25, 27, 28, 30, 31, 32, 41, 48, 49, 50, 51, 55, 56, 60, 82, 83
Avoiding	20	1, 2, 5, 15, 18, 58, 59, 61, 63, 64, 65, 66, 67, 68, 70, 71, 72, 74, 75, 81
Sensitivity	19	3, 4, 6, 7, 9, 13, 16, 19, 20, 44, 45, 46, 47, 52, 69, 73, 77, 78, 84
Registration	22	8, 12, 23, 24, 26, 33, 34, 35, 36, 37, 38, 39, 40, 53, 54, 57, 62, 76, 79, 80, 85, 86
Total	86	1–86

CBCL outcome			
S1	Anxious/depressed	S7	Rule-Breaking behavior
S2	Withdrawn/depressed	S8	Aggressive behavior
S3	Somatic complaints	Internal	Internalizing problems
S4	Social problems	External	Externalizing problems
S5	Thought problems	Total	Total problems
S6	Attention problems		

The lower part lists the 11 scales from the CBCL questionnaire (outcomes) to be predicted by the regressors.

quadrants, as well as touch processing, can be used to predict ASD behavioral problems, namely, anxious/depressed, withdrawn/depressed, rule-breaking behavior and aggressive behavior, as well as in internalizing and externalizing domains.

MATERIALS AND METHODS

Participants

Participants were 72 children and adolescents (21 females), aged between 6 and 14 years (mean = 7.83 years; SD = 2.80 years), diagnosed with ASD following the criteria established by the Diagnostic and Statistical Manual of Mental Disorders in its revised fourth version (DSM-IV-TR) or fifth version (DSM-5). Participants were part of a larger research project studying the association between phenotype and genotype characteristics in ASD. Qualified clinicians who were part of the research team confirmed the ASD diagnosis for research purposes, using the Autism Diagnostic Interview Revised, ADI-R (Rutter et al., 2006) and the Autism Diagnostic Observation Schedule, ADOS (Lord et al., 2008), both described in Sections Autism Diagnostic Interview Revised and Autism Diagnostic Observation Schedule−2, respectively, of the **Supplementary Material**. All parents who agreed to voluntarily participate gave the written informed consent, obtained in accordance with the Declaration of Helsinki.

Dataset Description

The Sections Sensory Profile−2 and Child Behavior Checklist of the **Supplementary Material** describe the SP2 (Dunn, 2014) and CBCL (Achenbach and Rescorla, 2001) questionnaires in detail, respectively. The six sets of items from SP2—touch processing, the four quadrants (seeking, avoiding, sensitivity, and registration) and the total SP2 score (all the items)—were used as inputs of the ML models for predicting the following 11 outcomes of the CBCL questionnaire (scale scores): withdrawn/depressed (S1), somatic complaints (S2), anxious/depressed (S3), social problems (S4), thought problems (S5), attention problems (S6), rule-breaking behavior (S7), aggressive behavior (S8), internalizing problems (internal), externalizing problems (external), and total problems (total). Raw scores for each scale were converted to standardized T-scores based on Spanish standards (Unitat d'Epidemiologia i de Diagnòstic en Psicopatologia del Desenvolupament, 2016), bounded between 0 and 100, considering age and sex of participants (6–11 and 12–18 years, separately). **Table 1** depicts the list of items included in each set. Each ML model predicts one of the 11 outcomes in CBCL using one of the six input sets in SP2, giving a total of $6{\cdot}11 = 66$ datasets. The influence of gender (denoted as G) was also investigated, as recent evidence (Osório et al., 2021) revealed that ASD females are more likely to be distressed by environmental stimuli, such as noise, and have more difficulties with movement coordination and postural control. Therefore, each set was analyzed with and without gender, thus obtaining $66{\cdot}2 = 132$ datasets. **Supplementary Figure 1** draws the boxplots that represent the distributions of values for the 11 outcomes. Although each outcome is a score on a scale from 1 to 100, the values are above 30–40 for all the outcomes and, in several cases, they do not reach 100. For each CBCL outcome, a value below 60 corresponds to a normative behavior, values between 60 and 70 correspond to preclinical behavior (i.e., near to require clinical treatment), and values above 70 correspond to a clinical diagnosis.

Machine Learning

The description of the ML regression models used to predict the CBCL outcomes automatically using the SP2 scores is detailed in Section Machine Learning Techniques of the **Supplementary Material**, whose **Supplementary Tables 1**, **2** list the details of these models, grouped by families. The family of linear and regularized regressors include simple linear regression (Chambers, 1992), namely, lm, lreg, lmreg, and pylm[1]; stochastic gradient descent (sgd); least absolute shrinkage and selection operator regression (lasso) and elasticnet (enet). Kernel and support vector regressors include kernel ridge regression (krr); ε-support vector regression (Chang and Lin, 2011) with radial basis function (RBF), svr and pysvr, and linear (lsvr) kernels; and Gaussian process regression (Rasmussen and Williams, 2006), named gpr. We also used the regression tree (named tree) and the M5 model tree (Cohen, 1995), named m5, implemented by the Weka library (Frank et al., 2016). The ensemble family includes bagging (Breiman, 1996); adaboost (Drucker, 1997); gradient boosting machine (Ridgeway, 1999), named gbm and pygbm; boosting of regression trees (Wang, 2011), named bstTree; cubist (Quinlan, 1992); random forest

[1]We used several implementations of linear regression because they achieved different results.

(Breiman, 2001), named rf and pyrf; extremely randomized regression trees (extraTrees); and voting committee (vote). We also used the multilayer perceptron neural network (pymlp). The models were selected due to their high performance in our exhaustive comparison (Fernández-Delgado et al., 2019), being implemented in the Python programming language with the Scikit-learn module (Pedregosa et al., 2011), in the R statistical and computing language (The R Team, 2022), and in the Octave (Eaton et al., 2022) and MATLAB (Mathworks, 2021) scientific programming languages.

Experimental Methodology

The classical K-fold cross-validation methodology, which splits the available dataset in training and test sets, is normally used to test the performance of ML models. The performance measurements commonly used in regression problems are the Pearson correlation coefficient (R), root mean squared error (RMSE), mean absolute error (MAE), and weighted absolute percentage error (WAPE), defined in Section Performance Measurements of the **Supplementary Material**. The reduced number ($N = 72$) of participants might lead to poorly significant training set and unreliable predictions using the K-fold cross validation with $K = 4$, 5, or 10. To avoid this drawback, we used leave-one-out cross validation, that is, a particular case of K-fold for $K = N$. In the i-th trial, with $i = 1...$ N, the i-th participant is left for testing, and the remaining N-1 participants are used to select adequate hyper-parameter values that achieve good performance (hyper-parameter tuning). The regressor is trained on a subset of the N-1 participants (training set) using a given combination of hyper-parameter values. The remaining participants (validation set) evaluate the regressor performance using that combination of values. In order to avoid biasing caused by splitting, the N-1 participants are sorted by increasing outcome value and participants with odd (even) index are assigned to the training (validation) set. Thus, each set roughly contains 50% of the N-1 participants with outcome values distributed across the whole range. The training/validation cycle is repeated for the different combinations of hyper-parameter values, and the combination with the lowest RMSE on the validation set is selected. Finally, the regressor is trained with both sets (training and validation, summing up N-1 participants), using the selected combination of hyper-parameter values, and tested on the i-th participant, which was devoted to testing. The tuning/testing process is repeated for each trial $i = 1,\ldots, N$, and the performance, measured by R, RMSE, MAE, and WAPE, is calculated over the N trials. The same process is executed for each model and CBCL outcome.

To measure the validity of the prediction to perform a diagnosis, each CBCL outcome is thresholded (see Section Dataset Description) and labeled as normative (preclinical or clinical) with values below (above) 60. The usual performance measurements are accuracy (ACC), sensitivity (Se), and specificity (Sp), defined in Section Performance Measurements of the **Supplementary Material**. This classification problem is not intended to replace the original prediction of the continuous CBCL outcome, but to estimate the impact of unreliable predictions on a final diagnostic (normative vs. preclinical and clinical).

RESULTS

Table 2 summarizes the best correlation R achieved by some regressors for each CBCL outcome (in columns) and the set of SP2 items (input, in rows) with and without gender. Each R value is the correlation between the true CBCL outcome values and the values predicted by the regressor for this outcome over the N patients, according to the abovementioned leave-one-out approach. These R values are not the correlations between CBCL outcomes and SP2 items. **Table 3** reports the best correlation R, and its corresponding RMSE, MAE, and WAPE values (in %), achieved by the best regressor for each outcome with and without gender (G), alongside the set of SP2 items that provided the best R. The last three rows of **Table 3** report the accuracy, sensitivity, and specificity classification.

According to the Colton criteria in Section Performance Measurements of the **Supplementary Material**, the prediction (**Table 2**) for externalization domain (external outcome, $R = 0.98$) is considered "very good to excellent" (labeled VGE in the table), while the prediction of anxious/depressed (S1) and social problems (S4), with $R = 0.72$, is "moderate to good" (MTG) but close to "very good to excellent." The prediction of withdrawn/depressed (S2), thought problems (S5), attention problems (S6), aggressive behavior (S8), internalizing and total problems is also "moderate to good" (MTG). Finally, the predictions of somatic complaints (S3) and rule-breaking (S7) behaviors are "bad to moderate" (BTM), and therefore fairly unreliable.

The avoiding quadrant is the most reliable in anxious/depressed (S1), aggressive behavior (S8), and internalizing problems as shown in **Table 2**. The registration quadrant best predicts withdrawn/depressed (S2), social problems (S4), and internalizing (same R as avoiding). Touch processing best predicts thought problems (S5), rule-breaking (S7, with low $R = 0.44$), and total problems. The seeking quadrant achieves low $R = 0.44$ in somatic complaints (S3) and $R = 0.51$ in attention problems (S6), so it is not very related to any of the problems. The sensitivity quadrant never gets the best reliability in prediction. The influence of gender on the prediction is marginal, with very small differences (about 0.02) in the best R for each outcome with and without gender, although this influence might be implicit on the remaining items of the questionnaire.

Table 3 lists the best R results, extracted from **Table 2**, alongside their corresponding RMSE, MAE, and WAPE values, best SP2 quadrant and regressor, and accuracy, sensitivity, and specificity of normative vs. preclinical and clinical classification. The MAE is below 10 for all the CBCL outcomes, except withdrawn/depressed (S2) and thought problems (S5), so the uncertainty prediction value for most outcomes is below 20. The outcome values range approximately between 35 and 100 (see **Supplementary Figure 1**), so these MAE values are comparatively small. The WAPE is very low in externalizing

TABLE 2 | The best *R* for each outcome over the scales is in bold, labeled by performance levels as: BTM (bad to moderate), MTG (moderate to good), and VGE (very good to excellent).

	CBCL outcome										
Item set	**S1**	**S2**	**S3**	**S4**	**S5**	**S6**	**S7**	**S8**	**Internal**	**External**	**Total**
Touch	0.54	0.3	0.21	0.68	**0.57 MTG**	0.5	**0.44 BTM**	0.47	0.49	0.4	**0.67 MTG**
Seeking	0.11	0.04	**0.44 BTM**	0.34	0.39	**0.51 MTG**	0.29	0.48	0.16	0.42	0.34
Avoiding	**0.72 MTG**	0.57	0.28	0.49	0.26	0.23	0.39	**0.55 MTG**	**0.63 MTG**	0.54	0.56
Sensitivity	0.43	0.36	0.2	0.51	0.41	0.4	0.35	0.36	0.43	0.37	0.47
Registration	0.69	**0.58 MTG**	0.35	**0.72 MTG**	0.38	0.43	0.32	0.48	**0.63 MTG**	0.42	0.58
Total	0.68	0.41	0.36	0.63	0.51	0.43	0.3	0.5	0.61	**0.98 VGE**	0.57

Best correlation (R) between true and predicted value for each CBCL outcome (in columns) and for each SP2 scale (touch, seeking, avoiding, sensitivity, registration, and total, in rows).

TABLE 3 | Correlation (*R*), RMSE, MAE, WAPE (in %), and input set that achieved the best performance for each CBCL outcome.

Outcome	**S1**	**S2**	**S3**	**S4**	**S5**	**S6**	**S7**	**S8**	**Internal**	**External**	**Total**
R	0.72	0.58	0.44	0.72	0.57	0.51	0.44	0.55	0.63	0.98	0.67
RMSE	8.56	16.30	10.05	9.93	21.98	8.67	9.46	12.05	9.89	2.32	9.16
MAE	6.39	12.44	7.71	8.05	18.15	6.6	7.42	9.12	7.79	1.07	7.07
WAPE (%)	11.9	18.93	14.22	11.9	25.8	10.1	13.6	15.95	13.18	1.86	11.20
Input set	Avoid	Reg+G	Seek	Reg	Touch	Seek+G	Touch+G	Avoid+G	Avoid	Total	Touch
Regressor	adaboost	pymlp	pygbm	pygbm	lreg	pyrf	extraTrees	tree	ridge	lm	pygbm
Acc (%)	87.5	70.8	79.2	66.7	70.8	77.8	77.8	73.6	79.2	97.2	73.6
Se (%)	56.2	77.5	41.2	82.9	68	87.7	35.7	54.2	78.6	100	78.4
Sp (%)	81.8	72.1	58.3	66.7	87.2	84.7	41.7	61.9	71	92.3	72.5

Besides, accuracy, sensitivity, and specificity (in %) and best regressor for the classification into normative range vs. pre-clinical and clinical.

problems (1.86%) and below 14% for most scales except withdrawn/depressed (S2), somatic complains (S3), thought problems (S5), and aggressive behavior (S8).

The pygbm (gradient boosting machine) is the regressor that achieves the best *R* in more (three) CBCL outcomes: somatic complains (S3), with low *R*, social problems (S4) and total, with higher *R*. Linear regression achieves the best *R* in thought (S5, regressor lreg), internalizing (ridge), and externalizing problems (lm, with high *R*). Regression trees and ensembles provide the best prediction for anxious/depressed (S1, adaboost); attention problems (S6, pyrf); rule-breaking (S7, extraTrees); and aggressive behavior (S8, tree). Neural network is the best for withdrawn/depressed behavior (S2, pymlp).

Regarding classification into normative vs. preclinical and clinical (last three rows of **Table 3**), accuracy is almost perfect (97.2%) in externalizing with linear regression, lm. Except social problems (S4), the accuracy is above 70% in all the outcomes, with values close to or above 80% for anxious/depressed (S1), somatic complains (S3), attention problems (S6), rule-breaking (S7), and internalizing. Overcoming sensitivity outcomes was 80% in social (S4) and attention (S6) problems, and 100% in externalizing, being close to or above 70% in the remaining CBCL scales except anxious/depressed (S1), somatic complains (S3), rule-breaking (S7), and aggressive behavior (S8). Specificity values were 80% in anxious/depressed (S1), thought (S5), and attention (S6) problems, and 92.3% in externalizing, being close to or above 70% for withdrawn/depressed (S2), social problems (S4), and internalizing and total problems. The lowest specificity values are achieved in somatic complaints (S3), rule-breaking (S7), and aggressive behavior (S8), which are globally the worst-performing CBCL outcomes.

Figure 1 plots the observed (horizontal axis) and predicted (vertical) values for externalizing (**Figure 1A**) and social problems (S4, **Figure 1B**) for all participants with the best regressor (lm and pygbm, respectively), and the best SP2 input set (total and registration, respectively). **Figure 1A** depicts the high coincidence between both values, with WAPE below 2%, while **Figure 1B** shows lower coincidence values, with WAPE around 12%, although the predicted values somehow raise with the true values, providing $R = 0.72$ (qualified as "moderate to good"). The CBCL values (blue squares) depicted on the right (left) of the red vertical line at 60 are participants who scored in the preclinical and clinical (in the normative) range. Likewise, the squares above (below) the horizontal red line at 60 are participants who are the best regressors predicted in the preclinical and clinical (in the normative) range. All the squares on the upper right and lower left areas defined by the horizontal and vertical red lines at 60 are predicted as the right class label, and only values on the upper-left and lower-right quadrants are predicted as the wrong class label. Thus, the number of classification errors is very

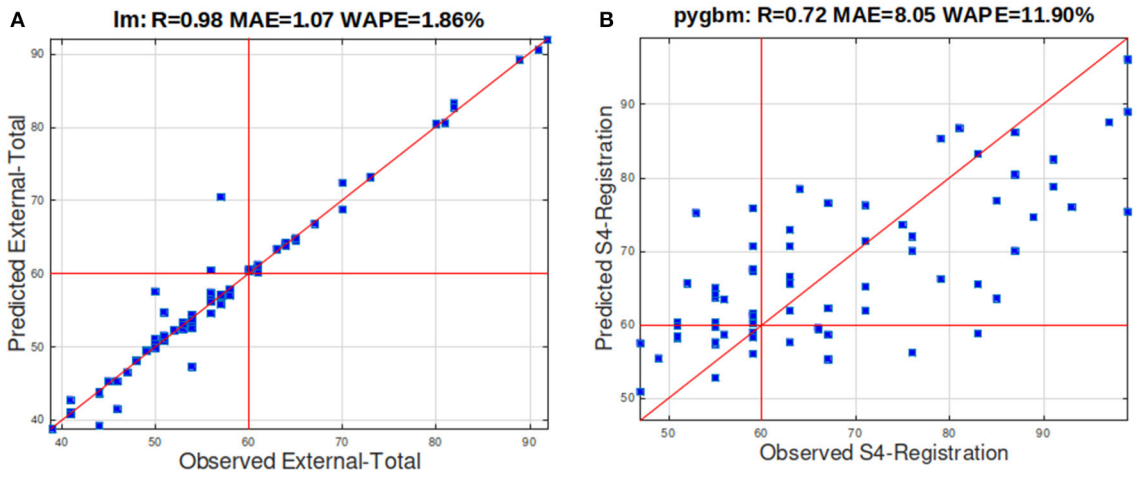

FIGURE 1 | (A) Scatterplot of the true values and values predicted by lm (linear regression) for the externalization domain. **(B)** Scatterplot of the true values and values predicted by pygbm for social problems (S4). The *R*, MAE, and WAPE values are reported in the title.

low in panel A (externalization domain), with no false negatives (dots in the lower right quadrant, 100% sensitivity) and just two false positives (upper left quadrant). In panel B, the number of dots in the upper left and lower right quadrants is higher, but much lower than in lower left and upper right quadrants (patients well-classified), with an accuracy of 66.7%, so the impact of unreliability in prediction ($R = 0.72$) over classification is low for this outcome.

DISCUSSION

This study investigated how sensory processing alterations predicted behavior problems in children and adolescents with ASD using ML models. This technique offers a new potential solution to classify ASD difficulties based on different dimensions, e.g., behavior, genetics, and neuroimaging data, among others (Georgescu et al., 2019). These artificial intelligence tools can be an important and useful approach to further explain how sensory processing abnormalities (one of the earliest clinical alterations in ASD) are predictive of social, behavior, and emotional problems in this population.

Overall, results revealed high correlation between some true behavioral (CBCL) scales and the values predicted by the regressors using some SP2 processing quadrants. The highest correlation was observed for total problems, anxiety/depression, social problems, and externalizing scales. The prediction was more reliable using certain SP2 scales, revealing strong relations with the predicted CBCL scales: CBCL externalizing problems and SP2 total scale score; CBCL social problems and SP2 registration quadrant; CBCL anxiety/depressed and SP2 avoiding quadrant; and CBCL total problems scale with SP2 touch scale. With this prediction, early indicative signs of the overall behavioral difficulties of children with an ASD diagnosis can be obtained from their response to sensory stimuli. Thus, these results can be extremely useful for clinical interventions. Considering the predicted information, early signs of altered sensory functioning would allow for incorporating personalized and early sensory-based care therapies for children with an ASD diagnosis, hence minimizing the affected areas of behavior, as much as possible.

Results obtained by the ML methods are consistent with other findings, suggesting an association between sensory processing and behavior problems in children and adolescents with ASD (Iarocci and McDonald, 2006). Patterns of sensory processing alterations, including touch processing, may imply difficulties in response to environmental cues and missing opportunities to learn from them, which is the foundation for the development of more complex processes, such as emotional regulation, and social interactions (Kojovic et al., 2019). These difficulties have cascade effects in daily life activities in ASD, manifested through a range of behavior problems such as hyperactivity, impulsivity, stereotyped and repetitive behaviors, as well as emotional and social distress (Thye et al., 2018). It may contribute to the emergence of anxious and depressive states, as dealing with sensory stimulation may be demanding for children and adolescents with ASD (Fernández-Prieto et al., 2021).

The results contribute to the existing evidence highlighting the detrimental impact of altered sensory processing on behavioral outcomes in children and adolescents with ASD (Foss-Feig et al., 2012; Uljarević et al., 2016; Miguel et al., 2017). These difficulties interfere with their adaptive functioning (McLean et al., 2014) and should be considered in interventional approaches with this population. Early intervention programs focused on addressing sensory difficulties may help prevent behavioral problems, alleviate behavioral difficulties, and, consequently, improve adaptive functioning of children and adolescents to environmental situations.

This work offers multiple strengths, of which how ML methods contribute to clarify the association between sensory processing impairments and behavioral difficulties in children and adolescents with ASD is highlighted, as these results can provide important clues for sensory-related intervention

approaches within this population. However, this study has some limitations. First is the reduced number of participants. Future studies should consider a larger sample to confirm the results. In addition, it would be important to replicate this investigation in ASD adult population to verify if similar outcomes are present. Also, it would be important that future studies address severity levels of ASD presentations, considering the high inter-individual variability observed in this population. Another limitation of this work refers to its cross-sectional design that does not allow for determining causal associations between the variables. Thus, future studies should consider assessing sensory processing and behavioral outcomes in a longitudinal manner to clarify the causal relationship between these dimensions. Also, future investigations should integrate brain imaging techniques to elucidate about the areas of the brain that pertain to sensory processing and/or behavior that are affected, which would strengthen these findings.

CONCLUSION

Autism spectrum disorders are associated with sensory processing abnormalities that often lead to behavioral alterations. The current study investigates the relations between the SP2 scales and the CBCL outcomes in order to study the association between sensory and behavior problems, using 26 machine learning regressors of different families: linear regression, kernel and support vector regression, ensembles including bagging, adaboost, gradient boosting machine and random forest, regression trees, and neural networks. Using a sample of 72 participants, the predicted outcomes are "from good to excellent" for externalization domain using all the SP2 items, and "from moderate to good" for anxious/depressed and social problems using avoiding and registration quadrants, respectively. The predictions are also "from moderate to good" for the remaining outcomes except somatic complaints and rule-breaking, where the predictions are "bad to moderate." Considering the classification into normative vs. preclinical and clinical, the accuracy reaches 97.2 and 87.5% for externalization and anxious/depressed, respectively. However, somatic complaints and rule-breaking outcomes, with low predictive reliability, still achieve accuracies near 80%, alongside with attention problems and internalization, while the remaining outcomes achieve accuracies above or near 70%.

DATA AVAILABILITY STATEMENT

The original contributions presented in the study are included in the article/**Supplementary Materials**, further inquiries can be directed to the corresponding author.

ETHICS STATEMENT

The studies involving human participants were reviewed and approved by the Research Ethics Committee of Santiago-Lugo. Written informed consent to participate in this study was provided by the participants' legal guardian/next of kin.

AUTHOR CONTRIBUTIONS

HA: article writing and experimental work with machine learning regressors. SC: article writing. EC: analysis of regression results. MT-F: conceptualization, methodology, investigation, and writing. AS: discussion of results in ASD context. AG-V: discussion of relations between sensory and behavior. AC: resources, writing, review, editing, and supervision. MF-D: execution of regression models. MF-P: writing of original draft and review, visualization, and project administration. All authors contributed to the article and approved the submitted version.

FUNDING

This work has received financial support from the Consellería de Educación, Universidade e Formación Profesional (accreditation 2019-2022 ED431G-2019/04) and the European Regional Development Fund (ERDF), which acknowledges the CiTIUS—Centro Singular de Investigación en Tecnoloxías Intelixentes da Universidade de Santiago de Compostela as a Research Center of the Galician University System. SC acknowledges the Centro de Investigação em Psicologia para o Desenvolvimento (CIPD) [The Psychology for Positive Development Research Center] (UID/PSI/04375), Lusíada University North, Porto, supported by national funds through the Portuguese Foundation for Science and Technology, I.P., and the Portuguese Ministry of Science, Technology, and Higher Education (UID/PSI/04375/2019). AS was supported by the Psychology Research Center (PSI/01662), School of Psychology, University of Minho, through the Foundation for Science and Technology (FCT) through the Portuguese State Budget (Ref.: UIDB/PSI/01662/2020). MT-F, AC, and MF-P were funded by Instituto de Salud Carlos III (PI19/00809 to AC) and co-funded by European Union (ERDF) A way of making Europe, and Fundación María José Jove.

SUPPLEMENTARY MATERIAL

The Supplementary Material for this article can be found online at: https://www.frontiersin.org/articles/10.3389/fnmol.2022.889641/full#supplementary-material

REFERENCES

Achenbach, T. M., and Rescorla, L. A. (2001). *Manual for the ASEBA School-Age Forms & Profiles: An Integrated System of Multi-Informant Assessment*. Burlington, VT: University of Vermont; Research Center for Children, Youth, & Families.

American Psychiatric Association (2013). *Diagnostic and Statistical Manual of Mental Disorders, 5th Edn.* Washington, DC: American Psychiatric Association. doi: 10.1176/appi.books.9780890425596

Ben-Sasson, A., Carter, A. S., and Briggs-Gowan, M. J. (2009). Sensory over-responsivity in elementary school: prevalence and social-emotional correlates. *J. Abnorm. Child. Psychol.* 37, 705–716. doi: 10.1007/s10802-008-9295-8

Bitsika, V., Sharpley, C. F., and Mills, R. (2016). Are sensory processing features associated with depressive symptoms in boys with an ASD? *J. Autism Dev. Disord.* 46, 242–252. doi: 10.1007/s10803-015-2569-4

Breiman, L. (1996). Bagging predictors. *Mach. Learn.* 24, 123–140. doi: 10.1007/BF00058655

Breiman, L. (2001). Random forests. *Mach. Learn.* 45, 5–32. doi: 10.1023/A:1010933404324

Briscoe, J., and Marín, O. (2020). Looking at neurodevelopment through a big data lens. *Science* 369, 1–10. doi: 10.1126/science.aaz8627

Chambers, J. M. (1992). "Linear models," in *Statistical Models in S*, eds J. M. Chambers, and T. J. Hastie (Pacific Grove, CA: Wadsworth & Brooks/Cole).

Chang, C. C., and Lin, C. J. (2011). LIBSVM: a library for support vector machines. *ACM T. Intel. Syst. Technol.* 2, 1–27. doi: 10.1145/1961189.1961199

Chiarotti, F., and Venerosi, A. (2020). Epidemiology of autism spectrum disorders: a review of worldwide prevalence estimates since 2014. *Brain Sci.* 10, 274–295. doi: 10.3390/brainsci10050274

Cidav, Z., Munson, J., Estes, A., Dawson, G., Rogers, S., and Mandell, D. (2017). Cost offset associated with early start Denver model for children with autism. *J. Am. Acad. Child. Psychol.* 56, 777–783. doi: 10.1016/j.jaac.2017.06.007

Cohen, W. (1995). "Fast effective rule induction," in *Proceedings International Conference Machine Learning*, eds A. Prieditis and E. Russell (Tahoe City, CA: Morgan Kaufmann), 115–123. doi: 10.1016/B978-1-55860-377-6.50023-2

Deb, B. K., and Bateup, H. S. (2022). Modeling somatic mutations associated with neurodevelopmental disorders in human brain organoids. *Front. Mol. Neurosci.* 14, 787243. doi: 10.3389/fnmol.2021.787243

Drucker, H. (1997). "Improving regressors using boosting techniques," in *Proceeding International Conference Machine Learning* (San Francisco, CA: Morgan Kaufmann), 107–115.

Dunn, W. (2014). *Sensory Profile 2 Manual.* San Antonio, TX: Pearson; The Psychological Corporation.

Eaton, J., Bateman, D., Hauberg, S., and Wehbring, R. (2022). *GNU Octave v. 5.2.0 Manual: A High-Level Interactive Language for Numerical Computations.* Available online at: http://www.octave.org (accessed March 3, 2022).

Fernández-Delgado,. M., Sirsat, M. S., Cernadas, E., Alawadi, S., Barro, S., and Febrero-Bande, M. (2019). An extensive experimental survey of regression methods. *Neural Netw.* 111, 11–34. doi: 10.1016/j.neunet.2018.12.010

Fernández-Prieto, M., Moreira, C., Cruz, S., Campos, V., Martínez-Regueiro, R., Taboada, M., et al. (2021). Executive functioning: a mediator between sensory processing and behaviour in autism spectrum disorder. *J. Autism Dev. Disord.* 51, 2091–2103. doi: 10.1007/s10803-020-04648-4

Foss-Feig, J. H., Heacock, J. L., and Cascio, C. J. (2012). Tactile responsiveness patterns and their association with core features in autism spectrum disorders. *Res. Autism Spectr. Disord.* 6, 337–344. doi: 10.1016/j.rasd.2011.06.007

Frank, E., Hall, M. A., and Witten, I. H. (2016). *The Weka Workbench. Online Appendix for "Data Mining: Practical Machine Learning Tools and Techniques"*. Burlington, MA: Morgan Kaufmann.

Georgescu, A.L., Koehler, J.C., Weiske, J., Vogeley, K., Koutsouleris, N., and Falter-Wagner, C. (2019). Machine learning to study social interaction difficulties in ASD. *Front. Robot. AI* 6, 132. doi: 10.3389/frobt.2019.00132

Gonthier, C., Longuépée, L., and Bouvard, M. (2016). Sensory processing in low-functioning adults with autism spectrum disorder: distinct sensory profiles and their relationships with behavioral dysfunction. *J. Autism Dev. Disord.* 46, 3078–3089. doi: 10.1007/s10803-016-2850-1

Iarocci, G., and McDonald, J. (2006). Sensory integration and the perceptual experience of persons with autism. *J. Autism Develop. Disord*. 36, 77–90. doi: 10.1007/s10803-005-0044-3

Kojovic, N., Ben Hadid, L., Franchini, M., and Schaer,. M. (2019). Sensory processing issues and their association with social difficulties in children with autism spectrum disorders. *J. Clin. Med.* 8, 1508. doi: 10.3390/jcm8101508

Lane, A. E., Young, R. L., Baker, A. E., and Angley, M. T. (2010). Sensory processing subtypes in autism: association with adaptive behavior. *J. Autism Dev. Disord.* 40, 112–122. doi: 10.1007/s10803-009-0840-2

Lombardo, M. V., Lai, M. C., and Baron-Cohen, S. (2019). Big data approaches to decomposing heterogeneity across the autism spectrum. *Mol. Psychiatry* 24, 1435–1450. doi: 10.1038/s41380-018-0321-0

Lord, C., Rutter, M., DiLavore, P. C., Risi, S., Gotham, K., Bishop, S. L., et al. (2008). *ADOS. Escala de Observación Para El Diagnóstico Del Autismo*. Madrid: TEA Editions.

Marco, E., Hinkley, L., Hill, S., and Nagarajan, S. (2011). Sensory processing in autism: a review of neurophysiologic findings. *Pediatr. Res.* 69, 48–54. doi: 10.1203/PDR.0b013e3182130c54

Mathworks (2021). *Matlab v. 9.10.0*. Mathworks. Available online at: http://www.mathworks.com (accessed March 3, 2022).

McLean, R. L., Johnson-Harrison, A., Zimak, E., Joseph, R. M., and Morrow, E.M. (2014). Executive function in probands with autism with average IQ and their unaffected first-degree relatives. *J. Am. Acad. Child Adolesc. Psychol.* 53, 1001–1009. doi: 10.1016/j.jaac.2014.05.019

Miguel, H. O., Sampaio, A., Martínez-Regueiro, R., Gómez-Guerrero, L., López-Dóriga, C. G., Gómez, S., et al. (2017). Touch processing and social behavior in ASD. *J. Autism Dev. Disord.* 47, 2425–2433. doi: 10.1007/s10803-017-3163-8

Mikkelsen, M., Wodka, E. L., Mostofsky, S. H., and Puts, N. A. J. (2018). Autism spectrum disorder in the scope of tactile processing. *Dev. Cogn. Neurosci.* 29, 140–150. doi: 10.1016/j.dcn.2016.12.005

Osório, J.M.A., Rodríguez-Herreros, B., Richetin, S., Junod, V., Romascano, D., Pittet, V., et al. (2021). Sex differences in sensory processing in children with autism spectrum disorder. *Autism Res.* 14, 2412–2423. doi: 10.1002/aur.2580

Parenti, I., Rabaneda, L. G., Schoen, H., and Novarino, G. (2021). Neurodevelopmental disorders: from genetics to functional pathways. *Trends Neurosci.* 43, 608–621. doi: 10.1016/j.tins.2020.05.004

Pedregosa, P., Varoquaux, G., Gramfort, A., Michel, V., Thirion, B., Grisel, O., et al. (2011). Scikit-learn: machine learning in Python. *J. Mach. Learn. Res.* 12, 2825–2830. Available online at: https://www.jmlr.org/papers/volume12/pedregosa11a/pedregosa11a.pdf

Piccardi, E. S., Begum, A. J., Jonesm, E. J. H., Mason, L., Charman, T., Johnson, M. H., et al. (2021). Behavioural and neural markers of tactile sensory processing in infants at elevated likelihood of autism spectrum disorder and/or attention deficit hyperactivity disorder. *J. Neurodev. Disord.* 13, 1. doi: 10.1186/s11689-020-09334-1

Puts, N. A., Wodka, E. L., Tommerdahl, M., Mostofsky, S. H., and Edden, R. A. (2014). Impaired tactile processing in children with autism spectrum disorder. *J. Neurophysiol.* 111, 1803–1811. doi: 10.1152/jn.00890.2013

Quinlan, R. J. (1992). "Learning with continuous classes," in *Proceeding Australian Journal Conference Artifical Intelligence* (Singapore: World Scientific), 343–348.

Rasmussen, C., and Williams, C. (2006). *Gaussian Processes for Machine Learning*. Cambridge, MA: MIT Press. doi: 10.7551/mitpress/3206.001.0001

Ridgeway, G. (1999). The state of boosting. *Comp. Sci. Stat.* 31, 172–181.

Rutter, M., Le Couteur, A., and Lord, C. (2006). *ADI-R: Entrevista Para el Diagnóstico del Autismo-Revisada*. Madrid: TEA Editions.

Tavassoli, T., Bellesheim, K., Tommerdahl, M., Holden, J. M., Kolevzon, A., and Buxbaum, J. D. (2016). Altered tactile processing in children with autism spectrum disorder. *Autism Res.* 9, 616–620. doi: 10.1002/aur.1563

Thabtah, T. (2019). Machine learning in autistic spectrum disorder behavioral research: a review and ways forward. *Inform. Health Soc. Care* 44, 278–297. doi: 10.1080/17538157.2017.1399132

The R Team (2022). *The R Project for Statistical Computing*. The R Team. Available online at: http://www.r-project.org (accessed March 3, 2022).

Thye, M. D., Bednarz, H. M., Herringshaw, A. J., Sartin, E. B., and Kana, R. K. (2018). The impact of atypical sensory processing on social impairments in autism spectrum disorder. *Dev. Cogn. Neurosci.* 29, 151–167. doi: 10.1016/j.dcn.2017.04.010

Tomcheck, S. D., and Dunn, W. (2007). Sensory processing in children with and without autism: a comparative study using the short sensory profile. *Am. J. Occup. Ther.* 61, 190–200. doi: 10.5014/ajot.61.2.190

Tseng, M. H., Fu, C. P., Cermak, S., Lu, L., and Shieh, J. Y. (2011). Emotional and behavioral problems in preschool children with autism: relationship with sensory processing dysfunction. *Res. Autism Spect. Dis.* 5, 1441–1450. doi: 10.1016/j.rasd.2011.02.004

Uljarević, M., Lane, A., Kelly, A., and Leekam, S. (2016). Sensory subtypes and anxiety in older children and adolescents with autism spectrum disorder. *Autism Res.* 9, 1073–1078. doi: 10.1002/aur.1602

Unitat d'Epidemiologia i de Diagnòstic en Psicopatologia del Desenvolupament (2016). *Norms of Achenbach's CBCL6-18 Forms in Spanish population*. Available onlineat: http://www.ued.uab.es (accessed March 3, 2022).

Wang, Z. (2011). HingeBoost: ROC-based boost for classification and variable selection. *Int. J. Biostat.* 7, 1–30. doi: 10.2202/1557-4679.1304

Zachor, D. A., and Curatolo, P. (2014). Participants of Italian-Israeli consensus conference. Recommendations for early diagnosis and intervention in autism spectrum disorders: an Italian-Israeli consensus conference. *Eur. J. Paediatr. Neurol.* 18, 107–118. doi: 10.1016/j.ejpn.2013.09.002

Conflict of Interest: The authors declare that the research was conducted in the absence of any commercial or financial relationships that could be construed as a potential conflict of interest.

Publisher's Note: All claims expressed in this article are solely those of the authors and do not necessarily represent those of their affiliated organizations, or those of the publisher, the editors and the reviewers. Any product that may be evaluated in this article, or claim that may be made by its manufacturer, is not guaranteed or endorsed by the publisher.

Copyright © 2022 Alateyat, Cruz, Cernadas, Tubío-Fungueiriño, Sampaio, González-Villar, Carracedo, Fernández-Delgado and Fernández-Prieto. This is an open-access article distributed under the terms of the Creative Commons Attribution License (CC BY). The use, distribution or reproduction in other forums is permitted, provided the original author(s) and the copyright owner(s) are credited and that the original publication in this journal is cited, in accordance with accepted academic practice. No use, distribution or reproduction is permitted which does not comply with these terms.

frontiers | Frontiers in Molecular Neuroscience

ORIGINAL RESEARCH
published: 23 June 2022
doi: 10.3389/fnmol.2022.912671

Impaired Neurodevelopmental Genes in Slovenian Autistic Children Elucidate the Comorbidity of Autism With Other Developmental Disorders

Danijela Krgovic[1,2], Mario Gorenjak[3], Nika Rihar[4], Iva Opalic[1], Spela Stangler Herodez[1,2], Hojka Gregoric Kumperscak[5], Peter Dovc[4] and Nadja Kokalj Vokac[1,2]*

[1] Laboratory of Medical Genetics, University Medical Centre Maribor, Maribor, Slovenia, [2] Department of Molecular Biology, Faculty of Medicine, University of Maribor, Maribor, Slovenia, [3] Centre for Human Molecular Genetics, and Pharmacogenomics, Faculty of Medicine, University of Maribor, Maribor, Slovenia, [4] Department of Animal Science, Biotechnical Faculty, University of Ljubljana, Ljubljana, Slovenia, [5] Department of Pediatrics, University Medical Centre Maribor, Maribor, Slovenia

OPEN ACCESS

Edited by:
Salam Salloum-Asfar, Qatar Biomedical Research Institute, Qatar

Reviewed by:
María Eugenia De La Morena-Barrio, University of Murcia, Spain
Branko Aleksic, Nagoya University, Japan

***Correspondence:**
Danijela Krgovic
danijela.krgovic1@um.si

Specialty section:
This article was submitted to Neuroplasticity and Development, a section of the journal Frontiers in Molecular Neuroscience

Received: *04 April 2022*
Accepted: *11 May 2022*
Published: *23 June 2022*

Citation:
Krgovic D, Gorenjak M, Rihar N, Opalic I, Stangler Herodez S, Gregoric Kumperscak H, Dovc P and Kokalj Vokac N (2022) Impaired Neurodevelopmental Genes in Slovenian Autistic Children Elucidate the Comorbidity of Autism With Other Developmental Disorders. Front. Mol. Neurosci. 15:912671. doi: 10.3389/fnmol.2022.912671

Autism spectrum disorders (ASD) represent a phenotypically heterogeneous group of patients that strongly intertwine with other neurodevelopmental disorders (NDDs), with genetics playing a significant role in their etiology. Whole exome sequencing (WES) has become predominant in molecular diagnostics for ASD by considerably increasing the diagnostic yield. However, the proportion of undiagnosed patients still remains high due to complex clinical presentation, reduced penetrance, and lack of segregation analysis or clinical information. Thus, reverse phenotyping, where we first identified a possible genetic cause and then determine its clinical relevance, has been shown to be a more efficient approach. WES was performed on 147 Slovenian pediatric patients with suspected ASD. Data analysis was focused on identifying ultrarare or "single event" variants in ASD-associated genes and further expanded to NDD-associated genes. Protein function and gene prioritization were performed on detected clinically relevant variants to determine their role in ASD etiology and phenotype. Reverse phenotyping revealed a pathogenic or likely pathogenic variant in ASD-associated genes in 20.4% of patients, with subsequent segregation analysis indicating that 14 were *de novo* variants and 1 was presumed compound heterozygous. The diagnostic yield was further increased by 2.7% by the analysis of ultrarare or "single event" variants in all NDD-associated genes. Protein function analysis established that genes in which variants of unknown significance (VUS) were detected were predominantly the cause of intellectual disability (ID), and in most cases, features of ASD as well. Using such an approach, variants in rarely described ASD-associated genes, such as *SIN3B*, *NR4A2*, and *GRIA1*, were detected. By expanding the analysis to include functionally similar NDD genes, variants in *KCNK9*, *GNE*, and other genes were identified. These would probably have been missed by classic genotype–phenotype analysis. Our study thus demonstrates that in patients with ASD, analysis of ultrarare or "single event" variants obtained using

WES with the inclusion of functionally similar genes and reverse phenotyping obtained a higher diagnostic yield despite limited clinical data. The present study also demonstrates that most of the causative genes in our cohort were involved in the syndromic form of ASD and confirms their comorbidity with other developmental disorders.

Keywords: reverse phenotyping, single event variants, NDD-associated genes, *GRIA1* gene, *NR4A2* gene, *SIN3B* gene

INTRODUCTION

Autism spectrum disorders (ASD) combine phenotypically heterogeneous groups that often co-occur with other neurodevelopmental disorders (NDDs) (Arteche-López et al., 2021). Clinically, two main features must be met for the diagnosis of ASD; the patient must present with difficulties in each of the three social communication subdomains and two of the four different restricted, repetitive sensory–motor behaviors in the past or present for both features (Lord et al., 2018). Variations in phenotype and their severity indicate that genetics and environmental factors are key players in the etiology of ASD (Rylaarsdam and Guemez-Gamboa, 2019). The size of genetic variants and mutation types vary from large chromosomal aberrations to single nucleotide variants (SNVs). They may also be rare or common risk variants (Balicza et al., 2019). Current guidelines for the detection of copy number variants (CNVs) with chromosomal microarray (CMA) in patients with NDDs, including ASD, as first-tier tests are still valid, although they were published over a decade ago (Miller et al., 2010).

Implementing next-generation sequencing (NGS) methods in the molecular diagnosis of NDDs has considerably increased the diagnostic yield (Lindstrand et al., 2019; Arteche-López et al., 2021). Whole exome sequencing (WES) enables the detection of rare or common small deletions, duplications, indels, synonymous, nonsense, splice, 3′-UTR, and missense or frameshift variants in the coding regions of the genome. The use of WES analysis in conjunction with CNV analysis enables a molecular diagnosis to be made in about 30% of patients with ASD and intellectual disability (ID) (Valentino et al., 2021). NGS methods have also enabled us to pinpoint genes implicated in ASD phenotypes (Bernier et al., 2014; Satterstrom et al., 2020). Trio-based WES analysis has proven to be successful in identifying rare inherited and *de novo* variants in genes involved in the etiology of ASD and novel ASD-associated genes (Satterstrom et al., 2020; Lintas et al., 2021). However, the inability to determine the origin of the suspected variant, reduced penetrance, broad clinical characterization of patients with ASD, or lack of clinical information aggravates the process of making proper genotype–phenotype correlations. Therefore, in these cases, it makes sense to reverse the diagnostic process by looking for ultrarare variants in the ASD-associated genes in the same group of patients and only then defining their clinical significance. This approach reduces the probability of an inaccurate analysis due to a highly heterogeneous phenotype or limited descriptions of patients by using simple algorithms. Following this approach, variants in rarely described ASD-associated genes, such as the *SIN3B*, *NR4A2*, and *GRIA1*, were detected, and a broad clinical phenotype combining ID and neurodevelopmental abnormalities, including ASD, was described in these patients (Geisheker et al., 2017; Lévy et al., 2018; Latypova et al., 2021). More importantly, the diagnostic yield was further increased using this type of analysis for potential causative variants in genes involved in other NDDs (the *KCNK9* and *GNE* genes). These genes were not linked to ASD according to ASD-associated genes listed in the Simons Foundation Autism Research Initiative (SFARI) database[1] (Graham, Zadeh et al., 2016; Yang et al., 2020). Variants of unknown significance (VUS) also represent a challenging category for clinical interpretation. Therefore, for genes with VUS, variant protein function predictions and gene prioritizations were performed to identify causative genes outside of the ASD-associated pool of genes.

The present study further endorses the comorbidity of ASD and NDDs, indicating that genetic analysis should not be limited only to the wide range of ASD-associated genes. We also demonstrated how phenotype-driven analysis is not always the optimal approach, especially in cases with limited clinical data. The present study also demonstrates how the usage of the obtained genetic data in combination with simple step algorithms and bioinformatics could increase the yield of molecular diagnostics for patients with ASD.

MATERIALS AND METHODS

Patient Enrollment

Patients with ASD from a large cohort of 439 Slovenian children with NDD were included (Krgovic et al., 2018). In this study, patients with ASD and their parents were re-invited to participate in the WES study. Written informed consent from their parents or legal guardians was obtained for all probands included in our cohort. This study is part of a larger study that was approved by the Commission of the Republic of Slovenia for Medical Ethics (KME No. 89/01/11). All experimental procedures were performed according to guidelines and regulations and abided by the tenets of the Declaration of Helsinki.

Patients

A WES analysis was carried out on DNA samples from 147 pediatric patients with a suspected diagnosis of ASD. The patient

[1] https://gene.sfari.org/tools/

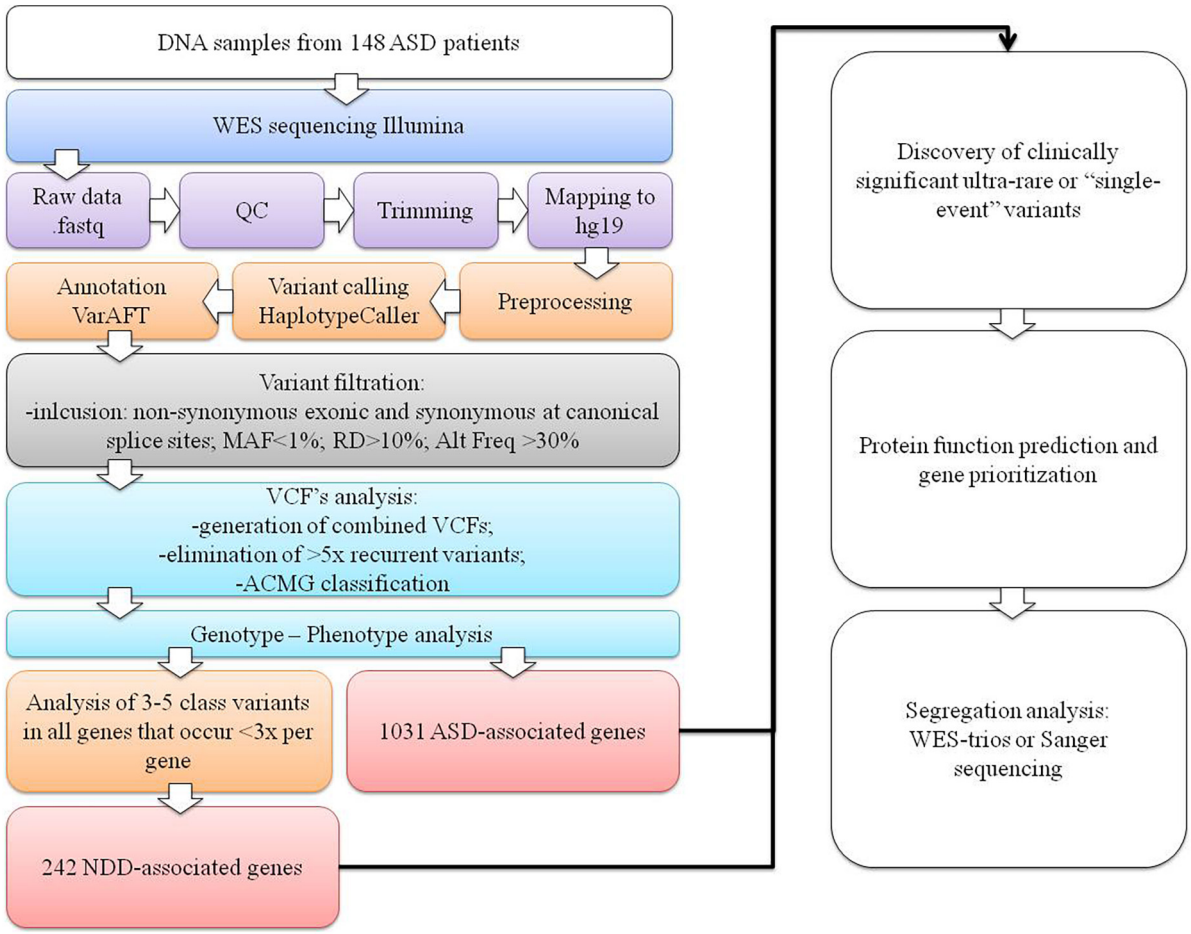

FIGURE 1 | The WES data variant analysis step-by-step workflow used in our cohort. The first section represents the NGS pipeline for generating VCF files. In the second section, variant filtering, identifying ultrarare or "single event" variants process, and data interpretation are presented.

TABLE 1 | Diagnostic yield obtained by WES in 147 patients with suspected ASD.

	1,031 ASD-associated genes		**242 NDD-associated genes**	
	LP/P	**VUS**	**LP/P**	**VUS**
No. of ASD patients	**30/147 (20.4%)**	**9/147 (6.1%)**	**4/147 (2.7%)**	**(6/147) 4.1%**
No. of patients with more than one variant	3		1	
No. of variants detected	31	12	4	6
Inheritance				
De novo	15*	1	1	/
Maternal	2*	/	1	1
Paternal	/	/	/	2
Not tested	13	10	1	3
Excluded from one parent	1	1	1	/

**One de novo and maternally inherited variant found in the same gene in a presumed compound heterozygous state.LP, likely pathogenic variant; P, pathogenic variant; VUS, variant of unknown significance.*

group consisted of 110 boys (74.8%) and 37 girls (25.2%) with a mean age of 8.2 ± 0.935 years (±SD) at molecular diagnostic referral. The main referral diagnosis was suspected ASD, usually with coexistent ID, development delay (DD), language impairment, attention deficit hyperactivity disorder (ADHD), and other disorders. The test group included 10 pairs of siblings, of which 2 sets were twins, and 2 families had more than 2 affected children.

Whole Exome Sequencing

Whole exome sequencing was performed on patients and, in some cases, their parents using DNA extracted from peripheral blood leukocytes with the QIAamp® DNA Blood Midi Kit (QIAGEN, Hilden, Germany). WES and library construction were performed by Novogene (Novogene Company Limited, Cambridge, United Kingdom) using the Agilent SureSelect Human All Exon Kit (Agilent Technologies, Santa Clara, CA, United States). The DNA libraries were then sequenced on an Illumina HiSeq 4000 platform (150-bp paired-end reads) (Illumina, San Diego, CA, United States) with an average depth coverage of 100× with an average 12 Gb output per sample.

Analysis Algorithm

Raw fastq reads were first assessed for quality control using FastQC v0.11.9 software (Wingett and Andrews, 2018). The Trimmomatic tool v0.39 was used to trim technical sequences and adapters from raw sequences (Bolger et al., 2014). The Burrows-Wheeler Aligner BWA v0.7.12-r1039 with the MEM algorithm was used for mapping the raw reads to the human reference genome (GRCh37/hg19) (Li and Durbin, 2010). PCR duplicates' marking and mate information fixation were performed using PicardTools v2.20.1. Base quality scores were additionally recalibrated using the genome analysis toolkit (GATK) v4.0 (McKenna et al., 2010; DePristo et al., 2011; Van der Auwera et al., 2013). Variant calling was performed using the HaplotypeCaller algorithm in genomic mode with joint calling (Poplin et al., 2018). Variant quality score recalibration using a GATK-implemented adaptive error model, a machine learning method with known genomic sites, was also used to establish a method for enabling variant filtering based on the fine balance between sensitivity and specificity for true or false genetic variants. Normalization with left trimming was also performed using GATK to obtain the final unfiltered VCF files. Variant annotation was performed using the VarAFT tool v2.17-2 (Desvignes et al., 2018). Machine learning algorithms using conservation profiles, such as SIFT and PolyPhen-2 conservation profiles, were used for the prediction of consequences of missense mutations (Kumar et al., 2009; Adzhubei et al., 2010, 2013). Subsequently, stepwise variant filtering was performed for variants with a read-depth coverage of >10× and an altered variant frequency of at least 30%. Variants with a frequency of more than 1% in the population variant databases [1,000 genome projects, Exome Aggregation Consortium (ExAC), and Exome Variant Server (EVS)] were excluded. Intergenic or 3′-UTR/5′-UTR untranslated region variants and non-splice–related intronic and synonymous variants were also filtered out, except for those located at canonical splice sites (**Figure 1**).

Variant Filtering and Classification

Filtered VCF files for all 147 patients were combined, generating a catalog of 39,668 variants (on average, 268 variants per patient), which were sorted by their canonical transcript and genomic position. All the recurrent variants that were present more than five times were eliminated as they were presumed to be sequence artifacts. We then obtained only ultrarare variants or "single event" variants that occurred only once per gene. Variants were then classified based on standards and guidelines of the American College of Medical Genetics and Genomics (ACMG) as pathogenic (class 5), likely pathogenic (class 4), variants of uncertain clinical significance (VUS) (class 3), likely benign (class 2), and benign (class 1) using the Franklin[2] tool (Richards et al., 2015). For all variants classified as possible causative (classes 3–5) in 1,031 genes listed in the SFARI database (SFARI-Gene_genes_01-11-2022release_03-23-2022export) (**Supplementary Table 1**), genotype–phenotype analysis was performed based on the clinical description of patients and a literature search. If parents' samples were available, segregation analysis with WES-trio for VUS or Sanger sequencing for likely pathogenic or pathogenic variants was carried out.

The analysis was further expanded for all class 3–5 variants in all genes, with the limitation that no more than three variants emerged per gene. This facilitated detection of the rare or "single event" variants in the gene that was more likely to be causal and reduced the scope of the analysis. For these genes, a subsequent extensive literature search was performed to determine whether the gene could be associated with NDDs, resulting in the inclusion of an additional 242 NDD-associated genes (**Supplementary Table 1**) in the genotype–phenotype analysis. The diagram of our analysis is presented in **Figure 1**.

Segregation Analysis

Segregation of the potential variant was performed in 32 trio-based WES analyses, 10 family WES analyses (siblings and parents), and Sanger sequencing in 14 families when pathogenic/likely pathogenic variants in ASD-associated genes were detected. All variants detected by WES analysis were then confirmed by Sanger sequencing using the Beckman Coulter CEQ 8000 Genetic Analysis System (Beckman Coulter Inc., Indianapolis, IN, United States).

Protein Function Predictions and Gene Prioritizations

The STRING[3] tool was used for generating functionally similar genes based on genomic and proteomic data for the detected pathogenic, likely pathogenic, and VUS variants (**Table 2**; Szklarczyk et al., 2019). The genes were clustered with *k*-means clustering into four groups to identify possible correlations in the same biological pathways and/or involvement in specific phenotypes (diseases).

The same set of genes was also used in enrichment and Gene Ontology (GO) analysis, employing the g:Profiler[4] tool to

[2]https://franklin.genoox.com/clinical-db/home

[3]https://string-db.org/

[4]https://biit.cs.ut.ee/gprofiler/gost

determine which Human Phenotype Ontology (HP) terms are most frequently linked with the analyzed genes, particularly for genes with VUS variants that are not listed in the SFARI database (Raudvere et al., 2019).

RESULTS

Whole Exome Sequencing and Segregation Analysis

With WES analysis focusing on ultrarare variants in 1,031 ASD-associated genes, we were able to identify pathogenic or likely pathogenic variants, 14 of which were *de novo*, in 20.4% (N 30/147) of patients. In two patients, two variants were identified. One of these patients was presumed to be compound heterozygous with *de novo* and maternally inherited variants, while the other patient had a likely pathogenic and a VUS variant in two different genes. One patient has a maternally inherited variant that was also present in the younger brother with phenotype consistency. In one patient, a variant was excluded in the mother but not in the father. Segregation was not tested in 13 patients as parental samples were not available for further analysis. One of these 13 patients was the carrier of both the likely pathogenic and VUS variants in 2 different genes. The diagnostic yield was further increased by 2.7% (N 4/147) by adding the analysis of ultrarare variants detected in an additional 242 NDDs genes not listed in the SFARI database (**Supplementary Table 1**). Of these genes, one variant was *de novo*, one was maternally inherited, one variant was not from the mother, and segregation was not analyzed in one variant. The overall diagnostic yield was estimated to be 23.1% (N 34/147). VUS variants were detected in 10.2% (N 15/147) of patients, of which 4.1% (N 6/147) were detected by adding additional NDDs gene analysis. In 11 patients with VUS variants in all genes together, segregation was not tested, 1 was maternally and 2 were paternally inherited. In one patient, inheritance was excluded from the mother but not from the father, and one had a *de novo* variant. Our results are summarized in **Table 1**. Patient characteristics and identified pathogenic, likely pathogenic, and VUS variants are listed in **Table 2**.

The occurrence of variants per gene for clinically significant variants analyzed in this cohort is presented in **Figure 2**. From the chart in the figure, it can be seen that in 18 out of 42 genes, the variant occurred as a "single event" (meaning we detected 1 variant per gene in all patients combined). Benign and likely benign variants were detected in the *ABCA13*, *DNMT3A*, *KMT2C*, and *TRIP12* genes. In the other genes, only ACMG class 3–5 variants were found.

Protein Function Predictions and Gene Prioritizations

Functional enrichment analysis of 42 genes showed that they were predominantly involved in the development of the nervous system with a *p*-value of 4.16e−06 (N 22/42). Genes can be ranked into three major groups according to their molecular function. The first group consists of chromatin-binding proteins (GO:0003682): ACTL6B, ADNP, CHD8, DNMT3A, KDM5A, KDM6B, MECP2, SIN3B, and STAG1. The second group consists of proteins with gate channel activity: GRIA1, GRIA4, GRIN2A, KCNK9, KCNQ2, KCNQ5, and SCN8A. The third group consists of proteins that share transcriptional regulatory function (GO:0140110) with ADNP, ACTL6B, KDM5A, MECP2, and SIN3B proteins, and they include DYRK1A, FOXP2, KMT2C, LZTR1, NR4A2, RAI1, and TBL1XR1. Other proteins are involved in processes, such as transmembrane transporter activity (GO:0022857) (ABCA13, MAGT1, and SLC2A1) and regulation of molecular functions (GO:0098772) (IQSEC2, PPP2R5D, RPS6KA3, and SOS2).

Disease-gene associations showed that 28 out of 42 genes analyzed were involved in mental health diseases (*p*-value of 4.97e−27), of which 22 genes were also linked to ID (*p*-value of 8.58e−23). Only four of these genes (*ADNP*, *CHD8*, *DYRK1A*, and *MECP2*) were linked to ASD (*p*-value of 7.9e−4). Clustering 42 genes using the STRING tool generated 4 gene clusters that were colored red (15 genes), yellow (11 genes), blue (8 genes), and green (8 genes). The largest red cluster consisted of three Noonan-causing genes *KRAS*, *LZTR1*, and *SOS2* (Johnston et al., 2018). The *KRAS* gene interacted with other genes in this node, as well as the shared ID in disease-gene association with six other genes (colored red in the isolated figure form). The yellow-colored node encompassed the three Rett syndrome-causing genes *MECP2*, *GRIN2A*, and *TBL1XR1* (colored red in **Figure 3A**), but mutations in other genes in this node were also involved in a Rett-like phenotype (Wang et al., 2019). The blue-colored node consists of the ASD-associated genes *ADNP*, *CHD8*, and *DYRK1A* (colored green in **Figure 3C**), but the majority of genes in this node are predominantly linked to ID (colored blue in **Figure 3C**). Functional enrichment analysis in this node also showed that five of the eight proteins (ACTL6B, ANDP, CHD8, KDM5A, and KDM6B) were chromatin binding (GO:0003682) (*p*-value of 3.6e−3). The green-colored node consists of eight genes, six of which code for proteins involved in transmembrane transporter activity (GO:0022857) (*p*-value of 3.6e−3) and were also linked to ID (colored red in the isolated figure form) with the exception of the *ABCA13* gene.

All four gene groups are presented in the center of **Figure 3**. Disease-gene associations are labeled for each group separately in **Figures 3A–D**.

On the contrary, using the g:Profiler tool for the same set of genes, it was clearly shown that ASD under HP:0000729 (purple bubble 2 in **Figure 4**) is the main feature (*p*-value of 2.457e−10) linked to the analyzed set of genes. Features, such as delayed speech and language, language impairment, global DD, neurodevelopmental delay, ID, and hyperactivity, and also the features observed in our patients, were significantly found less frequently than ASD (purple bubbles 3–8 in **Figure 4**). As observed in the STRING analysis, the GO biological process analysis showed that

TABLE 2 | Description of patients clinical characteristics for molecular diagnostic referral and identified as pathogenic, likely pathogenic, and VUS variants in the genes.

Patient ID	Sex	Age at referral (years)	Clinical indication for referral	Gene	HGVS nomenclature	Protein change	Zygosity/ origin	ACMG classification	OMIM and/or literature	DECIPHER[1] ID/HGDM[2] identifier
025244	F	14	Asperger syndrome, ADHD, OCD, psychiatric problems	*ABCA13*	NM_152701.5:c.8953dup	p.(Gln2985ProfsTer4)	het/NA	LP	Chen et al., 2017	480974/NA
033532	M	4	ASD, ID	*ACTL6B*	NM_016188.5:c.694C > A	p.(Pro232Thr)	het/NA	VUS	Bell et al., 2019	480976/NA
021055	M	10	ASD, ID	*ADNP*	NM_015339.4:c.2188C > T	p.(Arg730Ter)	het/*dn*	P	Arnett et al., 2018	480982/CM166963
027819	M	15	Suspected ASD, mild ID, ADHD, aggressive behavior, absent speech, bilateral hearing impairment, long face with prominent ears, micrognathia	*ADNP*	NM_015339.4:c.3071_3072del	p.(Glu1024AlafsTer7)	het/NA	LP	Arnett et al., 2018	480984/NA
020213	F	14	ASD, gross DD, ID, microcephaly, absent speech, low-set ears	*ADNP*	NM_015339.4:c.2496_2499del	p.(Asn832LysfsTer81)	het/*dn*	P	Arnett et al., 2018	480985/CD144180
035442	F	19	ASD, ID, aggressive, speech delay	*CAMK2B*	NM_001220.5:c.328G > A	p.(Glu110Lys)	het/NA	LP	Rizzi et al., 2020	480986/CM1716240
045750	F	2	ASD, DD, microcephaly	*CHD8*	NM_001170629.2:c.7181A > G	p.(Lys2394Arg)	het/NA	VUS	Du et al., 2018	480987/NA
041619	M	5	ASD, DD, speech delay, ADHD	*CSNK1E*	NM_001894.4:c.188-1G > T	p.?	het/NA	LP	Chen et al., 2019	480989/NA
046526	M	4	ASD, ID, ADHD	*CYFIP2**	NM_001037333.3:c.40G > A	p.(Val14Met)	het/NA	VUS	Begemann et al., 2021	480992/NA
040054	M	15	ASD, ID, disproportionate tall stature, arachnodactyly, downward slanting palpebral fissures, EEG abnormality, poor fine motor coordination, delayed speech and language development, OCD, dental crowding, flat face, kyphoscoliosis, joint hypermobility, increased arm span, abnormality of the sternum	*DNMT3A*	NM_175629.2:c.1969G > A	p.(Val657Met)	het/not inh mat and not present in healthy sister	VUS	Tatton-Brown et al., 2018	480994/NA
025324	M	8	ASD, ADHD, mild ID, speech delay	*DLG2*	NM_001142699.1:c.285A > G	p.(Gln95Gln)[a]	het/*dn*	VUS	Ruzzo et al., 2019	480996/NA

(Continued)

TABLE 2 | (Continued)

Patient ID	Sex	Age at referral (years)	Clinical indication for referral	Gene	HGVS nomenclature	Protein change	Zygosity/ origin	ACMG classification	OMIM and/or literature	DECIPHER[1] ID/HGDM[2] identifier
016930	F	7	ASD, ID/DD, microcephaly, hypotonia, epilepsy	*DYRK1A*	NM_001396.4:c.1316del	p.(Ala439ValfsTer12)	het/*dn*	P	Earl et al., 2017	480999/NA
047559	M	6	ASD, DD, speech delay, brachycephaly, twin brothers	*FGFR2**	NM_022970.3:c.1069G > T	p.(Val357Phe)	het/pat	VUS	Azoury et al., 2017; Szczurkowska et al., 2018	481000/NA
047560	M	6		*FGFR2**	NM_022970.3:c.1069G > T	p.(Val357Phe)	het/pat	VUS		481002/NA
024441	M	7	ASD, ID, psychosis	*FOXP2*	NM_148898.4:c.1674G > A	p.(Trp558Ter)	het/NA	LP	Trelles et al., 2021	481004/NA
039934	F	4	ASD, absent speech, poor eye contact, poor social contact	*FBXO11*	NM_001190274.1: c.1112G > T	p.(Ser371Ile)	het/NA	VUS	Jansen et al., 2019; Gregor et al., 2022	481005/NA/NA
				HECW2	NM_020760.3:c.4436G > A	p.(Arg1479Gln)	het/NA	LP	Ullman et al., 2018	
041707	M	6	ASD, DD, poor/absent speech	*HECW2*	NM_020760.3:c.4294-1G > T	p.?	het/NA	LP	Ullman et al., 2018	481007/NA
035247	M	5	ASD, DD	*GNE**	NM_001128227.2: c.1287dup	p.(Asp430ArgfsTer3)	het/NA	LP	Yang et al., 2020	481008/NA
045124	F	5	ASD, ID, global DD, delayed speech and language development	*GRIA1*	NM_001258021.1: c.1526G > A	p.(Arg509Gln)	het/*dn*	LP	Geisheker et al., 2017	481010/NA
045232	M	10	Suspected ASD, ADHD, mild ID [b]Younger brother with similar problems – not tested for variant in the *GRIA4* gene	*GRIA4**	NM_000829.4:c.627T > G	p.(Phe209Leu)	het/NA	VUS	Martin et al., 2017	481011/NA
046940	M	4	ASD	*GRIA4**	NM_000829.4:c.1064A > C	p.(Gln355Pro)	het/NA	VUS	Martin et al., 2017	481013/NA
018325	M	11	ASD, DD	*GRIN2A*	NM_000833.4:c.982G > T	p.(Glu328Ter)	het/NA	LP	Strehlow et al., 2019	481017/NA
016906	M	6	ASD, ID/DD, ADHD	*GRIN2A*	NM_000833.5:c.4204C > T NM_000833.5:c.2329C > G	p.(Arg1402Trp) p.(Leu777Val)	het/NA het/NA	VUS VUS	Strehlow et al., 2019	481018/NA/NA
027448	M	19	ASD, generalized-onset seizure, developmental regression, feeding difficulties, absent speech, poor fine motor coordination, progressive inability to walk, thoracolumbar scoliosis	*IQSEC2*	NM_001111125.3:c.2563C > T	p.(Arg855Ter)	hemy/*dn*	P	Lopergolo et al., 2021	481019/CM129316

(Continued)

TABLE 2 | (Continued)

Patient ID	Sex	Age at referral (years)	Clinical indication for referral	Gene	HGVS nomenclature	Protein change	Zygosity/ origin	ACMG classification	OMIM and/or literature	DECIPHER[1] ID/HGDM[2] identifier
019020	M	9	Autistic behavior, ID, long face, cleft palate, strabismus [b]Younger brother with ADHD but without *KCNK9* mutation	*KCNK9**	NM_001282534.2:c.392G > A	p.(Arg131His)	het/*dn*	LP	Graham, Zadeh et al., 2016	481021/NA
019450	M	13	ASD, epilepsy	*KCNQ2*	NM_172107.4:c.1997C > T	p.(Pro666Leu)	het/NA	VUS	van der Werf et al., 2020	481022/NA
037249	M	7	Asperger syndrome, ADHD, epilepsy	*KCNQ5*	NM_001160133.2:c.911G > C	p.(Trp304Ser)	het/NA	VUS	Lehman et al., 2017	481023/NA
033739	M	5	ASD, DD	*KDM5A*	NM_001042603.2:c.953A > G	p.(Tyr318Cys)	het/NA	VUS	El Hayek et al., 2020	481024/NA
040353	M	12	Autistic behavior, delayed speech and language development, stereotypical hand wringing, poor eye contact	*KDM6B*	NM_001080424.2:c.3196_3199dup	p.(Ala1067ValfsTer31)	het/*dn*	P	Stolerman et al., 2019	481025/NA
047960	M	5	Autistic behavior, ADHD, poor motor coordination, speech delay	*KMT2C*	NM_170606.3:c.11586_11587del	p.(Pro3863SerfsTer18)	het/NA	LP	Koemans et al., 2017	481026/NA
029613	M	3	Autistic behavior, abnormal aggressive, impulsive or violent behavior, neurodevelopmental delay	*LZTR1*	NM_006767.4:c.451G > A	p.(Asp151Asn)	het/*dn*	LP	Johnston et al., 2018	481035/NA/NA
				LZTR1	NM_006767.4:c.1672C > T	p.(Gln558Ter)	het/mat	LP		
037023	M	7	Autistic behavior, ID, global DD, language impairment, hypotonia, pain tolerance, sleep disturbance	*MAGT1**	NM_032121.5:c.527C > T	p.(Ala176Val)	hemy/mat	VUS	Blommaert et al., 2019	481036/NA
033763	F	12	Autistic behavior, ID/DD, delayed gross motor development, abnormal emotion/affect behavior, childhood stereotypy	*MECP2*	NM_001110792.2:c.961C > T	p.(Arg321Trp)	het/*dn*	P	Liyanage and Rastegar, 2014	481037/NA

(Continued)

TABLE 2 | (Continued)

Patient ID	Sex	Age at referral (years)	Clinical indication for referral	Gene	HGVS nomenclature	Protein change	Zygosity/ origin	ACMG classification	OMIM and/or literature	DECIPHER[1] ID/HGDM[2] identifier
018653	F	12	ASD, ID	*NR4A2*	NM_006186.4:c.571C > T	p.(Gln191Ter)	het/*dn*	P	Lévy et al., 2018; Guo et al., 2019	481038/NA
027329	M	5	ASD, ID, delayed speech and language development, high pain tolerance [b]Younger brother: ASD, DD, absent speech, stereotypic movement – *NRXN3* mutation carrier [b]Mother with mild ID, delayed speech and language development in childhood	*NRXN3*	NM_004796.6:c.526C > T	p.(Arg176Ter)	het/mat	LP	Wang et al., 2018	481039/NA
022629	M	11	ASD, ID	*PPP2R5D*	NM_006245.4:c.592G > A	p.(Glu198Lys)	het/*dn*	P	Biswas et al., 2020	481040/CM153575
038924	F	11	ASD, ID	*PPP2R5D*	NM_006245.4:c.758G > A	p.(Arg253Gln)	het/NA	LP	Biswas et al., 2020	481041/NA
035820	F	12	ASD, ADHD, ID/DD, motor delay, delayed speech and language development, muscular hypotonia	*RAI1*	NM_030665.4:c.1854del	p.(Ile618MetfsTer201)	het/*dn*	P	Abad et al., 2018	481042/NA
036247	M	4	Autistic behavior, DD, epilepsy	*RPS6KA3*	NM_004586.3:c.1631A > G	p.(Asn544Ser)	hemy/NA	LP	Field et al., 2006	481046/NA
018960	F	12	Autistic behavior, global DD, absent speech	*SCN8A*	NM_014191.4:c.57del	p.(Glu20SerfsTer70)	het/not inh mat	LP	Butler et al., 2017	481048/NA
027720	M	3	ASD, DD	*SIN3B*	NM_015260.4:c.1843G > A	p.(Asp615Asn)	het/*dn*	LP	Latypova et al., 2021	481049/NA
034742	F	13	Autistic behavior, cognitive impairment, short attention span, motor delay, visual impairment, delayed speech and language development, poor fine motor coordination, prominent nasal tip, microcephaly, recurrent infections, lactose intolerance	*SLC2A1**	NM_006516.4:c.667C > T	p.(Arg223Trp)	het/not inh mat	P	López-Rivera et al., 2020; Mir et al., 2022	481051/CM101705

(Continued)

TABLE 2 | (Continued)

Patient ID	Sex	Age at referral (years)	Clinical indication for referral	Gene	HGVS nomenclature	Protein change	Zygosity/ origin	ACMG classification	OMIM and/or literature	DECIPHER[1] ID/HGDM[2] identifier
023509	F	7	ASD	*SOS2*	NM_006939.4:c.791C > A	p.(Thr264Lys)	het/*dn*	P	Yamamoto et al., 2015	481052/CM1511144
019146	F	6	ASD, ID	*STAG1*	NM_005862.3:c.2672A > C	p.(Lys891Thr)	het/NA	VUS	Lehalle et al., 2017	481053/NA
022940	M	4	ASD, twin brothers	*TBL1XR1*	NM_024665.7:c.303_304del	p.(Asp101GlufsTer43)	het/NA	LP	Quan et al., 2020	481054/NA
022941	M	4		*TBL1XR1*	NM_024665.7:c.303_304del	p.(Asp101GlufsTer43)	het/NA	LP		481055/NA
040139	M	5	ASD, DD, neonatal hypertonia, poor fine motor coordination, delayed speech and language development, umbilical hernia, atopic dermatitis, dental hypoplasia, abnormal palate morphology	*TBL1XR1*	NM_024665.7:c.1183T > C	p.(Tyr395His)	het/*dn*	P	Quan et al., 2020	481056/NA
040110	M	14	ASD, ADHD, hearing impairment, obesity, panhypopituitarism	*TM4SF20*	NM_024795.4:c.184-2A > T	p.?	het/not inh mat	VUS	Andres et al., 2021	481057/CS1826517/NA
				*KRAS**	NM_033360.4:c.401C > G	p.(Ala134Gly)	het/mat	LP	Roberts, 2001; Struja and Capraro, 2021	
011139	M	7	Autistic behavior, ADHD, ID, motor delay, delayed speech and language development	*TRIP12*	NM_004238.3:c.4813dup	p.(Val1605GlyfsTer17)	het/*dn*	P	Louie et al., 2020	481059/NA

[1] *https://www.deciphergenomics.org/.*
[2] *http://www.hgmd.cf.ac.uk/ac/index.php.*
[a] *Synonymous variant with potential altered splice effect.*
[b] *Observed positive family history.*
**NDD-associated genes not listed in the SFARI gene list.*
HGVS, Sequence Variant Nomenclature; het, heterozygous; hemy, hemizygous; NA, not available; dn, de novo; mat, maternal; pat, paternal; not inh mat, excluded in the mother; P, pathogenic; LP, likely pathogenic; VUS, variant of unknown significance.

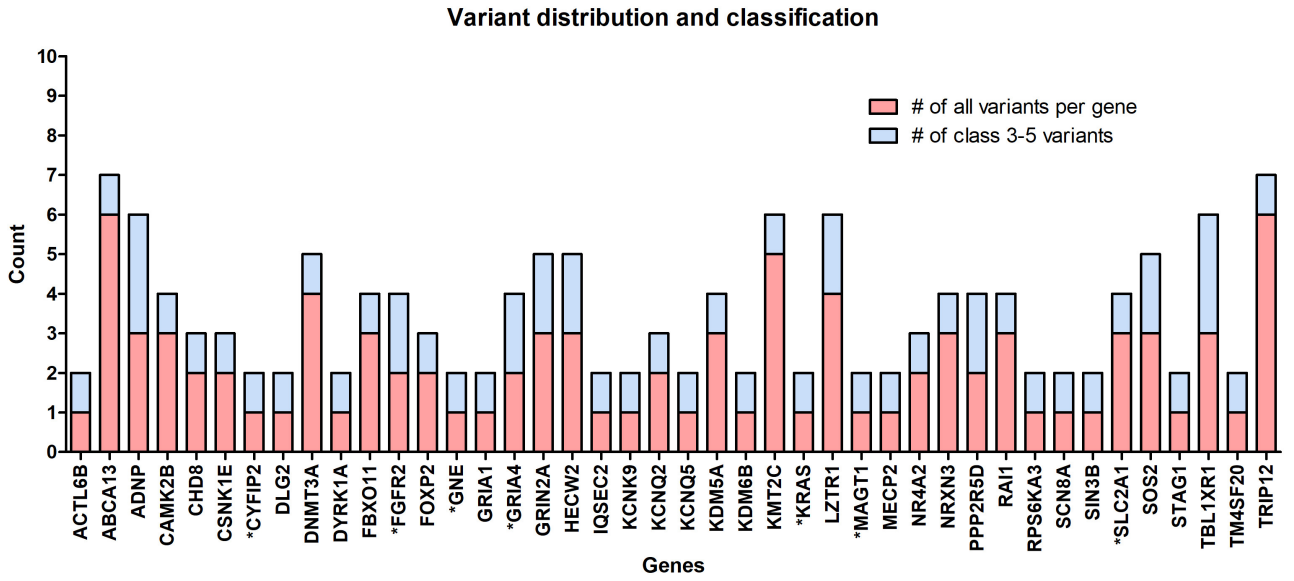

FIGURE 2 | The occurrence of all rare variants per gene (red) and the number of those classified as clinically significant variants (blue). In 18 out of 42 identified genes, 1 variant per gene occurred, the so-called "single event" variant. Genes marked with an asterisk (*) belong to the group of NDD-associated genes.

the analyzed genes were predominantly involved in the development of the nervous system (GO:0007399) (*p*-value of 1.878 × e−6). All the data from the g:Profiler analysis are available online.

DISCUSSION

The introduction of WES in the genetic diagnosis of ASD has significantly improved our knowledge of its etiology at the molecular level. The phenotype-driven analysis is often a limitation in the discovery of new disease-associated genes since the clinical presentation of patients with ASD is a key factor in genetic testing and data interpretation (Arteche-López et al., 2021; Lintas et al., 2021). The process of establishing an accurate diagnosis is further hindered by the lack of segregation analysis, reduced penetrance, limited data availability in the literature, as well as non-specific and limited clinical descriptions of patients. Therefore, reverse phenotyping and seeking the ultrarare variants in genes that are not only limited to ASD and then performing functional studies to obtain datasets should result in a higher diagnostic yield (Lintas et al., 2021).

In our study, a WES analysis was performed in 147 pediatric patients with suspected ASD. Genotype–phenotype analysis of 1,031 ASD-associated genes enabled the detection of pathogenic or likely pathogenic variants in 20.4% (N 30/147) of patients, of which almost half (N 14/30) were shown to be *de novo* in subsequent segregation analysis. The high incidence of *de novo* variants was expected in our study since it is estimated that *de novo* events contribute to autism in 30–39% of all patients with ASD (Yoon et al., 2021). In addition, one had a maternally inherited variant, and one patient was presumed to be a compound heterozygote, harboring one maternally inherited and one *de novo* variant. Adding 242 NDD-associated genes (**Supplementary Table 1**) to the genotype–phenotype analysis resulted in the detection of pathogenic/likely pathogenic variants in four more patients and increased the diagnostic yield to 23.1% (N 34/147). A VUS variant was detected in 10.2% (N 15/147) of patients. All the variants and patient clinical characteristics are listed in **Tables 1**, **2**.

Protein function predictions and gene prioritization analyses were performed for genes identified in our cohort to establish possible correlations between already known ASD-associated genes and those not listed in the SFARI database. The disease-gene associations analysis (**Figure 1**) shows that the majority of detected variants are associated with an ID phenotype, and thus we presumed that our patients mostly have a syndromic ASD since autistic behavior (HP:0000729) is strongly associated with all of the analyzed genes (**Figure 4**). According to the literature, ASD is comorbidity with ID in 32% of patients (Miot et al., 2019). Our disease-gene associations showed that 22 out of 42 genes analyzed were also linked to ID (*p*-value of 8.58e−23), whereas only 4 genes (*ADNP*, *CHD8*, *DYRK1A*, and *MECP2*) were linked to ASD (*p*-value of 7.9e−4). As expected, functional enrichment analysis confirmed that genes involved in the etiology of ASD were predominantly involved in the development of the nervous system, and mutations in these genes, in our cases, altered their transcriptional regulatory functions or transmembrane transporter activity, which are known molecular mechanisms in the etiology of ASD (Rylaarsdam and Guemez-Gamboa, 2019).

Functional enrichment analysis for genes not listed in the SFARI database also demonstrated their association with the already known ASD-associated genes. For example, based on their functional similarity, the *KRAS*, *SLC2A1*, and *FGFR2* genes were clustered in the red node. The *KRAS* gene, along with *LZTR1* and *SOS2*, is one of the three Noonan syndrome-causing

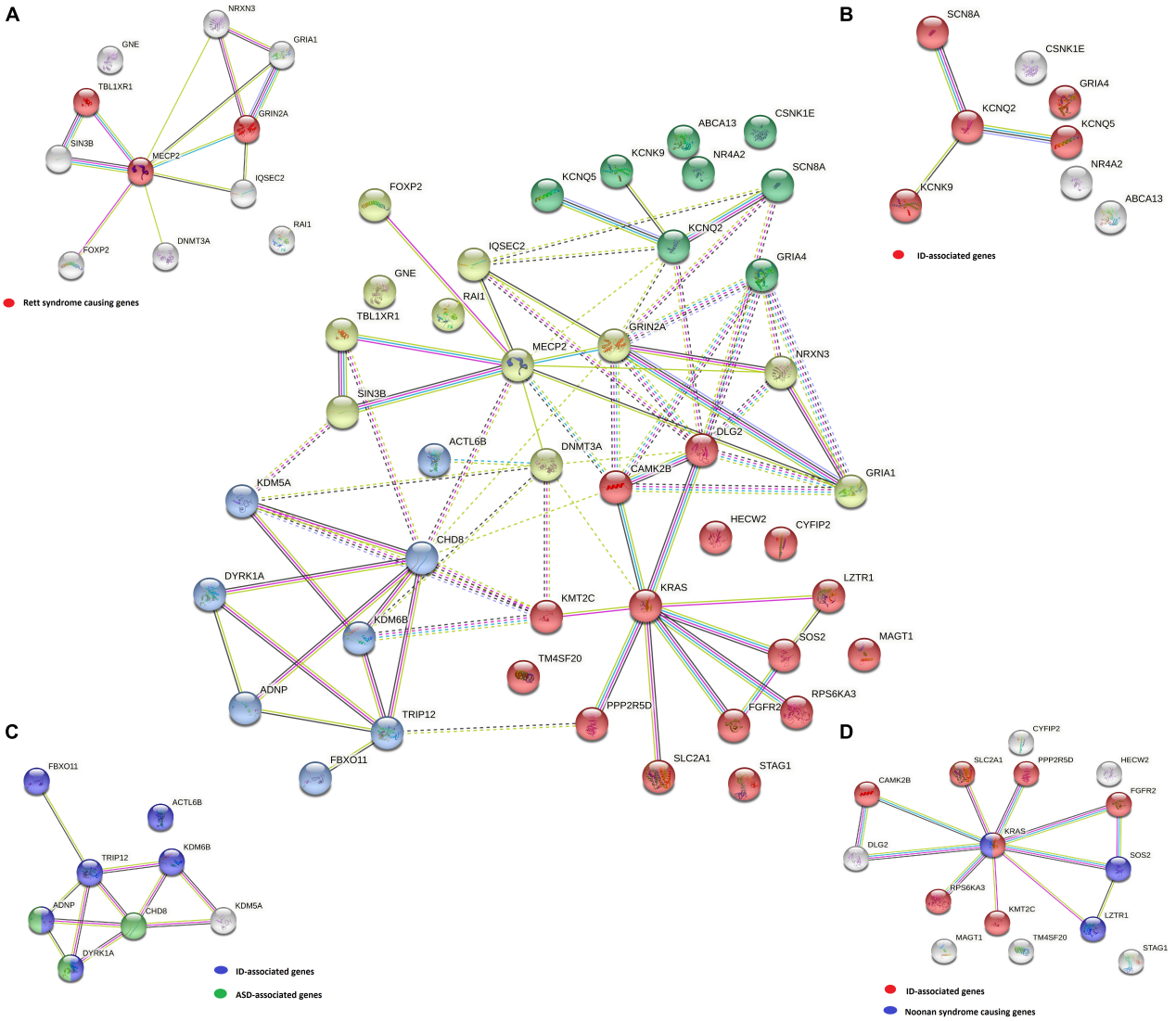

FIGURE 3 | A STRING *k*-means clustering classified the genes into four groups: yellow **(A)**, green **(B)**, blue **(C)**, and red **(D)** by possible correlation in the same biological pathways and/or involvement in specific phenotypes (diseases). For each group, specific disease-gene associations are marked on the isolated figure forms **(A–D)**.

genes in this group. They cause dysregulation of the RAS-MaPK signaling pathway (Tartaglia et al., 2011) and are also linked to ID (**Figure 3D**). The maternally inherited pathogenic variant in the *KRAS* gene explains the panhypopituitarism observed in our patient (Patient 040110) (Struja and Capraro, 2021). Although the *KRAS* gene is not linked to ASD, ASD was observed in Patient 040110, presumed compound heterozygous variants in *LZTR1* in Patient 029623, and a *de novo* variant in *SOS2* in Patient 023509, are a probably causative in all three patients since ADHD and behavioral problems are reported in the Noonan syndrome phenotype (Roberts, 2001). For Patient 029623, additional analyses should be performed to establish whether the variants are truly biallelic since compound heterozygosity was presumed based only on the genotype–phenotype correlation. Patient 040110 is also a carrier of a VUS variant in the *TM4SF20* gene with a predicted acceptor loss score of Δ0.99 using the SpliceAI tool,[5] associated with language impairment (Andres et al., 2021). However, this feature was not reported in our patient (**Table 2**). This can be explained by the reduced penetrance observed for *TM4SF20* truncation carriers (Wiszniewski et al., 2013). Our analysis showed that the *KRAS* gene is functionally linked to the *SLC2A1* gene, which is also not reported as an ASD-associated gene. The abovementioned connection stems from tumor genetics since glucose deprivation has been shown to contribute to the development of *KRAS* pathway mutations in tumor cells (Yun et al., 2009). A presumed *de novo* pathogenic mutation in the *SLC2A1* gene was detected in a 13-year-old girl (Patient 034742) with a severe phenotype, which reverse

[5] spliceailookup.broadinstitute.org

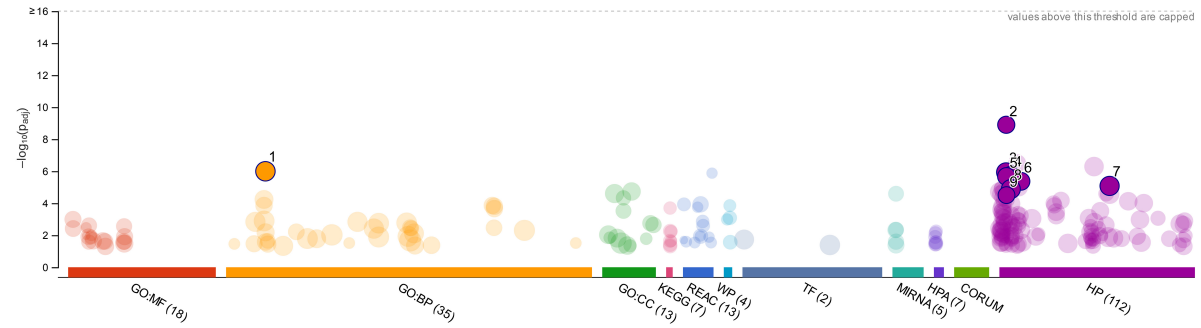

ID	Source	Term ID	Term Name	p_{adj} (query_1)
1	GO:BP	GO:0007399	nervous system development	1.011×10^{-6}
2	HP	HP:0000729	Autistic behavior	1.256×10^{-9}
3	HP	HP:0000708	Behavioral abnormality	1.168×10^{-6}
4	HP	HP:0001263	Global developmental delay	1.929×10^{-6}
5	HP	HP:0000750	Delayed speech and language development	2.130×10^{-6}
6	HP	HP:0002463	Language impairment	4.290×10^{-6}
7	HP	HP:0012758	Neurodevelopmental delay	8.300×10^{-6}
8	HP	HP:0001249	Intellectual disability	1.314×10^{-5}
9	HP	HP:0000752	Hyperactivity	3.119×10^{-5}

FIGURE 4 | g:Profiler analysis for the studied genes based on GO is presented for molecular function (MF), biological process (BP), cellular component (CC), biological pathways (KEGG, Reactome, and WikiPathways), regulatory motifs in DNA (TF and MIRNA), protein databases (HPA and CORUM), and Human Phenotype Ontology (HP). Only data for BP and HP were analyzed and represented in the figure.

phenotyping has shown, is a cause of the GLUT1 deficiency syndrome (López-Rivera et al., 2020; Mir et al., 2022). Another gene, not reported to be associated with ASD, but which can be linked to *KRAS*, is the *FGFR2* gene since they are both involved in the RTK/Ras/MAPK signaling pathway (Das et al., 2014). The paternally inherited VUS variant was detected by family-WES analyses in twin brothers with ASD, DD, speech delay, and brachycephaly. Mutations in the *FGFR2* gene with incomplete penetrance have been reported to cause a syndromic form of craniosynostosis with ID/DD (Azoury et al., 2017). To the best of our knowledge, no clear association of this gene with ASD has been established, although a functional study in mice has shown that dysregulation of the *Fgfr2* gene leads to impaired core behavior related to ASD (Szczurkowska et al., 2018). For all three abovementioned genes, the g:Profiler tool showed involvement with high significance in behavioral abnormalities (HP:0000708), DD (HP:0001263), ID (HP:0001249), and also in autistic behavior (HP:0000729) for the *SLC2A1* gene (**Figure 4** and data available online).

Similar correlations can be made for other non-SFARI genes in the other three clusters mentioned above. Two such genes are the *KCNK9* and *GRIA4* genes in the green cluster (**Figure 3B**). The pathogenic variant in the *KCNK9* gene was identified as a "single event" variant in NDD-associated genes (**Figure 2**). Reverse phenotyping revealed that Patient 019020 has a clinical feature of the *KCNK9* imprinting syndrome (Graham, Zadeh et al., 2016). Segregation analysis revealed a *de novo* variant, presumably on the maternal allele.

Two different VUS variants were detected in the *GRIA4* gene in two male patients (Patients 045232 and 046940) who share ASD as a common clinical feature. Segregation analysis was not performed in either case. Although the *GRIA4* gene is not listed in the SFARI database, *de novo* heterozygous pathogenic variants in the *GRIA4* gene have already been reported in patients with an ASD-like phenotype (Martin et al., 2017). The *KCNK9* and *GRIA4* genes were also clustered together with *KCNQ2*, *KCNQ5*, and *SCN8A* (**Figure 3B**). Five of eight genes in this cluster share gate channel activity (GO:0022836) and are involved in the ASD/ID/DD phenotype according to g:Profiler analysis (data available online).

Additional gene correlations were also identified by gene clustering. In the yellow node, according to WikiPathways data (Martens et al., 2021), there are three Rett syndrome-causing genes (**Figure 3A**). Genes, such as *IQSEC2* and even *KCNQ2* from the green node, are linked to these genes since both genes are involved in the Rett-like syndrome phenotype (Wang et al., 2019).

Despite an attempt to establish a true protein function prediction analysis for some genes in our cohort, no connection could be made. Their role in a patient's phenotype was set by focusing on "single event" variants. In almost half of the cases (18 out of 42 genes), the variant occurred as a "single event." This means that we detected one variant per gene in all patients combined (**Figure 2**), which confirms that ultrarare variants are a key factor in the etiology of ASD, and new genes will emerge by adding new patient cohorts. Among non-SFARI listed genes,

variants were detected in the *CYFIP2*, *GNE*, and *MAGT1* genes. Using the g:Profiler tool, all three genes were found to be linked to NDD features (data available online), while the same three genes have been described in patients with an ASD-associated phenotype in the literature in recent years (Blommaert et al., 2019; Yang et al., 2020; Begemann et al., 2021). In the future, functional studies, variant segregation, and better genotype–phenotype analysis should be performed for this category of genes to establish their true roles in a patient's phenotype.

These same studies should be performed for Patient 039934, a female with variants in both the *FBXO11* and *HECW2* genes, which are both associated with a complex NDD phenotype that includes autistic features, ID, and abnormalities in language development, features also present in our proband. A splice variant in the *HECW2* gene with a predicted acceptor loss score Δ of 1.00 using the SpliceAI tool was detected in Patient 041707 with a similar phenotype consisting of ASD, DD, and poor/absent speech. Since segregation analysis was not performed in either of these patients, the true significance of the variants for the patients' phenotype is not clear. For both genes, *de novo* variants in the genes were reported as causative, hence variant segregation and better genotype–phenotype analysis are essential (Ullman et al., 2018; Jansen et al., 2019). Therefore, despite both variants in the *HECW2* gene being classified as likely pathogenic, at present, they should be treated as VUS.

By defining ultrarare and "single event" variants in the ASD-associated genes, variants in rarely reported patients with ASD in the literature were identified.

A pathogenic variant, later established as *de novo* after reverse phenotyping and segregation, was detected in a 12-year-old girl (Patient 018653) with ASD and ID. The *NR4A2* gene encodes nuclear receptor 4A subfamily (Nr4a) of transcription factors involved in hippocampal synaptic plasticity and cognitive functions (Català-Solsona et al., 2021). *NR4A2* haploinsufficiency caused by deletions or a frameshift mutation in this gene and associated with ID and ASD has been reported in the literature (Lévy et al., 2018; Guo et al., 2019). To the best of our knowledge, our patient has the first stop-gain mutation reported in the literature that confirms a *de novo* loss-of-function (LoF) mutation involved in the etiology of ASD. A different variant (**Figure 2**), also found in the *NR4A2* gene in another patient, was marked as not causative since it was also present in the mother who had no health problems.

In a 5-year-old girl with ASD, ID/DD, and delayed speech and language development (Patient 045124), a "single event" variant is a likely pathogenic *de novo* variant in the *GRIA1* gene. The GRIA1 gene encoding the α-amino-3-hydroxy-5-methyl-4-isoxazolepropionic acid (AMPA) receptor subunit GLUA1 has been reported in wide neurological and psychiatric disorders, including schizophrenia (Bygrave et al., 2019). In a large study of 17,688 patients with NDDs, 21 patients were carriers of a mutation causing a 636 amino acid change from alanine to threonine in the GRIA1 protein. These patients showed evidence of specific learning disabilities and autism (Geisheker et al., 2017). Hence, our patient represents a new mutational and phenotypic spectrum of patients with *GRIA1* gene haploinsufficiency.

A missense variant in the *SIN3B* gene was also found as a "single event" variant in Patient 023509 with ASD and DD. This variant was classified as a VUS according to ACMG guidelines, but WES-trio showed that the variant occurred *de novo*. The *SIN3B* gene encodes a transcription corepressor which has an important role in histone deacetylation and transcriptional repression (Latypova et al., 2021). An animal model showed that *Sin3b* knockout mice and zebrafish *sin3b* mutants express skeletal and growth defects (David et al., 2008; Moravec et al., 2017). *Sin3b* knockout mice also showed defects in blood differentiation, whereas zebrafish *sin3b* mutants showed locomotor defects (Cantor and David, 2017; Moravec et al., 2017). Although STRING analysis did not show any correlation with a specific phenotype (data available online), both g:Profiler analysis and the literature have reported that haploinsufficiency of *SIN3B* causes an ID and ASD phenotypes (Latypova et al., 2021).

There are several limitations to our study. First and foremost, limitations are the limited sample size and the lack of segregation and functional studies, especially for VUS variants and variants in poorly researched genes. Second, we focused only on non-synonymous coding variants, and by using a filtering process, we probably eliminated variants that were poorly covered or were present with low allelic frequency. For genes where protein function predictions and gene prioritization analysis results were not obtained, functional enrichment analysis with all ASD-associated genes should be performed in the future.

The abovementioned cases demonstrate that by performing WES analysis for patients with ASD without focusing on ASD-associated genes but including gene lists for genes that are functionally similar or linked to them, we yielded a higher diagnostic output, despite the limited clinical data. Reverse phenotyping by a clinician can then be performed to determine whether the variant in the analyzed gene is clinically relevant for the patient. In our study, focusing on the ultrarare variants or "single event" variants per gene regardless of their previously known molecular function was crucial for patients with complex phenotypes. This is illustrated by the high proportion of *de novo* variants identified as causative. Our study also demonstrates that most of the causative genes are involved in a syndromic form of ASD. In most patients, this is not the main feature, but rather part of a more complicated phenotype seen in these patients. Thus, classical genotype–phenotype analysis of WES data would be time-consuming, and perhaps in some cases, proper genotype–phenotype correlation would not be made due to several factors: a variable phenotype in specific disorders, overlapping clinical features, the revolving phenotype in small children, or reduced penetrance.

DATA AVAILABILITY STATEMENT

The datasets presented in this study can be found in online repositories. The names of the repositories and accession numbers can be found in the article. The datasets analyzed for this study can be found on the g:Profiler website (https://biit.cs.ut.ee/gplink/l/iGN_PmjmTv).

ETHICS STATEMENT

The studies involving human participants were reviewed and approved by the Commission of the Republic of Slovenia for Medical Ethics. Written informed consent was obtained from the individual(s), and minor(s)' legal guardian/next of kin, for the publication of any potentially identifiable images or data included in this article.

AUTHOR CONTRIBUTIONS

DK designed the study, analyzed the NGS data, performed the functional enrichment analysis and data interpretation, performed the validation by Sanger sequencing and the segregation analysis, and wrote the manuscript. MG and NR performed the NGS variant analysis workflow. MG participated in the chart and figure formation. IO and HG evaluated the patients. SS performed the validation by Sanger sequencing. MG, IO, SS, HG, PD, and NK revised the manuscript. All authors have read and approved the manuscript.

FUNDING

The authors acknowledge that the Advanced Genomic Analyses of Slovenian Children With Autistic Spectrum Disorders project [grant number Z3-9294 (B)] and the Comparative Genomics and Genome Biodiversity Research Program (grant number P4-0220) were financially supported by the Slovenian Research Agency.

ACKNOWLEDGMENTS

We are grateful to all the patients and their families for their cooperation. We also like to express gratitude to our student Tim Ravnjak for his substantial assistance with NGS data analysis, to Barbara Stojanov for participating in the evaluation of patients, and to our colleagues Lara Forstner, Leon Maric, and Spela Buneto for performing Sanger sequencing.

SUPPLEMENTARY MATERIAL

The Supplementary Material for this article can be found online at: https://www.frontiersin.org/articles/10.3389/fnmol.2022.912671/full#supplementary-material

REFERENCES

Abad, C., Cook, M. M., Cao, L., Jones, J. R., Rao, N. R., Dukes-Rimsky, L., et al. (2018). A rare de novo RAI1 gene mutation affecting BDNF-enhancer-driven transcription activity associated with autism and atypical smith-magenis syndrome presentation. *Biology* 7:31. doi: 10.3390/biology7020031

Adzhubei, I., Jordan, D. M., and Sunyaev, S. R. (2013). Predicting functional effect of human missense mutations using PolyPhen-2. *Curr. Protoc. Hum. Genet.* 7:20. doi: 10.1002/0471142905.hg0720s76

Adzhubei, I. A., Schmidt, S., Peshkin, L., Ramensky, V. E., Gerasimova, A., Bork, P., et al. (2010). A method and server for predicting damaging missense mutations. *Nat. Methods* 7, 248–249. doi: 10.1038/nmeth0410-248

Andres, E. M., Neely, H. L., Hafeez, H., Yasmin, T., Kausar, F., Basra, M. A. R., et al. (2021). Study of rare genetic variants in TM4SF20, NFXL1, CNTNAP2, and ATP2C2 in Pakistani probands and families with language impairment. *Meta Gene* 30:100966. doi: 10.1016/j.mgene.2021.100966

Arnett, A. B., Rhoads, C. L., Hoekzema, K., Turner, T. N., Gerdts, J., Wallace, A. S., et al. (2018). The autism spectrum phenotype in ADNP syndrome. *Autism Res.* 11, 1300–1310. doi: 10.1002/aur.1980

Arteche-López, A., Gómez Rodríguez, M. J., Sánchez Calvin, M. T., Quesada-Espinosa, J. F., Lezana Rosales, J. M., Palma Milla, C., et al. (2021). Towards a change in the diagnostic algorithm of autism spectrum disorders: evidence supporting whole exome sequencing as a first-tier test. *Genes* 12:560. doi: 10.3390/genes12040560

Azoury, S. C., Reddy, S., Shukla, V., and Deng, C. X. (2017). Fibroblast growth factor receptor 2 (FGFR2) mutation related syndromic craniosynostosis. *Int. J. Biol. Sci.* 13, 1479–1488. doi: 10.7150/ijbs.22373

Balicza, P., Varga, N. Á, Bolgár, B., Pentelényi, K., Bencsik, R., Gál, A., et al. (2019). Comprehensive analysis of rare variants of 101 autism-linked genes in a hungarian cohort of autism spectrum disorder patients. *Front. Genet.* 10:434. doi: 10.3389/fgene.2019.00434

Begemann, A., Sticht, H., Begtrup, A., Vitobello, A., Faivre, L., Banka, S., et al. (2021). New insights into the clinical and molecular spectrum of the novel CYFIP2-related neurodevelopmental disorder and impairment of the WRC-mediated actin dynamics. *Genet. Med.* 23, 543–554. doi: 10.1038/s41436-020-01011-x

Bell, S., Rousseau, J., Peng, H., Aouabed, Z., Priam, P., Theroux, J. F., et al. (2019). Mutations in ACTL6B cause neurodevelopmental deficits and epilepsy and lead to loss of dendrites in human neurons. *Am. J. Hum. Genet.* 104, 815–834. doi: 10.1016/j.ajhg.2019.03.022

Bernier, R., Golzio, C., Xiong, B., Stessman, H. A., Coe, B. P., Penn, O., et al. (2014). Disruptive CHD8 mutations define a subtype of autism early in development. *Cell* 158, 263–276. doi: 10.1016/j.cell.2014.06.017

Biswas, D., Cary, W., and Nolta, J. A. (2020). PPP2R5D-related intellectual disability and neurodevelopmental delay: a review of the current understanding of the genetics and biochemical basis of the disorder. *Int. J. Mol. Sci.* 21:1286. doi: 10.3390/ijms21041286

Blommaert, E., Péanne, R., Cherepanova, N. A., Rymen, D., Staels, F., Jaeken, J., et al. (2019). Mutations in MAGT1 lead to a glycosylation disorder with a variable phenotype. *Proc. Natl. Acad. Sci. U.S.A.* 116, 9865–9870. doi: 10.1073/pnas.1817815116

Bolger, A. M., Lohse, M., and Usadel, B. (2014). Trimmomatic: a flexible trimmer for Illumina sequence data. *Bioinformatics* 30, 2114–2120. doi: 10.1093/bioinformatics/btu170

Butler, K. M., da Silva, C., Shafir, Y., Weisfeld-Adams, J. D., Alexander, J. J., Hegde, M., et al. (2017). De novo and inherited SCN8A epilepsy mutations detected by gene panel analysis. *Epilepsy Res.* 129, 17–25. doi: 10.1016/j.eplepsyres.2016.11.002

Bygrave, A. M., Jahans-Price, T., Wolff, A. R., Sprengel, R., Kullmann, D. M., Bannerman, D. M., et al. (2019). Hippocampal-prefrontal coherence mediates working memory and selective attention at distinct frequency bands and provides a causal link between schizophrenia and its risk gene GRIA1. *Transl. Psychiatry* 9:142. doi: 10.1038/s41398-019-0471-0

Cantor, D. J., and David, G. (2017). The chromatin-associated Sin3B protein is required for hematopoietic stem cell functions in mice. *Blood* 129, 60–70. doi: 10.1182/blood-2016-06-721746

Català-Solsona, J., Miñano-Molina, A. J., and Rodríguez-Álvarez, J. (2021). Nr4a2 transcription factor in hippocampal synaptic plasticity, memory and cognitive dysfunction: a perspective review. *Front. Mol. Neurosci.* 14:786226. doi: 10.3389/fnmol.2021.786226

Chen, J., Khan, R. A. W., Wang, M., He, K., Wang, Q., Li, Z., et al. (2017). Association between the variability of the ABCA13 gene and the risk of major

depressive disorder and schizophrenia in the Han Chinese population. *World J. Biol. Psychiatry* 18, 550–556. doi: 10.1080/15622975.2016.1245442

Chen, X., Jin, J., Wang, Q., Xue, H., Zhang, N., Du, Y., et al. (2019). A de novo pathogenic CSNK1E mutation identified by exome sequencing in family trios with epileptic encephalopathy. *Hum. Mutat.* 40, 281–287. doi: 10.1002/humu.23690

Das, K., Gunasegaran, B., Tan, I. B., Deng, N., Lim, K. H., and Tan, P. (2014). Mutually exclusive FGFR2, HER2, and KRAS gene amplifications in gastric cancer revealed by multicolour FISH. *Cancer Lett.* 353, 167–175. doi: 10.1016/j.canlet.2014.07.021

David, G., Grandinetti, K. B., Finnerty, P. M., Simpson, N., Chu, G. C., and Depinho, R. A. (2008). Specific requirement of the chromatin modifier mSin3B in cell cycle exit and cellular differentiation. *Proc. Natl. Acad. Sci. U.S.A.* 105, 4168–4172. doi: 10.1073/pnas.0710285105

DePristo, M. A., Banks, E., Poplin, R., Garimella, K. V., Maguire, J. R., Hartl, C., et al. (2011). A framework for variation discovery and genotyping using next-generation DNA sequencing data. *Nat. Genet.* 43, 491–498. doi: 10.1038/ng.806

Desvignes, J. P., Bartoli, M., Delague, V., Krahn, M., Miltgen, M., Béroud, C., et al. (2018). VarAFT: a variant annotation and filtration system for human next generation sequencing data. *Nucleic Acids Res.* 46, W545–W553. doi: 10.1093/nar/gky471

Du, X., Gao, X., Liu, X., Shen, L., Wang, K., Fan, Y., et al. (2018). Genetic diagnostic evaluation of trio-based whole exome sequencing among children with diagnosed or suspected autism spectrum disorder. *Front. Genet.* 9:594. doi: 10.3389/fgene.2018.00594

Earl, R. K., Turner, T. N., Mefford, H. C., Hudac, C. M., Gerdts, J., Eichler, E. E., et al. (2017). Clinical phenotype of ASD-associated DYRK1A haploinsufficiency. *Mol. Autism.* 8:54. doi: 10.1186/s13229-017-0173-5

El Hayek, L., Tuncay, I. O., Nijem, N., Russell, J., Ludwig, S., Kaur, K., et al. (2020). KDM5A mutations identified in autism spectrum disorder using forward genetics. *eLife* 9:e56883. doi: 10.7554/eLife.56883

Field, M., Tarpey, P., Boyle, J., Edkins, S., Goodship, J., Luo, Y., et al. (2006). Mutations in the RSK2(RPS6KA3) gene cause Coffin-Lowry syndrome and nonsyndromic X-linked mental retardation. *Clin. Genet.* 70, 509–515. doi: 10.1111/j.1399-0004.2006.00723.x

Geisheker, M. R., Heymann, G., Wang, T., Coe, B. P., Turner, T. N., Stessman, H. A. F., et al. (2017). Hotspots of missense mutation identify neurodevelopmental disorder genes and functional domains. *Nat. Neurosci.* 0, 1043–1051. doi: 10.1038/nn.4589

Graham, J. M. , Zadeh, N., Kelley, M., Tan, E. S., Liew, W., Tan, V., et al. (2016). KCNK9 imprinting syndrome-further delineation of a possible treatable disorder. *Am. J. Med. Genet. A* 170, 2632–2637. doi: 10.1002/ajmg.a.37740

Gregor, A., Meerbrei, T., Gerstner, T., Toutain, A., Lynch, S. A., Stals, K., et al. (2022). De novo missense variants in FBXO11 alter its protein expression and subcellular localization. *Hum. Mol. Genet.* 31, 440–454. doi: 10.1093/hmg/ddab265

Guo, H., Duyzend, M. H., Coe, B. P., Baker, C., Hoekzema, K., Gerdts, J., et al. (2019). Genome sequencing identifies multiple deleterious variants in autism patients with more severe phenotypes. *Genet. Med.* 21, 1611–1620. doi: 10.1038/s41436-018-0380-2

Jansen, S., van der Werf, I. M., Innes, A. M., Afenjar, A., Agrawal, P. B., Anderson, I. J., et al. (2019). De novo variants in FBXO11 cause a syndromic form of intellectual disability with behavioral problems and dysmorphisms. *Eur. J. Hum. Genet.* 27, 738–746. doi: 10.1038/s41431-018-0292-2

Johnston, J. J., van der Smagt, J. J., Rosenfeld, J. A., Pagnamenta, A. T., Alswaid, A., Baker, E. H., et al. (2018). Autosomal recessive Noonan syndrome associated with biallelic LZTR1 variants. *Genet. Med.* 20, 1175–1185. doi: 10.1038/gim.2017.249

Koemans, T. S., Kleefstra, T., Chubak, M. C., Stone, M. H., Reijnders, M. R. F., de Munnik, S., et al. (2017). Functional convergence of histone methyltransferases EHMT1 and KMT2C involved in intellectual disability and autism spectrum disorder. *PLoS Genet.* 13:e1006864. doi: 10.1371/journal.pgen.1006864

Krgovic, D., Kokalj Vokac, N., Zagorac, A., and Gregoric Kumperscak, H. (2018). Rare structural variants in the DOCK8 gene identified in a cohort of 439 patients with neurodevelopmental disorders. *Sci. Rep.* 8:9449. doi: 10.1038/s41598-018-27824-0

Kumar, P., Henikoff, S., and Ng, P. C. (2009). Predicting the effects of coding non-synonymous variants on protein function using the SIFT algorithm. *Nat. Protoc.* 4, 1073–1081. doi: 10.1038/nprot.2009.86

Latypova, X., Vincent, M., Mollé, A., Adebambo, O. A., Fourgeux, C., Khan, T. N., et al. (2021). Haploinsufficiency of the Sin3/HDAC corepressor complex member SIN3B causes a syndromic intellectual disability/autism spectrum disorder. *Am. J. Hum. Genet.* 108, 929–941. doi: 10.1016/j.ajhg.2021.03.017

Lehalle, D., Mosca-Boidron, A. L., Begtrup, A., Boute-Benejean, O., Charles, P., Cho, M. T., et al. (2017). STAG1 mutations cause a novel cohesinopathy characterised by unspecific syndromic intellectual disability. *J. Med. Genet.* 54, 479–488. doi: 10.1136/jmedgenet-2016-104468

Lehman, A., Thouta, S., Mancini, G. M. S., Naidu, S., van Slegtenhorst, M., McWalter, K., et al. (2017). Loss-of-function and gain-of-function mutations in KCNQ5 cause intellectual disability or epileptic encephalopathy. *Am. J. Hum. Genet.* 101, 65–74. doi: 10.1016/j.ajhg.2017.05.016

Lévy, J., Grotto, S., Mignot, C., Maruani, A., Delahaye-Duriez, A., Benzacken, B., et al. (2018). NR4A2 haploinsufficiency is associated with intellectual disability and autism spectrum disorder. *Clin. Genet.* 94, 264–268. doi: 10.1111/cge.13383

Li, H., and Durbin, R. (2010). Fast and accurate long-read alignment with Burrows-Wheeler transform. *Bioinformatics* 26, 589–595. doi: 10.1093/bioinformatics/btp698

Lindstrand, A., Eisfeldt, J., Pettersson, M., Carvalho, C. M. B., Kvarnung, M., Grigelioniene, G., et al. (2019). From cytogenetics to cytogenomics: whole-genome sequencing as a first-line test comprehensively captures the diverse spectrum of disease-causing genetic variation underlying intellectual disability. *Genome Med.* 11:68. doi: 10.1186/s13073-019-0675-1

Lintas, C., Sacco, R., Azzarà, A., Cassano, I., and Gurrieri, F. (2021). Genotype-phenotype correlations in relation to newly emerging monogenic forms of autism spectrum disorder and associated neurodevelopmental disorders: the importance of phenotype reevaluation after pangenomic results. *J. Clin. Med.* 10:5060. doi: 10.3390/jcm10215060

Liyanage, V. R., and Rastegar, M. (2014). Rett syndrome and MeCP2. *Neuromolecular Med.* 16, 231–264. doi: 10.1007/s12017-014-8295-9

Lopergolo, D., Privitera, F., Castello, G., Lo Rizzo, C., Mencarelli, M. A., Pinto, A. M., et al. (2021). IQSEC2 disorder: a new disease entity or a Rett spectrum continuum? *Clin. Genet.* 99, 462–474. doi: 10.1111/cge.13908

López-Rivera, J. A., Pérez-Palma, E., Symonds, J., Lindy, A. S., McKnight, D. A., Leu, C., et al. (2020). A catalogue of new incidence estimates of monogenic neurodevelopmental disorders caused by de novo variants. *Brain* 143, 1099–1105. doi: 10.1093/brain/awaa051

Lord, C., Elsabbagh, M., Baird, G., and Veenstra-Vanderweele, J. (2018). Autism spectrum disorder. *Lancet* 392, 508–520. doi: 10.1016/S0140-6736(18)31129-2

Louie, R. J., Friez, M. J., Skinner, C., Baraitser, M., Clark, R. D., Schwartz, C. E., et al. (2020). Clark-Baraitser syndrome is associated with a nonsense alteration in the autosomal gene TRIP12. *Am. J. Med. Genet. A* 182, 595–596. doi: 10.1002/ajmg.a.61443

Martens, M., Ammar, A., Riutta, A., Waagmeester, A., Slenter, D. N., Hanspers, K., et al. (2021). WikiPathways: connecting communities. *Nucleic Acids Res.* 49, D613–D621. doi: 10.1093/nar/gkaa1024

Martin, S., Chamberlin, A., Shinde, D. N., Hempel, M., Strom, T. M., and Schreiber, A. (2017). De novo variants in GRIA4 lead to intellectual disability with or without seizures and gait abnormalities. *Am. J. Hum. Genet.* 101, 1013–1020. doi: 10.1016/j.ajhg.2017.11.004

McKenna, A., Hanna, M., Banks, E., Sivachenko, A., Cibulskis, K., Kernytsky, A., et al. (2010). The genome analysis toolkit: a MapReduce framework for analyzing next-generation DNA sequencing data. *Genome Res.* 20, 1297–1303. doi: 10.1101/gr.107524.110

Miller, D. T., Adam, M. P., Aradhya, S., Biesecker, L. G., Brothman, A. R., Carter, N. P., et al. (2010). Consensus statement: chromosomal microarray is a first-tier clinical diagnostic test for individuals with developmental disabilities or congenital anomalies. *Am. J. Hum. Genet.* 2010, 749–764. doi: 10.1016/j.ajhg.2010.04.006

Miot, S., Akbaraly, T., Michelon, C., Couderc, S., Crepiat, S., Loubersac, J., et al. (2019). Comorbidity burden in adults with autism spectrum disorders and intellectual disabilities-a report from the EFAAR (frailty assessment in ageing adults with autism spectrum and intellectual disabilities) study. *Front. Psychiatry* 10:617. doi: 10.3389/fpsyt.2019.00617

Mir, A., Almudhry, M., Alghamdi, F., Albaradie, R., Ibrahim, M., Aldurayhim, F., et al. (2022). SLC gene mutations and pediatric neurological disorders: diverse clinical phenotypes in a Saudi Arabian population. *Hum. Genet.* 141, 81–99. doi: 10.1007/s00439-021-02404-x

Moravec, C. E., Yousef, H., Kinney, B. A., Salerno-Eichenholz, R., Monestime, C. M., Martin, B. L., et al. (2017). Zebrafish sin3b mutants are viable but have size, skeletal, and locomotor defects. *Dev. Dyn.* 246, 946–955. doi: 10.1002/dvdy.24581

Poplin, R., Ruano-Rubio, V., DePristo, M. A., Fennell, T. J., Carneiro, M. O., Van der Auwera, G. A., et al. (2018). Scaling accurate genetic variant discovery to tens of thousands of samples. *bioRXiv* [Preprint]. doi: 10.1101/201178v3

Quan, Y., Zhang, Q., Chen, M., Wu, H., Ou, J., Shen, Y., et al. (2020). Genotype and phenotype correlations for TBL1XR1 in neurodevelopmental disorders. *J. Mol. Neurosci.* 70, 2085–2092. doi: 10.1007/s12031-020-01615-7

Raudvere, U., Kolberg, L., Kuzmin, I., Arak, T., Adler, P., Peterson, H., et al. (2019). g:Profiler: a web server for functional enrichment analysis and conversions of gene lists (2019 update). *Nucleic Acids Res.* 47, W191–W198. doi: 10.1093/nar/gkz369

Richards, S., Aziz, N., Bale, S., Bick, D., Das, S., Gastier-Foster, J., et al. (2015). Standards and guidelines for the interpretation of sequence variants: a joint consensus recommendation of the American College of Medical Genetics and Genomics and the Association for Molecular Pathology. *Genet. Med.* 17, 405–424. doi: 10.1038/gim.2015.30

Rizzi, S., Spagnoli, C., Salerno, G. G., Frattini, D., Caraffi, S. G., Trimarchi, G., et al. (2020). Severe intellectual disability, absence of language, epilepsy, microcephaly and progressive cerebellar atrophy related to the recurrent de novo variant p.(P139L) of the CAMK2B gene: a case report and brief review. *Am. J. Med. Genet. A* 182, 2675–2679. doi: 10.1002/ajmg.a.61803

Roberts, A. E. (2001). "Noonan syndrome. [updated 2022 Feb 17]," in *GeneReviews§[Internet]*, eds M. P. Adam, H. H. Ardinger, R. A. Pagon, S. E. Wallace, L. J. H. Bean, K. W. Gripp, et al. (Seattle, WA: University of Washington), 1993–2022.

Ruzzo, E. K., Pérez-Cano, L., Jung, J. Y., Wang, L. K., Kashef-Haghighi, D., Hartl, C., et al. (2019). Inherited and de novo genetic risk for autism impacts shared networks. *Cell* 178, 850.e26–866.e26. doi: 10.1016/j.cell.2019.07.015

Rylaarsdam, L., and Guemez-Gamboa, A. (2019). Genetic causes and modifiers of autism spectrum disorder. *Front. Cell Neurosci.* 13:385. doi: 10.3389/fncel.2019.00385

Satterstrom, F. K., Kosmicki, J. A., Wang, J., Breen, M. S., De Rubeis, S., An, J. Y., et al. (2020). Large-scale exome sequencing study implicates both developmental and functional changes in the neurobiology of autism. *Cell* 180, 568.e23–584.e23. doi: 10.1016/j.cell.2019.12.036

Stolerman, E. S., Francisco, E., Stallworth, J. L., Jones, J. R., Monaghan, K. G., Keller-Ramey, J., et al. (2019). Genetic variants in the KDM6B gene are associated with neurodevelopmental delays and dysmorphic features. *Am. J. Med. Genet. A* 179, 1276–1286. doi: 10.1002/ajmg.a.61173

Strehlow, V., Heyne, H. O., Vlaskamp, D. R. M., Marwick, K. F. M., Rudolf, G., de Bellescize, J., et al. (2019). GRIN2A-related disorders: genotype and functional consequence predict phenotype. *Brain* 142, 80–92. doi: 10.1093/brain/awy304

Struja, T., and Capraro, J. (2021). Synchronous pituitary and pineal gland lesions presenting with panhypopituitarism in a patient with widespread colorectal cancer: a case report. *Oxf. Med. Case Rep.* 2021:omab030. doi: 10.1093/omcr/omab030

Szczurkowska, J., Pischedda, F., Pinto, B., Managò, F., Haas, C. A., Summa, M., et al. (2018). NEGR1 and FGFR2 cooperatively regulate cortical development and core behaviours related to autism disorders in mice. *Brain* 141, 2772–2794. doi: 10.1093/brain/awy190

Szklarczyk, D., Gable, A. L., Lyon, D., Junge, A., Wyder, S., Huerta-Cepas, J., et al. (2019). STRING v11: protein-protein association networks with increased coverage, supporting functional discovery in genome-wide experimental datasets. *Nucleic Acids Res.* 47, D607–D613. doi: 10.1093/nar/gky1131

Tartaglia, M., Gelb, B. D., and Zenker, M. (2011). Noonan syndrome and clinically related disorders. *Best Pract. Res. Clin. Endocrinol. Metab.* 25, 161–179. doi: 10.1016/j.beem.2010.09.002

Tatton-Brown, K., Zachariou, A., Loveday, C., Renwick, A., Mahamdallie, S., Aksglaede, L., et al. (2018). The tatton-brown-rahman syndrome: a clinical study of 55 individuals with de novo constitutive DNMT3A variants. *Wellcome Open Res.* 3:46. doi: 10.12688/wellcomeopenres.14430.1

Trelles, M. P., Levy, T., Lerman, B., Siper, P., Lozano, R., and Halpern, D. (2021). Individuals with FOXP1 syndrome present with a complex neurobehavioral profile with high rates of ADHD, anxiety, repetitive behaviors, and sensory symptoms. *Mol. Autism.* 12:61. doi: 10.1186/s13229-021-00469-z

Ullman, N. L., Smith-Hicks, C. L., Desai, S., and Stafstrom, C. E. (2018). De Novo HECW2 mutation associated with epilepsy, developmental decline, and intellectual disability: case report and review of literature. *Pediatr. Neurol.* 85, 76–78. doi: 10.1016/j.pediatrneurol.2018.03.005

Valentino, F., Bruno, L. P., Doddato, G., Giliberti, A., Tita, R., Resciniti, S., et al. (2021). Exome sequencing in 200 intellectual disability/autistic patients: new candidates and atypical presentations. *Brain Sci.* 11:936. doi: 10.3390/brainsci11070936

Van der Auwera, G. A., Carneiro, M. O., Hartl, C., Poplin, R., Del Angel, G., Levy-Moonshine, A., et al. (2013). From FastQ data to high-confidence variant calls: the genome analysis toolkit best practices pipeline. *Curr. Protoc. Bioinform.* 43, 11.10.1–11.10.33. doi: 10.1002/0471250953.bi1110s43

van der Werf, I. M., Jansen, S., de Vries, P. F., Gerstmans, A., van de Vorst, M., Van Dijck, A., et al. (2020). Overrepresentation of genetic variation in the AnkyrinG interactome is related to a range of neurodevelopmental disorders. *Eur. J. Hum. Genet.* 28, 1726–1733. doi: 10.1038/s41431-020-0682-0

Wang, J., Gong, J., Li, L., Chen, Y., Liu, L., Gu, H., et al. (2018). Neurexin gene family variants as risk factors for autism spectrum disorder. *Autism Res.* 11, 37–43. doi: 10.1002/aur.1881

Wang, J., Zhang, Q., Chen, Y., Yu, S., Wu, X., and Bao, X. (2019). Rett and Rett-like syndrome: expanding the genetic spectrum to KIF1A and GRIN1 gene. *Mol. Genet. Genomic Med.* 7:e968. doi: 10.1002/mgg3.968

Wingett, S. W., and Andrews, S. (2018). FastQ screen: a tool for multi-genome mapping and quality control. *F1000Research* 7:1338. doi: 10.12688/f1000research.15931.2

Wiszniewski, W., Hunter, J. V., Hanchard, N. A., Willer, J. R., Shaw, C., Tian, Q., et al. (2013). TM4SF20 ancestral deletion and susceptibility to a pediatric disorder of early language delay and cerebral white matter hyperintensities. *Am. J. Hum. Genet.* 93, 197–210. doi: 10.1016/j.ajhg.2013.05.027

Yamamoto, G. L., Aguena, M., Gos, M., Hung, C., Pilch, J., Fahiminiya, S., et al. (2015). Rare variants in SOS2 and LZTR1 are associated with Noonan syndrome. *J. Med. Genet.* 52, 413–421. doi: 10.1136/jmedgenet-2015-103018

Yang, X., Li, H., Ge, J., Chao, H., Li, G., Zhou, Z., et al. (2020). The level of GNE and its relationship with behavioral phenotypes in children with autism spectrum disorder. *Medicine* 99:e21013. doi: 10.1097/MD.0000000000021013

Yoon, S., Munoz, A., Yamrom, B., Lee, Y. H., Andrews, P., Marks, S., et al. (2021). Rates of contributory de novo mutation in high and low-risk autism families. *Commun. Biol.* 4:1026. doi: 10.1038/s42003-021-02533-z

Yun, J., Rago, C., Cheong, I., Pagliarini, R., Angenendt, P., Rajagopalan, H., et al. (2009). Glucose deprivation contributes to the development of KRAS pathway mutations in tumor cells. *Science* 325, 1555–1559. doi: 10.1126/science.1174229

Conflict of Interest: The authors declare that the research was conducted in the absence of any commercial or financial relationships that could be construed as a potential conflict of interest.

Publisher's Note: All claims expressed in this article are solely those of the authors and do not necessarily represent those of their affiliated organizations, or those of the publisher, the editors and the reviewers. Any product that may be evaluated in this article, or claim that may be made by its manufacturer, is not guaranteed or endorsed by the publisher.

Copyright © 2022 Krgovic, Gorenjak, Rihar, Opalic, Stangler Herodez, Gregoric Kumperscak, Dovc and Kokalj Vokac. This is an open-access article distributed under the terms of the Creative Commons Attribution License (CC BY). The use, distribution or reproduction in other forums is permitted, provided the original author(s) and the copyright owner(s) are credited and that the original publication in this journal is cited, in accordance with accepted academic practice. No use, distribution or reproduction is permitted which does not comply with these terms.

frontiers | Frontiers in Molecular Neuroscience

ORIGINAL RESEARCH
published: 13 July 2022
doi: 10.3389/fnmol.2022.901682

Autism-Risk Gene *necab2* Regulates Psychomotor and Social Behavior as a Neuronal Modulator of mGluR1 Signaling

Zexu Chen[1,2,3,4†], Han Long[1,2†], Jianhua Guo[1,2], Yiran Wang[1,2,5,6], Kezhe He[1,2], Chenchen Tao[5,7], Xiong Li[1,2,6], Keji Jiang[8], Su Guo[6] and Yan Pi[1,2*]*

[1] State Key Laboratory of Genetic Engineering, School of Life Sciences, Fudan University, Shanghai, China, [2] National Demonstration Center for Experimental Biology Education, School of Life Sciences, Fudan University, Shanghai, China, [3] Eye Institute and Department of Ophthalmology, Eye & ENT Hospital, Fudan University, Shanghai, China, [4] NHC Key Laboratory of Myopia (Fudan University), Key Laboratory of Myopia, Chinese Academy of Medical Sciences, Shanghai, China, [5] School of Clinical Medicine, Shanghai Medical College, Fudan University, Shanghai, China, [6] Department of Bioengineering and Therapeutic Sciences, Programs in Human Genetics and Biological Sciences, University of California, San Francisco, San Francisco, CA, United States, [7] Department of Pulmonary and Critical Care Medicine, Zhongshan Hospital, Fudan University, Shanghai, China, [8] East China Sea Fisheries Research Institute, Chinese Academy of Fishery Sciences, Shanghai, China

OPEN ACCESS

Edited by:
Jun Aruga,
Nagasaki University, Japan

Reviewed by:
Arturo Ortega,
Centro de Investigación y de Estudios Avanzados del Instituto Politécnico Nacional, Mexico
Akira Muto,
Toho University, Japan
Philippe Rondard,
Centre National de la Recherche Scientifique (CNRS), France

***Correspondence:**
Su Guo
su.guo@ucsf.edu
Yan Pi
yanpi@fudan.edu.cn

[†] These authors have contributed equally to this work

Specialty section:
This article was submitted to Brain Disease Mechanisms, a section of the journal Frontiers in Molecular Neuroscience

Received: 22 March 2022
Accepted: 07 June 2022
Published: 13 July 2022

Citation:
Chen Z, Long H, Guo J, Wang Y, He K, Tao C, Li X, Jiang K, Guo S and Pi Y (2022) Autism-Risk Gene necab2 Regulates Psychomotor and Social Behavior as a Neuronal Modulator of mGluR1 Signaling. Front. Mol. Neurosci. 15:901682. doi: 10.3389/fnmol.2022.901682

Background: *De novo* deletion of the *neuronal calcium-binding protein 2* (*NECAB2*) locus is associated with idiopathic autism spectrum disorders (ASDs). The *in vivo* function of *NECAB2* in the brain remains largely elusive.

Methods: We investigated the morphological and behavioral profiles of both *necab2* knock-out and overexpression zebrafish models. The expression pattern and molecular role of *necab2* were probed through a combination of *in vitro* and *in vivo* assays.

Results: We show that Necab2 is a neuronal specific, cytoplasmic, and membrane-associated protein, abundantly expressed in the telencephalon, habenula, and cerebellum. Necab2 is distributed peri-synaptically in subsets of glutamatergic and GABAergic neurons. CRISPR/Cas9-generated *necab2* knock-out zebrafish display normal morphology but exhibit a decrease in locomotor activity and thigmotaxis with impaired social interaction only in males. Conversely, *necab2* overexpression yields behavioral phenotypes opposite to the loss-of-function. Proteomic profiling uncovers a role of Necab2 in modulating signal transduction of G-protein coupled receptors. Specifically, co-immunoprecipitation, immunofluorescence, and confocal live-cell imaging suggest a complex containing NECAB2 and the metabotropic glutamate receptor 1 (mGluR1). *In vivo* measurement of phosphatidylinositol 4,5-bisphosphate further substantiates that Necab2 promotes mGluR1 signaling.

Conclusions: Necab2 regulates psychomotor and social behavior *via* modulating a signaling cascade downstream of mGluR1.

Keywords: autism spectrum disorders, calcium-binding protein, social behavior, metabotropic glutamate receptor 1, cerebellum

INTRODUCTION

Human genetics have uncovered many genes associated with complex neurodevelopmental disorders including intellectual disability, autism spectrum disorders (ASD), and schizophrenia (Sanders et al., 2011; De Rubeis et al., 2014; Iossifov et al., 2014; Schizophrenia Working Group of the Psychiatric Genomics Consortium, 2014; Niemi et al., 2018). The major challenges ahead are to establish efficient and cost-effective approaches to evaluate the mechanisms by which alterations of these genes may cause brain abnormalities, and devise potential therapeutic strategies harnessing this knowledge.

Zebrafish is a promising model system to perform such studies. As a vertebrate, zebrafish share considerable genomic similarities with mammals. There are zebrafish orthologues for about 82% of genes associated with human diseases (Howe et al., 2013). Also, tools for loss- (Hsu et al., 2014) and gain-of-function studies (Kawakami et al., 2016) have been well-established. Chemical treatment and behavioral tracking can be conveniently implemented in high-throughput studies, thereby linking genes to the brain and behavior (Guo, 2004; Thyme et al., 2019). Neural activity can be measured brain-wide at single-cell resolution (Chen et al., 2018).

Calcium is an important regulator of neuronal activity. Its dysregulation has been linked to neurological diseases (Schwaller, 2020). Calcium influx triggers exocytosis of neurotransmitter-containing synaptic vesicles at the presynaptic terminals (Neher and Sakaba, 2008). A transient rise of calcium levels in the dendritic spines post-synaptically induces activity-dependent synaptic plasticity (Zucker, 1999). Calcium signals can also regulate gene transcription at a slower time scale ranging from minutes to hours (Lyons and West, 2011). Complementing the omnipotence of Ca^{2+} as a neuronal regulator are a variety of calcium-binding proteins. *Neuronal Ca^{2+} binding proteins* (*NECABs*) are a protein family characterized by a single N-terminal EF-hand domain responsible for calcium binding, a putative antibiotic biosynthesis monooxygenase (ABM) domain at the C terminus, and a NECAB homology region (NHR) in between (Sugita et al., 2002; Kawasaki and Kretsinger, 2017). At least three members (*NECAB1-3*) are identified in humans that are conserved across vertebrates. NECABs are either expressed primarily in the nervous system (*NECAB1* and *NECAB2*) or the brain and muscle (*NECAB3*) (Zimmermann et al., 2013). *NECAB2* has been reported to interact with two G-protein coupled receptors in the human embryonic kidney cells in a calcium-regulated manner (Canela et al., 2007, 2009). At the spinal level, *necab2* is down-regulated by the peripheral nerve injury (Zhang et al., 2014) and functions as a critical determinant of pro-nociceptive neurotransmission (Zhang et al., 2018; Ma et al., 2021). A proteomic study involving yeast two-hybrid screening showed that *NECAB2* interacts with five autism-risk genes (*FMR1*, *FXR1*, *FXR2*, *SMARCA2,* and *TSC1*) (Sakai et al., 2011). A *de novo* deletion spanning the locus of *NECAB2* has been clinically detected in patients with idiopathic ASD (Itsara et al., 2010; Sakai et al., 2011; Sanders et al., 2011). However, the *in vivo* function of *NECAB2* in the brain remains elusive. As such, it remains speculative whether and how *NECAB2* might be involved in the pathogenesis of ASD.

In the present study, we performed *in vivo* functional analysis of *necab2* employing zebrafish. By generating knock-out and isoform-specific overexpression models, we showed that *necab2* played a critical role in regulating psychomotor and social behaviors. We further uncovered the molecular role that Necab2 interact with metabotropic glutamate receptor subtype 1 (mGluR1) and promote phosphatidylinositol 4,5-bisphosphate hydrolysis. These findings lay foundation for devising potential therapeutic strategies to combat the neurodevelopmental disorders involving *NECAB2* and its interacting molecular pathways.

RESULTS

necab2 Is Conserved in the Vertebrate Lineage and Expressed in the Developing Brain

NECAB2 belongs to a protein family with three recognizable domains: the EF-hand at the N-terminus, the middle NHR domain, and an ABM motif at the C-terminus (**Figure 1A**). In zebrafish, all three functional domains were conserved among Necab1-3, all of which have only one ortholog in the zebrafish genome (**Figure 1B**). The Necab2 protein sequence shares 44 and 38% of amino acid identity with Necab1 and Necab3. Multiple transcripts of *necab2* have been predicted in the Ensemble database (**Supplementary Figure 1A**). Two isoforms of Necab2 were confirmed at both RNA and protein levels. One of them possesses alternative splicing in the exon 9, which generated a premature stop codon before translating the ABM motif, named *necab2-201* (**Supplementary Figures 1B,C**). A phylogenetic analysis of the *necab2* orthologs across species revealed that NECAB2 is presented in *Homo sapiens* and at least 12 other vertebrates (**Figure 1C**) but is undetectable in the invertebrates such as *Drosophila* or *Caenorhabditis elegans*. The Necab2 protein sequences of zebrafish exhibit a relatively high level of amino acid identity with the corresponding human protein and the three typical conserved domains (EF-hand, NHR, ABM) exhibit 81, 86, and 60% amino acid identity respectively. Together, these findings indicate that NECAB2 is conserved in vertebrates and zebrafish is a potential model for studying the *in vivo* function of Necab2 in the intact brain.

The distribution of NECAB2 has been well-characterized in the spinal cord and peripheral nervous system (Zhang et al., 2014, 2016). However, its distribution in the brain remains largely unexplored. Using whole-mount *in situ* hybridization in embryonic and larval zebrafish, we found that *necab2* was expressed in the retina and subsets of brain regions examined from 24 hpf (hours post fertilization) to 96 hpf, resembling the distribution of nascent neurons (**Figure 1D**). Immunofluorescent labeling studies showed that the distribution of Necab2 protein was similar to its RNA transcripts but had stronger enrichment in the telencephalon, habenula, and cerebellum (**Figure 1E**). Subcellularly, immunofluorescent staining indicated Necab2 to

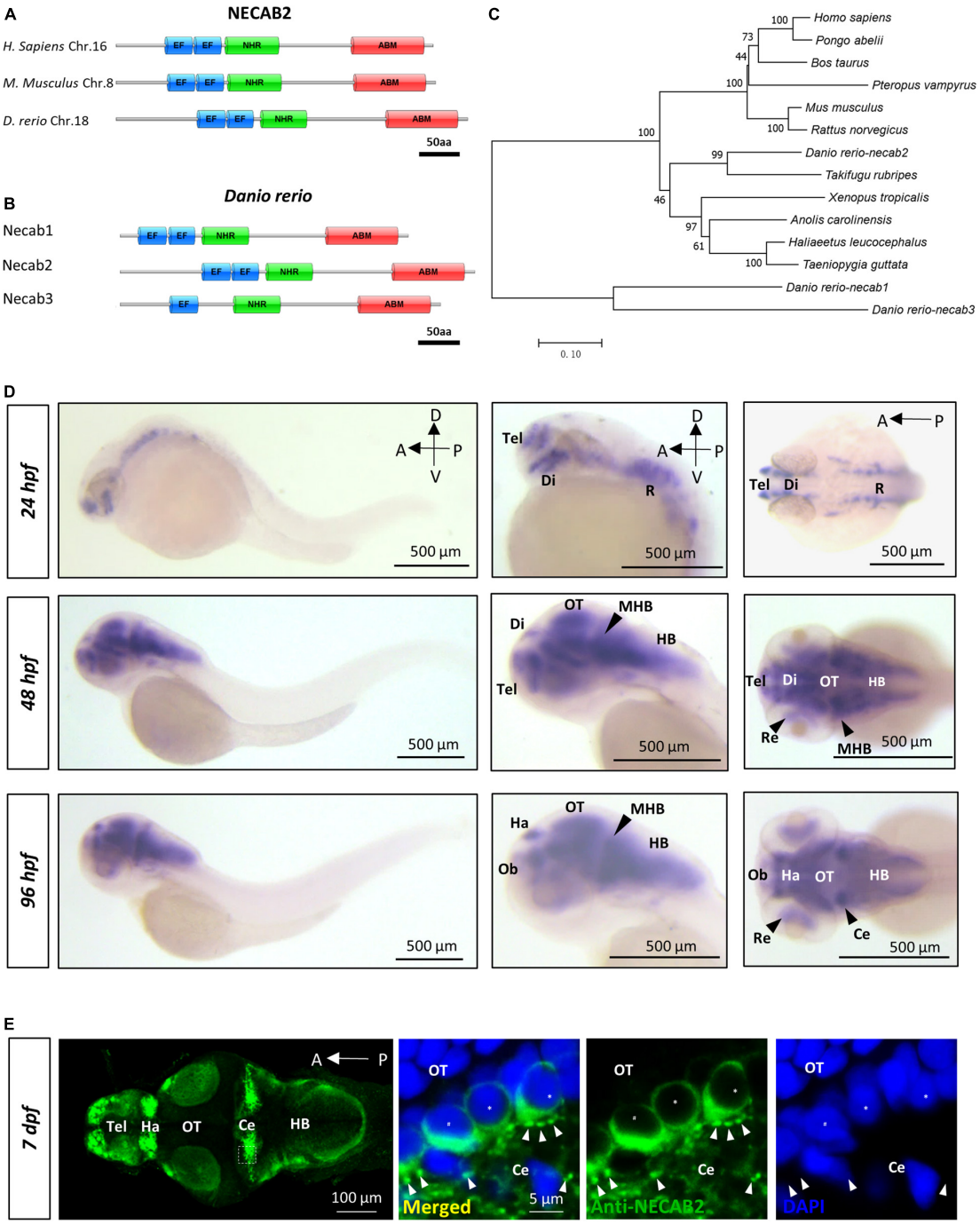

FIGURE 1 | *necab2*, conserved in the vertebrate lineage, is expressed in the developing zebrafish brain. **(A)** Protein Diagrams of NECAB2 orthologs in *H. sapiens*, *M. musculus,* and *D. rerio*. Diagrams represented the longest isoform. The diagrams were denoted by the species name and chromosome number (Chr.) All major functional domains are conserved. Scale bar = 50 amino acids (aa). **(B)** Protein Diagrams of the Necab family in *D. rerio*. Diagrams represented the longest isoforms. Diagrams are denoted by the gene name. All the major functional domains were conserved in Necab1, Necab2, and Necab3. Scale bar = 50 amino acids (aa). **(C)** The phylogenetic tree of the evolutionary relationship of *NECAB2*. Diverse animal phyla were identified by a best reciprocal BLAST search with human *NECAB2* and were mapped onto a phylogenetic tree. The tree was drawn to scale, with branch lengths in the same units as those of the evolutionary distances. All of the sequences were available from the NCBI protein database. Scale bar = 0.10. **(D)** Whole-mount *in situ* hybridization of *necab2* in wild-type embryos at 24, 48, and 96 hpf. *necab2* was expressed in selected brain regions reminiscent of the locations of nascent neurons. Scale bar = 500 μm. **(E)** Whole-mount immunofluorescence of Necab2 in wild-type larvae at 7 dpf. Necab2 was abundant in the telencephalon, habenula, and cerebellum. Scale bar = 100 μm. Necab2 was detected in structures reminiscent of synapse boutons (arrowheads) and the cell cytoplasm/membrane avoiding the nucleus (asterisks). The region in the dashed white box was shown at a higher magnification on the right. Scale bar = 5 μm. NECAB2 protein domains: EF, EF-Hand; NHR, NECAB Homologous Region; ABM, Antibiotic Biosynthesis Monooxygenase. hpf, hour post-fertilization; dpf, day post-fertilization; Tel, telencephalon; Di, diencephalon; Ce, cerebellum; Re, retina; Ha, habenula; OT, optic tectum; MHB, midbrain-hindbrain boundary; HB, hindbrain.

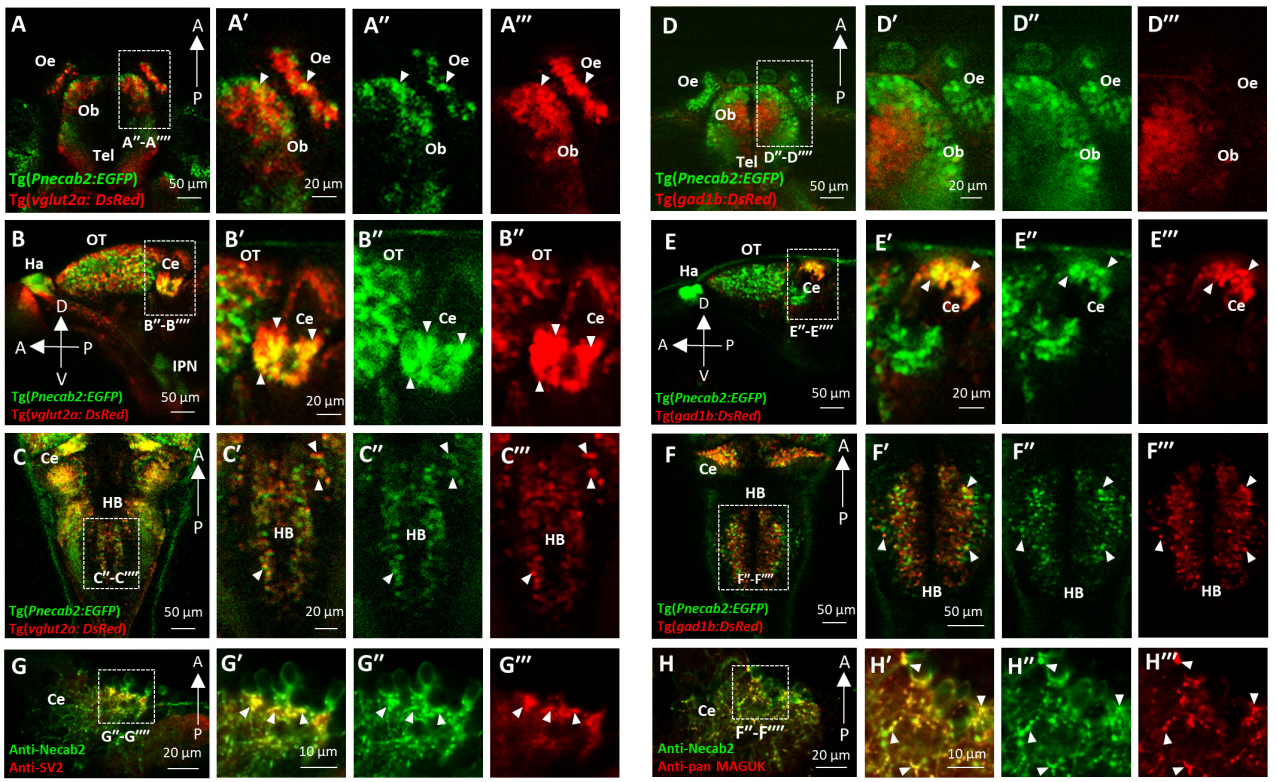

FIGURE 2 | Necab2 is expressed in subsets of glutamatergic and GABAergic neurons. **(A–A‴)** Confocal live imaging of the transgenic fish Tg(*Pnecab2:EGFP*) crossed with Tg(*vglut2a:DsRed*) at 5 dpf. Necab2 was expressed in subsets of glutamatergic neurons in the telencephalon, olfactory bulb, and olfactory epithelium (arrowheads, dorsal views). Scale bar = 50 μm **(A)**. The region in the dashed white box **(A)** was shown at higher magnification on the right **(A′–A‴)**. Scale bar = 20 μm. **(B–B‴)**. Necab2 was expressed in subsets of glutamatergic neurons in the optic tectum and cerebellum (arrowheads, lateral views). Scale bar = 50 μm **(B)**. The region in the dashed white box **(B)** was shown at higher magnification on the right **(B′–B‴)**. Scale bar = 20 μm. **(C–C‴)** Necab2 was expressed in subsets of glutamatergic neurons in the hindbrain (arrowheads, dorsal views). Scale bar = 50 μm **(C′)**. The region in the dashed white box **(C)** was shown at higher magnification on the right **(C′–C‴)**. Scale bar = 20 μm. **(D–D‴)** Confocal live imaging of the transgenic fish Tg(*Pnecab2:EGFP*) crossed with Tg(*gad1b:DsRed*) at 5 dpf. The Necab2-expressing neurons rarely overlapped with the gad1b-positive neurons in the telencephalon, olfactory bulb, or olfactory epithelium (arrowheads, dorsal views). Scale bar = 50 μm **(D)**. The region in the dashed white box **(D)** was shown at higher magnification on the right **(D′–D‴)**. Scale bar = 20 μm. **(E–E‴)** Necab2-expressing neurons strongly overlapped with gad1b-positive neurons in the cerebellum (arrowheads, lateral views). Scale bar = 50 μm **(E)**. The region in the dashed white box **(E)** was shown at higher magnification on the right **(E′–E‴′)**. Scale bar = 20 μm. **(F–F‴)** Necab2-expressing neurons overlapped with gad1b-positive neurons in the hindbrain (arrowheads, dorsal views). Scale bar = 50 μm **(F)**. The region in the dashed white box **(F)** was shown at higher magnification on the right **(F′–F‴)**. Scale bar = 50 μm. **(G–G‴)** Co-immunofluorescent staining of the anti-Necab2 with anti-SV2 in 7 dpf larvae showed that Necab2 was enriched in the pre-synaptic structures (arrowheads). Scale bar = 20 μm **(G)**. The region in the dashed white box **(G)** is shown at higher magnification on the right **(G′–G‴)**. Scale bar = 10 μm. **(H–H‴)** Co-immunofluorescent staining of anti-Necab2 with anti-pan MAGUK in the 7 dpf larvae showed that Necab2 was enriched in the postsynaptic structures (arrowheads). Scale bar = 20 μm **(H)**. The region in the dashed white box **(H)** was shown at higher magnification on the right **(H′–H‴)**. Scale bar = 10 μm. dpf, day post-fertilization; Tel, telencephalon; Ce, cerebellum; Hb, habenula; OT, optic tectum; IPN, interpeduncular nucleus.

be enriched in structures resembling the synapses (**Figure 1E**). All the RNA probes and antibodies used in this study were verified (**Supplementary Figure 2**). Thus, in contrast to other calcium-binding proteins that confine to cytoplasmic domains, these results suggest that Necab2 might not be merely a cytoplasmic calcium buffer.

necab2 Is Expressed Peri-Synaptically in Subsets of Glutamatergic and GABAergic Neurons

To further characterize Necab2 expression at the cellular level, we established a transgenic reporter line, Tg (*Pnecab2:EGFP*), expressing EGFP under the control of upstream regulatory elements of the *necab2* gene. The fidelity of transgene expression was verified (**Supplementary Figures 3A,B**), and the EGFP signal was detectable at single-cell resolution (**Supplementary Figure 3C**). By crossing the reporter line with those that labeled glutamatergic [Tg(*vglut2a:DsRed*)], GABAergic [Tg(*gad1b:DsRed*)], and glycinergic [Tg(*glyt2:DsRed*)] neurons as well as performing immunofluorescent labeling of dopaminergic (anti-TH) and serotonergic (anti-5-HT) neurons, we found that *necab2* was expressed in subsets of glutamatergic and GABAergic (**Figure 2**) but not in other types of neurons (**Supplementary Figure 4**). In the glutamatergic neurons, Necab2 co-localized with Vglut2a in sub-regions of the telencephalon (**Figure 2A**),

diencephalon, tectum, cerebellum (**Figure 2B**), and hindbrain (**Figure 2C**). Notably, the overlap between *necab2*-expressing and *gad1b*-expressing neurons was not detectable in the forebrain (**Figure 2D**) but was prominent in the cerebellum (**Figure 2E**), and the hindbrain (**Figure 2F**). We also examined whether Necab2 was located pre-synaptically (labeled by anti-SV2) or post-synaptically (labeled by anti-pan MAGUK). Necab2 was enriched in both the pre-synaptic (**Figure 2G**) and post-synaptic structures (**Figure 2H**) in the cerebellum. Taken together, Necab2 displays restricted expression in subsets of excitatory and inhibitory neuronal terminals, suggesting that it might play a role in modulating synaptic signaling.

Generation of a *necab2* Mutant *via* CRISPR/Cas9 and *necab2* Over-Expressing Lines *via in vivo* Transgenesis

The function of *necab2* was further elucidated by knocking out the gene using CRISPR/Cas9 genome editing. A mutant allele was generated, containing 2 bp insertion (c.308_309 insCG) in front of the EF-hand domain (**Figure 3A**), resulting in a frameshift and a putative premature stop codon (p.Arg98*fs) (**Figure 3B**). Applying *in situ* hybridization and qPCR, we detected a significant decrease in *necab2* transcript levels in the mutant larvae (**Figures 3C,D**). The diminished *necab2* transcript in the mutant was presumably due to non-sense mediated RNA decay (Lykke-Andersen and Jensen, 2015). Since *necab1, necab2,* and *necab3* all share conserved domains with overlapping expression, it was evaluated whether the upregulation of *necab1* and *necab3* might compensate for the loss of *necab2*. A statistically significant increase was detected for *necab1* ($p = 0.0255$) but not *necab3* ($p = 0.4238$) transcripts (**Figure 3D**), suggesting potentially minimal compensation effects from these genes.

For gain-of-function studies, we generated overexpression lines of the two *necab2* isoforms (*necab2-001 and 201*) under the control of *hsp70*, a heat shock promoter. EGFP linked to Necab2 *via* the viral E2A element was used as a marker for screening (**Figure 3E**). The validity of Tg(*hsp:necab2-001:E2A:EGFP*) and Tg(*hsp:necab2-201:E2A:EGFP*) was verified by fluorescent imaging and semi-quantitative RT-PCR after 1 h 37°C heat-shock at 1 dpf (**Figures 3F,G**).

The *necab2* Mutant Exhibits Decreased Baseline Locomotor Activity, Reduced Thigmotaxis Behavior, and Impaired Social Interactions

Many aspects of development examined in the *necab2* mutant so far appeared normal: the grossly normal appearance (**Figure 4A**), normal neural development and cytoarchitecture (**Figure 4B**), and the balanced composition of neuronal subtypes (**Figure 4C**), as well as good fertility in adulthood (data not shown). To determine whether the *necab2* mutant displayed altered behaviors as those commonly observed in ASD patients, we recorded larval locomotion and anxiety-associated behaviors, adapted as markers of ASD behaviors in zebrafish (Kozol et al., 2015; Zimmermann et al., 2015; Li et al., 2019; Maphanga et al., 2020). To control for possible differences in genetic backgrounds, behavioral tracking was performed on the progeny derived from heterozygous $necab2^{+/-}$ mating, followed by blind genotyping (**Figure 5A**). The *necab2* mutant larvae showed a decrease in baseline locomotor activity, measured by both the speed ($p = 0.0136$) and the frequency of high activity ($p = 0.0007$) (**Figure 5B**). Thigmotaxis (i.e., preference for edges) is used as a measure of anxiety in rodents (Treit and Fundytus, 1988; Simon et al., 1994). Larval zebrafish also display this anxiety-like behavior as young as 5 dpf (Schnörr et al., 2012; Lundegaard et al., 2015). The preference index (PI,% time in edge –% time in the center) (**Figure 5C**) was quantified, which revealed that the mutant larvae had significantly lower PI ($p = 0.0480$), indicating either a reduced fear-like response or decreased cognition needed for spatial navigation (**Figure 5D**). Strikingly, overexpression of *necab2-201* isoform in larval stage yielded behaviors opposite to that of the mutant (**Figures 5B″,D″**). Overexpression of the *necab2-001* isoform in larval stage had milder effects and at times did not reach significance (**Figures 5B′,D′**). Taken together, opposite behaviors in the loss-of-function and gain-of-function models suggest that *NECAB2* is necessary and sufficient for promoting locomotor and thigmotaxis behaviors.

Since the *NECAB2* loss-of-function was found in ASD patients, we wondered whether the *necab2* mutant might exhibit altered social behaviors as observed in many zebrafish autism models (Kim et al., 2017; Liu et al., 2018). For that, the three-chamber social preference test was used (**Figure 5E**; Lachlan et al., 1998). Wild-type adult zebrafish preferred to stay in the conspecific arm (**Figure 5F**). Similar to the larval assays above, behavior tracking was done blindly on the adult progeny derived from heterozygous $necab2^{+/-}$ mating, followed by genotyping. Given the 4:1 male/female ratio observed in human autism (Schaafsma and Pfaff, 2014), data in different sexes were analyzed. We found that adult $necab2^{-/-}$ males spent significantly less time in the conspecific arm ($p = 0.0400$) and comparatively more time in the center arm ($p = 0.0075$) as well as the empty arm ($p = 0.0530$) than their wild-type counterparts in total and throughout the examination window (**Figures 5G–G‴**). In contrast to males, adult $necab2^{-/-}$ females manifested similar social preference compared to their wild-type counterparts (**Figures 5H–H‴**). Together, *necab2* deficiency impairs social interaction in adult zebrafish in a male-specific manner.

Necab2 Had Potential Roles in Modulating the G-Protein Coupled Receptor Signaling

Thus far, our data showed that *necab2*, which was expressed in synaptic terminals of glutamatergic and GABAergic neuronal subtypes, played a critical role in regulating psychomotor behaviors in larval zebrafish and social interactions in adult male zebrafish. To further probe its molecular and biochemical actions, we performed co-immunoprecipitation (Co-IP) using the anti-Necab2 antibody in both $necab2^{+/+}$ and $necab2^{-/-}$ zebrafish larvae followed by mass spectrometry (MS) to identify

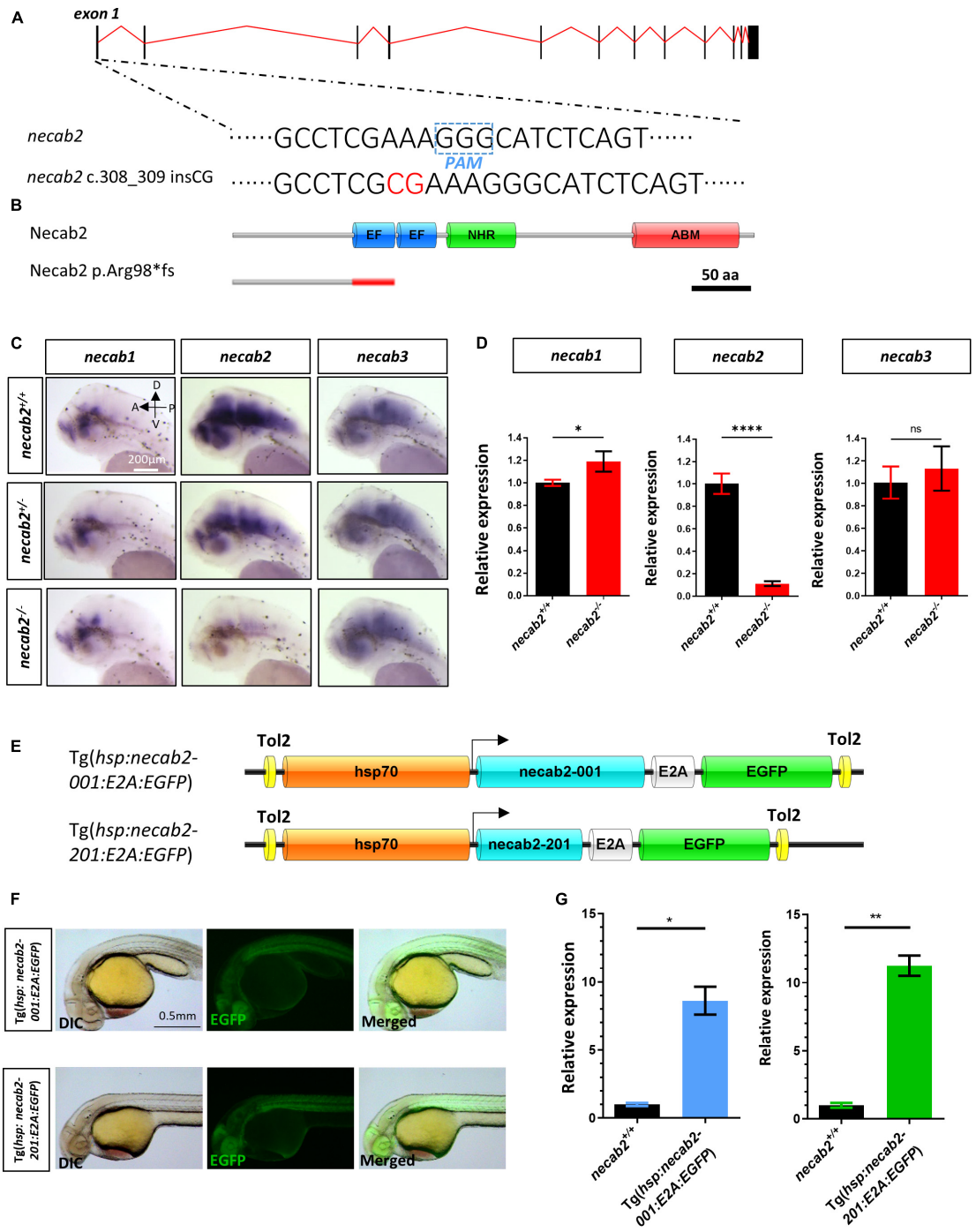

FIGURE 3 | Generation of a *necab2* mutant *via* CRISPR/Cas9 and necab2 over-expression lines by Tol2 transgenesis. **(A)** Schematic presentation of the genomic structure of *necab2* and a 2 bp insertion in exon1 generated by gene targeting *via* CRISPR. The PAM site was highlighted in the dashed blue box. The inserted base was shown in red. **(B)** Predicted structures of Necab2$^{+/+}$ and Necab2$^{-/-}$ proteins in zebrafish. The 2 bp insertion in exon 1 resulted in a frame-shift mutation and premature termination before the EF-hand domain. **(C)** Spatial analysis of *necab1*, *necab2*, and *necab3* mRNA by whole-mount *in situ* hybridization was performed blindly in the embryos derived from the in-cross of *necab2*$^{+/-}$ followed by genotyping. Scale bar = 200 μm. **(D)** Quantitative analysis of *necab1*, *necab2*, and *necab3* mRNA by qRT-PCR. The mRNA of *necab3* did not show a significant compensation effect while the upregulation of the *necab1* mRNA reached statistical significance. (ns $p \geq 0.05$, *$p < 0.05$, ****$p < 0.0001$, Student's *t*-test or Mann-Whitney *U* test). **(E)** Schematic presentation of the *Tol2* transgenic construction of Tg(*hsp:necab2-001:E2A:EGFP*) and Tg(*hsp:necab2-201:E2A:EGFP*). **(F)** Fluorescent imaging of the transgenic fish Tg(*hsp:necab2-001:E2A:EGFP*) and Tg(*hsp:necab2-201:E2A:EGFP*). Fish were processed for 37°C heat-shock for 1 h at 1 dpf. Scale bar = 0.5 mm. **(G)** Quantitative analysis of the *necab2* mRNA in Tg(*hsp:necab2-001:E2A:EGFP*) and Tg(*hsp:necab2-201:E2A:EGFP*) against their wild-type counterparts respectively by qRT-PCR. (*$p < 0.05$, **$p < 0.01$, Student's *t* test or Mann–Whitney U test.) dpf, day post-fertilization.

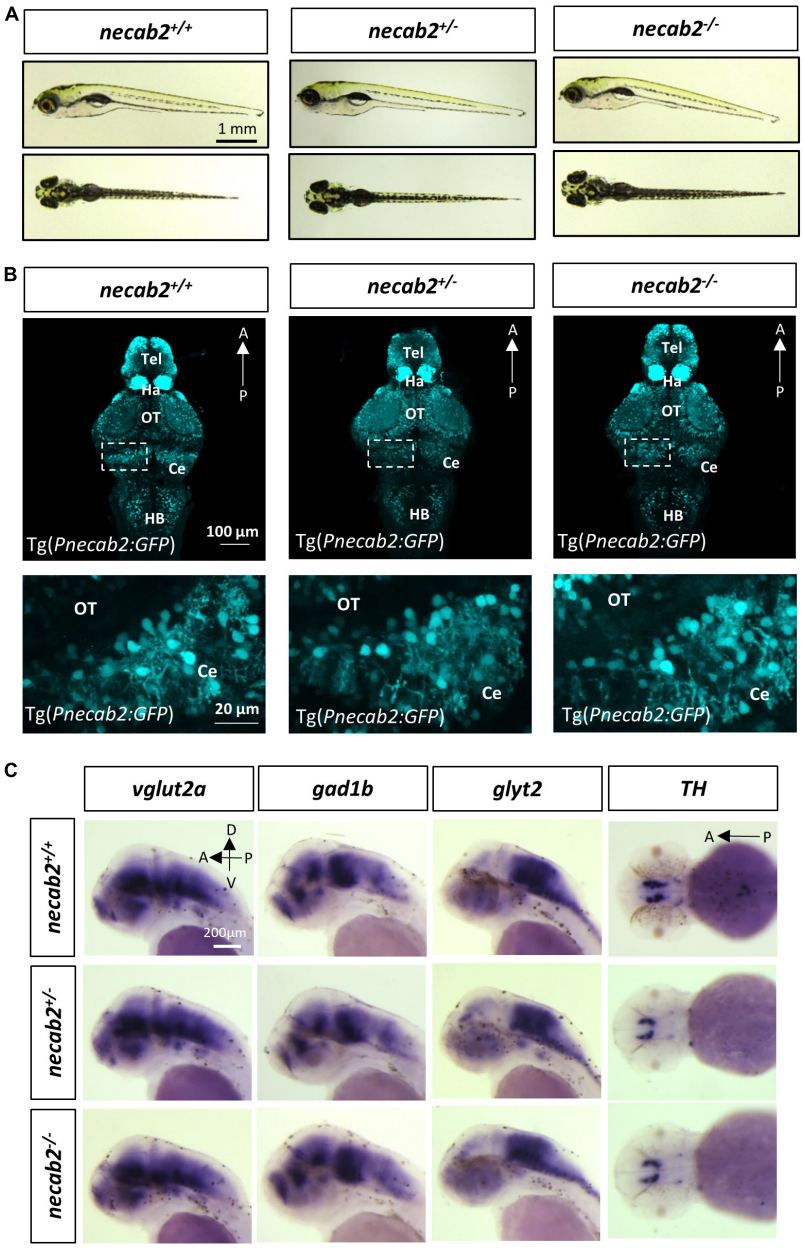

FIGURE 4 | The *necab2*$^{-/-}$ larvae display grossly normal morphology and neuronal marker expression. **(A)** The *necab2*$^{+/-}$ and *necab2*$^{-/-}$ larvae exhibited grossly normal appearance compared to wildtype siblings. The 7 dpf larvae derived from the heterozygous *necab2*$^{+/-}$ mating were imaged blindly and followed by genotyping. Scale bar = 1 mm. **(B)** The *necab2*$^{+/-}$ and *necab2*$^{-/-}$ larvae exhibited normal neural cytoarchitecture compared to wildtype siblings. A total of 7 dpf larvae were derived from heterozygous *necab2*$^{+/-}$ mating in the Tg(*Pnecab2:EGFP*) background. Genotyping using the dissected tail was done after fixation for anti-EGFP immunofluorescence staining. Scale bar = 100 μm. The region in the dashed white box was shown at higher magnification below. Scale bar = 20 μm. **(C)** The *necab2*$^{+/-}$ and *necab2*$^{-/-}$ larvae exhibit grossly normal composition of neuronal types. Spatial analysis of the glutamatergic (*vglut2a*), GABAergic (*gad1b*), glycinergic (*glyt2*), and dopaminergic (*TH*) neurons by whole-mount mRNA *in situ* hybridization was conducted blindly in the embryos derived from in-cross of *necab2*$^{+/-}$ followed by genotyping. For each group, a total of 20 larvae were processed for *in situ* hybridization in order to obtain at least three homozygous larvae respectively. Scale bar = 200 μm. dpf, day post-fertilization; Tel, telencephalon; Di, diencephalon; Ce, cerebellum; re, retina; Ha, habenula; OT, optic tectum; MHB, midbrain-hindbrain boundary; HB, hindbrain; lens, crystalline lens.

the Necab2 interactome *in vivo*. Coomassie blue staining on the Co-IP samples, followed by western blotting (WB), confirmed the presence of two Necab2 isoforms and the specificity of the antibody (**Supplementary Figure 5**). Proteins co-immunoprecipitated in the *necab2*$^{-/-}$ zebrafish larvae were presumed to be non-specific and therefore served as a control. A number of Necab2-interacting proteins were discovered using this approach (**Figure 6A**). Pathway enrichment analysis

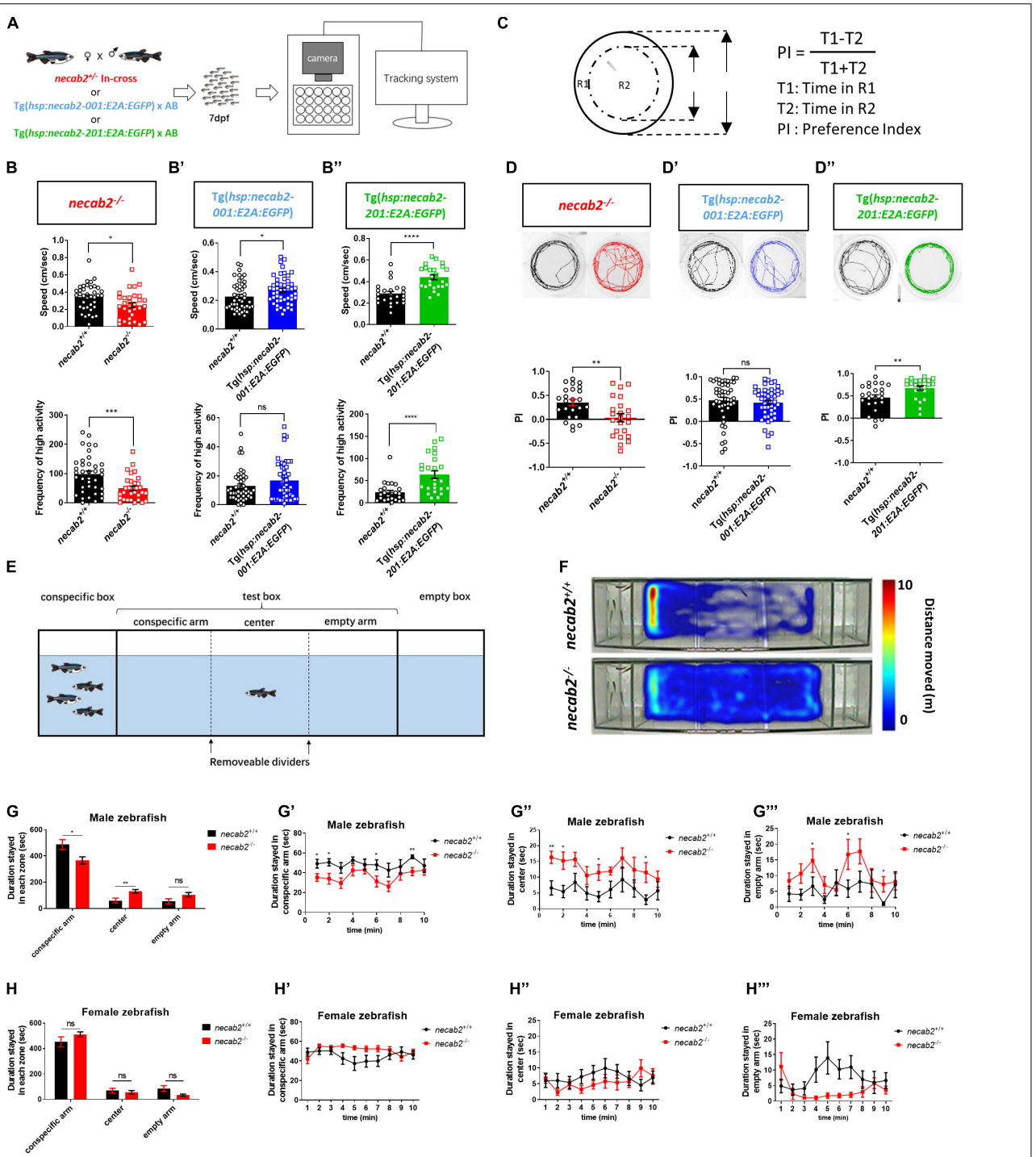

FIGURE 5 | Necab2 is necessary and sufficient to promote psychomotor, thigmotaxis, and social interaction. **(A)** Workflow and experimental setup. To control for potential differences in the genetic background, tracking experiments were performed blindly on the progeny from heterozygous *necab2*$^{+/-}$ mating. Genotyping was done after behavioral tracking by PCR. **(B–B′′)** *necab2*$^{-/-}$ (in red, $n = 31$, with sibling control $n = 38$) larvae exhibited locomotor hypo-activity while Tg(*hsp:necab2-001:E2A:EGFP*) larvae (in blue, $n = 48$, with sibling control $n = 45$) and Tg(*hsp:necab2-201:E2A:EGFP*) larvae (in green, $n = 24$, with sibling control $n = 24$) yielded the opposite. (ns $p \geq 0.05$, *$p < 0.05$, ***$p < 0.001$, ****$p < 0.0001$, Student's *t*-test or Mann-Whitney *U* test). **(C)** Diagram of the thigmotaxis behavior test. The equation for calculating the preference index (PI) was shown at right. PI was calculated as the subtraction of the locomotion duration in the outer region (R1) and inner region (R2) divided by the total duration. R1 and R2 were of the same area. **(D–D′′)** The *necab2*$^{-/-}$ (in red, $n = 23$, with sibling control $n = 24$) larvae exhibited decreased preference for the periphery region while Tg(*hsp:necab2-201:E2A:EGFP*) larvae (in green, $n = 23$, with sibling control $n = 24$) yields the opposite. Tg(*hsp:necab2-001:E2A:EGFP*) larvae (in blue, $n = 48$, with sibling control $n = 47$) showed no difference. (ns $p \geq 0.05$, **$p < 0.01$, Student's *t*-test or Mann-Whitney *U* test). **(E)** Diagram of the three-chamber social behavior test. Four unfamiliar conspecifics with mixed-sex were placed in the conspecific

(Continued)

FIGURE 5 | box while the box of the same size on the opposite end was empty. The test box in between was evenly divided into three zones—conspecific arm, center, and empty arm. The fish in the test was placed in the center bordered by two opaque dividers for one minute as adaption. **(F)** Representative heat maps of the duration stayed in each zone in the *necab2*$^{-/-}$ zebrafish and its wild-type sibling. **(G–G‴)** Duration stayed in each zone of the male progeny of in-crossed *necab2*$^{+/-}$ fish at 3 months old. Columns showed total duration spent in each zone of *necab2*$^{+/+}$ ($n = 9$) and *necab2*$^{-/-}$ ($n = 9$). Line diagrams showed the duration per minute spent in each zone. (ns $p \geq 0.05$, *$p < 0.05$, **$p < 0.01$ Student's *t*-test or Mann-Whitney *U* test). **(H–H‴)** Duration stayed in each zone of the female progeny of in-crossed *necab2*$^{+/-}$ fish at 3 months old. Columns showed total duration spent in each zone of *necab2*$^{+/+}$ ($n = 9$) and *necab2*$^{-/-}$ ($n = 9$). Line diagrams showed the duration per minute spent in each zone. (ns $p \geq 0.05$, Student's *t*-test or Mann-Whitney *U* test). The duration was not significantly different at each time point. Speed: average speed calculated by the computer in 15–30 min. Frequency of high activity: the times that more than 80% of the pixels from the zebrafish body moved per second.

identified significant interactions of Necab2 with proteins in several biological processes, including the protein lipase C-beta (PLCβ)-mediated events (R-DRE-112043), G-protein activation (R-DRE-202040), G-protein coupled serotonin receptor binding (GO:0031821), and G-protein beta/gamma-subunit complex binding (GO:0031683) (**Figures 6B,C**). These results indicate that Necab2 is involved in modulating signal transduction cascades of G-protein coupled receptors (GPCRs).

Necab2 Interacts With mGluR1 *in vitro*

Several studies have shown the emerging role of mGluR1, which is a member of the type I metabotropic glutamate receptors, in the development of ASD (Martin et al., 2010; Ribeiro et al., 2010; Tsai et al., 2012). Considering its abundance in the cerebellum and potential role as a GPCR modulator, we wondered whether Necab2 interacts with mGluR1. There are two paralogous loci of mGluR1, *grm1a* and *grm1b,* in the zebrafish genome (Haug et al., 2013). Due to the lack of full-length cDNA clones for the zebrafish genes, we performed co-IP using the mouse mGluR1 (*Grm1*) cDNA clone in cultured mammalian cells. In HEK293T cells, we detected an interaction between rodent NECAB2 and mGluR1 proteins (**Figure 6D**). To determine which NECAB2 domain(s) are responsible for mGluR1 binding, truncated forms of NECAB2 were combined with mGluR1 for transfecting HEK293T cells. Co-IP revealed that NECAB2 interacted with mGluR1 through the NHR domain (**Figure 6D″**), instead of the EF-hand domain (**Figure 6D′**) or the ABM domain (**Figure 6D‴**). To further explore the roles of NECAB2 domains, the Co-IP experiments between the NECAB2-Flag and EGFP-NECAB2, or the segmented domains with different tags, were performed. NECAB2s were able to interact with each other (**Figure 6E**), through either the NHR domain (**Figures 6E″,F**) or the ABM domain (**Figures 6E‴,F′**). The EF-hand domain did not participate in the self-interaction (**Figure 6E′**) and the NHR domain was not able to cross interact with the ABM domain (**Figure 6F″**). In summary, NECAB2 interacts with mGluR1 through the NHR domain *in vitro*. The NHR domain and the ABM domain probably play a role in the self-interaction of NECAB2.

Necab2 Interacts With mGluR1 *in vivo* and Is Sufficient to Promote mGluR1 Signaling

To explore whether Necab2 and mGluR1 interact *in vivo*, whole-mount immunofluorescent staining and confocal imaging were performed in the larval zebrafish cerebellar neurons. Since Grm1a, but not Grm1b has been identified in the cerebellum of zebrafish (Haug et al., 2013), a polyclonal antibody was raised in the rat against Grm1a, yielding good specificity (**Supplementary Figure 2C**). We first performed co-localization analysis of mouse Necab2 and Grm1a transfected into Hela cells. Strong co-localization of NECAB2 and mGluR1 was observed especially at the cell membrane (**Figures 7A–A″,B–B″**), which suggests possible membrane association of Necab2. We next identified *necab2*-expressing neuronal subtypes in the cerebellum by performing confocal live imaging in Tg(*Pnecab2:EGFP*) and Tg(*gad1b:DsRed*) backgrounds. The results indicated that necab2 is expressed both in the GABAergic Purkinje neurons or interneurons (**Supplementary Figures 6A–A‴**) and the glutamatergic granule neurons (**Supplementary Figures 6B–B‴,C–C‴**). More specifically, Necab2 was abundant in Pvalb7-positive Purkinje neurons (**Figures 7C–C‴**) and colocalized with mGluR1 (**Figures 7D–D‴**). Together, these results indicate that Necab2 is associated with mGluR1 at the membrane of GABAergic Purkinje cells.

To explore whether the interaction between Necab2 and mGluR1 has functional relevance, we measured the downstream effectors of mGluR1 signaling. Stimulation of type I mGluR1 activates phospholipase C (PLC), which hydrolyzes phosphatidylinositol 4,5-bisphosphate (PIP2) to produce inositol trisphosphate (InsP3) and diacylglycerol (DAG), thereby increasing intracellular calcium concentration, stimulating protein kinase C (PKC), and generating slow excitatory postsynaptic currents (Venkatachalam and Montell, 2007). Measurement of PIP2 hydrolysis *in vivo* has been developed by injecting mRNAs encoding the PH domain of PLC (*that is*, the PIP2 binding domain) into zebrafish embryos (Gong et al., 2017). By fusing with mCherry, the red fluorescent signal of PLC-PH-mCherry protein indicates the abundance of PIP2 in cell membrane. By generating the transgenic line Tg(*hsp:plc-ph:mCherry*), we measured the PLC-PH-mCherry signal in *necab2*$^{-/-}$ and WT siblings at 7dpf (**Figure 7E** and **Supplementary Figure 7**). The PLC-PH-mCherry protein was abundant in the cerebellum showing strong membrane association indicating a high content of PIP2 in this region (**Figures 7E–7E‴**). Confocal live imaging was performed on the progeny derived from the heterozygous *necab2*$^{+/-}$ mating, followed by blind genotyping. Compared to their *necab2*$^{+/+}$ siblings (**Figures 7F–F″**), *necab2*$^{-/-}$ larvae accumulated more PLC-PH-mCherry at the cell membrane of *necab2*-expressing cells identified by Tg(*Pnecab2:EGFP*) (**Figures 7G–G″**). Semi-quantitative measurement of the plasma/cytosol mCherry

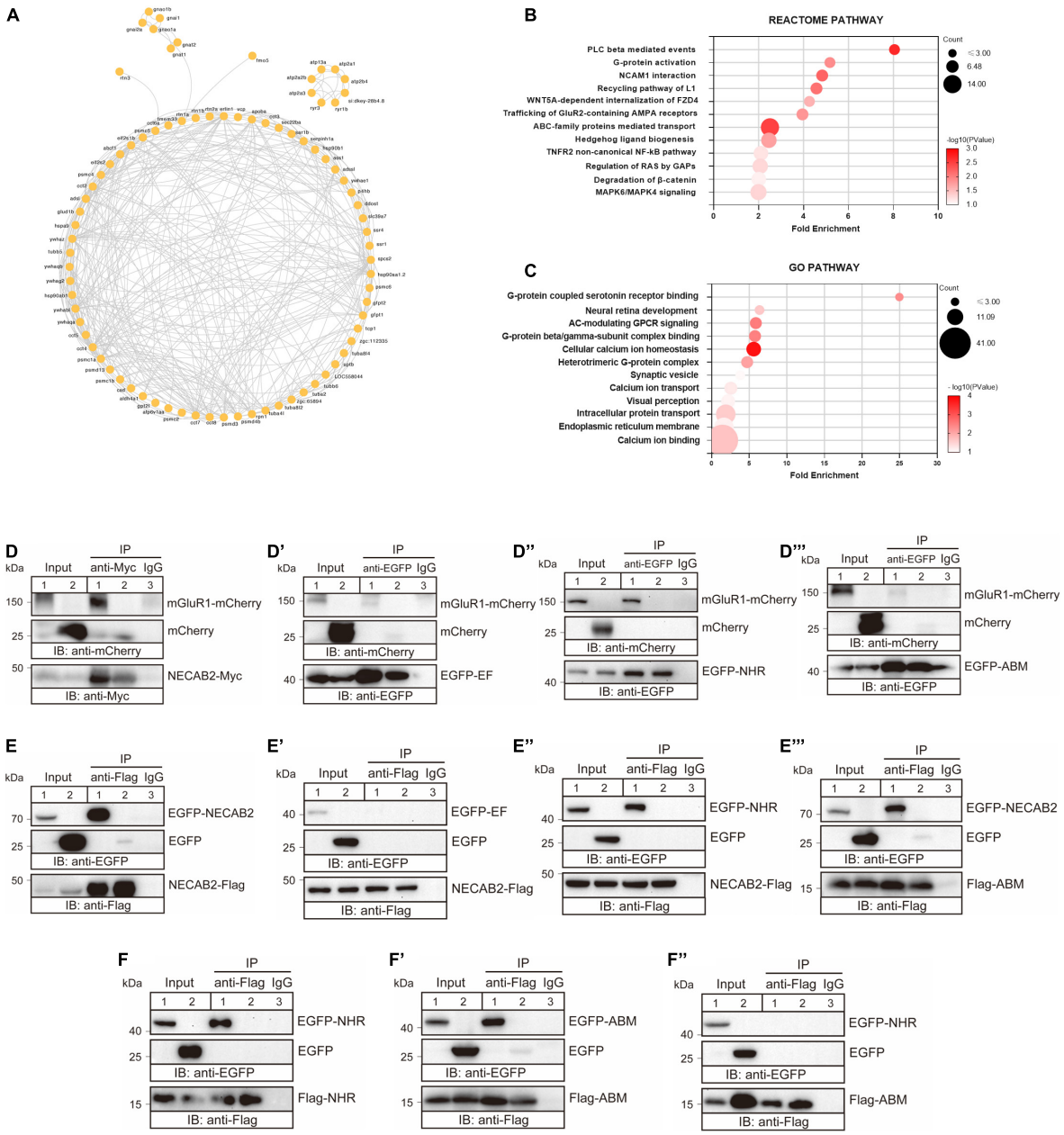

FIGURE 6 | NECAB2 interacts with mGluR1 *in vitro*. **(A)** Overview of the protein interaction network derived from the Necab2 co-immunoprecipitation and subsequent mass spectrometry in the *necab2*$^{+/+}$ and *necab2*$^{-/-}$ larvae. **(B)** REACTOME analysis revealed the significant biological processes detected in the *necab2*$^{+/+}$ larvae compared to the *necab2*$^{-/-}$ larvae. **(C)** Gene Ontology (GO) analysis revealed the significant biological processes detected in the *necab2*$^{+/+}$ larvae compared to the *necab2*$^{-/-}$ larvae. **(D–D‴)** NECAB2 interacts with mGluR1 through the NHR domain uncovered by co-immunoprecipitation analysis. The HEK293 cells were transiently transfected with mGluR1-mCherry plus NECAB2-Myc **(D)**, EGFP-EF **(D′)**, EGFP-NHR **(D″)**, or EGFP-ABM **(D‴)** for lane 1 and lane 3 respectively, and indicated vectors plus mCherry-vector for lane 2 and processed for immunoprecipitation using mouse anti-Myc antibody **(D)** or anti-EGFP antibody **(D–D‴)**, with normal mouse IgG for negative control in lane3. The crude extracts (Input) and immunoprecipitations (IP) were analyzed by SDS-PAGE and immunoblotted using the rabbit anti-mCherry antibody **(D–D‴)**, mouse anti-Myc antibody **(D)** or mouse anti-EGFP antibody **(D′–D‴)**. **(E–E‴)** NECAB2 has self-interaction through either NHR or ABM domain uncovered by co-immunoprecipitation analysis. The HEK293 cells were transiently transfected with NECAB2-Flag plus EGFP-NECAB2 **(E)**, NECAB2-Flag plus EGFP-EF **(E′)**, NECAB2-Flag plus EGFP-NHR **(E″)**, or NECAB2-Flag plus EGFP-ABM **(E‴)** for lane 1 and lane 3, and the indicated vectors plus EGFP-vector for lane 2 and processed for immunoprecipitation using mouse anti-Flag antibody, with normal mouse IgG for negative control in lane 3. The crude extracts (Input) and immunoprecipitations (IP) were analyzed by SDS-PAGE and immunoblotted using mouse anti-EGFP antibody **(E–E‴)** or mouse anti-Flag antibody **(E–E‴)**. **(F–F″)** Co-immunoprecipitation analysis of NHR and ABM domains showed self-interaction but no cross-interaction of the two domains. The HEK293 cells were transiently transfected with Flag-NHR plus EGFP-NHR **(F)**, Flag-ABM plus EGFP-ABM **(F′)**, and Flag-ABM plus EGFP-NHR **(F″)** for lane 1 and lane 3, and indicated vectors plus EGFP-vector for lane 2 and processed for immunoprecipitation using the mouse anti-Flag antibody, with normal mouse IgG for negative control in lane3. The crude extracts (Input) and immunoprecipitations (IP) were analyzed by SDS-PAGE and immunoblotted mouse anti-Flag antibody **(F–F″)** or mouse anti-EGFP antibody **(F–F″)**.

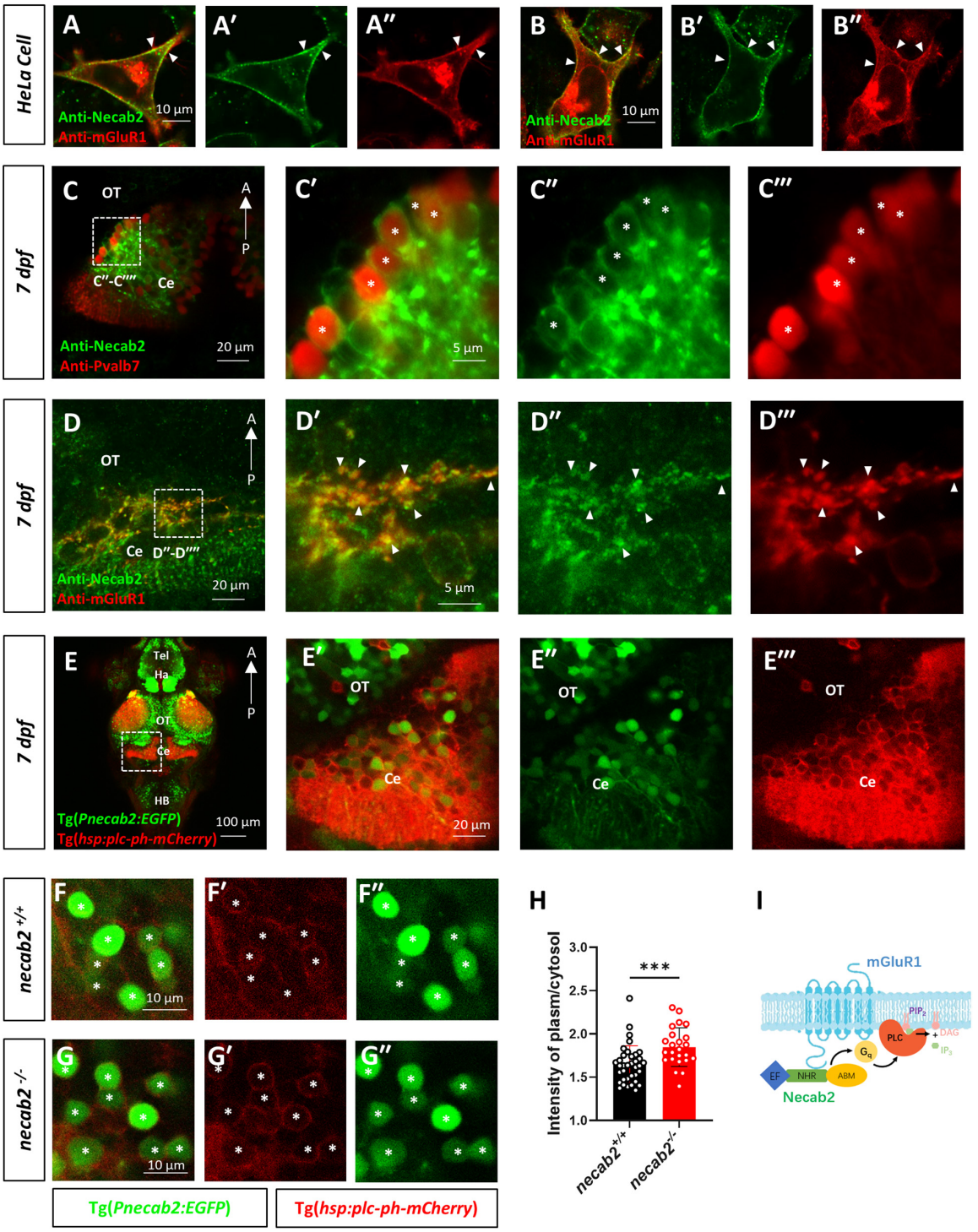

FIGURE 7 | Necab2 co-localizes with mGluR1 and promotes PIP2-PLC-PKC signaling. **(A–A″,B–B″)** NECAB2 and mGluR1 colocalize at the cell membrane of HeLa cells (arrowheads). The HeLa cells were transiently transfected with EGFP-NECAB2 and mGluR1-mCherry and live imaging was conducted with the confocal microscope. Scale bar = 10 μm. **(C–C‴)** Co-immunofluorescent staining of anti-Necab2 with anti-Pvalb7 in 7 dpf larvae showed that Necab2 was expressed in the Purkinje cells in the cerebellum (asterisks). Scale bar = 20 μm **(C)**. The region in the dashed white box **(C)** is shown at higher magnification on the right **(C′–C‴)**. Scale bar = 5 μm. **(D–D‴)** NECAB2 and mGluR1 co-localized in the cerebellum of the zebrafish larvae (arrowheads). The *necab2*$^{+/+}$ larvae at 7 dpf were processed for anti-Necab2 and anti-mGluR1 immunofluorescence staining following fixation. Scale bar = 20 μm **(D)**. The region in the dashed white box **(D)** was shown at higher magnification on the right **(D′–D‴)**. Scale bar = 5 μm. **(E–E‴)** Live imaging of *necab2*$^{+/+}$ larvae at 7 dpf in Tg(*hsp70:plc-ph-mCherry*) and Tg(*Pnecab2:EGFP*) background by confocal microscope. Z-stack, Maximum intensity projection. Scale bar = 100 μm **(E′)**. The cerebral region (in the dashed white box) was shown at higher magnification on the right **(E′–E‴)**. Scale bar = 20 μm. **(F–F″,G–G″)** The *necab2*$^{-/-}$ larvae accumulated more PLC-PH-mCherry at the

(Continued)

FIGURE 7 | cell membrane of the necab2-expressing cells (asterisks) than that of the *necab2*$^{+/+}$ larvae. Genotyping of the 7 dpf larvae derived from heterozygous *necab2*$^{+/-}$ in the Tg (*Pnecab2:EGFP*) and Tg(*hsp70:plc-ph-mCherry*) background mating was done after live imaging with the confocal microscope. Scale bar = 10 μm. **(H)** The quantification of the PLC-PH-mCherry intensity in the *necab2*$^{-/-}$ larvae ($n = 6$) and *necab2*$^{+/+}$ ($n = 4$) larvae by calculating the fluorescent intensity of plasma/cytosol. Two different sections per larva and three independent necab2-expressing cells per section were analyzed. (***$p < 0.001$, Mann–Whitney U test). **(I)** The summary of Necab2 interacting with mGluR1. Necab2 bound mGluR1 through the NHR domain. Necab2 was likely to facilitate the mGluR1 mediated PLC-PIP2-PKC signaling. dpf, day post-fertilization; Tel, telencephalon; Ha, habenula; OT, optic tectum; Ce, cerebellum; HB, hindbrain.

intensity suggested more PIP2 and reduced PLC-PIP2-PKC signaling in the *necab2*$^{-/-}$ larvae ($p = 0.0003$) (**Figure 7H**). In support of Necab2's role in regulating mGluR1 signaling rather than its synthesis or localization, we found that the expression of mGluR1 was unchanged in *necab2*$^{-/-}$ (**Supplementary Figures 6D,E**).

Thus, our data suggest that Necab2 interacts with mGluR1 to promote its signaling in cerebellar Purkinje and possible other neuronal types. Necab2 binds to mGluR1 through the NHR domain. The interaction facilitates the PIP2 hydrolysis and probable mGluR1 mediated downstream signal transductions to mediate neuronal activation (**Figure 7I**).

DISCUSSION

Genotypic and phenotypic complexities in ASD patients have been well recognized (Vorstman et al., 2017). Although the number of ASD candidate loci has expanded significantly, functional studies significantly lag behind. *NECAB2* is a potential risk gene for ASDs. A segmental deletion in the *NECAB2* gene spanning the human chromosome 16q23.3-q24.1 has been reported in a proband with idiopathic ASD (Sakai et al., 2011). Two individuals with deletions in chromosome 16q23.3 encompass *NECAB2* and three additional genes have also been reported (Itsara et al., 2010; Sanders et al., 2011; **Supplementary Table 1**). Meanwhile, missense mutations in *NECAB1* are associated with developmental language disorders, one of the frequent comorbidities in autism (Kornilov et al., 2016). Despite the roles in pro-nociceptive pain signaling in the spinal cord (Zhang et al., 2014, 2018; Ma et al., 2021), the potential role of *NECAB2* in the brain remains largely elusive. In this study, we have reported the *in vivo* brain distribution of *necab2* at both tissue, cellular, and subcellular levels. We have also investigated the morphological and behavioral phenotypes in both the loss-of-function and gain-of-function models of zebrafish. Furthermore, *necab2* was found to interact with mGluR1 both *in vitro* and *in vivo* and such interaction served to modulate mGluR1 signaling *via* the PLC-PIP2-PKC cascade in the cerebellum.

The *necab2* knock-out zebrafish generated *via* CRISPR developed normally but showed altered psychomotor and social behaviors. The double-blind, high-throughput behavior analysis in larvae demonstrated that the *necab2*$^{-/-}$ larvae were hypoactive, less anxious, or cognitively compromised in spatial navigation, while the *necab2*-overexpressing larvae demonstrated behavioral phenotypes that were opposite to the loss-of-function model. The impaired locomotor activity was commonly observed in other zebrafish models of autism (Bailey et al., 2016; Lee et al., 2018; Liu et al., 2018). The reduction in the thigmotaxis was also reported in some ASD models, such as the *shank3b* mutant (Liu et al., 2018). Therefore, the amenability to these behaviors as high-throughput assays for small molecule drug screening is a tremendous advantage of the zebrafish model. Importantly, the social deficits observed in the *necab2* knock-out zebrafish were reminiscent of that in ASD patients, reinforcing the notion that disruption of *necab2* causes ASD-relevant symptoms. It is interesting to note that only male zebrafish exhibit impaired social interaction, which correlates well with the high male/female ratio in ASD patients and lower penetrance of ASD in female patients (Lai et al., 2015). One possible explanation is that estrogen has a protective effect against ASD since estrogen was found to ameliorate ASD-like behaviors in zebrafish larva (Hoffman et al., 2016). Meanwhile, the interaction between estrogen receptors and mGluR1 could facilitate the glutamatergic neurotransmission at parallel fiber-Purkinje cell synapses (Hedges et al., 2018). However, the exact mechanism underlying the male-specific social defects in *necab2*$^{-/-}$ zebrafish warrants further investigations. Additional behavioral assays are certainly needed to further explore other ASD-related behaviors in the *necab2* mutants, such as learning and cognitive impairments.

It is interesting to note that Necab2 was abundant in the GABAergic cerebellar Purkinje cells. The cerebellum not only coordinates a person's motor ability but also plays an important role in language, emotion, and cognition (Wang et al., 2014). The cerebellar role in autism has been highlighted in neuroanatomical (Amaral et al., 2008), neuroimaging (D'Mello et al., 2015), and gene-expression studies (Menashe et al., 2013). The decrease in the number and activity of Purkinje cells was evident in either ASD patients (Ritvo et al., 1986) or gene knock-out models (Tsai et al., 2012). Subcellularly, Necab2 was not confined to cell bodies but was abundantly detected in peri-synaptic structures, leading to the hypothesis that Necab2 might be involved in synaptic signal transduction, the dysfunction of which has been regarded as one of the key features in ASD pathophysiology (Ebrahimi-Fakhari and Sahin, 2015; Masini et al., 2020). Combined with ASD-like behaviors in the *necab2*$^{-/-}$ model, our finding relating to cerebellar Purkinje cells provides an excellent cellular context to further probe Necab2's role in regulating synaptic physiology.

Although NECAB2 has been identified about 20 years ago (Sugita and Sudhof, 2000), the understanding of its molecular role and biochemical function is still limited. One of the most important aspects of our findings was the establishment of a physical interaction between Necab2 and mGluR1. Defects in the type I mGluRs and their downstream signaling events have been considered to be one of the major causes of autism (Zoghbi and Bear, 2012). In contrast to the ionotropic glutamate receptors that mediate fast excitatory synaptic transmission,

mGluRs modulate neuronal excitability and synaptic plasticity through a variety of intracellular second messengers (Niswender and Conn, 2010). mGluR1 couples to G_{α} q/G11 to activate the PLC-β, which cleaves PIP2 into DAG and InsP3. InsP3 then binds to its corresponding receptor on the ER membrane to increase the cytoplasmic Ca^{2+} ion levels (Katan and Cockcroft, 2020). Both Ca^{2+} and DAG stimulate PKC to phosphorylate AMPA, which leads to internalization and long-term depression. Our study found that the *necab2* knock-out accumulated PIP2 in the cell membrane, indicating a reduced PLC-β activity and in turn downstream PKC activity. This observation suggests that Necab2 facilitates the signaling transduction of mGluR1. Our study further showed that Necab2 bound mGluR1 through NHR domain. The NHR domain and ABM domain probably involve in the self-interaction of NECAB2, however, the exact roles warrant further studies. Previously, NECAB2 was found to interact with another type I mGluR member, mGluR5, and potentiate its subsequent IP3 accumulation (Canela et al., 2009). Though, the exact significance of the macromolecular complexes composed of mGluR1 and Necab2 remained to be clarified, we speculated that the interaction among mGluR1, Necab2, and other potential protein, similar to the interaction between mGluR5 and NECAB2, probably promote subsequent signaling by ensuring the proximity of G-proteins or PLCβ with mGluR1. However, testifying the above hypothesis demands additional experiments. For one thing, it will be interesting to find out whether an increase in cytoplasmic Ca^{2+} has a regulatory role over the interaction between Necab2 and mGluR1 *in vivo*.

LIMITATION

The significance of our study is limited by the following points: First, the expression of necab2 was only profiled in the larva stage. It remains to be investigated whether the expression pattern differs in the adult brain. Second, the interaction between Necab2 and mGluR1 is validated in both transfected cells and intact brains, but the evidence for Necab2 modulating mGluR1 signaling is still limited. Future biochemical experiments should be performed in the zebrafish model with a focus on how necab2 promotes mGluR1 signaling through the interaction and its downstream effects. Third, Necab2 has a relatively broad expression spectrum in the nervous system, and the role of Necab2 in other types of neurons should not be neglected. Another potential drawback of our study is the absence of the rescue experiment. Finally, the homology between zebrafish and humans should be cautioned especially when interpreting the behaviors.

CONCLUSION

In conclusion, this study has shed new light on the *in vivo* function of *necab2*, a locus associated with ASD risk. We characterized the phenotypes of *necab2* loss-of-function and gain-of-function in the zebrafish models and provided direct evidence for the interaction between Necab2 and mGluR1 both *in vitro* and *in vivo*. The domains involved in the interaction were also mapped. Manifestation of ASD-like behaviors in the *necab2* loss of function model further helps establish *necab2* as a disease-causing locus and provides a new avenue for mechanistic studies and therapeutic discovery.

MATERIALS AND METHODS

Protein Diagrams and Polygenetic Tree

Protein diagrams of the NECAB2 orthologs in *H. sapiens*, *M. musculus*, and *D. rerio* were generated using IBS 1.0 from published NCBI protein sequences (Liu et al., 2015). Phylogenetic tree of the evolutionary relationship of NECAB2 proteins and evolutionary analyses were conducted using the MEGA7 software (Kumar et al., 2016).

Zebrafish Maintenance and Strains

The zebrafish were raised and maintained in accordance with a standard protocol (Westerfield, 2000). All wildtype zebrafish used in the present study are AB strain. The *necab2* mutant was generated using the CRISPR/Cas9 technology as described previously (Hwang et al., 2013). The *necab2* sgRNA (AATTTAATACGACTCACTATAGGGCTTCGCGCCGGAGCC TCGAAGTTTAAGAGCTATGCT) was transcribed *in vitro* from the DNA templates of the amplified PCR products of the pMD19-T-gRNA vector (CZRC, China). The Cas9 mRNA was generated *in vitro* by transcription with a linearized plasmid pT3TS-nlszCas9-nls (CZRC, China). The *Cas9* mRNA and *necab2* sgRNA were co-injected into the one-cell stage embryos. The positive founders were mated with the wild-type fish to obtain F1 generation. The F1 heterozygous zebrafish with identical frameshift mutations were intercrossed to generate an F2 homozygous mutant.

The Tg (*hsp:necab2-001:E2A: EGFP*) and Tg (*hsp:necab2-201:E2A: EGFP*) were generated *via* the Tol2 transposition system as described previously (Kawakami et al., 2016). Briefly, the *necab2-001* or *necab2-201* cDNA fragment was cloned into the pT2KhspGFF. The transposase mRNA was generated by *in vitro* transcription with a linearized plasmid pCS-zTP. A Tol2-donor plasmid DNA and the transposase mRNA were introduced into the zebrafish fertilized eggs by microinjection. The positive founders were mated with wild-type fish to obtain F1 generation. The larvae were raised at 29°C and heat-shocked at 1 dpf for 1.5 h before screening or experiments. The Tg (*hsp:plc-ph:mCherry*) was produced by cloning the PH domain of the PLC fused with mCherry from pXT7-PLCδ1a-PH-mCherry into the pT2Khsp. The plasmid was obtained from the laboratory of the Shunji Jia at Tsinghua University.

The reporter line, Tg (*Pnecab2:EGFP*) was generated similarly. The full-length upstream promoter region was cloned into the pT2KhspGFF after being verified by the Sanger sequencing. The fragment length we cloned is 7848 bp located in Chromosome 18: 21,401,324-21,409,171 (NC_007129.7), which contains the potential regulating sequences spanning from the 3′UTR of the upstream gene (*hydin*) to the intron between exon 1 and exon 2 of *necab2*.

The Tg(*vglut2a:DsRed*), Tg(*gad1b: DsRed*), and Tg(*glyt2:DsRed*) lines were obtained from the National BioResource Project, Zebrafish, Core Institution (Saitama, Japan), and were deposited by the National Institute of Natural Science (Dr. Shin-ichi Higashijima) (Higashijima et al., 2004).

Behavior Profiling

The behavioral assays were conducted as described previously (Bai et al., 2016). Behavioral testing was performed in the *DanioVision* system at a constant water-bath temperature of 29°C and at time-points between 11:00 and 16:00 h to avoid unexpected factors that might contribute to locomotion. High activity is defined as more than 80% change of the pixels of the targeted larva during one frame, which is defined and measured by the built-in algorithm. All the behaviors were tracked at 60 frames per second. To control for potential differences in genetic backgrounds, all the tracking experiments for mutants were performed blindly on the progeny of heterozygous mating. After tracking, the genomic DNA was isolated from individual larvae and genotyping was done by PCR. Behavior profiling was done in 7 dpf larvae and 3-month-old zebrafish, respectively. Larvae of overexpression lines were derived from Tg(*hsp:necab2-001:E2A:EGFP*) and Tg(*hsp:necab2-201:E2A:EGFP*) mating with wildtype respectively, and were raised at 29°C and tested after 1.5 h at 37°C heat-shock and 1 h at 29°C for accommodation. The genotypes were identified by selecting the fluorescent larvae under the microscope after behavior tracking, while the larvae without fluorescent were identified as sibling controls.

In vivo PIP2 Assay and Confocal Live Imaging

The PIP2 assay was performed according to the previously study with some modifications (Haug et al., 2013). Confocal imaging and fluorescent quantitative analysis were performed blindly on the progeny of heterozygous *necab2*$^{+/-}$ mating. The larvae were mounted in low melt agarose and live-imaging was performed under the Zeiss LSM880 confocal microscope (Zeiss). Images were processed using the ZEN2012 software (Zeiss) and the quantification analysis was performed to measure the intensity of the plasma/cytosol using the ImageJ (64-bit Java 1.8.0_172). Specifically, the area and fluorescent intensity of the whole cell and the cytoplasm were outlined and measured manually. The intensity of the plasma membrane was calculated by subtraction: the plasma fluorescent intensity = (mean fluorescent intensity of whole cell × area of whole cell − mean fluorescent intensity of cytosol × area of cytosol)/(area of whole cell − area of cytosol). The plasma/cytosol intensity = mean fluorescent intensity of plasma/mean fluorescent intensity of cytosol. Subsequently, genomic DNA was isolated from individual larvae and genotyped *via* PCR.

In situ Hybridization and Immunohistochemistry

In situ hybridization was performed according to the previously described method with some modifications (Peng et al., 2009). Briefly, larvae were fixed in 4% PFA at different ages after PTU treatment to inhibit pigment synthesis. Embryos were hybridized with the designed digoxin-labeled RNA probe. After staining, embryos were washed in PBST and cleared in benzyl benzoate/benzyl alcohol for imaging.

Whole-mount antibody staining of dissected embryos was performed as previously described, with some modifications (Peng et al., 2009). Briefly, larvae were fixed in 4% PFA at different ages following PTU incubation. After fixation, embryos were washed in PBS, dissected, blocked for at least 1 h at room temperature, and incubated in the primary antibodies overnight at 4°C. Embryos were washed 4–6 times in PBT and incubated in secondary antibodies overnight at 4°C. Afterward, embryos were washed 4–6 times at room temperature and mounted for imaging in low melt agarose (0.8–1%). The tubes containing embryos were rotated at each step.

The primary antibodies used in this study were as follows: The polyclonal rabbit anti-Necab2 antibodies were raised against the full-length zebrafish Necab2 protein (1 aa–428 aa) in association with the GeneCreate Biological Engineering Co., Ltd., in Wuhan, China, and used in 1:500 dilution. The polyclonal rat anti-GRM1 antibodies were raised against the C-terminal zebrafish grm1a protein (GDGKPAPCQSNSILNMFRRKKNNNNATGST NPNGKSVSWSESGARPQGRGSSVFHRLSVHVRRQAVGQSQ TAVIRPLTNASQPPESEYGAGLNTAPNGSHPDDKDLYNLGEG HDGGPQHPTAQEGGLPPSY) in collaboration with Dia-An Biotech, Inc., in Wuhan, China, and used in a 1:500 dilution. Other primary antibodies included: the mouse IgG1 anti-SV2 (1:500 dilution, DSHB, AB_2315387), mouse anti-pan-MAGUK (1:500 dilution, Antibodies Inc., AB_10673115), chicken anti-EGFP (1:500 dilution, Aves Labs, AB_2307313), and mouse anti-Pvalb7 (1:1,500 dilution, MYBioSource, MBS1321475).

The secondary antibodies used in this study were as follows: goat anti-rabbit 647 (1:1,000 dilution, abcam, ab150079), Anti-rat 568 (1:1,000 dilution, abcam, ab175476), and goat anti-Chicken 568 (1:1000 dilution, abcam, ab175477).

Immunoprecipitation and Immunoblotting

For immunoprecipitation, HEK293 cells were transfected using the pCMV6 plasmids, into which cDNAs of truncated domains of NECAB2 and mGluR1 from mouse plus indicated tags were cloned, and Lipofectamine 2000 (Invitrogen) was used. The transiently-transfected HEK293 cells or zebrafish tissues were solubilized in the NETT lysis buffer (50 mM Tris-HCl, 150 mM NaCl, 0.1 mM EDTA, and 1% Triton X-100) following ultrasonic crushing. After centrifugation, supernatants were incubated overnight at 4°C with the mouse anti-Flag antibody (1 μg, Sigma, F1804), mouse anti-Myc antibody (1 μg, MBL, M192-3), mouse anti-EGFP antibody (1 μg, Abmart, M20004S), rabbit anti-Necab2 antibody (1 μg) or normal mouse IgG (1 μg, EMD Millipore Corporation, M12-371). Then, the protein A/G agarose beads (Santa Cruz Biotechnology) were added and rotated at 4°C for another 4 h. The beads were then washed by NETT buffer 5 times and finally boiled in the loading buffer for SDS-PAGE.

For immunoblotting, samples were fractionated on SDS polyacrylamide gels and transferred to PVDF membranes (Millipore). Afterward, membranes were immunoblotted with the mouse anti-Flag antibody (1:5,000 dilution, Sigma, F1804), mouse anti-Myc antibody (1:5,000 dilution, MBL, M192-3), mouse anti-EGFP antibody (1:5,000 dilution, Abmart, M20004S), rabbit anti-mCherry antibody (1:5,000 dilution, Abcam, ab183628), or rabbit anti-Necab2 antibody (1:5,000 dilution) followed by incubation in the correspondent secondary antibody (1:5,000 dilution, HRP-conjugated goat anti-mouse/rabbit IgG, CWbio, CW0102S/CW0103S). The immunoreactive bands were developed using an efficient chemiluminescence kit (Bio-Rad).

Mass Spectrometry

The PAGE-resolved proteins were identified by mass spectroscopy using the LTQ Orbitrap Elite (Thermo Fisher Scientific) from the State Key Laboratory of Genetic Engineering of the School of Life Sciences, Fudan University, Shanghai, China. The protein-protein interaction network was based on STRING (Search Tool for the Retrieval of Interacting Genes/Proteins, available online at website: www.string-db.org) and repainted by the RStudio. The pathway analysis was based on DAVID (the Database for Annotation, Visualization, and Integrated Discovery) Bioinformatics Resources using the Reactome V62 and Gene Ontology. All of the non-human identifiers were converted to their human equivalents.

Statistical Analysis

Statistical analyses were performed using SPSS version 25.0 (64-bit edition, IBM Corp., Armonk, NY, United States). The normality of the data was confirmed by the Shapiro-Wilk test and the quantitative variables were presented as mean ± standard error and median (quartiles) where appropriate. The descriptive variables were shown in the counts or proportions. The student's *t*-test or Mann–Whitney U test was applied as appropriate for comparing the two independent groups. The one-way analysis of variance or Kruskal–Wallis test was used to compare the three or more independent groups. All the analyses were two-tailed, and the statistical significance was set as a p-value of < 0.05. The results of the two-sided tests were considered significant at $p < 0.05$.

DATA AVAILABILITY STATEMENT

The datasets presented in this study can be found in online repositories. The names of the repository/repositories and accession number(s) can be found in the article/**Supplementary Material**.

ETHICS STATEMENT

The animal study was reviewed and approved by Human Research Ethics Committee of Fudan University.

AUTHOR CONTRIBUTIONS

ZC, JG, and HL constructed the zebrafish models. CT and HL performed the immunostaining. HL performed the behavior profiling. YW and HL carried out the western-blot and Co-IP. ZC and XL performed the confocal imaging. ZC and SG wrote the first draft of the manuscript. KH and KJ critically reviewed the manuscript. SG and YP supervised the project. All authors contributed to the study conception and design and read and approved the final manuscript.

FUNDING

This project was supported by the National Key Research and Development Program (2016YFC0906400).

ACKNOWLEDGMENTS

We thank Shouyi Qiao and Huijuan Gu for their generous support. We are grateful to Ruilin Zhang, Gang Wang, and their laboratory members for technical assistance and helpful discussion. We sincerely thank Jiajun Zhu for help of proteomic profiling.

SUPPLEMENTARY MATERIAL

The Supplementary Material for this article can be found online at: https://www.frontiersin.org/articles/10.3389/fnmol.2022.901682/full#supplementary-material

Supplementary Figure 1 | Multiple isoforms of NECAB2 in human, mouse, and zebrafish. **(A)** The protein diagrams of NECAB2 isoforms in human (*Homo sapiens*), mouse (*Mus musculus*), and zebrafish (*Danio rerio*) transcripts were shown, predicted from the Ensemble database. Scale bar = 50 amino acids (aa). **(B)** Transcript-specific primers were generated to confirm the existence of the two predicted transcripts of *necab2* in the Ensemble database. cDNA is obtained from AB zebrafish larvae at 1 hpf, 10 hpf, 2 dpf, 3 dpf, 4 dpf, and 5 dpf, respectively. The housekeeping gene β-*actin* was used as an internal reference. **(C)** Western blot analysis of Necab2 in the *necab2*$^{+/+}$ and *necab2*$^{-/-}$ larvae. Note the two isoforms of Necab2 in zebrafish (arrows). Necab2-001 is supposed to be 47.91 kDa. Necab2-201 is supposed to be 30.25kDa. The bands detected both in the *necab2*$^{+/+}$ and *necab2*$^{-/-}$ larvae were likely to be unspecific binding. hpf, hour post-fertilization.

Supplementary Figure 2 | Specificity of the RNA probes and antibodies used in this study. **(A)** Self-designed anti-sense and sense probe of *necab2* were used in whole-mount *in situ* hybridization from 24 to 120 hpf. The contrast of *in situ* hybridization signals between the anti-sense and sense-probe was evident, which confirmed the specificity of the RNA probe. Scale bar = 500 μm. **(B)** Custom-produced rabbit anti-Necab2 polyclonal antibody was performed in immunofluorescence in both the *necab2*$^{+/+}$ and *necab2*$^{-/-}$ larvae at 120 hpf. The contrast of immunofluorescent signals between the WT and the *necab2* mutant was evident though part of the forebrain showed slight residual immunoreactivity. This supported the specificity of the antibody with little cross-reactivity to Necab1 and Necab3. Scale bar = 100 μm. The region in the dashed white box was shown at higher magnification below. Scale bar = 20 μm. **(C)** Immuno-depletion analysis of the polyclonal rat anti-GRM1a antibody in the *necab2*$^{+/+}$ larvae at 120 hpf. The mixture of anti-Grm1a antibody and the Grm1a antigen (1:5) eliminated the immunofluorescent signaling in the anti-Grm1a antibody staining alone, suggesting that the immunoreactivity of anti-GRM1a

antibody staining was specific. Scale bar = 100 μm. The region in the dashed white box was shown at higher magnification below. Scale bar = 20 μm. hpf, day post-fertilization; Tel, telencephalon; Ce, cerebellum; Ha, habenula; OT, optic tectum; HB, hindbrain.

Supplementary Figure 3 | Tg(*Pnecab2:EGFP*) under the control of the upstream regulatory elements of *necab2* manifests good fidelity. **(A)** Comparison of transgenic EGFP expression with *in situ* hybridization in 120 hpf *necab2*$^{+/+}$ larvae. Scale bar = 100, 200 μm, respectively. **(B)** Co-immunostaining of the anti-Necab2 and anti-EGFP antibody in Tg(*Pnecab2:EGFP*) from whole-mount scale to cell-resolution. Scale bar = 50 μm. **(C)** Imaging at cellular resolution detected the necab2-expressing neuron projection from habenula in the diencephalon to the inter-peduncular nucleus (IPN) and expression in the spinal cord and retinal ganglion (arrowheads). Scale bar = 10, 50 μm, respectively. hpf, day post-fertilization; Tel, telencephalon; Di, diencephalon; Ce, cerebellum; Re, retina; Ha, habenula; OT, optic tectum; MHB, midbrain-hindbrain boundary; HB, hindbrain; lens, crystalline lens.

Supplementary Figure 4 | *necab2* expression is not detected in glycinergic, dopaminergic, or serotonergic neurons. **(A–A‴)** *necab2* was not detected in glycinergic neurons. High single-cell resolution images in the cerebellum of Tg(*Pnecab2:EGFP*) detected no co-localization between *necab2* with *glyt2*. Single section. Z-stack, Maximum intensity projection. Scale bar = 50 μm. **(B–B″,C–C″)** *necab2* was not detected in dopaminergic neurons. Co-immunofluorescent staining of anti-EGFP with anti-TH in Tg(*Pnecab2:EGFP*) showed no co-localization. Scale bar = 50 μm. **(D–D″)** *necab2* was not detected in serotonergic neurons. Co-immunofluorescent staining of anti-EGFP with anti-5-HT in Tg(*Pnecab2:EGFP*) showed no co-localization. Scale bar = 50 μm. hpf, day post-fertilization; Tel, telencephalon; Ce, cerebellum; Ha, habenula; OT, optic tectum; HB, hindbrain.

Supplementary Figure 5 | Verification of the co-immunoprecipitation products used for mass spectrometry. **(A)** Coomassie blue staining analysis. The *necab2*$^{+/+}$ and *necab2*$^{-/-}$ zebrafish were processed for immunoprecipitation using the polyclonal rabbit anti-Necab2 antibody and analyzed by Coomassie blue staining. Two biological replicates were performed for each group. **(B)** Western blot analysis. The *necab2*$^{+/+}$ and *necab2*$^{-/-}$ zebrafish were processed for immunoprecipitation by rabbit anti-Necab2 antibody and the crude extracts (Input), as well as immunoprecipitations (IP), were analyzed by the SDS-PAGE. Two biological replicates were performed for each group. Note that two NECAB2 isoforms (arrows) were identified by the antibody only in *necab2*$^{+/+}$ but not the *necab2*$^{-/-}$ zebrafish.

Supplementary Figure 6 | The expression of mGluR1 and the nature of neuronal subtypes expressing Necab2 in the larval zebrafish cerebellum. **(A–A‴)** Confocal live imaging of the *necab2*$^{+/+}$ larvae fish at 5 dpf in Tg(*Pnecab2:EGFP*) and Tg(*gad1b:DsRed*) background in the cerebellar gad1b-enriched area. The Necab2-expressing neurons strongly overlapped with the gad1b-positive neurons (arrowheads). Scale bar = 100 μm **(A)**. The region in the dashed white box **(A)** was shown at higher magnification on the right **(A′–A‴)**. Scale bar = 10 μm. **(B–B‴)** Confocal live imaging of the *necab2*$^{+/+}$ larvae fish at 5 dpf in Tg(*Pnecab2:EGFP*) and Tg(*vglut2a:DsRed*) background in the cerebellar gad1b-enriched area. The Necab2-expressing neurons overlapped with the vglut2a-positive neurons (arrowheads). Scale bar = 100 μm **(B)**. The region in the dashed white box **(B)** was shown at higher magnification on the right **(B′–B‴)**. Scale bar = 10 μm. **(C–C‴)** Confocal live imaging of the *necab2*$^{+/+}$ larvae fish at 5 dpf in Tg(*Pnecab2:EGFP*) and Tg(*vglut2a:DsRed*) background in the cerebellar vglut2a-enriched area. The Necab2-expressing neurons overlapped with the vglut2a-positive neurons (arrowheads). Scale bar = 100 μm **(C)**. The region in the dashed white box **(C)** was shown at higher magnification on the right **(C′–C‴)**. Scale bar = 10 μm. **(D,E)** Immunostaining of anti-Grm1a in the *necab2*$^{+/+}$ and *necab2*$^{-/-}$ larval cerebellum showed no difference in the mGluR1 expression. Scale bar = 20 μm. hpf, day post fertilization; Tel, telencephalon; Ce, cerebellum; ce-gad1b, cerebellar gad1b enriched area; ce-vglut2a, cerebellar vglut2a enriched area; Ha, habenula; OT, optic tectum; HB, hindbrain.

Supplementary Figure 7 | The quantification of the plasma/cytosol intensity in the *in vivo* PIP2 imaging by ImageJ. **(A)** The live fluorescence imaging of Tg(*hsp70:plc-ph-mCherry*) with the confocal microscope. Scale bar = 10 μm. **(B)** The outline of the selected cell was drawn manually. The mean fluorescent intensity was calculated by ImageJ, which is the mean fluorescent intensity of the whole cell (Area = 0.546, Mean value = 44.025). Scale bar = 2 μm. **(C)** The cytosol fluorescent intensity was calculated after the outline of the cytoplasm was sketched (Area = 0.355, Mean value = 33.500). The plasma fluorescent intensity was obtained by subtracting cytosol intensity from whole cell intensity: The plasma fluorescent intensity = (mean fluorescent intensity of whole cell * area of whole cell - mean fluorescent intensity of cytosol * area of cytosol)/(area of whole cell - area of cytosol). The plasma/cytosol intensity = mean fluorescent intensity of plasma/mean fluorescent intensity of cytosol. Scale bar = 2 μm.

REFERENCES

Amaral, D. G., Schumann, C. M., and Nordahl, C. W. (2008). Neuroanatomy of autism. *Trends Neurosci.* 31, 137–145. doi: 10.1016/j.tins.2007.12.005

Bai, Y., Liu, H., Huang, B., Wagle, M., and Guo, S. (2016). Identification of environmental stressors and validation of light preference as a measure of anxiety in larval zebrafish. *BMC Neurosci.* 17:63. doi: 10.1186/s12868-016-0298-z

Bailey, J. M., Oliveri, A. N., Karbhari, N., Brooks, R. A., De La Rocha, A. J., Janardhan, S., et al. (2016). Persistent behavioral effects following early life exposure to retinoic acid or valproic acid in zebrafish. *Neurotoxicology* 52, 23–33. doi: 10.1016/j.neuro.2015.10.001

Canela, L., Fernández-Dueñas, V., Albergaria, C., Watanabe, M., Lluís, C., Mallol, J., et al. (2009). The association of metabotropic glutamate receptor type 5 with the neuronal Ca2+-binding protein 2 modulates receptor function. *J. Neurochem.* 111, 555–567. doi: 10.1111/j.1471-4159.2009.06348.x

Canela, L., Lujan, R., Lluis, C., Burgueno, J., Mallol, J., Canela, E. I., et al. (2007). The neuronal Ca(2+) -binding protein 2 (NECAB2) interacts with the adenosine A(2A) receptor and modulates the cell surface expression and function of the receptor. *Mol. Cell Neurosci.* 36, 1–12. doi: 10.1016/j.mcn.2007.05.007

Chen, X., Mu, Y., Hu, Y., Kuan, A. T., Nikitchenko, M., Randlett, O., et al. (2018). Brain-wide Organization of Neuronal Activity and Convergent Sensorimotor Transformations in Larval Zebrafish. *Neuron* 100, 876–890. doi: 10.1016/j.neuron.2018.09.042

De Rubeis, S., He, X., Goldberg, A. P., Poultney, C. S., Samocha, K., Cicek, A. E., et al. (2014). Synaptic, transcriptional and chromatin genes disrupted in autism. *Nature* 515, 209–215. doi: 10.1038/nature13772

D'Mello, A. M., Crocetti, D., Mostofsky, S. H., and Stoodley, C. J. (2015). Cerebellar gray matter and lobular volumes correlate with core autism symptoms. *Neuroimage Clin.* 7, 631–639. doi: 10.1016/j.nicl.2015.02.007

Ebrahimi-Fakhari, D., and Sahin, M. (2015). Autism and the synapse: emerging mechanisms and mechanism-based therapies. *Curr. Opin. Neurol.* 28, 91–102. doi: 10.1097/WCO.0000000000000186

Gong, B., Shen, W., Xiao, W., Meng, Y., Meng, A., and Jia, S. (2017). The Sec14-like phosphatidylinositol transfer proteins Sec14l3/SEC14L2 act as GTPase proteins to mediate Wnt/Ca(2+) signaling. *Elife* 6:e26362. doi: 10.7554/eLife.26362

Guo, S. (2004). Linking genes to brain, behavior and neurological diseases: what can we learn from zebrafish? *Genes Brain Behav.* 3, 63–74. doi: 10.1046/j.1601-183x.2003.00053.x

Haug, M. F., Gesemann, M., Mueller, T., and Neuhauss, S. C. (2013). Phylogeny and expression divergence of metabotropic glutamate receptor genes in the brain of zebrafish (Danio rerio). *J. Comp. Neurol.* 521, 1533–1560. doi: 10.1002/cne.23240

Hedges, V. L., Chen, G., Yu, L., Krentzel, A. A., Starrett, J. R., Zhu, J. N., et al. (2018). Local Estrogen Synthesis Regulates Parallel Fiber-Purkinje Cell Neurotransmission Within the Cerebellar Cortex. *Endocrinology* 159, 1328–1338. doi: 10.1210/en.2018-00039

Higashijima, S., Mandel, G., and Fetcho, J. R. (2004). Distribution of prospective glutamatergic, glycinergic, and GABAergic neurons in embryonic and larval zebrafish. *J. Comp. Neurol.* 480, 1–18. doi: 10.1002/cne.20278

Hoffman, E. J., Turner, K. J., Fernandez, J. M., Cifuentes, D., Ghosh, M., Ijaz, S., et al. (2016). Estrogens Suppress a Behavioral Phenotype in Zebrafish Mutants of the Autism Risk Gene, CNTNAP2. *Neuron* 89, 725–733. doi: 10.1016/j.neuron.2015.12.039

Howe, K., Clark, M. D., Torroja, C. F., Torrance, J., Berthelot, C., Muffato, M., et al. (2013). The zebrafish reference genome sequence and its relationship to the human genome. *Nature* 496, 498–503. doi: 10.1038/nature12111

Hsu, P. D., Lander, E. S., and Zhang, F. (2014). Development and applications of CRISPR-Cas9 for genome engineering. *Cell* 157, 1262–1278. doi: 10.1016/j.cell.2014.05.010

Hwang, W. Y., Fu, Y., Reyon, D., Maeder, M. L., Tsai, S. Q., Sander, J. D., et al. (2013). Efficient genome editing in zebrafish using a CRISPR-Cas system. *Nat. Biotechnol.* 31, 227–229.

Iossifov, I., O'Roak, B. J., Sanders, S. J., Ronemus, M., Krumm, N., Levy, D., et al. (2014). The contribution of de novo coding mutations to autism spectrum disorder. *Nature* 515, 216–221. doi: 10.1038/nature13908

Itsara, A., Wu, H., Smith, J. D., Nickerson, D. A., Romieu, I., London, S. J., et al. (2010). De novo rates and selection of large copy number variation. *Genome Res.* 20, 1469–1481. doi: 10.1101/gr.107680.110

Katan, M., and Cockcroft, S. (2020). Phospholipase C families: common themes and versatility in physiology and pathology. *Prog. Lipid Res.* 80:101065. doi: 10.1016/j.plipres.2020.101065

Kawakami, K., Asakawa, K., Muto, A., and Wada, H. (2016). Tol2-mediated transgenesis, gene trapping, enhancer trapping, and Gal4-UAS system. *Methods Cell Biol.* 135, 19–37.

Kawasaki, H., and Kretsinger, R. H. (2017). Structural and functional diversity of EF-hand proteins: evolutionary perspectives. *Protein Sci.* 26, 1898–1920. doi: 10.1002/pro.3233

Kim, O. H., Cho, H. J., Han, E., Hong, T. I., Ariyasiri, K., Choi, J. H., et al. (2017). Zebrafish knockout of Down syndrome gene, DYRK1A, shows social impairments relevant to autism. *Mol. Autism* 8:50. doi: 10.1186/s13229-017-0168-2

Kornilov, S. A., Rakhlin, N., Koposov, R., Lee, M., Yrigollen, C., Caglayan, A. O., et al. (2016). Genome-Wide Association and Exome Sequencing Study of Language Disorder in an Isolated Population. *Pediatrics* 137:e20152469. doi: 10.1542/peds.2015-2469

Kozol, R. A., Cukier, H. N., Zou, B., Mayo, V., De Rubeis, S., Cai, G., et al. (2015). Two knockdown models of the autism genes SYNGAP1 and SHANK3 in zebrafish produce similar behavioral phenotypes associated with embryonic disruptions of brain morphogenesis. *Hum. Mol. Genet.* 24, 4006–4023. doi: 10.1093/hmg/ddv138

Kumar, S., Stecher, G., and Tamura, K. (2016). MEGA7: Molecular Evolutionary Genetics Analysis Version 7.0 for Bigger Datasets. *Mol. Biol. Evol.* 33, 1870–1874. doi: 10.1093/molbev/msw054

Lachlan, R. F., Crooks, L., and Laland, K. N. (1998). Who follows whom? Shoaling preferences and social learning of foraging information in guppies. *Anim. Behav.* 56, 181–190. doi: 10.1006/anbe.1998.0760

Lai, M. C., Lombardo, M. V., Auyeung, B., Chakrabarti, B., and Baron-Cohen, S. (2015). Sex/gender differences and autism: setting the scene for future research. *J. Am. Acad. Child. Adolesc. Psychiat.* 54, 11–24. doi: 10.1016/j.jaac.2014.10.003

Lee, S., Chun, H., Lee, J., Park, H., Kim, K., Kim, C. H., et al. (2018). Plausibility of the zebrafish embryos/larvae as an alternative animal model for autism: A comparison study of transcriptome changes. *PLoS One* 13:e203543. doi: 10.1371/journal.pone.0203543

Li, M., Liu, X., and Feng, X. (2019). Cardiovascular toxicity and anxiety-like behavior induced by deltamethrin in zebrafish (Danio rerio) larvae. *Chemosphere* 219, 155–164. doi: 10.1016/j.chemosphere.2018.12.011

Liu, C. X., Li, C. Y., Hu, C. C., Wang, Y., Lin, J., Jiang, Y. H., et al. (2018). CRISPR/Cas9-induced shank3b mutant zebrafish display autism-like behaviors. *Mol. Autism* 9:23. doi: 10.1186/s13229-018-0204-x

Liu, W., Xie, Y., Ma, J., Luo, X., Nie, P., Zuo, Z., et al. (2015). IBS: an illustrator for the presentation and visualization of biological sequences. *Bioinformatics* 31, 3359–3361.

Lundegaard, P. R., Anastasaki, C., Grant, N. J., Sillito, R. R., Zich, J., Zeng, Z., et al. (2015). MEK Inhibitors Reverse cAMP-Mediated Anxiety in Zebrafish. *Chem. Biol.* 22, 1335–1346. doi: 10.1016/j.chembiol.2015.08.010

Lykke-Andersen, S., and Jensen, T. H. (2015). Nonsense-mediated mRNA decay: an intricate machinery that shapes transcriptomes. *Nat. Rev. Mol. Cell Biol.* 16, 665–677. doi: 10.1038/nrm4063

Lyons, M. R., and West, A. E. (2011). Mechanisms of specificity in neuronal activity-regulated gene transcription. *Prog. Neurobiol.* 94, 259–295. doi: 10.1016/j.pneurobio.2011.05.003

Ma, Y., Deng, Q., Li, S., Chen, M., Jin, B., and Wang, M. (2021). TRPV1, Targeted by miR-338-3p, Induces Neuropathic Pain by Interacting with NECAB2. *J. Mol. Neurosci.* 71, 55–65. doi: 10.1007/s12031-020-01626-4

Maphanga, V. B., Skalicka-Woźniak, K., Budzynska, B., Enslin, G. M., and Viljoen, A. M. (2020). Screening selected medicinal plants for potential anxiolytic activity using an *in vivo* zebrafish model. *Psychopharmacology* 237, 3641–3652. doi: 10.1007/s00213-020-05642-5

Martin, L. A., Goldowitz, D., and Mittleman, G. (2010). Repetitive behavior and increased activity in mice with Purkinje cell loss: a model for understanding the role of cerebellar pathology in autism. *Eur. J. Neurosci.* 31, 544–555. doi: 10.1111/j.1460-9568.2009.07073.x

Masini, E., Loi, E., Vega-Benedetti, A. F., Carta, M., Doneddu, G., Fadda, R., et al. (2020). An Overview of the Main Genetic, Epigenetic and Environmental Factors Involved in Autism Spectrum Disorder Focusing on Synaptic Activity. *Int. J. Mol. Sci.* 21:8290. doi: 10.3390/ijms21218290

Menashe, I., Grange, P., Larsen, E. C., Banerjee-Basu, S., and Mitra, P. P. (2013). Co-expression profiling of autism genes in the mouse brain. *PLoS Comput. Biol.* 9:e1003128. doi: 10.1371/journal.pcbi.1003128

Neher, E., and Sakaba, T. (2008). Multiple roles of calcium ions in the regulation of neurotransmitter release. *Neuron* 59, 861–872.

Niemi, M., Martin, H. C., Rice, D. L., Gallone, G., Gordon, S., Kelemen, M., et al. (2018). Common genetic variants contribute to risk of rare severe neurodevelopmental disorders. *Nature* 562, 268–271. doi: 10.1038/s41586-018-0566-4

Niswender, C. M., and Conn, P. J. (2010). Metabotropic Glutamate Receptors: Physiology, Pharmacology, and Disease. *Annu. Rev. Pharmacol. Toxicol.* 50, 295–322.

Peng, J., Wagle, M., Mueller, T., Mathur, P., Lockwood, B. L., Bretaud, S., et al. (2009). Ethanol-modulated camouflage response screen in zebrafish uncovers a novel role for cAMP and extracellular signal-regulated kinase signaling in behavioral sensitivity to ethanol. *J. Neurosci.* 29, 8408–8418. doi: 10.1523/JNEUROSCI.0714-09.2009

Ribeiro, F. M., Paquet, M., Cregan, S. P., and Ferguson, S. S. (2010). Group I metabotropic glutamate receptor signalling and its implication in neurological disease. *CNS Neurol. Disord. Drug Targets* 9, 574–595. doi: 10.2174/187152710793361612

Ritvo, E. R., Freeman, B. J., Scheibel, A. B., Duong, T., Robinson, H., Guthrie, D., et al. (1986). Lower Purkinje cell counts in the cerebella of four autistic subjects: initial findings of the UCLA-NSAC Autopsy Research Report. *Am. J. Psychiat.* 143, 862–866. doi: 10.1176/ajp.143.7.862

Sakai, Y., Shaw, C. A., Dawson, B. C., Dugas, D. V., Al-Mohtaseb, Z., Hill, D. E., et al. (2011). Protein interactome reveals converging molecular pathways among autism disorders. *Sci. Transl. Med.* 3:86ra49.

Sanders, S. J., Ercan-Sencicek, A. G., Hus, V., Luo, R., Murtha, M. T., Moreno-De-Luca, D., et al. (2011). Multiple recurrent de novo CNVs, including duplications of the 7q11.23 Williams syndrome region, are strongly associated with autism. *Neuron* 70, 863–885. doi: 10.1016/j.neuron.2011.05.002

Schaafsma, S. M., and Pfaff, D. W. (2014). Etiologies underlying sex differences in Autism Spectrum Disorders. *Front. Neuroendocrinol.* 35:255–271. doi: 10.1016/j.yfrne.2014.03.006

Schnörr, S. J., Steenbergen, P. J., Richardson, M. K., and Champagne, D. L. (2012). Measuring thigmotaxis in larval zebrafish. *Behav. Brain Res.* 228, 367–374.

Schwaller, B. (2020). Cytosolic Ca(2+) Buffers Are Inherently Ca(2+) Signal Modulators. *Cold Spring Harb Perspect. Biol.* 12:a035543. doi: 10.1101/cshperspect.a035543

Simon, P., Dupuis, R., and Costentin, J. (1994). Thigmotaxis as an index of anxiety in mice. Influence of dopaminergic transmissions. *Behav. Brain Res.* 61, 59–64. doi: 10.1016/0166-4328(94)90008-6

Sugita, S., and Sudhof, T. C. (2000). Specificity of Ca2+-dependent protein interactions mediated by the C2A domains of synaptotagmins. *Biochemistry* 39, 2940–2949. doi: 10.1021/bi9920984

Sugita, S., Ho, A., and Sudhof, T. C. (2002). NECABs: a family of neuronal Ca(2+)-binding proteins with an unusual domain structure and a restricted expression pattern. *Neuroscience* 112, 51–63. doi: 10.1016/s0306-4522(02)00063-5

Thyme, S. B., Pieper, L. M., Li, E. H., Pandey, S., Wang, Y., Morris, N. S., et al. (2019). Phenotypic Landscape of Schizophrenia-Associated Genes Defines Candidates and Their Shared Functions. *Cell* 177, 478–491. doi: 10.1016/j.cell.2019.01.048

Treit, D., and Fundytus, M. (1988). Thigmotaxis as a test for anxiolytic activity in rats. *Pharmacol. Biochem. Behav.* 31, 959–962.

Tsai, P. T., Hull, C., Chu, Y., Greene-Colozzi, E., Sadowski, A. R., Leech, J. M., et al. (2012). Autistic-like behaviour and cerebellar dysfunction in Purkinje cell Tsc1 mutant mice. *Nature* 488, 647–651. doi: 10.1038/nature11310

Venkatachalam, K., and Montell, C. (2007). TRP channels. *Annu. Rev. Biochem.* 76, 387–417.

Vorstman, J., Parr, J. R., Moreno-De-Luca, D., Anney, R., Nurnberger, J. I. Jr., and Hallmayer, J. F. (2017). Autism genetics: opportunities and challenges for clinical translation. *Nat. Rev. Genet.* 18, 362–376.

Wang, S. S., Kloth, A. D., and Badura, A. (2014). The cerebellum, sensitive periods, and autism. *Neuron* 83, 518–532. doi: 10.1016/j.neuron.2014.07.016

Westerfield, M. (2000). *The Zebrafish Book: A Guide for the Laboratory Use of Zebrafish (Danio Rerio)*. Corvallis: University of Oregon Press.

Schizophrenia Working Group of the Psychiatric Genomics Consortium (2014). Biological insights from 108 schizophrenia-associated genetic loci. *Nature* 511, 421–427.

Zhang, M. D., Su, J., Adori, C., Cinquina, V., Malenczyk, K., Girach, F., et al. (2018). Ca2+-binding protein NECAB2 facilitates inflammatory pain hypersensitivity. *J. Clin. Invest.* 128, 3757–3768. doi: 10.1172/JCI120913

Zhang, M. D., Tortoriello, G., Hsueh, B., Tomer, R., Ye, L., Mitsios, N., et al. (2014). Neuronal calcium-binding proteins 1/2 localize to dorsal root ganglia and excitatory spinal neurons and are regulated by nerve injury. *Proc. Natl. Acad. Sci.* 111, E1149–E1158. doi: 10.1073/pnas.1402318111

Zhang, M., Barde, S., Szodorai, E., Josephson, A., Mitsios, N., Watanabe, M., et al. (2016). Comparative anatomical distribution of neuronal calcium-binding protein (NECAB) 1 and -2 in rodent and human spinal cord. *Brain Struct. Fun.* 221, 3803–3823. doi: 10.1007/s00429-016-1191-3

Zimmermann, B., Girard, F., Meszar, Z., and Celio, M. R. (2013). Expression of the calcium binding proteins Necab-1,-2 and -3 in the adult mouse hippocampus and dentate gyrus. *Brain Res.* 1528, 1–7. doi: 10.1016/j.brainres.2013.06.004

Zimmermann, F. F., Gaspary, K. V., Leite, C. E., De Paula, C. G., and Bonan, C. D. (2015). Embryological exposure to valproic acid induces social interaction deficits in zebrafish (Danio rerio): a developmental behavior analysis. *Neurotoxicol. Teratol.* 52, 36–41. doi: 10.1016/j.ntt.2015.10.002

Zoghbi, H. Y., and Bear, M. F. (2012). Synaptic Dysfunction in Neurodevelopmental Disorders Associated with Autism and Intellectual Disabilities. *Cold Spring Harbor Perspect. Biol.* 4:a9886. doi: 10.1101/cshperspect.a009886

Zucker, R. S. (1999). Calcium- and activity-dependent synaptic plasticity. *Curr. Opin. Neurobiol.* 9, 305–313. doi: 10.1016/S0959-4388(99)80045-2

Conflict of Interest: The authors declare that the research was conducted in the absence of any commercial or financial relationships that could be construed as a potential conflict of interest.

Publisher's Note: All claims expressed in this article are solely those of the authors and do not necessarily represent those of their affiliated organizations, or those of the publisher, the editors and the reviewers. Any product that may be evaluated in this article, or claim that may be made by its manufacturer, is not guaranteed or endorsed by the publisher.

Copyright © 2022 Chen, Long, Guo, Wang, He, Tao, Li, Jiang, Guo and Pi. This is an open-access article distributed under the terms of the Creative Commons Attribution License (CC BY). The use, distribution or reproduction in other forums is permitted, provided the original author(s) and the copyright owner(s) are credited and that the original publication in this journal is cited, in accordance with accepted academic practice. No use, distribution or reproduction is permitted which does not comply with these terms.

frontiers | Frontiers in Molecular Neuroscience

TYPE Original Research
PUBLISHED 10 August 2022
DOI 10.3389/fnmol.2022.901016

Check for updates

OPEN ACCESS

EDITED BY
Feng Zhao,
Shandong Institute of Business and Technology, China

REVIEWED BY
Manabu Makinodan,
Nara Medical University, Japan
Thorsten Rudroff,
The University of Iowa, United States
Franziska Scharkowski,
Charles River Discovery Research Services Germany GmbH, Germany

*CORRESPONDENCE
Paradee Auvichayapat
aparad@kku.ac.th

SPECIALTY SECTION
This article was submitted to Neuroplasticity and Development, a section of the journal Frontiers in Molecular Neuroscience

RECEIVED 21 March 2022
ACCEPTED 13 July 2022
PUBLISHED 10 August 2022

CITATION
Keeratitanont K, Theerakulpisut D, Auvichayapat N, Suphakunpinyo C, Patjanasoontorn N, Tiamkao S, Tepmongkol S, Khiewvan B, Raruenrom Y, Srisuruk P, Paholpak S and Auvichayapat P (2022) Brain laterality evaluated by F-18 fluorodeoxyglucose positron emission computed tomography in autism spectrum disorders. *Front. Mol. Neurosci.* 15:901016. doi: 10.3389/fnmol.2022.901016

COPYRIGHT
© 2022 Keeratitanont, Theerakulpisut, Auvichayapat, Suphakunpinyo, Patjanasoontorn, Tiamkao, Tepmongkol, Khiewvan, Raruenrom, Srisuruk, Paholpak and Auvichayapat. This is an open-access article distributed under the terms of the Creative Commons Attribution License (CC BY). The use, distribution or reproduction in other forums is permitted, provided the original author(s) and the copyright owner(s) are credited and that the original publication in this journal is cited, in accordance with accepted academic practice. No use, distribution or reproduction is permitted which does not comply with these terms.

Brain laterality evaluated by F-18 fluorodeoxyglucose positron emission computed tomography in autism spectrum disorders

Keattichai Keeratitanont[1,2], Daris Theerakulpisut[1], Narong Auvichayapat[2,3], Chanyut Suphakunpinyo[2,3], Niramol Patjanasoontorn[2,4], Somsak Tiamkao[2,5], Supatporn Tepmongkol[6,7], Benjapa Khiewvan[8], Yutapong Raruenrom[1], Piyawan Srisuruk[9,10], Suchat Paholpak[4,10] and Paradee Auvichayapat[2,11]*

[1]Division of Nuclear Medicine, Department of Radiology, Faculty of Medicine, Khon Kaen University, Khon Kaen, Thailand, [2]Noninvasive Brain Stimulation Research Group of Thailand, Faculty of Medicine, Khon Kaen University, Khon Kaen, Thailand, [3]Department of Pediatrics, Faculty of Medicine, Khon Kaen University, Khon Kaen, Thailand, [4]Department of Psychiatry, Faculty of Medicine, Khon Kaen University, Khon Kaen, Thailand, [5]Department of Medicine, Faculty of Medicine, Khon Kaen University, Khon Kaen, Thailand, [6]Division of Nuclear Medicine, Department of Radiology, Faculty of Medicine, Chulalongkorn University, Bangkok, Thailand, [7]Chulalongkorn University Biomedical Imaging Group (CUBIG), Faculty of Medicine, Chulalongkorn University, Bangkok, Thailand, [8]Division of Nuclear Medicine, Department of Radiology, Faculty of Medicine Siriraj Hospital, Mahidol University, Bangkok, Thailand, [9]Department of Educational Psychology and Counseling, Faculty of Education, Khon Kaen University, Khon Kaen, Thailand, [10]Research and Service Institute for Autism, Khon Kaen University, Khon Kaen, Thailand, [11]Department of Physiology, Faculty of Medicine, Khon Kaen University, Khon Kaen, Thailand

Background and rationale: Autism spectrum disorder (ASD) is a neuropsychiatric disorder that has no curative treatment. Little is known about the brain laterality in patients with ASD. F-18 fluorodeoxyglucose positron emission computed tomography (F-18 FDG PET/CT) is a neuroimaging technique that is suitable for ASD owing to its ability to detect whole brain functional abnormalities in a short time and is feasible in ASD patients. The purpose of this study was to evaluate brain laterality using F-18 FDG PET/CT in patients with high-functioning ASD.

Materials and methods: This case-control study recruited eight ASD patients who met the DSM-5 criteria, the recorded data of eight controls matched for age, sex, and handedness were also enrolled. The resting state of brain glucose metabolism in the regions of interest (ROIs) was analyzed using the Q.Brain software. Brain glucose metabolism and laterality index in each ROI of ASD patients were compared with those of the controls. The pattern of brain metabolism was analyzed using visual analysis and is reported in the data description.

Results: The ASD group's overall brain glucose metabolism was lower than that of the control group in both the left and right hemispheres, with mean differences of 1.54 and 1.21, respectively. We found statistically lower mean

glucose metabolism for ASD patients than controls in the left prefrontal lateral (Z = 1.96, p = 0.049). The left laterality index was found in nine ROIs for ASD and 11 ROIs for the control. The left laterality index in the ASD group was significantly lower than that in the control group in the prefrontal lateral (Z = 2.52, p = 0.012), precuneus (Z = 2.10, p = 0.036), and parietal inferior (Z = 1.96, p = 0.049) regions.

Conclusion: Individuals with ASD have lower brain glucose metabolism than control. In addition, the number of ROIs for left laterality index in the ASD group was lower than control. Left laterality defects may be one of the causes of ASD. This knowledge can be useful in the treatment of ASD by increasing the left-brain metabolism. This trial was registered in the Thai Clinical Trials Registry (TCTR20210705005).

KEYWORDS

F-18 FDG PET/CT, brain glucose metabolism, autism spectrum disorders, laterality, treatment by non-invasive brain stimulation, positron emission tomography

Introduction

Autism spectrum disorder (ASD) is a neurodevelopmental disorder. There are several aspects listed for the ASD pathology, i.e., the irregular arrangement of neural connections, neuronal migration defects, neurotransmitter imbalance, and altered dendritic morphology (John and Watts, 2008). A systematic review concluded that there is evidence of brain laterality related to ASD (Cara et al., 2022). In addition, a meta-analysis that recruited data from magnetic resonance imaging (MRI), functional MRI (fMRI), diffusion tensor imaging, and magnetoencephalography studies revealed a tentative decrease in the strength of laterality at the inferior frontal gyrus in ASD. However, the results showed an inclusive relationship between ASD and brain laterality (Preslar et al., 2014). Therefore, further studies about hemispheric specialization and brain laterality in ASD are warranted.

F-18 fluorodeoxyglucose positron emission computed tomography (F-18 FDG PET/CT) is another functional neuroimaging technique for evaluating brain metabolism, similar to resting-state fMRI. Previous studies have demonstrated a correlation between these two techniques (Soddu et al., 2016; Savio et al., 2017). However, PET/CT is superior with ASD individuals over resting state fMRI, because PET/CT requires a shorter time period and has no loud radio transmission sounds in the scanner to frighten ASD individuals and make them move. Therefore, PET/CT is more feasible than fMRI for individuals with ASD. In the cellular level, F-18 FDG PET/CT is also a well-established imaging modality for observing glucose metabolism within neuronal cells (Varrone et al., 2009).

Preliminary evidence supports brain laterality in PET scans for individual with normal brain function, which defined as persons without any mental illness or neurological deficit, Willis et al. (2002) reported left laterality in the medial frontal gyrus, posterior thalamus, lingual gyrus, cuneus, and superior cingulate cortex. Right laterality was found in the mesio-anterior cerebellum and lateral frontal and temporal regions normalized by global glucose metabolism during an auditory continuous performance task at 20–69 years old (Willis et al., 2002). Gur et al. (1995) assessed glucose metabolism during a resting state in individual with normal brain function with a mean age of 27.5 years and reported higher metabolism in the left hemisphere for the premotor, motor, and sensorimotor regions and higher right hemispheric glucose metabolism in the cerebellum (Gur et al., 1995). Azari et al. (1992) studied the resting state of brain glucose metabolism in healthy 18–40-year-old subjects using F-18 FDGPET/CT (Azari et al., 1992). They found no differences in the regional or right-left asymmetrical brain glucose metabolism between men and women. These heterogeneous findings resulted from a wide variety of measurement methods, that is, measurements at resting and functioning states, as well as a variety of normalized references.

At present, there are no studies on brain laterality in stocktickerASD patients. Although there was a report showing lower brain glucose metabolism in the medial frontal lobe and cingulate regions, compared to healthy controls (Hazlett et al., 2004). The previous PET scan studies provided basic information about glucose metabolism in the stocktickerASD brain but they did not focus on brain laterality. From the present data, there are some laterality studies on neuropsychiatric disorders (Savic and Lindström, 2008; Morimoto et al., 2013;

Pustina et al., 2015). However, to the best of our knowledge, there have been no any reports on brain laterality in individuals with stocktickerASD.

Given this lack of brain laterality information in ASD, we sought to determine a systematic brain laterality in ASD high-functioning individuals to facilitate further understanding of hemispheric specialization in the resting state of the ASD brain.

Materials and methods

Study design

This case-control study used F-18FDG PET/CT scans to investigate possible differences in resting-state brain laterality between eight high-functioning ASD individuals and eight matched controls. The study was conducted between July 7, 2020 and October 30, 2021, and all interventions were performed at the Srinagarind Hospital, Faculty of Medicine, Khon Kaen University, Thailand. This trial was registered in the Thai Clinical Trials Registry (TCTR20210705005).

Participant recruitment and informed consent

The study participants were recruited *via* advertisements at the Institute of Vocational Education Northeastern Region 3 and the Autism Parents Association of Khon Kaen Province, Thailand. The study procedures were described to any eligible participant who expressed an interest in participating in the study by a child psychiatrist (N.P.) according to the DSM-5 clinical assessment using the Autism Diagnostic Observation Schedule-2 (ADOS-2) (Lord et al., 2000).

The inclusion criteria were as follows: (a) mild to moderate autistic symptoms (Childhood Autism Rating Scale, CARS score 30–36.5) where the patient can stay still in the CT scanner during the examination; (b) aged between 15 and 30 years; (c) normal brain structure evaluated by MRI; and (d) the caregiver together with the patients consented to participate in the research.

The exclusion criteria were as follows: (a) severe neurological disorders such as brain tumor, intracranial infection, and uncontrollable epilepsy; (b) uncooperative parents; and (c) claustrophobia.

Prior to starting the study, each participant underwent history taking and physical examination by a neurologist (S.T. or N.A.) to detect comorbid neurological problems. The brain structures of the participants were assessed using MRI, and the ASD functioning class was assessed by a child psychiatrist (N.P.).

The study also included eight recorded images of non-ASD patients who underwent a whole-body F-18 FDG PET/CT scan as a control group (Sharma et al., 2018). All records of non-ASD patients were obtained from the Nuclear Medicine Unit, Khon Kaen University, Thailand. All patients in the control records met the inclusion criteria: (1) age, sex, and handedness matched to the ASD group; (2) use of the same imaging protocol as ASD participants; (3) complete documentation about patients' history, diagnosis, physical examination, and course of treatments; (4) normal neurologic examinations at the time of the study; (5) normal brain structure evaluated by MRI; and (6) complete image acquisition by PET/CT without significant artifacts. The exclusion criteria were as follows: (1) history of neuropsychiatric diseases such as ASD, depression, schizophrenia, ADHD, mania, and epilepsy; (2) undergoing treatment with neuropsychiatric medications; and (3) CNS impairment, brain structural abnormality, or brain metastasis. Information of the non-ASD patients and their F-18 FDG PET/CT brain images were reviewed and reanalyzed to obtain the uptake ratio in each brain region using Q.Brain software (by K.K.). Verbal consent *via* telephone (N.A.) was obtained from all participants in the control group before data extraction.

The study was conducted in accordance with the Declaration of Helsinki and approved by the Ethics Committee of Khon Kaen University (identifier number: HE 621277). Written informed consent was obtained from all the patients and their caregivers before participation.

Measures

Autism spectrum disorder functioning class

The ASD functioning class was classified as having low – or high-functioning autism. High-functioning autism is defined as an individual with ASD who has an intelligence quotient (IQ) above or equal 70. The Wechsler Adult Intelligence Scale fourth edition (WAIS-IV) was used for the IQ test in this study (Alvares et al., 2020).

PET scan procedure and data processing

The F-18 FDG was produced with a radiochemical purity of > 95%. The imaging equipment used was a PET/CT scanner (Discovery 690; GE Healthcare, WI, United States). Each participant underwent brain F-18 FDG PET/CT imaging after signing an informed consent form and at least 6 h of fasting. All brain F-18 FDG PET/CT images were acquired 45 min after intravenous injection of 7 mCi of F-18 FDG during the resting stage. CT image acquisition parameters were as follows: voltage, 120 kV; tube current, 10 mA; thickness of scanning slice, 3.27 mm; speed, 0.5 sec/rotation; pitch, 0.98; scanning

duration, 39.37 s. Third-dimensional PET image acquisition was performed in the same range as the CT scan. The ordered subset expectation maximization method was used for the image reconstruction. The reconstructed data were transferred to a dedicated workstation (GE Xeleris Workstation, version 4.0; GE Healthcare) for both qualitative and quantitative analyses. The 26 cortical regions of interest (ROIs) were automatically located after image fusion and anatomical standardization. The ROIs included the bilateral prefrontal lateral, prefrontal medial, sensorimotor, anterior cingulate, posterior cingulate, precuneus, parietal superior, parietal inferior, occipital lateral, primary visual, temporal lateral, temporal mesial, cerebellum, and pons regions.

Our study measured glucose uptake, which is the amount of the glucose (F-18 FDG) uptake by the neural cells. The glucose metabolism is the amount of glucose utilized by the cells. The neural cells firstly uptake (import) F-18 FDG *via* glucose transporter type 3 (GLUT-3) and then the F-18 FDG is metabolized by glycolysis pathway within the cytoplasm and is stored in the cell. Thus, the glucose (F-18 FDG) uptake directly indicates the brain glucose metabolism (utilization); two terms (glucose (F-18 FDG) metabolism and glucose uptake) can be interchangeable (Varrone et al., 2009).

Visual analysis

The patterns of brain metabolism were qualitatively assessed after adjusting thalamus and basal ganglia as the maximal intensity regions. Cross-sectional images of brain metabolism were independently reviewed and scored as normal, hypo-, or hypermetabolism by three expert nuclear medicine physicians (D.T., S.T., and B.K.). First, two experts (D.T. and S.T.) independently reviewed and sent the results to K.K., with discordant results sent to another expert (B.K.) who was blinded to the prior reviewers' results. The evaluation of a third expert was regarded as the final arbitration. The three expert nuclear medicine physicians were also blinded to each other and the clinical status of the participants.

Because of visual analysis was subjective and had no cut-off point, we measured assessor reliability to ensure the quality of the evaluation among the investigator as follows: three nuclear medicine physicians rated the same selected set of 28 brain pet scan images on an assessment document as hyper-, normal-, or hypo-metabolism twice with an inter-assessment interval of 2 months.

Quantitative analysis

Quantitative analysis of the brain glucose metabolism ratio was calculated for both ASD patients and controls in all predefined ROIs using commercial software with an available database, Q.Brain (GE Healthcare, Milwaukee, WI, United States). The previous studies found many hypometabolic brain areas involving cerebral cortex and cerebellum in patients with ASD (Hampson and Blatt, 2015). Using global metabolism as the reference while many brain areas were in hypometabolic state may cause overestimation of the metabolic value (Yakushev et al., 2008). Therefore, the pons was the most appropriate area to be the reference region (Verger et al., 2021).

Brain laterality

The 28 cortical ROIs of brain glucose metabolism in both the ASD and control groups were assessed for laterality (by K.K.) using the laterality index [100 × (left-right)/(mean left + mean right)/2] (Willis et al., 2002). Brain laterality is presented as left or right laterality. The laterality index was compared between the ASD and control groups using the Wilcoxon signed-rank test.

Overall brain glucose metabolism

To obtain an overview of the brain glucose metabolism in each hemisphere, we summed the brain glucose metabolism of all ROIs in each left or right hemisphere. We compared the overall brain glucose metabolism between the ASD and control groups, as well as between the left and right hemispheres of each group using the Wilcoxon signed-rank test.

Statistical analysis

A previous study reported that the effect size of the mean change difference in regional glucose metabolism was 0.09, with a pooled variance of 0.06 (Hazlett et al., 2004). We calculated that a sample size of eight patients was required to provide a statistical power of 90% to detect the difference between pre – and post-tDCS treatment with a two-sided alpha significance level of 0.05.

Regional brain glucose metabolism by visual analysis is presented as normal, hypo, or hypermetabolism. For other descriptive purposes, the mean and standard deviation of the demographic and outcome variables were calculated. For the validity test, changes in brain metabolism assessed by three independent observers were analyzed using Cronbach's alpha. The brain glucose metabolism ratio within the control group and ASD group, and the laterality index in each ROI between the ASD and control groups were compared using the Wilcoxon signed-rank test. The correlation between age and brain glucose metabolism (F-18 FDG uptake) across all ROIs has been evaluated using Spearman's correlation coefficient and the relationship was explored by regression analysis. Regarding to

the neuropsychiatric medications that can suppress the neuronal activity and can decrease overall brain glucose metabolism, the second analysis between ASD with medications and ASD without medications was performed using Wilcoxon signed-rank test. Analyses were conducted using SPSS Statistics (SPSS version 20), with the significance level set at $p < 0.05$. The data were monitored by P.A. and K.K.

Results

Demographic data

The eight ASD participants had a mean (± SD) age of 19.00 (± 3.02) years (range, 15–23) and a mean age of 4.87 (± 3.89) years at ASD diagnosis (range, 1.5–11). IQ means (± SD) is 86.45 (± 10.49) (range, 73–105). Most of the participants were male (87.5%) and left-handed (63%); one had an ASD family history (12.5%), one participant had a perinatal risk factor (12.5%), and six participants had idiopathic or no risk factors detected (75%). Four participants (50%) were born *via* cesarean section. There was nobody suffering from any psychiatric disorders. However, there was one participant who had focal epilepsy as the underlying disease. She was ensured by neurologists (S.T. and N.A.) that her status was controllable because she received only one antiepileptic drug (Lacosamide) and did not have any episode of epileptic attack for more than 1 year (Kwan et al., 2010). The mean blood glucose levels before performing F-18 FDG PET-CT were 96.75 ± 11.49 mg/dL.

The control group had a mean (± SD) age of 19.00 (± 2.83) years (range, 16 to 23). The participants were diagnosed with T-cell lymphoma (37.5%), Hodgkin lymphoma (12.5%), and non-Hodgkin lymphoma (50%), all of whom were in stage I with complete remission and were at the 1-year follow-up. None of the participants in the control group had neurological symptoms, and all participants (both the control and ASD groups) had normal brain structures as evaluated by MRI. The mean blood glucose levels before performing F-18 FDG PET-CT were 94.82 ± 15.31 mg/dL. The demographic data of the participants are presented in **Table 1**.

Brain glucose metabolism assessed by visual analysis

Prior to evaluating regional brain glucose metabolism, we assessed the inter-observer and intra-rater reliabilities for visual analysis. There was a very high degree of reliability among the three investigators ($r = 0.87$, 95%CI = 0.76 to 0.94, $p < 0.001$). The intra-rater reliability test was also high for D.T. ($r = 0.86$, 95%CI = 0.69 to 0.93, $p < 0.001$), S.T. ($r = 0.94$, 95%CI = 0.88 to 0.97, $p < 0.001$), and B.K. ($r = 1.00$, 95%CI = 1.00 to 0.98, $p < 0.001$). There were several hypometabolic areas, particularly

TABLE 1 Demographic data of participants.

Autism spectrum disorders ($n = 8$)														Control ($n = 8$)							
ID	Sex	Age (years)	Handedness	Age of diagnosis	Partuition	Maternal age at partuition	Paternal age at partuition	History of pregnancy	Family history for ASD	Medication	Behavioral therapy	Chemotherapy	Status	ID	Sex	Age (years)	Handedness	Diagnosis	Treatment		
ASD 01	F	19	R	3.5	C/S	33	40	Normal	Yes	Ri, B, L	SB	Complete	Remission	Ctrl 01	F	17	R	N-HL	Complete		Remission
ASD 02	M	15	L	11	C/S	28	38	PE	No	Ri	SB	Complete	Remission	Ctrl 02	M	16	L	TCL	Complete		Remission
ASD 03	M	16	R	3.25	N/L	34	34	Normal	No	No	SB	Complete	Remission	Ctrl 03	M	17	R	ALL	Complete		Remission
ASD 04	M	22	R	2.5	C/S	34	32	Normal	No	No	OT	Complete	Remission	Ctrl 04	M	22	R	N-HL	Complete		Remission
ASD 05	M	18	L	4.25	N/L	26	30	Normal	No	No	SB	Complete	Remission	Ctrl 05	M	18	L	HL	Complete		Remission
ASD 06	M	22	L	1.92	N/L	30	35	Normal	No	No	OT	Complete	Remission	Ctrl 06	M	22	L	N-HL	Complete		Remission
ASD 07	M	17	L	1.5	C/S	40	50	Normal	No	No	OT	Complete	Remission	Ctrl 07	M	17	L	N-HL	Complete		Remission
ASD 08	M	23	L	11	N/L	33	33	Normal	No	Ri	No	Complete	Remission	Ctrl 08	M	23	L	TCL	Complete		Remission

ASD, autism spectrum disorders; B, Benzhexol; C/S, cesarean section; Ctrl, control; F, female; HL, Hodgkin lymphoma; L, lacosamide; L, left; M, male; N-HL, non-Hodgkin lymphoma; N/L, normal labor; OT, occupational therapy; PE, pre-eclampsia; R, right; Ri, risperidone; SB, school base; TCL, T-cell lymphoma.

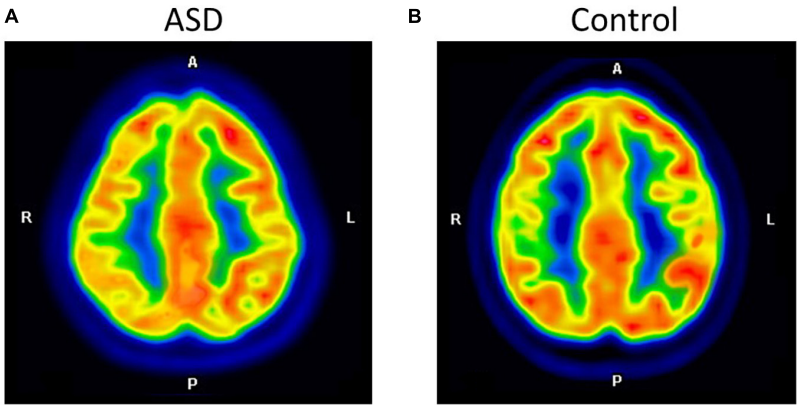

FIGURE 1
The axial images of the F-18 FDG PET/CT scan demonstrated relatively decreased FDG uptake at the right parietal inferior compared to the left parietal inferior in ASD **(A)**. The control participant shows normal FDG uptake in the same region **(B)**.

in the right cerebral hemisphere (8/8), in the ROIs examined by visual analysis in all eight ASD participants (Figure 1 and Table 2). Normal brain glucose metabolism was reported by reviewers in all ROIs of the control group.

Brain glucose metabolism comparing between autism spectrum disorder and control

Autism spectrum disorder overall brain glucose metabolism was lower than that of controls in both the left and right hemispheres, with mean differences of 1.54 and 1.21, respectively. For the left ROIs, the Wilcoxon signed-rank test showed statistically lower mean glucose metabolism for ASD patients than controls in the left prefrontal lateral (Z = 1.96, p = 0.049) and trends toward a lower mean glucose metabolism in the left anterior cingulate (Z = 1.68, p = 0.092), left posterior cingulate (Z = 1.68, p = 0.093), left parietal superior (Z = 1.68, p = 0.093), left parietal inferior (Z = 1.82, p = 0.069), and left temporal mesial area (Z = 1.68, p = 0.092).

For the right ROIs, there was no statistical difference in the mean glucose metabolism between the ASD and control groups. However, there was a trend of lower brain glucose metabolism for ASD than control in the right prefrontal lateral (Z = 1.82, p = 0.069), right anterior cingulate (Z = 1.68, p = 0.093), right posterior cingulate (Z = 1.68, p = 0.093), and right parietal inferior area (Z = 1.69, p = 0.091) (Figure 2 and Table 3).

Overall brain glucose metabolism between autism spectrum disorder with and without medications

Wilcoxon signed-rank test of the overall brain glucose metabolism showed no statistical difference between two groups (Z = 0.54, p = 0.593).

TABLE 2 Visual analysis of autism spectrum disorders' PET/CT image (n = 8).

ID	Area of hypometabolism	Area of hypermetabolism
ASD 01	R – Temporal lateral	Bi- Visual cortex
ASD 02	R – Parietal superior	Bi- Visual cortex
ASD 03	R – Parietal superior, R – Temporal lateral	Bi- Visual cortex
ASD 04	R – Parietal superior, R – Parietal inferior, R – Temporal lateral	Bi- Visual cortex
ASD 05	Bi – Posterior cingulate cortex, Bi – Precuneus, Bi – Parietal superior, Bi – Parietal inferior	Bi- Visual cortex
ASD 06	R – Parietal superior, R – Parietal inferior	Bi- Visual cortex
ASD 07	R – Parietal superior, R – Temporal lateral	Bi- Visual cortex
ASD 08	R – Parietal superior, R – Temporal lateral	Bi- Visual cortex

ASD, autism spectrum disorders; Bi, bilateral; L, left; R, right.

Brain laterality index

In the control group, our data showed left laterality index in 11 ROIs, that is, prefrontal lateral, prefrontal medial, sensorimotor, anterior cingulate, posterior cingulate, precuneus, parietal superior, parietal inferior, occipital lateral, temporal lateral, and temporal mesial. However, in the ASD group, the left laterality index was found in only nine ROIs: the prefrontal lateral, prefrontal medial, sensorimotor, anterior cingulate, posterior cingulate, parietal superior, parietal inferior, temporal lateral, and temporal mesial. Wilcoxon signed-rank test showed

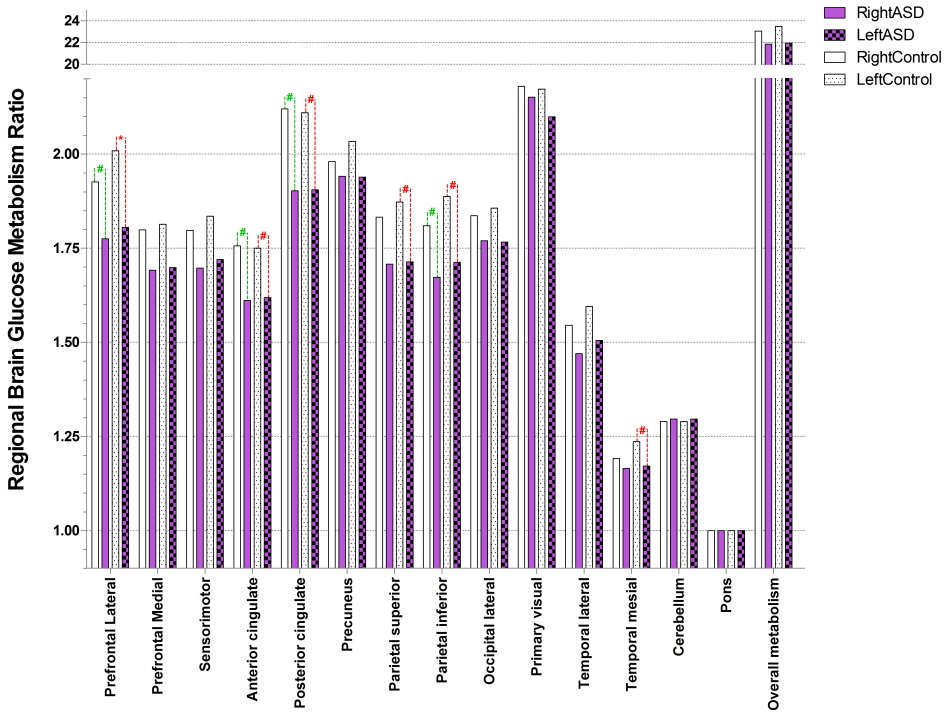

FIGURE 2
Ratio of brain glucose metabolism in regions of interest between control and ASD (* represents statistically significant, # tentative statistically significant by Wilcoxon signed-rank test).

a significantly lower degree of left laterality for ASD over controls in the prefrontal lateral ($Z = 2.52$, $p = 0.012$), precuneus ($Z = 2.10$, $p = 0.036$), and parietal inferior ($Z = 1.96$, $p = 0.049$). There was a trend toward a lower degree of left laterality in the parietal superior ($Z = 1.68$, $p = 0.093$) and temporal mesial regions in the ASD group than in the control group ($Z = 1.82$, $p = 0.069$). Brain laterality in the region of interest between the control and ASD groups is shown in **Figure 3**.

The correlation between age and brain glucose metabolism

In the control group, Spearman's correlation coefficient showed a trend toward association between age and brain glucose metabolism at the left prefrontal medial ($p = 0.071$, $r = 0.667$) and right temporal lateral ($p = 0.072$, $r = 0.665$). No association between age and brain glucose metabolism in any ROI of ASD group.

Discussion

To the best of our knowledge, this is the first study that aimed to study brain laterality using F-18 FDG PET/CT normalized by pons in high-functioning ASD individuals compared to controls (normal neurocognitive subjects matched for age, sex, and handedness). This study revealed that brain glucose metabolism at the left prefrontal lateral in the ASD group was lower than the control group. We also found a statistically significant decrease in left laterality in ASD patients compared to controls at the prefrontal lateral, precuneus, and parietal inferior regions.

Why brain glucose metabolism in autism spectrum disorder is lower than control?

Our visual analysis found hypometabolic areas (lower brain glucose metabolism or reduced glucose metabolism) at the right ROIs in all ASD participants than in controls. ASD pathology is the impairment of synaptogenesis (Courchesne et al., 2020), synaptic pruning (Tang et al., 2014; Kim et al., 2016), and alterations in neural network proliferation (Marchetto et al., 2016). The study using resting-state fMRI evidenced both hypo and hyper-connectivity in ASD. These findings indicated that one of the causes of ASD is abnormal neural connections (Haghighat et al., 2021). F-18 FDG PET/CT scan is one of the studies for detection of abnormal brain glucose metabolism. Neuronal cells that perform more action always

TABLE 3 Brain glucose metabolism in the right and left region of interest presented as ratio of brain glucose metabolism using Q.Brain software in ASD (n = 8) and control (n = 8).

	Prefrontal lateral		Prefrontal medial		Sensorimotor		Anterior cingulate		Posterior cingulate		Precuneus		Parietal superior		Parietal inferior		Occipital lateral		Primary visual		Temporal lateral		Temporal mesial		Cerebellum	Pons	Overall metabolism	
	R	L	R	L	R	L	R	L	R	L	R	L	R	L	R	L	R	L	R	L	R	L	R	L	M	M	R	L
ASD 01	1.5	1.54	1.43	1.44	1.48	1.52	1.31	1.3	1.69	1.7	1.76	1.73	1.51	1.5	1.47	1.5	1.6	1.61	1.96	1.9	1.28	1.32	1.01	1.03	1.2	1	19.2	19.29
ASD 02	1.88	1.91	1.8	1.79	1.74	1.76	1.6	1.64	2.08	2	2.03	2	1.84	1.9	1.83	1.85	1.87	1.84	2.04	1.86	1.64	1.65	1.28	1.2	1.28	1	22.91	22.68
ASD 03	1.96	1.96	1.8	1.82	1.84	1.84	1.71	1.74	1.88	1.89	1.88	1.89	1.61	1.62	1.77	1.79	1.84	1.83	2.3	2.15	1.57	1.6	1.27	1.28	1.4	1	22.83	22.81
ASD 04	1.74	1.72	1.67	1.67	1.7	1.69	1.77	1.78	1.72	1.76	1.89	1.78	1.69	1.62	1.6	1.63	1.73	1.73	2.26	2.14	1.45	1.47	1.13	1.18	1.36	1	21.71	21.53
ASD 05	1.69	1.72	1.55	1.56	1.58	1.63	1.52	1.54	1.84	1.8	1.78	1.79	1.58	1.65	1.54	1.56	1.69	1.71	1.94	2.08	1.38	1.4	1.13	1.16	1.25	1	20.47	20.85
ASD 06	1.64	1.73	1.66	1.63	1.6	1.61	1.48	1.45	1.85	1.91	1.96	2.01	1.71	1.67	1.6	1.67	1.68	1.67	2.16	2.1	1.35	1.42	1.11	1.13	1.26	1	21.06	21.26
ASD 07	1.8	1.84	1.72	1.74	1.71	1.81	1.71	1.71	1.92	1.95	1.96	1.97	1.73	1.76	1.72	1.75	1.81	1.79	2.15	2.2	1.47	1.52	1.11	1.14	1.25	1	22.06	22.43
ASD 08	1.99	2.02	1.9	1.94	1.93	1.9	1.79	1.79	2.24	2.23	2.27	2.28	1.99	1.99	1.85	1.95	1.94	1.95	2.4	2.36	1.62	1.66	1.28	1.25	1.37	1	24.57	24.69
Mean	**1.78**	**1.81**	**1.69**	**1.70**	**1.70**	**1.72**	**1.61**	**1.62**	**1.90**	**1.91**	**1.94**	**1.93**	**1.71**	**1.71**	**1.67**	**1.71**	**1.77**	**1.77**	**2.15**	**2.10**	**1.47**	**1.51**	**1.17**	**1.17**	**1.30**	**1.00**	**21.85**	**21.94**
SD	0.18	0.18	0.17	0.18	0.16	0.16	0.2	0.17	0.17	0.19	0.18	0.18	0.18	0.17	0.15	0.19	0.14	0.15	0.2	0.18	0.15	0.14	0.09	0.1	0.07	0	1.65	1.60
Control 01	2.02	2.09	1.93	1.93	1.95	1.99	1.75	1.80	2.15	2.15	2.11	2.17	1.94	1.99	1.9	1.94	2.02	2.01	2.27	2.29	1.64	1.70	1.25	1.30	1.33	1.00	24.26	24.69
Control 02	1.96	2.03	1.91	1.95	1.89	2.00	1.85	1.87	2.26	2.26	2.08	2.12	1.97	2.02	1.9	1.93	1.99	2.00	2.43	2.43	1.61	1.63	1.18	1.23	1.39	1.00	24.42	24.86
Control 03	2.30	2.35	2.02	2.02	1.99	2.02	2.08	1.99	2.50	2.58	2.04	2.25	1.92	1.97	2.05	2.17	1.81	1.88	2.17	2.03	1.66	1.67	1.30	1.30	1.19	1.00	25.03	25.42
Control 04	1.84	1.94	1.71	1.71	1.66	1.76	1.62	1.66	2.04	2.01	1.93	1.93	1.76	1.77	1.74	1.87	1.68	1.66	1.83	1.87	1.47	1.51	1.18	1.22	1.30	1.00	21.76	22.21
Control 05	1.78	1.83	1.75	1.75	1.72	1.69	1.76	1.77	2.06	1.99	1.94	1.96	1.75	1.82	1.7	1.74	1.77	1.78	2.19	2.13	1.46	1.50	1.14	1.18	1.31	1.00	22.33	22.45
Control 06	1.94	2.11	1.75	1.77	1.78	1.86	1.70	1.72	2.12	2.08	2.11	2.16	1.96	1.97	1.86	1.97	1.94	1.98	2.24	2.39	1.59	1.66	1.21	1.29	1.25	1.00	23.45	24.21
Control 07	1.82	1.89	1.62	1.66	1.71	1.73	1.60	1.65	1.96	2.05	1.88	1.89	1.68	1.70	1.72	1.79	1.69	1.73	2.01	2.01	1.48	1.54	1.15	1.23	1.26	1.00	21.58	22.13
Control 08	1.75	1.83	1.70	1.72	1.68	1.63	1.63	1.60	1.87	1.86	1.75	1.79	1.68	1.74	1.61	1.69	1.79	1.81	2.30	2.23	1.45	1.55	1.12	1.14	1.29	1.00	21.62	21.88
Mean	**1.93**	**2.01**	**1.80**	**1.81**	**1.80**	**1.84**	**1.75**	**1.76**	**2.12**	**2.12**	**1.98**	**2.03**	**1.83**	**1.87**	**1.81**	**1.89**	**1.84**	**1.86**	**2.18**	**2.17**	**1.55**	**1.60**	**1.19**	**1.24**	**1.29**	**1.00**	**23.06**	23.48
SD	0.18	0.18	0.14	0.13	0.13	0.15	0.16	0.13	0.19	0.22	0.13	0.16	0.13	0.13	0.14	0.15	0.13	0.13	0.19	0.20	0.09	0.08	0.06	0.06	0.06	0.00	1.40	1.45
C-ASD	0.151#	0.20*	0.11	0.12	0.10	0.12	0.14#	0.14#	0.22#	0.22#	0.04	0.10	0.13	0.159#	0.14#	0.18#	0.07	0.09	0.03	0.07	0.07	0.09	0.03	0.07#	−0.01	0.00	1.21	1.54

ASD, autism spectrum disorders group; C – ASD, mean of control group minus mean of ASD group; L, left; M, middle part; N/A, not applicable; R, right. * Represents statistical difference $p < 0.05$; # Represent tentative statistical difference $0.09 > p > 0.05$ by Wilcoxon signed-rank test. The bold values are the mean of brain glucose metabolism.

10.3389/fnmol.2022.901016

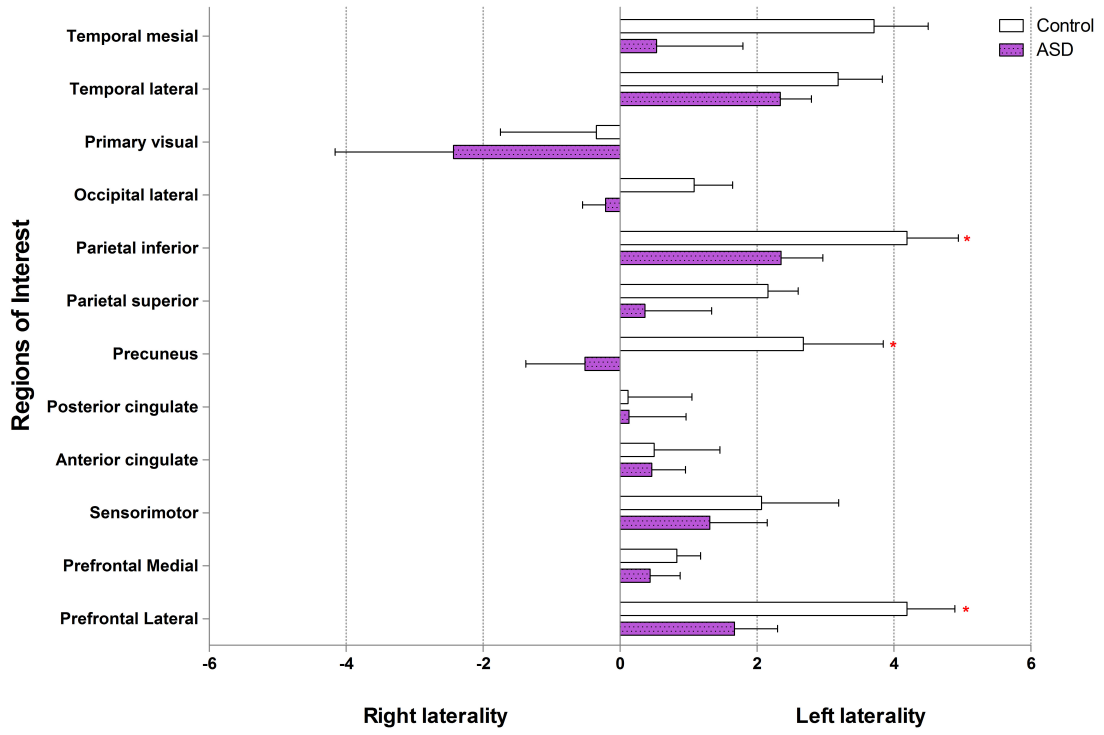

FIGURE 3
Brain laterality in regions of interest between control and ASD (* represents statistically significant by Wilcoxon signed-rank test).

have higher glucose metabolism, as shown in the PET images. In contrast, less active or non-functioning cells were identified as hypometabolic areas. Our observation revealed multiple areas with lower brain glucose metabolism, including the parietal superior, temporal lateral, parietal inferior, and precuneus regions in the ASD. These findings support those of previous studies, including Hazlett et al. (2004), who reported cortical lower glucose metabolism in the medial prefrontal and anterior cingulate regions in ASD patients compared with controls (Hazlett et al., 2004). Another study showed lower brain glucose metabolism in the amygdala, hippocampus, parahippocampal gyrus, caudate nucleus, cerebellum, mesial temporal, thalamus, superior temporal, and mesial temporal regions (Sharma et al., 2018). A lower brain metabolism had also been reported in the hippocampus, amygdala, parahippocampal gyrus, mesial temporal, parietal, cerebellum (Leblanc, 2017) parietal lobe, temporal lobe, anterior cingulate, posterior cingulate, and thalamus (Haznedar et al., 2006; Manglunia and Puranik, 2016; Mitelman et al., 2018). Our study could not focus on the hippocampus and amygdala due to limitation of the processing software. As we have already known, these two brain regions are very important for ASD pathology. As mentioned in the previous study, the volume of hippocampus combined with amygdala are approximately 87% of all element in mesial temporal region (Striepens et al., 2010). Therefore, decrease in both brain glucose metabolism and brain laterality at the left temporal mesial in our ASD participants was sufficient to infer that there was abnormal brain glucose metabolism at the hippocampus and amygdala. Nevertheless, using the specific software that can analyze the hippocampus and amygdala separately would be more accurate.

We also observed areas with higher brain glucose metabolism in both primary visual cortices. These finding may associate with local functional disruption within the occipital cortices, which could produce spontaneous brain activity or spontaneous ability to perform a given cognitive or physiological tasks, causing abnormally high brain glucose metabolism in these regions (Itahashi et al., 2015). Overall, the lower brain glucose metabolism in the ASD group compared to the control group in our study was probably due to abnormal neuronal connectivity (Billeci et al., 2013; Haghighat et al., 2021).

What is the pathophysiology of brain laterality?

Our data in the control (individual with normal brain function) group showed left laterality in almost all ROIs except primary visual area using Q.Brain software normalized by pons. The prefrontal lateral, prefrontal medial, sensorimotor, anterior cingulate, posterior cingulate, precuneus, parietal superior,

parietal inferior, occipital lateral, temporal lateral, and temporal mesial showed left laterality in various degree by which the prefrontal lateral was the most left lateralization.

At present, there are some studies that evaluate laterality in individual with normal brain function. They usually presented the laterality using three aspects (1) hemispheric lateralization; (2) functional lateralization, i.e., language, sensory, and motor lateralization; and (3) ROI lateralization. The hemispheric and functional lateralization are extensively used and usually measured by fMRI. The ROI lateralization, as used in our study, is rarely mentioned but it can be measured by PET scan (Gur et al., 1995; Willis et al., 2002). Among the ROI lateralization by PET scan studies, there was also a difference in reference region used in the study. Gur RC and colleagues demonstrated left laterality in almost all ROI including the premotor cortex, sensorimotor, and parietal superior in their study using global as a reference region. They also reported right laterality in the occipital lateral (Gur et al., 1995). Willis MW and colleagues, using global reference, demonstrated left laterality in the frontal medial and precuneus regions. However, they found right laterality in the frontal lateral and temporal regions (Willis et al., 2002). According to our study that used pons as a reference region, it was difficult to compare our results with these two studies. We therefore perform second analysis using global as reference region (**Table 4** in supplemental document) in order to compare the results. The results of our study were not different from our results that used pons as a reference region. Comparing with Gur's and Willis' studied, the left laterality was found in most of the ROIs in the individual with normal brain function. However, right laterality was found in different regions for example; Willis found right laterality in the frontal lateral, while our study and Gur evidenced left laterality in frontal lateral. This difference may be due to (1) Willis performed in volunteers with mean age of 40 years old, while Gur and our studies performed in the individual with normal brain function with mean age about 20 years old. Changes in glucose metabolism due to age-related differences could be affected frontal lateral region (Fujimoto et al., 2008; Hsieh et al., 2012); and (2) the differences in protocols; our study and Gur study measured brain glucose metabolism at the resting stage, while Willis' study measured during tasks assignment. Although studies in this area do not have enough evidences to draw a conclusion, individuals with normal brain function are likely to have left laterality in most ROIs.

Why is the left laterality usually found in the resting state of individual with normal brain function?

The lateralized circuits arise from the gene that regulates neural circuit formation but the core concept of genetic mechanism in brain laterality is still unknown (Francks, 2015). The primate mirror system responds to intentional movement in daily activity and imitation of another individual action (Rizzolatti and Sinigaglia, 2010). Moreover, the language circuit relates to the idea of language perception in both verbal and non-verbal communications (Corballis, 2017a). All of these features, located within the left cerebral hemisphere, have been developing over time since the beginning of humankind causing left lateralization (Corballis, 2017a,b).

Brain laterality in autism spectrum disorder vs. individual with normal brain function?

In the control group, our findings showed left laterality that was observed in all ROIs (except the primary visual region). The left laterality in ASD was found to be lower than that in the control group in the prefrontal lateral, precuneus, and parietal inferior. In addition, we found a trend toward association between age and brain glucose metabolism at the left prefrontal medial and right temporal lateral in the control group while there was no correlation between age and F-18 FDG PET/CT uptake in ASD group.

Brain glucose metabolism in ASD patients were lower than those in controls, as mentioned above. As there have been no previous studies on laterality by FDG PET/CT in individuals with ASD, it was impossible to compare results with the same neuroimaging method. fMRI is another neuroimaging modality similar to PET/CT, and for the ASD preliminary results, we found a decrease in the left laterality index in the prefrontal lateral, precuneus, and parietal inferior regions compared to the control. Our findings are in concordance with other evidence of less laterality in the frontal language areas detected by fMRI (Preslar et al., 2014). The explanation of abnormal left laterality occurring within the ASD brain is unclear, but there is a possibility that atypical early brain development occurred in those brain regions (Benkarim et al., 2021), resulting in abnormal functional lateralization for language and social function in ASD patients (Lindell and Hudry, 2013). As our findings showed decreased brain glucose metabolism of left prefrontal lateral in ASD. We also found decreasing of left laterality in prefrontal lateral. Therefore, this part of the brain is probably important for ASD pathophysiology. As we know that the dorsolateral prefrontal cortex plays an important role in executive function by connecting the frontal and parietal cortices *via* frontoparietal networks (Haber et al., 2021), enhancing working memory capacity (Osaka et al., 2021), and is related to human intelligence (Hearne et al., 2016). An irregular arrangement of neural connections is one of the proposed pathologies of ASD. This abnormal connection may occur mainly in the frontoparietal network and result in decreased brain glucose metabolism in both cerebral hemispheres, but more striking in the left hemisphere, leading to decreased left

TABLE 4 Brain laterality in control group using global as the reference region (n = 8).

	Prefrontal Lateral	Prefrontal medial	Sensori motor	Anterior cingulate	Posterior cingulate	Precu neus	Parietal superior	Parietal inferior	Occipital lateral	Primary visual	Temporal lateral	Temporal mesial
Control 01	3.75	0.00	2.03	2.10	0.00	2.71	2.95	2.00	0.00	0.86	3.52	4.57
Control 02	3.75	2.05	5.08	1.05	0.00	1.80	1.97	2.00	1.00	0.00	2.35	4.57
Control 03	2.81	0.00	2.03	−4.20	−0.86	−1.31	−1.95	2.99	4.01	−6.03	1.17	0.00
Control 04	3.75	0.00	6.09	2.10	−1.73	0.90	0.00	3.99	−1.00	1.72	2.35	3.05
Control 05	2.81	1.02	−1.02	0.00	−0.86	1.80	1.97	2.00	2.00	−0.86	3.52	3.05
Control 06	2.81	0.00	4.06	1.05	−1.73	−2.71	−2.92	4.99	2.00	6.90	4.70	0.00
Control 07	0.94	2.05	1.02	0.00	5.19	0.00	0.98	2.99	2.00	−0.86	3.52	7.62
Control 08	1.88	−2.05	−3.05	0.00	0.00	0.00	−1.97	3.99	1.00	−3.45	2.35	4.57
Mean	2.81	0.38	2.03	0.26	0.00	0.40	0.13	3.12	1.38	−0.22	2.94	3.43
SD	1.00	1.33	3.07	2.01	2.22	1.79	2.19	1.12	1.51	3.79	1.09	2.54

The negative values represent right laterality and the positive values represent left laterality.

laterality in the left precuneus and parietal inferior regions, as seen in our ASD participants.

Studies on laterality in individual with normal brain function show heterogeneity, and the results are inconclusive. Our study showed that ASD patients had a distinctive laterality trend compared to controls, that is, a lesser number of ROIs for left laterality. Moreover, among the areas of left laterality found in this study, ASD individuals showed lower brain glucose metabolism levels than control, that is, left laterality index in the prefrontal lateral in control was equal to 4 vs. ASD equal to 1.8. This finding is likely caused by abnormal brain development that results in abnormal left laterality through various mechanisms during the perinatal period (Wiper, 2017).

How is this new knowledge useful?

Currently, there is no curative treatment for ASDs. Non-invasive brain stimulation (NIBS) is an emerging tool for the treatment of ASDs. The main NIBS devices for ASD treatment are transcranial magnetic stimulation (TMS) and transcranial direct current stimulation (tDCS). A recent systematic review and meta-analysis suggested that TMS might be a novel technique which has therapeutic potential to correct the abnormal neuroplasticity in ASD (Huashuang et al., 2022). Same as TMS, systematic review and meta-analytic study of tDCS identified improvements in social, health, and behavioral problem domains of the Autism Treatment Evaluation Checklist (García-González et al., 2021).

Transcranial magnetic stimulation is neurostimulation using a magnetic field transmitted through the scalp, and induced an electric field to the neuronal cells. The magnitude of this electric field is enough to produce depolarization of neurons. Repetitive TMS (rTMS) delivers multiple series of short magnetic pulse over a specified brain region. The low frequency rTMS leads to long-term suppression of brain excitability, whereas at high frequency rTMS typically results in long-term facilitation of brain excitability by mechanisms associated with long-term potentiation (Khaleghi et al., 2020).

These after effects, which are mediated by glutamatergic synapses [especially the N-methyl-D-aspartate (NMDA) receptors], have been related to long-term potentiation and long-term depression-liked mechanisms. The tDCS is a neuromodulation method that modify neuronal membrane potential and thus affect spontaneous firing rates by applying a weak direct current *via* two electrodes. The anodal electrode will increase excitability of the underneath neurons; whereas, cathodal electrode will decrease excitability of the neuron cell due to hyperpolarization. The effects of tDCS are not only restricted to the area under the electrode but also transmitted by functional connection within the brain to distance areas. The neuroplasticity induced by tDCS might be associated with the increased functional connectivity in the brain (García-González et al., 2021). The primary treatment principle for both devices is to stimulate the less-active brain regions and inhibit the overactive brain regions. The currently targeted brain regions for the NIBS method in ASD patients remain diverse (Barahona-Corrêa et al., 2018). In general, positive clinical outcomes are associated with anodal (stimulation electrode) over the left DLPFC (Schneider and Hopp, 2011; Amatachaya et al., 2014, 2015; Gómez et al., 2017; Auvichayapat et al., 2020; Hadoush et al., 2020). However, another study also showed a positive effect of the cathodal (inhibitory electrode) over the left DLPFC (Rothärmel et al., 2019). To date, studies have been inconsistent regarding the appropriate regional protocol for NIBS electrode placement.

Our study suggests that ASD participants have lower regional brain glucose metabolism in many areas of the brain, as well as less left laterality, than controls. To induce normal brain metabolism, the application of anodal tDCS or high-frequency TMS over the left hemisphere of ASD patients might be more effective than over the right hemisphere or performing left-sided inhibition. Applying these knowledges may extend to the treatment of major depressive disorder, bipolar depression

(Cotovio et al., 2022), schizophrenia (Oertel et al., 2010), and other laterality abnormality (He et al., 2022). However, further in-depth studies, including clinical outcomes after non-invasive brain stimulation treatment should be evaluated by functional neuromolecular imaging study in the specific ROI such as MRS, are recommended.

Limitation of the study

This study could not include normal young-adult participants as the control due to the ethical concerning about radiation exposure. Although patients with lymphoma were found to have global brain hypometabolism, the previous study revealed that these hypometabolic states recovered after sessions of chemotherapy (Nonokuma et al., 2014). In addition, our control participants had completed a full course of chemotherapy before the time of the study and all of them were in the complete remission state. Therefore, in our opinion, it was acceptable to be the control group.

We did not find the difference of overall brain glucose metabolism between the medication and non-medication groups. However, the neuropsychological medications affect the neuronal activity by suppression of overall brain glucose metabolism. In order to precisely answer the research question, our suggestion is to exclude ASD with medications in the future functional neuroimaging study.

Summary

This study provides preliminary evidence showing lower resting brain glucose metabolism in ASD patients and less left laterality than controls when measured by F-18 FDG PET/CT. In addition, the degree of left laterality in ASD patients was also lower than that in controls. This preliminary knowledge could be usefully applied in ASD treatment by increasing left-brain metabolism and promoting more left laterality. Nonetheless, a larger sample size and clinical outcome-focused studies in combination with neuroimaging in terms of brain laterality are strongly suggested.

Data availability statement

The raw data supporting the conclusions of this article will be made available by the authors, without undue reservation.

Ethics statement

The studies involving human participants were reviewed and approved by the Ethics Committee of Khon Kaen University (Identifier number: HE 621277). Written informed consent to participate in this study was provided by the participants' legal guardian/next of kin.

Author contributions

PA, DT, NA, and KK: study design. PA, KK, NP, CS, NA, and STi: subject enrollment. CS, NP, KK, DT, STe, and BK: outcome evaluator. PA, KK, and YR: data collection. PA and KK: data analysis. KK, PA, NP, NA, and SP: manuscript writing. All authors contributed to the article and approved the submitted version.

Funding

This work was supported by grants from the following organization: the Research and Service Institute for Autism (RSIA Research Funding, RRF1), Research Assistantship (AS63206); Epilepsy Research Group, Srinagarind Hospital, Faculty of Medicine, Khon Kaen University, and Danapha Research Grant (2564) Thailand. The funders of the study had no role in study design, data collection, data analysis, data interpretation, or writing of the report.

Acknowledgments

We would like to thank director, teachers, staffs, and guardians of autistic children of the Institute of Vocational Education: Northeastern Region 3 and Autism Parents Association of Khon Kaen, Thailand in the very well co-operation and supports. We also thank John F. Smith and Editage (www.editage.com) for English language editing.

Conflict of interest

The authors declare that the research was conducted in the absence of any commercial or financial relationships that could be construed as a potential conflict of interest.

Publisher's note

All claims expressed in this article are solely those of the authors and do not necessarily represent those of their affiliated organizations, or those of the publisher, the editors and the reviewers. Any product that may be evaluated in this article, or claim that may be made by its manufacturer, is not guaranteed or endorsed by the publisher.

References

Alvares, G. A., Bebbington, K., Cleary, D., Evans, K., Glasson, E. J., Maybery, M. T., et al. (2020). The misnomer of "high functioning autism": intelligence is an imprecise predictor of functional abilities at diagnosis. *Autism* 24, 221–232. doi: 10.1177/1362361319852831

Amatachaya, A., Auvichayapat, N., Patjanasoontorn, N., Suphakunpinyo, C., Ngernyam, N., Aree-Uea, B., et al. (2014). Effect of anodal transcranial direct current stimulation on autism: a randomized double-blind crossover trial. *Behav. Neurol.* 2014:173073. doi: 10.1155/2014/173073

Amatachaya, A., Jensen, M. P., Patjanasoontorn, N., Auvichayapat, N., Suphakunpinyo, C., Janjarasjitt, S., et al. (2015). The short-term effects of transcranial direct current stimulation on electroencephalography in children with autism: a randomized crossover controlled trial. *Behav. Neurol.* 2015:928631. doi: 10.1155/2015/928631

Auvichayapat, N., Patjanasoontorn, N., Phuttharak, W., Suphakunpinyo, C., Keeratitanont, K., Tunkamnerdthai, O., et al. (2020). Brain metabolite changes after anodal transcranial direct current stimulation in autism spectrum disorder. *Front. Mol. Neurosci.* 13:70. doi: 10.3389/fnmol.2020.00070

Azari, N. P., Rapoport, S. I, Grady, C. L., DeCarli, C., Haxby, J. V., Schapiro, M. B., et al. (1992). Gender differences in correlations of cerebral glucose metabolic rates in young normal adults. *Brain Res.* 574, 198–208. doi: 10.1016/0006-8993(92)90817-S

Barahona-Corrêa, J. B., Velosa, A., Chainho, A., Lopes, R., and Oliveira-Maia, A. J. (2018). Repetitive transcranial magnetic stimulation for treatment of autism spectrum disorder: a systematic review and meta-analysis. *Front. Integr. Neurosci.* 12:27. doi: 10.3389/FNINT.2018.00027

Benkarim, O., Paquola, C., Park, B-y, Hong, S. J., Royer, J., Vos de Wael, R., et al. (2021). Connectivity alterations in autism reflect functional idiosyncrasy. *Commun. Biol.* 4, 1–15. doi: 10.1038/s42003-021-02572-6

Billeci, L., Sicca, F., Maharatna, K., Apicella, F., Narzisi, A., Campatelli, G., et al. (2013). On the application of quantitative EEG for characterizing autistic brain: a systematic review. *Front. Hum. Neurosci.* 7:442. doi: 10.3389/FNHUM.2013.00442

Cara, M. L., Streata, I., Buga, A. M., and Iliescu, D. G. (2022). Developmental brain asymmetry. the good and the bad sides. *Symmetry* 14:128. doi: 10.3390/SYM14010128

Corballis, M. C. (2017a). The evolution of lateralized brain circuits. *Front. Psychol.* 8:1021. doi: 10.3389/FPSYG.2017.01021

Corballis, M. C. (2017b). Language evolution: a changing perspective. *Trends Cogn. Sci.* 21, 229–236. doi: 10.1016/J.TICS.2017.01.013

Cotovio, G., Rodrigues da Silva, D., Real Lage, E., Seybert, C., and Oliveira-Maia, A. J. (2022). Hemispheric asymmetry of motor cortex excitability in mood disorders – Evidence from a systematic review and meta-analysis. *Clin. Neurophysiol.* 137, 25–37. doi: 10.1016/J.CLINPH.2022.01.137

Courchesne, E., Gazestani, V. H., and Lewis, N. E. (2020). Prenatal origins of ASD: the when, what, and how of ASD development. *Trends Neurosci.* 43, 326–342. doi: 10.1016/J.TINS.2020.03.005

Francks, C. (2015). Exploring human brain lateralization with molecular genetics and genomics. *Ann. N. Y. Acad. Sci.* 1359, 1–13. doi: 10.1111/NYAS.12770

Fujimoto, T., Matsumoto, T., Fujita, S., Takeuchi, K., Nakamura, K., Mitsuyama, Y., et al. (2008). Changes in glucose metabolism due to aging and gender-related differences in the healthy human brain. *Psychiatry Res.* 164, 58–72. doi: 10.1016/J.PSCYCHRESNS.2006.12.014

García-González, S., Lugo-Marín, J., Setien-Ramos, I., Gisbert-Gustemps, L., Arteaga-Henríquez, G., Díez-Villoria, E., et al. (2021). Transcranial direct current stimulation in Autism Spectrum Disorder: a systematic review and meta-analysis. *Eur. Neuropsychopharmacol.* 48, 89–109. doi: 10.1016/J.EURONEURO.2021.02.017

Gómez, L., Vidal, B., Maragoto, C., Morales, L. M., Berrillo, S., Vera Cuesta, H., et al. (2017). Non-invasive brain stimulation for children with autism spectrum disorders: a short-term outcome study. *Behav. Sci. (Basel, Switzerland)* 7:63. doi: 10.3390/bs7030063

Gur, R. C., Mozley, L. H., Mozley, P. D., Resnick, S. M., Karp, J. S., Alavi, A., et al. (1995). Sex differences in regional cerebral glucose metabolism during a resting state. *Science (New York, N.Y.)* 267, 528–531. doi: 10.1126/SCIENCE.7824953

Haber, S. N., Liu, H., Seidlitz, J., and Bullmore, E. (2021). Prefrontal connectomics: from anatomy to human imaging. *Neuropsychopharmacology* 47, 20–40. doi: 10.1038/s41386-021-01156-6

Hadoush, H., Nazzal, M., Almasri, N. A., Khalil, H., and Alafeef, M. (2020). Therapeutic effects of bilateral anodal transcranial direct current stimulation on prefrontal and motor cortical areas in children with autism spectrum disorders: a pilot study. *Autism Res.* 13, 828–836. doi: 10.1002/AUR.2290

Haghighat, H., Mirzarezaee, M., Araabi, B. N., and Khadem, A. (2021). Functional networks abnormalities in autism spectrum disorder: age-related hypo and hyper connectivity. *Brain Topogr.* 34, 306–322. doi: 10.1007/S10548-021-00831-7

Hampson, D. R., and Blatt, G. J. (2015). Autism spectrum disorders and neuropathology of the cerebellum. *Front. Neurosci.* 9:420. doi: 10.3389/FNINS.2015.00420/BIBTEX

Hazlett, E. A., Buchsbaum, M. S., Hsieh, P., Haznedar, M. M., Platholi, J., LiCalzi, E. M., et al. (2004). Regional glucose metabolism within cortical brodmann areas in healthy individuals and autistic patients. *Neuropsychobiology* 49, 115–125. doi: 10.1159/000076719

Haznedar, M., Buchsbaum, M. S., Hazlett, E. A., LiCalzi, E. M., Cartwright, C., and Hollander, E. (2006). Volumetric analysis and three-dimensional glucose metabolic mapping of the striatum and thalamus in patients with autism spectrum disorders. *Am. J. Psychiatry* 163:1252. doi: 10.1176/appi.ajp.163.7.1252

He, N., Palaniyappan, L., Linli, Z., and Guo, S. (2022). Abnormal hemispheric asymmetry of both brain function and structure in attention deficit/hyperactivity disorder: a meta-analysis of individual participant data. *Brain Imaging Behav.* 16, 54–68. doi: 10.1007/S11682-021-00476-X

Hearne, L. J., Mattingley, J. B., and Cocchi, L. (2016). Functional brain networks related to individual differences in human intelligence at rest. *Sci. Rep.* 6:32328. doi: 10.1038/srep32328

Hsieh, T. C., Lin, W. Y., Ding, H. J., Sun, S. S., Wu, Y. C., Yen, K. Y., et al. (2012). Sex- and age-related differences in brain FDG metabolism of healthy adults: an SPM analysis. *J. Neuroimaging?* 22, 21–27. doi: 10.1111/J.1552-6569.2010.00543.X

Huashuang, Z., Yang, L., Chensheng, H., Jing, X., Bo, C., Dongming, Z., et al. (2022). Prevalence of adverse effects associated with transcranial magnetic stimulation for autism spectrum disorder: a systematic review and meta-analysis. *Front. Psychiatry* 13:875591. doi: 10.3389/FPSYT.2022.875591

Itahashi, T., Yamada, T., Watanabe, H., Nakamura, M., Ohta, H., Kanai, C., et al. (2015). Alterations of local spontaneous brain activity and connectivity in adults with high-functioning autism spectrum disorder. *Mol. Autism* 6:30. doi: 10.1186/S13229-015-0026-Z

John, T., and Watts, T. J. (2008). The pathogenesis of autism. *Clin. Med. Pathol.* 1, 99–103.

Khaleghi, A., Zarafshan, H., Vand, S. R., and Mohammadi, M. R. (2020). Effects of non-invasive neurostimulation on autism spectrum disorder: a systematic review. *Clin. Psychopharmacol. Neurosci.* 18, 527–552. doi: 10.9758/CPN.2020.18.4.527

Kim, H. J., Cho, M. H., Shim, W. H., Kim, J. K., Jeon, E. Y., Kim, D. H., et al. (2016). Deficient autophagy in microglia impairs synaptic pruning and causes social behavioral defects. *Mol. Psychiatry* 22, 1576–1584. doi: 10.1038/mp.2016.103

Kwan, P., Arzimanoglou, A., Berg, A. T., Brodie, M. J., Hauser, W. A., Mathern, G., et al. (2010). Definition of drug resistant epilepsy: consensus proposal by the ad hoc task force of the ILAE Commission on Therapeutic Strategies. *Epilepsia* 51, 1069–1077. doi: 10.1111/J.1528-1167.2009.02397.X

Leblanc, H. (2017). Brain abnormality findings in F18-FDG PET/CT imaging and its role in the clinical diagnosis of autism. *J. Nuclear Med.* 58(Suppl. 1):828.

Lindell, A. K., and Hudry, K. (2013). Atypicalities in cortical structure, handedness, and functional lateralization for language in autism spectrum disorders. *Neuropsychology Review* 23, 257–270. doi: 10.1007/S11065-013-9234-5

Lord, C., Risi, S., Lambrecht, L., Cook, E. H., Leventhal, B. L., Dilavore, P. C., et al. (2000). The autism diagnostic observation schedule—generic: a standard measure of social and communication deficits associated with the spectrum of autism. *J. Autism Dev. Disord.* 30, 205–223. doi: 10.1023/A:1005592401947

Manglunia, A. S., and Puranik, A. D. (2016). FDG PET/CT findings in a clinically diagnosed case of childhood autism. *Indian J. Nuclear Med.* 31, 138–140. doi: 10.4103/0972-3919.178302

Marchetto, M. C., Belinson, H., Tian, Y., Freitas, B. C., Fu, C., Vadodaria, K. C., et al. (2016). Altered proliferation and networks in neural cells derived from idiopathic autistic individuals. *Mol. Psychiatry* 22, 820–835. doi: 10.1038/mp.2016.95

Mitelman, S. A., Bralet, M. C., Mehmet Haznedar, M., Hollander, E., Shihabuddin, L., Hazlett, E. A., et al. (2018). Positron emission tomography assessment of cerebral glucose metabolic rates in autism spectrum disorder and schizophrenia. *Brain Imaging Behav.* 12:532. doi: 10.1007/S11682-017-9721-Z

Morimoto, E., Okada, T., Kanagaki, M., Yamamoto, A., Fushimi, Y., Matsumoto, R., et al. (2013). Evaluation of focus laterality in temporal lobe epilepsy: a quantitative study comparing double inversion-recovery MR imaging at 3T with FDG-PET. *Epilepsia* 54, 2174–2183. doi: 10.1111/EPI.12396

Nonokuma, M., Kuwabara, Y., Takano, K., Tamura, K., Ishitsuka, K., and Yoshimitsu, K. (2014). Evaluation of regional cerebral glucose metabolism in patients with malignant lymphoma of the body using statistical image analysis. *Ann. Nuclear Med.* 28, 950–960. doi: 10.1007/S12149-014-0890-1

Oertel, V., Knöchel, C., Rotarska-Jagiela, A., Schönmeyer, R., Lindner, M., van de Ven, V., et al. (2010). Reduced laterality as a trait marker of schizophrenia–evidence from structural and functional neuroimaging. *J. Neurosci.* 30, 2289–2299. doi: 10.1523/JNEUROSCI.4575-09.2010

Osaka, M., Kaneda, M., Azuma, M., Yaoi, K., Shimokawa, T., and Osaka, N. (2021). Capacity differences in working memory based on resting state brain networks. *Sci. Rep.* 11:19502. doi: 10.1038/s41598-021-98848-2

Preslar, J., Kushner, H. I., Marino, L., and Pearce, B. (2014). Autism, lateralisation, and handedness: a review of the literature and meta-analysis. *Laterality* 19, 64–95. doi: 10.1080/1357650X.2013.772621

Pustina, D., Avants, B., Sperling, M., Gorniak, R., He, X., Doucet, G., et al. (2015). Predicting the laterality of temporal lobe epilepsy from PET, MRI, and DTI: a multimodal study. *NeuroImage* 9:20. doi: 10.1016/J.NICL.2015.07.010

Rizzolatti, G., and Sinigaglia, C. (2010). The functional role of the parieto-frontal mirror circuit: interpretations and misinterpretations. *Nat. Rev. Neurosci.* 11, 264–274. doi: 10.1038/NRN2805

Rothärmel, M., Moulier, V., Vasse, M., Isaac, C., Faerber, M., Bendib, B., et al. (2019). A prospective open-label pilot study of transcranial direct current stimulation in high-functioning autistic patients with a dysexecutive syndrome. *Neuropsychobiology* 78, 189–199. doi: 10.1159/000501025

Savic, I., and Lindström, P. (2008). PET and MRI show differences in cerebral asymmetry and functional connectivity between homo- and heterosexual subjects. *Proc. Natl. Acad. Sci. U.S.A.* 105, 9403–9408. doi: 10.1073/PNAS.0801566105

Savio, A., Fünger, S., Tahmasian, M., Rachakonda, S., Manoliu, A., Sorg, C., et al. (2017). Resting-state networks as simultaneously measured with functional MRI and PET. *J. Nuclear Med.* 58:1314. doi: 10.2967/JNUMED.116.185835

Schneider, H. D., and Hopp, J. P. (2011). The use of the Bilingual Aphasia Test for assessment and transcranial direct current stimulation to modulate language acquisition in minimally verbal children with autism. *Clin. Linguist. Phonetics* 25, 640–654. doi: 10.3109/02699206.2011.570852

Sharma, A., Gokulchandran, N., Sane, H., Nivins, S., Paranjape, A., and Badhe, P. (2018). The baseline pattern and age-related developmental metabolic changes in the brain of children with autism as measured on positron emission tomography/computed tomography scan. *World J. Nuclear Med.* 17, 94–101. doi: 10.4103/wjnm.WJNM_29_17

Soddu, A., Gómez, F., Heine, L., di Perri, C., Bahri, M. A., Voss, H. U., et al. (2016). Correlation between resting state fMRI total neuronal activity and PET metabolism in healthy controls and patients with disorders of consciousness. *Brain Behavior* 6, 1–15. doi: 10.1002/BRB3.424

Striepens, N., Scheef, L., Wind, A., Popp, J., Spottke, A., Cooper-Mahkorn, D., et al. (2010). Volume loss of the medial temporal lobe structures in subjective memory impairment. *Dement. Geriatr. Cogn. Disord.* 29, 75–81. doi: 10.1159/000264630

Tang, G., Gudsnuk, K., Kuo, S. H., Cotrina, M. L., Rosoklija, G., Sosunov, A., et al. (2014). Loss of mTOR-dependent macroautophagy causes autistic-like synaptic pruning deficits. *Neuron* 83, 1131–1143. doi: 10.1016/J.NEURON.2014.07.040

Varrone, A., Asenbaum, S., vander Borght, T., Booij, J., Nobili, F., Någren, K., et al. (2009). EANM procedure guidelines for PET brain imaging using [18F]FDG, version 2. *Eur. J. Nuclear Med. Mol. Imaging* 36, 2103–2110. doi: 10.1007/S00259-009-1264-0

Verger, A., Doyen, M., Campion, J. Y., and Guedj, E. (2021). The pons as reference region for intensity normalization in semi-quantitative analysis of brain 18 FDG PET: application to metabolic changes related to ageing in conventional and digital control databases. *EJNMMI Res.* 11:31. doi: 10.1186/S13550-021-00771-0

Willis, M. W., Ketter, T. A., Kimbrell, T. A., George, M. S., Herscovitch, P., Danielson, A. L., et al. (2002). Age, sex and laterality effects on cerebral glucose metabolism in healthy adults. *Psychiatry Res.* 114, 23–37. doi: 10.1016/S0925-4927(01)00126-3

Wiper, M. L. (2017). Evolutionary and mechanistic drivers of laterality: a review and new synthesis. *Laterality* 22, 740–770. doi: 10.1080/1357650X.2017.1291658

Yakushev, I., Landvogt, C., Buchholz, H. G., Fellgiebel, A., Hammers, A., Scheurich, A., et al. (2008). Choice of reference area in studies of Alzheimer's disease using positron emission tomography with fluorodeoxyglucose-F18. *Psychiatry Res.* 164, 143–153. doi: 10.1016/J.PSCYCHRESNS.2007.11.004

frontiers | Frontiers in Molecular Neuroscience

TYPE Original Research
PUBLISHED 15 August 2022
DOI 10.3389/fnmol.2022.947513

Check for updates

OPEN ACCESS

EDITED BY
Salam Salloum-Asfar,
Qatar Biomedical Research Institute, Qatar

REVIEWED BY
Sara A. Abdulla,
Qatar Biomedical Research Institute, Qatar
Edward Quadros,
Downstate Health Sciences University, United States
Dongchuan Yu,
Southeast University, China

*CORRESPONDENCE
Changlian Zhu
changlian.zhu@neuro.gu.se;
zhuc@zzu.edu.cn

SPECIALTY SECTION
This article was submitted to Neuroplasticity and Development, a section of the journal Frontiers in Molecular Neuroscience

RECEIVED 18 May 2022
ACCEPTED 18 July 2022
PUBLISHED 15 August 2022

CITATION
Li B, Xu Y, Pang D, Zhao Q, Zhang L, Li M, Li W, Duan G and Zhu C (2022) Interrelation between homocysteine metabolism and the development of autism spectrum disorder in children. *Front. Mol. Neurosci.* 15:947513. doi: 10.3389/fnmol.2022.947513

COPYRIGHT
© 2022 Li, Xu, Pang, Zhao, Zhang, Li, Li, Duan and Zhu. This is an open-access article distributed under the terms of the Creative Commons Attribution License (CC BY). The use, distribution or reproduction in other forums is permitted, provided the original author(s) and the copyright owner(s) are credited and that the original publication in this journal is cited, in accordance with accepted academic practice. No use, distribution or reproduction is permitted which does not comply with these terms.

Interrelation between homocysteine metabolism and the development of autism spectrum disorder in children

Bingbing Li[1], Yiran Xu[1], Dizhou Pang[2], Qiang Zhao[3], Lingling Zhang[1], Ming Li[1], Wenhua Li[1], Guiqin Duan[2] and Changlian Zhu[1,4]*

[1]Henan Key Laboratory of Child Brain Injury and Henan Pediatric Clinical Research Center, Third Affiliated Hospital and Institute of Neuroscience, Zhengzhou University, Zhengzhou, China, [2]Center for Child Behavioral Development, Third Affiliated Hospital of Zhengzhou University, Zhengzhou, China, [3]Key Clinical Laboratory of Henan Province, Department of Clinical Laboratory, First Affiliated Hospital of Zhengzhou University, Zhengzhou, China, [4]Center for Brain Repair and Rehabilitation, Institute of Neuroscience and Physiology, University of Gothenburg, Sahlgrenska Academy, Gothenburg, Sweden

Evidence is emerging that dysregulation of circulating concentrations of homocysteine, an important intermediate in folate and vitamin B12 metabolism, is associated with autism spectrum disorder (ASD), but comprehensive assessments and correlations with disease characteristics have not been reported. Multivariate ordinal regression and restricted cubic spline (RCS) models were used to estimate independent correlations between serum homocysteine, folate, and vitamin B12 levels and clinical outcomes and severity of children with ASD. After adjusting for confounding factors, serum homocysteine levels were significantly higher in children with ASD than in healthy controls (β: 0.370; 95% CI: 0.299∼0.441, $p < 0.001$). Moreover, homocysteine had a good diagnostic ability for distinguishing children with ASD from healthy subjects (AUC: 0.899, $p < 0.001$). The RCS model indicated a positive and linear association between serum homocysteine and the risk of ASD. The lowest quartile of folate was positively associated with ASD severity (OR: 4.227, 95% CI: 1.022∼17.488, $p = 0.041$) compared to the highest quartile, and serum folate showed a negative and linear association with ASD severity. In addition, decreased concentrations of folate and vitamin B12 were associated with poor adaptive behavior developmental quotients of the Gesell Developmental Schedules ($p < 0.05$). Overall, an increased homocysteine level was associated with ASD in a linear manner and is thus a novel diagnostic biomarker for ASD. Decreased concentrations of folate and vitamin B12 were associated with poor clinical profiles of children with ASD. These findings suggest that homocysteine-lowering interventions or folate and vitamin B12 supplementation might be a viable treatment strategy for ASD.

KEYWORDS

homocysteine, folate, vitamin B12, autism spectrum disorder, biomarkers

Introduction

Autism spectrum disorder (ASD) is an early-onset neurodevelopmental disorder characterized by problems with social communication, repetitive behavior, and restricted interests, and patients can manifest a comprehensive array of additional symptoms such as intellectual disabilities and gastrointestinal disorders (Lai et al., 2014). Although heredity is widely recognized as one of the major causes of ASD (Sandin et al., 2017), it cannot explain the recent increase in ASD prevalence (Maenner et al., 2020). Therefore, more and more attention has been paid to the study of environmental factors in the etiology of ASD.

Homocysteine, a sulfur-containing amino acid, is a metabolic intermediate in methionine metabolism and is crucial for methionine availability, nucleotide synthesis, and methylation reactions (Koklesova et al., 2021). Elevated serum homocysteine levels have been identified as a risk factor for several neurological and psychiatric disorders, including cognitive impairment (Zhou et al., 2021), dementia (Chen et al., 2020), and bipolar disorders (Salagre et al., 2017), and they have been shown to have direct neurotoxicity and to induce oxidative stress and mitochondrial dysfunction, both of which are implicated in ASD (Frye et al., 2013a; Balachandar et al., 2021). These observations have raised questions regarding whether elevated serum homocysteine is a biomarker or a therapeutic target of ASD. However, previous observational studies generated contrasting results, with some showing significant positive associations (Altun et al., 2018; Chen et al., 2021) and others showing no associations (Main et al., 2015; Saha et al., 2022). More importantly, no studies assessed the specific shape of this association while controlling for confounding factors that might affect the serum concentrations of homocysteine such as age, sex, and the use of vitamin supplements. All these factors might lead to some bias and preclude an exhaustive evaluation of the role of homocysteine in ASD. Also, prior studies did not fully examine the relationship between homocysteine levels and clinical severity of ASD symptoms and neurodevelopment in children with ASD.

In addition, levels of homocysteine are inversely correlated with levels of folate and vitamin B12 in the blood (Refsum et al., 2004), which are cofactors for the folate-dependent methylation of homocysteine to methionine (Škovierová et al., 2016) and are required for the synthesis of both phospholipids and myelin, and are crucial for the normal functioning of the brain (Hassan et al., 2019). Folate and vitamin B12 deficiencies have been linked to cognitive impairment (Dror and Allen, 2008; Michelakos et al., 2013) and ASD (Al-Farsi et al., 2013; Li et al., 2021). Moreover, 38% of children with ASD have cerebral folate deficiency syndrome (Rossignol and Frye, 2021a), which is a new emerging group of syndromes that are characterized by low cerebral folate levels under normal blood folate levels. The most common cause of low cerebral folate in this syndrome is the presence of folate receptor autoantibodies that can block folate transport across the blood–brain barrier to the brain and thus influence the development of the central nervous system (Ramaekers et al., 2005; Bobrowski-Khoury et al., 2021). Animal models demonstrated that a decrease in brain folate resulted in homocysteine accumulation and changes in neuronal excitability and maintenance, which contributed to the development of cognitive deficits (Kruman et al., 2005; Mann et al., 2018). Furthermore, owing to gastrointestinal disorders and/or picky eating (Sharp et al., 2013), children with ASD often have inadequate dietary intakes, leading to severe vitamin B12 and folate deficiencies (Ranjan and Nasser, 2015), which might further increase serum homocysteine levels and worsen autism symptoms. It can thus be debated whether it is low levels of folate or vitamin B12 that play an important role in the etiology of ASD. Thus, more extensive well-designed studies are needed to clarify this association.

The primary aim of the present study was to comprehensively investigate the relationship of homocysteine levels with the risk and clinical severity of ASD and its potential role as a diagnostic marker of the risk of developing ASD or for predicting the severity of ASD, which may pave the way for new therapeutic strategies for ASD. Owing to the interrelatedness of homocysteine, folate, and vitamin B12 levels as discussed earlier, we additionally examined the associations between serum folate and vitamin B12 levels and the risk and severity of ASD.

Methods

Participants

In this case–control study, 135 patients who were diagnosed with ASD were consecutively recruited from the inpatient department of the Third Affiliated Hospital of Zhengzhou University from August 2019 to November 2021. The inclusion criteria were age from 1 year to 6 years, patients having completed questionnaires on diet and medical history, those having anthropometric measurements recorded, and those not having consumed vitamin B for more than 3 months prior to the blood sample collection. Children with other developmental disorders or psychiatric diseases such as Rett syndrome, cerebral palsy, or chronic seizures were excluded from the study. A total of 84 healthy individuals were recruited from the community as volunteers with their parents' consent, and these individuals had no physical or neurological disorders and had not received vitamin B supplementation in the previous 3 months. This study was designed and conducted in accordance with the Declaration of Helsinki. All subjects were recruited during the same period, and written informed consent was obtained from the primary caregivers of all participants. The study protocol was approved

by the ethics committee of the Third Affiliated Hospital of Zhengzhou University (Approval # 2020-126-01).

Data collection

Information on demographics, dietary preference for meat and vegetables, medical history, and family or personal history from the two groups of children was collected by well-trained nurses using a pre-tested questionnaire. Anthropometric assessments were performed by trained health professionals following a standardized protocol. The body mass index (BMI) was calculated and expressed as kg/m^2. The z-score of BMI-for-age (ZBMIA) was calculated, and overweight was defined as a ZBMIA > 2 according to the WHO criteria (WHO, 2008). Information on the history of vitamin supplements was recorded because this could affect the participants' levels of homocysteine, folate, and vitamin B12.

Diagnosis and behavioral assessments

Children in the ASD group were diagnosed by using the Diagnostic and Statistical Manual of Mental Disorders, 5th Edition (Regier et al., 2013) for the first time without systemic intervention, and ASD symptoms were assessed by using the Childhood Autism Rating Scale (CARS) by two experienced psychiatrists (Schopler et al., 1980). CARS is an assessment scale of the severity of autistic symptomatology and consists of 15 items that are rated on a four-point scale, and the higher the score, the more severe the symptoms. Children with scores between 30 and 36 are considered to having mild to moderate autism, and those with scores between 37 and 60 are considered severe autism. Neurodevelopmental levels of children with ASD were evaluated using the Gesell Developmental Schedules (GDS), which have been widely used to evaluate the development of children aged from 16 days to 6 years (Liu et al., 2016, 2022). The GDS include five subscales, namely, adaptive, gross motor, fine motor, language, and personal–social behavior. The developmental quotient (DQ) of the five domains was used to evaluate the level of neurodevelopment, and a DQ ≤ 75 for two or more subscales of the GDS indicates a developmental delay.

Sample collection and measurements

A measure of 2 mL of venous blood was drawn into a serum separation tube and immediately centrifuged (1,500 $\times$ g for 5 min) to separate the serum from the cells, after which 0.2 mL of serum was pipetted into several vials and stored at $-80^{\circ}C$ until being assayed. Serum homocysteine levels were measured using the enzyme cycling assay (Roche Diagnostics, Cobas e 801, Switzerland), and serum folate and vitamin B12 levels were analyzed using automated electrochemiluminescence immunoassays (Roche Diagnostics, Cobas 8000, Switzerland).

Statistics

Statistical analyses were performed using SPSS version 23 (SPSS Inc., Chicago, IL, USA), SAS version 14 (SAS Institute, Cary, North Carolina, USA), and Stata version 12 (Stata Corporation, College Station, TX, USA). The characteristics of all the subjects are presented as numbers (percentages) for categorical variables, as means $\pm$ standard deviations for parametrically distributed variables or as medians (interquartile ranges) for non-parametrically distributed variables. The differences between the ASD group and control group were analyzed by using the Student's *t*-test or the Wilcoxon rank sum test for comparisons of the continuous variables according to the data distribution and by using the chi-squared tests for the categorical variables. The Spearman correlation test was applied to examine the correlations between serum homocysteine, folate, and vitamin B12 levels and the neurodevelopmental level of children with ASD.

Univariate and multivariate linear regression models were applied to compare serum homocysteine, folate, and vitamin B12 levels between the ASD group and the control group. The confounding factors adjusted in the multivariate linear regression models were as follows: model 1 included age, sex, BMI, picky eating, and use of vitamins, and model 2 included all the covariates in model 1 and was additionally adjusted for the combined effects of serum homocysteine, folate, or vitamin B12 levels, which were included in the linear model as continuous variables and were natural logarithm-transformed in order to meet normal distribution.

Multivariable regression analysis models were used to assess the correlations between serum homocysteine and folate levels and the severity of ASD symptoms in children with ASD after adjusting for age, sex, BMI, picky eating, use of vitamins, and serum homocysteine, folate, or vitamin B12 levels (continuous, ln-transformed). The trends across the quartiles of serum homocysteine and folate levels were tested by treating the quartiles as a continuous variable and assigning the midpoint concentration for each quartile. The RCS model was used to show the shape of these associations between homocysteine levels and ASD and between homocysteine and folate levels and the severity of ASD symptoms, respectively. Spearman's correlation analysis and multivariate linear regression models were used to assess the relationship between serum homocysteine, folate, and vitamin B12 levels and neurodevelopmental outcomes in children with ASD.

Cumulative frequency distributions were calculated to show the distribution of serum homocysteine levels in children with

TABLE 1 General characteristics of the participants in the study.

Variables	Total population ($n = 219$)	ASD ($n = 135$)	Controls ($n = 84$)	p-value
Age, years	3.25 (3.00,3.83)	3.25 (2.75,4.25)	3.33 (3.50,3.00)	0.647
≤ 3	82 (37.4)	55 (40.7)	27 (32.1)	0.251
>3	137 (62.6)	80 (59.3)	57 (67.9)	–
Men, n (%)	181 (82.60)	117 (86.70)	64 (76.20)	0.066
BMI, kg/m^2	16.09 ± 1.90	16.39 ± 1.90	15.59 ± 1.81	<0.001
ZBMIA	0.38 ± 1.40	0.65 ± 1.33	−0.05 ± 1.40	0.001
Overweight	26 (11.87)	23 (9.6)	3 (3.6)	0.002
Developmental delay, *n* (%)	115 (52.51)	115 (85.2)	0	–
Picky eating, *n* (%)	97 (44.29)	77 (79.40)	20 (20.60)	0.001
Resistance to vegetables, *n* (%)	70 (31.96)	57 (81.4)	13 (18.6)	<0.001
Resistance to meats, *n* (%)	36 (16.44)	27 (75.0)	9 (25.0)	0.091
Resistance to fruits, *n* (%)	14 (6.40)	11 (78.60)	3 (21.40)	0.258
History of taking vitamins, *n* (%)	86 (39.27)	71 (82.6)	15 (17.4)	<0.001
Severity of ASD, *n* (%)				
Mild to moderate	65 (29.68)	65 (48.1)	0	–
Severe	70 (31.96)	70 (51.9)	0	–
Hcy, μmol/L	6.68 (5.30, 7.95)	7.50 (6.70, 8.90)	5.15 (4.49, 6.03)	0.005
Folate, nmol/L	29.3 (19.6, 37.7)	27.6 (17.6, 34.8)	31.4 (23.5, 40.5)	0.003
VitB12, pmol/L	583 (415, 772)	530 (369, 708)	649 (478, 839)	0.005

BMI, body mass index; ZBMIA, z score for BMI-for-age; ASD, autism spectrum disorder; Hcy, homocysteine; VitB12, vitamin B12. Overweight is defined as a ZBMIA > 2. Data are presented as number (percentage) for categorical data, mean ± standard deviation for parametrically distributed data, or median (interquartile range) for non-parametrically distributed data. Student's t-test or the Wilcoxon rank sum test was used for comparison of the continuous variables according to the data distribution, and chi-square tests were used for the categorical variables.

ASD and healthy controls. Finally, the predictive value of serum homocysteine, folate, and vitamin B12 levels and their combination for developing ASD was analyzed by receiver operating characteristic (ROC) analysis. A two-tailed p-value <0.05 and a 95% CI not covering the null value were considered statistically significant for all analyses.

Results

Characteristics of the participants

The general characteristics and serum homocysteine, folate, and vitamin B12 concentrations of the study population are shown in Table 1. There were no significant differences in age or sex between the children with ASD and healthy controls ($p > 0.05$). The children with ASD had significantly higher values of BMI (16.39 ± 1.90 vs. 15.59 ± 1.81) and a higher prevalence of overweight (9.6 vs. 3.6%), food selectivity (79.4 vs. 20.6%), resistance to vegetables (81.4 vs. 18.6%), and history of taking vitamins (82.6 vs. 17.4%) than the healthy controls. Moreover, 51.9% of the children with ASD had severe symptoms of ASD, and 85.2% had developmental delays. The serum levels of homocysteine were significantly higher ($p = 0.0048$) in the ASD group than in the control group, while the serum levels of folate ($p = 0.003$) and vitamin B12 ($p = 0.0048$) were lower in the ASD group (Figure 1A). The Spearman correlation coefficient (r_s) between serum homocysteine and folate was −0.560 and that for vitamin B12 was −0.318 (Figure 1B).

Association of serum homocysteine, folate, and vitamin B12 levels in children with ASD

We used linear regression models to analyze the correlation of serum homocysteine, folate, and vitamin B12 with ASD. As seen in Figure 2 and Supplementary Table 1, after adjusting for age, sex, BMI, picky eating, and history of use of vitamins in model 1, high levels of serum homocysteine (β: 0.370; 95% CI: 0.299 ∼ 0.441, $p < 0.001$) and low levels of serum folate (β:

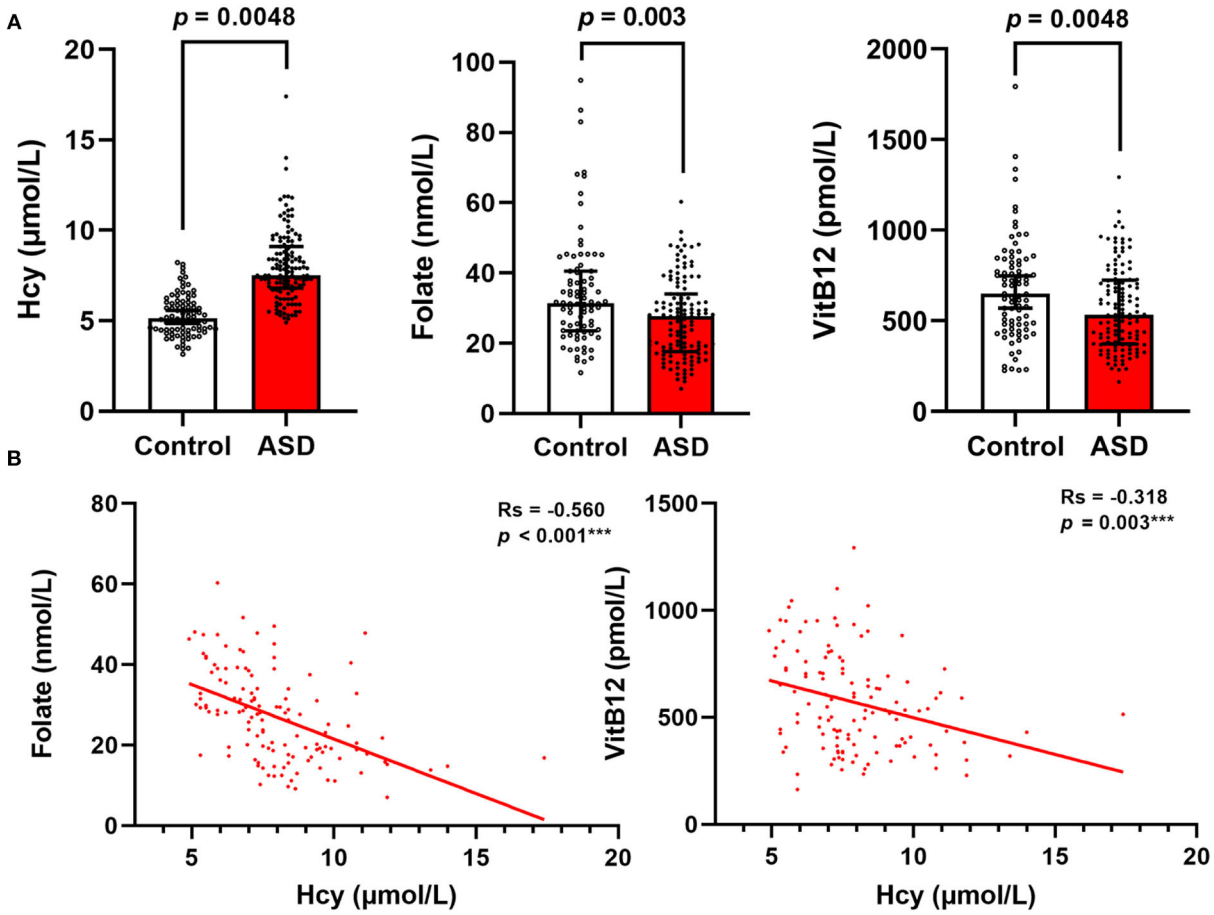

FIGURE 1
Serum Hcy, folate, and VitB12 levels differ between children with ASD and healthy controls. **(A)** Comparison of Hcy, folate, and VitB12 levels between the two groups. **(B)** Correlations between serum Hcy, folate, and VitB12 levels in children with ASD. Results are presented as Spearman correlation coefficients (r_s) and p-values. Hcy, homocysteine; VitB12, vitamin B12.

−0.238; 95% CI: −0.369 ∼ −0.107, $p < 0.001$) and vitamin B12 (β: −0.188; 95% CI: −0.327 ∼ −0.048, $p = 0.009$) were significantly associated with ASD. Notably, increased levels of serum homocysteine (β: 0.299; 95% CI: 0.235 ∼ 0.363, $p < 0.001$) remained significantly correlated with ASD even after successively adjusting for serum folate and vitamin B12 levels in model 2. However, the associations between low serum folate levels and vitamin B12 levels were no longer significant after adjusting for all confounding variables in model 2.

The cumulative frequency distribution of serum homocysteine concentrations in the ASD and control groups is shown in Figure 3A. There was a clear distinction between the two groups, and there was a marked increase in the distribution of the homocysteine concentration in children with ASD compared with healthy controls. Furthermore, in the subgroup analyses, sex, age (≤ 3 years vs. > 3 years), ZBMIA (≤ 2 vs. > 2), dietary preference for meat and vegetables, and use of vitamins in the children with ASD all exhibited significantly higher serum homocysteine levels than healthy controls for each covariate (all $p < 0.05$, Figures 3B–I).

The ROC analysis of serum homocysteine, folate, and vitamin B12 to distinguish children with ASD from healthy controls

The optimum cutoff points for serum homocysteine, folate, and vitamin B12 levels were set at the maximum value of the Youden index. These values are presented in Figure 4, along with the area under the ROC curve (AUC), sensitivity and specificity in detecting ASD, and the associated p-values. The AUC of homocysteine was 0.899 (95% CI: 0.859 ∼ 0.939), and the cutoff was 6.69 μmol/L (sensitivity: 77%, specificity: 89%), which indicated a relatively high discrimination ability.

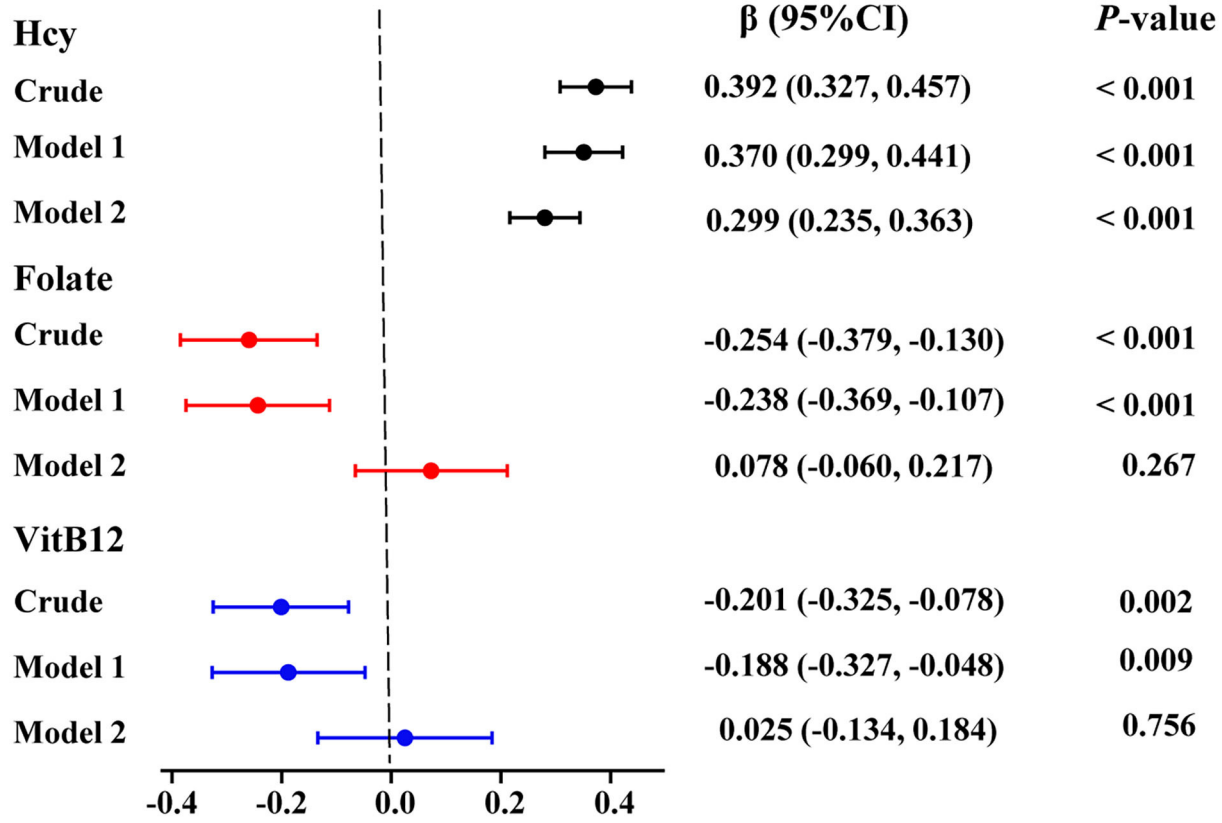

FIGURE 2
Multivariate linear logistic regression analysis for the associations between serum Hcy, folate, and VitB12 levels and ASD. Colored points represent the adjusted regression coefficient (β), and horizontal lines represent the 95% CI. "Crude" means no adjustment. Model 1 was adjusted for age, sex, BMI, picky eating, and use of vitamins. Model 2 was adjusted for model 1 and the other two metabolites. Hcy, homocysteine; VitB12, vitamin B12.

Because the AUCs of folate and vitamin B12 were 0.646 and 0.615, respectively, they could not differentiate the children with ASD from the healthy controls. Furthermore, the AUCs of the combination of homocysteine and folate with or without vitamin B12 were both 0.902, which was slighter higher than the AUC of serum homocysteine alone, thus showing better diagnostic ability. This indicates that the diagnostic performance of serum homocysteine alone was equivalent to that of the combination of the three biomarkers, suggesting that homocysteine alone might be a potential biomarker for ASD.

Association of serum homocysteine, folate, and vitamin B12 levels with ASD severity

The baseline demographic, clinical, and laboratory characteristics of the children with ASD grouped by the severity of ASD symptoms according to CARS scores are given in Table 2. The median values of serum homocysteine levels increased significantly across the groups of ASD severity, while the median values of serum folate levels decreased significantly across the groups of ASD severity. No significant differences in age, sex, BMI, food selectivity, history of birth asphyxia, or other clinical characteristics were observed between the two groups ($p > 0.05$). In addition, we further analyzed the impact of age, sex, BMI, dietary habits, and comorbidity on serum homocysteine and folate levels in children with ASD. As seen in Supplementary Figure 1, serum homocysteine ($r_s = 0.334$, $p < 0.001$) and folate levels ($r_s = -0.438$, $p < 0.001$) were associated with age, and children with ASD older than 3 years exhibited higher serum homocysteine and lower folate levels than children with ASD younger than 3 years ($p < 0.05$). Interestingly, serum folate levels were lower in children with ASD who resisted vegetables and who did not take vitamins before this analysis ($p < 0.05$, Supplementary Figure 2). No significant correlations were found for serum homocysteine with dietary preferences in children with ASD.

According to the aforementioned results, a further multiple logistic regression analysis was carried out to analyze the

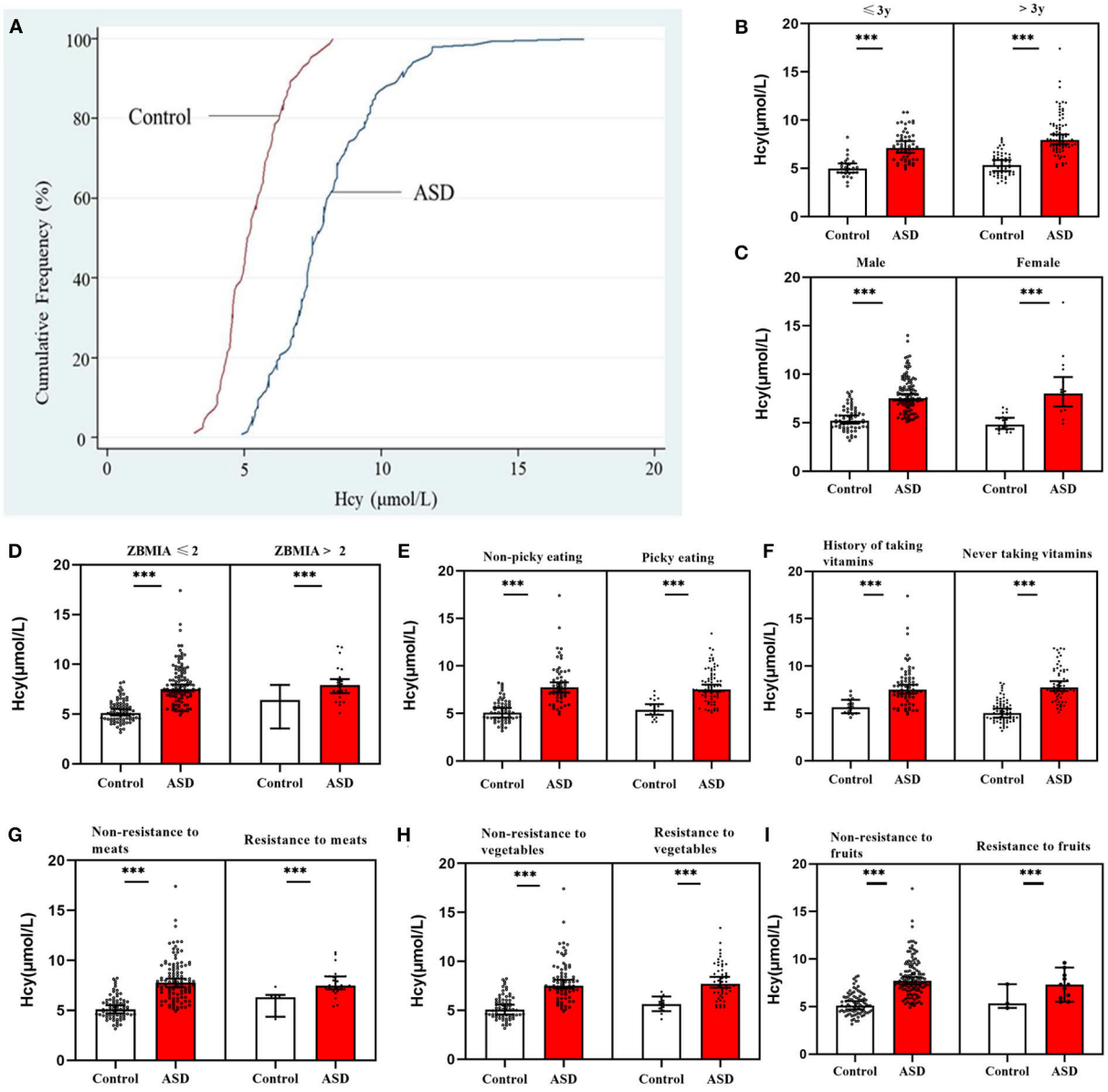

FIGURE 3
Serum homocysteine (Hcy) levels in children with ASD and controls. **(A)** Cumulative frequency distributions of Hcy levels in both groups. **(B–I)** Serum Hcy levels were stratified by age, sex, BMI, food selectivity, and use of vitamins. In both groups, there were significant differences between serum Hcy levels in children with ASD for each covariate (***$p < 0.001$). Hcy, homocysteine; VitB12, vitamin B12.

correlation between serum homocysteine and folate levels and ASD symptom severity (Figure 5). After adjusting for age, sex, BMI, picky eating, and use of multivitamins (model 1), the highest homocysteine quartile was independently associated with the severity of ASD (OR: 11.769, 95% CI: 1.207 ∼ 114.784) compared with the lowest homocysteine quartile. However, the correlation between the highest homocysteine quartile and ASD symptom severity was no longer significant after additionally adjusting for serum folate and vitamin B12 levels in model 2. The multivariate-adjusted OR (95% CI) of ASD severity was 7.116 (1.954 ∼ 25.910) for serum folate levels when comparing the lowest versus the highest quartile, and the relationships were still significant after adjustment for all of the confounding factors in model 2 (OR: 4.227, 95%CI: 1.022 ∼ 17.488). The linear model also showed a negative association of the serum folate level with ASD severity (p-trend < 0.05).

Because we found that folate concentrations were associated with age in children with ASD, an age-stratified analysis was

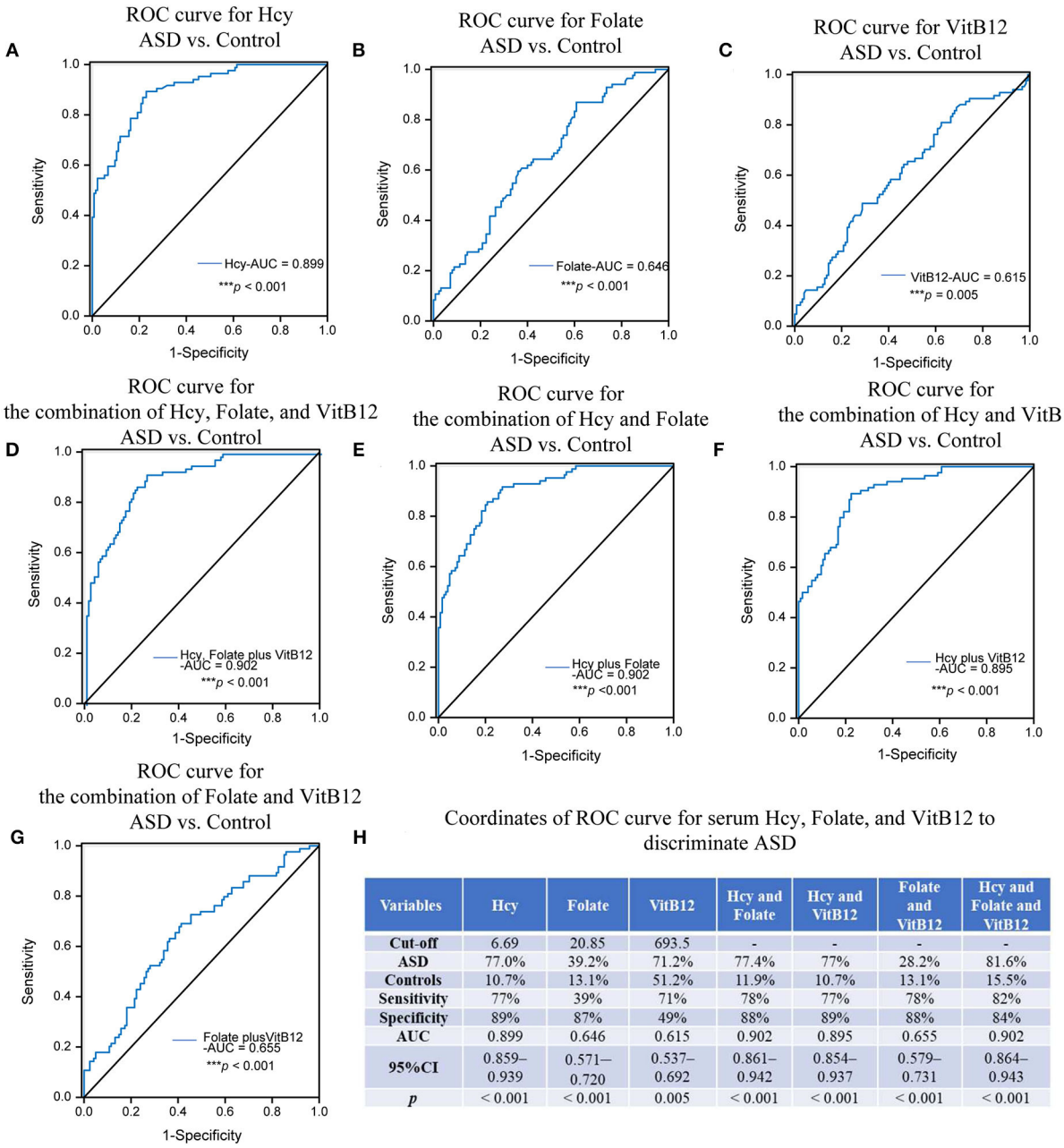

Variables	Hcy	Folate	VitB12	Hcy and Folate	Hcy and VitB12	Folate and VitB12	Hcy and Folate and VitB12
Cut-off	6.69	20.85	693.5	-	-	-	-
ASD	77.0%	39.2%	71.2%	77.4%	77%	28.2%	81.6%
Controls	10.7%	13.1%	51.2%	11.9%	10.7%	13.1%	15.5%
Sensitivity	77%	39%	71%	78%	77%	78%	82%
Specificity	89%	87%	49%	88%	89%	88%	84%
AUC	0.899	0.646	0.615	0.902	0.895	0.655	0.902
95%CI	0.859–0.939	0.571–0.720	0.537–0.692	0.861–0.942	0.854–0.937	0.579–0.731	0.864–0.943
p	< 0.001	< 0.001	0.005	< 0.001	< 0.001	< 0.001	< 0.001

FIGURE 4
ROC analysis of Hcy, folate, and VitB12. The AUCs of the ROC curves for **(A)** Hcy, **(B)** folate, and **(C)** VitB12 were 0.899 (***$p < 0.001$), 0.646 ($p = 0.230$), and 0.615 (***$p < 0.001$), respectively. The AUCs of the ROC curves for **(D)** Hcy+folate+VitB12, **(E)** Hcy+folate, **(F)** Hcy+VitB12, and **(G)** folate+VitB12 were 0.902 (***$p < 0.001$), 0.902 (***$p < 0.001$), 0.895 (***$p < 0.001$) and 0.655 (***$p < 0.001$), respectively. **(H)** Coordinates of ROC curve for Hcy, folate, and VitB12 to discriminate ASD from heathy controls. Hcy, homocysteine; VitB12, vitaminB12.

performed to moderate the confounding effect of age. The results showed that serum folate levels were negatively but not strongly associated with the severity of ASD in both age groups. Serum folate levels in the younger age group (≤ 3 years) showed a higher tendency for the risk of severe ASD (Supplementary Table 2).

The RCS analysis of serum homocysteine, folate, and vitamin B12 levels and ASD risk and severity

As seen in Figure 6, a positive linear association was observed between the serum homocysteine concentration and

TABLE 2 Baseline characteristics of patients with ASD grouped by severity of clinical symptoms according to CARS.

Variables	Total ($n = 135$)	CARS < 36 ($n = 65$)	CARS ≥ 36 ($n = 70$)	p-value
Age, years	3.25 (2.75–4.25)	3.25 (2.75–3.96)	3.29 (2.67–4.50)	0.346
Male, *n* (%)	117 (86.7)	56 (86.2)	61 (87.1)	1.0
BMI, kg/m^2	16.39 (1.90)	16.56 (2.05)	16.24 (1.75)	0.34
Overweight, *n* (%)	23 (17.0)	14 (21.5)	9 (12.9)	0.252
History of birth asphyxia, *n* (%)	19 (14.1)	10 (15.4)	9 (12.9)	0.805
Natural labor, *n* (%)	61 (45.2)	33 (50.8)	28 (40)	0.229
Birth weight, kg	3.30 (3.10–3.60)	3.30 (2.95–3.58)	3.30 (3.10–3.70)	0.141
History of neonatal care, *n* (%)	15 (11.1)	8 (12.3)	7 (10.0)	0.786
Siblings ≥1, *n* (%)	71 (52.6)	30 (46.2)	41 (58.6)	0.170
Breast-fed, *n* (%)	95 (70.4)	45 (69.2)	50 (71.4)	0.851
Severe jaundice, *n* (%)	11 (8.1)	8 (12.3)	3 (4.3)	0.118
Picky eating, n (%)	77 (57.0)	38 (58.5)	39 (55.7)	0.862
Resistance to vegetables, *n* (%)	57 (42.2)	25 (38.5)	32 (45.7)	0.486
Resistance to meats, *n* (%)	27 (20.0)	14 (21.5)	13 (18.6)	0.674
Resistance to fruits, *n* (%)	11 (8.1)	8 (12.3)	3 (4.3)	0.118
History of taking vitamins, *n* (%)	71 (53.4)	34 (54.0)	37 (52.9)	1.0
Developmental delay, *n* (%)	115 (85.2)	54 (83.1)	61 (87.1)	0.629
Language regression, *n* (%)	15 (11.1)	6 (9.2)	9 (12.9)	0.590
Hcy, μmol/L	7.5 (6.70–8.90)	7.1 (6.20–8.32)	8.24 (7.30–9.51)	0.005
Folate, nmol/L	27.6 (17.6–34.8)	30.6 (20.0–39.4)	22.3 (15.6–29.5)	0.001
VitB12, pmol/L	530 (369–70)	587 (408–783)	444 (342–676)	0.140

BMI, body mass index; Hcy, homocysteine; VitB12, vitamin B12; ASD, autism spectrum disorder; CARS, Childhood Autism Rating Scale.

the risk of ASD ($p_{overall} < 0.001$, $p_{nonlinearity} = 0.182$), while serum folate levels showed a negative linear association with the risk of ASD ($p_{overall} = 0.003$, $p_{nonlinearity} = 0.086$). In addition, the results of RCS regression of ASD severity showed similar linear relationships between serum homocysteine ($p_{overall} = 0.025$, $p_{nonlinearity} = 0.689$) and folate ($p_{overall} = 0.018$, $p_{nonlinearity} = 0.910$) and severity of ASD symptoms. No association was observed between serum vitamin B12 levels and ASD risk ($p_{overall} > 0.05$, $p_{nonlinearity} = 0.732$).

Associations of serum homocysteine, folate, and vitamin B12 levels with neurodevelopment in children with ASD

We performed the Spearman correlation analysis to identify the relationship between serum homocysteine, folate, and vitamin B12 levels and Gesell DQ scores in children with ASD. As seen in Supplementary Figure 3, the serum homocysteine level was negatively correlated with adaptive behavior DQ ($r_s = -0.181$, $p = 0.05$) and gross motor DQ ($r_s = -0.216$, $p = 0.019$). Serum folate levels were positively correlated with adaptive behavior DQ ($r_s = 0.365$, $p < 0.001$), gross motor DQ ($r_s = 0.349$, $p < 0.001$), fine motor DQ ($r_s = 0.211$, $p = 0.027$), language DQ ($r_s = 0.229$, $p = 0.016$), and personal–social DQ ($r_s = 0.186$, $p = 0.052$). Serum vitamin B12 levels were positively correlated with adaptive behavior DQ ($r_s = 0.323$, $p = 0.001$), gross motor DQ ($r_s = 0.246$, $p = 0.009$), and language DQ ($r_s = 0.192$, $p = 0.044$). The associations between serum homocysteine, folate, and vitamin B12 levels and adaptive behavior, gross motor, fine motor, language, and social behavior DQs in the multiple linear regression model are shown in Supplementary Table 3 and Figure 7. Serum folate (β = 8.687, 95% CI: 0.217∼17.158) and vitamin B12 (β = 8.320, 95% CI: 0.940∼15.70) levels were significantly positively related to the adaptive behavior DQ. No significant association was found between homocysteine and Gesell DQ scores. Stratified analyses by age showed that serum vitamin B12 was positively related to adaptive behavior (β = 16.476, 95% CI: 5.076∼27.876) and

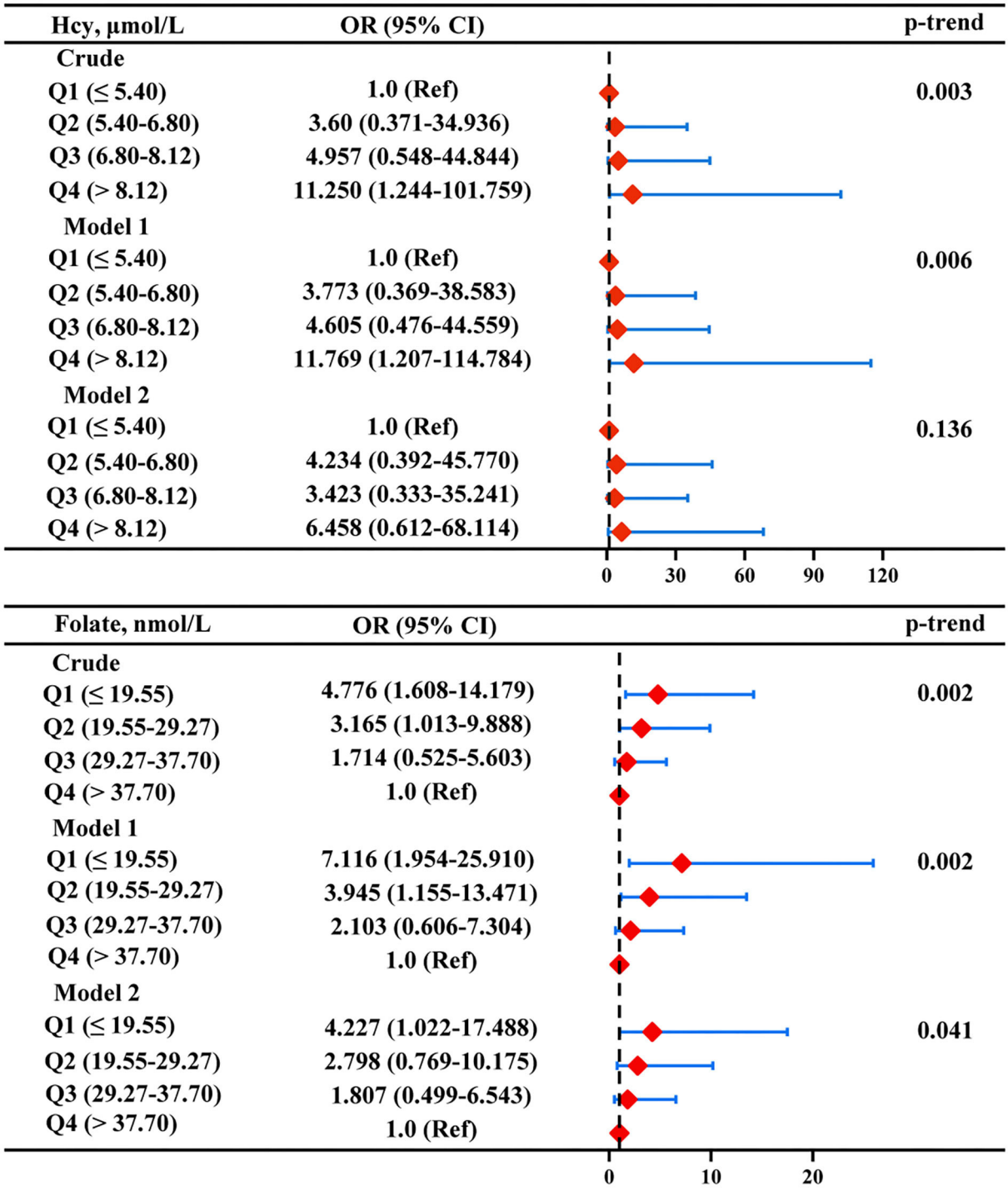

FIGURE 5
Multiple logistic regression analysis for the associations between serum Hcy and folate and severity of ASD. Model 1 was adjusted for age, sex, BMI, picky eating, and use of vitamins. Model 2 was adjusted for model 1 and the other two metabolites. Red diamonds represent the adjusted OR, and horizon lines represent 95% CI. P-values for the trend test (p-trend) were obtained from the multiple logistic regression models by using the median of each parameter quartile (ln-transformed serum homocysteine and folate concentrations) as a continuous variable. Hcy, homocysteine.

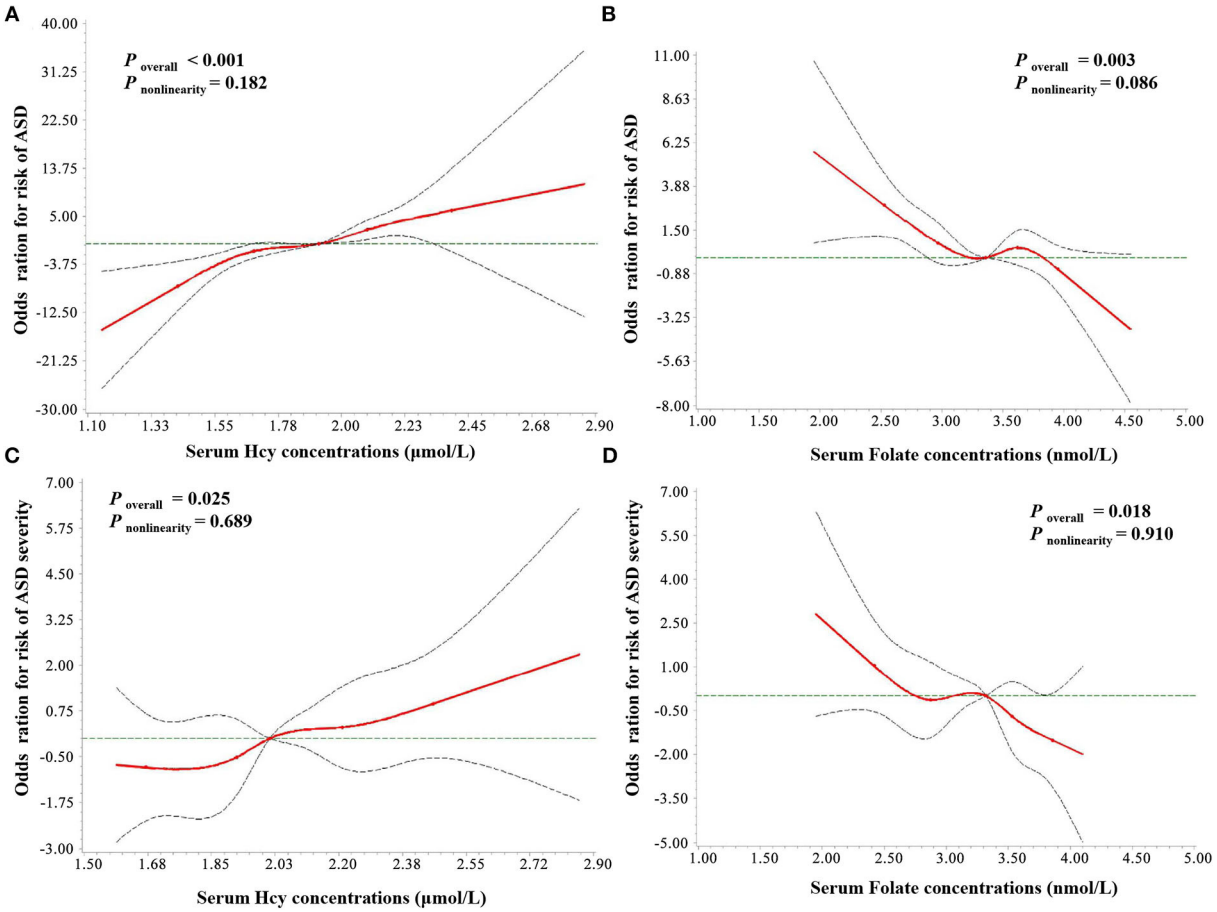

FIGURE 6
RCS regression analysis of serum Hcy and folate concentrations with ASD risk and severity. The risk estimates for ASD risk **(A,B)** and severity **(C,D)** were adjusted for age, sex, BMI, picky eating, use of vitamins, and the other two metabolites. Lines represent adjusted odds ratios (solid red lines) and 95% CIs (long dashed lines) based on the RCS models for the ln-transformed concentrations of serum Hcy and folate. The reference values were set at the 25th percentiles, and the knots were set at 5th, 25th, 50th, 75th, and 95th percentiles of the ln-transformed concentrations, respectively. Hcy, homocysteine; VitB12, vitamin B12.

language (β = 15.186, 95%CI: 1.581∼28.791) DQs in children aged >3 years (Supplementary Table 4).

Discussion

Numerous epidemiological studies reported a connection between homocysteine/folate/vitamin B12 and ASD, but there has been a lack of adequate controls for confounding variables, a large sample size, and rigorous statistical analyses that might influence the interpretation of the results. As far as we know, this is the first study to comprehensively evaluate the interrelations between serum homocysteine, folate, and vitamin B12 levels and their associations with the clinical outcomes and severity of ASD after adjusting for known confounding variables such as age, sex, BMI, use of vitamins, and dietary preference. We further confirmed whether this association between homocysteine/folate/vitamin B12 levels and ASD is linear or nonlinear.

Our findings from this study strengthen the evidence that increased homocysteine is associated with ASD linearly and may serve as a novel and sensitive biomarker for distinguishing children with ASD from healthy subjects. The finding that serum homocysteine was higher in children with ASD was robust after adjustment for relevant covariates, which was in line with a recently published meta-analysis that examined 31 articles involving 3304 subjects (Guo et al., 2020a). The difference in serum homocysteine levels between children with ASD and healthy controls was stable and was not changed by clinical characteristics such as age, sex, or eating habits. In addition, our study revealed that homocysteine showed a good diagnostic ability to discriminate children with ASD from healthy controls. Overall, homocysteine could be considered a stable biomarker to predict ASD risk prior to the onset of behavioral abnormalities.

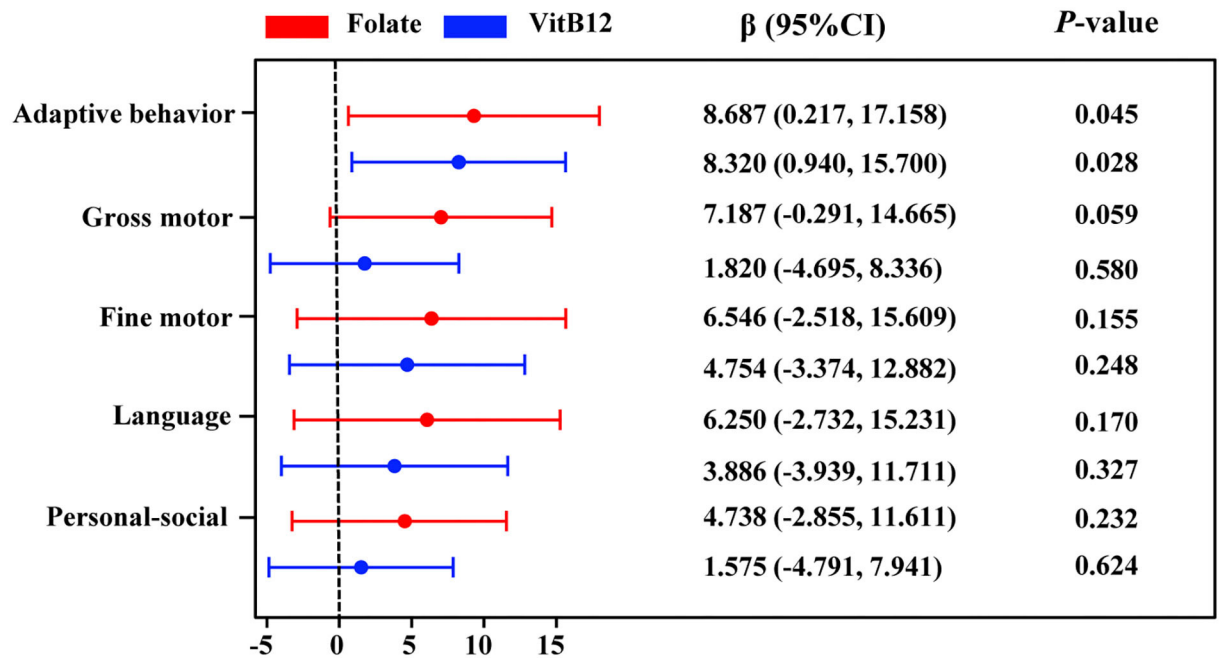

FIGURE 7
Multiple linear regression for adaptive behavior, gross motor, fine motor, language, and personal–social behavior DQs with serum folate and VitB12 concentrations. Colored points represent the adjusted regression coefficient (β), and horizontal lines represent 95% CI adjusted for age, sex, BMI, picky eating, use of vitamins, and the other two metabolites. VitB12, vitamin B12.

To date, few epidemiological studies focused on the specific shape of relationships between homocysteine and ASD. Our results identified a linear association between homocysteine and ASD, which could be in part explained by previously reported *in vitro* experiments showing that higher homocysteine levels exhibited neurotoxicity in a dose-dependent manner (Fan et al., 2017). Regarding the potential biological mechanisms supporting these findings, emerging evidence suggests that impaired homocysteine metabolism is linked to induced oxidative stress, mitochondrial impairment, and methylation impairment, all of which are involved in autism pathology (Rossignol and Frye, 2014). Moreover, elevated homocysteine levels have been found to show toxic effects on the nervous system and accumulate in the brain of animals, resulting in abnormal brain energy metabolism, neural or cognitive dysfunction, and behavioral alterations (Dos Santos et al., 2019; Wyse et al., 2020).

On the other hand, the optimal cutoff value for serum homocysteine levels to distinguish ASD was 6.69 μmol/L based on the Youden index. As is well known, the cutoff value of 15 μmol/L for serum homocysteine levels is used to define hyperhomocysteinemia (>15 μmol/L) in adults (Yang et al., 2014), but this is not suitable for children because serum homocysteine levels may differ between age groups (Setién-Suero et al., 2016). We also observed an age difference in serum homocysteine levels of the children with ASD. There is currently no accepted cutoff value for elevated homocysteine levels in children, but our results provide some evidence for developing age-dependent homocysteine cutoff values.

Because serum folate and vitamin B12 levels are the important determinants of homocysteine levels in children (González-Gross et al., 2012) and are negatively associated with homocysteine levels, which was also verified in our studies, we examined the association of folate and vitamin B12 levels with ASD. However, the finding that serum folate and vitamin B12 levels were lower in the children with ASD did not hold after additional adjustment for the combined effects of homocysteine/folate/vitamin B12 levels, which was in contrast to previous research (Zhu et al., 2020). It is worth noting that higher homocysteine levels were strongly and independently associated with ASD, but not with folate and vitamin B12 levels, which could be explained by several mechanisms involved in the disruption of homocysteine metabolism. One intriguing possibility is that cerebral folate deficiency under normal blood folate levels caused by the impaired transport of folate across the blood–brain barrier (Frye et al., 2013c; Ramaekers et al., 2020), leads to homocysteine accumulation (Ramaekers et al., 2014). Another possible reason is that homocysteine levels are strictly controlled by two metabolic pathways

(Azzini et al., 2020), of which dysfunction in folate-independent remethylation and transsulfuration pathways, but not in folate and vitamin B12-dependent pathways, leads to elevated serum homocysteine concentrations. Human and animal experiments have reported an association between dysfunction in folate-independent pathways and increased homocysteine levels. One experiment in an animal model of ASD showed elevated serum homocysteine concentrations due to decreased betaine homocysteine methyltransferase expression, which is one of the folate-independent remethylation-related enzymes (Huang et al., 2019). An open-label trial in children with ASD who were treated with folic acid and methylcobalamin showed that excess intake of folate and vitamin B12 did not significantly change homocysteine levels (James et al., 2009). Other factors like MTHFR gene mutations can also induce elevated homocysteine without folate or B12 deficiency in children with ASD (Paşca et al., 2009).

Only a few studies examined the association between serum homocysteine, folate, and vitamin B12 and the severity of ASD, as evaluated by CARS scores, and these studies consistently lacked clinical characteristics and nutritional factors as control covariates. Some studies (Han et al., 2015; Altun et al., 2018), but not all (Guo et al., 2020b; Li et al., 2021), showed that high levels of homocysteine and low levels of folate and vitamin B12 are associated with ASD severity. Such data would be of interest to determine if the three metabolites can be used as markers for ASD severity. Our analyses demonstrated that children with severe ASD symptoms had a higher mean homocysteine level but a lower mean folate level than children with mild ASD symptoms, but no significant difference in serum vitamin B12 levels was observed between the two groups. Moreover, we also observed a negative association between folate levels and the severity of ASD independent of confounding factors. Recent findings of greater improvement in autism symptoms following folate supplementation in children with ASD partly support our results (Sun et al., 2016; Hoxha et al., 2021). In addition, ASD symptoms may vary between age groups (Guthrie et al., 2013), and serum folate levels were associated with age and were relatively higher in children aged $\leq$ 3 years, which was consistent with some previous studies (González-Gross et al., 2012; Li et al., 2021). Our age-stratified analysis suggested that folate deficiency at younger ages might lead to a higher risk of severe ASD, which might be associated with the role of folate in the formation of synapses, which peaks before the age of 3 years (Nelson, 2007). Furthermore, we observed a strong, linear, and independent association between low folate levels and ASD severity in RCS models, indicating that serum folate might act as a predictor for ASD severity. An *in vitro* study has also suggested that folate had a dose-dependent protective effect on neurons (Chen et al., 2013). In summary, although no significant differences in folate levels between children with ASD and healthy children were found in our study, children with ASD had folate deficiencies on a larger scale, which were related to autism symptoms. Thus, high folate concentrations, especially in children younger than 3 years, may be a protective factor against autism.

Previous epidemiological research mainly explored the relationship between homocysteine, folate, and vitamin B12 and neurodevelopment in children with ASD using correlation analyses (Guo et al., 2020b; Ljungblad et al., 2021). For example, a previous study found that high homocysteine levels were associated with motor scores using the Ages and Stages Questionnaire in presumed healthy infants aged 3–7 months (Ljungblad et al., 2021), which was in line with our results. Another study found that folate levels were positively correlated with Gesell DQ scores in children with ASD, but vitamin B12 levels were not significantly correlated with neurodevelopment in children with ASD (Guo et al., 2020b). However, some studies reported that decreased serum vitamin B12 levels were correlated with neurodevelopment disorders (Kvestad et al., 2017; Hope et al., 2020). These inconsistent results seem to be related to heterogeneity in the methodological design. Thus, by using a multiple linear regression model, we further demonstrated that both serum folate and vitamin B12 levels were positively associated with adaptive behavior in children with ASD. Well-designed clinical trials have also indicated that supplementation with vitamin B12 and folate can be beneficial for neurodevelopment in children with ASD, especially in adaptive behavior (Frye et al., 2013b; Rossignol and Frye, 2021b). Folate and vitamin B12 are crucial for normal neuron function, and serious deficiencies of these vitamins might directly affect brain function by disrupting myelination and synapse formation during neural development in the brain (Prado and Dewey, 2014). Notably, a higher vitamin B12 level at age >3 years was associated with higher adaptive behavior DQ and language DQ in children with ASD. James et al. also reported that vitamin B12 supplementation in children with ASD aged >3 years is effective in improving autism symptoms (Adams et al., 2018). However, larger studies in future are needed to verify these associations. This finding suggests that serum folate and vitamin B12 concentrations are closely related to cognitive functioning.

The major strength of our study was that multiple variable regression models with confounder control were used to assess the associations between serum homocysteine, folate, and vitamin B12 levels and the outcomes and severity of ASD. Moreover, RCS regression was used to analyze the dose–response relationships of serum homocysteine, folate, and vitamin B12 with ASD. In addition, diverse statistical methods were applied to examine the utility of the three parameters as multidimensional biomarkers for predicting ASD risk prior to the onset of behavioral abnormalities or for predicting the developmental trajectory of children with ASD. However, there are some limitations to this study. First, this study was a case–control study and could not directly analyze the relative risk, thus limiting the attribution of

causality in the results. Second, the sample numbers were limited in the stratified analysis (sex, BMI, and dietary habits); thus, the statistical efficiency was reduced and multivariate analyses could not be performed. Thus, further longitudinal studies with larger sample sizes and functional experiments are necessary to verify the results of this study. Third, there are still some confounding factors that were not considered, such as genetic factors, types of vitamin supplementation, and drug treatments, which might have biased our results. Therefore, we cannot rule out residual confounding by unmeasured factors.

In summary, this study showed that an increased homocysteine level was associated with the risk of ASD in a linear manner and is thus a novel diagnostic biomarker for ASD. Decreased concentrations of folate and vitamin B12 were associated with poor clinical profiles of children with ASD. Our findings suggest that serum homocysteine, folate, and vitamin B12 can be used as biomarkers to predict the development profile and clinical severity of children with ASD. Homocysteine-lowering interventions or folate and vitamin B12 supplementation might be a viable treatment strategy for ASD. However, additional research needs to confirm the observed associations and to clarify if they may serve as new therapeutic targets for ASD.

Data availability statement

The original contributions presented in the study are included in the article/Supplementary material, further inquiries can be directed to the corresponding author.

Ethics statement

The studies involving human participants were reviewed and approved by the Ethics Committee of the Third Affiliated Hospital of Zhengzhou University. Written informed consent to participate in this study was provided by the participants' legal guardian/next of kin. Written informed consent was obtained from the minor(s)' legal guardian/next of kin for the publication of any potentially identifiable images or data included in this article.

Author contributions

CZ conceptualized and designed the study and critically reviewed and revised the manuscript. BL conceptualized and designed the study, performed the statistical analysis, and drafted the initial manuscript. YX and QZ conducted data analyses and blood measurements. DP, LZ, ML, WL, and GD were involved in the collection of blood and clinical data. All authors read and approved the final manuscript.

Funding

This work was supported by the National Nature Science Foundation of China (81902162, U21A20347), the Swedish Research Council (2018-02267), Swedish governmental grants to scientists working in healthcare (ALFGBG-965197), the Henan Provincial Science and Technology Department (222102310161, 182102310688, 202102310221), and the Henan Province Medical Research Project (LHGJ20190349).

Conflict of interest

The authors declare that the research was conducted in the absence of any commercial or financial relationships that could be construed as a potential conflict of interest.

Publisher's note

All claims expressed in this article are solely those of the authors and do not necessarily represent those of their affiliated organizations, or those of the publisher, the editors and the reviewers. Any product that may be evaluated in this article, or claim that may be made by its manufacturer, is not guaranteed or endorsed by the publisher.

Supplementary material

The Supplementary Material for this article can be found online at: https://www.frontiersin.org/articles/10.3389/fnmol.2022.947513/full#supplementary-material

References

Adams, J. B., Audhya, T., Geis, E., Gehn, E., Fimbres, V., Pollard, E. L., et al. (2018). Comprehensive nutritional and dietary intervention for autism spectrum disorder-a randomized, controlled 12-month trial. *Nutrients.* 10, 369. doi: 10.3390/nu10030369

Al-Farsi, Y. M., Waly, M. I., Deth, R. C., Al-Sharbati, M. M., Al-Shafaee, M., Al-Farsi, O., et al. (2013). Low folate and vitamin B12 nourishment is common in Omani children with newly diagnosed autism. *Nutrition.* 29,537–541. doi: 10.1016/j.nut.2012.09.014

Altun, H., Kurutaş, E. B., Sahin, N., Güngör, O, and Findikli, E. (2018). The levels of vitamin D, vitamin D receptor, homocysteine and complex B vitamin in children with autism spectrum disorders. *Clin. Psychopharmacol. Neurosci.* 16,383–390. doi: 10.9758/cpn.2018.16.4.383

Azzini, E., Ruggeri, S., and Polito, A. (2020). Homocysteine: its possible emerging role in at-risk population groups. *Int. J. Mol. Sci.* 21, 1421. doi: 10.3390/ijms21041421

Balachandar, V., Rajagopalan, K., Jayaramayya, K., Jeevanandam, M., and Iyer, M. (2021). Mitochondrial dysfunction: a hidden trigger of autism? *Genes. Dis.* 8,629–639. doi: 10.1016/j.gendis.2020.07.002

Bobrowski-Khoury, N., Ramaekers, V. T., Sequeira, J. M., and Quadros, E. V. (2021). Folate receptor alpha autoantibodies in autism spectrum disorders: diagnosis, treatment and prevention. *J. Pers. Med.* 11, 710. doi: 10.3390/jpm11080710

Chen, L., Shi, X. J., Liu, H., Mao, X., Gui, L. N., Wang, H., et al. (2021). Oxidative stress marker aberrations in children with autism spectrum disorder: a systematic review and meta-analysis of 87 studies ($N = 9109$). *Transl. Psychiat.* 11, 15. doi: 10.1038/s41398-020-01135-3

Chen, S., Honda, T., Ohara, T., Hata, J., Hirakawa, Y., Yoshida, D., et al. (2020). Serum homocysteine and risk of dementia in Japan. *J. Neurol. Neurosurg. Psychiat.* 91, 540–546. doi: 10.1136/jnnp-2019-322366

Chen, T. F., Tang, M. C., Chou, C. H., Chiu, M. J., and Huang, R. F. (2013). Dose-dependent folic acid and memantine treatments promote synergistic or additive protection against Aβ (25-35) peptide-induced apoptosis in SH-SY5Y cells mediated by mitochondria stress-associated death signals. *Food Chem. Toxicol.* 62, 538–547. doi: 10.1016/j.fct.2013.09.015

Dos Santos, T. M., Siebert, C., De Oliveira, M. F., Manfredini, V., and Wyse, A. T. S. (2019). Chronic mild hyperhomocysteinemia impairs energy metabolism, promotes DNA damage and induces a Nrf2 response to oxidative stress in rats brain. *Cell Mol. Neurobiol.* 39, 687–700. doi: 10.1007/s10571-019-00674-8

Dror, D. K., and Allen, L. H. (2008). Effect of vitamin B12 deficiency on neurodevelopment in infants: current knowledge and possible mechanisms. *Nutr. Rev.* 66, 250–255. doi: 10.1111/j.1753-4887.2008.00031.x

Fan, C. D., Sun, J. Y., Fu, X. T., Hou, Y. J., Li, Y., Yang, M. F., et al. (2017). Astaxanthin attenuates homocysteine-induced cardiotoxicity *in vitro* and *in vivo* by inhibiting mitochondrial dysfunction and oxidative damage. *Front. Physiol.* 8, 1041. doi: 10.3389/fphys.2017.01041

Frye, R. E., Delatorre, R., Taylor, H., Slattery, J., Melnyk, S., Chowdhury, N., et al. (2013a). Redox metabolism abnormalities in autistic children associated with mitochondrial disease. *Transl. Psychiat.* 3, e273. doi: 10.1038/tp.2013.51

Frye, R. E., Melnyk, S., Fuchs, G., Reid, T., Jernigan, S., Pavliv, O., et al. (2013b). Effectiveness of methylcobalamin and folinic acid treatment on adaptive behavior in children with autistic disorder is related to glutathione redox status. *Autism Res. Treat* 2013, 609705. doi: 10.1155/2013/609705

Frye, R. E., Sequeira, J. M., Quadros, E. V., James, S. J., and Rossignol, D. A. (2013c). Cerebral folate receptor autoantibodies in autism spectrum disorder. *Mol. Psychiat.* 18, 369–381. doi: 10.1038/mp.2011.175

González-Gross, M., Benser, J., Breidenassel, C., Albers, U., Huybrechts, I., Valtueña, J., et al. (2012). Gender and age influence blood folate, vitamin B12, vitamin B6, and homocysteine levels in European adolescents: the Helena study. *Nutr. Res.* 32, 817–826. doi: 10.1016/j.nutres.2012.09.016

Guo, B. Q., Li, H. B., and Ding, S. B. (2020a). Blood homocysteine levels in children with autism spectrum disorder: an updated systematic review and meta-analysis. *Psychiatry Res.* 291, 113283. doi: 10.1016/j.psychres.2020.113283

Guo, M., Li, L., Zhang, Q., Chen, L., Dai, Y., Liu, L., et al. (2020b). Vitamin and mineral status of children with autism spectrum disorder in Hainan province of China: associations with symptoms. *Nutr. Neurosci.* 23, 803–810. doi: 10.1080/1028415X.2018.1558762

Guthrie, W., Swineford, L. B., Nottke, C., and Wetherby, A. M. (2013). Early diagnosis of autism spectrum disorder: stability and change in clinical diagnosis and symptom presentation. *J. Child Psychol. Psychiat.* 54, 582–590. doi: 10.1111/jcpp.12008

Han, Y., Xi, Q. Q., Dai, W., Yang, S. H., Gao, L., Su, Y. Y., et al. (2015). Abnormal transsulfuration metabolism and reduced antioxidant capacity in Chinese children with autism spectrum disorders. *Int. J. Dev. Neurosci.* 46, 27–32. doi: 10.1016/j.ijdevneu.2015.06.006

Hassan, Z., Coelho, D., Kokten, T., Alberto, J. M., Umoret, R., Daval, J. L., et al. (2019). Brain susceptibility to methyl donor deficiency: from fetal programming to aging outcome in rats. *Int J. Mol. Sci.* 20, 5692. doi: 10.3390/ijms20225692

Hope, S., Naerland, T., Høiland, A. L., Torske, T., Malt, E., Abrahamsen, T., et al. (2020). Higher vitamin B12 levels in neurodevelopmental disorders than in healthy controls and schizophrenia: a comparison among participants between 2 and 53 years. *Faseb J.* 34, 8114–8124. doi: 10.1096/fj.201900855RRR

Hoxha, B., Hoxha, M., Domi, E., Gervasoni, J., Persichilli, S., Malaj, V., et al. (2021). Folic acid and autism: a systematic review of the current state of knowledge. *Cells.* 10, 1976. doi: 10.3390/cells10081976

Huang, F., Chen, X., Jiang, X., Niu, J., Cui, C., Chen, Z., et al. (2019). Betaine ameliorates prenatal valproic-acid-induced autism-like behavioral abnormalities in mice by promoting homocysteine metabolism. *Psychiatry Clin. Neurosci.* 73, 317–322. doi: 10.1111/pcn.12833

James, S. J., Melnyk, S., Fuchs, G., Reid, T., Jernigan, S., Pavliv, O., et al. (2009). Efficacy of methylcobalamin and folinic acid treatment on glutathione redox status in children with autism. *Am. J. Clin. Nutr.* 89, 425–430. doi: 10.3945/ajcn.2008.26615

Koklesova, L., Mazurakova, A., Samec, M., Biringer, K., Samuel, S. M., Büsselberg, D., et al. (2021). Homocysteine metabolism as the target for predictive medical approach, disease prevention, prognosis, and treatments tailored to the person. *Epma J.* 12, 1–29. doi: 10.1007/s13167-021-00263-0

Kruman, I. I., Mouton, P. R., Emokpae, R. Jr., Cutler, R. G., and Mattson, M. P. (2005). Folate deficiency inhibits proliferation of adult hippocampal progenitors. *Neuroreport* 16, 1055–1059. doi: 10.1097/00001756-200507130-00005

Kvestad, I., Hysing, M., Shrestha, M., Ulak, M., Thorne-Lyman, A. L., Henjum, S., et al. (2017). Vitamin B-12 status in infancy is positively associated with development and cognitive functioning 5 y later in Nepalese children. *Am. J. Clin. Nutr.* 105, 1122–1131. doi: 10.3945/ajcn.116.144931

Lai, M. C., Lombardo, M. V., and Baron-Cohen, S. (2014). Autism. *Lancet* 383, 896–910. doi: 10.1016/S0140-6736(13)61539-1

Li, Q., Yang, T., Chen, L., Dai, Y., Wu, L. J., Jia, F. Y., et al. (2021). Serum folate status is primarily associated with neurodevelopment in children with autism spectrum disorders aged three and under-a multi-center study in China. *Front. Nutr.* 8, 661223. doi: 10.3389/fnut.2021.661223

Liu, C., Huang, L., Huang, S., Wei, L., Cao, D., Zan, G., et al. (2022). Association of both prenatal and early childhood multiple metals exposure with neurodevelopment in infant: a prospective cohort study. *Environ. Res.* 205, 112450. doi: 10.1016/j.envres.2021.112450

Liu, P., Wu, C., Chang, X., Qi, X., Zheng, M., and Zhou, Z. (2016). Adverse associations of both prenatal and postnatal exposure to organophosphorous pesticides with infant neurodevelopment in an agricultural area of Jiangsu Province, China. *Environ. Health Perspect.* 124, 1637–1643. doi: 10.1289/EHP196

Ljungblad, U. W., Paulsen, H., Mørkrid, L., Pettersen, R. D., Hager, H. B., Lindberg, M., et al. (2021). The prevalence and clinical relevance of hyperhomocysteinemia suggesting vitamin B12 deficiency in presumed healthy infants. *Eur. J. Paediatr. Neurol.* 35, 137–146. doi: 10.1016/j.ejpn.2021.10.008

Maenner, M. J., Shaw, K. A., Baio, J., Washington, A., Patrick, M., DiRienzo, M., et al. (2020). Prevalence of autism spectrum disorder among children aged 8 years - autism and developmental disabilities monitoring network, 11 sites, united states, 2016. *MMWR Surveill Summ.* 69, 1–12. doi: 10.15585/mmwr.ss6904a1

Main, P. A., Thomas, P., Angley, M. T., Young, R., Esterman, A., King, C. E., et al. (2015). Lack of evidence for genomic instability in autistic children as measured by the cytokinesis-block micronucleus cytome assay. *Autism Res.* 8, 94–104. doi: 10.1002/aur.1428

Mann, A., Portnoy, E., Han, H., Inbar, D., Blatch, D., Shmuel, M. et al. (2018). Folate homeostasis in epileptic rats. *Epilepsy Res.* 142, 64–72. doi: 10.1016/j.eplepsyres.2018.03.014

Michelakos, T., Kousoulis, A. A., Katsiardanis, K., Dessypris, N., Anastasiou, A., Katsiardani, K. P., et al. (2013). Serum folate and B12 levels in association with cognitive impairment among seniors: results from the VELESTINO study in Greece and meta-analysis. *J. Aging Health* 25, 589–616. doi: 10.1177/0898264313482488

Nelson, C. A. (2007). A neurobiological perspective on early human deprivation. *Child Dev. Perspect.* 1, 13–18. doi: 10.1111/j.1750-8606.2007.00004.x

Paşca, S. P., Dronca, E., Kaucsár, T., Craciun, E. C., Endreffy, E., Ferencz, B. K., et al. (2009). One carbon metabolism disturbances and the C677T MTHFR gene polymorphism in children with autism spectrum disorders. *J. Cell. Mol. Med.* 13, 4229–4238. doi: 10.1111/j.1582-4934.2008.00463.x

Prado, E. L., and Dewey, K. G. (2014). Nutrition and brain development in early life. *Nutr. Rev.* 72, 267–284. doi: 10.1111/nure.12102

Ramaekers, V. T., Rothenberg, S. P., Sequeira, J. M., Opladen, T., Blau, N., Quadros, E. V., et al. (2005). Autoantibodies to folate receptors in the cerebral folate deficiency syndrome. *N. Engl. J. Med.* 352, 1985–1991. doi: 10.1056/NEJMoa043160

Ramaekers, V. T., Sequeira, J. M., Thöny, B., and Quadros, E. V. (2020). Oxidative stress, folate receptor autoimmunity, and CSF findings in severe infantile autism. *Autism Res. Treat* 2020, 9095284. doi: 10.1155/2020/9095284

Ramaekers, V. T., Thöny, B., Sequeira, J. M., Ansseau, M., Philippe, P., Boemer, F., et al. (2014). Folinic acid treatment for schizophrenia associated with folate receptor autoantibodies. *Mol. Genet. Metab.* 113, 307–314. doi: 10.1016/j.ymgme.2014.10.002

Ranjan, S., and Nasser, J. A. (2015). Nutritional status of individuals with autism spectrum disorders: do we know enough? *Adv. Nutr.* 6, 397–407. doi: 10.3945/an.114.007914

Refsum, H., Smith, A. D., Ueland, P. M., Nexo, E., Clarke, R., McPartlin, J., et al. (2004). Facts and recommendations about total homocysteine determinations: an expert opinion. *Clin. Chem.* 50, 3–32. doi: 10.1373/clinchem.2003.021634

Regier, D. A., Kuhl, E. A., and Kupfer, D. J. (2013). The DSM-5: Classification and criteria changes. *World psychiatry* 12, 92–98. doi: 10.1002/wps.20050

Rossignol, D. A., and Frye, R. E. (2014). Evidence linking oxidative stress, mitochondrial dysfunction, and inflammation in the brain of individuals with autism. *Front. Physiol.* 5, 150. doi: 10.3389/fphys.2014.00150

Rossignol, D. A., and Frye, R. E. (2021a). Cerebral folate deficiency, folate receptor alpha autoantibodies and leucovorin (folinic acid) treatment in autism spectrum disorders: a systematic review and meta-analysis. *J. Pers. Med.* 11, 1141. doi: 10.3390/jpm11111141

Rossignol, D. A., and Frye, R. E. (2021b). The effectiveness of cobalamin (B12) treatment for autism spectrum disorder: a systematic review and meta-analysis. *J. Pers. Med.* 11, 784. doi: 10.3390/jpm11080784

Saha, S., Saha, T., Rajamma, U., Sinha, S., and Mukhopadhyay, K. (2022). Analysis of association between components of the folate metabolic pathway and autism spectrum disorder in eastern Indian subjects. *Mol. Biol. Rep.* 49, 1281–1293. doi: 10.1007/s11033-021-06956-z

Salagre, E., Vizuete, A. F., Leite, M., Brownstein, D. J., McGuinness, A., Jacka, F., et al. (2017). Homocysteine as a peripheral biomarker in bipolar disorder: a meta-analysis. *Eur. Psychiatry* 43, 81–91. doi: 10.1016/j.eurpsy.2017.02.482

Sandin, S., Lichtenstein, P., Kuja-Halkola, R., Hultman, C., Larsson, H., and Reichenberg, A. (2017). The heritability of autism spectrum disorder. *JAMA* 318, 1182–1184. doi: 10.1001/jama.2017.12141

Schopler, E., Reichler, R. J., DeVellis, R. F., and Daly, K. (1980). Toward objective classification of childhood autism: childhood autism rating scale (CARS). *J. Autism Dev. Disord.* 10, 91–103. doi: 10.1007/BF02408436

Setién-Suero, E., Suárez-Pinilla, M., Suárez-Pinilla, P., Crespo-Facorro, B., and Ayesa-Arriola, R. (2016). Homocysteine and cognition: a systematic review of 111 studies. *Neurosci. Biobehav. Rev.* 69, 280–298. doi: 10.1016/j.neubiorev.2016.08.014

Sharp, W. G., Berry, R. C., McCracken, C., Nuhu, N. N., Marvel, E., Saulnier, C. A., et al. (2013). Feeding problems and nutrient intake in children with autism spectrum disorders: a meta-analysis and comprehensive review of the literature. *J. Autism Dev. Disord.* 43, 2159–2173. doi: 10.1007/s10803-013-1771-5

Škovierová, H., Vidomanová E, Mahmood, S., Sopková J., Drgová A., and Cervenová, T. et al. (2016). The molecular and cellular effect of homocysteine metabolism imbalance on human health. *Int. J. Mol. Sci.* 17, 1733. doi: 10.3390/ijms17101733

Sun, C., Zou, M., Zhao, D., Xia, W., and Wu, L. (2016). Efficacy of folic acid supplementation in autistic children participating in structured teaching: an open-label trial. *Nutrients.* 8, 337. doi: 10.3390/nu8060337

WHO. (2008). *Training Course on Child Growth Assessment WHO Official Website. WHO*. Available online at: https://www.who.int/publications-detail-redirect/9789241595070 (accessed December 1, 2008).

Wyse, A. T. S., Sanches, E. F., Dos Santos, T. M., Siebert, C., Kolling, J., and Netto, C. A. (2020). Chronic mild hyperhomocysteinemia induces anxiety-like symptoms, aversive memory deficits and hippocampus atrophy in adult rats: new insights into physiopathological mechanisms. *Brain Res.* 1728, 146592. doi: 10.1016/j.brainres.2019.146592

Yang, B., Fan, S., Zhi, X., Wang, Y., Wang, Y., Zheng, Q., et al. (2014). Prevalence of hyperhomocysteinemia in China: a systematic review and meta-analysis. *Nutrients* 7, 74–90. doi: 10.3390/nu7010074

Zhou, S., Chen, J., Cheng, L., Fan, K., Xu, M., Ren, W., et al. (2021). Age-dependent association between elevated homocysteine and cognitive impairment in a post-stroke population: a prospective study. *Front. Nutr.* 8, 691837. doi: 10.3389/fnut.2021.691837

Zhu, J., Guo, M., Yang, T., Lai, X., Tang, T., Chen, J., et al. (2020). Nutritional status and symptoms in preschool children with autism spectrum disorder: a two-center comparative study in Chongqing and Hainan Province, China. *Front. Pediatr.* 8, 469. doi: 10.3389/fped.2020.00469

frontiers | Frontiers in Molecular Neuroscience

TYPE Brief Research Report
PUBLISHED 18 August 2022
DOI 10.3389/fnmol.2022.932305

Check for updates

OPEN ACCESS

EDITED BY
Salam Salloum-Asfar,
Qatar Biomedical Research Institute, Qatar

REVIEWED BY
Mazahir T. Hasan,
Achucarro Basque Center for Neuroscience, Spain
Sowmyashree Mayur Kaku,
St John's National Academy of Health Sciences, India

*CORRESPONDENCE
Astrid Moura Vicente
astrid.vicente@insa.min-saude.pt

SPECIALTY SECTION
This article was submitted to Neuroplasticity and Development, a section of the journal Frontiers in Molecular Neuroscience

RECEIVED 29 April 2022
ACCEPTED 18 July 2022
PUBLISHED 18 August 2022

CITATION
Vilela J, Martiniano H, Marques AR, Santos JX, Rasga C, Oliveira G and Vicente AM (2022) Disease similarity network analysis of Autism Spectrum Disorder and comorbid brain disorders.
Front. Mol. Neurosci. 15:932305.
doi: 10.3389/fnmol.2022.932305

COPYRIGHT
© 2022 Vilela, Martiniano, Marques, Santos, Rasga, Oliveira and Vicente. This is an open-access article distributed under the terms of the Creative Commons Attribution License (CC BY). The use, distribution or reproduction in other forums is permitted, provided the original author(s) and the copyright owner(s) are credited and that the original publication in this journal is cited, in accordance with accepted academic practice. No use, distribution or reproduction is permitted which does not comply with these terms.

Disease similarity network analysis of Autism Spectrum Disorder and comorbid brain disorders

Joana Vilela[1,2], Hugo Martiniano[1,2], Ana Rita Marques[1,2], João Xavier Santos[1,2], Célia Rasga[1,2], Guiomar Oliveira[3,4] and Astrid Moura Vicente[1,2]*

[1]Departamento de Promoção da Saúde e Doenças Não Transmissíveis, Instituto Nacional de Saúde Doutor Ricardo Jorge, Lisbon, Portugal, [2]Faculty of Sciences, BioISI-Biosystems & Integrative Sciences Institute, University of Lisboa, Lisbon, Portugal, [3]Unidade de Neurodesenvolvimento e Autismo, Serviço do Centro de Desenvolvimento da Criança, Centro de Investigação e Formação Clínica, Hospital Pediátrico, Centro Hospitalar e Universitário de Coimbra, Coimbra, Portugal, [4]Faculty of Medicine, University Clinic of Pediatrics and Coimbra Institute for Biomedical Imaging and Translational Research, University of Coimbra, Coimbra, Portugal

Autism Spectrum Disorder (ASD) is a neurodevelopmental disorder with heterogeneous clinical presentation, variable severity, and multiple comorbidities. A complex underlying genetic architecture matches the clinical heterogeneity, and evidence indicates that several co-occurring brain disorders share a genetic component with ASD. In this study, we established a genetic similarity disease network approach to explore the shared genetics between ASD and frequent comorbid brain diseases (and subtypes), namely Intellectual Disability, Attention-Deficit/Hyperactivity Disorder, and Epilepsy, as well as other rarely co-occurring neuropsychiatric conditions in the Schizophrenia and Bipolar Disease spectrum. Using sets of disease-associated genes curated by the DisGeNET database, disease genetic similarity was estimated from the Jaccard coefficient between disease pairs, and the Leiden detection algorithm was used to identify network disease communities and define shared biological pathways. We identified a heterogeneous brain disease community that is genetically more similar to ASD, and that includes Epilepsy, Bipolar Disorder, Attention-Deficit/Hyperactivity Disorder combined type, and some disorders in the Schizophrenia Spectrum. To identify loss-of-function rare *de novo* variants within shared genes underlying the disease communities, we analyzed a large ASD whole-genome sequencing dataset, showing that ASD shares genes with multiple brain disorders from other, less genetically similar, communities. Some genes (e.g., *SHANK3, ASH1L, SCN2A, CHD2,* and *MECP2*) were previously implicated in ASD and these disorders. This approach enabled further clarification of genetic sharing between ASD

and brain disorders, with a finer granularity in disease classification and multi-level evidence from DisGeNET. Understanding genetic sharing across disorders has important implications for disease nosology, pathophysiology, and personalized treatment.

KEYWORDS

Autism Spectrum Disorder (ASD), Psychiatric genetics, cross-disorder genetics, brain disorders, disease similarity, network analysis, disease community, *de novo* mutations

Introduction

Autism Spectrum Disorder (ASD) is a neurodevelopmental brain disorder characterized by communication deficits and repetitive behavioral patterns (American Psychiatric Association, 2013). ASD presents as a clinical spectrum, with patients exhibiting variable degrees of clinical severity, compounded by various comorbidities. No single neurobiology underlies ASD, as many molecular mechanisms and biological processes have previously been implicated and are likely reflected in the spectrum of clinical phenotypes observed in patients. ASD segregates in families and a complex genetic architecture is clear, with estimates of up to 1,000 genes potentially implicated (Ramaswami and Geschwind, 2018). While high-risk rare variants in many different genes can be identified in up to 40% of cases, a substantial proportion of ASD risk variance is attributed to common genetic variants with small risk effects (Gaugler et al., 2014), and is still not clearly determined.

A range of brain diseases can co-occur with ASD, which frequently share traits or symptoms (White et al., 2020). However, the combination of comorbid conditions can vary largely between patients, possibly due to different combinations of genetic risk factors. Multiple studies have addressed the genetic overlap between ASD and neuropsychiatric and neurologic conditions, mostly focusing on common genetic variants, uncovering intriguing evidence, particularly for Attention-Deficit/Hyperactivity Disorder (ADHD), Epilepsy, and Schizophrenia (SCZ). Common rare genetic variants have also been identified for Intellectual Disability (ID), one of the most common ASD comorbidities and its subtypes.

For instance, the exome sequencing analysis of approximately 8,000 ASD children, with or without ADHD, discovered a similar burden of rare protein-truncating variants in very conserved genes in both diseases (Satterstrom et al., 2019). ASD frequently co-occurs with ADHD and Epilepsy in children, with rare damaging chromosomal alterations combined with the exposure to environmental factors possibly contributing to the risk of co-occurrence of ASD, ADHD, and Epilepsy (Lo-Castro and Curatolo, 2014). Evidence suggests that ASD and Epilepsy have significant genetic overlap (Novarino et al., 2013). Interestingly, children who have an older sibling diagnosed with ASD have a 70% more chance to have Epilepsy than controls (Christensen et al., 2016).

A Genome-Wide Association Study (GWAS) of over 16,000 ASD cases identified significant genetic overlap between ASD and SCZ (Autism Spectrum Disorders Working Group of The Psychiatric Genomics Consortium, 2017). A common variant genetic overlap between ASD and SCZ was also detected by heritability and correlation analysis based on GWAS studies in very large datasets (Anttila et al., 2018). *Loci* such as 10q24.32 and genes implicated in ASD are also associated with SCZ (Autism Spectrum Disorders Working Group of The Psychiatric Genomics Consortium, 2017). Interestingly, these disorders share a genetic component associated with impairments in social communication; however, they exhibit distinct developmental profiles which are consistent with the different onset of clinical symptoms (St Pourcain et al., 2018). Exome sequencing of 57 trios with sporadic or familial SCZ identified a high proportion of nonsense *de novo* mutations (McCarthy et al., 2014), several in genes implicated in ASD (e.g., *AUTS2, CDH8, MECP2*) and ID (e.g., *HUWE1* and *TRAPPC9*), supporting a shared genetic etiology between these disorders. Exome sequencing of familial Bipolar Disorder (BP) also suggests an overlap with rare genetic variations implicated in SCZ and ASD (Goes et al., 2016). This study identified 84 rare damaging variants that segregated with BP in genes, which were previously reported to have *de novo* variants in ASD and SCZ.

Analysis of sequencing data in large datasets shows that ASD and ID share multiple genes (Satterstrom et al., 2020). This overlap is more evident in syndromes in which patients have both ASD and ID, such as Phelan-McDermid syndrome. This syndrome implicates structural alterations in a chromosomic region that contains the gene *SHANK3* that is strongly associated with ID and ASD. Evidence suggests that mutations in this gene occur in about 1.7% of patients with ID, 0.5% of individuals with ASD, and up to 2% of people with ASD who also have moderate to profound ID (Soorya et al., 2018).

Individuals diagnosed with ASD are two times more likely than control subjects to be diagnosed with Obsessive-Compulsive Disorder (OCD), according to a longitudinal study of nearly 3.4 million people in Denmark over 18 years

(Meier et al., 2015). A combined GWAS study of ASD and OCD identified a significant polygenic component of ASD, predicting 0.11% of the phenotypic variance in an independent OCD dataset (Guo et al., 2017).

Given the previous evidence for shared genetic influences between ASD and several comorbid brain disorders, in this study, we sought to further explore the genetic similarity with ASD across a range of brain disorders, using multi-level evidence from well-curated databases and a machine learning approach. Appreciating these genetic overlaps has important implications for disease diagnostic classifications, for understanding the underlying pathophysiology, and for the eventual development of personalized treatment approaches. The specific objectives of the present study were (1) to infer the genetic similarity between ASD and other brain disorders co-occurring with ASD, including disease subtypes; (2) to identify the communities of diseases that have higher genetic similarity with ASD; and (3) to identify likely pathogenic mutations in a large ASD sequencing dataset that may explain the genetic similarities conferred by rare variants across ASD and comorbid brain disorders.

Methods

The overall methodological process followed in this study is represented in **Supplementary File 1**.

Selection of diseases in the DisGeNET database

In this step, we used the DisGeNET database as the data source for disease-disease associations and gene-disease associations (**Supplementary File 1**). The DisGeNET database includes genetic data on the full spectrum of human diseases as well as normal and abnormal traits (Piñero et al., 2015, 2017, 2020). This database integrates data of human gene-disease associations from several repositories including single gene, complex multigenic, and environmental diseases, integrated by gene and disease vocabulary mapping. We analyzed the DisGeNET dataset of disease-disease associations based on previously implicated genes (file *disease_to_disease_ALL.tsv.gz* from the DisGeNET website[1]), and performed analyses using packages implemented in R studio 2022.02.0 Build 443, R version 4.1.2.[2] For each pair of diseases, DisGeNET provides the Jaccard Index of disease similarity, which assesses the fraction of shared genes among the diseases according to the proportion of the number of shared genes by the total number of genes implicated in both diseases.

From the DisGeNET file, we selected the disease terms related to ASD and 28 co-occurring psychiatric disorders (White et al., 2020), shown in **Table 1**. We also selected DisGeNET terms related to Epilepsy, as this neurologic disorder frequently co-occurs with ASD and other psychiatric disorders. Correspondence between the Unified Medical Language System (UMLS) nomenclature used in DisGeNET and the Diagnostic and Statistical Manual of Mental Disorders, Fifth Edition, Text Revision (DSM-V; American Psychiatric Association, 2013), was done using the codes from the International Classification of Diseases ICD-10/ICD-10-CM, which belong to the medical coding system designed by the World Health Organization (World Health Organization, 2004).

Construction of a network of disease gene-based similarities between Autism Spectrum Disorder and comorbid brain disorders and disease community detection

The input data source for this analysis is the filtered DisGeNET file of disease-disease associations from the previous step (**Supplementary File 1**). The network of disease-disease similarities was produced using the DisGeNET Jaccard Index, which calculates the genetic similarity for each disease pair, as the weight of the edge connecting each pair of diseases. The network was generated using the igraph R package.[3] Network disease communities were identified using the Leiden community detection algorithm (Traag et al., 2019) implemented in the R package LeidenAlg (Kharchenko et al., 2022). This algorithm identifies network communities based on modularity optimization. Modularity compares the number of connections inside a community with the expected number of connections for that community in a random network with the same number of nodes and keeping the same degree (number of connections of a node with other nodes). Using this method, we constructed a network of disease-disease similarities and calculated the number of disease communities optimizing the modularity parameter. Network edition and visualization were done with Cytoscape v 3.7.2 (Shannon et al., 2003).

Analysis of gene sets underlying disease communities, and pathway and molecular function enrichment analysis

In this step, we identified several gene sets: (1) genes shared within each community; (2) genes that overlap among different

1 https://www.disgenet.org/downloads

2 http://www.rstudio.com/

3 https://igraph.org/

TABLE 1 Disease terms selected according to the International Classification of Diseases ICD-10/ICD-10-CM codes (the latest release, ICD-11, is not yet available in DisGeNET), the medical coding system designed by the World Health Organization to catalog health conditions by categories of similar diseases under which more specific conditions are listed. All the disease categories were obtained from the DSM-5, except Epilepsy, which is a neurologic disorder.

ICD-10/ICD-10-CM code	Unified Medical Language System (UMLS) nomenclature	DSM-5 disease category
F23; F23.9	Acute transient psychotic disorder	Schizophrenia Spectrum Disorder and other psychotic disorders
F90; F90.9	Attention-Deficit/Hyperactivity Disorder	Neurodevelopmental disorders
F90.2	Attention-Deficit/Hyperactivity Disorder, combined type	Neurodevelopmental disorders
F84.0	Autism Spectrum Disorders (the term Autistic Disorder is not in use in DSM-5)	Neurodevelopmental disorders
F31; F31.9	Bipolar Disorder	Bipolar and related disorders
F31.81	Bipolar II Disorder	Bipolar and related disorders
F06.1	Catatonia, Organic*	Occurs in the context of disorders from different disease categories*
F06.1	Catatonia**	Occurs in the context of disorders from different disease categories**
F34.0	Cyclothymic Disorder	Bipolar and related disorders
F22.0	Delusional disorder	Schizophrenia Spectrum Disorder and other psychotic disorders
G40; G40.9; G40.909	Epilepsy	–
F90.1	Hyperkinetic conduct disorder	Neurodevelopmental disorders
F21	Incipient Schizophrenia	Schizophrenia Spectrum Disorder and other psychotic disorders/Personality Disorders
F22	Involutional paraphrenia	Schizophrenia Spectrum Disorder and other psychotic disorders
F79	Intellectual Disability (substitutes the term Mental deficiency, not in use in DSM-5)***	Neurodevelopmental disorders
F79	Intellectual Disability (substitutes the term Mental handicap, not in use in DSM-5)***	Neurodevelopmental disorders
F70-F79.9	Intellectual Disability (substitutes the term Mental Retardation, not in use in DSM-5)***	Neurodevelopmental disorders
F79	Intellectual Disability (substitutes the term Mental Retardation, not in use in DSM-5)***	Neurodevelopmental disorders
F70	Mild Intellectual Disability (substitutes the term Mild Mental Retardation, not in use in DSM-5)***	Neurodevelopmental disorders
F71	Moderate Intellectual Disability	Neurodevelopmental disorders
F29	Nonorganic psychosis	Schizophrenia Spectrum Disorder and other psychotic disorders
F42; F42.9; F42.8	Obsessive-Compulsive Disorder	Obsessive-compulsive and related disorders
F22	Paranoia	Schizophrenia Spectrum Disorder and other psychotic disorders
F73	Profound Intellectual Disability (the term Profound Mental Retardation is not in use in DSM-5)***	Neurodevelopmental disorders
F23	Psychosis, Brief Reactive	Schizophrenia Spectrum Disorder and other psychotic disorders
F25.0	Schizoaffective disorder, bipolar type	Schizophrenia Spectrum Disorder and other psychotic disorders
F20.81	Schizophreniform Disorders	Schizophrenia Spectrum Disorder and other psychotic disorders
F20.81	Schizophreniform psychosis NOS	Schizophrenia Spectrum Disorder and other psychotic disorders
F21	Schizotypal Personality Disorder	Schizophrenia Spectrum Disorder and other psychotic disorders/Personality Disorders
F72	Severe Intellectual Disability	Neurodevelopmental disorders

Correspondence between the Unified Medical Language System (UMLS) nomenclature used in DisGeNET and DSM-5 was done by the ICD-10/ICD-10-CM codes.
*The nosology used in DisGeNET with respect to Catatonia, follows a classification that was present in the previous version of the Diagnostic and Statistical Manual of Mental Disorders (DSM-IV), which defined that Organic Catatonia was related to the occurrence of Catatonia due to a General Medical Condition, clearly distinct from a Schizophrenia subtype.
**The Catatonia here is not the Organic Catatonia but includes Catatonia present in psychotic and mood disorders, which includes the catatonic subtype of Schizophrenia from the DSM-IV (Tandon et al., 2013). The catatonic subtype of Schizophrenia from the DSM-IV will be deleted in the DSM-5 revision along with other Schizophrenia subtypes (Tandon and Carpenter, 2012), and Catatonia is currently a specifier for Schizophrenia.
***Intellectual Disability is the term used in this study in substitution to the DisGeNET terms Mental deficiency, Mental handicap, and Mental retardation as these terms are no longer in use in DSM-5.

disease communities; and (3) genes that are exclusive from each community (**Supplementary File 1**). After performing disease community detection, we analyzed the DisGeNET dataset *all_gene_disease_associations.tsv.gz* available at https://www.disgenet.org/downloads to identify the gene sets. This dataset contains all gene-disease associations in the database.

Pathway and molecular function enrichment used the list of genes that are exclusive to each disease community and was performed using Reactome pathways (Jassal et al., 2020) and Gene Ontology (GO; Carbon et al., 2009) molecular functions, using g:Profiler (Raudvere et al., 2019; **Supplementary File 1**). The Gene Ontology (GO) resource[4] develops structured controlled ontologies to characterize genes and their products. The GO Consortium has developed AmiGO, a web-based application that allows users to search, sort, analyze, visualize, and download the data of interest. Reactome[5] is a manually

4 http://geneontology.org/

5 https://reactome.org/

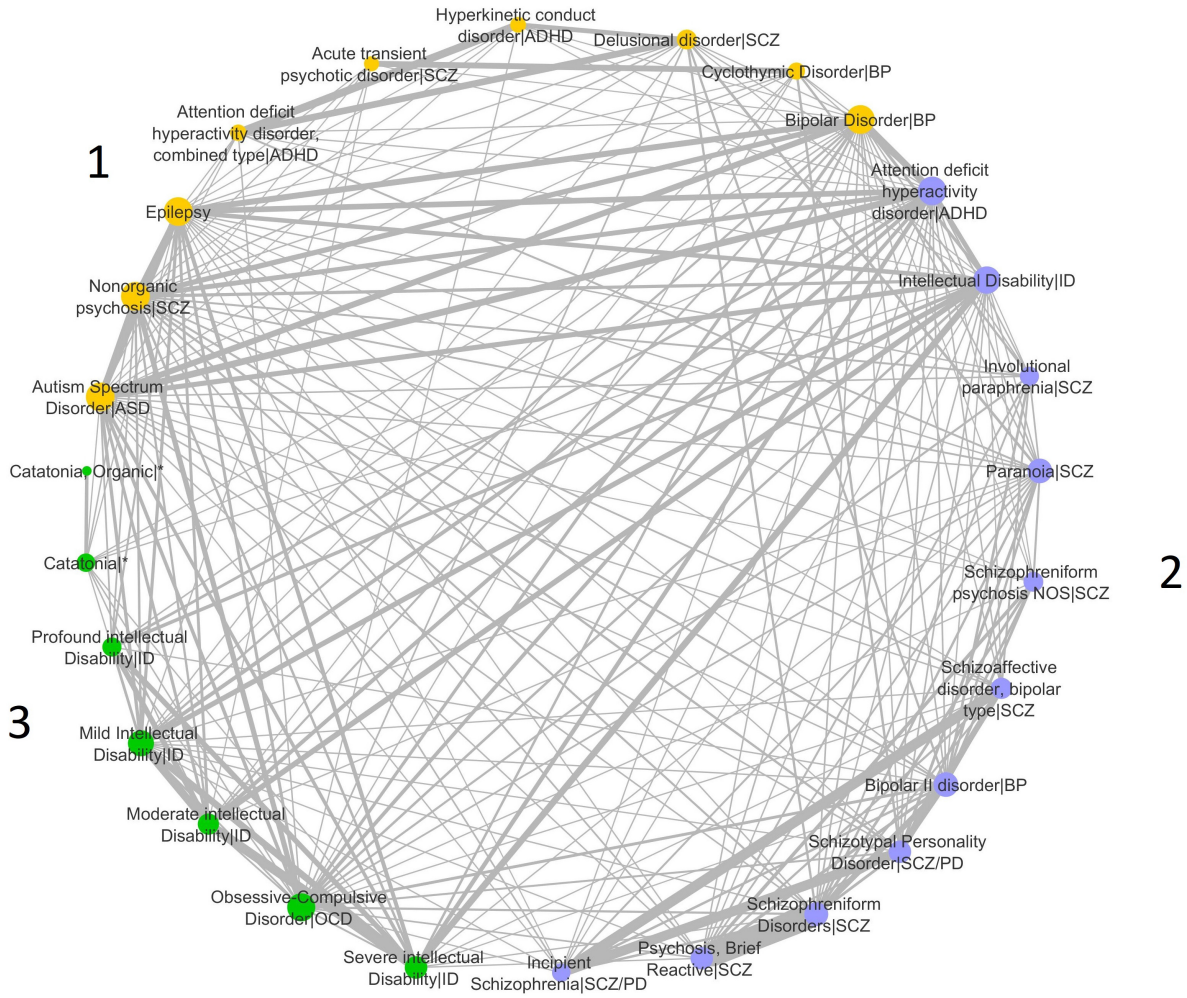

FIGURE 1

Disease similarity network. The implementation of the Leiden algorithm for the identification of disease communities in the network identified three disease communities. The different communities are indicated with different colors in the network, and the diseases included in each community are shown in the figure. Network nodes (or vertices) represent diseases. Edges (or links) represent disease-disease associations. Edge thickness is proportional to weight and represents the degree of similarity between disease pairs computed by the Jaccard index. Circles sizes reflect the node degree (**Supplementary Table 1**), which represents the number of connections the node has to other network nodes. ASD, Autism Spectrum Disorder; ADHD, Attention-Deficit/Hyperactivity Disorder; SCZ, Disease included under the Schizophrenia Spectrum Disorder and other psychotic disorders diagnosis; ID, Disease included under the Intellectual Disability diagnosis; BP, Disease included in the Bipolar and related disorders diagnosis; SCZ/PD, Disease included under the Personality Disorder diagnosis and under the Schizophrenia Spectrum Disorder and other psychotic disorders diagnosis; OCD, Disease included under the Obsessive-Compulsive and related disorders diagnosis; *Occurs in the context of disorders from different disease categories. Duplicate nodes in the same community were omitted from the figure but used in the analyses: for ASD—nodes from obsolete disease terms that are not used in the DSM-5 edition; for Intellectual Disability—nodes from disease terms that are not present in the DSM-5 edition are substituted for updated DSM-5 terms.

curated and peer-reviewed pathway database that provides bioinformatic tools for the visualization, interpretation, and analysis of pathway information with applications in genome analysis, modeling, and systems biology. Only results below a threshold of 0.05 for the False Discovery Rate were considered.

Identification of rare *de novo* loss of function Single Nucleotide Variants within genes from network disease communities, in Autism Spectrum Disorder patients

To validate the prediction that ASD patients have mutations in genes shared among comorbid brain disorders, we searched for Single Nucleotide Variants (SNVs), namely *de novo* loss of function (LoF) mutations, in an ASD Whole Genome Sequencing (WGS) public dataset. We focused on rare *de novo* mutations because this class of variants plays an important role in neurodevelopmental diseases, including ASD, ID, ADHD, and others. For this purpose, we searched the large dataset of genomic variants from WGS of ASD subjects available in the MSSNG database[6] (Yuen et al., 2017; **Supplementary File 1**). MSSNG is a collaboration between the ASD organization Autism Speaks,[7] Google, and the research community to create the world's largest genomic database on ASD. MSSNG seeks to make data available from the WGS of 10,000 individuals from ASD families. The omitted letters in MSSNG (pronounced "missing") represent the missing information about ASD that the project seeks to deliver (Yuen et al., 2017).

The dataset was already filtered for quality parameters (Yuen et al., 2017), namely: (1) variants with genotype quality of at least 99 (GQ for Illumina; VAF for Complete Genomics); (2) variants with Minor Allele Frequency (MAF) below 1%; and (3) variant call more than 95% of the time as a reference allele and less than 1% of the time as a variant in the parents. We performed a systematic analysis of data of 3,881 ASD individuals. For the selection of rare *de novo* predicted LoF SNVs, we inspected the variants with predicted pathogenic effect in protein function or structure, according to the Ensembl Variant Effect Predictor (VEP; McLaren et al., 2016), and only LoF variants of frameshift, stop gain and stop loss, were present in the dataset. Finally, we identified the proportion of rare *de novo* LoF SNVs present in genes from each disease community of the network, identified genes with variants in all disease communities, and characterized the genes from the ASD disease community (**Supplementary File 1**).

Genes from the ASD disease community with more than one rare *de novo* LoF SNV were also characterized according to the Simons Foundation Autism Research Initiative (SFARI) gene scoring module.[8] SFARI is an ASD-dedicated database that incorporates a gene scoring module to establish a gene rank according to the strength of the evidence that associates a given gene with ASD. The Syndromic category (Category S) includes mutations that are associated with a substantial degree of increased risk and consistently linked to additional traits not required for an ASD diagnosis. If there is independent evidence implicating a gene in idiopathic ASD, it is listed as "#S" (e.g., 1S, 2S). If there is no independent evidence, the gene is listed only as "S." Category 1 genes have been clearly implicated in ASD (presence of at least three *de novo* likely-gene-disrupting mutations) and are also found in the gene list of a large ASD research study, SPARK[9] (SPARK Consortium, 2018), or on the list of genes reported by Satterstrom et al. (2020). All the genes in this category reach a False Discovery Rate threshold of < 0.1 (threshold used in Satterstrom et al. (2020) for the identification of ASD risk genes in a large exome sequencing ASD cohort), and some reach the threshold of genome-wide significance. Genes from the SFARI 3 category were not used, as they constitute weaker ASD candidates.

Results

Construction of a network of gene-based disease similarities between Autism Spectrum Disorder and comorbid brain disorders and disease community detection

We analyzed 309 disease-disease associations based on the genetic similarity of a set of 31 brain disease terms from the DisGeNET dataset of disease-disease associations (**Table 1**). We constructed a network of disease-disease similarities and calculated the number of disease communities optimizing the modularity parameter of the Leiden algorithm (**Figure 1**). The highest modularity positive score for the dataset was 0.06, indicating that the number of connections within groups exceeds the number of expected connections by chance.

Three disease communities were identified (**Figure 1**). ASD is placed in Community 1 with Epilepsy, ADHD combined type, Hyperkinetic conduct disorder (HC), and some of the diseases included in the SCZ Spectrum, Bipolar Disorder (BP), and Cyclothymic Disorder (CD). Community 2 integrates the majority of the diseases in the SCZ spectrum, as well as ADHD, BP type II disorder, and Intellectual Disability (ID). Subtypes of ID are also present in Community 3, along with Obsessive-Compulsive Disorder (OCD) and Catatonia.

6 https://research.mss.ng/

7 https://www.autismspeaks.org/

8 https://gene.sfari.org/database/gene-scoring/

9 https://sparkforautism.org/

Network connectivity for each disease is measured by the node degree. ASD, BP, Epilepsy, and Nonorganic psychosis (NP) in Community 1 are the diseases with the highest node degree, indicative of the largest number of connections to other diseases in the entire network. The strength of disease connections is represented by line widths, as thicker lines represent stronger connections. The strongest ASD intra-community connections are with Epilepsy and BP. ASD also shows very strong connections to ADHD and ID in Community 2. A strong connection is also found between ASD and BP in Community 1. ADHD and ID are the diseases with the highest node degree in Community 2, while OCD, Mild ID, and severe ID in Community 3 show the highest number of connections to other diseases (**Figure 1** and **Supplementary Table 1**). ID subtypes are mostly clustered in Community 3, and we can observe a strong connection between ID (in Community 2) and most of these subtypes, independently of severity level. Strong connections are also detected between ADHD and Delusional disorder/SCZ, and Epilepsy and BP.

Analysis of gene sets underlying disease communities, and pathway and molecular function enrichment analyses

Community 1 has the largest number of genes (3,191 genes), while Community 2 includes a total of 1,276 genes, and Community 3 has 1,045 genes (**Supplementary File 2**). The three gene lists partially overlap (**Supplementary File 2**). However, some of the genes implicated in the disease-disease associations analyzed are exclusive from each community. The proportion of the number of exclusive genes by the total number of genes for each community is 67.63% for Community 1, 30.49% for Community 2, and 39.90% for Community 3 (**Supplementary File 2**).

For the pathway enrichment analyses, we focused on the list of exclusive genes from each disease community and, for all three gene lists, calculated the enrichment in GO molecular functions (GO:MF) and Reactome pathways (REAC) (**Supplementary File 3**). Some of these pathways were previously associated with disorders in each of these communities. The top five enriched terms for each community are shown in **Table 2**.

Identification of rare *de novo* loss of function Single Nucleotide Variants in Autism Spectrum Disorder datasets

We analyzed 3,881 ASD cases from the MSSNG whole genome sequencing dataset and identified 366 rare (MAF < 1%) *de novo* LoF SNVs, within 336 genes (Yuen et al., 2017; **Supplementary Table 2**). The majority of these variants (43.32%) fall in the predicted effect category of *stop gain* variants, followed by *frameshift deletions* (36.51%) and *frameshift insertions* (17.71%; **Supplementary File 4**).

We further searched this ASD dataset specifically for rare *de novo* LoF SNVs within the genes associated with each disease community of the network. As expected, we found that Community 1 diseases share the largest proportion (33.61%) of rare *de novo* LoF SNVs, followed by Community 3 (22.68%) and Community 2 (18.85%; **Supplementary File 5**).

The genes with rare *de novo* LoF SNVs that are shared among all communities are shown in **Figure 2A**. The genes *SHANK3, ASH1L, SCN2A,* and *CHD2* have the highest number of rare *de novo* LoF SNVs (three to five variants) in ASD patients. The genes with more than one rare *de novo* LoF SNV in Community 1 are shown in **Figure 2B**. Genes that are also in the SFARI gene scoring module as candidate genes for ASD are shown. Most of the 15 genes shared by Community 1 diseases with more than one variant are included in the SFARI ASD list of candidate genes in high evidence categories, namely category 1 (five genes) and category 1S (eight genes). Genes with more than one rare *de novo* LoF SNV in communities 2 and 3 are shown in **Supplementary File 5**. A summary of the results of this study can be found in **Supplementary Table 3**.

Discussion

In this study, we investigated the shared genetic component between ASD and other brain disorders that often co-occur in ASD patients. We hypothesize that the clinical variability that characterizes ASD, and the occurrence of comorbidities, may be partially explained by shared genetic components among these disorders and ASD. To further understand this question, we explored whether some of these disorders are genetically more similar to ASD than others that do not frequently co-occur with this disorder. For this purpose, we built a disease similarity network, using the shared genetic architecture as a means to assess disease-disease similarities.

Using this approach, we showed that ASD is one of the five disorders with more connections in the disease similarity network. This result indicates that ASD indeed shares genes that have been previously implicated in its etiology with many of the 29 co-occurring brain disorders analyzed.

We next used the Leiden community detection algorithm to cluster all diseases into three communities, according to gene-based genetic similarity. ASD is included in Community 1, which encompasses a heterogeneous group of diseases, namely Epilepsy, ADHD subtypes, and some of the conditions that are part of the BD and the SCZ spectra. This community also shows the largest number of shared genes. Most of the disorders of Community 2 are SCZ subtypes, and ID is highly represented in Community 3 and shares a fewer number of

TABLE 2 Top five Gene Ontology molecular functions and Reactome pathways enrichment for communities' exclusive genes.

Community 1			
Source	**Term_name**	**Term_id**	**Adjusted_*p*_value**
REAC	Signal Transduction	REAC:R-HSA-162582	1.95E-12
REAC	Neuronal System	REAC:R-HSA-112316	1.31E-09
REAC	Signaling by GPCR	REAC:R-HSA-372790	4.57E-08
REAC	GPCR downstream signalling	REAC:R-HSA-388396	4.91E-08
REAC	Signaling by Nuclear Receptors	REAC:R-HSA-9006931	3.81E-07
GO:MF	signaling receptor binding	GO:0005102	7.68E-19
GO:MF	enzyme binding	GO:0019899	5.55E-16
GO:MF	ion binding	GO:0043167	6.16E-15
GO:MF	ion transmembrane transporter activity	GO:0015075	1.64E-14
GO:MF	signaling receptor activity	GO:0038023	5.67E-13
Community 2			
Source	**Term_name**	**Term_id**	**Adjusted_*p*_value**
REAC	Diseases of Mismatch Repair (MMR)	REAC:R-HSA-5423599	1.20E-03
REAC	RHOQ GTPase cycle	REAC:R-HSA-9013406	2.31E-02
REAC	Diseases of DNA repair	REAC:R-HSA-9675135	2.36E-02
REAC	RHOJ GTPase cycle	REAC:R-HSA-9013409	3.04E-02
REAC	RAC3 GTPase cycle	REAC:R-HSA-9013423	3.04E-02
GO:MF	single base insertion or deletion binding	GO:0032138	1.71E-02
GO:MF	mismatch repair complex binding	GO:0032404	1.71E-02
GO:MF	DNA insertion or deletion binding	GO:0032135	3.87E-02
Community 3			
Source	**Term_name**	**Term_id**	**Adjusted_*p*_value**
REAC	Respiratory electron transport. ATP synthesis by chemiosmotic coupling and heat production by uncoupling proteins.	REAC:R-HSA-163200	1.18E-04
REAC	Complex I biogenesis	REAC:R-HSA-6799198	1.18E-04
REAC	Respiratory electron transport	REAC:R-HSA-611105	1.18E-04
REAC	The citric acid (TCA) cycle and respiratory electron transport	REAC:R-HSA-1428517	1.18E-04
REAC	Post-translational modification: synthesis of GPI-anchored proteins	REAC:R-HSA-163125	9.86E-03
GO:MF	catalytic activity	GO:0003824	1.44E-07
GO:MF	oxidoreduction-driven active transmembrane transporter activity	GO:0015453	4.97E-06
GO:MF	NADH dehydrogenase (ubiquinone) activity	GO:0008137	4.97E-06
GO:MF	NADH dehydrogenase (quinone) activity	GO:0050136	4.97E-06
GO:MF	NADH dehydrogenase activity	GO:0003954	5.08E-06

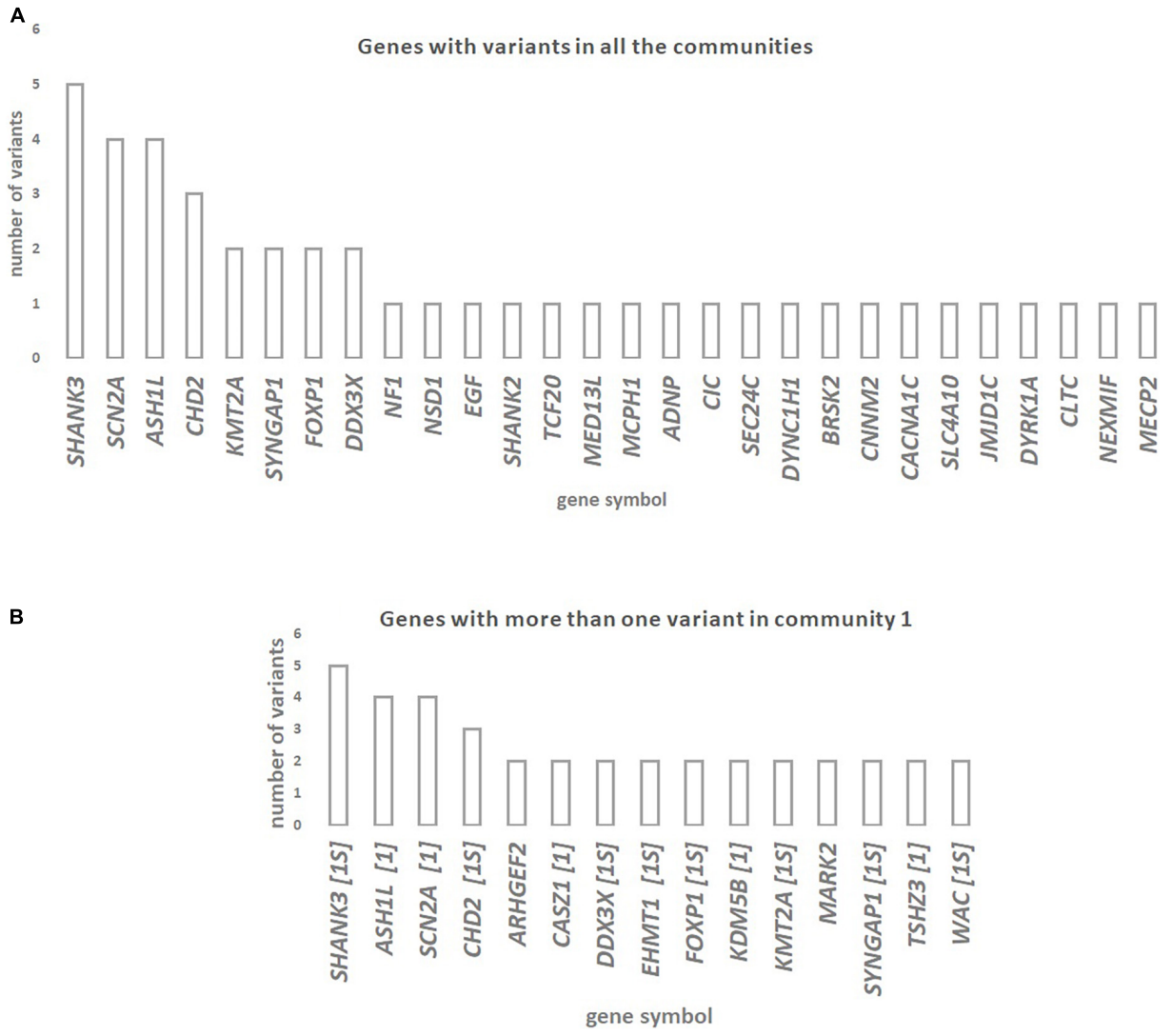

FIGURE 2
(A) Genes with rare *de novo* LoF SNVs in ASD patients are shared across diseases from the three communities of the network of disease-disease similarities. **(B)** Genes with more than one rare *de novo* LoF SNV in ASD patients that are shared across Community 1 diseases (which includes ASD) of the network of disease-disease similarities. Whenever genes are also in the SFARI gene scoring module as candidate genes for ASD (https://gene.sfari.org/database/gene-scoring/), we display the evidence score next to the gene symbols.

genes. The heterogeneous nature of Community 1 suggests that ASD has genetic similarities with a larger number of disorders than SCZ, BP, and ID. This is expected and in accordance with our hypothesis, given that the clinical presentation of ASD is so variable, compounded by multiple comorbidities, and that this variability is frequently attributed to the large number of genes that have been implicated in its etiology (Ramaswami and Geschwind, 2018). It is somewhat unexpected that both ADHD and ID cluster in Community 2, which generally groups other neuropsychiatric diseases with a late adolescent or adult-onset. Furthermore, ID subtypes are mostly clustered in Community 3, and we can observe a strong connection between ID (in Community 2) and most of these subtypes, independently of severity level. This unexpected community formation may reflect some bias in the terminology used by DisGeNET, as ID encompasses all the ID subtypes, and fewer genetic studies may be available for each of the subtypes.

The strongest ASD intra-community connections are with Epilepsy and BD. While Epilepsy is a common comorbidity of ASD, the connection with BD is not frequently reported. ASD also shows very strong connections to two diseases in Community 2, namely ADHD and ID. These two neurodevelopmental disorders are, together with Epilepsy, the most common comorbidities of ASD. The finer nosological granularity provided by this approach may also be revealing previously less clear genetic similarities. For instance, a strong

connection is found between ASD and BD in Community 1. It is worth noting that ASD, ADHD, ID, and Epilepsy are normally diagnosed early in life and, as such, most studies are carried out in children. On the other hand, SCZ, psychosis, and BP are later onset diseases. Because few studies are focusing on adults with ASD (Forde et al., 2021), not much clinical evidence is available regarding the co-occurrence of these adult diseases and ASD, but it can be detected using this approach based on gene sharing. Interestingly, the approach also detects strong connections and community grouping between other childhood onset and adult onset brain diseases, for instance, between ADHD and Delusional disorder/SCZ, and Epilepsy and BD. These findings provide evidence for genetic relationships that were previously not considered and suggest that is worth exploring further the comorbidities in datasets of adults diagnosed with childhood-onset disorders.

The community detection algorithm assigns ID and ASD to separate communities. Even though ASD and ID are known to share candidate genes, the results show that there is enough genetic distance to place both disorders in separate communities. This may indicate that ASD patients with ID may have mutations in a subset of genes that are more related to ID than ASD patients without ID. This is in accordance with previous evidence that showed that some ASD-risk genes have higher frequencies of disruptive *de novo* variants in people ascertained for developmental delay (Satterstrom et al., 2020).

Previous work on clustering analysis of psychiatric disorders suggested that ASD and mood and psychotic disorders (which included SCZ and BP) cluster in different groups (Lee et al., 2019). Our results have some degree of overlap with previous evidence as we identify a community composed of most of the SCZ spectrum disorders (Community 2). However, as we have genetic annotations for disease subtypes as input data, we were also able to infer which SCZ-related disorders have more genetic similarity with ASD than others.

Enrichment analysis using genes exclusively from each of the three communities allowed the identification of shared biological pathways and molecular functions among these brain disorders. Community 1 is enriched in signal transduction and neuronal system mechanisms. These pathways have been implicated in some diseases from Community 1, for instance, the *dysfunction in neuronal activity-dependent signaling pathways* in ASD (Ebert and Greenberg, 2013), the *dysregulation in neuronal apoptosis-regulatory pathways* in Epilepsy (Bozzi et al., 2011), or alterations in *G-protein-coupled receptors (GPCRs)* in ASD, SCZ, and BP (Monfared et al., 2021). The top five terms enriched in GO molecular functions and Reactome pathways for genes exclusive of Community 2 are related to DNA repair and mismatch repair. Mismatch repair is a cellular pathway that corrects base mispairs occurring during DNA replication (Graham et al., 2019). High-level DNA damage has been implicated in psychiatric disorders (Raza et al., 2016), and candidate genes suggesting a role for this mechanism in Schizophrenia have been identified (Odemis et al., 2015). Genes exclusive of Community 3 are enriched in terms related to mitochondrial complex 1 NADH dehydrogenase, a finding in accordance with the typical association of Mitochondrial complex I deficiency with severe ID, encephalopathy, ataxia, and dystonia (Loeffen et al., 2000; Distelmaier et al., 2009; Pagniez-Mammeri et al., 2012; Valiente-Pallejà et al., 2018).

We further analyzed rare *de novo* LoF SNVs in 3,881 ASD cases from the MSSNG WGS cohort, to explore whether ASD patients have pathogenic mutations in genes implicated in multiple brain disorders. *de novo* mutations in ASD, and in human disease in general, are maintained at low frequencies in the population by natural selection (Alonso-Gonzalez et al., 2018), and therefore, rare risk alleles tend to be eliminated, while common alleles that are benign or neutral show signs of positive selection (Polimanti and Gelernter, 2017). However, *de novo* mutations can have strong effects on protein structure and/or function and, despite being rare individually, may capture an important component of the heritability for complex genetic diseases (Veltman and Brunner, 2012). Supporting this hypothesis, we identified, in these ASD subjects, rare *de novo* LoF SNVs within genes previously associated with other disorders in all three communities.

We observed that the genes *SHANK3, ASH1L, SCN2A,* and *CHD2,* which are candidate genes for diseases in all three communities, have a higher number of *de novo* rare LoF SNVs in ASD subjects. These genes are strong candidates for ASD, according to the SFARI gene category scoring. These observations suggest that ASD patients have deleterious mutations in genes shared with other brain disorders from the same or different communities. In fact, previous reports implicate these genes in several of the disorders analyzed. For instance, mutations in *SHANK3* (SH3 and Multiple Ankyrin Repeat Domains 3), which encodes a synaptic scaffold protein supporting the organization of hundreds of other synaptic proteins, have been reported in patients with ASD, ID, and SCZ (Durand et al., 2012; Monteiro and Feng, 2017). The *ASH1L* gene (ASH1-Like Histone Lysine Methyltransferase), that encodes a histone methyltransferase involved in chromatin modification, binds to the promoter region of *NRXN1* (Neurexin 1) inhibiting the transcriptional activity of *NRXN1* and dysregulating synapse formation (Zhu, 2016; Zhang et al., 2021). Several reports associate this gene with ID, delayed speech, and seizures (Okamoto et al., 2017). Mutations in the *CHD2* gene (Chromodomain Helicase DNA Binding Protein 2), which encodes a member of the chromodomain helicase DNA-binding (CHD) family of proteins, have been identified in ASD, ID, and Epilepsy (Luo et al., 2022). The present approach was therefore successful in identifying genes underlying the shared genetic component between ASD and the diseases analyzed.

Previous studies have addressed the question of cross-disorder genetic overlap, mainly focusing on common genetic variation resulting from Genome-Wide Association Studies (GWAS; Autism Spectrum Disorders Working Group of The Psychiatric Genomics Consortium, 2017; Anttila et al., 2018; Lee et al., 2019). Instead of addressing common variations shared between disorders, this study complemented the previous evidence by focusing on rare *de novo* variants. Rare *de novo* mutations contribute substantially to an individual's ASD risk (Iossifov, 2012; Neale, 2012; Genovese and Butler, 2020), and altogether explain ASD in a significant fraction of patients (Sanders, 2012). Furthermore, rare *de novo* mutations are extremely useful to identify biological pathways that can be disrupted by different mutations in multiple genes. Understanding which genes mutated in ASD are shared by co-occurring brain conditions is an important step to understanding the clinical variability of ASD, and eventually to defining targets for therapeutic development.

Our methodological approach improves previous studies in several aspects. First, the data on gene-disease associations comes from a wide range of sources, including curated genetic databases, animal models, or GWAS data, and therefore provides converging evidence from multiple sources. Second, we used gene-disease annotations to several disorders that compose larger disease classes, for instance, multiple levels of ID disease severity, several disorders in the SCZ spectrum, or different ADHD and BP clinical profiles. We, therefore, took advantage of existing fine-grained disease classifications, gaining resolution to explain the architecture of disease subtypes and variable clinical presentations, as we did not assume that the genetic component of a disease is equally distributed across disease subtypes. Third, we characterized the genes implicated in a disease community-driven framework, by analyzing disease pairs in the context of their genetic relationships with several other disorders in the network instead of analyzing pairs of diseases independently. The methodology developed still has some limitations, as the annotation coverage of gene-disease association is uneven among diseases, which can lead to under or overestimated disease similarities. Improved annotation and curation of databases is crucial for approaches based on the analysis of large datasets and needs to be addressed very seriously for medical use of results from artificial intelligence approaches.

Overall, this work provided further evidence for a shared genetic architecture between ASD and several other brain disorders, including some frequent comorbidities of ASD. It also identified genes and biological processes that overlap between brain disease communities and showed that ASD patients present rare *de novo* LoF variants in genes previously associated with frequent comorbid disorders. Future studies on the analysis of disease-disease similarities should be developed with the aim of expanding this analysis to other ASD co-occurring conditions that are not in the scope of the mental illness, in particular, diseases that affect the immune system (Meltzer and van de Water, 2017) and the gastrointestinal tract, and may be related with genetically determined microbiome constitution (Liu et al., 2021).

Importantly, this study showed the value of a data-driven approach, using data from heterogeneous sources to characterize the genetic overlap between diseases and, in particular, to gain insights into the shared genetic architecture of ASD and other brain disorders.

Data availability statement

ASD whole-genome sequencing dataset analysed annotated_de_novo_variants_20200624.xls was obtained from the MSSNG web-site (https://research.mss.ng/).

Ethics statement

The studies involving human participants were reviewed and approved by the Institutional Review Boards or Ethical Committees of the participating sites. Written informed consent to participate in this study was provided by the participants' legal guardian/next of kin.

Author contributions

JV, HM, and AV developed the concept for this work. Data curation, methodological development, and formal analysis were carried out by JV, with strong support from HM and contributions from JS, AM, CR, and GO. GO and AV provided resources. AV and HM provided overall supervision and coordination. JV wrote the initial draft, revised, and edited by HM and AV. All authors contributed and revised the article, and approved the submitted version.

Funding

This research was supported by Fundação para a Ciência e a Tecnologia (UIDB/04046/2020 and UIDP/04046/2020 Center grants to BioISI), by PAC-POCI-01-0145-FEDER-016428 MEDPERSYST, by DeePer—Deep graph learning approaches to personalized medicine (EXPL/CCI-BIO/0126/2021), and by National Institute of Health Doutor Ricardo Jorge. JV, AM, and JS are recipients of a fellowship from BioSys PhD programme PD65-2012 (JV Ref: PD/BD/131390/2017; AM Ref: PD/BD/113773/2015; and JS Ref: PD/BD/114386/2016) from Fundação para a Ciência e a Tecnologia (Portugal).

Acknowledgments

We wish to acknowledge the resources of MSSNG (www.mss.ng), Autism Speaks, and The Centre for Applied Genomics at The Hospital for Sick Children, Toronto, Canada. We also thank the participating families for their time and contributions to this database, as well as the generosity of the donors who supported this program.

Conflict of interest

The authors declare that the research was conducted in the absence of any commercial or financial relationships that could be construed as a potential conflict of interest.

Publisher's note

All claims expressed in this article are solely those of the authors and do not necessarily represent those of their affiliated organizations, or those of the publisher, the editors and the reviewers. Any product that may be evaluated in this article, or claim that may be made by its manufacturer, is not guaranteed or endorsed by the publisher.

Supplementary material

The Supplementary Material for this article can be found online at: https://www.frontiersin.org/articles/10.3389/fnmol.2022.932305/full#supplementary-material

References

Alonso-Gonzalez, A., Rodriguez-Fontenla, C., and Carracedo, A. (2018). De novo mutations (DNMs) in autism spectrum disorder (ASD): Pathway and network analysis. *Front. Genet.* 9:406. doi: 10.3389/fgene.2018.00406

American Psychiatric Association. *Diagnostic and statistical manual of mental disorders: DSM-5*. 5th ed. Arlington. VA: American Psychiatric Association (2013).

Anttila, V., Bulik-Sullivan, B., Finucane, H. K., Walters, R. K., Bras, J., Duncan, L., et al. (2018). Analysis of shared heritability in common disorders of the brain. *Science* 360:eaa8757. doi: 10.1126/science.aap8757

Autism Spectrum Disorders Working Group of The Psychiatric Genomics Consortium (2017). Meta-analysis of GWAS of over 16,000 individuals with autism spectrum disorder highlights a novel locus at 10q24.32 and a significant overlap with schizophrenia. *Mol. Autism* 8:21. doi: 10.1186/s13229-017-0137-9

Bozzi, Y., Dunleavy, M., and Henshall, D. C. (2011). Cell signaling underlying epileptic behavior. *Front. Behav. Neurosci.* 5:45. doi: 10.3389/fnbeh.2011.00045

Carbon, S., Ireland, A., Mungall, C. J., Shu, S., Marshall, B., Lewis, S., et al. (2009). AmiGO: Online access to ontology and annotation data. *Bioinformatics* 25, 288–289. doi: 10.1093/bioinformatics/btn615

Christensen, J., Overgaard, M., Parner, E. T., Vestergaard, M., and Schendel, D. (2016). Risk of epilepsy and autism in full and half siblings-a population-based cohort study. *Epilepsia* 57, 2011–2018. doi: 10.1111/epi.13595

Distelmaier, F., Koopman, W. J. H., van den Heuvel, L. P., Rodenburg, R. J., Mayatepek, E., Willems, P. H., et al. (2009). Mitochondrial complex I deficiency: From organelle dysfunction to clinical disease. *Brain* 132, 833–842. doi: 10.1093/brain/awp058

Durand, C. M., Perroy, J., Loll, F., Perrais, D., Fagni, L., Bourgeron, T., et al. (2012). SHANK3 mutations identified in autism lead to modification of dendritic spine morphology via an actin-dependent mechanism. *Mol. Psychiatry* 17, 71–84. doi: 10.1038/mp.2011.57

Ebert, D. H., and Greenberg, M. E. (2013). Activity-dependent neuronal signalling and autism spectrum disorder. *Nature* 493, 327–337. doi: 10.1038/nature11860

Forde, J., Bonilla, P. M., Mannion, A., Coyne, R., Haverty, R., and Leader, G. (2021). Health status of adults with autism spectrum disorder. *Rev. J. Autism Dev. Dis.* 2021, 1–11.

Gaugler, T., Klei, L., Sanders, S. J., Bodea, C. A., Goldberg, A. P., Lee, A. B., et al. (2014). Most genetic risk for autism resides with common variation. *Nature genetics*, 46, 881–885.

Genovese, A., and Butler, M. G. (2020). Clinical assessment, genetics, and treatment approaches in autism spectrum disorder (ASD). *Int. J. Mol. Sci.* 21:E4726. doi: 10.3390/ijms21134726

Goes, F. S., Pirooznia, M., Parla, J. S., Kramer, M., Ghiban, E., Mavruk, S., et al. (2016). Exome sequencing of familial bipolar disorder. *JAMA Psychiatry* 73, 590–597. doi: 10.1001/jamapsychiatry.2016.0251

Graham, V. W. J., Putnam, C. D., and Kolodner, R. D. (2019). "DNA mismatch repair: Mechanisms and cancer genetics?," in *Encyclopedia of Cancer*, eds P. Boffetta and P. Hainaut (Academic Press), 530–538. doi: 10.1016/B978-0-12-801238-3.96130-0

Guo, W., Samuels, J. F., Wang, Y., Cao, H., Ritter, M., Nestadt, P. S., (2017). Polygenic risk score and heritability estimates reveals a genetic relationship between ASD and OCD. *Eur. Neuropsychopharmacol.* 27, 657–666. doi: 10.1016/j.euroneuro.2017.03.011

Iossifov, I. (2012). De novo gene disruptions in children on the autistic spectrum. *Neuron* 2012, 285–299.

Jassal, B., Matthews, L., Viteri, G., Gong, C., Lorente, P., Fabregat, A., (2020). The reactome pathway knowledgebase. *Nucleic Acids Res.* 48, D498–D503. doi: 10.1093/nar/gkz1031

Kharchenko, P., Petukhov, V., Traag, V. A., Csárdi, G., Nepusz, T., Nguyen, M. V., (2022). *leidenAlg: Implements the Leiden Algorithm via an R Interface (1.0.2)*. Available online at: https://CRAN.R-project.org/package=leidenAlg (accessed March, 2022).

Lee, P. H., Anttila, V., Won, H., Feng, Y.-C. A., Rosenthal, J., Zhu, Z., (2019). Genomic relationships, novel loci, and pleiotropic mechanisms across eight psychiatric disorders. *Cell* 179, 1469–1482.e11. doi: 10.1016/j.cell.2019.11.020

Liu, Z., Mao, X., Dan, Z., Pei, Y., Xu, R., Guo, M., (2021). Gene variations in autism spectrum disorder are associated with alternation of gut microbiota, metabolites and cytokines. *Gut Microbes* 13, 1854967. doi: 10.1080/19490976.2020.1854967

Lo-Castro, A., and Curatolo, P. (2014). Epilepsy associated with autism and attention deficit hyperactivity disorder: Is there a genetic link? *Brain Dev.* 36, 185–193. doi: 10.1016/j.braindev.2013.04.013

Loeffen, J. L., Smeitink, J. A., Trijbels, J. M., Janssen, A. J., Triepels, R. H., Sengers, R. C., et al. (2000). Isolated complex I deficiency in children: Clinical, biochemical and genetic aspects. *Hum. Mutat.* 15, 123–134. doi: 10.1002/(SICI)1098-1004(200002)15:23.0.CO;2-P

Luo, X., Sun, X., Wang, Y., Lin, L., Yuan, F., Wang, S., et al. (2022). Clinical study of 8 cases of CHD2 gene mutation–related neurological diseases and their mechanisms. *Front. Cell Dev. Biol.* 10:853127. doi: 10.3389/fcell.2022.853127

McCarthy, S. E., Gillis, J., Kramer, M., Lihm, J., Yoon, S., Berstein, Y., (2014). De novo mutations in schizophrenia implicate chromatin remodeling and support a genetic overlap with autism and intellectual disability. *Mol. Psychiatry* 19, 652–658. doi: 10.1038/mp.2014.29

McLaren, W., Gil, L., Hunt, S. E., Riat, H. S., Ritchie, G. R. S., Thormann, A., et al. (2016). The ensembl variant effect predictor. *Gen. Biol.* 17:122. doi: 10.1186/s13059-016-0974-4

Meier, S. M., Petersen, L., Schendel, D. E., Mattheisen, M., Mortensen, P. B., and Mors, O. (2015). Obsessive-compulsive disorder and autism spectrum disorders: longitudinal and offspring risk. *PLoS One* 10:e0141703. doi: 10.1371/journal.pone.0141703

Meltzer, A., and van de Water, J. (2017). The role of the immune system in autism spectrum disorder. *Neuropsychopharmacology* 42, 284–298.

Monfared, R. V., Alhassen, W., Truong, T. M., Gonzales, M. A. M., Vachirakorntong, V., Chen, S., (2021). Transcriptome profiling of dysregulated GPCRs reveals overlapping patterns across psychiatric disorders and age-disease interactions. *Cells* 10:2967. doi: 10.3390/cells10112967

Monteiro, P., and Feng, G. (2017). SHANK proteins: Roles at the synapse and in autism spectrum disorder. *Nat. Rev. Neurosci.* 18, 147–157. doi: 10.1038/nrn.2016.183

Neale, B. M. (2012). Patterns and rates of exonic de novo mutations in autism spectrum disorders. *Nature* 485, 242–245.

Novarino, G., Baek, S. T., and Gleeson, J. G. (2013). The sacred disease: the puzzling genetics of epileptic disorders. *Neuron* 80, 9–11. doi: 10.1016/j.neuron.2013.09.019

Odemis, S., Tüzün, E., Güleç, H., Semiz, U., Dasdemir, S., Kucuk, M., (2015). Association between polymorphisms of DNA repair genes and risk of schizophrenia. *Genet. Test. Mol. Biomark.* 20:168. doi: 10.1089/gtmb.2015.0168

Okamoto, N., Miya, F., Tsunoda, T., Kato, M., Saitoh, S., Yamasaki, M., (2017). Novel MCA/ID syndrome with ASH1L mutation. *Am. J. Med. Genet. Part A* 173, 1644–1648. doi: 10.1002/ajmg.a.38193

Pagniez-Mammeri, H., Loublier, S., Legrand, A., Bénit, P., Rustin, P., and Slama, A. (2012). Mitochondrial complex I deficiency of nuclear origin: I. structural genes. *Mol. Genet. Metab.* 105, 163–172. doi: 10.1016/j.ymgme.2011.11.188

Piñero, J., Bravo, À, Queralt-Rosinach, N., Gutiérrez-Sacristán, A., Deu-Pons, J., Centeno, E., (2017). DisGeNET: A comprehensive platform integrating information on human disease-associated genes and variants. *Nucleic Acids Res.* 45, D833–D839. doi: 10.1093/nar/gkw943

Piñero, J., Queralt-Rosinach, N., Bravo, À, Deu-Pons, J., Bauer-Mehren, A., Baron, M., (2015). DisGeNET: A discovery platform for the dynamical exploration of human diseases and their genes. *Database J. Biol. Databases Curat.* 2015:bav028. doi: 10.1093/database/bav028

Piñero, J., Ramírez-Anguita, J. M., Saüch-Pitarch, J., Ronzano, F., Centeno, E., Sanz, F., (2020). The DisGeNET knowledge platform for disease genomics: 2019 update. *Nucleic Acids Res.* 48, D845–D855. doi: 10.1093/nar/gkz1021

Polimanti, R., and Gelernter, J. (2017). Widespread signatures of positive selection in common risk alleles associated to autism spectrum disorder. *PLoS Genet.* 13:e1006618. doi: 10.1371/journal.pgen.1006618

Ramaswami, G., and Geschwind, D. H. (2018). Genetics of autism spectrum disorder. *Handbook Clin. Neurol.* 147, 321–329. doi: 10.1016/B978-0-444-63233-3.00021-X

Raudvere, U., Kolberg, L., Kuzmin, I., Arak, T., Adler, P., Peterson, H., (2019). g:Profiler: A web server for functional enrichment analysis and conversions of gene lists (2019 update). *Nucleic Acids Res.* 47, W191–W198. doi: 10.1093/nar/gkz369

Raza, M. U., Tufan, T., Wang, Y., Hill, C., and Zhu, M.-Y. (2016). DNA damage in major psychiatric diseases. *Neurot. Res.* 30, 251–267. doi: 10.1007/s12640-016-9621-9

Sanders, S. J. (2012). De novo mutations revealed by whole-exome sequencing are strongly associated with autism. *Nature* 485, 237–241.

Satterstrom, F. K., Kosmicki, J. A., Wang, J., Breen, M. S., De Rubeis, S., An, J.-Y., (2020). Large-scale exome sequencing study implicates both developmental and functional changes in the neurobiology of autism. *Cell* 56:e23. doi: 10.1016/j.cell.2019.12.036

Satterstrom, F. K., Walters, R. K., Singh, T., Wigdor, E. M., Lescai, F., Demontis, D., (2019). Autism spectrum disorder and attention deficit hyperactivity disorder have a similar burden of rare protein-truncating variants. *Nat. Neurosci.* 22, 1961–1965. doi: 10.1038/s41593-019-0527-8

Shannon, P., Markiel, A., Ozier, O., Baliga, N. S., Wang, J. T., Ramage, D., (2003). Cytoscape: A software environment for integrated models of biomolecular interaction networks. *Geno. Res.* 13, 2498–2504. doi: 10.1101/gr.1239303

Soorya, L., Leon, J., Trelles, M. P., and Thurm, A. (2018). Framework for assessing individuals with rare genetic disorders associated with profound intellectual and multiple disabilities (PIMD): The example of Phelan McDermid syndrome. *Clin. Neuropsychol.* 32, 1226–1255. doi: 10.1080/13854046.2017.1413211

SPARK Consortium (2018). Spark: A US cohort of 50,000 families to accelerate autism research. *Neuron* 97, 488–493. doi: 10.1016/j.neuron.2018.01.015

St Pourcain B, Robinson EB, Anttila V, Sullivan BB, Maller J, Golding J, et al. ASD and schizophrenia show distinct developmental profiles in common genetic overlap with population-based social communication difficulties. *Mol Psychiatry*. (2018) 23:263–70.

Tandon, R., and Carpenter, W. T. Jr. (2012). DSM-5 status of psychotic disorders: 1 year prepublication. *Schizop. Bull.* 38, 369–370. doi: 10.1093/schbul/sbs048

Tandon, R., Heckers, S., Bustillo, J., Barch, D. M., Gaebel, W., Gur, R. E., (2013). Catatonia in DSM-5. *Schizoph. Res.* 150, 26–30. doi: 10.1016/j.schres.2013.04.034

Traag, V. A., Waltman, L., and van Eck, N. J. (2019). From louvain to leiden: Guaranteeing well-connected communities. *Sci. Rep.* 9:5233. doi: 10.1038/s41598-019-41695-z

Valiente-Pallejà, A., Torrell, H., Muntané, G., Cortés, M. J., Martínez-Leal, R., Abasolo, N., (2018). Genetic and clinical evidence of mitochondrial dysfunction in autism spectrum disorder and intellectual disability. *Hum. Mol. Genet.* 27, 891–900. doi: 10.1093/hmg/ddy009

Veltman, J. A., and Brunner, H. G. (2012). De novo mutations in human genetic disease. *Nat. Rev. Genet.* 13, 565–575. doi: 10.1038/nrg3241

White, S. W., Maddox, B. B., and Mazefsky, C. A. (2020). *The Oxford Handbook of Autism and Co-Occurring Psychiatric Conditions*. Oxford: Oxford University Press, doi: 10.1093/oxfordhb/9780190910761.001.0001

World Health Organization. *International statistical classification of diseases and related health problems: Alphabetical index*. (Vol. 3). Geneva: World Health Organization (2004).

Yuen, R. K., Merico, D., Bookman, M., Howe, J. L., Thiruvahindrapuram, B., Patel, R. V., (2017). Whole genome sequencing resource identifies 18 new candidate genes for autism spectrum disorder. *Nat. Neurosci.* 20, 602–611. doi: 10.1038/nn.4524

Zhang, C., Xu, L., Zheng, X., Liu, S., and Che, F. (2021). Role of Ash1l in tourette syndrome and other neurodevelopmental disorders. *Dev. Neurobiol.* 81, 79–91. doi: 10.1002/dneu.22795

Zhu, T. (2016). Histone methyltransferase Ash1L mediates activity-dependent repression of neurexin-1α. *Sci. Rep.* 6:26597. doi: 10.1038/srep26597

frontiers | Frontiers in Molecular Neuroscience

TYPE Hypothesis and Theory
PUBLISHED 16 September 2022
DOI 10.3389/fnmol.2022.974890

Check for updates

OPEN ACCESS

EDITED BY
Michael E. Cahill,
University of Wisconsin-Madison,
United States

REVIEWED BY
Sara Lagalwar,
Skidmore College, United States
Kwok-On Lai,
City University of Hong Kong,
Hong Kong SAR, China

*CORRESPONDENCE
Robert A. Sweet
sweetra@upmc.edu

SPECIALTY SECTION
This article was submitted to
Brain Disease Mechanisms,
a section of the journal
Frontiers in Molecular Neuroscience

RECEIVED 21 June 2022
ACCEPTED 29 July 2022
PUBLISHED 16 September 2022

CITATION
DeGiosio RA, Grubisha MJ,
MacDonald ML, McKinney BC,
Camacho CJ and Sweet RA
(2022) More than a marker: potential
pathogenic functions of MAP2.
Front. Mol. Neurosci. 15:974890.
doi: 10.3389/fnmol.2022.974890

COPYRIGHT
© 2022 DeGiosio, Grubisha,
MacDonald, McKinney, Camacho and
Sweet. This is an open-access article
distributed under the terms of the
Creative Commons Attribution License
(CC BY). The use, distribution or
reproduction in other forums is
permitted, provided the original
author(s) and the copyright owner(s)
are credited and that the original
publication in this journal is cited, in
accordance with accepted academic
practice. No use, distribution or
reproduction is permitted which does
not comply with these terms.

More than a marker: potential pathogenic functions of MAP2

Rebecca A. DeGiosio[1], Melanie J. Grubisha[1],
Matthew L. MacDonald[1], Brandon C. McKinney[1],
Carlos J. Camacho[2] and Robert A. Sweet[1,3]*

[1]Department of Psychiatry, University of Pittsburgh, Pittsburgh, PA, United States, [2]Department of Computational and Systems Biology, University of Pittsburgh, Pittsburgh, PA, United States, [3]Department of Neurology, University of Pittsburgh, Pittsburgh, PA, United States

Microtubule-associated protein 2 (MAP2) is the predominant cytoskeletal regulator within neuronal dendrites, abundant and specific enough to serve as a robust somatodendritic marker. It influences microtubule dynamics and microtubule/actin interactions to control neurite outgrowth and synaptic functions, similarly to the closely related MAP Tau. Though pathology of Tau has been well appreciated in the context of neurodegenerative disorders, the consequences of pathologically dysregulated MAP2 have been little explored, despite alterations in its immunoreactivity, expression, splicing and/or stability being observed in a variety of neurodegenerative and neuropsychiatric disorders including Huntington's disease, prion disease, schizophrenia, autism, major depression and bipolar disorder. Here we review the understood structure and functions of MAP2, including in neurite outgrowth, synaptic plasticity, and regulation of protein folding/transport. We also describe known and potential mechanisms by which MAP2 can be regulated *via* post-translational modification. Then, we assess existing evidence of its dysregulation in various brain disorders, including from immunohistochemical and (phospho) proteomic data. We propose pathways by which MAP2 pathology could contribute to endophenotypes which characterize these disorders, giving rise to the concept of a "MAP2opathy"—a series of disorders characterized by alterations in MAP2 function.

KEYWORDS

MAP2, cytoskeleton, psychiatric disorder, neurodevelopment, neurodegeneration

Introduction

The microtubule (MT) cytoskeleton is a fundamental coordinator of neuronal structure and function. MTs, comprised of heterodimers of α- and β-tubulin subunits, are present in all cell types and provide dynamic support to enable cell migration/division, modify and maintain cellular shape, and serve as tracks for intracellular trafficking (Goodson and Jonasson, 2018). In neurons, the MT network critically defines neurite morphology and mediates trafficking processes essential for synaptic transmission (Kapitein and Hoogenraad, 2015). This network is carefully regulated by a series of proteins which manipulate MT stability and/or arrangement.

Among these, the microtubule-associated proteins (MAPs) define a set of proteins which directly bind MTs, typically serving to stabilize them (Bodakuntla et al., 2019). MAPs additionally can have scaffolding functions, recruiting other cytoskeleton-modifying proteins or signaling pathway components to specific subcellular locations. Given the essential roles the MT cytoskeleton plays in neurons, it is unsurprising that pathology of both tubulin and various MAPs have been identified as direct precipitants of various brain disorders. The tubulinopathies, for instance, describe a set of cortical malformations caused by mutations in the several tubulin genes, while the tauopathies define a group of neurodegenerative diseases—most notably Alzheimer's Disease—characterized by pathology of the axonal MAP Tau.

These conditions overlap in part with "opathies" generated by dysfunction of intrinsically disordered proteins (IDPs), which have several features that confer unique pathogenic potential (**Box 1**). The structurally fluid nature of IDPs, including Tau, makes them well suited to play roles in numerous, diverse signaling pathways (Dunker et al., 2005); thus, depending on the exact pathology, a range of pleiotropic effects can be observed in IDP pathogenesis. For instance, tauopathies are distinguishable by differences in the affected Tau isoform(s), affected cell type(s), and/or fibrillar Tau aggregate structure. A similar degree of heterogeneity exists in the synucleopathies, resulting from pathologies in the IDP alpha-synuclein. In such disorders, the IDP does not represent a specific locus of defined pathogenesis, but rather a shared hub of pathology which can lead to various effects depending on the exact nature of the pathology and what upstream factors precipitated it.

MAP2 is an abundant dendritic MAP as well as an IDP which is closely related to Tau. It has been long appreciated for its roles in defining and maintaining dendritic structure; however, its neuropathological potential has been minimally explored. Evidence is beginning to suggest that MAP2 can be a similar pathogenic hub to other IDPs and MAPs, with various forms of MAP2 dysfunction having distinct causal factors and outcomes. For instance, ischemia leads to calpain-induced MAP2 cleavage which is thought to disrupt cytoskeletal integrity and may contribute to neuronal atrophy (Pettigrew et al., 1996). Similar MAP2 degradation occurs in prion disease (Guo et al., 2012). In contrast, in Huntington's Disease, MAP2 splicing is altered, leading to an imbalance between high and low molecular weight MAP2 forms that is thought to contribute to the dendritic atrophy which characterizes the disorder (Cabrera and Lucas, 2017). Alternatively, our recent work in primary auditory cortex indicates that in schizophrenia, MAP2 is hyperphosphorylated, leading to changes in dendritic architecture (Grubisha et al., 2021).

The goal of this review is to summarize the current understanding of MAP2 function and regulation and review the existing evidence for MAP2 dysregulation in disorder, discussing potential forms and consequences of MAP2 pathology. From this, we contemplate a new conceptual framework for schizophrenia and other disorders as "MAP2opathies" in parallel to the tauopathies, bearing implications for their study and treatment.

MAP2 structure and function

Domains and isoforms of MAP2

MAP2 is comprised of five functionally distinct domains: the N-terminus, a projection domain, a proline-rich domain, the MT-binding domain, and the C-terminus (**Figure 1A**). The MT-binding domain in turn contains 3–4 MT binding imperfect repeats, though only the last of these seems to be necessary for the MT bundling activity of the protein (Ludin et al., 1996). Though this domain was originally identified as the critical domain for MT-binding functionality based on its affinity for bovine MTs (Lewis et al., 1988), subsequent data has suggested that it alone is not sufficient for full MT-binding of MAP2. Indeed, addition of flanking sequences from both the proline-rich and C-terminal domains is necessary to match full-length MT-binding activity in transfected HeLa cells (Ferralli et al., 1994). Though the

BOX 1 | Features of intrinsically disordered proteins and their pathology.

IDPs are proteins which lack a stable tertiary structure. They are present in all organisms, being particularly abundant in eukaryotes, where over 30% of all proteins are estimated to have disordered regions (Ward et al., 2004). Their ability to adopt a variety of transient conformations tailored to different interacting partners enables their engagement in both "one-to-many" and "many-to-one" signaling, as well as their ability to scaffold together proteins, e.g., components of a particular signaling pathway. IDPs are heavily modified by post-translational modification (Pejaver et al., 2014) and alternative splicing (Romero et al., 2006), and tend to have relatively low rates of synthesis and short half-lives (Gsponer et al., 2008), ensuring tight regulation of their expression and activity.

These features make IDPs efficient master regulators of diverse signaling pathways, but also leave them more prone to potential dysregulations which can give rise to disease. Genetic mutations or changes in expression, splicing, modifications, trafficking and/or degradation all can lead to aberrant complex formation, signaling activity, and/or folding. The "IDPopathies" encompass a large group of human disorders which include various cancers, neurodegenerative diseases, diabetes, and cardiovascular disease (Uversky, 2014). Frequently the misfolding of proteins including IDPs also leads to their aggregation, giving rise to the amyloidoses, in which more than 37 distinct proteins have been implicated (Chiti and Dobson, 2017).

precise mechanism of MAP2/MT interaction remains unknown, the "jaws" model proposed for MT binding by Tau (Gustke et al., 1994)—with which MAP2 shares 90% sequence homology (**Figure 1B**) —may provide a framework to visualize this interaction, wherein flanking domains are responsible for positioning MAP2/Tau on the MT while the MT-binding domain mediates tubulin polymerization.

In addition to facilitating MT binding, these flanking domains are likely to serve roles in mediating interactions with key binding partners. The closely homologous proline-rich domain of Tau, for instance, mediates interaction with SH3 domain-containing proteins, and MAP2 is known to interact with several such proteins such as the +TIP protein EB3 (Kapitein et al., 2011), Src and Grb2 (Lim and Halpain, 2000). The N-terminus of MAP2 also notably contains a binding site for the PKA regulatory subunit subtype II. As such, MAP2 is the primary dendritic A-kinase anchoring protein (AKAP; Zhong et al., 2009). In contrast, the projection domain appears to regulate MT spacing (Chen et al., 1992).

MAP2 has four major isoforms *in vivo* derived from alternative splicing: high molecular weight (HMW) MAP2A

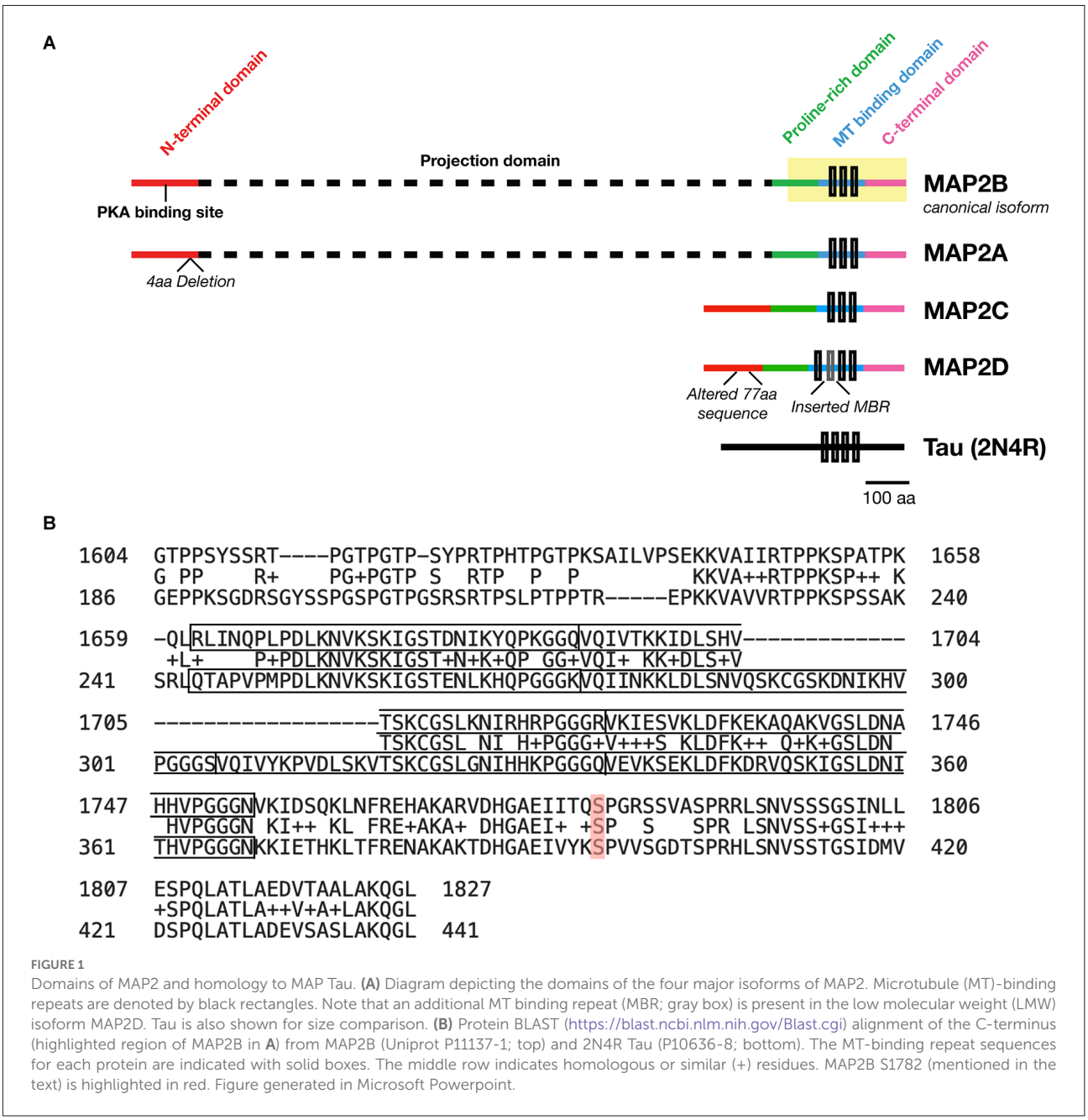

FIGURE 1
Domains of MAP2 and homology to MAP Tau. **(A)** Diagram depicting the domains of the four major isoforms of MAP2. Microtubule (MT)-binding repeats are denoted by black rectangles. Note that an additional MT binding repeat (MBR; gray box) is present in the low molecular weight (LMW) isoform MAP2D. Tau is also shown for size comparison. **(B)** Protein BLAST (https://blast.ncbi.nlm.nih.gov/Blast.cgi) alignment of the C-terminus (highlighted region of MAP2B in **A**) from MAP2B (Uniprot P11137-1; top) and 2N4R Tau (P10636-8; bottom). The MT-binding repeat sequences for each protein are indicated with solid boxes. The middle row indicates homologous or similar (+) residues. MAP2B S1782 (mentioned in the text) is highlighted in red. Figure generated in Microsoft Powerpoint.

and MAP2B (the canonical isoform), and low molecular weight (LMW) MAP2C and MAP2D. These four MAP2 isoforms share four of the five functional domains, with the projection domain being selective to the HMW forms. In human, MAP2A possesses a 4-residue deletion relative to MAP2B, and MAP2D contains an additional MT-binding repeat and a modified 77-residue segment in the N-terminal domain relative to the other three isoforms (see **Figure 1A**). Whereas the subcellular localization of Tau is predominantly axonal (although some Tau has been observed in dendrites and dendritic spines), MAP2 are predominantly somatodendritic (Caceres et al., 1984), although MAP2C can be detected in axons (Meichsner et al., 1993), and MAP2D may be expressed in some glia (Doll et al., 1993). Additional splice variants—including protein coding transcripts—of MAP2 may also exist but remain uncharacterized (Howe et al., 2021).

Following transcription, *MAP2* mRNA localizes to neuronal dendrites for local translation (Garner et al., 1988). In rat neurons, translocation of this mRNA is dependent upon the *trans*-acting protein MARTA2—which has high affinity for a *cis*-acting 3' UTR dendritic targeting element (Blichenberg et al., 1999)—as well as the kinesin KIF5 (Rehbein et al., 2000; Zivraj et al., 2013). Evidence suggests that local MAP2 protein translation in dendrites can be activity-dependent; prolonged high-frequency stimulation of the middle molecular layer of rat dentate gyrus causes an increase in MAP2 immunoreactivity in surrounding lamina, which is diminished by inhibition of protein synthesis (Steward and Halpain, 1999). This may be mediated by mTOR signaling, as rapamycin blocks tetanus-induced dendritic synthesis of MAP2 protein in hippocampal slice (Gong et al., 2006).

An enhanced selectivity of the HMW forms for the dendritic compartment may be due to presence of the projection domain, which inhibits MAP2A/B access to axons (Kanai and Hirokawa, 1995), perhaps *via* interactions with axonal initial segment proteins such as AnkyrinG (Hedstrom et al., 2008). Differential MT organization in dendrites and axons is subsequently thought to result from MAP2 vs. Tau binding (Chen et al., 1992). In addition to the dendritic shaft, MAP2 has also been observed in dendritic spines as early as 1989 by immunogold electron microscopy (Morales and Fifkova, 1989), though it is found less abundantly in spines in the absence of synaptic stimulus (see Section "Synaptic plasticity").

MAP2 is expressed shortly after the switch from neuronal precursor to neuron, and its isoforms are differentially expressed across neurodevelopment. MAP2B is expressed throughout development; MAP2A levels increase during development; MAP2C levels decrease during development, although it remains present in adulthood (Jalava et al., 2007). As a result, HMW MAP2 forms the vast majority of MAP2 in adulthood. In addition, MAP2C is expressed in the mature testis where it is involved in spermatogenesis (Sun and Handel, 2011).

Functions of MAP2

Interactions with cytoskeletal filaments

It has been long accepted that the primary function of MAP2, like Tau, is to bind MTs to increase their polymerization and bundling (Herzog and Weber, 1978; Stearns and Brown, 1979; Lewis et al., 1989). MAP2 is also commonly called an MT stabilizer, though importantly it does not suppress MT dynamics; rather, it reduces the frequency of depolymerizing "catastrophe" events in assembling MTs to enable their growth (Itoh and Hotani, 1994). This mechanism of MAP2 (and Tau; Baas and Qiang, 2019) can be thought of as a "dynamics-preserving" stabilization, as opposed to that of the "genuine" stabilizer MAP6, knockdown of which increases MT dynamics in the axonal compartment (Tortosa et al., 2017).

In addition to MTs, MAP2 can also bind and bundle actin, like Tau (Correas et al., 1990; Moraga et al., 1993; Roger et al., 2004). Thus, both proteins act as cross-linkers between the MT and actin networks (Mohan and John, 2015). Such crosstalk is important for various aspects of fundamental cellular functions such as cell motility and division. However, both proteins may affect actin filaments differently; for instance, phosphatidylinositol disrupts MAP2C- but not Tau-induced actin bundles (Yamauchi and Purich, 1993).

Process formation

The MT polymerizing and bundling effects of MAP2 facilitate process formation and maintain mature dendritic structure. Indeed, expression of MAP2 has repeatedly been shown to induce process formation in multiple heterologous cell lines (Edson et al., 1993; Leclerc et al., 1996). In neurons, MAP2 may act as the primary target of a number of endogenous agents which affect neurite structure *via* MT dynamics. For instance, pregnenolone—a neurosteroid with potential antidepressant and neuroprotective properties (Osuji et al., 2010; Marx et al., 2011, 2014)—enhances neurite growth by binding directly to MAP2 to simulate tubulin polymerization (Murakami et al., 2000; Fontaine-Lenoir et al., 2006). Melatonin increases neurite length, cellular MT content and MAP2 expression in a variety of contexts (Meléndez et al., 1996; Prieto-Gómez et al., 2008; Shu et al., 2016).

The neurite-forming and elongating effects of MAP2 can be disrupted by multiple interventions. The process appears to be negatively regulated by the projection domain, as MAP2B has a lower capacity for process formation than MAP2C in Sf9 cells (Bélanger et al., 2002). Expression of antisense oligonucleotides against MAP2 reduces the number of neurites and MTs within neurites in primary cortical cultures (Sharma et al., 1994). Similarly, *in vivo* knockout of MAP2 decreases dendritic length and MT density in hippocampal neurons

(Harada et al., 2002). Expression of mutant MAP2 constructs can also be used to disrupt dendritic morphogenesis; overexpression of a phosphomimetic MAP2C construct which cannot bind to MTs (S319E/S350E/S382E; Ozer and Halpain, 2000) yields shortened neurites both in dissociated neuronal culture (Huang et al., 2013) and in Neuro-2a cells (Dehmelt et al., 2003) relative to wild-type MAP2C expression. Therefore, changes in MAP2 expression, splicing, or phosphorylation could drive pathological changes in dendritic morphology, namely in reduced dendritic outgrowth.

Synaptic plasticity

MAP2 disruption can also affect structural and functional plasticity of synapses. As shown in the work of Kim et al. (2020), HMW MAP2 is recruited to spines following chemical long-term potentiation (LTP) induction, whereas knockdown of HMW MAP2 impairs LTP induction, LTP-induced growth of dendritic spines, and AMPAR recruitment to spines. This function appears to be selective to the HMW forms of MAP2, as MAP2C-GFP fails to translocate into spines in an activity-dependent manner. Notably, knockdown of HMW MAP2 did not alter spine density in this study; however, we have recently established that at least one MAP2 phosphomimetic mutant (S1782E) is associated with a reduction in spine density in cortical pyramidal neurons of CRISPR knock-in mice (Grubisha et al., 2021). Thus, MAP2 can also contribute to spine formation and/or maintenance, however these functions may be compensated for by related cytoskeletal proteins (such as MAP1B; Teng et al., 2001) in the case of knockdown/knockout.

The role of MT dynamics in mediating the structural and functional plasticity of dendritic spines has become well-appreciated following the discovery that MTs transiently invade spines in an activity-dependent manner (Gu et al., 2008; Hu et al., 2008; Mitsuyama et al., 2008; Jaworski et al., 2009). Such invasions facilitate NMDAR-dependent spine head growth (Merriam et al., 2011), delivering cargo to the spine head in response to synaptic activity (McVicker et al., 2016). The link between regulation of MT dynamics and spine structure is further supported by findings that inhibition of MT polymerization leads to impaired LTP, regression of mature-appearing spines to immature spine shapes, and loss of spines (Jaworski et al., 2009). Thus, it is plausible that MAP2 mediates its effects on synaptic plasticity *via* MT dynamics. Indeed, the binding of MAP2 to MTs is itself an activity-dependent process (Vaillant et al., 2002), likely guided *via* phosphorylation (see below). Recent studies have also illuminated the importance of MT-actin crosstalk to spine morphogenesis, with actin remodeling at activated spines promoting MT entry (Merriam et al., 2013; Schätzle et al., 2018), although to date it is unknown if the MT-actin crosslinking function of MAP2 plays a role in this process.

In addition to its direct interaction with cytoskeletal networks, MAP2 also may mediate its effects on plasticity *via* its interactome. MAP2 creates local dendritic reservoirs of proteins critical to LTP/LTD, including PKA, EB3, RNA particles and polyribosomes (Lim and Halpain, 2000; Nielsen et al., 2002; Ostroff et al., 2002; Angenstein et al., 2005; Farah et al., 2005; Zhong et al., 2009; Kapitein et al., 2011; Sontag et al., 2012; Chirillo et al., 2019; Kim et al., 2020). MAP2 is known to mediate the relocalization of EB3 to the dendritic shaft following chemical long-term depression (cLTD) stimulus, concurrent with a reduction in MT invasion events (Kapitein et al., 2011). Conversely, translocation of HMW MAP2 to spine heads following chemical LTP (Kim et al., 2020) raises the possibility that MAP2 may contribute to activity-dependent protein trafficking into spines. Additionally, as an AKAP, MAP2 is thought to contribute to a spatial gradient of type II PKA formed between the dendritic shaft and spines following cAMP elevation, which in turn impacts synaptic strength and LTP induction (Zhong et al., 2009). Moreover, our own proteomic screen of the MAP2 interactome identified MAP2 interactions with RNA binding proteins regulating translation which served to inhibit protein synthesis (Grubisha et al., 2021), potentially impacting dendritic spine plasticity. Such proteins included FMR1, PCBP1–3, and hnRNPK, which has been previously shown to regulate spine density and LTP as well as mediate the effects of BDNF on dendritic mRNA metabolism and NMDAR function (Folci et al., 2014; Leal et al., 2017). MAP2 protein has previously been shown to interact directly with IMP1 *via* its KH domains, which facilitate nucleic acid binding in a number of RNA-binding proteins (Nielsen et al., 2002). Thus, at least some of the observed interactions with RNA-binding proteins may be direct as opposed to indirect associations *via* tubulin or associated motor proteins. However, these interactions remain to be verified.

Regulation of protein folding and transport

The association of MAP2 with ribosomal proteins is not a novel discovery (Farah et al., 2005) but has remained a relatively underappreciated aspect of the protein. We have found that this association has functional consequence, as overexpressed MAP2C inhibits protein synthesis in HEK cells (Grubisha et al., 2021). The mechanism of such regulation is unknown, but may depend on its association with RNA-binding proteins (see above). Overexpression of MAP2 may ultimately sequester such proteins to disrupt typical RNA trafficking and subsequently, protein synthesis. In addition to regulating protein synthesis, MAP2 has also been shown to exhibit chaperone-like qualities, preventing protein aggregation and facilitating enzyme refolding

(Sarkar et al., 2004; Mitra et al., 2015). Of particular interest is the association MAP2 shares with Tau; MAP2 prevents the arachidonic acid-induced aggregation of Tau protein (Mitra et al., 2015), although the mechanism thereof is still unclear. MAP2 also regulates protein transport, predominantly by steric inhibition of the MT motors kinesin and dynein (Lopez and Sheetz, 1993; Hagiwara et al., 1994; Seitz et al., 2002). This can also contribute to selective axonal transport; using a sensory neuron model, Gumy et al. (2017) demonstrated that MAP2B generates a pre-axonal filtering zone controlling the activity of kinesin-1 and -5. Thus, MAP2 can shape the expression, conformation and transport of other proteins. However, these capacities remain understudied, particularly in the context of synaptic plasticity, where it may facilitate protein translocation into spines (Kim et al., 2020).

Neuronal death—marker or effector?

Neuron loss, regardless of cause, will be accompanied by corresponding loss of MAP2. However, in the context of induced brain injury, loss of MAP2 has been observed at early time points which precede neuronal death (Deshpande et al., 1992), raising the question of whether MAP2 loss may be involved casually in such death, presumably *via* disruption of the cytoskeletal network. MAP2 expression is significantly and consistently reduced early after induction of ischemia in both rodents (Dawson and Hallenbeck, 1996; Mages et al., 2021) and humans (Kühn et al., 2005), a loss which is thought to occur through calpain-mediated proteolysis (Pettigrew et al., 1996). However, the loss is also transient (Huh et al., 2003), suggesting that it does not correspond strictly to neuronal death. Moreover, MAP2 loss can be observed in regions of minimal cell death in mild traumatic brain injury models (Folkerts et al., 1998). Thus, whether MAP2 loss can precipitate or exacerbate neuronal death remains an open question which warrants further investigation, e.g., through characterization of neuronal survival following MAP2 knockout/knockdown, and/or rescue experiments exogenously expressing MAP2 during or post-injury. Such studies can illuminate whether MAP2 itself may represent a viable target for novel neuroprotective agents and strategies.

Regulation of MAP2 functions

Significantly, many MAP2 functions—such as its interactions with MTs and actin, as well as its chaperone-like properties—are regulated by phosphorylation. Phosphosites span the entirety of MAP2; however, phosphosites in the proline-rich, MT-binding and C-terminal domains share a higher degree of conservation across species and with Tau (Sánchez et al., 2000). Generally, phosphorylation tends to reduce the MT-binding affinity of MAP2 and therefore inhibit its MT bundling and polymerization-promoting functions, though the exact effects are site-specific. MAP2 phosphorylation is developmentally regulated (Riederer et al., 1995; Quinlan and Halpain, 1996; Sánchez et al., 2000), presumably mediating different phases of MT growth state and organization as neurons mature. Moreover, long-standing findings have established that MAP2 is also phosphorylated in response to synaptic activity that induces plasticity (Quinlan and Halpain, 1996; Li et al., 2016). This activity-dependent phosphorylation appears to be mediated at least in part by the Ras-MAPK pathway (Llansola et al., 2001; Kim et al., 2020), though to our knowledge, activity-dependent phosphosites of MAP2 have not yet been confirmed. Conversely, sensory deprivation appears to affect MAP2 phosphorylation as well; for instance, olfactory restriction sharply reduces immunoreactivity of AP18, a MAP2 antibody which recognizes pS136 (Philpot et al., 1997).

Other kinases known to phosphorylate MAP2 include PKA, CaMKII, PKC, GSK-3β, CDKs, and MARKs (Sánchez et al., 2000) as well as JNK1. JNK1 represents a notable exception to the general principle of MAP2 phosphorylation in that its phosphorylation of several proline-rich domain residues (T1619, T1622, and T1625) increases—rather than decreases—the protein's binding to MTs, as well as enhances dendritic arborization (Komulainen et al., 2014). This diversity of upstream regulators allows highly precise regulation of MAP2 function under a variety of cellular conditions. Notably, while phosphosites in MAP2 are frequently conserved in Tau, the position of sites phosphorylated in each MAP by a single kinase can differ, even in regions of high homology. This is the case for PKA, which mainly phosphorylates MAP2C at S435, whereas its major phosphosite in Tau is S214 (Jansen et al., 2017). Thus, the two can be differentially regulated by shared upstream kinases.

Interestingly, upstream kinases of MAP2 overlap substantially with those implicated in neuropsychiatric and neurodegenerative disorders. For instance, MAPK3 (ERK1), a component of the Ras-MAPK pathway, has been identified as the probable causal gene underlying the association signal at its locus in the largest schizophrenia genome-wide association study conducted to date (Schizophrenia Working Group of the Psychiatric Genomics Consortium et al., 2020). MAPK3 is also present at the 16p.11.2 locus, deletion of which is associated with autism (Pucilowska et al., 2015). GSK-3β, another kinase of MAP2, is a major regulator of neuronal development and has been strongly implicated in Alzheimer's disease (Maqbool et al., 2016). It is also thought to be a major effective target of various antipsychotics, antidepressants and mood stabilizers such as lithium (Beaulieu et al., 2009). PKA, a binding partner and kinase of MAP2, acts downstream of voltage-gated calcium channels (Davare et al., 1999), which are now clearly identified by unbiased genomic studies as contributing to risk in schizophrenia, bipolar disorder, depression, and autism

spectrum disorders (Psychiatric GWAS Consortium Bipolar Disorder Working Group, 2011; Lu et al., 2012; Schizophrenia Working Group of the Psychiatric Genomics Consortium, 2014; Rao et al., 2016).

In addition to phosphorylation, MAP2 is likely regulated through other PTMs. Glycosylation (Ding and Vandré, 1996), ADP-ribosylation (Scaife et al., 1992), and lysine acetylation (Hwang et al., 2016) of MAP2 have all been described, though their functions are unclear. One study found that phosphorylation of MAP2 by GSK3β and/or PKA inhibited its O-glycosylation by 50%-90% (Khatra et al., 2013), suggesting that these regulatory mechanisms share an inverse relationship. Similarly, Tau is significantly less O-GlcNAc glycosylated when hyperphosphorylated (Lefebvre et al., 2003; Robertson et al., 2004). Beyond PTMs, functions of MAP2 are also regulated by alterative splicing. Besides the differences between HMW and LMW MAP2 described here (see Section "Domains and isoforms of MAP2"), alternative splice variants (Howe et al., 2021) have yet to be confirmed and/or characterized, but could also have distinct functions. Finally, interacting partners, including proteins and other biomolecules, can affect the actions of MAP2. For instance, as previously mentioned, Tau and phosphatidylinositol influence the MT-binding and actin-bundling properties of MAP2, respectively. Phosphatidylinositol additionally inhibits its MT assembling ability (Yamauchi and Purich, 1987).

MAP2 in disorder

The first half of this review has highlighted the diverse roles MAP2 plays in the development and maintenance of neuronal function, including in neurite extension/outgrowth, synaptic plasticity, and protein folding/transport. We have also described how these functions can be modified by a series of mechanisms, including downregulation/knockdown, splicing variants, and PTMs. Below we review the evidence of dysregulated MAP2 present in neuropsychiatric and neurodegenerative disorders (summarized in **Table 1**), and further discuss how

TABLE 1 Evidence of MAP2 dysfunction in neuropsychiatric and neurodegenerative disorder.

Disorder	Region	Finding	References
Schizophrenia	DLPFC	Reduced MAP2-IR intensity	DeGiosio et al. (2019)
	Lateral intraparietal cortex	Reduced MAP2-IR intensity	DeGiosio et al. (2019)
	Primary visual cortex	Reduced MAP2-IR intensity	DeGiosio et al. (2019)
	Hippocampus	Qualitative absence of MAP2-IR in subset of subjects	Arnold et al. (1991) and Rosoklija et al. (2005)
	Olfactory bulb	Reduced MAP2-IR intensity	Rioux et al. (2004)
	DLPFC	Reduced MAP2-IR+ area fraction	Somenarain and Jones (2010)
	Anterior cingulate cortex (BA32)	Reduced MAP2-IR+ area fraction	Jones et al. (2002)
	Primary auditory cortex	Reduced MAP2-IR intensity	Shelton et al. (2015) and McKinney et al. (2019)
	Primary auditory cortex	Increased MAP2 phosphorylation	Grubisha et al. (2021)
	Hippocampus	Reduced MAP2-IR by phospho-specific antibody	Cotter et al. (1997)
	Corpus callosum	Increased MAP2 phosphorylation	Saia-Cereda et al. (2016)
Autism spectrum disorders	DLPFC	Reduced MAP2-IR+ neurons/dendrites	Mukaetova-Ladinska et al. (2004)
	Neocortex	Qualitative reduction of MAP2-IR	Kaufmann et al. (1995)
	n/a	2q34 deletion encompasses *MAP2* gene and causes Rett-like features	Pescucci et al. (2003) and Westphal et al. (2018)
Mood disorders major depressive/bipolar disorders	Subiculum	Qualitative absence of MAP2-IR in subset of subjects	Rosoklija et al. (2005)
	DLPFC	Qualitative reduction of MAP2-IR	Kang et al. (2012)
	DLPFC	Reduced MAP2 protein	Kang et al. (2012)
	DLPFC	Decreased MAP2 phosphorylation at S233, S1031	Martins-de-Souza et al. (2012)
	Various regions	Reduced MAP2 mRNA in males with major depressive disorder	Labonté et al. (2017)
	Anterior cingulate cortex	Reduced MAP2 protein	Föcking et al. (2016)
Huntington's Disease	Striatum	Altered MAP2 splicing	Cabrera and Lucas (2017)
	Striatum	Qualitative loss of dendritic MAP2-IR	Cabrera and Lucas (2017)
	DLPFC	Reduced MAP2-IR+ area fraction	Somenarain and Jones (2010)
Prion Disease	n/a brain homogenate	Reduced MAP2 protein (coincident with increase in calpain)	Guo et al. (2012)
Tauopathy	n/a	MAP2 phosphopeptides (T350, S1702, S1706) identified in purified NFTs	Rudrabhatla et al. (2011)

Evidence of MAP2 dysfunction in these disorders includes various irregularities in MAP2 immunoreactivity, expression level, and/or modification.

MAP2 may contribute to their characteristic endophenotypes based on the known functions of the protein.

MAP2 in neuropsychiatric disorder

Schizophrenia

Schizophrenia is a psychiatric disorder characterized by psychotic symptoms as well as a variety of cognitive dysfunctions. Reduced MAP2 immunoreactivity (MAP2-IR) has been reported in diverse brain regions in schizophrenia and has been described as a "molecular hallmark" of the disorder (Marchisella et al., 2016). This observation has been made in the subiculum, the olfactory bulbs, entorhinal cortex, BA9, BA32 and, in our studies, dorsolateral prefrontal cortex (DLPFC), lateral intraparietal cortex, primary visual cortex, and primary auditory cortex (BA41; Arnold et al., 1991; Jones et al., 2002; Rioux et al., 2004; Rosoklija et al., 2005; Somenarain and Jones, 2010; Shelton et al., 2015; DeGiosio et al., 2019; McKinney et al., 2019). The reduced MAP2-IR does not appear to result from reductions in neuron number/density, as this remains unchanged in areas where MAP2-IR loss is profound (Jones et al., 2002; Dorph-Petersen et al., 2009; Somenarain and Jones, 2010). In our own studies we have also excluded potential effects of several clinical and technical confounds such as postmortem interval (the time from death until tissue fixation), duration of tissue freezer storage, use of psychotropic medications, or substance use status at time of death (Shelton et al., 2015; DeGiosio et al., 2019; McKinney et al., 2019). While lower tissue pH (a possible indicator of brain health prior to death) was correlated with lower MAP2-IR in one study, this effect did not account for reductions present across the cortex in schizophrenia (DeGiosio et al., 2019). As previously alluded to (see Section "Neuronal death—marker or effector?"), cerebral ischemia/hypoxia have previously been shown to reduce numbers of MAP2-IR-positive neurons in human neocortex and hippocampus; however, although causes of death associated with cerebral hypoxia or ischemia were more common in our schizophrenia subjects, they also did not explain the differences in MAP2-IR (DeGiosio et al., 2019). These analyses indicate that MAP2-IR deficit can represent a selective impairment in MAP2 that is not simply consequential to common factors affecting neuronal health.

With the additional power available from a combined cohort of 45 schizophrenia subjects paired with non-psychiatric comparison subjects, we were able to conduct formal mediation tests demonstrating that lower MAP2-IR mediated reductions in the density of dendritic spines in primary auditory cortex, suggesting that pathology of MAP2 is related, potentially in a causal manner, to pathogenic processes. Interestingly, in this study we determined that MAP2 protein levels were not reduced (McKinney et al., 2019). Moreover, MAP2 mRNA levels are unchanged in the hippocampal formation in schizophrenia subjects (Law et al., 2004). Therefore, MAP2-IR loss in schizophrenia does not appear to reflect reductions in mRNA/protein levels. Instead, MAP2 may undergo aberrant PTM to change its function. This could also preclude homeostatic compensation by other MAPs, previously proposed to occur in MAP2 knockout mice, which have shown that MAP2 expression is dispensable to mouse survival (Teng et al., 2001; Harada et al., 2002).

In support of this idea, several studies have suggested that the phosphorylation state of MAP2 is altered in schizophrenia. The immunohistochemical studies of Cotter et al. (1997) showed a trend toward decreased immunoreactivity by Ab305—a MAP2 antibody which recognizes pT1616/pT1619 in the proline-rich domain—in hippocampus of individuals with schizophrenia. The findings of Saia-Cereda et al. (2016) indicate that MAP2 phosphorylation is globally altered in the corpus callosum of schizophrenia subjects. In addition, using phosphoproteomics methods we have recently shown that MAP2 is differentially phosphorylated in primary auditory cortex, with phosphorylation events tending to be upregulated in disorder. Moreover, in this study we demonstrated that a subset of identified MAP2 phosphopeptides were significantly correlated with dendritic spine density and synaptic protein levels in BA41 (Grubisha et al., 2021).

This provided the first evidence indicating a potential pathogenic role for MAP2 phosphorylation in schizophrenia. As a proof of concept, we showed that a MAP2 mutant mimicking the most highly upregulated phosphorylation event identified, pS1782 (pS426 in MAP2C; **Figure 1B**), reduced the MT binding affinity of the protein, and that CRISPR mice harboring this mutation displayed reduced spine density and dendritic complexity in auditory cortex (Grubisha et al., 2021), paralleling findings from postmortem tissue (reviewed in Glausier and Lewis, 2013). This indicates that at least one schizophrenia-associated MAP2 phosphorylation event may be capable of causing dendritic pathology *in vivo*. Interestingly, this residue is homologous to S396 in Tau-a residue which is associated with AD and regulates Tau localization as well as LTD (Bramblett et al., 1993; Mondragón-Rodríguez et al., 2014; Regan et al., 2015; Xia et al., 2015; Wesseling et al., 2020). We further found that levels of the pS1782-bearing phosphopeptide were significantly lower in schizophrenia subjects on antipsychotic medication at time of death, suggesting that this phosphorylation event may represent a target of antipsychotic treatment, although the effect was not recapitulated in a monkey model of long-term antipsychotic exposure (Grubisha et al., 2021). In summary, aberrant MAP2 phosphorylation in schizophrenia may both underlie the profound reductions in MAP2-IR observed

postmortem and have direct consequences for neuronal structure and function.

Autism

Autism spectrum disorders are neurodevelopmental disorders characterized by alterations in social communication and repetitive behaviors, as well as varying levels of intellectual disability. In several case reports of intellectual disability and autism, reduced numbers of MAP2-IR+ neurons and dendrites has been noted, without a change in total neuron number (Kaufmann et al., 1995; Mukaetova-Ladinska et al., 2004). Interestingly, a significant change in MAP2 expression was noted in a recent proteomic analysis of autism (though this did not survive correction for false discovery rate; Abraham et al., 2019). Moreover, case study reports of rare 2q34 deletions—which encompass the *MAP2* gene—have described autism-like outcomes (Pescucci et al., 2003; Westphal et al., 2018). Though inconclusive, these data raise the possibility that MAP2 levels are reduced in at least some cases of autism. Such change, however, is likely to originate post-transcriptionally, as mRNA levels appear to be unaltered (Gandal et al., 2018).

A depletion of MAP2, even partial, could feasibly contribute to endophenotypes which characterize autism spectrum disorders, particularly with respect to synaptic plasticity. As described earlier, knockdown of MAP2 demonstrably impairs functional and structural plasticity of dendritic spines (Kim et al., 2020), which can be expected to alter learning and memory. Indeed, deficits in verbal learning/memory and working memory are among the most consistently impaired cognitive domains in adults with autism (Velikonja et al., 2019). Additionally, in postmortem brain tissue from individuals with autism, dendritic spine morphology shifts towards more immature phenotypes (Martínez-Cerdeño, 2017), which could result from a lack of MAP2-mediated activity-dependent spine growth. This may warrant further investigation of MAP2 abundance and function in autism.

Mood disorders

MAP2-IR reduction has additionally been reported in the DLPFC of individuals with major depressive disorder (Kang et al., 2012) and in the hippocampus of major depression and bipolar disorder subjects (Rosoklija et al., 2005). The origin of this reduction is unclear. In the work of Kang et al. (2012), reduced DLPFC MAP2 levels were observed by western blot; however, it is unclear from these data if this is solely the result of reduced neuron density, which has also been noted in the region (Rajkowska et al., 1999). In contrast, microarray data indicates no change in MAP2 mRNA expression in depression (Seney et al., 2018). However, a separate study utilizing RNA sequencing to study sex-specific transcriptomic changes in depression identified a male-specific reduction in MAP2 mRNA level in multiple cortical regions (Labonté et al., 2017). Decreased MAP2 was also recently observed in bipolar disorder *via* proteomic analysis of the postsynaptic density (Föcking et al., 2016)—though not, to date, at the whole homogenate level—while it fails to exhibit change at the mRNA level by RNA sequencing (Gandal et al., 2018).

Two MAP2 phosphorylation events in the projection domain (pS233 and pS1031) have been reported to be decreased (case:control ratio = 0.82–0.83) in DLPFC of individuals with major depression, though these changes did not remain significant after controlling for false discovery rate (Martins-de-Souza et al., 2012). Interestingly, however, chronic antidepressant treatment has been observed to affect MAP2 expression and/or phosphorylation and subsequently, tubulin polymerization kinetics. Subchronic treatment of naïve rats with imipramine increases MAP2-IR in hippocampus (Iwata et al., 2006), while treatments with fluvoxamine, desipramine, maprotiline, and citalopram increase MAP2 phosphorylation (as assessed using phosphospecific antibodies or ^{32}P incorporation), in turn suppressing tubulin polymerization (Miyamoto et al., 1995, 1997; Perez et al., 1995). It is unknown if and how such modification of MAP2 might contribute to antidepressant effects; however, previous data indicates that transient phosphorylation of MAP2 could support the dendritic outgrowth observed in response to antidepressant treatment (Seo et al., 2014). Indeed, ^{32}P incorporation in MAP2 has previously been shown to correlate with dendritic arborization across time in cultured hippocampal neurons (Díez-Guerra and Avila, 1993). This observation was soon after substantiated by data indicating that treatment with protein kinase inhibitors reduces dendritic branching in these cells, while protein phosphatase inhibitors increase branching (Audesirk et al., 1997). However, our work on MAP2 S1782E—in which pseudo-phosphorylation of MAP2 reduced dendritic length and branching (Grubisha et al., 2021)—suggests that effects of MAP2 phosphorylation on dendritic arborization are complex and could depend on site, brain area and/or duration of signal. These data warrant further investigation of MAP2 phosphorylation state in depression, and of the specific interactions between MAP2 and antidepressants to better understand their mechanism of action.

MAP2 in neurodegenerative disorder

Huntington's disease

Huntington's disease is a heritable neurodegenerative disorder caused by mutation in huntingtin, a microtubule-associated protein involved in axonal transport. The work of

Cabrera and Lucas (2017) established that MAP2 splicing is altered in striatum of Huntington's subjects, favoring the LMW forms and reducing overall MAP2 levels. The authors proposed that this aberrant splicing of MAP2 results from altered activity of splicing factor SRSF6, previously implicated in the disease. The loss of MAP2 protein was accompanied by a substantial loss of MAP2-IR in the region, complimenting prior work showing reduced MAP2-IR in Brodmann area 9 of Huntington's subjects (Somenarain and Jones, 2010).

As described above (see Section "Domains and isoforms of MAP2"), the HMW and LMW forms of the protein differ by inclusion or exclusion of the projection domain. This yields differential subcellular localization patterns and MT spacing characteristics. Additionally, they appear to differ in their ability to support activity-dependent spine plasticity, with HMW forms selectively translocating into spines following chemical LTP stimulus (Kim et al., 2020). In Huntington's, such MAP2-mediated plasticity may be diminished, with consequences for learning and memory. Additionally, LMW forms appear to have greater affinity for neurite formation than HMW forms (Bélanger et al., 2002). Thus, the shift towards LMW MAP2 could be expected to yield more dendrites, and indeed this has been reported in prefrontal cortex of a small cohort of Huntington's subjects (Sotrel et al., 1993). Therefore, aberrant MAP2 splicing may represent a crucial precipitant to the structural and functional abnormalities seen in neurons affected by Huntington's disease.

Prion disease

Prion diseases are a group of transmissible neurodegenerative diseases caused by prions—misfolded proteins which can transmit their misfolded shape onto normal variants of the same protein, causing aggregation and altered protein function. Work by Guo et al. (2012) described significant reductions of MAP2 protein in scrapies-infected hamsters, attributable to a concomitant increase in the protease calpain. Interestingly, this parallels findings from brain injury models, such as ischemia and traumatic spinal cord injury, which also describe calpain-mediated MAP2 degradation (Pettigrew et al., 1996; Springer et al., 1997). Aβ oligomers can similarly induce such degradation (Fifre et al., 2006). Further, one recent study has demonstrated the downregulation of MAP2 protein in SMN-deficient motor neuron-like cells modeling spinal muscular atrophy, which the authors speculate may also be due to calpain hyperactivity (Özer et al., 2022). Thus, MAP2 appears to be a frequent target of calpain to mediate MT destabilization and potentially cell death under a variety of circumstances. Further study can clarify what therapeutic value MAP2 may have in preventing neuron loss (see Section "Neuronal death—marker or effector?").

Tauopathies

The tauopathies are a group of neurodegenerative disorders characterized by the hyperphosphorylation of MAP Tau and its subsequent assembly into neurofibrillary tangles (NFTs). MAP2 has generally not been considered as a potential pathogenic agent in the tauopathies, as its presence in NFTs has been a subject of some debate (Xie et al., 2014) and it forms no analogous aggregates. However, recent works have called into question whether NFTs themselves drive neuropathology, or if they are by products of pathology which is driven by soluble tau forms (Kopeikina et al., 2012). Indeed, the work of Xie et al. (2014) showed that while MAP2 and Tau have different aggregation properties, pan-neuronal expression of either can elicit severe neurotoxic effects. In this revised framework, interactions between MAP2 and soluble Tau may be important in shaping tauopathy. MAP2 and Tau have been known to cross-regulate each other; for instance, hyperphosphorylated Tau can sequester HMW MAP2 and thereby inhibit MT assembly (Alonso et al., 1997). Conversely, MAP2 prevents the arachidonic acid-induced aggregation of Tau, though MAP2 phosphorylation impairs this chaperoning ability (Mitra et al., 2015). Thus, MAP2 and Tau seem to share a reciprocal relationship whereby dysregulation of one can lead to that of the other. Mass spectrometry methods have revealed the presence of MAP2 phosphopeptides in purified Alzheimer's NFTs (Rudrabhatla et al., 2011), indicating that MAP2 may be hyperphosphorylated in the disorder. Thus, MAP2 remains an active element to consider in the pathogenesis of tauopathies. Better understanding the origin of its aberrant phosphorylation in tauopathies and the nature of its interactions with Tau could lead to new therapeutic targets for the prevention of Tau aggregation.

The "MAP2opathy"—limitations and future directions

MAP2 is often viewed solely as an endpoint marker of neuronal health. However, it is also a critical cytoskeletal regulator, dysfunction of which drastically affects neuronal structure and function. We have here described the known roles of MAP2 in neurite outgrowth, synaptic plasticity and protein folding/transport, as well as mechanisms of its regulation, including most prominently alternative splicing and phosphorylation. As such, MAP2 is poised to become dysregulated in various ways, potentially leading to distinct, pleiotropic effects. We have reviewed the current evidence for alterations in MAP2 function present in various neuropsychiatric and neurodegenerative disorders such as schizophrenia and Huntington's disease. MAP2 pathology appears to originate at different levels

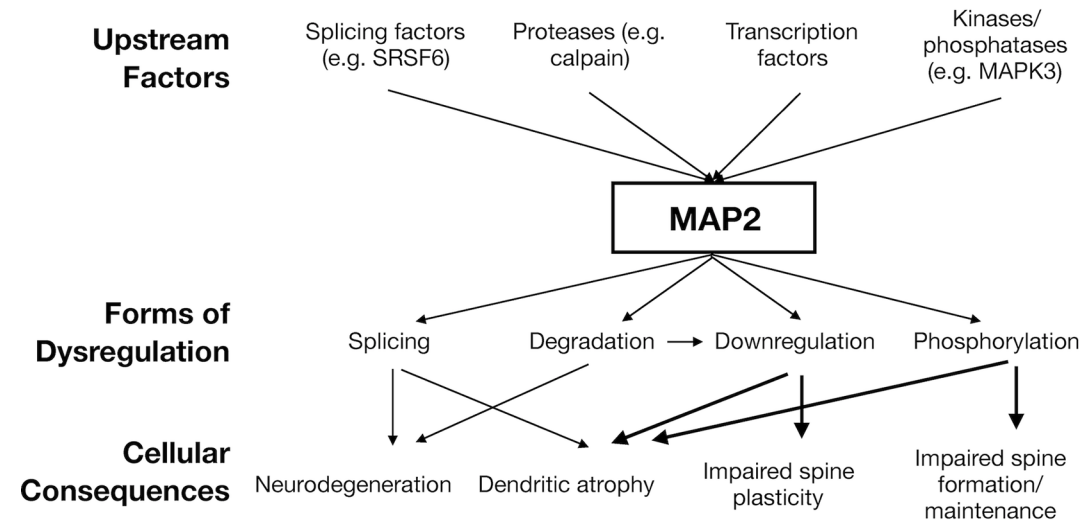

FIGURE 2
Hypothesized model of "MAP2opathy". Genetically- or environmentally-precipitated upstream risk factors are expected to affect MAP2 in a variety of ways, leading to diverse, overlapping cellular consequences. Thick arrows indicate causal relationships established in *in vivo* models (Harada et al., 2002; Kim et al., 2020; Grubisha et al., 2021). Thin arrows indicate noted correlational relationships (Pettigrew et al., 1996; Guo et al., 2012; Cabrera and Lucas, 2017). Figure generated in Microsoft Powerpoint.

across these disorders; for instance, Huntington's is marked by aberrant RNA splicing, autism may be associated with lowered MAP2 protein abundance, while schizophrenia is distinguished by aberrant post-translational modification of MAP2.

This parallels the multiple distinct mechanisms by which tau can become dysregulated in tauopathy, which is not limited to mutations in MAPT genes, but also includes protein modification (particularly phosphorylation), *cis/trans* isomerization, and more. Thus, a "MAP2opathy" may similarly exist, characterizing varied neurodevelopmental and neurodegenerative disorders; akin to Tau, MAP2 could represent a molecular bottleneck situated downstream of genetic and environmental risk factors and upstream of neuronal pathology (**Figure 2**). This would position MAP2 as a flexible therapeutic target, able to ameliorate pathology while remaining effective in a large proportion of affected individuals regardless of their unique set of risk factors. However, classification of MAP2opathy as a genuine proteinopathy is still premature and awaits further research. **Table 2** outlines various forms of evidence in favor of classification of a proteinopathy, comparing the existing evidence in the case of either tau or MAP2. An overall lack of genetic evidence implicating MAP2 mutation in disorder distinguishes it from tau and requires consideration. This could be due to the role of LMW MAP2 in spermatogenesis (Sun and Handel, 2011), which may make the gene mutation-intolerant [loss of function observed/expected upper bound fraction (LOEUF) = 0.1 (Karczewski et al., 2020)] and limit the ability of organisms to transmit MAP2 mutations that could later cause neuropathology. Instead, pathogenic MAP2 is more likely to arise from integrated upstream processes including kinase/phosphatase function, splicing machinery and proteolytic processes, analogous to those at play in tauopathy.

Existing data regarding MAP2 pathology is largely limited to correlational study, leaving open the possibility that changes to MAP2 immunoreactivity, expression or modification do not contribute to pathogenesis, but instead are merely incidental changes incurred by upstream processes. Despite clear evidence that disruptions to MAP2 expression and/or modification can lead to changes in dendritic and synaptic structure and function (Sharma et al., 1994; Ozer and Halpain, 2000; Harada et al., 2002; Akulinin and Dahlstrom, 2003; Dehmelt et al., 2003; Huang et al., 2013; Kim et al., 2020; Grubisha et al., 2021), this largely remains to be demonstrated in disease-relevant contexts. For example, our modeling of a schizophrenia-associated MAP2 phosphorylation event demonstrates a potential causal role of dysregulated MAP2 in the altered dendritic outgrowth which characterizes this disorder (Grubisha et al., 2021). Similarly, the altered splicing of MAP2 observed in Huntington's might be modeled experimentally by manipulation of SRSF6 splicing factor, and rescue experiments can be performed by exogenous expression of HMW MAP2 to observe consequential effects on dendritic growth. Better understanding patterns of calpain-mediated cleavage of MAP2 could enable modeling of its degradation using truncation-inducing mutations or overexpression of truncated MAP2 constructs to explore roles of MAP2 degradation in neuronal atrophy of prion diseases

TABLE 2 Evidences of proteinopathy for tau vs. MAP2.

Evidence of proteinopathy	Tau	MAP2
Mutation of the encoding gene is associated with disease	Mutations in *MAPT* gene lead to FTDP-17 as well as other neurodegenerative disorders similar to Pick's disease, corticobasal degeneration and supranuclear palsy (Strang et al., 2019)	Autism-associated rare 2q34 microdeletions encompass the *MAP2* gene (Pescucci et al., 2003); however, **mutations selective to *MAP2* have not to date been associated with disorder**
Modifications of transcript or protein are associated with disease	Tau protein hyperphosphorylation is a hallmark of tauopathy, contributing to its aggregation/formation of NFTs (Noble et al., 2013). Missplicing of Tau pre-mRNA- in some cases associated with *MAPT* mutation- is also associated with various tauopathies (Park et al., 2016)	Changes in expression, post-translational modification and/or splicing of MAP2 have been described in various disorders (see **Table 1**)
Experimental manipulation of the protein causes disease-associated pathology	Mutant Tau mouse lines such as rTg4150 can replicate key features of tauopathy including neuron loss and memory impairments (Denk and Wade-Martins, 2009). Phosphomimicry of Tau can lead to learning and memory deficits in *Drosophila* and mice (Beharry et al., 2013; Di et al., 2016)	MAP2 knockdown can lead to impairments in LTP and dendritic outgrowth, which are implicated in neurodevelopmental and neurodegenerative disorder (Kim et al., 2020). Mimicry of a schizophrenia-associated MAP2 phosphorylation event leads to reduced dendritic arborization and spine density (Grubisha et al., 2021). **Other disease-relevant modifications of MAP2, such as altered splicing or cleavage, have not been modeled. Behavioral/cognitive outcomes of mutant MAP2 animals have not yet been reported**
Protein dysregulation precedes functional impairments	Tau deposition precedes clinical symptoms of disorder in humans (Jack et al., 2010)	**Time course of MAP2 PTMs, splicing alterations, etc remain unknown**
Degree of protein dysregulation scales with disease pathology	Burden of tau PET binding correlates with cognitive symptoms and severity of regional atrophy (Cho et al., 2016). Higher NFT burden is also associated with faster cognitive decline (Jefferson-George et al., 2017)	MAP2 phosphopeptide levels correlate with dendritic spine density and socioeconomic status in individuals with schizophrenia (Grubisha et al., 2021). Additionally, MAP2-IR loss statistically mediates dendritic spine loss in primary auditory cortex of subjects with schizophrenia (McKinney et al., 2019). **Associations of MAP2 expression/phosphorylation with pathology in other disorders remains uninvestigated**

Bold face text highlights current gaps in knowledge regarding MAP2 pathology.

or brain injury. MAP2 phosphorylation events observed in NFTs also have yet to be modeled, which could be used to illuminate what roles—if any—MAP2 phosphorylation plays in Tau aggregation/pathology.

Additionally, recent works revealing new or understudied functions of MAP2, such as that in LTP induction and AMPAR translocation (Kim et al., 2020), neuronal polarization *via* axonal filtering (Gumy et al., 2017), and our own work on phosphomimetic MAP2 (Grubisha et al., 2021) make clear that there is still much to learn about the basic biology of MAP2 protein. Firstly, thorough characterization of MAP2 PTM state on a residue-specific level in both healthy and diseased contexts will prove informative and can be readily achieved through modern mass spectrometry methods. Roles of such modifications in cytoskeletal filament organization, neurite outgrowth, synaptic plasticity and neuronal viability remain to be examined. Such studies will likely benefit from the extant literature regarding Tau, as these proteins structurally and functionally parallel one another—for example, through conserved phosphosites such as S396Tau/S1782MAP2 (Grubisha et al., 2021). Further, a bias exists in the literature favoring the *in vitro* study of immature MAP2c relative to mature, HMW forms of the protein, likely due to its ease of production and purification. However, these forms have differential structure and functions that remain to be fully understood. Such distinctions will provide insights to the developmental regulation of MAP2 functions. In conclusion, future studies of MAP2 will not only enhance our understanding of basic neurobiology but can also shed light on pathogenesis of a potential therapeutic target in neuropsychiatric and neurodegenerative disorders.

Data availability statement

The original contributions presented in the study are included in the article, further inquiries can be directed to the corresponding author.

Author contributions

RD and RS conceived the idea for this manuscript. RD performed the literature search and drafted the work with assistance from RS. MG, MM, BM, and CC critically revised the work. All authors contributed to the article and approved the submitted version.

Funding

This work was supported by National Institute of Mental Health (grant numbers: MH116046, MH071533, MH118497, and MH125235), National Institute on Aging (grant number: AG027224), and National Institutes of Health (grant number: GM97082).

Conflict of interest

The authors declare that the research was conducted in the absence of any commercial or financial relationships that could be construed as a potential conflict of interest.

Publisher's note

All claims expressed in this article are solely those of the authors and do not necessarily represent those of their affiliated organizations, or those of the publisher, the editors and the reviewers. Any product that may be evaluated in this article, or claim that may be made by its manufacturer, is not guaranteed or endorsed by the publisher.

References

Abraham, J. R., Szoko, N., Barnard, J., Rubin, R. A., Schlatzer, D., Lundberg, K., et al. (2019). Proteomic investigations of autism brain identify known and novel pathogenetic processes. *Sci. Rep.* 9:13118. doi: 10.1038/s41598-019-49533-y

Akulinin, V. A., and Dahlstrom, A. (2003). Quantitative analysis of MAP2 immunoreactivity in human neocortex of three patients surviving after brain ischemia. *Neurochem. Res.* 28, 373–378. doi: 10.1023/a:1022401922669

Alonso, A. D., Grundke-Iqbal, I., Barra, H. S., and Iqbal, K. (1997). Abnormal phosphorylation of tau and the mechanism of Alzheimer neurofibrillary degeneration: sequestration of microtubule-associated proteins 1 and 2 and the disassembly of microtubules by the abnormal tau. *Proc. Natl. Acad. Sci. U S A* 94, 298–303. doi: 10.1073/pnas.94.1.298

Angenstein, F., Evans, A. M., Ling, S.-C., Settlage, R. E., Ficarro, S., Carrero-Martinez, F. A., et al. (2005). Proteomic characterization of messenger ribonucleoprotein complexes bound to nontranslated or translated poly(A) mRNAs in the rat cerebral cortex. *J. Biol. Chem.* 280, 6496–6503. doi: 10.1074/jbc.M412742200

Arnold, S. E., Lee, V. M., Gur, R. E., and Trojanowski, J. Q. (1991). Abnormal expression of two microtubule-associated proteins (MAP2 and MAP5) in specific subfields of the hippocampal formation in schizophrenia. *Proc. Natl. Acad. Sci. U S A* 88, 10850–10854. doi: 10.1073/pnas.88.23.10850

Audesirk, G., Cabell, L., and Kern, M. (1997). Modulation of neurite branching by protein phosphorylation in cultured rat hippocampal neurons. *Brain Res. Dev. Brain Res.* 102, 247–260. doi: 10.1016/s0165-3806(97)00100-4

Baas, P. W., and Qiang, L. (2019). Tau: it's not what you think. *Trends Cell Biol.* 29, 452–461. doi: 10.1016/j.tcb.2019.02.007

Beaulieu, J.-M., Gainetdinov, R. R., and Caron, M. G. (2009). Akt/GSK3 signaling in the action of psychotropic drugs. *Ann. Rev. Pharmacol. Toxicol.* 49, 327–347. doi: 10.1146/annurev.pharmtox.011008.145634

Beharry, C., Alaniz, M. E., and Alonso, A. D. C. (2013). Expression of Alzheimer-like pathological human tau induces a behavioral motor and olfactory learning deficit in *Drosophila melanogaster*. *J. Alzheimers Dis.* 37, 539–550. doi: 10.3233/JAD-130617

Bélanger, D., Farah, C. A., Nguyen, M. D., Lauzon, M., Cornibert, S., and Leclerc, N. (2002). The projection domain of MAP2b regulates microtubule protrusion and process formation in Sf9 cells. *J. Cell Sci.* 115, 1523–1539. doi: 10.1242/jcs.115.7.1523

Blichenberg, A., Schwanke, B., Rehbein, M., Garner, C. C., Richter, D., and Kindler, S. (1999). Identification of a cis-acting dendritic targeting element in MAP2 mRNAs. *J. Neurosci.* 19, 8818–8829. doi: 10.1523/JNEUROSCI.19-20-08818.1999

Bodakuntla, S., Jijumon, A., Villablanca, C., Gonzalez-Billault, C., and Janke, C. (2019). Microtubule-associated proteins: structuring the cytoskeleton. *Trends Cell Biol.* 29, 804–819. doi: 10.1016/j.tcb.2019.07.004

Bramblett, G. T., Goedert, M., Jakes, R., Merrick, S. E., Trojanowski, J. Q., and Lee, V. M. Y. (1993). Abnormal tau phosphorylation at Ser396 in Alzheimer's disease recapitulates development and contributes to reduced microtubule binding. *Neuron* 10, 1089–1099. doi: 10.1016/0896-6273(93)90057-x

Cabrera, J. R., and Lucas, J. J. (2017). MAP2 splicing is altered in Huntington's disease. *Brain Pathol.* 27, 181–189. doi: 10.1111/bpa.12387

Caceres, A., Binder, L., Payne, M., Bender, P., Rebhun, L., and Steward, O. (1984). Differential subcellular localization of tubulin and the microtubule-associated protein MAP2 in brain tissue as revealed by immunocytochemistry with monoclonal hybridoma antibodies. *J. Neurosci.* 4, 394–410. doi: 10.1523/JNEUROSCI.04-02-00394.1984

Chen, J., Kanai, Y., Cowan, N., and Hirokawa, N. (1992). Projection domains of MAP2 and tau determine spacings between microtubules in dendrites and axons. *Nature* 360, 674–677. doi: 10.1038/360674a0

Chirillo, M. A., Waters, M. S., Lindsey, L. F., Bourne, J. N., and Harris, K. M. (2019). Local resources of polyribosomes and SER promote synapse enlargement and spine clustering after long-term potentiation in adult rat hippocampus. *Sci. Rep.* 9:3861. doi: 10.1038/s41598-019-40520-x

Chiti, F., and Dobson, C. M. (2017). Protein misfolding, amyloid formation and human disease: a summary of progress over the last decade. *Annu. Rev. Biochem.* 86, 27–68. doi: 10.1146/annurev-biochem-061516-045115

Cho, H., Choi, J. Y., Hwang, M. S., Lee, J. H., Kim, Y. J., Lee, H. M., et al. (2016). Tau PET in Alzheimer disease and mild cognitive impairment. *Neurology* 87, 375–383. doi: 10.1212/WNL.0000000000002892

Correas, I., Padilla, R., and Avila, J. (1990). The tubulin-binding sequence of brain microtubule-associated proteins, tau and MAP-2, is also involved in actin binding. *Biochem. J.* 269, 61–64. doi: 10.1042/bj2690061

Cotter, D., Kerwin, R., Doshi, B., Martin, C. S., and Everall, I. P. (1997). Alterations in hippocampal non-phosphorylated MAP2 protein expression in schizophrenia. *Brain Res.* 765, 238–246. doi: 10.1016/s0006-8993(97)00575-1

Díez-Guerra, F. J., and Avila, J. (1993). MAP2 phosphorylation parallels dendrite arborization in hippocampal neurones in culture. *Neuroreport* 4, 419–422. doi: 10.1097/00001756-199304000-00020

Davare, M. A., Dong, F., Rubin, C. S., and Hell, J. W. (1999). The A-kinase anchor protein MAP2B and cAMP-dependent protein kinase are associated with class C L-type calcium channels in neurons. *J. Biol. Chem.* 274, 30280–30287. doi: 10.1074/jbc.274.42.30280

Dawson, D. A., and Hallenbeck, J. M. (1996). Acute focal ischemia-induced alterations in MAP2 immunostaining: description of temporal changes and utilization as a marker for volumetric assessment of acute brain injury. *J. Cereb. Blood Flow Metab.* 16, 170–174. doi: 10.1097/00004647-199601000-00020

DeGiosio, R., Kelly, R. M., DeDionisio, A. M., Newman, J. T., Fish, K. N., Sampson, A. R., et al. (2019). MAP2 immunoreactivity deficit is conserved across the cerebral cortex within individuals with schizophrenia. *NPJ Schizophr.* 5:13. doi: 10.1038/s41537-019-0081-0

Dehmelt, L., Smart, F. M., Ozer, R. S., and Halpain, S. (2003). The role of microtubule-associated protein 2c in the reorganization of microtubules and lamellipodia during neurite initiation. *J. Neurosci.* 23, 9479–9490. doi: 10.1523/JNEUROSCI.23-29-09479.2003

Denk, F., and Wade-Martins, R. (2009). Knock-out and transgenic mouse models of tauopathies. *Neurobiol. Aging* 30, 1–13. doi: 10.1016/j.neurobiolaging.2007.05.010

Deshpande, J., Bergstedt, K., Lindén, T., Kalimo, H., and Wieloch, T. (1992). Ultrastructural changes in the hippocampal CA1 region following transient

cerebral ischemia: evidence against programmed cell death. *Exp. Brain Res.* 88, 91–105. doi: 10.1007/BF02259131

Di, J., Cohen, L., Corbo, C., Phillips, G. R., El Idrissi, A., and Alonso, A. D. (2016). Abnormal tau induces cognitive impairment through two different mechanisms: synaptic dysfunction and neuronal loss. *Sci. Rep.* 6:20833. doi: 10.1038/srep20833

Ding, M., and Vandré, D. D. (1996). High molecular weight microtubule-associated proteins contain O-linked-N-acetylglucosamine. *J. Biol. Chem.* 271, 12555–12561. doi: 10.1074/jbc.271.21.12555

Doll, T., Meichsner, M., Riederer, B., Honegger, P., and Matus, A. (1993). An isoform of microtubule-associated protein 2 (MAP2) containing four repeats of the tubulin-binding motif. *J. Cell Sci.* 106, 633–639. doi: 10.1242/jcs.106.2.633

Dorph-Petersen, K.-A., Delevich, K. M., Marcsisin, M. J., Zhang, W., Sampson, A. R., Gundersen, H. J. G., et al. (2009). Pyramidal neuron number in layer 3 of primary auditory cortex of subjects with schizophrenia. *Brain Res.* 1285, 42–57. doi: 10.1016/j.brainres.2009.06.019

Dunker, A. K., Cortese, M. S., Romero, P., Iakoucheva, L. M., and Uversky, V. N. (2005). Flexible nets: the roles of intrinsic disorder in protein interaction networks. *FEBS J.* 272, 5129–5148. doi: 10.1111/j.1742-4658.2005.04948.x

Edson, K., Weisshaar, B., and Matus, A. (1993). Actin depolymerisation induces process formation on MAP2-transfected non-neuronal cells. *Development* 117, 689–700. doi: 10.1242/dev.117.2.689

Farah, C. A., Liazoghli, D., Perreault, S., Desjardins, M., Guimont, A., Anton, A., et al. (2005). Interaction of Microtubule-associated Protein-2 and p63: a new link between microtubules and rough endoplasmic reticulum membranes in neurons. *J. Biol. Chem.* 280, 9439–9449. doi: 10.1074/jbc.M412304200

Ferralli, J., Doll, T., and Matus, A. (1994). Sequence analysis of MAP2 function in living cells. *J. Cell Sci.* 107, 3115–3125. doi: 10.1242/jcs.107.11.3115

Fifre, A., Sponne, I., Koziel, V., Kriem, B., Potin, F. T. Y., Bihain, B. E., et al. (2006). Microtubule-associated protein MAP1A, MAP1B and MAP2 proteolysis during soluble amyloid β-peptide-induced Neuronal apoptosis: synergistic involvement of calpain and caspase-3. *J. Biol. Chem.* 281, 229–240. doi: 10.1074/jbc.M507378200

Föcking, M., Dicker, P., Lopez, L. M., Hryniewiecka, M., Wynne, K., English, J. A., et al. (2016). Proteomic analysis of the postsynaptic density implicates synaptic function and energy pathways in bipolar disorder. *Transl. Psychiatry* 6:e959. doi: 10.1038/tp.2016.224

Folci, A., Mapelli, L., Sassone, J., Prestori, F., D'Angelo, E., Bassani, S., et al. (2014). Loss of hnRNP K impairs synaptic plasticity in hippocampal neurons. *J. Neurosci.* 34, 9088–9095. doi: 10.1523/JNEUROSCI.0303-14.2014

Folkerts, M. M., Berman, R. F., Muizelaar, J. P., and Rafols, J. A. (1998). Disruption of MAP-2 immunostaining in rat hippocampus after traumatic brain injury. *J. Neurotrauma* 15, 349–363. doi: 10.1089/neu.1998.15.349

Fontaine-Lenoir, V., Chambraud, B., Fellous, A., David, S., Duchossoy, Y., Baulieu, E.-E., et al. (2006). Microtubule-associated protein 2 (MAP2) is a neurosteroid receptor. *Proc. Natl. Acad. Sci. U S A* 103, 4711–4716. doi: 10.1073/pnas.0600113103

Gandal, M. J., Zhang, P., Hadjimichael, E., Walker, R. L., Chen, C., Liu, S., et al. (2018). Transcriptome-wide isoform-level dysregulation in ASD, schizophrenia and bipolar disorder. *Science* 362:eaat8127. doi: 10.1126/science.aat8127

Garner, C. C., Tucker, R. P., and Matus, A. (1988). Selective localization of messenger RNA for cytoskeletal protein MAP2 in dendrites. *Nature* 336, 674–677. doi: 10.1038/336674a0

Glausier, J. R., and Lewis, D. A. (2013). Dendritic spine pathology in schizophrenia. *Neuroscience* 251, 90–107. doi: 10.1016/j.neuroscience.2012.04.044

Gong, R., Park, C. S., Abbassi, N. R., and Tang, S.-J. (2006). Roles of glutamate receptors and the mammalian target of rapamycin (mTOR) signaling pathway in activity-dependent dendritic protein synthesis in hippocampal neurons. *J. Biol. Chem.* 281, 18802–18815. doi: 10.1074/jbc.M512524200

Goodson, H. V., and Jonasson, E. M. (2018). Microtubules and microtubule-associated proteins. *Cold Spring Harb. Perspect. Biol.* 10:a022608. doi: 10.1101/cshperspect.a022608

Grubisha, M., Sun, X., MacDonald, M., Garver, M., Sun, Z., Paris, K., et al. (2021). MAP2 is differentially phosphorylated in schizophrenia, altering its function. *Mol. Psychiatry* 26, 5371–5388. doi: 10.1038/s41380-021-01034-z

Gsponer, J., Futschik, M. E., Teichmann, S. A., and Babu, M. M. (2008). Tight regulation of unstructured proteins: from transcript synthesis to protein degradation. *Science* 322, 1365–1368. doi: 10.1126/science.1163581

Gu, J., Firestein, B. L., and Zheng, J. Q. (2008). Microtubules in dendritic spine development. *J. Neurosci.* 28, 12120–12124. doi: 10.1523/JNEUROSCI.2509-08.2008

Gumy, L. F., Katrukha, E. A., Grigoriev, I., Jaarsma, D., Kapitein, L. C., Akhmanova, A., et al. (2017). MAP2 defines a pre-axonal filtering zone to regulate KIF1- versus KIF5-dependent cargo transport in sensory neurons. *Neuron* 94, 347–362.e7. doi: 10.1016/j.neuron.2017.03.046

Guo, Y., Gong, H.-S., Zhang, J., Xie, W.-L., Tian, C., Chen, C., et al. (2012). Remarkable reduction of MAP2 in the brains of scrapie-infected rodents and human prion disease possibly correlated with the increase of calpain. *PLoS One* 7:e30163. doi: 10.1371/journal.pone.0030163

Gustke, N., Trinczek, B., Biernat, J., Mandelkow, E.-M., and Mandelkow, E. (1994). Domains of tau protein and interactions with microtubules. *Biochemistry* 33, 9511–9522. doi: 10.1021/bi00198a017

Hagiwara, H., Yorifuji, H., Sato-Yoshitake, R., and Hirokawa, N. (1994). Competition between motor molecules (kinesin and cytoplasmic dynein) and fibrous microtubule-associated proteins in binding to microtubules. *J. Biol. Chem.* 269, 3581–3589. doi: 10.1016/S0021-9258(17)41903-X

Harada, A., Teng, J., Takei, Y., Oguchi, K., and Hirokawa, N. (2002). MAP2 is required for dendrite elongation, PKA anchoring in dendrites and proper PKA signal transduction. *J. Cell Biol.* 158, 541–549. doi: 10.1083/jcb.200110134

Hedstrom, K. L., Ogawa, Y., and Rasband, M. N. (2008). AnkyrinG is required for maintenance of the axon initial segment and neuronal polarity. *J. Cell. Biol.* 183, 635–640. doi: 10.1083/jcb.200806112

Herzog, W., and Weber, K. (1978). Fractionation of brain microtubule-associated proteins: isolation of two different proteins which stimulate tubulin polymerization *in vitro*. *Eur. J. Biochem.* 92, 1–8. doi: 10.1111/j.1432-1033.1978.tb12716.x

Howe, K. L., Achuthan, P., Allen, J., Allen, J., Alvarez-Jarreta, J., Amode, M. R., et al. (2021). Ensembl 2021. *Nucleic Acids Res.* 49, D884–D891. doi: 10.1093/nar/gkaa942

Hu, X., Viesselmann, C., Nam, S., Merriam, E., and Dent, E. W. (2008). Activity-dependent dynamic microtubule invasion of dendritic spines. *J. Neurosci.* 28, 13094–13105. doi: 10.1523/JNEUROSCI.3074-08.2008

Huang, Y.-A., Kao, J.-W., Tseng, D. T.-H., Chen, W.-S., Chiang, M.-H., and Hwang, E. (2013). Microtubule-associated type II protein kinase A is important for neurite elongation. *PLoS One* 8:e73890. doi: 10.1371/journal.pone.0073890

Huh, J., Raghupathi, R., Laurer, H. L., Helfaer, M. A., and Saatman, K. E. (2003). Transient loss of microtubule-associated protein 2 immunoreactivity after moderate brain injury in mice. *J. Neurotrauma* 20, 975–984. doi: 10.1089/089771503770195821

Hwang, A. W., Trzeciakiewicz, H., Friedmann, D., Yuan, C.-X., Marmorstein, R., Lee, V. M. Y., et al. (2016). Conserved lysine acetylation within the microtubule-binding domain regulates MAP2/tau family members. *PLoS One* 11:e0168913. doi: 10.1371/journal.pone.0168913

Itoh, T. J., and Hotani, H. (1994). Microtubule-stabilizing activity of microtubule-associated proteins (MAPs) is due to increase in frequency of rescue in dynamic instability: shortening length decreases with binding of MAPs onto microtubules. *Cell Struct. Funct.* 19, 279–290. doi: 10.1247/csf.19.279

Iwata, M., Shirayama, Y., Ishida, H., and Kawahara, R. (2006). Hippocampal synapsin I, growth-associated protein-43 and microtubule-associated protein-2 immunoreactivity in learned helplessness rats and antidepressant-treated rats. *Neuroscience* 141, 1301–1313. doi: 10.1016/j.neuroscience.2006.04.060

Jack, C. R., Jr., Knopman, D. S., Jagust, W. J., Shaw, L. M., Aisen, P. S., Weiner, M. W., et al. (2010). Hypothetical model of dynamic biomarkers of the Alzheimer's pathological cascade. *Lancet Neurol.* 9, 119–128. doi: 10.1016/S1474-4422(09)70299-6

Jalava, N. S., Lopez-Picon, F. R., Kukko-Lukjanov, T.-K., and Holopainen, I. E. (2007). Changes in microtubule-associated protein-2 (MAP2) expression during development and after status epilepticus in the immature rat hippocampus. *Int. J. Dev. Neurosci.* 25, 121–131. doi: 10.1016/j.ijdevneu.2006.12.001

Jansen, S., Melková, K., Trošanová, Z., Hanáková, K., Zachrdla, M., Nováček, J., et al. (2017). Quantitative mapping of microtubule-associated protein 2c (MAP2c) phosphorylation and regulatory protein 14-3-3ζ-binding sites reveals key differences between MAP2c and its homolog Tau. *J. Biol. Chem.* 292:10316. doi: 10.1074/jbc.A116.771097

Jaworski, J., Kapitein, L. C., Gouveia, S. M., Dortland, B. R., Wulf, P. S., Grigoriev, I., et al. (2009). Dynamic microtubules regulate dendritic spine morphology and synaptic plasticity. *Neuron* 61, 85–100. doi: 10.1016/j.neuron.2008.11.013

Jefferson-George, K. S., Wolk, D. A., Lee, E. B., and McMillan, C. T. (2017). Cognitive decline associated with pathological burden in primary age-related tauopathy. *Alzheimers Dement.* 13, 1048–1053. doi: 10.1016/j.jalz.2017.01.028

Jones, L. B., Johnson, N., and Byne, W. (2002). Alterations in MAP2 immunocytochemistry in areas 9 and 32 of schizophrenic prefrontal cortex. *Psychiatry Res.* 114, 137–148. doi: 10.1016/s0925-4927(02)00022-7

Kanai, Y., and Hirokawa, N. (1995). Sorting mechanisms of tau and MAP2 in neurons: suppressed axonal transit of MAP2 and locally regulated microtubule binding. *Neuron* 14, 421–432. doi: 10.1016/0896-6273(95)90298-8

Kang, H. J., Voleti, B., Hajszan, T., Rajkowska, G., Stockmeier, C. A., Licznerski, P., et al. (2012). Decreased expression of synapse-related genes and loss of synapses in major depressive disorder. *Nat. Med.* 18, 1413–1417. doi: 10.1038/nm.2886

Kapitein, L. C., and Hoogenraad, C. C. (2015). Building the neuronal microtubule cytoskeleton. *Neuron* 87, 492–506. doi: 10.1016/j.neuron.2015.05.046

Kapitein, L. C., Yau, K. W., Gouveia, S. M., van der Zwan, W. A., Wulf, P. S., Keijzer, N., et al. (2011). NMDA receptor activation suppresses microtubule growth and spine entry. *J. Neurosci.* 31, 8194–8209. doi: 10.1523/JNEUROSCI.6215-10.2011

Karczewski, K. J., Francioli, L. C., Tiao, G., Cummings, B. B., Alföldi, J., Wang, Q., et al. (2020). The mutational constraint spectrum quantified from variation in 141,456 humans. *Nature* 581, 434–443. doi: 10.1038/s41586-020-2308-7

Kaufmann, W. E., Naidu, S., and Budden, S. (1995). Abnormal expression of microtubule-associated protein 2 (MAP-2) in neocortex in rett syndrome. *Neuropediatrics* 26, 109–113. doi: 10.1055/s-2007-979738

Khatra, B. S., Juarez, M., Johnson, D., and DeTure, M. (2013). Phosphorylation of tau-4R and microtubule binding region of MAP-2C by PKA and GSK-3β inhibits their O-glycosylation by OGT. *FASEB J.* 27:1038.8. doi: 10.1096/fasebj.27.1_supplement.1038.8

Kim, Y., Jang, Y.-N., Kim, J.-Y., Kim, N., Noh, S., Kim, H., et al. (2020). Microtubule-associated protein 2 mediates induction of long-term potentiation in hippocampal neurons. *FASEB J.* 34, 6965–6983. doi: 10.1096/fj.201902122RR

Komulainen, E., Zdrojewska, J., Freemantle, E., Mohammad, H., Kulesskaya, N., Deshpande, P., et al. (2014). JNK1 controls dendritic field size in L2/3 and L5 of the motor cortex, constrains soma size and influences fine motor coordination. *Front. Cell Neurosci.* 8:272. doi: 10.3389/fncel.2014.00272

Kopeikina, K., Hyman, B., and Spires-Jones, T. (2012). Soluble forms of tau are toxic in Alzheimer's disease. *Transl. Neurosci.* 3, 223–233. doi: 10.2478/s13380-012-0032-y

Kühn, J., Meissner, C., and Oehmichen, M. (2005). Microtubule-associated protein 2 (MAP2)—a promising approach to diagnosis of forensic types of hypoxia-ischemia. *Acta Neuropathol.* 110, 579–586. doi: 10.3174/ajnr.A7606

Labonté, B., Engmann, O., Purushothaman, I., Menard, C., Wang, J., Tan, C., et al. (2017). Sex-specific transcriptional signatures in human depression. *Nat. Med.* 23, 1102–1111. doi: 10.1038/nm.4386

Law, A. J., Weickert, C. S., Hyde, T. M., Kleinman, J. E., and Harrison, P. J. (2004). Reduced spinophilin but not microtubule-associated protein 2 expression in the hippocampal formation in schizophrenia and mood disorders: molecular evidence for a pathology of dendritic spines. *Am. J. Psychiatry* 161, 1848–1855. doi: 10.1176/ajp.161.10.1848

Leal, G., Comprido, D., de Luca, P., Morais, E., Rodrigues, L., Mele, M., et al. (2017). The RNA-binding protein hnRNP K mediates the effect of BDNF on dendritic mRNA metabolism and regulates synaptic NMDA receptors in hippocampal neurons. *eNeuro* 4:ENEURO.0268-17.2017. doi: 10.1523/ENEURO.0268-17.2017

Leclerc, N., Baas, P. W., Garner, C. C., and Kosik, K. S. (1996). Juvenile and mature MAP2 isoforms induce distinct patterns of process outgrowth. *Mol. Biol. Cell* 7, 443–455. doi: 10.1091/mbc.7.3.443

Lefebvre, T., Ferreira, S., Dupont-Wallois, L., Bussière, T., Dupire, M.-J., Delacourte, A., et al. (2003). Evidence of a balance between phosphorylation and O-GlcNAc glycosylation of Tau proteins—a role in nuclear localization. *Biochim. Biophys. Acta* 1619, 167–176. doi: 10.1016/s0304-4165(02)00477-4

Lewis, S. A., Ivanov, I. E., Lee, G. H., and Cowan, N. J. (1989). Organization of microtubules in dendrites and axons is determined by a short hydrophobic zipper in microtubule-associated proteins MAP2 and tau. *Nature* 342, 498–505. doi: 10.1038/342498a0

Lewis, S. A., Wang, D. H., and Cowan, N. J. (1988). Microtubule-associated protein MAP2 shares a microtubule binding motif with tau protein. *Science* 242, 936–939. doi: 10.1126/science.3142041

Li, J., Wilkinson, B., Clementel, V. A., Hou, J., O'Dell, T. J., and Coba, M. P. (2016). Long-term potentiation modulates synaptic phosphorylation networks and reshapes the structure of the postsynaptic interactome. *Sci. Signal.* 9:rs8. doi: 10.1126/scisignal.aaf6716

Lim, R. W. L., and Halpain, S. (2000). Regulated association of microtubule-associated protein 2 (MAP2) with Src and Grb2: evidence for MAP2 as a scaffolding protein. *J. Biol. Chem.* 275, 20578–20587. doi: 10.1074/jbc.M001887200

Llansola, M., Sáez, R., and Felipo, V. (2001). NMDA-induced phosphorylation of the microtubule-associated protein MAP-2 is mediated by activation of nitric oxide synthase and MAP kinase. *Eur. J. Neurosci.* 13, 1283–1291. doi: 10.1046/j.0953-816x.2001.01497.x

Lopez, L. A., and Sheetz, M. P. (1993). Steric inhibition of cytoplasmic dynein and kinesin motility by MAP2. *Cell Motil. Cytoskeleton* 24, 1–16. doi: 10.1002/cm.970240102

Lu, A. T.-H., Dai, X., Martinez-Agosto, J. A., and Cantor, R. M. (2012). Support for calcium channel gene defects in autism spectrum disorders. *Mol. Autism.* 3:18. doi: 10.1186/2040-2392-3-18

Ludin, B., Ashbridge, K., Funfschilling, U., and Matus, A. (1996). Functional analysis of the MAP2 repeat domain. *J. Cell Sci.* 109, 91–99. doi: 10.1242/jcs.109.1.91

Mages, B., Fuhs, T., Aleithe, S., Blietz, A., Hobusch, C., Härtig, W., et al. (2021). The cytoskeletal elements MAP2 and NF-L show substantial alterations in different stroke models while elevated serum levels highlight especially MAP2 as a sensitive biomarker in stroke patients. *Mol. Neurobiol.* 58, 4051–4069. doi: 10.1007/s12035-021-02372-3

Maqbool, M., Mobashir, M., and Hoda, N. (2016). Pivotal role of glycogen synthase kinase-3: a therapeutic target for Alzheimer's disease. *Eur. J. Med. Chem.* 107, 63–81. doi: 10.1016/j.ejmech.2015.10.018

Marchisella, F., Coffey, E. T., and Hollos, P. (2016). Microtubule and microtubule associated protein anomalies in psychiatric disease. *Cytoskeleton (Hoboken)* 73, 596–611. doi: 10.1002/cm.21300

Martínez-Cerdeño, V. (2017). Dendrite and spine modifications in autism and related neurodevelopmental disorders in patients and animal models. *Dev. Neurobiol.* 77, 393–404. doi: 10.1002/dneu.22417

Martins-de-Souza, D., Guest, P. C., Vanattou-Saifoudine, N., Rahmoune, H., and Bahn, S. (2012). Phosphoproteomic differences in major depressive disorder postmortem brains indicate effects on synaptic function. *Eur. Arch. Psychiatry Clin. Neurosci.* 262, 657–666. doi: 10.1007/s00406-012-0301-3

Marx, C. E., Bradford, D. W., Hamer, R. M., Naylor, J. C., Allen, T. B., Lieberman, J. A., et al. (2011). Pregnenolone as a novel therapeutic candidate in schizophrenia: emerging preclinical and clinical evidence. *Neuroscience* 191, 78–90. doi: 10.1016/j.neuroscience.2011.06.076

Marx, C. E., Lee, J., Subramaniam, M., Rapisarda, A., Bautista, D. C. T., Chan, E., et al. (2014). Proof-of-concept randomized controlled trial of pregnenolone in schizophrenia. *Psychopharmacology (Berl)* 231, 3647–3662. doi: 10.1007/s00213-014-3673-4

McKinney, B. C., MacDonald, M. L., Newman, J. T., Shelton, M. A., DeGiosio, R. A., Kelly, R. M., et al. (2019). Density of small dendritic spines and microtubule-associated-protein-2 immunoreactivity in the primary auditory cortex of subjects with schizophrenia. *Neuropsychopharmacology* 44, 1055–1061. doi: 10.1038/s41386-019-0350-7

McVicker, D. P., Awe, A. M., Richters, K. E., Wilson, R. L., Cowdrey, D. A., Hu, X., et al. (2016). Transport of a kinesin-cargo pair along microtubules into dendritic spines undergoing synaptic plasticity. *Nat. Commun.* 7:12741. doi: 10.1038/ncomms12741

Meichsner, M., Doll, T., Reddy, D., Weisshaar, B., and Matus, A. (1993). The low molecular weight form of microtubule-associated protein 2 is transported into both axons and dendrites. *Neuroscience* 54, 873–880. doi: 10.1016/0306-4522(93)90581-y

Meléndez, J., Maldonado, V., and Ortega, A. (1996). Effect of melatonin on β-tubulin and MAP2 expression in NIE-115 cells. *Neurochem. Res.* 21, 653–658. doi: 10.1007/BF02527721

Merriam, E. B., Lumbard, D. C., Viesselmann, C., Ballweg, J., Stevenson, M., Pietila, L., et al. (2011). Dynamic microtubules promote synaptic NMDA receptor-dependent spine enlargement. *PLoS One* 6:e27688. doi: 10.1371/journal.pone.0027688

Merriam, E. B., Millette, M., Lumbard, D. C., Saengsawang, W., Fothergill, T., Hu, X., et al. (2013). Synaptic regulation of microtubule dynamics in dendritic spines by calcium, F-actin and drebrin. *J. Neurosci.* 33, 16471–16482. doi: 10.1523/JNEUROSCI.0661-13.2013

Mitra, G., Gupta, S., Poddar, A., and Bhattacharyya, B. (2015). MAP2c prevents arachidonic acid-induced fibril formation of tau: role of chaperone activity and phosphorylation. *Biophys. Chem.* 205, 16–23. doi: 10.1016/j.bpc.2015.06.003

Mitsuyama, F., Niimi, G., Kato, K., Hirosawa, K., Mikoshiba, K., Okuya, M., et al. (2008). Redistribution of microtubules in dendrites of hippocampal CA1 neurons

after tetanic stimulation during long-term potentiation. *Ital. J. Anat. Embryol.* 113, 17–27.

Miyamoto, S., Asakura, M., Sasuga, Y., Imafuku, J., Gamo, Y., and Osada, K. (1995). Chronic antidepressant administration inhibits microtubule assembly in rat cerebral cortex. *Eur. Neuropsychopharmacol.* 5:280.

Miyamoto, S., Asakura, M., Sasuga, Y., Osada, K., Bodaiji, N., Imafuku, J., et al. (1997). Effects of long-term treatment with desipramine on microtubule proteins in rat cerebral cortex. *Eur. J. Pharmacol.* 333, 279–287. doi: 10.1016/s0014-2999(97)01140-0

Mohan, R., and John, A. (2015). Microtubule-associated proteins as direct crosslinkers of actin filaments and microtubules. *IUBMB Life* 67, 395–403. doi: 10.1002/iub.1384

Mondragón-Rodríguez, S., Perry, G., Luna-Muñoz, J., Acevedo-Aquino, M. C., and Williams, S. (2014). Phosphorylation of tau protein at sites Ser396–404 is one of the earliest events in Alzheimer's disease and Down syndrome. *Neuropathol. Appl. Neurobiol.* 40, 121–135. doi: 10.1111/nan.12084

Moraga, D. M., Nuñez, P., Garrido, J., and Maccioni, R. B. (1993). A τ fragment containing a repetitive sequence induces bundling of actin filaments. *J. Neurochem.* 61, 979–986. doi: 10.1111/j.1471-4159.1993.tb03611.x

Morales, M., and Fifkova, E. (1989). Distribution of MAP 2 in dendritic spines and its colocalization with actin. *Cell Tissue Res.* 256, 447–456. doi: 10.1007/BF00225592

Mukaetova-Ladinska, E. B., Arnold, H., Jaros, E., Perry, R., and Perry, E. (2004). Depletion of MAP2 expression and laminar cytoarchitectonic changes in dorsolateral prefrontal cortex in adult autistic individuals. *Neuropathol. Appl. Neurobiol.* 30, 615–623. doi: 10.1111/j.1365-2990.2004.00574.x

Murakami, K., Fellous, A., Baulieu, E.-E., and Robel, P. (2000). Pregnenolone binds to microtubule-associated protein 2 and stimulates microtubule assembly. *Proc. Natl. Acad. Sci. U S A* 97, 3579–3584. doi: 10.1073/pnas.97.7.3579

Nielsen, F. C., Nielsen, J., Kristensen, M. A., Koch, G., and Christiansen, J. (2002). Cytoplasmic trafficking of IGF-II mRNA-binding protein by conserved KH domains. *J. Cell Sci.* 115, 2087–2097. doi: 10.1242/jcs.115.10.2087

Noble, W., Hanger, D. P., Miller, C. C., and Lovestone, S. (2013). The importance of tau phosphorylation for neurodegenerative diseases. *Front. Neurol.* 4:83. doi: 10.3389/fneur.2013.00083

Ostroff, L. E., Fiala, J. C., Allwardt, B., and Harris, K. M. (2002). Polyribosomes redistribute from dendritic shafts into spines with enlarged synapses during LTP in developing rat hippocampal slices. *Neuron* 35, 535–545. doi: 10.1016/s0896-6273(02)00785-7

Osuji, I. J., Vera-Bolaños, E., Carmody, T. J., and Brown, E. S. (2010). Pregnenolone for cognition and mood in dual diagnosis patients. *Psychiatry Res.* 178, 309–312. doi: 10.1016/j.psychres.2009.09.006

Ozer, R. S., and Halpain, S. (2000). Phosphorylation-dependent localization of microtubule-associated protein MAP2c to the actin cytoskeleton. *Mol. Biol. Cell* 11, 3573–3587. doi: 10.1091/mbc.11.10.3573

Özer, P. Z., Koyunoğlu, D., Son, Ç. D., Yurter, H. E., and Bora, G. (2022). SMN loss dysregulates microtubule-associated proteins in spinal muscular atrophy model. *Mol. Cell. Neurosci.* 120:103725. doi: 10.1016/j.mcn.2022.103725

Park, S. A., Ahn, S. I., and Gallo, J.-M. (2016). Tau mis-splicing in the pathogenesis of neurodegenerative disorders. *BMB Rep.* 49, 405–413. doi: 10.5483/bmbrep.2016.49.8.084

Pejaver, V., Hsu, W. L., Xin, F., Dunker, A. K., Uversky, V. N., and Radivojac, P. (2014). The structural and functional signatures of proteins that undergo multiple events of post-translational modification. *Protein Sci.* 23, 1077–1093. doi: 10.1002/pro.2494

Perez, J., Mori, S., Caivano, M., Popoli, M., Zanardi, R., Smeraldi, E., et al. (1995). Effects of fluvoxamine on the protein phosphorylation system associated with rat neuronal microtubules. *Eur. Neuropsychopharmacol.* 5, 65–69. doi: 10.1016/0924-977x(95)00024-j

Pescucci, C., Meloni, I., Bruttini, M., Ariani, F., Longo, I., Mari, F., et al. (2003). Chromosome 2 deletion encompassing the MAP2 gene in a patient with autism and Rett-like features. *Clin. Genet.* 64, 497–501. doi: 10.1046/j.1399-0004.2003.00176.x

Pettigrew, L. C., Holtz, M. L., Craddock, S. D., Minger, S. L., Hall, N., and Geddes, J. W. (1996). Microtubular proteolysis in focal cerebral ischemia. *J. Cereb. Blood Flow Metab.* 16, 1189–1202. doi: 10.1097/00004647-199611000-00013

Philpot, B. D., Lim, J. H., Halpain, S., and Brunjes, P. C. (1997). Experience-dependent modifications in MAP2 phosphorylation in rat olfactory bulb. *J. Neurosci.* 17, 9596–9604. doi: 10.1523/JNEUROSCI.17-24-09596.1997

Prieto-Gómez, B., Velázquez-Paniagua, M., Cisneros, L. O., Reyes-Vázquez, C., Jiménez-Trejo, F., Reyes, M. E., et al. (2008). Melatonin attenuates the decrement of dendritic protein MAP-2 immuno-staining in the hippocampal CA1 and CA3 fields of the aging male rat. *Neurosci. Lett.* 448, 56–61. doi: 10.1093/brain/awac191

Psychiatric GWAS Consortium Bipolar Disorder Working Group (2011). Large-scale genome-wide association analysis of bipolar disorder identifies a new susceptibility locus near ODZ4. *Nat. Genet.* 43, 977–983. doi: 10.1038/ng.943

Pucilowska, J., Vithayathil, J., Tavares, E. J., Kelly, C., Karlo, J. C., and Landreth, G. E. (2015). The 16p11.2 deletion mouse model of autism exhibits altered cortical progenitor proliferation and brain cytoarchitecture linked to the ERK MAPK pathway. *J. Neurosci.* 35, 3190–3200. doi: 10.1523/JNEUROSCI.4864-13.2015

Quinlan, E. M., and Halpain, S. (1996). Emergence of activity-dependent, bidirectional control of microtubule-associated protein MAP2 phosphorylation during postnatal development. *J. Neurosci.* 16, 7627–7637. doi: 10.1523/JNEUROSCI.16-23-07627.1996

Rajkowska, G., Miguel-Hidalgo, J. J., Wei, J., Dilley, G., Pittman, S. D., Meltzer, H. Y., et al. (1999). Morphometric evidence for neuronal and glial prefrontal cell pathology in major depression. *Biol. Psychiatry* 45, 1085–1098. doi: 10.1016/s0006-3223(99)00041-4

Rao, S., Yao, Y., Zheng, C., Ryan, J., Mao, C., Zhang, F., et al. (2016). Common variants in CACNA1C and MDD susceptibility: a comprehensive meta-analysis. *Am. J. Med. Genet. B Neuropsychiatr. Genet.* 171, 896–903. doi: 10.1002/ajmg.b.32466

Regan, P., Piers, T., Yi, J.-H., Kim, D.-H., Huh, S., Park, S. J., et al. (2015). Tau phosphorylation at serine 396 residue is required for hippocampal LTD. *J. Neurosci.* 35, 4804–4812. doi: 10.1523/JNEUROSCI.2842-14.2015

Rehbein, M., Kindler, S., Horke, S., and Richter, D. (2000). Two trans-acting rat-brain proteins, MARTA1 and MARTA2, interact specifically with the dendritic targeting element in MAP2 mRNAs. *Mol. Brain Res.* 79, 192–201. doi: 10.1016/s0169-328x(00)00114-5

Riederer, B. M., Draberova, E., Viklicky, V., and Draber, P. (1995). Changes of MAP2 phosphorylation during brain development. *J. Histochem. Cytochem.* 43, 1269–1284. doi: 10.1177/43.12.8537643

Rioux, L., Ruscheinsky, D., and Arnold, S. E. (2004). Microtubule-associated protein MAP2 expression in olfactory bulb in schizophrenia. *Psychiatry Res.* 128, 1–7. doi: 10.1016/j.psychres.2004.05.022

Robertson, L. A., Moya, K. L., and Breen, K. C. (2004). The potential role of tau protein O-glycosylation in Alzheimer's disease. *J. Alzheimers Dis.* 6, 489–495. doi: 10.3233/jad-2004-6505

Roger, B., Al-Bassam, J., Dehmelt, L., Milligan, R. A., and Halpain, S. (2004). MAP2c, but not tau, binds and bundles F-actin via its microtubule binding domain. *Curr. Biol.* 14, 363–371. doi: 10.1016/j.cub.2004.01.058

Romero, P. R., Zaidi, S., Fang, Y. Y., Uversky, V. N., Radivojac, P., Oldfield, C. J., et al. (2006). Alternative splicing in concert with protein intrinsic disorder enables increased functional diversity in multicellular organisms. *Proc. Natl. Acad. Sci. U S A* 103, 8390–8395. doi: 10.1073/pnas.0507916103

Rosoklija, G., Keilp, J. G., Toomayan, G., Mancevski, B., Haroutunian, V., Liu, D., et al. (2005). Altered subicular MAP2 immunoreactivity in schizophrenia. *Prilozi* 26, 13–34. doi: 10.1097/00005072-199505000-00212

Rudrabhatla, P., Jaffe, H., and Pant, H. C. (2011). Direct evidence of phosphorylated neuronal intermediate filament proteins in neurofibrillary tangles (NFTs): phosphoproteomics of Alzheimers NFTs. *FASEB J.* 25, 3896–3905. doi: 10.1096/fj.11-181297

Sánchez, C., Díaz-Nido, J., and Avila, J. (2000). Phosphorylation of microtubule-associated protein 2 (MAP2) and its relevance for the regulation of the neuronal cytoskeleton function. *Prog. Neurobiol.* 61, 133–168. doi: 10.1016/s0301-0082(99)00046-5

Saia-Cereda, V. M., Cassoli, J. S., Schmitt, A., Falkai, P., and Martins-de-Souza, D. (2016). Differential proteome and phosphoproteome may impact cell signaling in the corpus callosum of schizophrenia patients. *Schizophr. Res.* 177, 70–77. doi: 10.1016/j.schres.2016.03.022

Sarkar, T., Mitra, G., Gupta, S., Manna, T., Poddar, A., Panda, D., et al. (2004). MAP2 prevents protein aggregation and facilitates reactivation of unfolded enzymes. *Eur. J. Biochem.* 271, 1488–1496. doi: 10.1111/j.1432-1033.2004.04053.x

Scaife, R. M., Wilson, L., and Purich, D. L. (1992). Microtubule protein ADP-ribosylation in vitro leads to assembly inhibition and rapid depolymerization. *Biochemistry* 31, 310–316. doi: 10.1021/bi00116a042

Schätzle, P., Esteves da Silva, M., Tas, R. P., Katrukha, E. A., Hu, H. Y., Wierenga, C. J., et al. (2018). Activity-dependent actin remodeling at the base

of dendritic spines promotes microtubule entry. *Curr. Biol.* 28, 2081–2093. doi: 10.1016/j.cub.2018.05.004

Schizophrenia Working Group of the Psychiatric Genomics Consortium (2014). Biological insights from 108 schizophrenia-associated genetic loci. *Nature* 511, 421–427. doi: 10.1038/nature13595

Schizophrenia Working Group of the Psychiatric Genomics Consortium, Ripke, S., Walters, J. T. R., and O'Donovan, M. C. (2020). Mapping genomic loci prioritises genes and implicates synaptic biology in schizophrenia. *medRxiv* [Preprint]. doi: 10.1101/2020.09.12.20192922

Seitz, A., Kojima, H., Oiwa, K., Mandelkow, E.-M., Song, Y.-H., and Mandelkow, E. (2002). Single-molecule investigation of the interference between kinesin, tau and MAP2c. *EMBO J.* 21, 4896–4905. doi: 10.1093/emboj/cdf503

Seney, M. L., Huo, Z., Cahill, K., French, L., Puralewski, R., Zhang, J., et al. (2018). Opposite molecular signatures of depression in men and women. *Biol. Psychiatry* 84, 18–27. doi: 10.1016/j.biopsych.2018.01.017

Seo, M. K., Lee, C. H., Cho, H. Y., Lee, J. G., Lee, B. J., Kim, J. E., et al. (2014). Effects of antidepressant drugs on synaptic protein levels and dendritic outgrowth in hippocampal neuronal cultures. *Neuropharmacology* 79, 222–233. doi: 10.1016/j.neuropharm.2013.11.019

Sharma, N., Kress, Y., and Shafit-Zagardo, B. (1994). Antisense MAP-2 oligonucleotides induce changes in microtubule assembly and neuritic elongation in pre-existing neurites of rat cortical neurons. *Cell Motil. Cytoskeleton* 27, 234–247. doi: 10.1002/cm.970270305

Shelton, M. A., Newman, J. T., Gu, H., Sampson, A. R., Fish, K. N., MacDonald, M. L., et al. (2015). Loss of microtubule-associated protein 2 immunoreactivity linked to dendritic spine loss in schizophrenia. *Biol. Psychiatry* 78, 374–385. doi: 10.1016/j.biopsych.2014.12.029

Shu, T., Wu, T., Pang, M., Liu, C., Wang, X., Wang, J., et al. (2016). Effects and mechanisms of melatonin on neural differentiation of induced pluripotent stem cells. *Biochem. Biophys. Res. Commun.* 474, 566–571. doi: 10.1016/j.bbrc.2016.04.108

Somenarain, L., and Jones, L. B. (2010). A comparative study of MAP2 immunostaining in areas 9 and 17 in schizophrenia and Huntington chorea. *J. Psychiatr. Res.* 44, 694–699. doi: 10.1016/j.jpsychires.2009.12.006

Sontag, J.-M., Nunbhakdi-Craig, V., White, C. L., III, Halpain, S., and Sontag, E. (2012). The protein phosphatase PP2A/Bα binds to the microtubule-associated proteins tau and MAP2 at a motif also recognized by the kinase Fyn. *J. Biol. Chem.* 287, 14984–14993. doi: 10.1074/jbc.M111.338681

Sotrel, A., Williams, R. S., Kaufmann, W. E., and Myers, R. H. (1993). Evidence for neuronal degeneration and dendritic plasticity in cortical pyramidal neurons of Huntington's disease: A quantitative Golgi study. *Neurology* 43:2088. doi: 10.1212/wnl.43.10.2088

Springer, J. E., Azbill, R. D., Kennedy, S. E., George, J., and Geddes, J. W. (1997). Rapid calpain I activation and cytoskeletal protein degradation following traumatic spinal cord injury: attenuation with riluzole pretreatment. *J. Neurochem.* 69, 1592–1600. doi: 10.1046/j.1471-4159.1997.69041592.x

Stearns, M. E., and Brown, D. L. (1979). Purification of a microtubule-associated protein based on its preferential association with tubulin during microtubule initiation. *FEBS Lett.* 101, 15–20.

Steward, O., and Halpain, S. (1999). Lamina-specific synaptic activation causes domain-specific alterations in dendritic immunostaining for MAP2 and CAM kinase II. *J. Neurosci.* 19, 7834–7845. doi: 10.1523/JNEUROSCI.19-18-07834.1999

Strang, K. H., Golde, T. E., and Giasson, B. I. (2019). MAPT mutations, tauopathy and mechanisms of neurodegeneration. *Lab. Investig.* 99, 912–928. doi: 10.1038/s41374-019-0197-x

Sun, F., and Handel, M. A. (2011). A mutation in Mtap2 is associated with arrest of mammalian spermatocytes before the first meiotic division. *Genes (Basel)* 2, 21–35. doi: 10.3390/genes2010021

Teng, J., Takei, Y., Harada, A., Nakata, T., Chen, J., and Hirokawa, N. (2001). Synergistic effects of MAP2 and MAP1B knockout in neuronal migration, dendritic outgrowth and microtubule organization. *J. Cell Biol.* 155, 65–76. doi: 10.1083/jcb.200106025

Tortosa, E., Adolfs, Y., Fukata, M., Pasterkamp, R. J., Kapitein, L. C., and Hoogenraad, C. C. (2017). Dynamic palmitoylation targets MAP6 to the axon to promote microtubule stabilization during neuronal polarization. *Neuron* 94, 809–825. doi: 10.1016/j.neuron.2017.04.042

Uversky, V. N. (2014). Wrecked regulation of intrinsically disordered proteins in diseases: pathogenicity of deregulated regulators Front. *Front. Mol. Biosci.* 1:6. doi: 10.3389/fmolb.2014.00006

Vaillant, A. R., Zanassi, P., Walsh, G. S., Aumont, A., Alonso, A., and Miller, F. D. (2002). Signaling mechanisms underlying reversible, activity-dependent dendrite formation. *Neuron* 34, 985–998. doi: 10.1016/s0896-6273(02)00717-1

Velikonja, T., Fett, A.-K., and Velthorst, E. (2019). Patterns of nonsocial and social cognitive functioning in adults with autism spectrum disorder: a systematic review and meta-analysis. *JAMA Psychiatry* 76, 135–151. doi: 10.1001/jamapsychiatry.2018.3645

Ward, J. J., Sodhi, J. S., McGuffin, L. J., Buxton, B. F., and Jones, D. T. (2004). Prediction and functional analysis of native disorder in proteins from the three kingdoms of life. *J. Mol. Biol.* 337, 635–645. doi: 10.1016/j.jmb.2004.02.002

Wesseling, H., Mair, W., Kumar, M., Schlaffner, C. N., Tang, S., Beerepoot, P., et al. (2020). Tau PTM profiles identify patient heterogeneity and stages of Alzheimer's disease. *Cell* 183, 1699–1713.e13. doi: 10.1016/j.cell.2020.10.029

Westphal, D. S., Andres, S., Makowski, C., Meitinger, T., and Hoefele, J. (2018). MAP2 - a candidate gene for epilepsy, developmental delay and behavioral abnormalities in a patient with microdeletion 2q34 [case report]. *Front. Genet.* 9, 927–936. doi: 10.3389/fgene.2018.00099

Xia, D., Li, C., and Götz, J. (2015). Pseudophosphorylation of Tau at distinct epitopes or the presence of the P301L mutation targets the microtubule-associated protein Tau to dendritic spines. *Biochim. Biophys. Acta* 1852, 913–924. doi: 10.1016/j.bbadis.2014.12.017

Xie, C., Miyasaka, T., Yoshimura, S., Hatsuta, H., Yoshina, S., Kage-Nakadai, E., et al. (2014). The homologous carboxyl-terminal domains of microtubule-associated protein 2 and TAU induce neuronal dysfunction and have differential fates in the evolution of neurofibrillary tangles. *PLoS One* 9:e89796. doi: 10.1371/journal.pone.0089796

Yamauchi, P. S., and Purich, D. L. (1987). Modulation of microtubule assembly and stability by phosphatidylinositol action on microtubule-associated protein-2. *J. Biol. Chem.* 262, 3369–3375.

Yamauchi, P. S., and Purich, D. L. (1993). Microtubule-associated protein interactions with actin filaments: evidence for differential behavior of neuronal MAP-2 and tau in the presence of phosphatidylinositol. *Biochem. Biophys. Res. Commun.* 190, 710–715. doi: 10.1006/bbrc.1993.1107

Zhong, H., Sia, G.-M., Sato, T. R., Gray, N. W., Mao, T., Khuchua, Z., et al. (2009). Subcellular dynamics of type II PKA in neurons. *Neuron* 62, 363–374. doi: 10.1016/j.neuron.2009.03.013

Zivraj, K. H., Rehbein, M., Ölschläger-Schütt, J., Schob, C., Falley, K., Buck, F., et al. (2013). The RNA-binding protein MARTA2 regulates dendritic targeting of MAP2 mRNAs in rat neurons. *J. Neurochem.* 124, 670–684. doi: 10.1111/jnc.12079

frontiers | Frontiers in Molecular Neuroscience

TYPE Review
PUBLISHED 04 October 2022
DOI 10.3389/fnmol.2022.999605

Check for updates

OPEN ACCESS

EDITED BY
Dezhi Liao,
University of Minnesota Twin Cities,
United States

REVIEWED BY
Y. Y. Cai,
Nanyang Technological University,
Singapore
Yu-Dong Zhang,
University of Leicester,
United Kingdom

*CORRESPONDENCE
Afshin Shoeibi
Afshin.shoeibi@gmail.com
Sara A. Abdulla
saabdulla@hbku.edu.qa

SPECIALTY SECTION
This article was submitted to Neuroplasticity and Development, a section of the journal Frontiers in Molecular Neuroscience

RECEIVED 21 July 2022
ACCEPTED 09 August 2022
PUBLISHED 04 October 2022

CITATION
Moridian P, Ghassemi N, Jafari M, Salloum-Asfar S, Sadeghi D, Khodatars M, Shoeibi A, Khosravi A, Ling SH, Subasi A, Alizadehsani R, Gorriz JM, Abdulla SA and Acharya UR (2022) Automatic autism spectrum disorder detection using artificial intelligence methods with MRI neuroimaging: A review. *Front. Mol. Neurosci.* 15:999605. doi: 10.3389/fnmol.2022.999605

COPYRIGHT
© 2022 Moridian, Ghassemi, Jafari, Salloum-Asfar, Sadeghi, Khodatars, Shoeibi, Khosravi, Ling, Subasi, Alizadehsani, Gorriz, Abdulla and Acharya. This is an open-access article distributed under the terms of the Creative Commons Attribution License (CC BY). The use, distribution or reproduction in other forums is permitted, provided the original author(s) and the copyright owner(s) are credited and that the original publication in this journal is cited, in accordance with accepted academic practice. No use, distribution or reproduction is permitted which does not comply with these terms.

Automatic autism spectrum disorder detection using artificial intelligence methods with MRI neuroimaging: A review

Parisa Moridian[1], Navid Ghassemi[2], Mahboobeh Jafari[3], Salam Salloum-Asfar[4], Delaram Sadeghi[5], Marjane Khodatars[5], Afshin Shoeibi[6]*, Abbas Khosravi[7], Sai Ho Ling[8], Abdulhamit Subasi[9,10], Roohallah Alizadehsani[7], Juan M. Gorriz[6], Sara A. Abdulla[4]* and U. Rajendra Acharya[11,12,13]

[1]Faculty of Engineering, Science and Research Branch, Islamic Azad University, Tehran, Iran, [2]Department of Computer Engineering, Ferdowsi University of Mashhad, Mashhad, Iran, [3]Faculty of Electrical and Computer Engineering, Semnan University, Semnan, Iran, [4]Neurological Disorders Research Center, Qatar Biomedical Research Institute, Hamad Bin Khalifa University, Qatar Foundation, Doha, Qatar, [5]Department of Medical Engineering, Mashhad Branch, Islamic Azad University, Mashhad, Iran, [6]Data Science and Computational Intelligence Institute, University of Granada, Granada, Spain, [7]Institute for Intelligent Systems Research and Innovation (IISRI), Deakin University, Geelong, VIC, Australia, [8]Faculty of Engineering and IT, University of Technology Sydney (UTS), Ultimo, NSW, Australia, [9]Faculty of Medicine, Institute of Biomedicine, University of Turku, Turku, Finland, [10]Department of Computer Science, College of Engineering, Effat University, Jeddah, Saudi Arabia, [11]Ngee Ann Polytechnic, Singapore, Singapore, [12]Department of Biomedical Informatics and Medical Engineering, Asia University, Taichung, Taiwan, [13]Department of Biomedical Engineering, School of Science and Technology, Singapore University of Social Sciences, Singapore, Singapore

Autism spectrum disorder (ASD) is a brain condition characterized by diverse signs and symptoms that appear in early childhood. ASD is also associated with communication deficits and repetitive behavior in affected individuals. Various ASD detection methods have been developed, including neuroimaging modalities and psychological tests. Among these methods, magnetic resonance imaging (MRI) imaging modalities are of paramount importance to physicians. Clinicians rely on MRI modalities to diagnose ASD accurately. The MRI modalities are non-invasive methods that include functional (fMRI) and structural (sMRI) neuroimaging methods. However, diagnosing ASD with fMRI and sMRI for specialists is often laborious and time-consuming; therefore, several computer-aided design systems (CADS) based on artificial intelligence (AI) have been developed to assist specialist physicians. Conventional machine learning (ML) and deep learning (DL) are the most popular schemes of AI used for diagnosing ASD. This study aims to review the automated detection of ASD using AI. We review several CADS that have been developed using ML techniques for the automated diagnosis of ASD using MRI modalities. There has been very limited work on the use of DL

techniques to develop automated diagnostic models for ASD. A summary of the studies developed using DL is provided in the Supplementary Appendix. Then, the challenges encountered during the automated diagnosis of ASD using MRI and AI techniques are described in detail. Additionally, a graphical comparison of studies using ML and DL to diagnose ASD automatically is discussed. We suggest future approaches to detecting ASDs using AI techniques and MRI neuroimaging.

KEYWORDS

ASD diagnosis, neuroimaging, MRI modalities, machine learning, deep learning

Introduction

A complex intricate network of millions of neurons is responsible for monitoring and controlling each part of the human body and brain (Sparks et al., 2002; Brieber et al., 2007; Ecker et al., 2015). These networks consist of many neurons that need to be directly interconnected and synchronized (Sato et al., 2012; Hernandez et al., 2015). It has been suggested that certain disorders in the human body arise when brain networks are incorrectly connected to manage a specific activity (Gautam and Sharma, 2020; Noor et al., 2020; Khodatars et al., 2021; Loh et al., 2022). Disorders of this type can be classified into three groups based on their psychological or neural characteristics and threaten the health of many individuals across the globe. Autism spectrum disorder (ASD) (Yang et al., 2022), schizophrenia (Sadeghi et al., 2022), attention deficit hyperactivity disorder (ADHD) (Bakhtyari and Mirzaei, 2022), epilepsy (Shoeibi et al., 2021a), Parkinson's disease (Sahu et al., 2022), and bipolar disorder (BD) (Highland and Zhou, 2022) are some of the most known neurodevelopmental disorders.

Autism spectrum disorder is a neurodevelopmental disorder that manifests in childhood and causes a variety of challenges to individuals (Ecker et al., 2015). Those with ASD have difficulties with verbal and non-verbal communication, cognitive skills, social behavior, and entertaining activities (Aghdam et al., 2019; Ahmed et al., 2020a,b). ASD begins in the early stages of embryonic development, according to research results. Autism is thought to be caused by specific signal patterns in the cortex, abnormalities in the immune system, growth hormone fluctuations, and abnormalities in the neural mirror system in the embryonic stage (Chen et al., 2022; Jayanthy and Din, 2022). The overall ASD prevalence is one in 44 children aged 8 years, and ASD is around 4 times as prevalent among boys as among girls (Rakić et al., 2020; Maenner et al., 2021). In addition to lifelong social and adaptive disorders, one of the major consequences of autism is its negative impact on quality of life (Choi, 2017; Brown et al., 2018; Bengs et al., 2020; Byeon et al., 2020; D'Souza et al., 2020; Cao et al., 2021; Chen Y. et al., 2021; Chen H. et al., 2021; Chu et al., 2022). Therefore, early diagnosis and treatment of ASD are paramount for improving the quality of life of ASD children and their families (Kasari and Smith, 2013).

According to the DSM-3, mental health professionals originally divided autism into five categories, including Asperger's syndrome, Rett syndrome, childhood disintegrative disorder (CDD), autistic disorder, and Pervasive developmental disorder-not otherwise specified (PDD-NOS) (Volkmar et al., 1992; Matson et al., 2009). Using this method, physicians observed the symptoms of autistic individuals and compared their observations to those in the DSM-3 to diagnose the specific type of autism (Volkmar et al., 1986, 1992; Matson et al., 2009). In 2013, the DSM-5 was published, making significant changes to the categorization of autism (Volkmar and Mcpartland, 2014). DSM-5 categorizes autism severity into three levels, and more information is given in Volkmar and Mcpartland (2014). According to DSM-5, the lower the severity level of autism, the less support the child requires. Autism individuals with the second and third severity levels show moderate to severe symptoms and therefore require more frequent support. Although the DSM-5 provides explanations of the autism spectrum, these explanations are incomplete and do not provide guidance on the specific support that autistic children may require. In addition, some individuals simply do not fall into any of these categories, and ASD can change and intensify over time (Kim et al., 2014; Volkmar and Mcpartland, 2014).

Early diagnosis of ASD is of utmost importance for specialist physicians (Akhavan Aghdam et al., 2018; Anirudh and Thiagarajan, 2019; Arya et al., 2020; Al-Hiyali et al., 2021; Almuqhim and Saeed, 2021; Bayram et al., 2021). Hereafter, clinical screening methods for diagnosing ASD are introduced, including autism diagnostic interview-revised (ADI-R), childhood autism rating scale (CARS), social responsiveness scale, autism diagnostic observation schedule (ADOS), and Joseph picture self-concept scale (Thabtah and Peebles, 2019). Clinical screening methods have been proven effective in diagnosing ASD and are of great interest to specialist physicians.

Additionally, these methods assist in treating and preventing the development of ASD in the early stages (Thabtah and Peebles, 2019). As well as their many advantages, the mentioned methods always pose challenges for specialists (Thabtah and Peebles, 2019). These procedures involve long questionnaires, so they are very time-consuming and require different specialist physicians to analyze the questionnaire, which has led to many criticisms of clinical screening methods.

Additionally, some ASD diagnosis tools have been provided by neurologists and psychologists, including autism spectrum quotient (AQ), a modified checklist for autism in toddlers (M-CHAT), and a childhood Asperger syndrome test (CAST) (Thabtah and Peebles, 2019). Various items in these tools can be used to diagnose different types of autism; however, these methods face different challenges in the diagnosis of ASD (Thabtah and Peebles, 2019). These tools, for example, are not considered definitive screening methods for diagnosing ASD. Because, in most cases, ASD is diagnosed by them without the presence of a specialist physician (Thabtah and Peebles, 2019). However, some of these methods do not meet DSM-5 requirements (Thabtah and Peebles, 2019). Due to this, it is necessary to provide tools that are compatible with DSM-5.

Neuroimaging techniques are one group of methods used for diagnosing neurological and mental disorders such as ASD. These methods comprise structural and functional neuroimaging modalities, which are of special interest to physicians, particularly in diagnosing various brain disorders (Shoeibi et al., 2021b, 2022c). The fMRI is one of the major functional neuroimaging methods that records data in a non-invasive manner. fMRI has a high spatial resolution, making it an excellent method for examining functional connectivity in the brain. fMRI data is classified into two categories: T-fMRI and rs-fMRI. Furthermore, fMRI data are composed of a 4-dimensional tensor, which permits the 3D volume of the brain to be segmented into smaller areas, and the activity of each area is recorded for a predetermined time period. Although fMRI has provided satisfactory results in diagnosing a variety of brain disorders, these techniques are costly and too sensitive to motion artifacts (Ghassemi et al., 2020; Shoeibi et al., 2022b).

Structural and DTI have been used to examine brain anatomy and the interaction between brain regions, respectively. The structural neuroimaging modalities offer the advantage of cost-effectiveness and the availability of imaging protocols in most treatment facilities (Ghassemi et al., 2020). Physicians use sMRI modalities to diagnose autism in autistic individuals using (i) geometric features and (ii) volumetric features, which physicians have used to demonstrate that autistic people demonstrate superior brain development in comparison to normal people (Brambilla et al., 2003; Siewertsen et al., 2015; Zürcher et al., 2015; Zhang and Roeyers, 2019). Hazlett et al. (2005) studied the brain structure of 51 autistic children and 25 normal children (1.5–3 years of age). Their findings indicated that the Cerebellum white matter volume of autistic children was 2–4 times greater than that of normal children.

Although MRIs offer many advantages, MRI artifacts reduce the accuracy with which clinicians are able to diagnose autism. Additionally, ASD individuals' MRI data is recorded with multiple slices and different protocols. Consequently, it takes considerable time to examine all MRI slices accurately, and clinicians should be highly precise. The fatigue of the physician may lead to an incorrect diagnosis of ASD in many cases. In addition, MRI data is problematic because most physicians are inexperienced in interpreting these images and may find diagnosing ASD in its early stages difficult.

Numerous treatment methods have also been provided for ASD patients so far, some of which are listed here. Transcranial magnetic stimulation (TMS) and transcranial direct current stimulation (tDCS) are two non-invasive methods to diagnose and treat various neurological and mental disorders such as ASD (Khodatars et al., 2021). Using them, the areas of the brain where ASD occurs are selected by specialist physicians. Electrical pulses are then applied to these areas to treat or control ASD (Khodatars et al., 2021). Additionally, some researchers have provided rehabilitation systems based on AI techniques to treat ASD. For example, Cai et al. (2013) presented a virtual reality (VR) system for treating ASD. They proposed a VR program for people with ASD to interact with dolphins in their work. This tool enables people with ASD to virtually be at the pool as dolphin trainers, aiming to help people with ASD learn different types of non-verbal communication through hand movements with virtual dolphins.

To improve the accuracy of ASD diagnosis, AI techniques can be used. The use of AI in diagnosing various diseases has been studied (Nogay and Adeli, 2020; Ahmadi-Dastgerdi et al., 2021; Shoeibi et al., 2022a). Several studies have demonstrated that AI techniques, along with MRI neuroimaging modalities, increase the accuracy of ASD diagnosis (Nogay and Adeli, 2020; Ahmadi-Dastgerdi et al., 2021). An increasing number of studies have been conducted on detecting ASD using ML and DL methods. Researchers first demonstrated that ASD could be diagnosed from ML using MRI neuroimaging technologies (Shoeibi et al., 2022a). Based on ML algorithms, feature extraction, dimension reduction, and classification algorithms in CADS are selected through trial and error (Parikh et al., 2019; Alizadehsani et al., 2021). Choosing an appropriate algorithm for each CADS section can be challenging without adequate knowledge of AI (Mohammadpoor et al., 2016; Parikh et al., 2019; Alizadehsani et al., 2021; Wang et al., 2021a,c). Furthermore, ML techniques are not suitable for small data sets (Ghassemi et al., 2021). Therefore, these methods do not contribute to developing software for detecting ASDs using MRI neuroimaging modalities.

Various studies are being conducted to diagnose various diseases and disorders by using these methods to overcome the challenges inherent in ML techniques (Noor et al., 2019;

Al-Shoukry et al., 2020; Altinkaya et al., 2020; Yao et al., 2020). For example, in contrast to ML methods, DL uses deep layers for feature extraction and classification and requires fewer implementation steps in diagnosing ASD (Goodfellow et al., 2016). Furthermore, DL-based CADS can be more efficient and accurate with large input data.

An overview of studies relating to the detection of ASD using MRI neuroimaging methods is presented in this comprehensive systematic review. The first step was to systematically review all publications on ASD detection using MRI modalities and ML techniques. A recent review by the authors of this review discussed the use of different neuroimaging modalities and DL architectures to detect ASD (Khodatars et al., 2021). **Supplementary Appendix A** presents a review paper describing ASD detection in different neuroimaging modalities using DL techniques to compare ML and DL studies.

The following sections describe the following. Section 2 is a search Strategy based on PRISMA guidelines. Section 3 reviews the review papers in AI techniques for ASD diagnosis. Section 4 describes the CADS based on AI to detect ASD from MRI neuroimaging images. Section 5 presents a comparison between ML and DL studies to ASD detection using MRI modalities. Section 6 examines the most critical challenges for detecting ASD using AI methods. Future directions and conclusion sections are presented in sections 7 and 8, respectively.

Search strategy based on PRISMA guideline

The PRISMA protocol was used to select and review papers in this study (Sadeghi et al., 2022). Papers on the diagnosis of ASD by MRI modalities and AI models (ML and DL) published from 2016 to 2022 were included in this study. In this review paper, various citation databases, including IEEE, Wiley, Frontiers, ScienceDirect, SpringerLink, ACM, and ArXiv were used to search for papers in the field of ASD detection. Furthermore, Google Scholar has been used to search for the article entirety. Here are the keywords, including "ASD classification," "Feature extraction," "fMRI," "sMRI," and "Autism Spectrum Disorder," which were used to search for articles relating to the diagnosis of ASD using ML algorithms. To search for articles related to DL, the keywords used were "Autism Spectrum Disorder," "ASD," fMRI," "sMRI," and "Deep Learning."

As stated above, papers were selected and reviewed based on the PRISMA protocol at three different levels. In the first level, 34 out of 316 downloaded papers were eliminated as they were out of the scope of this study. Then, 28 papers were also excluded as they did not use MRI datasets in the ASD diagnosis, followed by excluding further 21 papers due to no use of AI techniques. Therefore, 233 papers were finally selected and used in this review paper. **Figure 1** shows the selection procedure of papers based on the PRISMA protocol on three levels. The key criteria for the inclusion and exclusion of papers on the ASD diagnosis based on the PRISMA protocol are shown in **Table 1**.

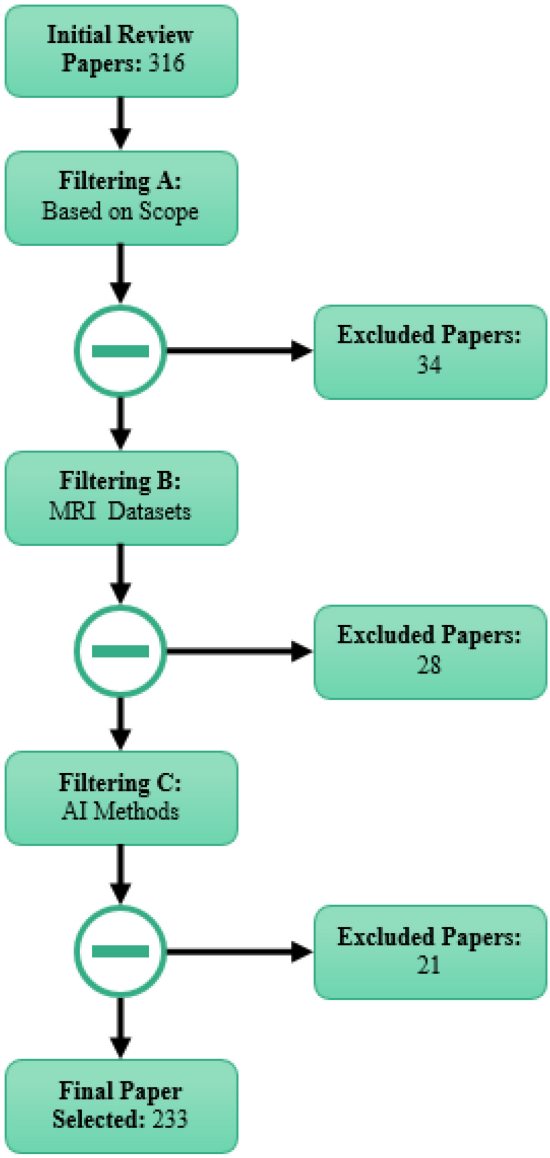

FIGURE 1
Papers selection process based on the PRISMA guidelines.

Artificial intelligence techniques for autism spectrum disorder diagnosis

For researchers in cognitive sciences, autism is a well-recognized neurodevelopmental disorder with a high prevalence in recent years. Challenges in the ASD diagnosis for physicians have resulted in extensive studies on this brain disorder.

TABLE 1 The exclusion and inclusion criteria for diagnosis of ASD.

Inclusion	Exclusion
1. sMRI neuroimaging modalities	1. Treatment of ASD
2. fMRI neuroimaging modalities	2. Clinical methods for ASD treatment
3. Different Types of Autism	3. Rehabilitation systems for ASD detection (Without AI techniques)
4. DL models	
5. Feature extraction methods	
6. Dimension reduction methods	
7. Classification methods	

Scholars in AI, and cognitive sciences seek to develop a real diagnostic tool for ASD using various AI techniques. Accordingly, extensive studies have focused on ASD diagnosis using neuroimaging modalities and AI techniques, outlined in this section by reviewing articles in the field of ASD diagnosis using these techniques.

Pagnozzi et al. (2018) reviewed 123 articles on ASD diagnosis using sMRI modalities and reported further developments in some brain areas of ASD individuals than those of HC. They also explained that ASD caused changes in the structure of patients' brains, including increased volume of frontal and temporal lobes, increased thickness of the frontal cortex, and increased cerebrospinal fluid volume. This study assists scholars in applying AI techniques in ASD diagnosis from sMRI modalities in future studies.

Nogay and Adeli (2020) published a review article on ASD diagnosis using brain imaging and ML techniques. They reviewed studies on ASD diagnosis for sMRI, fMRI and combined data using ML techniques and found a higher accuracy of ASD diagnosis at younger ages. They hope to develop a practical ASD diagnostic tool based on ML techniques from MRI modalities.

In another study, Xu et al. (Shoeibi et al., 2022a) reported methods and tools associated with ASD diagnosis from MRI data based on ML techniques. Initially, they introduced the most important ML-based algorithms, including feature extraction, feature selection and reduction, training and test models, and evaluation parameters.

Parlett-Pellerit et al. (Ahmadi-Dastgerdi et al., 2021) reviewed studies on unsupervised ML techniques for ASD diagnosis. In this study, various clinical data and medical imaging data were discussed for ASD diagnosis using unsupervised ML techniques.

The most important feature selection and classification algorithms for ASD diagnosis were studied in Rahman et al. (2020) paper. Their input data comprises various psychological tests such as ADOS and MRI modalities. They claimed that this study could assist scholars in developing future studies on ADS diagnosis.

A review article on the diagnosis of ASD and ADHD using AI techniques was published by Eslami et al. (2021a). They discussed DL and ML-based studies on ASD and ADHD diagnosis from MRI modalities and the most important AI techniques (DL and ML). In the ML section, the authors presented the most important feature extraction techniques, such as effective dynamic connectivity, and outlined various popular DL techniques.

Khodatars et al. (2021) presented a review paper on ASD diagnosis and rehabilitation using DL techniques. They initially introduced the public neuroimaging modalities datasets, such as MRI, pre-processing techniques, and DL models, an ASD diagnosis. Then, they summarized the studies conducted in this field in a table. They also discussed studies in the field of autism rehabilitation using DL techniques.

In this section, the most important review papers on ASD diagnosis from various data and AI techniques were discussed. In our study, ASD diagnosis papers using MRI data and various AI techniques (ML and DL) were reviewed. This paper reports all ASD diagnosis articles from 2010 to 2022. Also, the most important challenges and future works for diagnosing ASD from MRI modalities are presented. To the best of our knowledge, no similar review article has been provided, and our review article has outstanding innovations.

Computer-aided design systems for aided design systems diagnosis by magnetic resonance imaging neuroimaging modalities

The application of CADS based on AI techniques is presented in this section and illustrated in **Figure 2**. The steps involved in CADS using ML for ASD detection are outlined in **Figure 2**. As shown in **Figure 2**, CADS input consists of datasets containing MRI modalities. Standard preprocessing (low-level) methods for MRI neuroimaging modalities were demonstrated as a second step. Next, we will discuss these preprocessing methods for MRI neuroimaging modalities. The third step involves feature extraction. Feature reduction or selection techniques (dimension reduction) are considered to be the fourth step in the CADS based on ML. The final step involves the use of classification algorithms. The only difference between DL-based and ML-based CADS is the feature extraction to the classification step. This procedure is carried out in deep layers in CADS based on DL. This enables the extraction of features from MRI data without the user's intervention. Moreover, in CADS based on DL, diagnostics of ASD may be possible in case there are more input data, allowing the development of actual software for the detection of ASD. The details of ASD detection from MRI neuroimaging modalities using DL architectures are given in **Supplementary Appendix (A)**. Here we present the

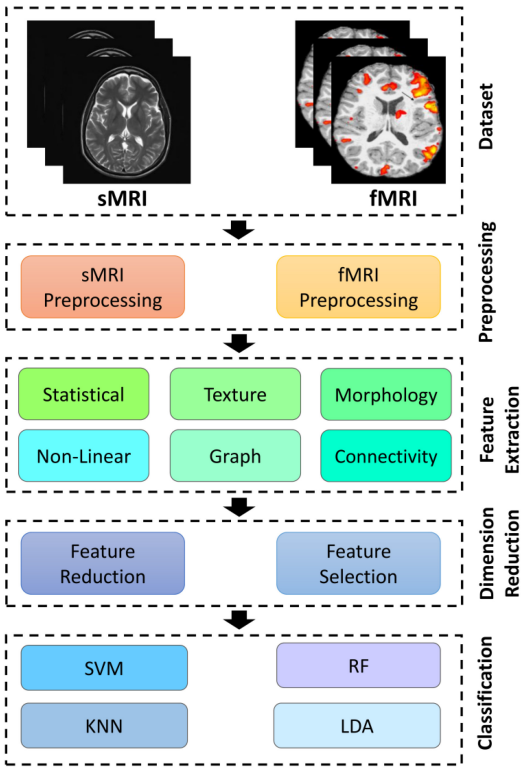

FIGURE 2
Block diagram of CADS- based on ML techniques for automated ASD diagnosis.

details of CADS based on ML and some of the most important algorithms in each section.

Magnetic resonance imaging neuroimaging autism spectrum disorder datasets

Various MRI modalities datasets for ASD diagnosis are available to researchers, including UCI (Last Access 19/07/2022a), NDAR (Last access 19/07/2022b), AGRE (Last access 19/07/2022d), NIMH Repository and Genomics Resource, n.d. (Last access 19/07/2022f), Gene Expression Omnibus [GEO], n.d. (Last access 19/07/2022e), SSC (Last access 19/07/2022h), Simons VIP SFARI (Last access 19/07/2022g), and autism brain imaging data exchange (ABIDE/) (Khodatars et al., 2021). **Table 2** and **Supplementary Table 1** summarize studies of ASD diagnosis using ML and DL techniques. As can be seen, the ABIDE database has a special place in research. ABIDE is recognized as the most complete and freely available database of MRI modalities for the automatic diagnosis of ASD (Khodatars et al., 2021). This dataset has two parts, ABIDE 1 and ABIDE-II, containing sMRI data, rs-fMRI data, and phenotypic data. 1112 datasets are involved in ABIDE I, and 1114 datasets are included in ABIDE II (Khodatars et al., 2021). ABIDE 1 also contains preprocessed data from MRI modalities for research, known as the preprocessed connectomes project (PCP) (Khodatars et al., 2021). Additionally, other available datasets, such as NDAR, UCI, and NRGR, have been used in ASD diagnostic. The results show that these datasets have been able to achieve satisfactory results. The datasets used for each study are summarized in **Table 2** and **Supplementary Table 1**.

Preprocessing techniques for functional and structural modalities

Preprocessing techniques are needed to help CADS to achieve promising results. The sMRI and fMRI neuroimaging modalities have implemented fixed preprocessing steps using different software packages. The most common software packages are brain extraction tools (BET) (Soltaninejad et al., 2014), FMRIB software libraries (FSL), statistical parametric mapping (SPM), and FreeSurfer (Khodatars et al., 2021). The following is the standard preprocessing steps for fMRI and sMRI neuroimaging modalities. Some of them are common for both fMRI and sMRI modalities, so we will introduce them in the fMRI-related section. **Figure 3** shows the standard fMRI and sMRI techniques. Also, the pipeline preprocessing techniques for ABIDE datasets will be introduced in another section.

The standard Preprocessing is a necessary step in fMRI, and if preprocessing is not carried out properly, it will lead to reduced performance of automated diagnosis of ASD. This step aims to extract regions suspected of having ASD and examine the function of brain neurons in those regions. The preprocessing steps of fMRI include delineation of the brain region, removal of the first few volumes, slice timing correction, inhomogeneity correction, motion correction, intensity normalization, temporal filtering, spatial smoothing, and ultimately registration standard atlas (Khodatars et al., 2021). As mentioned earlier, this step is usually carried out by a toolbox, including BET (Khodatars et al., 2021), FSL (Khodatars et al., 2021), SPM (Anand and Sahambi, 2010; Khodatars et al., 2021), FreeSurfer (Lee and Xue, 2017; Khodatars et al., 2021), etc. In reference (Khodatars et al., 2021), the details for standard preprocessing steps of fMRI modalities are elaborately explained.

The preprocessing of sMRI data extracts helps physicians examine regions with suspected ASD more accurately. Besides, low-level sMRI preprocessing methods help AI-based CADS to process important information. This process increases the accuracy and efficiency of diagnosis of ASD CADS. The most important standard sMRI covers intensity standardization, de-oblique, re-orientation, Denoising, and segmentation (Khodatars et al., 2021). In reference (Khodatars et al., 2021), each step of standard preprocessing for sMRI modalities is explained.

TABLE 2 Automated diagnosis of ASD with MRI neuroimaging modalities using ML methods.

References	Dataset	Number of cases	Modalities	Atlas + Pipeline	Feature extraction	Feature selection	Classification	The best performance criteria (%)
Haweel et al., 2020	NDAR	39 ASD	rs-fMRI	Brainnetome (BNT) Atlas	GLM Features	RFE	RF	Acc = 72
			sMRI	MNI-152 Atlas				
Yang X. et al., 2019	ABIDE	505 ASD, 530 HC	rs-fMRI	CC400 Atlas + CPAC Pipeline	Different Features	Nilearn	Ridge	Acc = 71.98 Pre = 71.53 Rec = 70.89
Zhang X. et al., 2020	NDAR	30 ASD, 30 HC	sMRI	NA	Cortical Path Signature Features	–	Siamese Verification Model	Acc = 87 Sen = 83 Spe = 90
Bi et al., 2019	ABIDE	103 ASD, 106 HC	rs-fMRI	AAL Atlas + DPARSF Pipeline	Graph-Theoretic Indicators (Dimensional Features)	–	GERSVMC	Acc = 96.8
Sartipi et al., 2018	ABIDE	222 ASD, 246 HC	rs-fMRI	HO Atlas + CPAC Pipeline	GARCH Model	*T*-test	SVM	Acc = 75.3
Saad and Islam, 2019	UMCD	51 ASD, 41 HC	DTI	NA	Graph Theory-based Features	PCA	SVM	Acc = 75 Sen = 81.94 Spe = 70 Pre = 70.42
Liu W. et al., 2020	ABIDE	250 ASD, 218 HC	rs-fMRI	AAL Atlas + CPAC Pipeline	Dimensional Feature Vectors	–	Elastic Net	Acc = 83.33
Zhuang et al., 2018b	Clinical	20 ASD	sMRI	NA	GLM	Different Feature Selection Methods	RF	NA
			rs-fMRI					
Zheng et al., 2019	ABIDE	66 ASD, 66 HC	sMRI	NA	Morphological and MFN Features	RFE	SVM	Acc = 78.63 Sen = 80 Spe = 77.27
ElNakieb et al., 2019	NDAR	122 ASD, 141 HC	DTI	MNI-152 Atlas	Global and Local Feature Extraction	Signal to Noise Ratio (s2n) Filter Based Feature Ranking	SVM	Acc = 71 Sen = 72 Spe = 70
Ge et al., 2018	NDAR	57 ASD, 34 HC	sMRI	NA	Morphometrical Features	–	K-Means Clustering	NA
Stevens et al., 2019	NA	2400 ASD	Different modalities	NA	Latent Clusters	+Bayesian Information Criterion	Linear Regression (LR)	Intensity = 94.29
Wang J. et al., 2020	ABIDE	175 ASD, 234 HC	rs-fMRI	AAL Atlas	Patch-based Functional Correlation Tensor (PBFCT) Features, FC Features	MSLRDA, *T*-test	Multi-View Sparse Representation Classifier (MVSRC)	NA
Dekhil et al., 2019	NDAR	72 ASD, 113 HC	sMRI	Desikan-Killiany (DK) Atlas	Morphological, Volumetric, and Functional Connectivity Features	–	KNN, RF	Acc = 81 Sen = 84 Spe = 79.2
			rs-fMRI					
Abdullah et al., 2019	NA	189 ASD, 515 HC	AQ	NA	Different Features	Chi-Squared Test, LASSO	LR	Acc = 97.54 Sen = 100 Spe = 96.59
Demirhan, 2018	UCI	104 ASD	ASD Scan Data	NA	Different Features	Grid Search Method	RF	Acc = 100 Sen = 100 Spe = 100
Syed et al., 2017	ABIDE	392 ASD, 407 HC	rs-fMRI	DPARSF Pipeline	ICA + Different Features (Reproducible REs, NMI Values, AC Maps)	gRAICAR	K-Means Clustring	Acc = 82.4 Sen = 77 Spe = 87
Liu W. et al., 2020	ABIDE 1	403ASD, 468 HC	rs-fMRI	AAL Atlas + CPAC Pipeline	Dynamic Functional Connectivity (DFC) and Mean Time Series Features	MTFS-EM	SVM	Acc = 76.8 Sen = 72.5 Spe = 79.9
Wang Y. et al., 2020	ABIDE	255 ASD, 276 HC	rs-fMRI	DPARSF Pipeline	Functional Connectivity Features	RFE	SVM	Acc = 90.6 Sen = 90.62 Spe = 90.58
Xiao et al., 2017	Clinical	46 ASD, 39 DD (Developmental Delay)	sMRI	DK Atlas	Neuroanatomical Features (Regional Cortical Thickness, Cortical Volume, Cortical Surface Area)	–	RF	Acc = 80.9 Sen = 81.3 Spe = 81 AUC = 88
Eill et al., 2019	CFMRI	46 ASD, 47 HC	Different Modalities	Johns Hopkins (JH), HO Atlas	Anatomical Variables, Cortical, Mean Diffusivity Values, Connectivity Matrices, and DTI Features	–	Conditional Random Forest (CRF)	Acc = 92.5 Sen = 97.8 Spe = 87.2

(Continued)

TABLE 2 (Continued)

References	Dataset	Number of cases	Modalities	Atlas + Pipeline	Feature extraction	Feature selection	Classification	The best performance criteria (%)
Sarovic et al., 2020	Clinical	24 ASD, 21 HC	sMRI	NA	Morphological Features of Subcortical Volumes	–	LR	Acc = 73.2
Zhao F. et al., 2017	ABIDE	54 ASD, 57 HC	sMRI	Different Atlase + DPARSF Pipeline	Regional Morphological Features	HSL-CCA, PCA	Linear SVM	Acc = 81.6 F1-S = 81.4
			t-fMRI					
Dekhil et al., 2018	NDAR	123 ASD, 160 HC	sMRI	All Atlases	PICA (Spatial Components, Correlation Values, Power Spectral Densities)	SAE	SVM	Acc = 92 Sen = 93 Spe = 89
			rs-fMRI					
Yang M. et al., 2019	ABIDE 1	260 ASD, 308 HC	rs-fMRI	AAL Pipeline	–	–	Attention Based Semi-Supervised Dictionary Learning (ASSDL) Model	Acc = 98.2
Jiang et al., 2019	ABIDE 1	250 ASD, 218 HC	rs-fMRI	AAL Atlas + CPAC Pipeline	Multi-Center Domain Adaptation (MCDA) Method	–	KNN	Acc = 73.45 Sen = 69.23 Spe = 79.17
Madine et al., 2020	ABIDE 1	155 ASD, 186 HC	sMRI	DK Atlas	Low-Order Morphological Connectivity Network (LON), Single Cell Interpretation *via* Multi-Kernel Learning (SIMLR), Similarity Matrix	–	Hypergraph Neural Network (HGNN)	Acc = 75.2
Thomas and Chandran, 2018	ABIDE	NA	sMRI	NA	GLCM	–	ANN	NA
			rs-fMRI					
Haweel et al., 2019b	Clinical	30 ASD, 30 HC	t-fMRI	BNT Atlas	GLM Feature Extraction	–	Stacked Non-negativity Constraint Auto-Encoder (SNCAE)	Acc = 75.8 Sen = 74.8 Spe = 76.7
Huang F. et al., 2019	ABIDE 1	109 ASD, 144 HC	rs-fMRI	AAL, Dosenbach 160, CC 200 Atlas + DPARSF Pipeline	Sparse Low-Rank Functional Connectivity Network	Different Feature Selection Methods	SVM	Acc = 81.74 Sen = 71.83 Spe = 89.50
Benabdallah et al., 2018	ABIDE 1	870 Subjects	rs-fMRI	AAL, multi-subject dictionary learning (MSDL) Atlas + CPAC Pipeline	ROIs Extraction, Connectivity Graphs Construction + Minimum Spanning Trees Extraction	MSTs Elimination	SVM	Acc = 74,89 Sen = 24,19 Spe = 93,59
Haweel et al., 2019a	Clinical	30 Subjects	t-fMRI	BNT Atlas	Multi-Level GLM + GLM3 Parameters, Z-Stats Maps for All Brain Areas	RFE	RF	Acc = 78
Alvarez-Jimenez et al., 2020	NDAR	22 ASD, 25 HC	t-fMRI	Proposed Atlas	GLM Analysis	–	Stacked Autoencoder With Non-Negativity Constraint (SNCAE)	Acc = 94.7
			sMRI					
Chaitra et al., 2020	ABIDE 1	34 ASD, 34 HC	sMRI	HO Atlas	Curvelet Transform + Coefficient Distribution Per Curvelet Sub-Band	Generalized Gaussian Distribution (GGD)	SVM	Different Results
	ABIDE II	42 ASD, 41 HC						
Fan et al., 2020	ABIDE 1	432 ASD, 556 HC	rs-fMRI	CC200 Atlas + DPARSF Pipeline	Graph-Theoretic Measures, Traditional FC Data	Recursive-Cluster-Elimination (RCE)	SVM	Acc = 70.1

(Continued)

TABLE 2 (Continued)

References	Dataset	Number of cases	Modalities	Atlas + Pipeline	Feature extraction	Feature selection	Classification	The best performance criteria (%)
Mellema et al., 2020	ABIDE 1	145 ASD, 157 HC	rs-fMRI	CC200 Atlas + CPAC Pipeline	Two-Group Cross-Localized Hidden Markov Model	Likelihood Values	SVM	Acc = 74.9
ElNakieb et al., 2018	IMPAC	418 ASD, 497 HC	rs-fMRI	All Atlases	Tangent-Space Embedding Metric	Permutation Feature Importance (PFI)	DenseFFwd	Acc = 75.4–80.4
Ke et al., 2019	Different Datasets	72 ASD, 113 HC	sMRI rs-fMRI	DK Atlas	Anatomical and Connectivity Matrix Features	–	KNN, RF, and SVM	Acc = 81 Sen = 78 Spe = 83.5
Ke et al., 2019	Different Datasets	97 ASD, 56 HC	DTI	JH Atlas	Global Features (FA, MD, AD) + Feature Mapping to Atlas + Local Feature Extraction (PDFs of Features for Each WM Area in the Atlas)	–	KNN, RF, and SVM	Acc = 81 Sen = 78 Spe = 83.5
Mostafa et al., 2019a	NAMIC	2 ASD, 2 HC	sMRI	NA	Adaptive Independent Subspace Analysis (AISA) Method, Texture Analysis + Different Features	t-SNE	KNN	Acc = 94.7 Sen = 92.29 Spe = 94.82 F1-S = 93.56
Bernas et al., 2018	ABIDE 1	403 ASD, 468 HC	rs-fMRI sMRI	NA	Eigenvalues and Topology Centralities Features	Backward Sequential Feature Selection Algorithm	LDA	Acc = 77.7
Dekhil et al., 2020	Clinical ABIDE	12 ASD, 12 HC 12 ASD, 18 HC	rs-fMRI	NA	Group Independent Component Analysis (gICA) + Wavelet Coherence Maps Extraction	–	SVM	Acc = 86.7 Sen = 91.7 Spe = 83.3
Yassin et al., 2020	ABIDE 1	561 ASD, 521 HC	sMRI rs-fMRI	DK, AAL Atlas + CCS Pipeline	Anatomical Feature Extraction + Functional Connectivity Analysis	–	KNN	Different Results
Soussia and Rekik, 2018	Clinical	36 ASD, 106 HC	sMRI	NA	Cortical Thickness, Surface Area, and Subcortical Volume Features	PCA	SVM	Different Results
Xiao et al., 2017	ABIDE 1	155 ASD, 186 HC	sMRI	DK Atlas	Low-Order Morphological Network Construction (LON), High-Order Morphological Network Construction (HON) Features	t-SNE, K-Means Clustering	SVM	Acc = 61.7
Zhao F. et al., 2018	Clinical	46 ASD, 39 DD	sMRI	Talairach, DK Atlas	Regional Cortical Thickness, Cortical Volume, And Cortical Surface Area	–	RF	Acc = 80.9 Sen = 81.3 Spe = 81
Fredo et al., 2018	ABIDE	54 ASD, 46 HC	rs-fMRI	AAL Atlas + DPARSF Pipeline	LON and HONs Features	LASSO	Ensemble Classifier with Multiple Linear SVMs	Acc = 81
Bi et al., 2018	ABIDE	160 ASD, 160 HC	rs-fMRI	HO Atlas	Functional Connectivity Matrix	CRF	SVM	Acc = 65 Sen = 65 Spe = 65
Tejwani et al., 2017	ABIDE	61 ASD, 46 HC	rs-fMRI	AAL Atlas	Graph Theory	–	Random SVM Cluster	Acc = 96.15
Tang et al., 2019	ABIDE	147 ASD, 146 HC	rs-fMRI	CC200 Atlas + DPARSF Pipeline	Two Different Features Sets	–	SVM	Acc = 61.1 Sen = 61.8 Spe = 60
Reiter et al., 2021	ABIDE	42 ASD, 37 HC	rs-fMRI	NA	Functional Connectivity Matrix	–	Different Classifiers	AUC = 97.75
Rane et al., 2017	ABIDE	306 ASD, 350 HC	rs- fMRI	NA	Functional Connectivity Matrix	CRF	RF	Acc = 73.75
Tolan and Isik, 2018	ABIDE 1	539 ASD, 573 HC	rs-fMRI	CPAC Pipeline	Feature Extraction (All Voxels Within Gray Matter Template Mask in MNI152 Space)	–	SVM	Acc = 62

(Continued)

TABLE 2 (Continued)

References	Dataset	Number of cases	Modalities	Atlas + Pipeline	Feature extraction	Feature selection	Classification	The best performance criteria (%)
Elnakieb et al., 2020	UMCD	79 Functional and 94 Structural Connectomes	rs-fMRI	NA	Graph Theory + Global, Nodal Measurements, and Gender Information	Relief Algorithm	Ensemble Learning	Acc = 67 pre = 0.67 Recall = 70
			DTI					Acc = 68 Pre = 0.73 Rec = 70
Crimi et al., 2017	NDAR	124 ASD, 139 HC	DTI	JH Atlas	Global and Local Features	Signal to Noise Ratio (S2n) Filter	SVM	Acc = 73 Sen = 70 Spe = 76
Jahedi et al., 2017	ABIDE II	31 ASD, 23 HC	rs-fMRI	AAL Atlas	Connectivity Matrix	–	SVM	Acc = 72.34
			DTI sMRI					
Bhaumik et al., 2018	ABIDE	126 ASD, 126 HC	rs- fMRI	NA	Functional Connectivity Matrix	CRF	SVM	Acc > 90
	Clinical	42 ASD, 30 HC						
Savva et al., 2020	ABIDE	167 ASD, 205 HC	rs-fMRI	CCS Pipeline	Functional Connectivity Matrix	–	SVM	Different Results
Mathur and Lindberg,	ABIDE 1	403 ASD, 465 HC	rs-fMRI	HO Atlas + CPAC Pipeline	sFC, dFC, and Haralick Texture Features	–	SVM	–
Eill et al., 2019	ABIDE	Whole Dataset	rs-fMRI	AAL Atlas + DPARSF Pipeline	Pearson Correlation Coefficient, Graph Measures, and Mean Intensities Features	–	Adaboost	Acc = 66.08
Zhuang et al., 2018a	Clinical	46 ASD, 47 HC	sMRI	JH Atlas	Functional Connectivity Matrix Features	–	CRF	Acc = 92.5 Sen = 97.8 Spe = 87.2
			DWI rs-fMRI	HO Atlas				
Kazeminejad and Sotero, 2019	Clinical	19 ASD	t-fMRI	NA	Elastic Net Regression	–	RF	NA
	ABIDE	64 ASD	rs-fMRI					
[129]	ABIDE 1	816 Subjects	rs-fMRI	AAL Atlas + CPAC Pipeline	Graph Theoretical Metrics	Sequential Forward Floating Algorithm	SVM	Acc = 95 Sen = 97 Spe = 91
Song et al., 2019	ABIDE 1	119 ASD, 116 HC	rs-fMRI	AAL, CC200 Atlas + DPARSF Pipeline	Community Pattern Quality Metrics Features	–	LDA, KNN	Acc = 75 Prec = 76.07 Rec = 71.67
	ABIDE II	97 ASD, 117 HC						
Cordova et al., 2020	Clinical	64 ASD, 66 ADHD, 28 HC	rs-fMRI	NA	43 Executive Functions (EF)	–	Functional Random Forest (FRF)	Different Results
Sadeghi et al., 2017	Clinical	29 ASD, 31 HC	sMRI	Different Atlas	Graph Theory + Different Features	Statistical Analysis	SVM	Acc = 92
		20 ASD, 20 HC	t-fMRI					
Zhang L. et al., 2020	ABIDE 1	21 ASD, 26 HC	rs-fMRI	AAL Atlas + DPARSF Pipeline	Fast Entropy Algorithm + Important Entropy	–	SVM	AUC = 62
Shi et al., 2020	ABIDE 1	59 ASD, 46 HC	rs-fMRI	AAL Atlas + DPARSF Pipeline	Function Connectivity + Minimum Spanning Tree (MST)	–	SVM	Acc = 86.7 Sen = 87.5 Spec = 85.7
Richards et al., 2020	ABIDE 1	437 ASD, 511 HC	sMRI	–	Computing the Brain Asymmetry with The BrainPrint + Asymmetry Values	–	LR Models	NA
Payabvash et al., 2019	Clinical	14 ASD, 33 HC	MRI, DTI	DK Atlas	Different Features	–	Naïve Bayes, RF, SVM, NN	Acc = 75.3 Sen = 51.4 Spec = 97.0
Huang H. et al., 2019	ABIDE	45 ASD, 47 HC	rs-fMRI	AAL Atlas	Modified Weighted Clustering Coefficients	*T*-test and SVM-RFE	Multi-Kernel Fusion SVM	Acc = 79.35 Sen = 82.22 Spec = 76.60
Huang et al., 2020a	ABIDE I	505 ASD, 530 HC	rs-fMRI	CC200 Atlas + CPAC Pipeline	Functional Connectivity	Graph-Based Feature Selection	MMoE Model	Acc = 68.7 Sen = 68.9 Spec = 68.6
Jung et al., 2019	ABIDE,	86 ASD, 83 ADHD, 125 HC	sMRI, rs-fMRI	DK Atlas	Functional Connectivity	Univariate *T*-test and Multivariate SVM-RFE	SVM	Acc = 76.3 Sen = 79.2 Spec = 63.9

(Continued)

TABLE 2 (Continued)

References	Dataset	Number of cases	Modalities	Atlas + Pipeline	Feature extraction	Feature selection	Classification	The best performance criteria (%)
DSouza et al., 2019	ABIDE	24 ASD, 35 HC	rs-fMRI	AAL Atlas	Mutual Connectivity Analysis with Local Models (MCA-LM)	Kendall's τ Coefficient	RF and AdaBoost	Acc = 81
Devika and Oruganti, 2021	ABIDE II	23 ASD, 15 HC	rs-fMRI	AAL Atlas + AFNI Pipeline	Functional Connectivity	ANOVA F-Score	SVM	Acc = 80.76
Ahammed et al., 2021	ABIDE 1	74 ASD, 74 HC	fMRI	DPARSF, CCS Pipeline	Bag-of-Feature (BoF) Extraction	–	SVM	Acc = 81 Sen = 81 Spec = 86
Yap and Chan, 2020	ABIDE	70 ASD, 74 HC	fMRI	NA	Functional Connectivity	Elastic SCAD SVM	SVM	Acc = 90.85 Sen = 90.86 Spec = 90.90
Wang et al., 2019c	ABIDE	250 ASD, 218 HC	rs-fMRI	AAL Atlas + CPAC Pipeline	Functional Connectivity + Low-Rank Representation Decomposition (maLRR)	–	KNN, SVM	Acc = 73.44 Sen = 75.79 Spec = 69.52
Karampasi et al., 2020	ABIDE	399 ASD, 472 HC	rs-fMRI	CC200 Atlas + CPAC Pipeline	Feature Extraction (Static FC, Demographic Information, Haralick Texture Features, Kullback-Leibler Divergence)	Feature Selection Algorithms (RFE-CBR, LLCFS, InfFS, mRMR, Laplacian Score)	SVM, KNN, LDA, Ensemble Trees	Acc = 72.5 Sen = 94 Spec = 64.7
Graña and Silva, 2021	ABIDE	408 ASD, 476 HC	rs-fMRI	CPAC Atlas	5 Methods for Functional Connectivity Matrix Construction	6 Feature Extraction/ Selection Approaches	9 Classifiers	–
Yamagata et al., 2019	Clinical	30 Pairs of Biological Siblings	rs-fMRI	Social Brain Connectome Atlas	Functional Connectivity	Sparse LR (SLR)	Bootstrapping Approach	Acc = 75 Sen = 76.67 Spec = 73.33
Conti et al., 2020	Clinical	26 ASD, 24 CAS, 18 HC	sMRI	–	Feature Extraction	Statistical Analysis	SVM	AUC = 73
Deshpande et al., 2013	Clinical	15 ASD, 15 HC	Task-fMRI	–	Functional Connectivity + Effective Connectivity	–	RCE-SVM	Acc = 95.9 Sen = 96.9 Spec = 94.8
Kazeminejad and Sotero, 2020	ABIDE 1	–	rs-fMRI	CC200, AAL Atlas + CPAC Pipeline	Graph Extraction + Feature Extraction	PCA	MLP	Different Results
Song et al., 2019	ABIDE	119 ASD, 116 HC	rs-fMRI	AAL Atlas + DPARSF Pipeline	Resting-State Functional Network Community Pattern Analysis	RFE	LDA	Acc = 74.86 Prec = 76.07 Recall = 71.67
Tang et al., 2019	ABIDE	42 ASD, 37 HC	rs-fMRI	–	Functional Connectivity + Joint Symmetrical Non-Negative Matrix Factorization (JSNMF)	–	SVM	AUC = 97.75
Mhiri and Rekik, 2020	ABIDE	245 ASD, 272 NC	rs-fMRI	DPARSF Pipeline	Different Features	NAG-FS	SVM	Acc = 65.03
Itani and Thanou, 2021	ABIDE 1	201 ASD, 251 HC	rs-fMRI	AAL Atlas + CPAC Pipeline	Graph Construction + Graph Signal Processing (GSP)	Fukunaga-Koontz Transform (FKT)	DT	Acc = 75
Zhan et al., 2021	ABIDE 1	133 ASD, 203 HC	rs-fMRI, sMRI	–	Functional Connectivity	Statistical Analysis	Sparse LR	Acc = 82.14 Sen = 79.70 Spec = 83.74
	ABIDE II	60 ASD, 89 HC						
Wismüller et al., 2020	ABIDE II	24 ASD, 35 HC	rs-fMRI	AAL Atlas	large-scale Extended Granger Causality (lsXGC)	Kendall's Tau rank correlation coefficient	SVM	Acc = 79
Deshpande et al., 2013	Clinical	15 ASD, 15 HC	fMRI	NA	Functional Connectivity, Effective Connectivity, and Fractional anisotropy (FA) From DTI, Behavioral Scores	Recursive Cluster Elimination	SVM	Acc = 95.9
Jiao et al., 2010	Clinical	22 ASD, 16 HC	MRI	Cortical Atlas	Thickness and Volume-Based Features	Surface-Based Morphometry	Different Classifiers (SVM,FT, LMT)	Acc = 87 Sen = 95 Spe = 75
Ecker et al., 2010b	Clinical	22 ASD, 22 HC	MRI	NA	GLM, Different Features	RFE-SVM	SVM	Spe = 86 Sen = 88
Chen et al., 2013	ABIDE	126 ASD, 126 HC	rs-fMRI	NA	Pearson Correlation Matrix, Connectivity Measures	PSO-SVM	SVM -RFE	Acc = 66 Sen = 60 Spe = 72

(Continued)

TABLE 2 (Continued)

References	Dataset	Number of cases	Modalities	Atlas + Pipeline	Feature extraction	Feature selection	Classification	The best performance criteria (%)
Uddin et al., 2011	ABIDE	24 ASD, 24 HC	sMRI	NA	Multivariate Statistical Pattern, Morphological Feature	NA	SVM	Acc = 80
Ingalhalikar et al., 2011	Clinical	45 ASD, 30 HC	DTI	EVE	FA (Fractional Anisotropy), MD Mean diffusivity, Anatomical ROI's	Signal-To-Noise (s2n) Ratio Coefficient Filter	SVM	Spe = 84 Sen = 74
Varol et al., 2012	Clinical	81 ASD, 50 HC	MRI	NA	Feature Extraction [Voxelwise Tissue Density Maps For GM, WM, and ventricles (VN)]	Welch's *T*-test	SVM	Acc = 73.28 Sen = 71.6 Spe = 76
Murdaugh et al., 2012	Clinical	13 ASD,15 HC	fMRI	NA	Functional ROIs, Functional Connectivity, Seed-Based Connectivity	*T*-test	Logistic regression	Acc > 96.3
Bloy et al., 2011	Clinical	23ASD,22 HC	MRI	NA	Orientation Invariant Features of Each ROI's Mean FOD	PCA	SVM	Acc = 77
Giuliano et al., 2013	Clinical	76 ASD,76 HC	sMRI	NA	Sequences Of The Intensity Values Of The GM Segments	SVM-RFE	SVM	Sen = 82 Spe = 80
Deshpande et al., 2013	Clinical	15 ASD, 15 HC	Task-fMRI	NA	Functional Connectivity, Effective Connectivity	NA	RCE-SVM	Acc = 95.9 Sen = 96.9 Spec = 94.8
Ecker et al., 2010a	Clinical	20 ASD, 20 HC	MRI	NA	Morphological Parameters Including Volumetric and Geometric Features	NA	SVM	Sen = 90 Spe = 80
Li et al., 2012	Clinical	10 ASD,10 HC	DTI	JHU-DTI-MNI	Brain Connectivity Network	Network Regularized SVM-RFE	SVM	Acc = 100
Bryant et al., 2012	Clinical	31 Klinefelter syndrome, 8 XYY Syndrome 75 HC	sMRI	NA	Statistical Parametric Mapping [Gray Matter Volume (TGMV) A Volume (TWMV) Measures]	RFE	SVM	NA
Vigneshwaran et al., 2013	Clinical, ABIDE	79 ASD,105 HC	MRI	NA	Voxel Locations of VBM Detected Brain Region	*T*-test	PBL-McRBFN	Acc (Mean) = 70 Sen (Mean) = 53 Spe (Mean) = 72
Sato et al., 2013	Clinical	82 ASD, 84 HC	sMRI	NA	Inter-Regional Thickness Correlation (IRTC) Using Pearson Correlation Between the Cortical Thicknesses of Each Region.	NA	Support Vector Reression	NA
An et al., 2010	Clinical	DTI Data: 5 b0 iImages, followed by 30 Diffusion Weighted Images, Child Control dataset	fMRI DTI	Brodmann	Fiber Connectivity Feature, ROIs Extraction, Functional Connectivity Information	NA	mv-EM	Max Percent Error: mv-EM: 8.55
Sadato and Tanabe, 2012	Clinical	21 ASD,21HC	fMRI	NA	Neural Substrates And Inter-Individual Functional Connectivity	*T*-test	NA	Acc = 74.2∓1.9
Filipovych et al., 2012	BLSA	17 MCI (mild cognitive impairment)	MRI	NA	Tissue Density Maps, Top-Ranked Features Wavelet Decomposition Level	Wavelet-Based Data Compression	JointMMCC	Different Results
Calderoni et al., 2012	Clinical	38 ASD, 38 HC	sMRI	NA	Volumetric Variables (GM, WM, CSF, TIV),	SVM-RFE, *T*-test	SVM	AUC = 80
Jiao et al., 2011	Clinical	13 ASD	MRI	NA	Regional Cortical Thicknesses And Volumes	NA	Three Decision-Tree-Based Models, SVM, logistic Model Tree	Acc > 80 Spe > 34 Sen > 92
Nielsen et al., 2013	ABIDE	447 ASD, 517 HC	rs-fMRI	NA	Functional Connectivity From a lattice of ROIs Covering The Gray Matter	NA	leave-one-out	Acc = 60 Spe = 58 Sen = 62

(Continued)

TABLE 2 (Continued)

References	Dataset	Number of cases	Modalities	Atlas + Pipeline	Feature extraction	Feature selection	Classification	The best performance criteria (%)
Jiao and Lu, 2011	Clinical	22 ASD, 16 HC	MRI	NA	Using Surface-based morphometry For Cortical Features (Average thickness, Mean Curvature, Gaussian curvature, Folding index, Curvature index)	NA	SVM,FT,LMT	Acc (SVM) = 74 Acc (FT) = 76 Acc (LMT) = 76
Retico et al., 2016a	Clinical	76 ASD, 76 HC	sMRI	NA	GM Volumes	RFE	SVM	AUC = 82
Retico et al., 2016b	Clinical	41 ASD, 40 HC	sMRI	NA	Regional Features	–	SVM	AUC = 81
Subbaraju et al., 2017	ABIDE	505 ASD, 530 Neurotypical Subjects	rs-fMRI	NA	Spatial Feature-based Detection Method (SFM) (Mean Connectivity Matrices, Discriminative Log-variance Features)	Feature Selection Based on top m Signals	SVM	Acc = 95
Gori et al., 2016	Clinical	41 ASD, 40 HC	sMRI	NA	ROI Features	–	SVM	AUC = 74
Lu et al., 2015	Clinical	35 ASD, 51 TD, 39 No Known Neuropsychiatric Disorders	fMRI	NA	Individual Difference Measures in BOLD Signals	–	LR	Sen = 63.64 Spe = 73.68
Chen et al., 2016	ABIDE	112 ASD, 128 HC	rs-fMRI	NA	Functional Connectivity Values	F-score Method	SVM	Acc = 79.17
Wee et al., 2014	NDAR	58 ASD, 59 HC	sMRI	NA	Regional and Interregional Morphological Features	*T*-test mRMR	SVM	Acc = 96.27 AUC = 99.52
Zhou et al., 2014	ABIDE	127 ASD, 153 TD	sMRI	NA	Quantitative Imaging Features (Regional Gray Matter and Cortical Thickness Volumes)	mRMR	SVM	Acc = 70

Pipeline methods

The pipelines are a preprocessed version of ABIDE data using standard preprocessing procedures, which researchers can use to avoid the problems of variations in the output between different studies as a result of preprocessing. The most popular ABIDE pipelines include neuroimaging analysis kit (NIAK), data processing assistant for rs- fMRI (DPARSF), the configurable pipeline for the analysis of connectomes (CPAC), and connectome computation system (CCS) (Khodatars et al., 2021).

Feature extraction

Representing data that allows ML algorithms to reason about them is the key to any related research. If this is not done, high performance cannot be achieved. Most commonly used feature extraction schemes for fMRI and sMRI are statistical, texture, morphological, non-linear, graph, functional connectivity, and structural connectivity schemes.

Statistical features

Autism spectrum disorder is typically detected with MRI modalities using statistical features, the most straightforward group of features. Despite their simplicity, these features are usually informative and can also serve as a benchmark for evaluating other methods of feature extraction as well. Additionally, the process of extracting these features is not time-consuming in comparison to other methods. However, these methods do not reveal non-linear or subtle patterns in data. Using statistical features for ASD diagnosis, Dekhil et al. (2019) extracted various statistical features from MRI data and then applied KNN and SVM algorithms in the classification step. The authors reported 81% accuracy.

Texture features

As a group of features, spatial patterns form an indispensable group, possibly the most important group, since the cognitive system of the human is mostly dependent on them. Gray-level co-occurrence matrix (GLCM) (Jafarpour et al., 2012) feature extraction is one of the most widely used methods in various research studies (Thomas and Chandran, 2018) among various textures-based features. Haweel et al. (2020) presented an ASD diagnostic method based on MRI data. Texture features and the RFE technique were used in the feature extraction and feature selection steps. Then, the authors used the RF technique for classifying features and reached an accuracy of 72%. In another study, scholars used various methods, such as Haralick, in the feature extraction step from sMRI data. Then, the authors tested different feature selection methods and reached an accuracy of 72.5%.

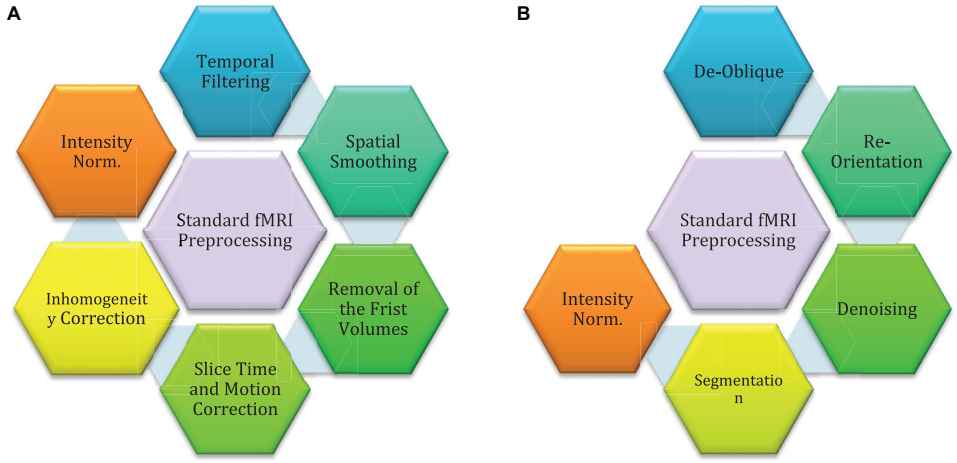

FIGURE 3
Standard preprocessing methods for MRI neuroimaging modalities: **(A)** preprocessing for fMRI data, **(B)** preprocessing for sMRI data.

Morphological features

Morphological operation is an important feature extraction technique frequently used in image processing (Usha and Perumal, 2019). In these methods, features are extracted from the appearance and shape of the image. Morphological operation is often used to process binary images, but they can also be used for gray and color-level images (Gupta et al., 2019). Morphological features are also commonly used for diagnosing brain diseases from sMRI modalities. Zheng et al. (2019) proposed the idea of ASD diagnosis using morphological features. After feature extraction, RFE and SVM were tested for feature selection and classification, respectively. An accuracy of 78.63% was obtained.

Non-linear features

A non-linear characteristic of biological data is emphasized when considering non-linear features. The performance of CADS for ASD is significantly enhanced through the use of these features (Anand and Sahambi, 2010). In reference (Mellema et al., 2020), non-linear-based features of likelihood are used to detect autism using MRI neuroimaging methods. Entropies are one of the most important non-linear methods that are widely used to extract features from signals and brain images (Georgiadis et al., 2008). Functional imaging modalities are non-linear and chaotic, which has led researchers to use entropy-based non-linear features to diagnose brain disorders (Saritha et al., 2013; Wang et al., 2022). Zhang L. et al. (2020) introduced a novel ASD diagnostic method using fMRI data and a new entropy method. This study initially used fast entropy for feature extraction from preprocessed fMRI data. Then, they used the SVM algorithm for feature classification and obtained satisfactory results.

Graph features

This group of features is highly relevant to the analysis of MRI data. Graph-based features are derived first by shaping the data into a graph, and then, from the constructed graph, local and global features are extracted (Lee and Xue, 2017). Researchers have explored graph features to diagnose ASD using fMRI data in many studies. Bi et al. (2019) employed rs-fMRI from the ABIDE database for ASD diagnosis using graph and genetic-evolutionary random SVM cluster (GERSVMC) for feature extraction and classification steps, respectively, and obtained an accuracy of 62%. Saad and Islam (2019) presented an ASD diagnostic method based on graph features in another study. After feature extraction *via* the graph method, PCA and SVM techniques were used for feature reduction and classification, which resulted in an accuracy of 75% for ASD diagnosis.

Connectivity matrix

In order to process sMRI and fMRI neuroimaging images, feature extraction methods based on connectivity matrix methods are typically employed (Zeng et al., 2018; Yeh et al., 2021). Such features provide information about the brain's structure and function. The functional connectivity matrix (FCM) (Zhou and Wang, 2007; Yan and Zhang, 2015) and structural connectivity matrix (SCM) (Yang et al., 2016; Ma et al., 2019) are the measures employed for fMRI and sMRI modalities, respectively. Connectivity features are mostly used in diagnosing brain disorders. **Table 2** and **Supplementary Table 1** outline studies on ASD diagnosis from MRI modalities using various AI techniques. **Table 2** shows that connectivity methods are most frequently used for feature extraction from MRI modalities. Liu W. et al. (2020) used dynamic functional connectivity (DFC) in the feature extraction step of rs-fMRI data. The feature selection step was also conducted by the MTFS-EM

method. Finally, they used the SVM method for classification and obtained an accuracy of 76.84%. In another study, Mathur and Lindberg, utilized DFC and static functional connectivity (SFC) in the feature extraction step. Then, the SVM was tested for connectivity-based classification of features. Authors could finally obtain satisfactory results for ASD diagnosis using connectivity features.

Feature reduction/selection methods

It has been shown that increasing the number of extracted features can help algorithms to represent data in a more meaningful and robust way; however, the curse of dimensionality (Fodor, 2002) may cause it to backfire and reduce performance. Several methods for reducing dimensionality and selecting features have been proposed to prevent this from occurring. In addition, these methods are widely used to increase the performance of CADS for detecting autism spectrum disorders. Several methods have previously been used in research papers, including principal component analysis (PCA) (Wold et al., 1987), recursive feature elimination (RFE) (Yan and Zhang, 2015), *T*-test (Zhou and Wang, 2007), autoencoder (AE) (Yang et al., 2016), conditional random forest (CRF) (Ma et al., 2019), Chi-squared (Ye and Yang, 2010), and least absolute shrinkage and selection operator (LASSO) (Muthukrishnan and Rohini, 2016). The following is a brief description of these methods.

Principal component analysis

Principal component analysis is arguably the most common dimensionality reduction method (Wold et al., 1987). It works by finding and representing data by the principal components, i.e., the vectors that preserve the most data variance. One of the benefits of PCA is its ability to find a minimal number of features required to preserve a specified variance ratio (Wold et al., 1987). Principal component analysis (PCA) is one of the most popular feature reduction techniques in medical applications and has also been used in ASD diagnosis research (Zhao F. et al., 2017; Soussia and Rekik, 2018; Saad and Islam, 2019; Kazeminejad and Sotero, 2020).

Recursive feature elimination

Recursive feature elimination is more of a wrapper-type algorithm, meaning that it is applied to a classification algorithm to find the best subset of features. As the name explains, this algorithm works by eliminating features one by one to reach the optimal number. First, a classification algorithm is trained on the dataset, ranking feature importance's. The least important feature is then eliminated and repeated until the number of remaining features matches the desired number (Yan and Zhang, 2015). Haweel et al. (2020) proposed a novel ASD diagnostic method using the GLM feature extraction technique. After feature extraction from MRI data, the RFE technique was used for feature reduction. The RF method was also tested in the classification step with an accuracy of 72%.

T-test

To find the best set of features, *T*-test calculates a score for each feature, then ranks them based on that score and picks the top features as selected ones. The score shows whether the values of a feature for a class are significantly different from those for another class by calculating the mean and standard division (STD) of each feature in each class (Zhou and Wang, 2007). A new ASD diagnostic method from MRI data was introduced by Sartipi et al. (2018). First, the graph technique was used for feature extraction from sMRI modalities. Then, they applied the *T*-test and SVM algorithms for the feature selection and classification steps and acquired an accuracy of 75%.

Chi-squared

Chi-Square is suitable when the features are categorical, and the target variable is also categorical, such as classification. Chi-Squared measures the degree of association between two variables; thus, features that connect with the targets can be picked (Ye and Yang, 2010). When the features are numerical, we can use a *T*-test, or Chi-Square can be used for the numerical variable by discretizing them (Ye and Yang, 2010). In reference (Dekhil et al., 2019). The authors proposed a new ASD diagnostic method using various ML techniques from MRI data. Various methods were used for feature extraction. Then, the Chi-squared method was tested for the feature selection step. Next, the LR classification algorithm was applied, which resulted in a promising performance.

Least absolute shrinkage and selection operator

Least absolute shrinkage and selection operator is mainly a regression method; however, this algorithm can also be used for feature selection (Muthukrishnan and Rohini, 2016). Notably, linear regression with L1 regularization is called Lasso. After training, the lasso assigns a weight to each feature for the regression (Muthukrishnan and Rohini, 2016). Using these weights, there are two methods to pick the best features, first, pick the K highest valued weights; second, pick all the weights which have a value higher than a specified threshold (Muthukrishnan and Rohini, 2016). Fredo et al. (2018) proposed a new ASD diagnostic method based on Hons and Lon features. Their paper used LASSO and SVM methods for feature selection and classification. They reported an accuracy of 81%.

Classification methods

This section discusses the various classification algorithms used in CADS for ASD. As mentioned earlier, classification is the last step in a CADS based on ML methods. Support

vector machine (SVM) (Noble, 2006; Suthaharan, 2016), linear discriminant analysis (LDA) (Zhang et al., 2007), k-nearest neighbor (KNN) (Liao and Vemuri, 2002), and random forest (RF) (Oshiro et al., 2012) are arguably among the most popular methods used in CADS created for ASD. **Table 2** and **Supplementary Table 1** show the classification algorithms used for ASD detection. A summary of classification algorithms used for automated detection of ASD are presented below.

Support vector machine

Support vector machines are among the oldest classification and has been widely used in many applications (Noble, 2006; Suthaharan, 2016). SVM tries to find the best hyperplane to separate data points; however, it only needs the dot product between every two data points (Noble, 2006; Suthaharan, 2016). Consequently, to transform data into another space, only a function that gives the dot product of two points in that space would suffice; this is also named kernel trick and is used widely in other fields. Using an appropriate kernel, SVM can usually yield high classification performances (Noble, 2006; Suthaharan, 2016).

Random forest

Random forests are an ensemble learning-based method proposed to make the decision trees robust to outliers (Oshiro et al., 2012). The basic idea is to train many trees and determine the final output based on voting among their outputs. To make the final results robust, each tree is trained only on a fraction of the data, and also each tree sees a fraction of all features. The picked ratio for both of these is the square root of the available number.

Linear discriminant analysis

Used as a tool for dimension reduction, classification, and data visualization (Zhang et al., 2007). It is simple and robust and yields interpretable classification results (Zhang et al., 2007). It works by dividing the data space into K disjoint regions that represent all the classes; then, in the testing phase, the label is determined by finding the region in which the data belongs. LDA can be used as the first benchmarking baseline before other, more complicated ones are employed for real-world classification problems (Zhang et al., 2007).

K-nearest neighbor

This classifier is among the simplest yet efficient algorithms; its main idea is to assign the label of each data point based on the label of those closest (Liao and Vemuri, 2002). Consequently, there is no training phase; however, for each test subject, the distance to all training points must be calculated, which scales with the size of the dataset; thus, this method is not applicable to enormous datasets. After finding the closest points, the final label is determined using a voting scheme (Liao and Vemuri, 2002).

Challenges in detecting autism spectrum disorder with magnetic resonance imaging neuroimaging modalities and artificial intelligence techniques

This section introduces the challenges facing ASD detection from MRI neuroimaging modalities and AI techniques. The challenges mentioned in this section cover dataset limitations, lack of access to multimodal datasets, AI techniques, and suitable hardware resources. They are briefly described below.

Unavailable magnetic resonance imaging neuroimaging datasets with different autism spectrum disorder patient

All datasets available involve two classes of ASD and control fMRI or sMRI modalities (Heinsfeld et al., 2018; El-Gazzar et al., 2019; Felouat and Oukid-Khouas, 2020). However, there are different types of ASD, and this poses a serious obstacle for researchers in AI wishing to develop systems that can detect different types of disorders. Datasets with different types of ASD can help pave the way for accurate diagnosis of various types of ASD.

Unavailable multi-modalities datasets for autism spectrum disorder diagnosis

In medical research, specialists have shown that neuroimaging multimodalities can effectively improve diagnosis of brain disorders. Neuroimaging modality fusion is one of the newest methods for diagnosing brain disorders such as ASD (Jones et al., 2011), SZ (Bora et al., 2011), and ADHD (Sibley et al., 2022). Physicians usually use MRI data with other neuroimaging modalities to diagnose brain disorders. To diagnose neurological and mental disorders, fMRI-MEG (Kober et al., 1993), MRI-PET (Loeffelbein et al., 2012), and EEG-fMRI (Valdes-Sosa et al., 2009) are the most important multimodalities. Unfortunately, the neuroimaging multimodalities datasets are not available for studies on ASD diagnosis. Such datasets might lead to practical and interesting studies in ASD diagnosis.

Challenges in artificial intelligence algorithms in diagnosing autism spectrum disorder

Computer-aided design systems based on ML algorithms are highly time-consuming and complex to design. However, if the

appropriate algorithms are selected, it can accurately diagnose ASD (Iglesias et al., 2017; Khosla et al., 2019; Hiremath et al., 2020; Leming et al., 2020, 2021). DL methods automatically perform the steps from feature extraction to classification. By using intelligent feature extraction, DL eliminates the need for supervision on features, which may reduce the performance of a CADS based on DL compared to ML. Therefore, when ML methods are combined with DL, promising results can be obtained in CADS for the diagnosis of ASD.

Challenges in hardware's

The lack of access to appropriate hardware resources is another problem encountered by researchers in the field of automated ASD detection. ASD detection datasets that are available publicly, such as ABIDE, have a lot of data; this poses many challenges for storing and processing these datasets on ordinary computers. In contrast, research in CAD implementation on cloud servers has not been seriously conducted to eliminate hardware resource problems. As a result, cloud servers are not yet extensively used for data storage and processing. Recently, some DL models called deep compact CNN models have been introduced to be implemented on hardware systems with limited resources (Zhang Z. et al., 2020). Deep compact-size CNN models require fewer hardware sources than other CNN methods (Tian et al., 2018; Wong et al., 2019). Some deep compact-size CNN methods include FBNetV3 (Srinivas et al., 2019), MobileNet (Michele et al., 2019), and TinyNet (Wu et al., 2018).

Discussion

This paper presents and compares the research about automated ASD detection with MRI neuroimaging modalities and AI methods. First, this section comprehensively compares the conducted studies on ASD detection using ML and DL techniques. In subsection one, the number of studies conducted annually in ASD detection from MRI neuroimaging modalities using different ML and DL techniques is presented. In subsection two, the MRI datasets employed in studies on the automated diagnosis of ASD using ML and DL techniques are compared. In subsection three, the number of MRI studies conducted annually on ASD detection from MRI neuroimaging modalities is discussed. The employed atlas in ML and DL studies for ASD detection is introduced in subsection four. Finally, section five discusses MRI pipeline techniques in the diagnosis of ASD research using ML and DL methods. Ultimately, different classification algorithms for ML and DL-based diagnosis of ASD are compared.

Comparison between the numbers of papers published each year for machine learning and deep learning research

This section presents the number of published papers annually on ASD detection using AI techniques. Studies on the ASD detection from MRI modalities and ML and DL techniques began in 2017. **Table 2** represents the papers on ASD detection in MRI neuroimaging modalities using ML methods. In addition, articles in ASD detection in MRI neuroimaging modalities using DL techniques are introduced in **Supplementary Appendix A**. **Figure 4** illustrates the number of papers published annually on ML and DL techniques for ASD detection.

As demonstrated in recent years, researchers' interest in using DL architectures has significantly grown compared to

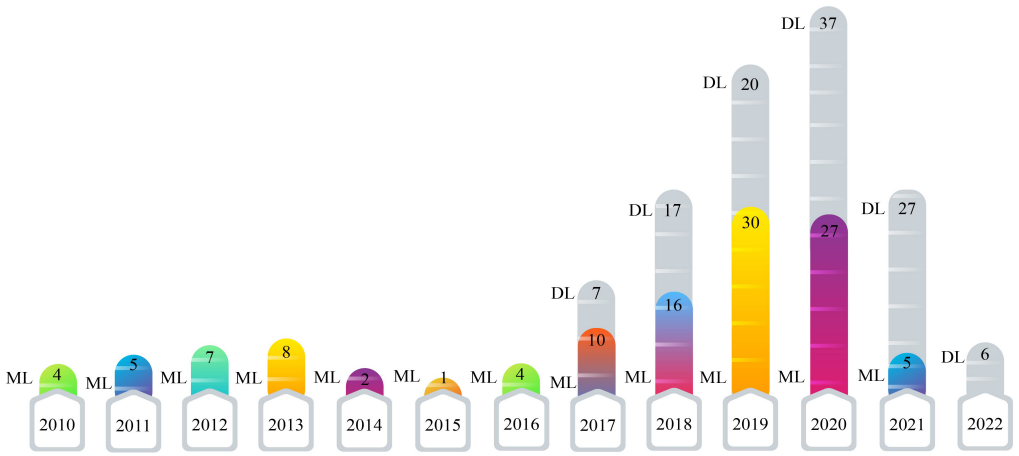

FIGURE 4
Shows the number of papers published in ASD detection using ML and DL methods.

ML techniques. According to Figure 4, DL models are used more in studies on the automated diagnosis of ASD with MRI modalities than ML models. Therefore, implementing CADS based on DL techniques is promising for developing applied software for ASD detection with MRI neuroimaging modalities in the future. For automated diagnosis of ASD with MRI modalities, various datasets are proposed in ABIDE. Besides, various toolboxes are available for the implementation of different DL models. These reasons are the foundation for many studies on the automated diagnosis of ASD using DL models.

Comparison between the numbers of datasets used in the machine learning and deep learning research

As stated in the neuroimaging modalities section, limited datasets are accessible. ABIDE is the most important dataset available in this field, which includes two datasets, ABIDE I and ABIDE II. Figure 5 demonstrates the types of datasets employed in the automated ASD diagnostic research using DL and ML techniques.

It can be noted from Figures 5A,B that a greater number of ABIDE datasets are employed in studies on the automated diagnosis of ASD. The major reason for the wide use of this dataset in various studies on the automated diagnosis of ASD is the availability of many subjects and different MRI modalities.

Comparison between the numbers of neuroimaging modalities used in the machine learning and deep learning research

The different structural and functional MRI neuroimaging modalities and ML and DL methods play an essential role in automated ASD detection. Table 2, reports studies on automated ASD detection using ML techniques and different MRI neuroimaging modalities have been presented. Moreover, Supplementary Table 1 discusses ASD detection using DL techniques. Figures 6A,B describes the annual research carried out to detect automated ASD using sMRI and fMRI neuroimaging modalities.

As shown in Figures 6A,B, the rs-fMRI modalities are most used in studies on ASD detection using ML and DL methods. As mentioned earlier, ASD is a neurological disorder that negatively affects brain function. Accordingly, researchers have used rs-fMRI modalities most widely in studies on ASD detection using AI methods.

Comparison between the numbers of atlases used in the machine learning and deep learning research

In another part of Table 2 and Supplementary Table 1, the types of Atlases for MRI neuroimaging modalities have been provided. Atlases are considered an important preprocessing

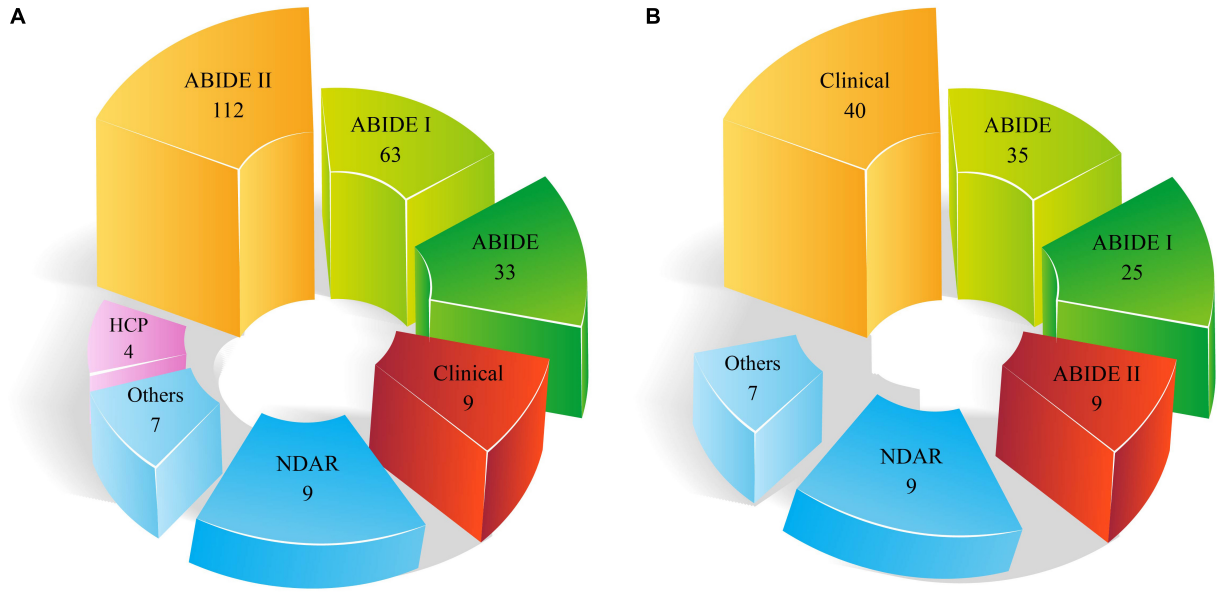

FIGURE 5
Number of datasets used for automated ASD detection. **(A)** DL and **(B)** ML methods.

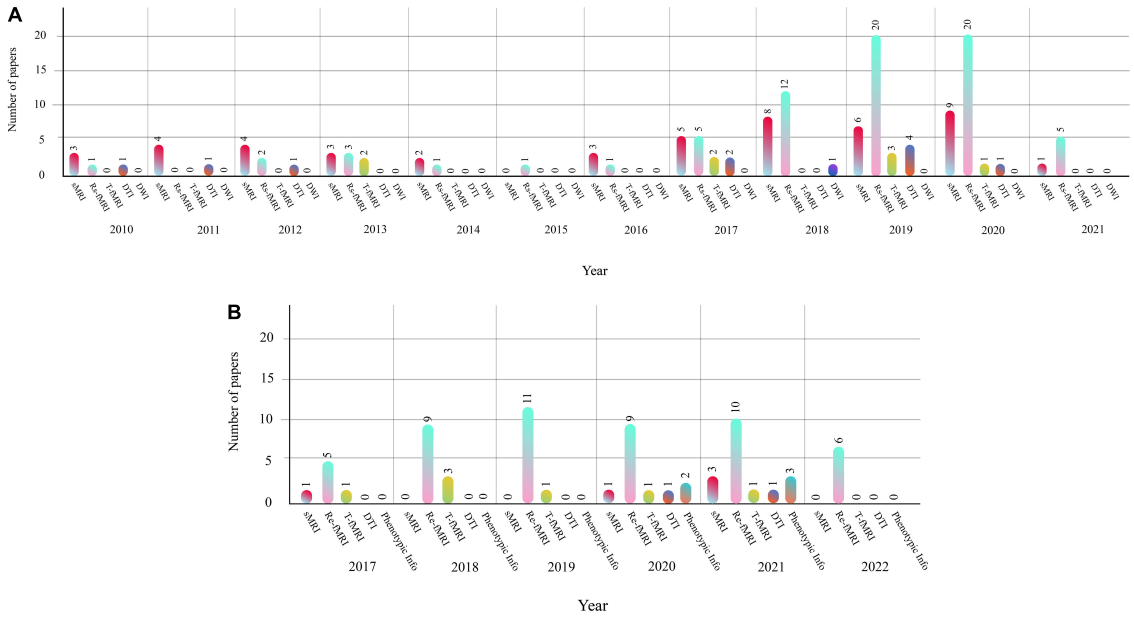

FIGURE 6
(A) Shows the number of MRI neuroimaging modalities used in the CADS based on ML methods. **(B)** Shows the number of MRI neuroimaging modalities used in the CADS based on DL methods.

step discussed in part of this section. The number of atlases employed in ML and DL research are described in Figure 7.

As shown in Figures 7A,B, the AAL atlas is most used in studies for ASD detection in MRI neuroimaging modalities using AI methods.

Comparison between the numbers of pipelines used in the machine learning and deep learning research

Pipelines play a significant role in preprocessing of MRI modalities. The pipelines employed in ASD data preprocessing are presented in Table 2 and Supplementary Table 1. The number of pipelines utilized in DL and ML research is shown in Figure 8. The results of the studies reveal that the CPAC pipeline is the most widely used.

Comparison between the numbers of classification methods in the machine learning and deep learning research

Classification is the last step of CADS with ML or DL methods. So far, various classification methods have been proposed in ML and DL, presented in Table 2 and Supplementary Table 1. The types of classification algorithms applied in CADS using DL and ML are depicted in Figure 9. As shown in this Figures 9A,B, it may be noted that the Softmax method is most used in DL architectures. In addition, SVM is the most widely applied in ML methods compared to other classification methods.

Future works

Lack of access to huge public datasets with various ASD disorders researchers is a big challenge. As mentioned in the introduction, autism has different types (Sparks et al., 2002), and the availability of datasets containing different types of ASD is of paramount importance for researchers. Hence, presenting MRI datasets of different types of autism disorder need to be addressed in future works. These datasets help researchers conduct more studies and compare their studies with other researchers on the automated diagnosis of ASD. As mentioned in previous sections, ABIDE is a free dataset available for researchers and consists of different cases and MRI modalities of ASD patients. But it does not have many cases of DTI modalities for the diagnosis of ASD. DTI modality is one of the popular methods in ASD detection. Publicly providing more datasets of this type of modality could increase research in the ASD diagnosis field using the DTI modality.

Another future work is to provide multimodal datasets, such as fMRI-EEG, for the diagnosis of ASD. In clinical studies (Cociu et al., 2017), it has been indicated that using multimodal neuroimaging, such as fMRI-EEG, plays a pivotal role in diagnosing ASD. In addition, providing datasets with combined

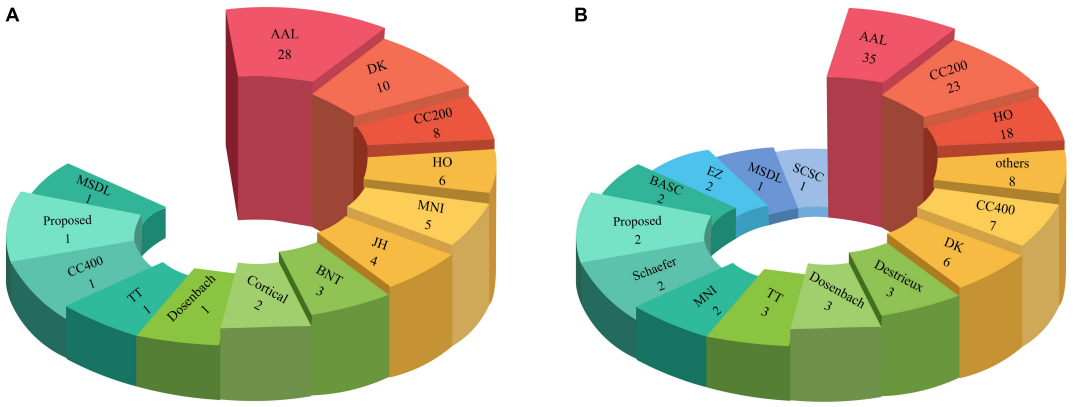

FIGURE 7
Number of Atlas used for ASD detection. **(A)** ML and **(B)** DL methods.

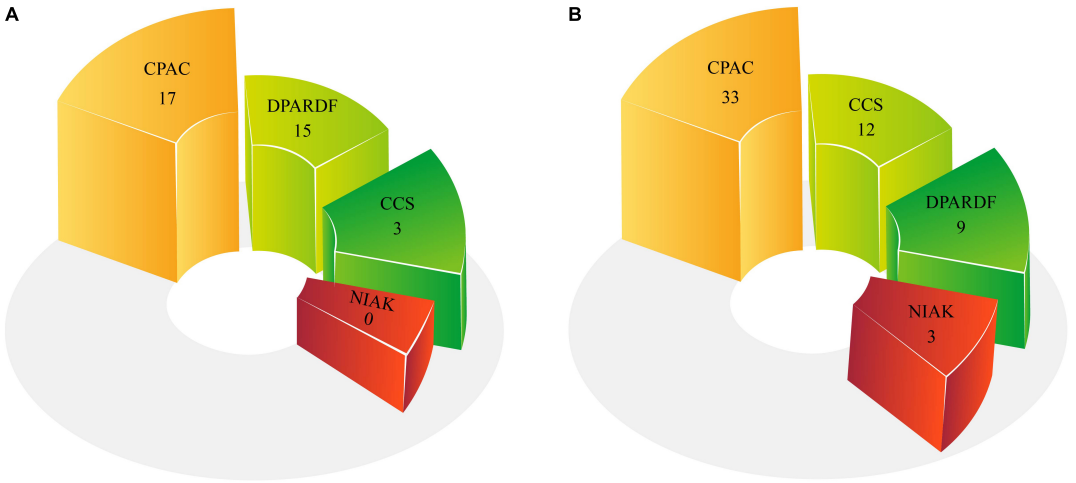

FIGURE 8
Number of pipelines used for ASD Detection: **(A)** ML and **(B)** DL methods.

modalities paves the way for new studies on the diagnosis of ASD using different AI methods.

Automated diagnosis of ASD with MRI using ML techniques can be the other future work. Various methods have been proposed for feature extraction from MRI data for the diagnosis of ASD, which are summarized in **Table 2**. According to **Table 2**, fuzzy-based feature extraction techniques have not been used in the diagnosis of ASD, and they can be introduced in future work. Fuzzy techniques are important in medical applications and allow researchers to develop software close to human logic (Chanussot et al., 1999; Davidson et al., 2001; Javed et al., 2013; Jiang et al., 2017; Meena and Agilandeeswari, 2020; Ullah et al., 2020). Hence, providing graph models based on fuzzy theory can be addressed in the future, leading to the accurate diagnosis of ASD with MRI modalities. Connectivity techniques are an essential feature extraction method for structural and functional neuroimaging modalities (Bhattacharya et al., 2006; Rowe et al., 2010; Smith et al., 2012; Gilson et al., 2018; Park et al., 2018; Zarghami and Friston, 2020). Proposing new feature extraction methods based on connectivity for structural and functional neuroimaging modalities is another field for future work. **Table 2** also indicates classification algorithms. In this section, fuzzy type 1 and 2 techniques can be used for data classification as future work on the diagnosis of ASD (Melin and Castillo, 2013, 2014; de Aguiar et al., 2017). Furthermore, in the future, graph theory-based classification methods can also be used to increase the performance of the CADS for automated diagnosis of ASD (Cai et al., 2018; Wu et al., 2020).

The reliability of AI models for medical diagnosis (Balagurunathan et al., 2021; Durán and Jongsma, 2021) poses another challenge for researchers, which needs to be

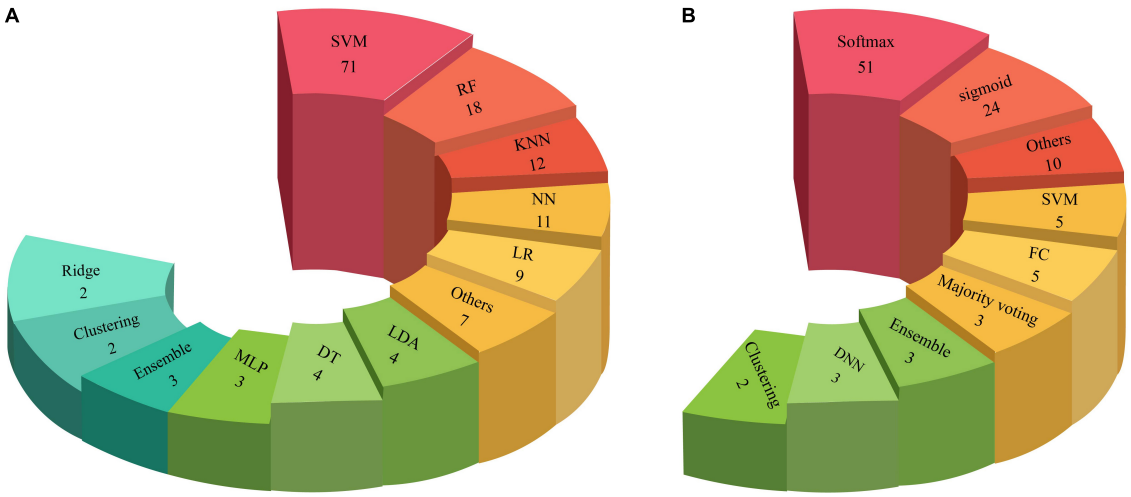

FIGURE 9
Number of classifiers used in CADS for ASD detection: **(A)** ML and **(B)** DL methods.

solved before these models are usable in real-life. There is more than one direction that contributes toward this end, such as designing test and validation protocols to ensure the validity of reported results, necessitating papers to include enough information to make results reproducible (such as protocols used in top-tier conferences such as NeurIPS) and also working on explainability and interpretability of models in addition to their performances (Afnan et al., 2021).

In **Supplementary Appendix (A)**, different studies on the automated diagnosis of ASD using MRI modalities and DL techniques is presented. It may be noted that conducted studies have used standard DL methods to diagnose ASD. In future works, graph theory (Zhang Z. et al., 2020; Ma et al., 2021), representation learning (Hamilton et al., 2017; Zhang et al., 2018), zero-shot learning (Wang et al., 2019d), Q-learning (Jang et al., 2019), attention learning (Li et al., 2018c), and advanced models of adversarial networks (Liu and Tuzel, 2016; Creswell et al., 2018) can be used for the automated diagnosis of ASD with MRI modalities.

Feature fusion technique is a new field in diagnosing different diseases, and many studies are being conducted in this field (Antropova et al., 2017; Fan et al., 2018; Hermessi et al., 2019; Liu et al., 2021; Wang et al., 2021b; Amemiya et al., 2022). The DL features can be extracted from MRI images for automated ASD detection. Ultimately, ML and DL features can be used to obtain high performance in the automated diagnosis of ASD.

Conclusion

Autism spectrum disorder is a neurological disorder with unknown symptoms that begins in childhood and cause problems in communication, social relationships, perception processing, and repetitive behaviors. In few studies, physicians have stated that ASD usually occurs due to genetic mutations or the inability of the fetus's brain cells to obey regular growth patterns during the first steps (Sparks et al., 2002; Brieber et al., 2007; Sato et al., 2012; Ecker et al., 2015; Hernandez et al., 2015).

Physicians use different ASD detection methods, among which different neuroimaging modalities are of paramount importance (Parisot et al., 2018; Mellema et al., 2019; Ronicko et al., 2020). Among different neuroimaging modalities, MRI-based functional and structural modalities are mostly used to diagnose ASD. sMRI and fMRI provide physicians with important information on the structure and function of the brain, respectively (Sserwadda and Rekik, 2021; Tummala, 2021). However, accurate diagnosis of ASD from sMRI and fMRI is sometimes time-consuming and challenging. Moreover, factors such as tiredness or different noises in MRI modalities may lead to clinicians' wrong diagnosis of ASD.

For this purpose, many studies are being conducted on the automated diagnosis of ASD using AI techniques, aiming to increase the performance of automated diagnosis of ASD. In general, studies on the automated diagnosis of ASD from MRI modalities using AI cover ML and DL methods. In few papers, researchers have conducted a review study in ASD detection based on DL (Khodatars et al., 2021) and ML (Brihadiswaran et al., 2019; de Belen et al., 2020; Hosseinzadeh et al., 2021; Kollias et al., 2021; Song et al., 2021; Tawhid et al., 2021) methods with different neuroimaging modalities.

This work is a comprehensive review of studies conducted on ASD detection using AI methods in different MRI neuroimaging modalities. First, AI-based CADS for ASD detection from different MRI neuroimaging modalities was introduced. Then, the steps of the CADS based on ML

algorithms for automated ASD detection in MRI neuroimaging modalities were studied. Also, in this section, papers on the automated ASD detection in MRI neuroimaging modalities using ML methods are summarized in **Table 2**. Previously, some authors of this study previously published a review paper about automatic ASD detection in different neuroimaging modalities using DL techniques (Khodatars et al., 2021), which is summarized in **Supplementary Table 1**.

The most critical challenges in ASD detection in MRI neuroimaging modalities and AI methods were presented in another section. Also, this section studied the most important challenges in the automated diagnosis of ASD using MRI modalities and AI techniques. The most important challenges in the diagnosis of ASD are the lack of access to public datasets with different MRI modalities, multimodal datasets, such as fMRI-EEG, AI algorithms, and hardware resources.

In the discussion section, first, the number of published annual papers on ASD detection using ML methods and DL techniques were discussed. Then, the number of datasets used in ML and DL studies was presented. In addition, the number of different MRI neuroimaging modalities with ML and DL methods used in annual studies in ML and DL was also indicated. Also, a comparison was made between different atlases used in MRI neuroimaging preprocessing for ASD detection. In another subsection, the number of pipelines in the preprocessing step of the MRI neuroimaging modalities for CADS based on various AI methods is also examined and compared. Finally, the number of classifier algorithms used in ML and DL studies for ASD detection was discussed.

In section 7, the future works for ASD detection in MRI neuroimaging modalities and AI methods were addressed. In this section, future works on MRI datasets for the diagnosis of ASD were first discussed. Then, future works on the diagnosis of ASD using AI techniques were addressed. Besides, future works on the automated diagnosis of ASD with MRI modalities were introduced. The final section also recommended the idea of using feature fusion for the diagnosis of ASD with MRI modalities in future works. Studies on ASD detection using AI techniques indicate that researchers will use the proposed methods in the future. The proposed methods are promising in developing real software for ASD detection using MRI modalities and help clinicians quickly diagnose ASD in the early stage.

Also, research on DL-based methods for the diagnosis of ASD has experienced significant attention in recent years. In standard mode, sMRI and fMRI data are recorded in 3D and 4D. However, in most papers, researchers have utilized 2D DL models to diagnose ASD using MRI neuroimaging modalities. Due to the high computational cost of 3D DL models for diagnosing ASD, there has been less research in this field. Providing 3D DL models based on quantization techniques reduces hardware resources and increases speed. Thus, DL models using quantization techniques (Liang et al., 2021) can be exploited to diagnose ASD in the future. Memory constraints are one of the research challenges of ASD diagnosis using MRI neuroimaging modalities. In medicine, cloud computing is one of the novel technologies to address storage and data processing issues (Chen and Ran, 2019). Using cloud computing in future work may lead to other valuable research in ASD diagnosis. In this way, MRI data is first sent to the cloud for storage. Next, the implementation of DL algorithms for the diagnosis of ASD can be carried out on their computing servers.

Author contributions

ASh, NG, PM, DS, RA, and UA contributed to conceptualization. ASh, SL, AK, JG, and ASu contributed to methodology. SL, AK, SS-A, SA, ASu, JG, RA, and UA contributed to validation. MJ, RA, DS, PM, and SA contributed to formal analysis. ASh, SS-A, SA, MK, MJ, and PM contributed to writing—original draft preparation. ASu, SS-A, SA, and MK contributed to writing—review and editing. All authors have read and agreed to the published version of the manuscript.

Funding

Open Access funding provided by the Qatar National Library.

Conflict of interest

The authors declare that the research was conducted in the absence of any commercial or financial relationships that could be construed as a potential conflict of interest.

Publisher's note

All claims expressed in this article are solely those of the authors and do not necessarily represent those of their affiliated organizations, or those of the publisher, the editors and the reviewers. Any product that may be evaluated in this article, or claim that may be made by its manufacturer, is not guaranteed or endorsed by the publisher.

Supplementary material

The Supplementary Material for this article can be found online at: https://www.frontiersin.org/articles/10.3389/fnmol.2022.999605/full#supplementary-material

References

Abdullah, A. A., Rijal, S., and Dash, S. R. (2019). Evaluation on machine learning algorithms for classification of autism spectrum disorder (ASD). *J. Phys. Conf. Ser.* 1372:012052.

Afnan, M. A. M., Liu, Y., Conitzer, V., Rudin, C., Mishra, A., Savulescu, J., et al. (2021). Interpretable, not black-box, artificial intelligence should be used for embryo selection. *Hum. Rep. Open* 2021:hoab040.

Aghdam, M. A., Sharifi, A., and Pedram, M. M. (2019). Diagnosis of autism spectrum disorders in young children based on resting-state functional magnetic resonance imaging data using convolutional neural networks. *J. Dig. Imaging* 32, 899–918. doi: 10.1007/s10278-019-00196-1

AGRE (n.d.). Available Online at: https://www.autismspeaks.org/agre (accessed July 19, 2022).

Ahammed, M. S., Niu, S., Ahmed, M. R., Dong, J., Gao, X., and Chen, Y. (2021). "Bag-of-features model for ASD fMRI classification using SVM," in *Proceedings of the 2021 Asia-Pacific Conference on Communications Technology and Computer Science (ACCTCS)*, (Shenyang: IEEE), 52–57.

Ahmadi-Dastgerdi, N., Hosseini-Nejad, H., Amiri, H., Shoeibi, A., and Gorriz, J. M. (2021). A vector quantization-based spike compression approach dedicated to multichannel neural recording microsystems. *Int. J. Neural Syst.* 32:2250001. doi: 10.1142/S0129065722500010

Ahmed, M. R., Zhang, Y., Liu, Y., and Liao, H. (2020b). Single volume image generator and deep learning-based ASD classification. *IEEE J. Biomed. Health Inf.* 24, 3044–3054. doi: 10.1109/JBHI.2020.2998603

Ahmed, M. R., Ahammed, M. S., Niu, S., and Zhang, Y. (2020a). "Deep learning approached features for ASD classification using SVM," in *Proceedings of the 2020 IEEE International Conference on Artificial Intelligence and Information Systems (ICAIIS)*, (Dalian: IEEE), 287–290. doi: 10.1155/2020/1394830

Akhavan Aghdam, M., Sharifi, A., and Pedram, M. M. (2018). Combination of rs-fMRI and sMRI data to discriminate autism spectrum disorders in young children using deep belief network. *J. Dig. Imaging* 31, 895–903. doi: 10.1007/s10278-018-0093-8

Al-Hiyali, M. I., Yahya, N., Faye, I., Khan, Z., and Alsaih, K. (2021). "Classification of BOLD FMRI signals using wavelet transform and transfer learning for detection of autism spectrum disorder," in *Proceedings of the 2020 IEEE-EMBS Conference on Biomedical Engineering and Sciences (IECBES)*, (Langkawi: IEEE), 94–98.

Alizadehsani, R., Khosravi, A., Roshanzamir, M., Abdar, M., Sarrafzadegan, N., Shafie, D., et al. (2021). Coronary artery disease detection using artificial intelligence techniques: A survey of trends, geographical differences and diagnostic features 1991–2020. *Comput. Biol. Med.* 128:104095. doi: 10.1016/j.compbiomed.2020.104095

Almuqhim, F., and Saeed, F. (2021). ASD-SAENet: A sparse autoencoder, and deep-neural network model for detecting autism spectrum disorder (ASD) using fMRI data. *Front. Comput. Neurosci.* 15:654315. doi: 10.3389/fncom.2021.654315

Al-Shoukry, S., Rassem, T. H., and Makbol, N. M. (2020). Alzheimer's diseases detection by using deep learning algorithms: A mini-review. *IEEE Access* 8, 77131–77141.

Altinkaya, E., Polat, K., and Barakli, B. (2020). Detection of Alzheimer's disease and dementia states based on deep learning from MRI images: A comprehensive review. *J. Inst. Electr. Comput.* 1, 39–53. doi: 10.3389/fnagi.2021.720226

Alvarez-Jimenez, C., Múnera-Garzón, N., Zuluaga, M. A., Velasco, N. F., and Romero, E. (2020). Autism spectrum disorder characterization in children by capturing local-regional brain changes in MRI. *Med. Phys.* 47, 119–131. doi: 10.1002/mp.13901

Amemiya, S., Takao, H., Kato, S., Yamashita, H., Sakamoto, N., and Abe, O. (2022). Feature-fusion improves MRI single-shot deep learning detection of small brain metastases. *J. Neuroimaging* 32, 111–119. doi: 10.1111/jon.12916

An, M., Ho, H. P., Staib, L., Pelphrey, K., and Duncan, J. (2010). "Multimodal MRI analysis of brain subnetworks in autism using multi-view EM," in *Proceedings of the 2010 Conference Record of the Forty Fourth Asilomar Conference on Signals, Systems and Computers*, (Pacific Grove, CA: IEEE), 786–789.

Anand, C. S., and Sahambi, J. S. (2010). Wavelet domain non-linear filtering for MRI denoising. *Magn. Reson. Imaging* 28, 842–861. doi: 10.1016/j.mri.2010.03.013

Anirudh, R., and Thiagarajan, J. J. (2019). "Bootstrapping graph convolutional neural networks for autism spectrum disorder classification," in *Proceedings of the ICASSP 2019-2019 IEEE International Conference on Acoustics, Speech and Signal Processing (ICASSP)*, (Piscataway, NJ: IEEE), 3197–3201.

Antropova, N., Huynh, B. Q., and Giger, M. L. (2017). A deep feature fusion methodology for breast cancer diagnosis demonstrated on three imaging modality datasets. *Med. Phys.* 44, 5162–5171. doi: 10.1002/mp.12453

Arya, D., Olij, R., Gupta, D. K., El Gazzar, A., Wingen, G., Worring, M., et al. (2020). "Fusing structural and functional MRIs using graph convolutional networks for autism classification," in *Proceedings of Medical imaging with deep learning*, (Birmingham: PMLR), 44–61. doi: 10.1016/j.compbiomed.2022.105823

Bakhtyari, M., and Mirzaei, S. (2022). ADHD detection using dynamic connectivity patterns of EEG data and ConvLSTM with attention framework. *Biomed. Signal Process. Control* 76:103708.

Balagurunathan, Y., Mitchell, R., and El Naqa, I. (2021). Requirements and reliability of AI in the medical context. *Phys. Med.* 83, 72–78.

Bayram, M. A., Ýlyas, Ö, and Temurtaş, F. (2021). Deep learning methods for autism spectrum disorder diagnosis based on fMRI images. *Sakarya Univ. J. Comput. Inf. Sci.* 4, 142–155.

Benabdallah, F. Z., El Maliani, A. D., Lotfi, D., Jennane, R., and El Hassouni, M. (2018). "Analysis of under-connectivity in autism using the minimum spanning tree: Application on large multi-site dataset," in *Proceedings 2018 9th International Symposium on Signal, Image, Video and Communications (ISIVC)*, (Rabat: IEEE), 296–299.

Bengs, M., Gessert, N., and Schlaefer, A. (2020). 4d spatio-temporal deep learning with 4d fmri data for autism spectrum disorder classification. *arXiv* [Preprint]. doi: 10.48550/arXiv.2004.10165

Bernas, A., Aldenkamp, A. P., and Zinger, S. (2018). Wavelet coherence-based classifier: A resting-state functional MRI study on neurodynamics in adolescents with high-functioning autism. *Comput. Methods Programs Biomed.* 154, 143–151. doi: 10.1016/j.cmpb.2017.11.017

Bhattacharya, S., Ho, M.-H. R., and Purkayastha, S. (2006). A Bayesian approach to modeling dynamic effective connectivity with fMRI data. *Neuroimage* 30, 794–812.

Bhaumik, R., Pradhan, A., Das, S., and Bhaumik, D. K. (2018). Predicting autism spectrum disorder using domain-adaptive cross-site evaluation. *Neuroinformatics* 16, 197–205. doi: 10.1007/s12021-018-9366-0

Bi, X.-A., Liu, Y., Sun, Q., Luo, X., Tan, H., Chen, J., et al. (2019). The genetic-evolutionary random support vector machine cluster analysis in autism spectrum disorder. *IEEE Access* 7, 30527–30535. doi: 10.3389/fphys.2018.01646

Bi, X.-A., Wang, Y., Shu, Q., Sun, Q., and Xu, Q. (2018). Classification of autism spectrum disorder using random support vector machine cluster. *Front. Genet.* 9:18. doi: 10.3389/fgene.2018.00018

Bloy, L., Ingalhalikar, M., Eavani, H., Roberts, T. P., Schultz, R. T., and Verma, R. (2011). HARDI based pattern classifiers for the identification of white matter pathologies. *Med. Image Comput. Comput. Assist. Interv.* 14, 234–241. doi: 10.1007/978-3-642-23629-7_29

Bora, E., Fornito, A., Radua, J., Walterfang, M., Seal, M., Wood, S. J., et al. (2011). Neuroanatomical abnormalities in schizophrenia: A multimodal voxelwise meta-analysis and meta-regression analysis. *Schizophr. Res.* 127, 46–57. doi: 10.1016/j.schres.2010.12.020

Brambilla, P., Hardan, A., Di Nemi, S. U., Perez, J., Soares, J. C., and Barale, F. (2003). Brain anatomy and development in autism: Review of structural MRI studies. *Brain Res. Bull.* 61, 557–569.

Brieber, S., Neufang, S., Bruning, N., Kamp-Becker, I., Remschmidt, H., Herpertz-Dahlmann, B., et al. (2007). Structural brain abnormalities in adolescents with autism spectrum disorder and patients with attention deficit/hyperactivity disorder. *J. Child Psychol. Psychiatry* 48, 1251–1258.

Brihadiswaran, G., Haputhanthri, D., Gunathilaka, S., Meedeniya, D., and Jayarathna, S. (2019). EEG-based processing and classification methodologies for autism spectrum disorder: A review. *J. Comput. Sci.* 15, 1161–1183. doi: 10.1109/TBCAS.2021.3089132

Brown, C. J., Kawahara, J., and Hamarneh, G. (2018). "Connectome priors in deep neural networks to predict autism," in *2018 IEEE 15th international symposium on biomedical imaging (ISBI 2018)*, (Washington, DC: IEEE), 110–113.

Bryant, D. M., Hoeft, F., Lai, S., Lackey, J., Roeltgen, D., Ross, J., et al. (2012). Sex chromosomes and the brain: A study of neuroanatomy in XYY syndrome. *Dev. Med. Child Neurol.* 54, 1149–1156. doi: 10.1111/j.1469-8749.2012.04418.x

Byeon, K., Kwon, J., Hong, J., and Park, H. (2020). "Artificial neural network inspired by neuroimaging connectivity: Application in autism spectrum disorder," in *2020 IEEE International Conference on Big Data and Smart Computing (BigComp)*, (Busan: IEEE), 575–578.

Cai, H., Zheng, V. W., and Chang, K. C.-C. (2018). A comprehensive survey of graph embedding: Problems, techniques, and applications. *IEEE Trans. Knowl. Data Eng.* 30, 1616–1637.

Cai, Y., Chia, N. K., Thalmann, D., Kee, N. K., Zheng, J., and Thalmann, N. M. (2013). Design and development of a virtual dolphinarium for children with autism. *IEEE Trans. Neural Syst. Rehab. Eng.* 21, 208–217. doi: 10.1109/TNSRE.2013.2240700

Calderoni, S., Retico, A., Biagi, L., Tancredi, R., Muratori, F., and Tosetti, M. (2012). Female children with autism spectrum disorder: An insight from mass-univariate and pattern classification analyses. *Neuroimage* 59, 1013–1022. doi: 10.1016/j.neuroimage.2011.08.070

Cao, M., Yang, M., Qin, C., Zhu, X., Chen, Y., Wang, J., et al. (2021). Using DeepGCN to identify the autism spectrum disorder from multi-site resting-state data. *Biomed. Signal Process. Control* 70:103015.

Chaitra, N., Vijaya, P., and Deshpande, G. (2020). Diagnostic prediction of autism spectrum disorder using complex network measures in a machine learning framework. *Biomed. Signal Process. Control* 62:102099.

Chanussot, J., Mauris, G., and Lambert, P. (1999). Fuzzy fusion techniques for linear features detection in multitemporal SAR images. *IEEE Trans. Geosci. Remote Sens.* 37, 1292–1305.

Chen, C. P., Keown, C. L., and Müller, R.-A. (2013). Towards Understanding autism Risk Factors: A Classification of Brain Images with Support Vector Machines. *Int. J. Semant. Comput.* 7, 205–213.

Chen, H., Duan, X., Liu, F., Lu, F., Ma, X., Zhang, Y., et al. (2016). Multivariate classification of autism spectrum disorder using frequency-specific resting-state functional connectivity—a multi-center study. *Prog. Neuropsychopharmacol. Biol. Psychiatry* 64, 1–9. doi: 10.1016/j.pnpbp.2015.06.014

Chen, H., Zhuang, F., Xiao, L., Ma, L., Liu, H., Zhang, R., et al. (2021). AMA-GCN: Adaptive Multi-layer Aggregation Graph Convolutional Network for Disease Prediction. *arXiv* [Preprint]. doi: 10.48550/arXiv.2106.08732

Chen, J., and Ran, X. (2019). Deep learning with edge computing: A review. *Proc. IEEE* 107, 1655–1674.

Chen, X., Wang, Z., Zhan, Y., Cheikh, F. A., and Ullah, M. (2022). "Interpretable learning approaches in structural MRI: 3D-ResNet fused attention for autism spectrum disorder classification," in *Proceedings of Medical Imaging 2022: Computer-Aided Diagnosis*, (Bellingham, WA: SPIE), 611–618.

Chen, Y., Liu, A., Fu, X., Wen, J., and Chen, X. (2021). An Invertible Dynamic Graph Convolutional Network for Multi-Center ASD Classification. *Front. Neurosci.* 15:828512. doi: 10.3389/fnins.2021.828512

Choi, H. (2017). Functional connectivity patterns of autism spectrum disorder identified by deep feature learning. *arXiv* [Preprint]. doi: 10.48550/arXiv.1707.07932

Chu, Y., Wang, G., Cao, L., Qiao, L., and Liu, M. (2022). Multi-Scale Graph Representation Learning for Autism Identification With Functional MRI. *Front. Neuroinform.* 15:802305. doi: 10.3389/fninf.2021.802305

Cociu, B. A., Das, S., Billeci, L., Jamal, W., Maharatna, K., Calderoni, S., et al. (2017). Multimodal functional and structural brain connectivity analysis in autism: A preliminary integrated approach with EEG, fMRI, and DTI. *IEEE Trans. Cogn. Dev. Syst.* 10, 213–226.

Conti, E., Retico, A., Palumbo, L., Spera, G., Bosco, P., Biagi, L., et al. (2020). Autism Spectrum Disorder and Childhood Apraxia of Speech: Early language-related hallmarks across structural MRI study. *J. Pers. Med.* 10:275. doi: 10.3390/jpm10040275

Cordova, M., Shada, K., Demeter, D. V., Doyle, O., Miranda-Dominguez, O., Perrone, A., et al. (2020). Heterogeneity of executive function revealed by a functional random forest approach across ADHD and ASD. *Neuroimage Clin.* 26:102245. doi: 10.1016/j.nicl.2020.102245

Creswell, A., White, T., Dumoulin, V., Arulkumaran, K., Sengupta, B., and Bharath, A. A. (2018). Generative adversarial networks: An overview. *IEEE Signal Process. Mag.* 35, 53–65.

Crimi, A., Dodero, L., Murino, V., and Sona, D. (2017). "Case-control discrimination through effective brain connectivity," in *2017 IEEE 14th International Symposium on Biomedical Imaging (ISBI 2017)*, (Melbourne, VIC: IEEE), 970–973.

D'Souza, N. S., Nebel, M. B., Crocetti, D., Wymbs, N., Robinson, J., Mostofsky, S., et al. (2020). "A deep-generative hybrid model to integrate multimodal and dynamic connectivity for predicting spectrum-level deficits in autism," in *International Conference on Medical Image Computing and Computer-Assisted Intervention*, (Berlin: Springer), 437–447.

Darweesh, A. N., Salem, N., and Al-Atabany, W. (2022). Classification of autism spectrum disorder using convolutional neural network. *SSRN Electron. J.* doi: 10.2139/ssrn.4057056

Davidson, V. J., Ryks, J., and Chu, T. (2001). Fuzzy models to predict consumer ratings for biscuits based on digital image features. *IEEE Trans. Fuzzy Syst.* 9, 62–67.

de Aguiar, E. P., Fernando, M. D. A., Vellasco, M. M., and Ribeiro, M. V. (2017). Set-membership type-1 fuzzy logic system applied to fault classification in a switch machine. *IEEE Trans. Intell. Transp. Syst.* 18, 2703–2712.

de Belen, R. A. J., Bednarz, T., Sowmya, A., and Del Favero, D. (2020). Computer vision in autism spectrum disorder research: A systematic review of published studies from 2009 to 2019. *Transl. Psychiatry* 10:333. doi: 10.1038/s41398-020-01015-w

Dekhil, O., Ali, M., El-Nakieb, Y., Shalaby, A., Soliman, A., Switala, A., et al. (2019). A personalized autism diagnosis CAD system using a fusion of structural MRI and resting-state functional MRI data. *Front. Psychiatry* 10:392. doi: 10.3389/fpsyt.2019.00392

Dekhil, O., Ali, M., Haweel, R., Elnakib, Y., Ghazal, M., Hajjdiab, H., et al. (2020). "A comprehensive framework for differentiating autism spectrum disorder from neurotypicals by fusing structural MRI and resting state functional MRI. *Semin. Pediatr. Neurol.* 34:100805. doi: 10.1016/j.spen.2020.100805

Dekhil, O., Hajjdiab, H., Shalaby, A., Ali, M. T., Ayinde, B., Switala, A., et al. (2018). Using resting state functional mri to build a personalized autism diagnosis system. *PLoS One* 13:e0206351. doi: 10.1371/journal.pone.0206351

Dekhil, O., Ismail, M., Shalaby, A., Switala, A., Elmaghraby, A., Keynton, R., et al. (2017). "A novel CAD system for autism diagnosis using structural and functional MRI," in *2017 IEEE 14th international symposium on biomedical imaging (ISBI 2017)*, (Melbourne, VIC: IEEE), 995–998.

Demirhan, A. (2018). Performance of machine learning methods in determining the autism spectrum disorder cases. *Mugla J. Sci. Technol.* 4, 79–84.

Deshpande, G., Libero, L. E., Sreenivasan, K. R., Deshpande, H. D., and Kana, R. K. (2013). Identification of neural connectivity signatures of autism using machine learning. *Front. Hum. Neurosci.* 7:670. doi: 10.3389/fnhum.2013.00670

Devika, K., and Oruganti, V. R. M. (2021). "A Machine Learning Approach for Diagnosing Neurological Disorders using Longitudinal Resting-State fMRI," in *2021 11th International Conference on Cloud Computing, Data Science & Engineering (Confluence)*, (Noida: IEEE), 494–499. doi: 10.1007/s10916-019-1475-2

Dolz, J., Desrosiers, C., and Ayed, I. B. (2018). 3D fully convolutional networks for subcortical segmentation in MRI: A large-scale study. *Neuroimage* 170, 456–470. doi: 10.1016/j.neuroimage.2017.04.039

Dominic, N., Cenggoro, T. W., Budiarto, A., and Pardamean, B. (2021). Transfer learning using inception-ResNet-v2 model to the augmented neuroimages data for autism spectrum disorder classification. *Commun. Math. Biol. Neurosci.* 2021:39.

DSouza, A. M., Abidin, A. Z., and Wismüller, A. (2019). "Classification of autism spectrum disorder from resting-state fMRI with mutual connectivity analysis," in *Proceedings of the Medical Imaging 2019: Biomedical Applications in Molecular, Structural, and Functional Imaging*, San Diego, CA, 292–299.

DSouza, N. S., Nebel, M. B., Crocetti, D., Robinson, J., Mostofsky, S., and Venkataraman, A. (2021). M-gcn: A multimodal graph convolutional network to integrate functional and structural connectomics data to predict multidimensional phenotypic characterizations. *Proc. Mach. Learn. Res.* 143, 119–130.

Du, Y., Li, B., Hou, Y., and Calhoun, V. D. (2020). "A deep learning fusion model for brain disorder classification: Application to distinguishing schizophrenia and autism spectrum disorder," in *Proceedings of the 11th ACM International Conference on Bioinformatics, Computational Biology and Health Informatics*, (New York, NY: ACM), 1–7. doi: 10.1145/3388440.3412478

Durán, J. M., and Jongsma, K. R. (2021). Who is afraid of black box algorithms? On the epistemological and ethical basis of trust in medical AI. *J. Med. Ethics* 47, 329–335.

Dvornek, N. C., Li, X., Zhuang, J., and Duncan, J. S. (2019). "Jointly discriminative and generative recurrent neural networks for learning from fMRI," in *Proceedings of the International Workshop on Machine Learning in Medical Imaging*, (Berlin: Springer), 382–390.

Dvornek, N. C., Yang, D., Ventola, P., and Duncan, J. S. (2018b). "Learning generalizable recurrent neural networks from small task-fmri datasets," in *Proceedings of the International Conference on Medical Image Computing and Computer-Assisted Intervention*, eds A. Frangi, J. Schnabel, C. Davatzikos, C. Alberola-López, and G. Fichtinger (Berlin: Springer), 329–337. doi: 10.1007/978-3-030-00931-1_38

Dvornek, N. C., Ventola, P., and Duncan, J. S. (2018a). "Combining phenotypic and resting-state fMRI data for autism classification with recurrent neural networks," in *Proceedings of the 2018 IEEE 15th International Symposium on Biomedical Imaging (ISBI 2018)*, (Washington, DC: IEEE), 725–728. doi: 10.1109/ISBI.2018.8363676

Dvornek, N. C., Ventola, P., Pelphrey, K. A., and Duncan, J. S. (2017). "Identifying autism from resting-state fMRI using long short-term memory networks," in *Proceedings of the 2017 International Workshop on Machine Learning in Medical Imaging*, Quebec, QC, 362–370.

Ecker, C., Bookheimer, S. Y., and Murphy, D. G. (2015). Neuroimaging in autism spectrum disorder: Brain structure and function across the lifespan. *Lancet Neurol.* 14, 1121–1134. doi: 10.1016/S1474-4422(15)00050-2

Ecker, C., Rocha-Rego, V., Johnston, P., Mourao-Miranda, J., Marquand, A., Daly, E. M., et al. (2010b). Investigating the predictive value of whole-brain structural MR scans in autism: A pattern classification approach. *Neuroimage* 49, 44–56. doi: 10.1016/j.neuroimage.2009.08.024

Ecker, C., Marquand, A., Mourão-Miranda, J., Johnston, P., Daly, E. M., Brammer, M. J., et al. (2010a). Describing the brain in autism in five dimensions—magnetic resonance imaging-assisted diagnosis of autism spectrum disorder using a multiparameter classification approach. *J. Neurosci.* 30, 10612–10623. doi: 10.1523/JNEUROSCI.5413-09.2010

Eill, A., Jahedi, A., Gao, Y., Kohli, J. S., Fong, C. H., Solders, S., et al. (2019). Functional connectivities are more informative than anatomical variables in diagnostic classification of autism. *Brain Connect.* 9, 604–612. doi: 10.1089/brain.2019.0689

El Gazzar, A., Cerliani, L., Van Wingen, G., and Thomas, R. M. (2019). "Simple 1-D convolutional networks for resting-state fMRI based classification in autism," in *Proceedings of the 2019 International Joint Conference on Neural Networks (IJCNN)*, (Piscataway, NJ: IEEE), 1–6.

El-Gazzar, A., Quaak, M., Cerliani, L., Bloem, P., Wingen, G. V., and Mani Thomas, R. (2019). "A hybrid 3DCNN and 3DC-LSTM based model for 4D spatio-temporal fMRI data: an ABIDE autism classification study," in *Proceedings of the OR 2.0 Context-Aware Operating Theaters and Machine Learning in Clinical Neuroimaging*, Shenzhen, 95–102.

Elnakieb, Y. A., Ali, M. T., Soliman, A., Mahmoud, A. H., Shalaby, A. M., Alghamdi, N. S., et al. (2020). Computer aided autism diagnosis using diffusion tensor imaging. *IEEE Access* 8, 191298–191308.

ElNakieb, Y., Ali, M. T., Dekhil, O., Khalefa, M. E., Soliman, A., Shalaby, A., et al. (2018). "Towards accurate personalized autism diagnosis using different imaging modalities: sMRI, fMRI, and DTI," in *Proceedings of the 2018 IEEE International Symposium on Signal Processing and Information Technology (ISSPIT)*, (Louisville, KY: IEEE), 447–452.

ElNakieb, Y., Soliman, A., Mahmoud, A., Dekhil, O., Shalaby, A., Ghazal, M., et al. (2019). "Autism spectrum disorder diagnosis framework using diffusion tensor imaging," in *Proceedings of the 2019 IEEE International Conference on Imaging Systems and Techniques (IST)*, (Piscataway, NJ: IEEE), 1–5.

Eslami, T., Almuqhim, F., Raiker, J. S., and Saeed, F. (2021a). Machine learning methods for diagnosing autism spectrum disorder and attention-deficit/hyperactivity disorder using functional and structural MRI: A survey. *Front. Neuroinform.* 14:575999. doi: 10.3389/fninf.2020.575999

Eslami, T., Raiker, J. S., and Saeed, F. (2021b). Explainable and scalable machine learning algorithms for detection of autism spectrum disorder using fMRI data. *Neural Eng. Tech. Autism Spectr. Disord.* 1, 39–54.

Eslami, T., and Saeed, F. (2019). "Auto-ASD-network: A technique based on deep learning and support vector machines for diagnosing autism spectrum disorder using fMRI data," in *Proceedings of the 10th ACM International Conference on Bioinformatics, Computational Biology and Health Informatics*, Niagara Falls, NY, 646–651. doi: 10.1155/2020/1394830

Eslami, T., Mirjalili, V., Fong, A., Laird, A. R., and Saeed, F. (2019). ASD-DiagNet: A hybrid learning approach for detection of autism spectrum disorder using fMRI data. *Front. Neuroinform.* 13:70. doi: 10.3389/fninf.2019.00070

Fan, G., Chen, Y., Chen, Y., Yang, M., Wang, J., Li, C., et al. (2020). Abnormal brain regions in two-group cross-location dynamics model of autism. *IEEE Access* 8, 94526–94534.

Fan, Z., Sun, L., Ding, X., Huang, Y., Cai, C., and Paisley, J. (2018). "A segmentation-aware deep fusion network for compressed sensing MRI," in *Proceedings of the European Conference on Computer Vision (ECCV)*), Munich, 55–70. doi: 10.1016/j.mri.2022.08.007

Felouat, H., and Oukid-Khouas, S. (2020). "Graph convolutional networks and functional connectivity for identification of autism spectrum disorder," in *Proceedings of the 2020 Second International Conference on Embedded & Distributed Systems (EDiS)*, (Piscataway, NJ: IEEE), 27–32.

Filipovych, R., Resnick, S. M., and Davatzikos, C. (2012). JointMMCC: Joint maximum-margin classification and clustering of imaging data. *IEEE Trans. Med. Imaging* 31, 1124–1140. doi: 10.1109/TMI.2012.2186977

Fodor, I. K. (2002). *A survey of dimension reduction techniques*. Livermore, CA: Lawrence Livermore National Lab.

Fredo, A., Jahedi, A., Reiter, M., and Müller, R.-A. (2018). Diagnostic classification of autism using resting-state fMRI data and conditional random forest. *Age* 12, 6–41.

Gao, J., Chen, M., Li, Y., Gao, Y., Li, Y., Cai, S., et al. (2021). Multisite autism spectrum disorder classification using convolutional neural network classifier and individual morphological brain networks. *Front. Neurosci.* 14:629630. doi: 10.3389/fnins.2020.629630

Gautam, R., and Sharma, M. (2020). Prevalence and diagnosis of neurological disorders using different deep learning techniques: A meta-analysis. *J. Med. Syst.* 44:29.

Ge, F., Chen, H., Zhang, T., Wang, X., Yuan, L., Hu, X., et al. (2018). "A novel framework for analyzing cortical folding patterns based on sulcal baselines and gyral crestlines," in *Proceedings of the 2018 IEEE 15th International Symposium on Biomedical Imaging (ISBI 2018)*, (Piscataway, NJ: IEEE), 1043–1047.

Gene Expression Omnibus [GEO]. (n.d.). *Gene Expression Omnibus*. Available online at: https://www.ncbi.nlm.nih.gov/geo (accessed July 19, 2022).

Geng, X., Yao, Q., Jiang, K., and Zhu, Y. (2020). "Deep neural generative adversarial model based on VAE+ GAN for disorder diagnosis," in *Proceedings of the 2020 International Conference on Internet of Things and Intelligent Applications (ITIA)*, (Piscataway, NY: IEEE), 1–7.

Georgiadis, P., Cavouras, D., Kalatzis, I., Daskalakis, A., Kagadis, G. C., Sifaki, K., et al. (2008). Improving brain tumor characterization on MRI by probabilistic neural networks and non-linear transformation of textural features. *Comput. Methods Programs Biomed.* 89, 24–32. doi: 10.1016/j.cmpb.2007.10.007

Ghassemi, N., Shoeibi, A., and Rouhani, M. (2020). Deep neural network with generative adversarial networks pre-training for brain tumor classification based on MR images. *Biomed. Signal Process. Control* 57:101678.

Ghassemi, N., Shoeibi, A., Khodatars, M., Heras, J., Rahimi, A., Zare, A., et al. (2021). Automatic diagnosis of covid-19 from ct images using cyclegan and transfer learning. *arXiv* [Preprint]. doi: 10.48550/arXiv.2104.11949

Gilson, M., Deco, G., Friston, K. J., Hagmann, P., Mantini, D., Betti, V., et al. (2018). Effective connectivity inferred from fMRI transition dynamics during movie viewing points to a balanced reconfiguration of cortical interactions. *Neuroimage* 180, 534–546. doi: 10.1016/j.neuroimage.2017.09.061

Giuliano, A., Calderoni, S., Muratori, F., Biagi, L., Tosetti, M., and Retico, A. (2013). "Multivariate analysis of structural MRI data to detect gender-related brain abnormalities in children with autism spectrum disorder," in *Proceedings of the 2013 european congress of radiology-ECR 2013*, Vienna.

Goodfellow, I., Bengio, Y., and Courville, A. (2016). *Deep learning*. Cambridge, MA: MIT press.

Gori, I., Giuliano, A., Oliva, P., Tosetti, M., Muratori, F., Calderoni, S., et al. (2016). "Processing Magnetic Resonance Image Features with One-class Support Vector Machines-Investigation of the Autism Spectrum Disorder Heterogeneity," in *Proceedings of the 2016 International Conference on Bioimaging*, (Setúbal: SciTePress), 111–117.

Graña, M., and Silva, M. (2021). Impact of machine learning pipeline choices in autism prediction from functional connectivity data. *Int. J. Neural Syst.* 31:2150009. doi: 10.1142/S012906572150009X

Guo, X., Dominick, K. C., Minai, A. A., Li, H., Erickson, C. A., and Lu, L. J. (2017). Diagnosing autism spectrum disorder from brain resting-state functional connectivity patterns using a deep neural network with a novel feature selection method. *Front. Neurosci.* 11:460. doi: 10.3389/fnins.2017.00460

Gupta, D., Vij, I., and Gupta, M. (2020). Autism detection using r-fMRI: Subspace approximation and CNN based approach. *Int. J. Adv. Trends Comput. Sci. Eng.* 9, 1029–1036.

Gupta, N., Bhatele, P., and Khanna, P. (2019). Glioma detection on brain MRIs using texture and morphological features with ensemble learning. *Biomed. Signal Process. Control* 47, 115–125.

Hamilton, W. L., Ying, R., and Leskovec, J. (2017). Representation learning on graphs: Methods and applications. *arXiv* [Preprint]. doi: 10.48550/arXiv.1709.05584

Haweel, R., Dekhil, O., Shalaby, A., Mahmoud, A., Ghazal, M., Khalil, A., et al. (2019b). "Functional magnetic resonance imaging based framework for autism diagnosis," in *Proceedings of the 2019 Fifth International Conference on Advances in Biomedical Engineering (ICABME)*, (Tripoli: IEEE), 1–4.

Haweel, R., Dekhil, O., Shalaby, A., Mahmoud, A., Ghazal, M., Keynton, R., et al. (2019a). "A machine learning approach for grading autism severity levels using task-based functional MRI," in *Proceedings of the 2019 IEEE International Conference on Imaging Systems and Techniques (IST)*, (Abu Dhabi: IEEE), 1–5.

Haweel, R., Dekhil, O., Shalaby, A., Mahmoud, A., Ghazal, M., Khalil, A., et al. (2020). "A novel framework for grading autism severity using task-based fMRI," in

Proceedings of the 2020 IEEE 17th International Symposium on Biomedical Imaging (ISBI), (Iowa City, IA: IEEE), 1404–1407.

Haweel, R., Shalaby, A., Mahmoud, A., Seada, N., Ghoniemy, S., Ghazal, M., et al. (2021b). A robust DWT–CNN-based CAD system for early diagnosis of autism using task-based fMRI. *Med. Phys.* 48, 2315–2326. doi: 10.1002/mp.14692

Haweel, R., Shalaby, A., Mahmoud, A., Ghazal, M., Seada, N., Ghoniemy, S., et al. (2021a). "A Novel Dwt-Based Discriminant Features Extraction From Task-Based FMRI: An ASD diagnosis study using CNN," in *Proceedings of the 2021 IEEE 18th International Symposium on Biomedical Imaging (ISBI)*, (Nice: IEEE), 196–199.

Hazlett, H. C., Poe, M., Gerig, G., Smith, R. G., Provenzale, J., Ross, A., et al. (2005). Magnetic resonance imaging and head circumference study of brain size in autism: Birth through age 2 years. *Arch. Gen. Psychiatry* 62, 1366–1376.

Heinsfeld, A. S., Franco, A. R., Craddock, R. C., Buchweitz, A., and Meneguzzi, F. (2018). Identification of autism spectrum disorder using deep learning and the ABIDE dataset. *Neuroimage Clin.* 17, 16–23.

Henschel, L., Conjeti, S., Estrada, S., Diers, K., Fischl, B., and Reuter, M. (2020). Fastsurfer-a fast and accurate deep learning based neuroimaging pipeline. *NeuroImage* 219:117012.

Hermessi, H., Mourali, O., and Zagrouba, E. (2019). Deep feature learning for soft tissue sarcoma classification in MR images via transfer learning. *Expert Systems with Applications* 120, 116–127.

Hernandez, L. M., Rudie, J. D., Green, S. A., Bookheimer, S., and Dapretto, M. (2015). Neural signatures of autism spectrum disorders: Insights into brain network dynamics. *Neuropsychopharmacology* 40, 171–189.

Highland, D., and Zhou, G. (2022). A review of detection techniques for depression and bipolar disorder. *Smart Health*.

Hiremath, Y., Ismail, M., Verma, R., Antunes, J., and Tiwari, P. (2020). "Combining deep and hand-crafted MRI features for identifying sex-specific differences in autism spectrum disorder versus controls," in *Proceedings of the Medical Imaging 2020: Computer-Aided Diagnosis*, (Bellingham, WA: SPIE), 445–451.

Hosseinzadeh, M., Koohpayehzadeh, J., Bali, A. O., Rad, F. A., Souri, A., Mazaherinezhad, A., et al. (2021). A review on diagnostic autism spectrum disorder approaches based on the Internet of Things and Machine Learning. *J. Supercomput.* 77, 2590–2608.

Hu, J., Cao, L., Li, T., Liao, B., Dong, S., and Li, P. (2020). Interpretable learning approaches in resting-state functional connectivity analysis: The case of autism spectrum disorder. *Comput. Math. Methods Med.* 2020:1394830. doi: 10.1155/2020/1394830

Huang, F., Elazab, A., Ouyang, L., Tan, J., Wang, T., and Lei, B. (2019). "Sparse low-rank constrained adaptive structure learning using multi-template for autism spectrum disorder diagnosis," in *Proceedings of the 2019 IEEE 16th International Symposium on Biomedical Imaging (ISBI 2019)*, (Venice: IEEE), 1555–1558.

Huang, H., Liu, X., Jin, Y., Lee, S. W., Wee, C. Y., and Shen, D. (2019). Enhancing the representation of functional connectivity networks by fusing multi-view information for autism spectrum disorder diagnosis. *Hum. Brain Mapp.* 40, 833–854. doi: 10.1002/hbm.24415

Huang, Z.-A., Zhu, Z., Yau, C. H., and Tan, K. C. (2020b). Identifying autism spectrum disorder from resting-state fMRI using deep belief network. *IEEE Trans. Neural Netw. Learn. Syst.* 32, 2847–2861.

Huang, Z.-A., Liu, R., and Tan, K. C. (2020a). "Multi-Task learning for efficient diagnosis of ASD and ADHD using Resting-State fMRI data," in *Proceedings of the 2020 International Joint Conference on Neural Networks (IJCNN)*, (Glasgow: IEEE), 1–7.

Husna, R. N. S., Syafeeza, A., Hamid, N. A., Wong, Y., and Raihan, R. A. (2021). Functional magnetic resonance imaging for autism spectrum disorder detection using deep learning. *Jurnal Teknologi* 83, 45–52.

Iglesias, J. E., Lerma-Usabiaga, G., Garcia-Peraza-Herrera, L. C., Martinez, S., and Paz-Alonso, P. M. (2017). "Retrospective head motion estimation in structural brain MRI with 3D CNNs," in *Proceedings of the International Conference on Medical Image Computing and Computer-Assisted Intervention*, (Berlin: Springer), 314–322.

Ingalhalikar, M., Parker, D., Bloy, L., Roberts, T. P., and Verma, R. (2011). Diffusion based abnormality markers of pathology: Toward learned diagnostic prediction of ASD. *Neuroimage* 57, 918–927. doi: 10.1016/j.neuroimage.2011.05.023

Ismail, M., Barnes, G., Nitzken, M., Switala, A., Shalaby, A., Hosseini-Asl, E., et al. (2017). "A new deep-learning approach for early detection of shape variations in autism using structural MRI," in *Proceedings of the2017 IEEE International Conference on Image Processing (ICIP)*, (Beijing: IEEE), 1057–1061.

Itani, S., and Thanou, D. (2021). Combining anatomical and functional networks for neuropathology identification: A case study on autism spectrum disorder. *Med. Image Anal.* 69:101986. doi: 10.1016/j.media.2021.101986

Jafarpour, S., Sedghi, Z., and Amirani, M. C. (2012). A robust brain MRI classification with GLCM features. *Int. J. Comput. Appl.* 37, 1–5.

Jahedi, A., Nasamran, C. A., Faires, B., Fan, J., and Müller, R.-A. (2017). Distributed intrinsic functional connectivity patterns predict diagnostic status in large autism cohort. *Brain Connect.* 7, 515–525. doi: 10.1089/brain.2017.0496

Jang, B., Kim, M., Harerimana, G., and Kim, J. W. (2019). Q-learning algorithms: A comprehensive classification and applications. *IEEE Access* 7, 133653–133667.

Javed, U., Riaz, M. M., Ghafoor, A., and Cheema, T. A. (2013). MRI brain classification using texture features, fuzzy weighting and support vector machine. *Prog. Electromagnet. Res. B* 53, 73–88.

Jayanthy, A., and Din, Q. M. U. (2022). "Early detection of autism spectrum disorder using behavioral data EEG, MRI and Behavioral Data: A Review," in *Assistive Technology Intervention in Healthcare*, eds S. Jain and S. Paul (Boca Raton, FL: CRC Press), 245–267.

Jha, R. R., Bhardwaj, A., Garg, D., Bhavsar, A., and Nigam, A. (2021). MHATC: Autism Spectrum Disorder identification utilizing multi-head attention encoder along with temporal consolidation modules. *arXiv* [Preprint]. doi: 10.48550/arXiv.2201.00404

Ji, J., and Yao, Y. (2020). Convolutional neural network with graphical Lasso to extract sparse topological features for brain disease classification. *IEEE/ACM Trans. Comput. Biol. Bioinformatics* 18, 2327–2338. doi: 10.1109/TCBB.2020.2989315

Ji, J., Xing, X., Yao, Y., Li, J., and Zhang, X. (2021). Convolutional kernels with an element-wise weighting mechanism for identifying abnormal brain connectivity patterns. *Pattern Recogn.* 109:107570.

Jiang, Q., Jin, X., Lee, S.-J., and Yao, S. (2017). A novel multi-focus image fusion method based on stationary wavelet transform and local features of fuzzy sets. *IEEE Access* 5, 20286–20302.

Jiang, Y., Li, Z., and Zhang, D. (2019). "Unsupervised domain adaptation for multi-center autism spectrum disorder identification," in *Proceedings of the 2019 IEEE SmartWorld, ubiquitous intelligence & computing, advanced & trusted computing, scalable computing & communications, cloud & big data computing, internet of people and smart city innovation (SmartWorld/SCALCOM/UIC/ATC/CBDCom/IOP/SCI)*, (Leicester: IEEE), 1608–1613.

Jiao, Y., and Lu, Z. (2011). "Predictive models for autism spectrum disorder based on multiple cortical features," in *Proceedings of the 2011 Eighth International Conference on Fuzzy Systems and Knowledge Discovery (FSKD)*, (Shanghai: IEEE), 1611–1615.

Jiao, Y., Chen, R., Ke, X., Cheng, L., Chu, K., Lu, Z., et al. (2011). Predictive models for subtypes of autism spectrum disorder based on single-nucleotide polymorphisms and magnetic resonance imaging. *Adv. Med. Sci.* 56, 334–342. doi: 10.2478/v10039-011-0042-y

Jiao, Y., Chen, R., Ke, X., Chu, K., Lu, Z., and Herskovits, E. H. (2010). Predictive models of autism spectrum disorder based on brain regional cortical thickness. *Neuroimage* 50, 589–599.

Jiao, Z., Li, H., and Fan, Y. (2020). "Improving diagnosis of autism spectrum disorder and disentangling its heterogeneous functional connectivity patterns using capsule networks," in *Proceedings of the 2020 IEEE 17th International Symposium on Biomedical Imaging (ISBI)*, (Iowa City, IA: IEEE), 1331–1334. doi: 10.1109/isbi45749.2020.9098524

Jönemo, J., Abramian, D., and Eklund, A. (2021). Evaluation of augmentation methods in classifying autism spectrum disorders from fMRI data with 3D convolutional neural networks. *arXiv* [Preprint]. doi: 10.48550/arXiv.2110.10489

Jones, C. R., Pickles, A., Falcaro, M., Marsden, A. J., Happé, F., Scott, S. K., et al. (2011). A multimodal approach to emotion recognition ability in autism spectrum disorders. *J. Child Psychol. Psychiatry* 52, 275–285.

Jung, M., Tu, Y., Park, J., Jorgenson, K., Lang, C., Song, W., et al. (2019). Surface-based shared and distinct resting functional connectivity in attention-deficit hyperactivity disorder and autism spectrum disorder. *Br. J. Psychiatry* 214, 339–344. doi: 10.1192/bjp.2018.248

Karampasi, A., Kakkos, I., Miloulis, S.-T., Zorzos, I., Dimitrakopoulos, G. N., Gkiatis, K., et al. (2020). "A machine learning fMRI approach in the diagnosis of autism," in *Proceedings of the 2020 IEEE International Conference on Big Data (Big Data)*, (Atlanta, GA: IEEE), 3628–3631.

Kasari, C., and Smith, T. (2013). Interventions in schools for children with autism spectrum disorder: Methods and recommendations. *Autism* 17, 254–267.

Kazeminejad, A., and Sotero, R. C. (2019). Topological properties of resting-state fMRI functional networks improve machine learning-based autism classification. *Front. Neurosci.* 12:1018. doi: 10.3389/fnins.2018.01018

Kazeminejad, A., and Sotero, R. C. (2020). The importance of anti-correlations in graph theory based classification of autism spectrum disorder. *Front. Neurosci.* 14:676. doi: 10.3389/fnins.2020.00676

Ke, F., Choi, S., Kang, Y. H., Cheon, K.-A., and Lee, S. W. (2020). Exploring the structural and strategic bases of autism spectrum disorders with deep learning. *IEEE Access* 8, 153341–153352.

Ke, Q., Zhang, J., Wei, W., Damaševičius, R., and Woźniak, M. (2019). Adaptive independent subspace analysis of brain magnetic resonance imaging data. *IEEE Access* 7, 12252–12261.

Khodatars, M., Shoeibi, A., Sadeghi, D., Ghaasemi, N., Jafari, M., Moridian, P., et al. (2021). Deep learning for neuroimaging-based diagnosis and rehabilitation of autism spectrum disorder: A review. *Computers in Biology and Medicine* 139, 104949. doi: 10.1016/j.compbiomed.2021.104949

Khosla, M., Jamison, K., Kuceyeski, A., and Sabuncu, M. R. (2018). "3D convolutional neural networks for classification of functional connectomes," in *Deep Learning in Medical Image Analysis and Multimodal Learning for Clinical Decision Support*, (Cham: Springer), 137–145.

Khosla, M., Jamison, K., Kuceyeski, A., and Sabuncu, M. R. (2019). Ensemble learning with 3D convolutional neural networks for functional connectome-based prediction. *NeuroImage* 199, 651–662. doi: 10.1016/j.neuroimage.2019.06.012

Kim, Y. S., Fombonne, E., Koh, Y.-J., Kim, S.-J., Cheon, K.-A., and Leventhal, B. L. (2014). A comparison of DSM-IV pervasive developmental disorder and DSM-5 autism spectrum disorder prevalence in an epidemiologic sample. *J. Am. Acad. Child Adolesc. Psychiatry* 53, 500–508. doi: 10.1016/j.jaac.2013.12.021

Kober, H., Grummich, P., and Vieth, J. (1993). Precise fusion of MEG and MRI tomography using a surface fit. *Biomed Eng.* 38, 355–356.

Kollias, K.-F., Syriopoulou-Delli, C. K., Sarigiannidis, P., and Fragulis, G. F. (2021). The contribution of machine learning and eye-tracking technology in autism spectrum disorder research: A systematic review. *Electronics* 10:2982.

Kong, Y., Gao, J., Xu, Y., Pan, Y., Wang, J., and Liu, J. (2019). Classification of autism spectrum disorder by combining brain connectivity and deep neural network classifier. *Neurocomputing* 324, 63–68.

Lee, T.-W., and Xue, S.-W. (2017). Linking graph features of anatomical architecture to regional brain activity: A multi-modal MRI study. *Neurosci. Lett.* 651, 123–127. doi: 10.1016/j.neulet.2017.05.005

Leming, M. J., Baron-Cohen, S., and Suckling, J. (2021). Single-participant structural similarity matrices lead to greater accuracy in classification of participants than function in autism in MRI. *Mol. Autism* 12, 1–15. doi: 10.1186/s13229-021-00439-5

Leming, M., Górriz, J. M., and Suckling, J. (2020). Ensemble deep learning on large, mixed-site fMRI datasets in autism and other tasks. *Int. J. Neural Syst.* 30:2050012. doi: 10.1142/S0129065720500124

Li, G., Chen, M.-H., Li, G., Wu, D., Sun, Q., Shen, D., et al. (2019). "A preliminary volumetric MRI study of amygdala and hippocampal subfields in autism during infancy," in *Proceedings of the 2019 IEEE 16th International Symposium on Biomedical Imaging (ISBI 2019)*, (Venice: IEEE), 1052–1056. doi: 10.1109/ISBI.2019.8759439

Li, X., Dvornek, N. C., Papademetris, X., Zhuang, J., Staib, L. H., Ventola, P., et al. (2018c). "2-channel convolutional 3D deep neural network (2CC3D) for fMRI analysis: ASD classification and feature learning," in *Proceedings of the 2018 IEEE 15th International Symposium on Biomedical Imaging (ISBI 2018)*, (Washington, DC: IEEE), 1252–1255. doi: 10.1109/isbi.2018.8363798

Li, G., Liu, M., Sun, Q., Shen, D., and Wang, L. (2018a). "Early diagnosis of autism disease by multi-channel CNNs," in *Proceedings of the International Workshop on Machine Learning in Medical Imaging*, (Berlin: Springer), 303–309. doi: 10.1007/978-3-030-00919-9_35

Li, H., Parikh, N. A., and He, L. (2018b). A novel transfer learning approach to enhance deep neural network classification of brain functional connectomes. *Front. Neurosci.* 12:491. doi: 10.3389/fnins.2018.00491

Li, X., Dvornek, N. C., Zhou, Y., Zhuang, J., Ventola, P., and Duncan, J. S. (2018d). "Efficient interpretation of deep learning models using graph structure and cooperative game theory: Application to ASD biomarker discovery," in *Proceedings of the International Conference on Information Processing in Medical Imaging*, (Berlin: Springer), 718–730. doi: 10.1007/978-3-030-20351-1_56

Li, X., Dvornek, N. C., Zhuang, J., Ventola, P., and Duncan, J. S. (2018e). "Brain biomarker interpretation in ASD using deep learning and fMRI," in *Proceedings of the International conference on medical image computing and computer-assisted intervention*, (Berlin: Springer), 206–214.

Li, H., Xue, Z., Ellmore, T. M., Frye, R. E., and Wong, S. T. (2012). "Identification of faulty DTI-based sub-networks in autism using network regularized SVM," in *Proceedings of the 2012 9th IEEE International Symposium on Biomedical Imaging (ISBI)*, (Barcelona: IEEE), 550–553.

Li, J., Wang, F., Pan, J., and Wen, Z. (2021). Identification of autism spectrum disorder with functional graph discriminative network. *Front. Neurosci.* 15:729937. doi: 10.3389/fnins.2021.729937

Li, R., Xian, K., Shen, C., Cao, Z., Lu, H., and Hang, L. (2019). "Deep attention-based classification network for robust depth prediction," in *Asian Conference on Computer Vision*, eds C. Jawahar, H. Li, G. Mori, and K. Schindler (Berlin: Springer), 663–678.

Li, X., Hect, J., Thomason, M., and Zhu, D. (2020). "Interpreting age effects of human fetal brain from spontaneous fMRI using deep 3D convolutional neural networks," in *Proceedings of the 2020 IEEE 17th International Symposium on Biomedical Imaging (ISBI)*, (Piscataway, NJ: IEEE), 1424–1427.

Liang, T., Glossner, J., Wang, L., Shi, S., and Zhang, X. (2021). Pruning and quantization for deep neural network acceleration: A survey. *Neurocomputing* 461, 370–403.

Liao, D., and Lu, H. (2018). "Classify autism and control based on deep learning and community structure on resting-state fMRI," in *Proceedings of the 2018 Tenth International Conference on Advanced Computational Intelligence (ICACI)*, (Xiamen: IEEE), 289–294.

Liao, Y., and Vemuri, V. R. (2002). Use of k-nearest neighbor classifier for intrusion detection. *Comput. Security* 21, 439–448.

Liu, J., Sheng, Y., Lan, W., Guo, R., Wang, Y., and Wang, J. (2020). Improved ASD classification using dynamic functional connectivity and multi-task feature selection. *Pattern Recogn. Lett.* 138, 82–87.

Liu, M.-Y., and Tuzel, O. (2016). Coupled generative adversarial networks. *Proceedings of the 30th International Conference on Neural Information Processing Systems*, Barcelona.

Liu, W., Liu, M., Yang, D., Wang, M., and Tao, T. (2020). "Automatic diagnosis of autism based on functional magnetic resonance imaging and elastic net," in *Proceedings of the 2020 IEEE 5th Information Technology and Mechatronics Engineering Conference (ITOEC)*, (Chongqing: IEEE), 104–108.

Liu, X., Wang, J., Sun, H., Chandra, S. S., Crozier, S., and Liu, F. (2021). On the regularization of feature fusion and mapping for fast MR multi-contrast imaging via iterative networks. *Magn. Reson. Imaging* 77, 159–168. doi: 10.1016/j.mri.2020.12.019

Loeffelbein, D. J., Souvatzoglou, M., Wankerl, V., Martinez-Möller, A., Dinges, J., Schwaiger, M., et al. (2012). PET-MRI fusion in head-and-neck oncology: current status and implications for hybrid PET/MRI. *J. Oral Maxillofac. Surgery* 70, 473–483. doi: 10.1016/j.joms.2011.02.120

Loh, H. W., Ooi, C. P., Barua, P. D., Palmer, E. E., Molinari, F., and Acharya, U. (2022). Automated detection of ADHD: Current trends and future perspective. *Comput. Biol. Med.* 146:105525. doi: 10.1016/j.compbiomed.2022.105525

Lu, H., Liu, S., Wei, H., and Tu, J. (2020). Multi-kernel fuzzy clustering based on auto-encoder for fMRI functional network. *Expert Syst. Appl.* 159: 113513.

Lu, J. T., Kishida, K. T., De Asis-Cruz, J., Lohrenz, T., Treadwell-Deering, D., Beauchamp, M., et al. (2015). Single-stimulus functional MRI produces a neural individual difference measure for autism spectrum disorder. *Clin. Psychol. Sci.* 3, 422–432. doi: 10.1177/2167702614562042

Ma, F., Gao, F., Sun, J., Zhou, H., and Hussain, A. (2019). Weakly supervised segmentation of SAR imagery using superpixel and hierarchically adversarial CRF. *Remote Sens.* 11:512.

Ma, X., Wu, J., Xue, S., Yang, J., Zhou, C., Sheng, Q. Z., et al. (2021). A comprehensive survey on graph anomaly detection with deep learning. *IEEE Trans. Knowl. Data Eng.*

Madine, M., Rekik, I., and Werghi, N. (2020). "Diagnosing autism using T1-W MRI with multi-kernel learning and hypergraph neural network," in *Proceedings of the 2020 IEEE International Conference on Image Processing (ICIP)*, (Abu Dhabi: IEEE), 438–442.

Maenner, M. J., Shaw, K. A., Bakian, A. V., Bilder, D. A., Durkin, M. S., Esler, A., et al. (2021). Prevalence and characteristics of autism spectrum disorder among children aged 8 years—autism and developmental disabilities monitoring network, 11 sites, United States, 2018. *MMWR Surveill. Summ.* 70, 1–16. doi: 10.15585/mmwr.mm6745a7

Mahmoud, A. M., Karamti, H., and Alrowais, F. (2020a). A two consequent multi-layers deep discriminative approach for classifying fMRI images. *Int. J. Artif. Intell. Tools* 29:2030001.

Mahmoud, A. M., Karamti, H., and Alrowais, F. M. (2020b). "An effective sparse autoencoders based deep learning framework for fMRI scans classification," in *Proceedings of the 22nd International Conference on Enterprise Information Systems (ICEIS 2020),* Prague, 540–547.

Mathur, M., and Lindberg, T. (n.d.). *Autism Spectrum Disorder classification using Machine Learning techniques on fMRI*. Available online at: https://mihirmathur.com/asd_classification.pdf

Matson, M. L., Mahan, S., and Matson, J. L. (2009). Parent training: A review of methods for children with autism spectrum disorders. *Research in Autism Spectrum Disorders* 3, 868–875.

Meena, D., and Agilandeeswari, L. (2020). Invariant features-based fuzzy inference system for animal detection and recognition using thermal images. *Int. J. Fuzzy Syst.* 22, 1868–1879.

Melin, P., and Castillo, O. (2013). A review on the applications of type-2 fuzzy logic in classification and pattern recognition. *Expert Syst. Appl.* 40, 5413–5423.

Melin, P., and Castillo, O. (2014). A review on type-2 fuzzy logic applications in clustering, classification and pattern recognition. *Appl. Soft Comput.* 21, 568–577.

Mellema, C. J., Treacher, A., Nguyen, K. P., and Montillo, A. (2020). "Architectural configurations, atlas granularity and functional connectivity with diagnostic value in Autism Spectrum Disorder," in *Proceedings of the 2020 IEEE 17th International Symposium on Biomedical Imaging (ISBI)*, (Piscataway, NJ: IEEE), 1022–1025. doi: 10.1109/ISBI45749.2020.9098555

Mellema, C., Treacher, A., Nguyen, K., and Montillo, A. (2019). "Multiple deep learning architectures achieve superior performance diagnosing autism spectrum disorder using features previously extracted from structural and functional MRI," in *Proceedings of the 2019 IEEE 16th International Symposium on Biomedical Imaging (ISBI 2019)*, (Venice: IEEE), 1891–1895. doi: 10.1109/ISBI.2019.8759193

Mhiri, I., and Rekik, I. (2020). Joint functional brain network atlas estimation and feature selection for neurological disorder diagnosis with application to autism. *Med. Image Anal.* 60:101596. doi: 10.1016/j.media.2019.101596

Michele, A., Colin, V., and Santika, D. D. (2019). Mobilenet convolutional neural networks and support vector machines for palmprint recognition. *Procedia Comput. Sci.* 157, 110–117.

Mohammadpoor, M., Shoeibi, A., and Shojaee, H. (2016). A hierarchical classification method for breast tumor detection. *Iran. J. Med. Phys.* 13, 261–268.

Mostafa, S., Tang, L., and Wu, F.-X. (2019a). Diagnosis of autism spectrum disorder based on eigenvalues of brain networks. *IEEE Access* 7, 128474–128486.

Mostafa, S., Yin, W., and Wu, F.-X. (2019b). "Autoencoder based methods for diagnosis of autism spectrum disorder," in *International Conference on Computational Advances in Bio and Medical Sciences*, eds I. Măndoiu, T. Murali, G. Narasimhan, S. Rajasekaran, P. Skums, and A. Zelikovsky (Cham: Springer), 39–51.

Mozhdefarahbakhsh, A., Chitsazian, S., Chakrabarti, P., Rao, K. J., Kateb, B., and Nami, M. (2021). "A Convolutional neural network model to differentiate attention deficit hyperactivity disorder and autism spectrum disorder based on the resting State fMRI data," in *Proceedings of the 2018 Tenth International Conference on Advanced Computational Intelligence (ICACI)*, (Xiamen: IEEE).

Murdaugh, D. L., Shinkareva, S. V., Deshpande, H. R., Wang, J., Pennick, M. R., and Kana, R. K. (2012). Differential deactivation during mentalizing and classification of autism based on default mode network connectivity. *PLoS One* 7:e50064. doi: 10.1371/journal.pone.0050064

Muthukrishnan, R., and Rohini, R. (2016). "LASSO: A feature selection technique in predictive modeling for machine learning," in *Proceedings of the 2016 IEEE international conference on advances in computer applications (ICACA)*, (Coimbatore: IEEE), 18–20.

NDAR (n.d.). *Welcome to the NIMH Data Archive*. Available online at: https://ndar.nih.gov (accessed July 19, 2022).

Nielsen, J. A., Zielinski, B. A., Fletcher, P. T., Alexander, A. L., Lange, N., Bigler, E. D., et al. (2013). Multisite functional connectivity MRI classification of autism: ABIDE results. *Front. Hum. Neurosci.* 7:599. doi: 10.3389/fnhum.2013.00599

NIMH Repository and Genomics Resource, (n.d.). *Comprehensive Data + Tools to Support Your Research*. Available online at: https://www.nimhgenetics.org (accessed July 19, 2022).

Niu, K., Guo, J., Pan, Y., Gao, X., Peng, X., Li, N., et al. (2020). Multichannel deep attention neural networks for the classification of autism spectrum disorder using neuroimaging and personal characteristic data. *Complexity* 2020:1357853. doi: 10.1155/2020/1357853

Noble, W. S. (2006). What is a support vector machine? *Nat. Biotechnol.* 24, 1565–1567. doi: 10.1038/nbt1206-1565

Nogay, H. S., and Adeli, H. (2020). Machine learning (ML) for the diagnosis of autism spectrum disorder (ASD) using brain imaging. *Rev. Neurosci.* 31, 825–841. doi: 10.1515/revneuro-2020-0043

Noor, M. B. T., Zenia, N. Z., Kaiser, M. S., Mahmud, M., and Mamun, S. A. (2019). "Detecting neurodegenerative disease from MRI: A brief review on a deep learning perspective," in *International conference on brain informatics*, eds P. Liang, V. Goel, and C. Shan (Cham: Springer), 115–125. doi: 10.1007/978-3-030-37078-7_12

Noor, M. B. T., Zenia, N. Z., Kaiser, M. S., Mamun, S. A., and Mahmud, M. (2020). Application of deep learning in detecting neurological disorders from magnetic resonance images: A survey on the detection of Alzheimer's disease, Parkinson's disease and schizophrenia. *Brain Informatics* 7, 1–21. doi: 10.1186/s40708-020-00112-2

Oshiro, T. M., Perez, P. S., and Baranauskas, J. A. (2012). "How many trees in a random forest?" in *International workshop on machine learning and data mining in pattern recognition*, ed. P. Perner (Berlin: Springer), 154–168. doi: 10.1007/978-3-642-31537-4_13

Pagnozzi, A. M., Conti, E., Calderoni, S., Fripp, J., and Rose, S. E. (2018). A systematic review of structural MRI biomarkers in autism spectrum disorder: A machine learning perspective. *Int. J. Dev. Neurosci.* 71, 68–82. doi: 10.1016/j.ijdevneu.2018.08.010

Parikh, M. N., Li, H., and He, L. (2019). Enhancing diagnosis of autism with optimized machine learning models and personal characteristic data. *Front. Comput. Neurosci.* 13:9. doi: 10.3389/fncom.2019.00009

Parisot, S., Ktena, S. I., Ferrante, E., Lee, M., Guerrero, R., Glocker, B., et al. (2018). Disease prediction using graph convolutional networks: Application to autism spectrum disorder and Alzheimer's disease. *Med. Image Anal.* 48, 117–130. doi: 10.1016/j.media.2018.06.001

Park, H.-J., Friston, K. J., Pae, C., Park, B., and Razi, A. (2018). Dynamic effective connectivity in resting state fMRI. *NeuroImage* 180, 594–608. doi: 10.1016/j.neuroimage.2017.11.033

Payabvash, S., Palacios, E. M., Owen, J. P., Wang, M. B., Tavassoli, T., Gerdes, M., et al. (2019). White matter connectome edge density in children with autism spectrum disorders: Potential imaging biomarkers using machine-learning models. *Brain Connect.* 9, 209–220. doi: 10.1089/brain.2018.0658

Pinaya, W. H., Mechelli, A., and Sato, J. R. (2019). Using deep autoencoders to identify abnormal brain structural patterns in neuropsychiatric disorders: A large-scale multi-sample study. *Hum. Brain Mapp.* 40, 944–954. doi: 10.1002/hbm.24423

Pominova, M., Kondrateva, E., Sharaev, M., Bernstein, A., and Burnaev, E. (2021). "Fader networks for domain adaptation on fMRI: Abide-ii study," in *Proceedings of the Thirteenth International Conference on Machine Vision*, (Bellingham, WA: SPIE), 570–577. doi: 10.1117/12.2587348

Pugazhenthi, B., Senapathy, G., and Pavithra, M. (2019). "Identification of autism in MR brain images using deep learning networks," in *Proceedings of the 2019 International Conference on Smart Structures and Systems (ICSSS)*, (Chennai: IEEE), 1–7. doi: 10.3389/fnins.2021.756868

Rahman, M. M., Usman, O. L., Muniyandi, R. C., Sahran, S., Mohamed, S., and Razak, R. A. (2020). A Review of machine learning methods of feature selection and classification for autism spectrum disorder. *Brain Sci.* 10:949. doi: 10.3390/brainsci10120949

Rakić, M., Cabezas, M., Kushibar, K., Oliver, A., and Lladó, X. (2020). Improving the detection of autism spectrum disorder by combining structural and functional MRI information. *Neuroimage Clin.* 25:102181. doi: 10.1016/j.nicl.2020.102181

Rane, S., Jolly, E., Park, A., Jang, H., and Craddock, C. (2017). Developing predictive imaging biomarkers using whole-brain classifiers: Application to the ABIDE I dataset. *Res. Ideas Outcomes* 3:e12733. doi: 10.3897/rio.3.e12733

Reiter, M. A., Jahedi, A., Fredo, A., Fishman, I., Bailey, B., and Müller, R.-A. (2021). Performance of machine learning classification models of autism using resting-state fMRI is contingent on sample heterogeneity. *Neural Comput. Appl.* 33, 3299–3310. doi: 10.1007/s00521-020-05193-y

Retico, A., Giuliano, A., Tancredi, R., Cosenza, A., Apicella, F., Narzisi, A., et al. (2016a). The effect of gender on the neuroanatomy of children with autism spectrum disorders: A support vector machine case-control study. *Mol. Autism* 7, 1–20. doi: 10.1186/s13229-015-0067-3

Retico, A., Gori, I., Giuliano, A., Muratori, F., and Calderoni, S. (2016b). One-class support vector machines identify the language and default mode regions as common patterns of structural alterations in young children with autism spectrum disorders. *Front. Neurosci.* 10:306. doi: 10.3389/fnins.2016.00306

Richards, R., Greimel, E., Kliemann, D., Koerte, I. K., Schulte-Körne, G., Reuter, M., et al. (2020). Increased hippocampal shape asymmetry and volumetric ventricular asymmetry in autism spectrum disorder. *Neuroimage Clin.* 26:102207. doi: 10.1016/j.nicl.2020.102207

Ronicko, J. F. A., Thomas, J., Thangavel, P., Koneru, V., Langs, G., and Dauwels, J. (2020). Diagnostic classification of autism using resting-state fMRI data improves with full correlation functional brain connectivity compared to

partial correlation. *J. Neurosci. Methods* 345:108884. doi: 10.1016/j.jneumeth.2020.108884

Rowe, J. B., Hughes, L. E., Barker, R. A., and Owen, A. M. (2010). Dynamic causal modelling of effective connectivity from fMRI: Are results reproducible and sensitive to Parkinson's disease and its treatment? *Neuroimage* 52, 1015–1026. doi: 10.1016/j.neuroimage.2009.12.080

Saad, M., and Islam, S. M. R. (2019). "Brain connectivity network analysis and classifications from diffusion tensor imaging," in *Proceedings of the 2019 International Conference on Robotics, Electrical and Signal Processing Techniques (ICREST)*, (Dhaka: IEEE), 422–427. doi: 10.1109/ICREST.2019.8644080

Sadato, N., and Tanabe, H. C. (2012). "Neural substrates and inter-individual functional connectivity during mutual gaze and joint attention using dual functional MRI," in *Proceedings of the 2012 ICME International Conference on Complex Medical Engineering (CME)*, (Kobe: IEEE), 527–530. doi: 10.1109/ICCME.2012.6275596

Sadeghi, D., Shoeibi, A., Ghassemi, N., Moridian, P., Khadem, A., Alizadehsani, R., et al. (2022). An overview of artificial intelligence techniques for diagnosis of Schizophrenia based on magnetic resonance imaging modalities: Methods, challenges, and future works. *Comput. Biol. Med.* 146:105554. doi: 10.1016/j.compbiomed.2022.105554

Sadeghi, M., Khosrowabadi, R., Bakouie, F., Mahdavi, H., Eslahchi, C., and Pouretemad, H. (2017). Screening of autism based on task-free fMRI using graph theoretical approach. *Psychiatry Res. Neuroimaging* 263, 48–56. doi: 10.1016/j.pscychresns.2017.02.004

Sahu, L., Sharma, R., Sahu, I., Das, M., Sahu, B., and Kumar, R. (2022). Efficient detection of Parkinson's disease using deep learning techniques over medical data. *Expert Syst.* 39:e12787. doi: 10.1111/exsy.12787

Sairam, K., Naren, J., Vithya, G., and Srivathsan, S. (2019). Computer aided system for autism spectrum disorder using deep learning methods. *Int. J. Psychosoc. Rehabil* 23, 418–425. doi: 10.1371/journal.pone.0253094

Saritha, M., Joseph, K. P., and Mathew, A. T. (2013). Classification of MRI brain images using combined wavelet entropy based spider web plots and probabilistic neural network. *Pattern Recogn. Lett.* 34, 2151–2156. doi: 10.1016/j.patrec.2013.08.017

Sarovic, D., Hadjikhani, N., Schneiderman, J., Lundström, S., and Gillberg, C. (2020). Autism classified by magnetic resonance imaging: A pilot study of a potential diagnostic tool. *Int. J. Methods Psychiatr. Research* 29, 1–18. doi: 10.1002/mpr.1846

Sartipi, S., Shayesteh, M. G., and Kalbkhani, H. (2018). "Diagnosing of autism spectrum disorder based on GARCH variance series for rs-fMRI data," in *Proceedings of the 2018 9th International Symposium on Telecommunications (IST)*, (Tehran: IEEE), 86–90. doi: 10.1109/ISTEL.2018.8661147

Sato, J. R., Hoexter, M. Q., De Magalhães Oliveira, P. P. Jr., Brammer, M. J., Murphy, D., Ecker, C., et al. (2013). Inter-regional cortical thickness correlations are associated with autistic symptoms: A machine-learning approach. *J. Psychiatr. Res.* 47, 453–459. doi: 10.1016/j.jpsychires.2012.11.017

Sato, W., Toichi, M., Uono, S., and Kochiyama, T. (2012). Impaired social brain network for processing dynamic facial expressions in autism spectrum disorders. *BMC Neurosci.* 13:99. doi: 10.1186/1471-2202-13-99

Savva, A. D., Karampasi, A. S., and Matsopoulos, G. K. (2020). "Deriving resting-state fMRI biomarkers for classification of autism spectrum disorder," in *Autism 360°*, eds U. Das, N. Papaneophytou and T. El-Kour (Amsterdam: Elsevier), 101–123. doi: 10.1016/B978-0-12-818466-0.00006-X

Sewani, H., and Kashef, R. (2020). An autoencoder-based deep learning classifier for efficient diagnosis of autism. *Children* 7:182. doi: 10.3390/children7100182

SFARI (n.d.). Available online at: https://www.sfari.org/funded-project/simons-variation-in-individualsproject-simons-vip (accessed July 19, 2022).

Shahamat, H., and Abadeh, M. S. (2020). Brain MRI analysis using a deep learning based evolutionary approach. *Neural Netw.* 126, 218–234. doi: 10.1016/j.neunet.2020.03.017

Shao, L., Fu, C., You, Y., and Fu, D. (2021). Classification of ASD based on fMRI data with deep learning. *Cogn. Neurodyn.* 15, 961–974. doi: 10.1007/s11571-021-09683-0

Sherkatghanad, Z., Akhondzadeh, M., Salari, S., Zomorodi-Moghadam, M., Abdar, M., Acharya, U. R., et al. (2020). Automated detection of autism spectrum disorder using a convolutional neural network. *Front. Neurosci.* 13:325. doi: 10.3389/fnins.2019.01325

Shi, C., Zhang, J., and Wu, X. (2020). An fMRI feature selection method based on a minimum spanning tree for identifying patients with autism. *Symmetry* 12:1995. doi: 10.3390/sym12121995

Shoeibi, A., Sadeghi, D., Moridian, P., Ghassemi, N., Heras, J., Alizadehsani, R., et al. (2021b). Automatic diagnosis of schizophrenia in EEG signals using CNN-LSTM models. *Front. Neuroinform.* 15:777977. doi: 10.3389/fninf.2021.777977

Shoeibi, A., Rezaei, M., Ghassemi, N., Namadchian, Z., Zare, A., and Gorriz, J. M. (2022c). "Automatic Diagnosis of Schizophrenia in EEG Signals Using Functional Connectivity Features and CNN-LSTM Model," in *Proceedings of the International Work-Conference on the Interplay Between Natural and Artificial Computation*, (Berlin: Springer), 63–73. doi: 10.1007/978-3-031-06242-1_7

Shoeibi, A., Ghassemi, N., Khodatars, M., Moridian, P., Khosravi, A., Zare, A., et al. (2022b). Automatic diagnosis of schizophrenia and attention deficit hyperactivity disorder in rs-fMRI modality using convolutional autoencoder model and interval type-2 Fuzzy Regression. *arXiv* [Preprint]. doi: 10.48550/arXiv.2205.15858

Shoeibi, A., Ghassemi, N., Khodatars, M., Jafari, M., Moridian, P., Alizadehsani, R., et al. (2021a). Applications of epileptic seizures detection in neuroimaging modalities using deep learning techniques: methods, challenges, and future works. *arXiv* [Preprint]. doi: 10.48550/arXiv.2105.14278

Shoeibi, A., Ghassemi, N., Khodatars, M., Moridian, P., Alizadehsani, R., Zare, A., et al. (2022a). Detection of epileptic seizures on EEG signals using ANFIS classifier, autoencoders and fuzzy entropies. *Biomed. Signal Process. Control* 73:103417. doi: 10.1016/j.bspc.2021.103417

Shrivastava, S., Mishra, U., Singh, N., Chandra, A., and Verma, S. (2020). "Control or autism-classification using convolutional neural networks on functional MRI," in *Proceedings of the 2020 11th International Conference on Computing, Communication and Networking Technologies (ICCCNT)*, (Kharagpur: IEEE), 1–6. doi: 10.1109/ICCCNT49239.2020.9225506

Sibley, M. H., Arnold, L. E., Swanson, J. M., Hechtman, L. T., Kennedy, T. M., Owens, E., et al. (2022). Variable patterns of remission from ADHD in the multimodal treatment study of ADHD. *Am. J. Psychiatry* 179, 142–151. doi: 10.1176/appi.ajp.2021.21010032

Siewertsen, C. M., French, E. D., and Teramoto, M. (2015). Autism spectrum disorder and pet therapy. *Adv. Mind Body Med.* 29, 22–25.

Smith, J. F., Pillai, A., Chen, K., and Horwitz, B. (2012). Effective connectivity modeling for fMRI: Six issues and possible solutions using linear dynamic systems. *Front. Syst. Neurosci.* 5:104. doi: 10.3389/fnsys.2011.00104

Soltaninejad, M., Ye, X., Yang, G., Allinson, N., and Lambrou, T. (2014). *Brain tumour grading in different MRI protocols using SVM on statistical features*. Egham: British Machine Vision Association.

Song, D.-Y., Topriceanu, C.-C., Ilie-Ablachim, D. C., Kinali, M., and Bisdas, S. (2021). Machine learning with neuroimaging data to identify autism spectrum disorder: A systematic review and meta-analysis. *Neuroradiology* 63, 2057–2072. doi: 10.1007/s00234-021-02774-z

Song, Y., Epalle, T. M., and Lu, H. (2019). Characterizing and predicting autism spectrum disorder by performing resting-state functional network community pattern analysis. *Front. Hum. Neurosci.* 13:203. doi: 10.3389/fnhum.2019.00203

Soussia, M., and Rekik, I. (2018). Unsupervised manifold learning using high-order morphological brain networks derived from T1-w MRI for autism diagnosis. *Front. Neuroinform.* 12:70. doi: 10.3389/fninf.2018.00070

Sparks, B., Friedman, S., Shaw, D., Aylward, E. H., Echelard, D., Artru, A., et al. (2002). Brain structural abnormalities in young children with autism spectrum disorder. *Neurology* 59, 184–192. doi: 10.1212/WNL.59.2.184

Srinivas, S. V. K., Nair, H., and Vidyasagar, V. (2019). Hardware aware neural network architectures using FbNet. *arXiv* [Preprint]. doi: 10.48550/arXiv.1906.07214

SSC. (n.d.). *Preclinical diagnosis of magnetic resonance (MR) brain images via discrete wavelet packet transform with Tsallis entropy and generalized eigenvalue proximal support vector machine (GEPSVM)*. Available online at: https://www.sfari.org/resource/simons-simplex-collection

Sserwadda, A., and Rekik, I. (2021). Topology-guided cyclic brain connectivity generation using geometric deep learning. *J. Neurosci. Methods* 353:108988. doi: 10.1016/j.jneumeth.2020.108988

Stevens, E., Dixon, D. R., Novack, M. N., Granpeesheh, D., Smith, T., and Linstead, E. (2019). Identification and analysis of behavioral phenotypes in autism spectrum disorder via unsupervised machine learning. *Int. J. Medical Inf.* 129, 29–36. doi: 10.1016/j.ijmedinf.2019.05.006

Subah, F. Z., Deb, K., Dhar, P. K., and Koshiba, T. (2021). A deep learning approach to predict autism spectrum disorder using multisite resting-state fMRI. *Appl. Sci.* 11:3636. doi: 10.1186/s12868-016-0283-6

Subbaraju, V., Suresh, M. B., Sundaram, S., and Narasimhan, S. (2017). Identifying differences in brain activities and an accurate detection of autism spectrum disorder using resting state functional-magnetic resonance imaging: A spatial filtering approach. *Med. Image Anal.* 35, 375–389. doi: 10.1016/j.media.2016.08.003

Sujit, S. J., Coronado, I., Kamali, A., Narayana, P. A., and Gabr, R. E. (2019). Automated image quality evaluation of structural brain MRI using an ensemble of deep learning networks. *J. Magn. Reson. Imaging* 50, 1260–1267. doi: 10.1002/jmri.26693

Suthaharan, S. (2016). "Support vector machine," in *Machine learning models and algorithms for big data classification*, (Berlin: Springer), 207–235. doi: 10.1007/978-1-4899-7641-3_9

Syed, M. A., Yang, Z., Hu, X. P., and Deshpande, G. (2017). Investigating brain connectomic alterations in autism using the reproducibility of independent components derived from resting state functional MRI data. *Front. Neurosci.* 11:459. doi: 10.3389/fnins.2017.00459

Tang, L., Mostafa, S., Liao, B., and Wu, F.-X. (2019). A network clustering based feature selection strategy for classifying autism spectrum disorder. *BMC Med. Genomics* 12, (Suppl. 7):153. doi: 10.1186/s12920-019-0598-0

Tang, M., Kumar, P., Chen, H., and Shrivastava, A. (2020). Deep multimodal learning for the diagnosis of autism spectrum disorder. *J. Imaging* 6:47. doi: 10.3390/jimaging6060047

Tawhid, M. N. A., Siuly, S., Wang, H., Whittaker, F., Wang, K., and Zhang, Y. (2021). A spectrogram image based intelligent technique for automatic detection of autism spectrum disorder from EEG. *PLoS One* 16:e0253094. doi: 10.1371/journal.pone.0253094

Tejwani, R., Liska, A., You, H., Reinen, J., and Das, P. (2017). Autism classification using brain functional connectivity dynamics and machine learning. *arXiv* [Preprint]. doi: 10.48550/arXiv.1712.08041

Thabtah, F., and Peebles, D. (2019). Early autism screening: a comprehensive review. *Int. J. Environ. Res. Public Health* 16:3502. doi: 10.3390/ijerph16183502

Thomas, M., and Chandran, A. (2018). "Artificial neural network for diagnosing autism spectrum disorder," in *Proceedings of the 2018 2nd International Conference on Trends in Electronics and Informatics (ICOEI)*, (Tirunelveli: IEEE), 930–933. doi: 10.1109/ICOEI.2018.8553781

Thomas, R. M., Gallo, S., Cerliani, L., Zhutovsky, P., El-Gazzar, A., and Van Wingen, G. (2020). Classifying autism spectrum disorder using the temporal statistics of resting-state functional MRI data with 3D convolutional neural networks. *Front. Psychiatry* 11:440. doi: 10.3389/fpsyt.2020.00440

Thyreau, B., and Taki, Y. (2020). Learning a cortical parcellation of the brain robust to the MRI segmentation with convolutional neural networks. *Med. Image Anal.* 61:101639. doi: 10.1016/j.media.2020.101639

Tian, Y., Gelernter, J., Wang, X., Chen, W., Gao, J., Zhang, Y., et al. (2018). Lane marking detection via deep convolutional neural network. *Neurocomputing* 280, 46–55. doi: 10.1016/j.neucom.2017.09.098

Tolan, E., and Isik, Z. (2018). "Graph theory based classification of brain connectivity network for autism spectrum disorder," in *Proceedings of the International Conference on Bioinformatics and Biomedical Engineering*, (Berlin: Springer), 520–530. doi: 10.1007/978-3-319-78723-7_45

Tummala, S. (2021). "Deep learning framework using siamese neural network for diagnosis of autism from brain magnetic resonance imaging," in *Proceedings of the 2021 6th International Conference for Convergence in Technology (I2CT)*, (Piscataway, NJ: IEEE), 1–5. doi: 10.1002/aur.2626

UCI (n.d.). *Center for Machine Learning and Intelligent Systems*. Available online at: https://archive.ics.uci.edu/ml/datasets.php (Accessed July 19, 2022).

Uddin, L. Q., Menon, V., Young, C. B., Ryali, S., Chen, T., Khouzam, A., et al. (2011). Multivariate searchlight classification of structural magnetic resonance imaging in children and adolescents with autism. *Biol. Psychiatry* 70, 833–841. doi: 10.1016/j.biopsych.2011.07.014

Ullah, H., Ullah, B., Wu, L., Abdalla, F. Y., Ren, G., and Zhao, Y. (2020). Multi-modality medical images fusion based on local-features fuzzy sets and novel sum-modified-Laplacian in non-subsampled shearlet transform domain. *Biomed. Signal Process. Control* 57:101724. doi: 10.1016/j.bspc.2019.101724

Usha, R., and Perumal, K. (2019). SVM classification of brain images from MRI scans using morphological transformation and GLCM texture features. *Int. J. Comput. Systems Eng.* 5, 18–23. doi: 10.1504/IJCSYSE.2019.098415

Valdes-Sosa, P. A., Sanchez-Bornot, J. M., Sotero, R. C., Iturria-Medina, Y., Aleman-Gomez, Y., Bosch-Bayard, J., et al. (2009). Model driven EEG/fMRI fusion of brain oscillations. *Hum. Brain Mapp.* 30, 2701–2721. doi: 10.1002/hbm.20704

Varol, E., Gaonkar, B., Erus, G., Schultz, R., and Davatzikos, C. (2012). "Feature ranking based nested support vector machine ensemble for medical image classification," in *Proceedings of the 2012 9Th IEEE international symposium on biomedical imaging (ISBI)*, (Piscataway, NJ: IEEE), 146–149. doi: 10.1109/ISBI.2012.6235505

Vigneshwaran, S., Mahanand, B., Suresh, S., and Savitha, R. (2013). "Autism spectrum disorder detection using projection based learning meta-cognitive RBF network," in *Proceedings of the 2013 International Joint Conference on Neural Networks (IJCNN)*, (Dallas, TX: IEEE), 1–8. doi: 10.1109/IJCNN.2013.6706777

Volkmar, F. R., and Mcpartland, J. C. (2014). From Kanner to DSM-5: autism as an evolving diagnostic concept. *Annu. Rev. Clin. Psychol.* 10, 193–212. doi: 10.1146/annurev-clinpsy-032813-153710

Volkmar, F. R., Cicchetti, D. V., Bregman, J., and Cohen, D. J. (1992). Three diagnostic systems for autism: DSM-III, DSM-III-R, and ICD-10. *J. Autism Dev. Disord.* 22, 483–492.

Volkmar, F. R., Cohen, D. J., and Paul, R. (1986). An evaluation of DSM-III criteria for infantile autism. *J. Am. Acad. Child Psychiatry* 25, 190–197. doi: 10.1016/S0002-7138(09)60226-0

Wang, W., Zheng, V. W., Yu, H., and Miao, C. (2019d). A survey of zero-shot learning: Settings, methods, and applications. *ACM Trans. Intell. Syst. Technol.* 10, 1–37. doi: 10.1145/3293318

Wang, C., Xiao, Z., and Wu, J. (2019b). Functional connectivity-based classification of autism and control using SVM-RFECV on rs-fMRI data. *Physica Med.* 65, 99–105. doi: 10.1016/j.ejmp.2019.08.010

Wang, C., Xiao, Z., Wang, B., and Wu, J. (2019a). Identification of autism based on SVM-RFE and stacked sparse auto-encoder. *IEEE Access* 7, 118030–118036. doi: 10.1109/ACCESS.2019.2936639

Wang, M., Zhang, D., Huang, J., Yap, P.-T., Shen, D., and Liu, M. (2019c). Identifying autism spectrum disorder with multi-site fMRI via low-rank domain adaptation. *IEEE Trans. Med. Imaging* 39, 644–655. doi: 10.1109/TMI.2019.2933160

Wang, J., Zhang, L., Wang, Q., Chen, L., Shi, J., Chen, X., et al. (2020). Multi-class ASD classification based on functional connectivity and functional correlation tensor via multi-source domain adaptation and multi-view sparse representation. *IEEE Trans. Med. Imaging* 39, 3137–3147. doi: 10.1109/TMI.2020.2987817

Wang, L., Li, K., and Hu, X. P. (2021a). Graph convolutional network for fMRI analysis based on connectivity neighborhood. *Netw. Neurosci.* 5, 83–95. doi: 10.1162/netn_a_00171

Wang, S. H., Nayak, D. R., Guttery, D. S., Zhang, X., and Zhang, Y. D. (2021c). COVID-19 classification by CCSHNet with deep fusion using transfer learning and discriminant correlation analysis. *Information Fusion* 68, 131–148. doi: 10.1016/j.inffus.2020.11.005

Wang, S.-H., Du, J., Xu, H., Yang, D., Ye, Y., Chen, Y., et al. (2021b). Automatic discrimination of different sequences and phases of liver MRI using a dense feature fusion neural network: A preliminary study. *Abdom. Radiol.* 46, 4576–4587. doi: 10.1007/s00261-021-03142-4

Wang, Y., Liu, J., Xiang, Y., Wang, J., Chen, Q., and Chong, J. (2022). MAGE: Automatic diagnosis of autism spectrum disorders using multi-atlas graph convolutional networks and ensemble learning. *Neurocomputing* 469, 346–353. doi: 10.1016/j.neucom.2020.06.152

Wang, Y., Wang, J., Wu, F.-X., Hayrat, R., and Liu, J. (2020). AIMAFE: Autism spectrum disorder identification with multi-atlas deep feature representation and ensemble learning. *J. Neurosci. Methods* 343:108840. doi: 10.1016/j.jneumeth.2020.108840

Wee, C. Y., Wang, L., Shi, F., Yap, P. T., and Shen, D. (2014). Diagnosis of autism spectrum disorders using regional and interregional morphological features. *Hum. Brain Mapp.* 35, 3414–3430. doi: 10.1002/hbm.22411

Wen, G., Cao, P., Bao, H., Yang, W., Zheng, T., and Zaiane, O. (2022). MVS-GCN: A prior brain structure learning-guided multi-view graph convolution network for autism spectrum disorder diagnosis. *Comput. Biol. Med.* 142:105239. doi: 10.1016/j.compbiomed.2022.105239

Wismüller, A., Foxe, J. J., Geha, P., and Saboksayr, S. S. (2020). "Large-scale Extended Granger Causality (lsXGC) for classification of Autism Spectrum Disorder from resting-state functional MRI," in *Proceedings of the Medical Imaging 2020: Computer-Aided Diagnosis*, (Bellingham, WA: SPIE), 458–465. doi: 10.1117/12.2550027

Wold, S., Esbensen, K., and Geladi, P. (1987). Principal component analysis. *Chemometr. Intell. Lab. Syst.* 2, 37–52. doi: 10.1016/0169-7439(87)80084-9

Wong, A., Famuori, M., Shafiee, M. J., Li, F., Chwyl, B., and Chung, J. (2019). "Yolo nano: A highly compact you only look once convolutional neural network for object detection," in *Proceedings of the 2019 Fifth Workshop on Energy Efficient Machine Learning and Cognitive Computing-NeurIPS Edition (EMC2-NIPS)*, (Piscataway, NJ: IEEE), 22–25. doi: 10.1109/EMC2-NIPS53020.2019.00013

Wu, W., Wu, A., and Zheng, W.-S. (2018). "Light person re-identification by multi-cue tiny net," in *Proceedings of the 2018 25th IEEE International Conference on Image Processing (ICIP)*, (Athens: IEEE), 1643–1647. doi: 10.1109/ICIP.2018.8451738

Wu, Z., Pan, S., Chen, F., Long, G., Zhang, C., and Philip, S. Y. (2020). A comprehensive survey on graph neural networks. *IEEE Trans. Neural Netw. Learn. Syst.* 32, 4–24. doi: 10.1109/TNNLS.2020.2978386

Xiao, X., Fang, H., Wu, J., Xiao, C., Xiao, T., Qian, L., et al. (2017). Diagnostic model generated by MRI-derived brain features in toddlers with autism spectrum disorder. *Autism Res.* 10, 620–630. doi: 10.1002/aur.1711

Xiao, Z., Wang, C., Jia, N., and Wu, J. (2018). SAE-based classification of school-aged children with autism spectrum disorders using functional magnetic resonance imaging. *Multimed. Tools Appl.* 77, 22809–22820. doi: 10.1007/s11042-018-5625-1

Xu, L., Geng, X., He, X., Li, J., and Yu, J. (2019). Prediction in autism by deep learning short-time spontaneous hemodynamic fluctuations. *Front. Neurosci.* 13:1120. doi: 10.3389/fnins.2019.01120

Xu, L., Liu, Y., Yu, J., Li, X., Yu, X., Cheng, H., et al. (2020). Characterizing autism spectrum disorder by deep learning spontaneous brain activity from functional near-infrared spectroscopy. *J. Neurosci. Methods* 331:108538. doi: 10.1016/j.jneumeth.2019.108538

Yamagata, B., Itahashi, T., Fujino, J., Ohta, H., Nakamura, M., Kato, N., et al. (2019). Machine learning approach to identify a resting-state functional connectivity pattern serving as an endophenotype of autism spectrum disorder. *Brain Imaging Behav.* 13, 1689–1698. doi: 10.1007/s11682-018-9973-2

Yan, K., and Zhang, D. (2015). Feature selection and analysis on correlated gas sensor data with recursive feature elimination. *Sens. Actuat. B Chem.* 212, 353–363. doi: 10.1016/j.snb.2015.02.025

Yang, M., Zhong, Q., Chen, L., Huang, F., and Lei, B. (2019). "Attention based semi-supervised dictionary learning for diagnosis of autism spectrum disorders," in *Proceedings of the 2019 IEEE International Conference on Multimedia & Expo Workshops (ICMEW)*, (Piscataway, NJ: IEEE), 7–12. doi: 10.1109/ICMEW.2019.00009

Yang, R., Ke, F., Liu, H., Zhou, M., and Cao, H.-M. (2021). Exploring sMRI biomarkers for diagnosis of autism spectrum disorders based on multi class activation mapping models. *IEEE Access* 9, 124122–124131. doi: 10.1109/ACCESS.2021.3069211

Yang, X., Islam, M. S., and Khaled, A. A. (2019). "Functional connectivity magnetic resonance imaging classification of autism spectrum disorder using the multisite ABIDE dataset," in *Proceedings of the 2019 IEEE EMBS International Conference on Biomedical & Health Informatics (BHI)*, (Chicago, IL: IEEE), 1–4.

Yang, X., Sarraf, S., and Zhang, N. (2018). Deep learning-based framework for Autism functional MRI image classification. *J. Arkansas Acad. Sci.* 72, 47–52. doi: 10.1016/j.neunet.2020.03.017

Yang, X., Schrader, P. T., and Zhang, N. (2020). A deep neural network study of the ABIDE repository on autism spectrum classification. *Int. J. Adv. Comput. Sci. Appl.* 11. doi: 10.3389/fnins.2018.00491

Yang, X., Zhang, N., and Schrader, P. (2022). A study of brain networks for autism spectrum disorder classification using resting-state functional connectivity. *Mach. Lear. Appl.* 8:100290. doi: 10.1016/j.mlwa.2022.100290

Yang, Y., Wu, Q. J., and Wang, Y. (2016). Autoencoder with invertible functions for dimension reduction and image reconstruction. *IEEE Trans. Syst. Man Cybern. Syst.* 48, 1065–1079. doi: 10.1109/TSMC.2016.2637279

Yao, A. D., Cheng, D. L., Pan, I., and Kitamura, F. (2020). Deep learning in neuroradiology: A systematic review of current algorithms and approaches for the new wave of imaging technology. *Radiol. Artif. Intell.* 2:e190026. doi: 10.1148/ryai.2020190026

Yap, S. Y., and Chan, W. H. (2020). Elastic SCAD SVM cluster for the selection of significant functional connectivity in autism spectrum disorder classification. *Acad. Fundam. Comput. Res.* 1.

Yassin, W., Nakatani, H., Zhu, Y., Kojima, M., Owada, K., Kuwabara, H., et al. (2020). Machine-learning classification using neuroimaging data in schizophrenia, autism, ultra-high risk and first-episode psychosis. *Transl. Psychiatry* 10, 1–11. doi: 10.1038/s41398-020-00965-5

Ye, Z., and Yang, J. (2010). Sliced inverse moment regression using weighted chi-squared tests for dimension reduction. *J. Statis. Plann. Inference* 140, 3121–3131. doi: 10.1016/j.jspi.2010.04.015

Yeh, C. H., Jones, D. K., Liang, X., Descoteaux, M., and Connelly, A. (2021). Mapping structural connectivity using diffusion MRI: Challenges and opportunities. *J. Magn. Reson. Imaging* 53, 1666–1682.

Yin, W., Li, L., and Wu, F.-X. (2022). A semi-supervised autoencoder for autism disease diagnosis. *Neurocomputing* 483, 140–147. doi: 10.1016/j.neucom.2022.02.017

Yin, W., Mostafa, S., and Wu, F.-X. (2021). Diagnosis of autism spectrum disorder based on functional brain networks with deep learning. *J. Comput. Biol.* 28, 146–165. doi: 10.1089/cmb.2020.0252

You, Y., Liu, H., Zhang, S., and Shao, L. (2020). "Classification of autism based on fMRI data with feature-fused convolutional neural network," in *Proceedings of the Cyberspace Data and Intelligence, and Cyber-Living, Syndrome, and Health*, (Berlin: Springer), 77–88. doi: 10.1007/978-981-33-4336-8_7

Zarghami, T. S., and Friston, K. J. (2020). Dynamic effective connectivity. *Neuroimage* 207:116453. doi: 10.1016/j.neuroimage.2019.116453

Zeng, L.-L., Wang, H., Hu, P., Yang, B., Pu, W., Shen, H., et al. (2018). Multi-site diagnostic classification of schizophrenia using discriminant deep learning with functional connectivity MRI. *EBioMedicine* 30, 74–85.

Zhan, Y., Wei, J., Liang, J., Xu, X., He, R., Robbins, T. W., et al. (2021). Diagnostic classification for human autism and obsessive-compulsive disorder based on machine learning from a primate genetic model. *Am. J. Psychiatry* 178, 65–76. doi: 10.1176/appi.ajp.2020.19101091

Zhang, D., Yin, J., Zhu, X., and Zhang, C. (2018). Network representation learning: A survey. *IEEE Trans. Big Data* 6, 3–28. doi: 10.1109/TBDATA.2018.2850013

Zhang, F., and Roeyers, H. (2019). Exploring brain functions in autism spectrum disorder: A systematic review on functional near-infrared spectroscopy (fNIRS) studies. *Int. J. Psychophysiol.* 137, 41–53. doi: 10.1016/j.ijpsycho.2019.01.003

Zhang, F., Wei, Y., Liu, J., Wang, Y., Xi, W., and Pan, Y. (2022). Identification of Autism spectrum disorder based on a novel feature selection method and Variational Autoencoder. *arXiv* [Preprint]. doi: 10.48550/arXiv.2204.03654

Zhang, L., Wang, X.-H., and Li, L. (2020). Diagnosing autism spectrum disorder using brain entropy: A fast entropy method. *Comput. Methods Programs Biomed.* 190:105240. doi: 10.1016/j.cmpb.2019.105240

Zhang, Z., Cui, P., and Zhu, W. (2020). Deep learning on graphs: A survey. *IEEE Trans. Knowl. Data Eng.* 34, 249–270. doi: 10.1109/TKDE.2020.2981333

Zhang, M., Zhao, X., Zhang, W., Chaddad, A., Evans, A., and Poline, J. B. (2020). "Deep discriminative learning for autism spectrum disorder classification," in *Proceedings of the International Conference on Database and Expert Systems Applications*, (Berlin: Springer), 435–443. doi: 10.1007/978-3-030-59003-1_29

Zhang, X., Ding, X., Wu, Z., Xia, J., Ni, H., Xu, X., et al. (2020). "Siamese verification framework for autism identification during infancy using cortical path signature features," in *Proceedings of the 2020 IEEE 17th International Symposium on Biomedical Imaging (ISBI)*, (Piscataway, NJ: IEEE), 1–4. doi: 10.1109/isbi45749.2020.9098385

Zhang, Y. D., Dong, Z., Wang, S. H., Yu, X., Yao, X., Zhou, Q., et al. (2020). Advances in multimodal data fusion in neuroimaging: Overview, challenges, and novel orientation. *Inf. Fusion* 64, 149–187. doi: 10.1016/j.inffus.2020.07.006

Zhang, Y., Zhou, X., Witt, R. M., Sabatini, B. L., Adjeroh, D., and Wong, S. T. (2007). Dendritic spine detection using curvilinear structure detector and LDA classifier. *Neuroimage* 36, 346–360. doi: 10.1016/j.neuroimage.2007.02.044

Zhao, F., Qiao, L., Shi, F., Yap, P.-T., and Shen, D. (2017). Feature fusion via hierarchical supervised local CCA for diagnosis of autism spectrum disorder. *Brain Imaging Behav.* 11, 1050–1060. doi: 10.1007/s11682-016-9587-5

Zhao, F., Zhang, H., Rekik, I., An, Z., and Shen, D. (2018). Diagnosis of autism spectrum disorders using multi-level high-order functional networks derived from resting-state functional MRI. *Front. Hum. Neurosci.* 12:184. doi: 10.3389/fnhum.2018.00184

Zhao, Y., Dai, H., Zhang, W., Ge, F., and Liu, T. (2019). "Two-stage spatial temporal deep learning framework for functional brain network modeling," in *Proceedings of the 2019 IEEE 16th International Symposium on Biomedical Imaging (ISBI 2019)*, (Venice: IEEE), 1576–1580.

Zhao, Y., Dong, Q., Zhang, S., Zhang, W., Chen, H., Jiang, X., et al. (2017). Automatic recognition of fMRI-derived functional networks using 3-D convolutional neural networks. *IEEE Trans. Biomed. Eng.* 65, 1975–1984. doi: 10.1109/TBME.2017.2715281

Zhao, Y., Ge, F., Zhang, S., and Liu, T. (2018). "3D deep convolutional neural network revealed the value of brain network overlap in differentiating autism spectrum disorder from healthy controls," in *Proceedings of the International Conference on Medical Image Computing and Computer-Assisted Intervention*, (Berlin: Springer), 172–180. doi: 10.1007/978-3-030-00931-1_20

Zheng, W., Eilam-Stock, T., Wu, T., Spagna, A., Chen, C., Hu, B., et al. (2019). Multi-feature based network revealing the structural abnormalities in autism spectrum disorder. *IEEE Trans. Affect. Comput.* 12, 732–742. doi: 10.1109/TAFFC.2018.2890597

Zhou, N., and Wang, L. (2007). A modified T-test feature selection method and its application on the HapMap genotype data. *Genomics Proteomics Bioinformatics* 5, 242–249. doi: 10.1016/S1672-0229(08)60011-X

Zhou, Y., Yu, F., and Duong, T. (2014). Multiparametric MRI characterization and prediction in autism spectrum disorder using graph theory and machine learning. *PLoS One* 9:e90405. doi: 10.1371/journal.pone.0090405

Zhuang, J., Dvornek, N. C., Li, X., Yang, D., Ventola, P., and Duncan, J. S. (2018b). "Prediction of pivotal response treatment outcome with task fMRI using random forest and variable selection," in *Proceedings of the 2018 IEEE 15th International Symposium on Biomedical Imaging (ISBI 2018)*, (Piscataway, NJ: IEEE), 97–100. doi: 10.1109/ISBI.2018.8363531

Zhuang, J., Dvornek, N. C., Li, X., Ventola, P., and Duncan, J. S. (2018a). "Prediction of severity and treatment outcome for ASD from fMRI," in *Proceedings of the International workshop on predictive intelligence in medicine*, (Berlin: Springer), 9–17. doi: 10.1007/978-3-030-00320-3_2

Zürcher, N. R., Bhanot, A., Mcdougle, C. J., and Hooker, J. M. (2015). A systematic review of molecular imaging (PET and SPECT) in autism spectrum disorder: Current state and future research opportunities. *Neurosci. Biobehav. Rev.* 52, 56–73. doi: 10.1016/j.neubiorev.2015.02.002

frontiers | Frontiers in Molecular Neuroscience

TYPE Original Research
PUBLISHED 06 October 2022
DOI 10.3389/fnmol.2022.979061

Check for updates

OPEN ACCESS

EDITED BY
Javier Corral,
University of Murcia, Spain

REVIEWED BY
Ferdinando Di Cunto,
University of Turin, Italy
Ángel Esteban-Gil,
University of Murcia, Spain

*CORRESPONDENCE
Hyung-Goo Kim
hkim@hbku.edu.qa

†These authors have contributed equally to this work

SPECIALTY SECTION
This article was submitted to Neuroplasticity and Development, a section of the journal Frontiers in Molecular Neuroscience

RECEIVED 27 June 2022
ACCEPTED 30 August 2022
PUBLISHED 06 October 2022

CITATION
Ben-Mahmoud A, Jun KR, Gupta V, Shastri P, de la Fuente A, Park Y, Shin KC, Kim CA, da Cruz AD, Pinto IP, Minasi LB, Silva da Cruz A, Faivre L, Callier P, Racine C, Layman LC, Kong I-K, Kim C-H, Kim W-Y and Kim H-G (2022) A rigorous *in silico* genomic interrogation at 1p13.3 reveals 16 autosomal dominant candidate genes in syndromic neurodevelopmental disorders. *Front. Mol. Neurosci.* 15:979061. doi: 10.3389/fnmol.2022.979061

COPYRIGHT
© 2022 Ben-Mahmoud, Jun, Gupta, Shastri, de la Fuente, Park, Shin, Kim, da Cruz, Pinto, Minasi, Silva da Cruz, Faivre, Callier, Racine, Layman, Kong, Kim, Kim and Kim. This is an open-access article distributed under the terms of the Creative Commons Attribution License (CC BY). The use, distribution or reproduction in other forums is permitted, provided the original author(s) and the copyright owner(s) are credited and that the original publication in this journal is cited, in accordance with accepted academic practice. No use, distribution or reproduction is permitted which does not comply with these terms.

A rigorous *in silico* genomic interrogation at 1p13.3 reveals 16 autosomal dominant candidate genes in syndromic neurodevelopmental disorders

Afif Ben-Mahmoud[1†], Kyung Ran Jun[2†], Vijay Gupta[1], Pinang Shastri[3], Alberto de la Fuente[4], Yongsoo Park[1], Kyung Chul Shin[1], Chong Ae Kim[5], Aparecido Divino da Cruz[6,7], Irene Plaza Pinto[6,7], Lysa Bernardes Minasi[6,7], Alex Silva da Cruz[6,7], Laurence Faivre[8,9], Patrick Callier[10], Caroline Racine[10], Lawrence C. Layman[11,12], Il-Keun Kong[13], Cheol-Hee Kim[14], Woo-Yang Kim[15] and Hyung-Goo Kim[1*]

[1]Neurological Disorders Research Center, Qatar Biomedical Research Institute, Hamad Bin Khalifa University, Doha, Qatar, [2]Department of Laboratory Medicine, Inje University Haeundae Paik Hospital, Busan, South Korea, [3]Department of Cardiovascular Medicine, Cape Fear Valley Medical Center, Fayetteville, NC, United States, [4]Diabetes Research Center, Qatar Biomedical Research Institute, Hamad Bin Khalifa University, Doha, Qatar, [5]Faculdade de Medicina, Unidade de Genética do Instituto da Criança – Hospital das Clínicas HCFMUSP, Universidade de São Paulo, São Paulo, Brazil, [6]School of Medical and Life Sciences, Genetics Master Program, Replicon Research Group, Pontifical Catholic University of Goiás, Goiânia, Brazil, [7]Genetics Master Program, Replicon Research Nucleus, School of Agrarian and Biological Sciences, Pontifical Catholic University of Goias, Goiás, Brazil, [8]Inserm UMR 1231 GAD, Genetics of Developmental Disorders, Université de Bourgogne-Franche Comté, Dijon, France, [9]Centre de Référence Anomalies du Développement et Syndromes Malformatifs, Hôpital d'Enfants, Dijon, France, [10]UMR 1231 GAD, Inserm – Université Bourgogne-Franche Comté, Dijon, France, [11]Section of Reproductive Endocrinology, Infertility and Genetics, Department of Obstetrics and Gynecology, Augusta University, Augusta, GA, United States, [12]Department of Neuroscience and Regenerative Medicine, Augusta University, Augusta, GA, United States, [13]Department of Animal Science, Division of Applied Life Science (BK21 Four), Gyeongsang National University, Jinju, South Korea, [14]Department of Biology, Chungnam National University, Daejeon, South Korea, [15]Department of Biological Sciences, Kent State University, Kent, OH, United States

Genome-wide chromosomal microarray is extensively used to detect copy number variations (CNVs), which can diagnose microdeletion and microduplication syndromes. These small unbalanced chromosomal structural rearrangements ranging from 1 kb to 10 Mb comprise up to 15% of human mutations leading to monogenic or contiguous genomic disorders. Albeit rare, CNVs at 1p13.3 cause a variety of neurodevelopmental disorders (NDDs) including development delay (DD), intellectual disability (ID), autism, epilepsy, and craniofacial anomalies (CFA). Most of the 1p13.3 CNV cases reported in the pre-microarray era encompassed a large number of genes and lacked the demarcating genomic coordinates, hampering the discovery of positional candidate genes within the boundaries. In this study, we present

four subjects with 1p13.3 microdeletions displaying DD, ID, autism, epilepsy, and CFA. *In silico* comparative genomic mapping with three previously reported subjects with CNVs and 22 unreported DECIPHER CNV cases has resulted in the identification of four different sub-genomic loci harboring five positional candidate genes for DD, ID, and CFA at 1p13.3. Most of these genes have pathogenic variants reported, and their interacting genes are involved in NDDs. RT-qPCR in various human tissues revealed a high expression pattern in the brain and fetal brain, supporting their functional roles in NDDs. Interrogation of variant databases and interacting protein partners led to the identification of another set of 11 potential candidate genes, which might have been dysregulated by the position effect of these CNVs at 1p13.3. Our studies define 1p13.3 as a genomic region harboring 16 NDD candidate genes and underscore the critical roles of small CNVs in *in silico* comparative genomic mapping for disease gene discovery. Our candidate genes will help accelerate the isolation of pathogenic heterozygous variants from exome/genome sequencing (ES/GS) databases.

KEYWORDS

1p13.3 deletion, intellectual disability, autism, *VAV3*, *WDR47*, *ELAPOR1*, *GSTM5*, *LRIF1*

Introduction

Chromosomal deletions and duplications, called copy number variations (CNVs), are unbalanced chromosomal structural abnormalities that may result in genomic disorders, the manifestations of which are frequently syndromic neurodevelopmental disorders (NDDs) (Lee et al., 2015). With its genomic length of 249 Mb, chromosome 1 is the largest human chromosome and contains about 2,000 human genes comprising about 9% of the total human genes (Murphy et al., 2003). A large number of genes on this chromosome are involved in mental and physical development, and thus, large heterozygous deletions or duplications can cause congenital abnormalities or pregnancy loss (Chen et al., 2017).

Subjects with CNVs within the proximal short arm of chromosome 1, specifically in the 1p13.3 region, are rare, and only seven cases have been reported so far (Tabata et al., 1991; Mattia et al., 1992; Lo et al., 1998; Utkus et al., 1999; Bisgaard et al., 2007; van Kuilenburg et al., 2009; Piccione et al., 2010). Importantly, these seven subjects share an overlapping phenotype of developmental delay (DD), intellectual disability (ID), epilepsy, and craniofacial anomalies (CFA) (Cases 1–7), suggesting the presence of syndromic NDD disease genes within 1p13.3. Four of them (Cases 4–7) are from the pre-comparative genomic hybridization (CGH) era without demarcating coordinates and thus not very informative (**Table 1**).

In this study, we describe the clinical phenotype of four subjects having microdeletions of different sizes at 1p13.3 with an overlapping phenotype of DD, ID, autism, epilepsy, and CFA. *In silico* comparative genomic mapping of these four subjects (Subjects 1–4 on **Figure 1A** and **Table 1**) with three reported demarcated deletions and duplication (Cases 1-3 on **Table 1** and **Figure 1A**) alongside twenty-two informative DECIPHER cases[1], version 11.14) (Firth et al., 2009; **Figure 1A** and **Supplementary Table 3**) has allowed us to narrow down the 1p13.3 genomic region harboring approximately 59 genes to four sub-genomic segments that encompass five positional candidate genes for syndromic NDDs at 1p13.3 (**Figure 1A** and **Table 2**). Upon analyzing various human disease databases including Human Gene Mutation Database (HGMD, [2]version Professional 2022.2), MGI (Mouse Genome Informatics[3], version 6.21), BioGrid[4] (version 4.4.212), and STRING[5] (version 11.5), we found that these five candidate genes have either NDD-associated nucleotide variants reported in them or their interactors, and a behavioral phenotype was shown in KO mice (**Table 2**). A high RNA expression pattern of these five positional

Abbreviations: CNV, copy number variation; NDDs, neurodevelopmental disorders; DD, development delay; ASD, autism spectrum disorder; ID, intellectual disability; CFA, craniofacial anomalies; ADHD, attention deficit hyperactivity disorder; NGS, next-generation sequencing.

1 https://decipher.sanger.ac.uk/
2 https://my.qiagendigitalinsights.com/bbp/view/hgmd/pro/start.php
3 http://www.informatics.jax.org/
4 https://thebiogrid.org/
5 https://string-db.org/

TABLE 1 Clinical features of eleven CNV subjects with 1p13.3 microdeletion/microduplication. Our four CNV carriers 1–4 are indicated here as Subjects 1–4.

Subjects ID	Subject 1 DGDP030	Subject 2	Subject 3	Subject 4	Case 1 Bisgaard et al., 2007	Case 2 van Kuilenburg et al., 2009	Case 3 Piccione et al., 2010	Case 4 Tabata et al., 1991	Case 5 Mattia et al., 1992	Case 6 Lo et al., 1998	Case 7 Utkus et al., 1999
Genomic coordinates [hg19]	chr1:107,240, 429-110,671,860	chr1:108,726, 456-108,853,796	chr1:108,729, 365-108,853,796	chr1:109,878, 638-110,200,728	chr1:104,092, 487-116,035,695	chr1:95,558,073-109,584,850 (personal communication, May 19, 2022)	chr1:102,540, 642-112,979,474	Unknown	Unknown	Unknown	Unknown
Cytogenetic Band	del(1)(p13.3)	del(1)(p13.3)	del(1)(p13.3)	del(1)(p13.3)*mat*	del(1)(p13.3p21.1)	del(1)(p13.3p21.3)	dup(1)(p21.2p13.2)	del(1)(p13.3p22.3)	del(1)(p13.3p22.3)	dup(1)(p13.1p22.1)	46,XY,der(6),ins(6;1)(q25;p13.3p22.1)*pat*
CNV	Deletion	Deletion	Deletion	Deletion	Deletion	Deletion	Duplication	Deletion	Deletion	Duplication	Duplication
Size (Mb)	3.4	0.13	0.12	0.322	11.9	14	10.44	>18.8	>18.8	>21.4	>12.4
Inheritance	Adopted	*de novo*	*de novo*	Maternal with the same phenotype	*de novo*	*de novo*	*de novo*	*de novo*	*de novo*	*de novo*	Paternal insertional translocation 46,XY,ins(6;1)(q25;p13.3p22.1)mat
Method of detection	FISH and array-CGH	Array-CGH	Array-CGH	Array-CGH	Array-CGH	FISH and array-CGH	Array-CGH	karyotyping	karyotyping	karyotyping	GTG banding and FISH
Age	44 years	11 years 6 months	6 years	22 years	13 years	3.5 years Patient 5	17 years	Died at 7 months	2 years	8 years	3 years
Sex	F	M	F	F	F	M	M	F	M	M	M
Ethnicity	Asian	European	European	European	N/A	European	N/A	N/A	European	Chinese	N/A
Developmental delay	+ Teeth did not appear until 20 months of age, severely developmentally delayed	+ Sat independently at around 12 months, walked at 24 months	+ Sat independently at around 10 months and walked at 16 months, no sucking reflex as new born	+ Walked at 18 months	+ No toilet trained, at 4.5 years, she was able to sit by herself and to walk for a short distance with support, failed to thrive until she received a gastrostomy at the age of eight years, first signs of puberty at the age of 12 years	+ Psychomotor impairment, feeding difficulties	+ Psychomotor retardation, walking independently occurred when he was one year old	+ Growth and psychomotor retardation	+ Early delays in motor skills	+	+ Sat at 9 months and walked independently at 17 months of age
Speech/ language delay	+ Talked to some extent until 3 year, only a few words	+ Spoke his first words at 36 months and was not speaking full sentences until 11 years of age	N/A	N/A	+ Never learned language	N/A	+ Language retardation	N/A	+ Delay	N/A	+ No speech

(Continued)

10.3389/fnmol.2022.979061

TABLE 1 (Continued)

Subjects ID	Subject 1 DGDP030	Subject 2	Subject 3	Subject 4	Case 1 Bisgaard et al., 2007	Case 2 van Kuilenburg et al., 2009	Case 3 Piccione et al., 2010	Case 4 Tabata et al., 1991	Case 5 Mattia et al., 1992	Case 6 Lo et al., 1998	Case 7 Utkus et al., 1999
Intellectual disability	+	+	+	+	+ Severe	+	+ IQ -64	N/A Died at seven months	N/A	+	+
Learning disability	+	+ Severe learning difficulties	N/A	N/A	N/A	N/A	N/A	N/A	N/A	N/A	N/A
Autism	+ Did not make eye contact, autistic	_	_	_	N/A	+	+ Difficulty with establishing relationships	N/A	N/A	N/A	N/A
Cranial anomalies	+ Asymmetrical skull with smaller right parietal area	_	_	+ Microcephaly OFC < -2DS	+ Microcephaly head circumference was 49.5 cm (<3rd centile)	+ Macrocephaly, epiphyseal dysplasia of the femoral head, frontal bossing, prominent forehead	+ Microcephaly (25th–50th centile)	_	+ At birth macrocephaly, OFC (90th centile) and at 22 months normocephaly, frontal bossing with ridged metopic suture, prominent occiput	+ Microcephaly (<3rd centile)	+ Microcephaly at 38 weeks and macrocephaly at three years age, wide prominent forehead with high frontal hairline, flat occiput, one occipital hair whorl in the midline
Facial dysmorphism	+ Ptosis, low-set ears, unfolded ears, and high arched palate	+ Bulbous nasal tip, epicanthal folds, downslanted palpebral fissure, low anterior hairline, long philtrum, wide nasal bridge, thin upper lip vermilion, long ears, micrognathi, and hypertelorism	+ Epicanthal folds, downslanted palpebral fissure, long philtrum, wide nasal bridge, hypertelorism, and micrognathia	+ Long face, epicanthus, prominent nose, posteriorly rotated ears	+ The extremities were short compared with the body, the shoulders were narrow and the neck was webbed, the hairlines, front and back were low, and the hair and eyebrows were thick and dark, the ears were low set, the ear lobes broad and the crus helix on the left ear was prominent, a broad nasal bridge and tip, anteverted nares, a prominent premaxillary region and an open mouth with an everted lower lip, her palate was high arched and there was space between her upper incisors	+ Hypertelorism, downward slanted palpebral fissures, low nasal bridge, full nasal tip, anteverted nares, long and prominent philtrum, open mouth appearance, everted lower vermillion, a highly arched palate and large lobules, large anterior fontanel, epicanthal folds, broad flat root of nose	+ Small receding chin, prominent nasal bridge, flat nose, short philtrum, midface hypoplasia	+ Upper and lower eyelids connected to each other by a string-like epithelium, low hairline, epicanthal folds, saddle nose with a broad, flat root, micrognathia, short neck, high-arched palate	+ Large anterior fontanelle, forehead nevus flammeus, low set ears with overlapping helices, bilateral ptosis (right greater than left), deeply set eyes, downward slanting palpebral fissures, arched eyebrows, long eyelashes, prominent nasal bridge and nasal tip, thick columella, and mild micrognathia, moderate right ptosis, short neck	+ Flare of the lateral eyebrows, eversion of the lateral part of lower eyelids, long eyelashes, epicanthic folds, blue sclerae, flat nose with short columella, prominent ears, mild micrognathia, bilateral ptosis	+ Hypertelorism, horizontal palpebral fissures, small lower incisors with diastema, narrow and high palate, large and prominent, but not misshapen ears

(Continued)

10.3389/fnmol.2022.979061

TABLE 1 (Continued)

Subjects ID	Subject 1 DGDP030	Subject 2	Subject 3	Subject 4	Case 1 Bisgaard et al., 2007	Case 2 van Kuilenburg et al., 2009	Case 3 Piccione et al., 2010	Case 4 Tabata et al., 1991	Case 5 Mattia et al., 1992	Case 6 Lo et al., 1998	Case 7 Utkus et al., 1999
Epilepsy /seizures /spasms	+ Suffered febrile seizures at 18 months, possible myoclonic seizures,	_	+ Episode of seizure and her MRI indicated a small arachnoid cyst in the posterior fossa	_	+ Epilepsy	+	N/A	+ Several episodes of generalized tonic clonic convulsions without high fever	N/A	+ Several tonic seizures at age 7 years	N/A
Cardiac anomalies	_	N/A	N/A	N/A	N/A	N/A	_	+ Extreme tetralogy of Fallot	_	_	+ Cardiac sonography disclosed a chorda running through the left ventricle
Short stature	+	+	_	+	+ <5th centile	+ 50th centile height	N/A	N/A	_	_	_
Hearing loss	+	N/A	N/A	N/A	N/A	N/A	N/A	N/A	N/A	+ Hearing deficit on the left side	N/A
Behavioral problems	+ Childhood schizophrenia, hallucinations, obsessive compulsive, wide mood swings, being in a room with people but did not make much effort to interact, complete emotional breakdown and increased violent behavior, strange night terror episodes	+ Deficits in attention and executive functions	_	+ Anxiety	+	+ Psychomotor retardation	+ Stereotyped movements finger snapping and repeated mannerism with obsessive–compulsive behavior	N/A	N/A	N/A	+ Constantly moving around

(Continued)

10.3389/fnmol.2022.979061

TABLE 1 (Continued)

Subjects ID	Subject 1 DGDP030	Subject 2	Subject 3	Subject 4	Case 1 Bisgaard et al., 2007	Case 2 van Kuilenburg et al., 2009	Case 3 Piccione et al., 2010	Case 4 Tabata et al., 1991	Case 5 Mattia et al., 1992	Case 6 Lo et al., 1998	Case 7 Utkus et al., 1999
Hand/finger /feet/toe anomalies	+ Walk with arched feet, cramps in her legs and arms, held her hands at odd angles and held objects with her fingertips, jerky gait	N/A	N/A	+ Short fingers brachydactyly	+ Valgus feet, a groove between the first and second toes, and minimal 2–3 syndactyly on the right foot, hypermobility	+ Nails were short and thin, tapering fingers (Figure 1)	+ Arachnodactyly of the fingers, fingers and toes with joint hyperlaxity	+ Bilateral pes equinovarus, fifth toes that overlapped the fourth toes bilaterally, a deep fissure between the first and second toes bilaterally, and abnormal flexions of fingers and toes, bilateral flexions of the radiocarpal, first metacarpophalangeal, hallucal interphalangealjoints, overextension of the first metatarsophalangeal joint	+ Arched feet, joint laxity and a high arched right foot, dermal ridge patterns showed a central whorl on the right thumb, second, and fifth digits, a biradial loop on the left thumb, ulnar loops on the right fourth and left	+ Persistent fetal finger pads, mild joint laxity, and mild cutaneous syndactyly between all fingers and toes	+ Flat arches of the feet, and irregular position of toes with tibial deviation of the second toes, gait was peculiar with outward rotation of the feet, small hands, brachydactyly, clinodactyly of 5th fingers
Muscle disorder	+ Mild fiber atrophy and random variation in muscle fiber size, motor milestones were of poor quality and out of the usual order	_	_	_	+ hypotonia, diplegia	+ Hypertonia and hyperreflexia changed into severe hypotonia and areflexia	N/A	N/A	+ Mild hypotonia, most notably in the upper limbs	N/A	+ Hypotonia
Eye disorder	+ Strabismus, astigmatism	N/A	N/A	N/A	+ Coloboma of both irides, central vision impairment	+ Myopia, astigmatism and nystagmus	+ Astigmatism	N/A	+ Ptosis with deeply set eyes	+ Long eye-lashes, eversion of the lateral part of lower eye-lids, bilateral ptosis	+ Mild exophthalmos
Other	Mild anemia, recurring petechial rash, kyphosis, lordosis		Loose skin	Mother and oldest brother show similar neurodevelop-mental phenotypes	Respiratory infections	Respiratory problems and eruption of his dentition was delayed,		Prominent xiphisternum, wide-spaced nipples, cyanosis and multiple congenital anomalies, hypoxia and metabolic acidosis	High-pitched cry showed mild gastroesopha geal reflux and an asymptomatic malrotation with a left-sided appendix	Kabuki make-up syndrome, episode of gastroenteritis at 5 months, recurrent otitis media with residual high-tone	Umbilical hernia, hypoplastic nipples, sacral dimple

These three published subjects (Cases 1–3) have been featured in Figure 1A, whereas the other four subjects (Cases 4–7) from pre-microarray era with no demarcation are not. Genomic coordinates of Case 2 were solicited from the author, and "tapering fingers" of Case 2 were deduced from Figure 1 of the article. N/A denotes not available, while (-) represents absence of the corresponding phenotype. Not tested; some cases are before the microarray era and without genomic coordinates.

10.3389/fnmol.2022.979061

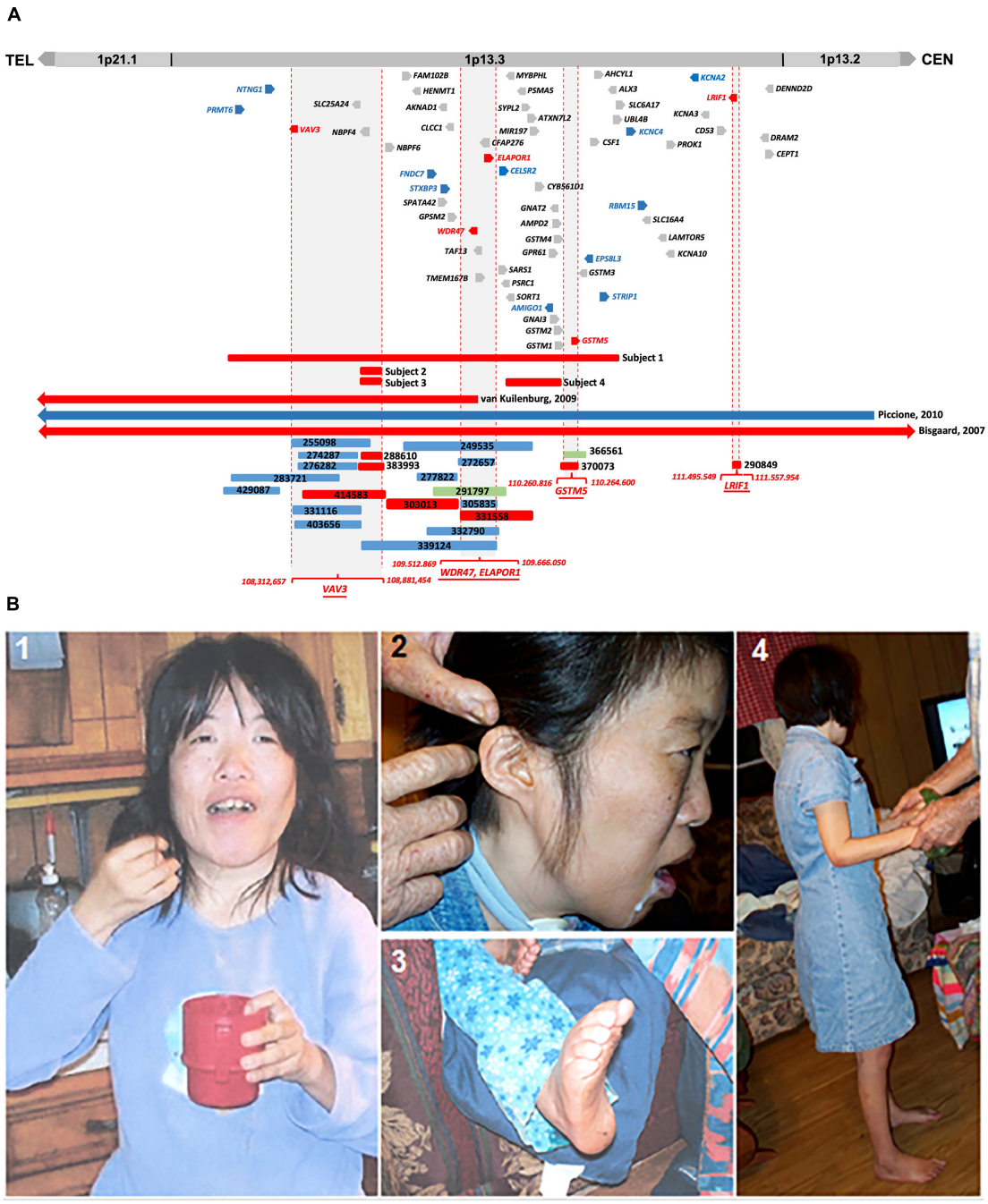

FIGURE 1
(A) Comparative CNV mapping of subjects with CNVs at 1p13.3. Deletions are represented by red bars and duplications are represented by blue bars. CNV cases from the DECIPHER database are denoted by a six-digit reference number. The sizes of the deleted and duplicated regions from Bisgaard et al. (2007) (Case 1), van Kuilenburg et al. (2009) (Case 2), Piccione et al. (2010) (Case 3), and 22 DECIPHER cases are presented relative to our four subjects. Vertical dotted red lines flanking gray background represent the refined four candidate gene loci; 59 genes located within the 4.6 Mb genomic region at 1p13.3 are depicted either in red for positional candidate genes, blue for functional candidate genes, or gray for the remaining genes. **(B)** Phenotypic features of Subject 1. **(1)** Picture shows facial dysmorphism, asymmetrical head, and small hands; **(2)** Low set, small, and unfolded ears; **(3)** arched feet; and **(4)** full body picture showing short stature.

candidate genes in human adult and fetal brain further supported this postulate (Figures 2, 3). Individual interrogation of the 54 remaining genes identified another set of 11 candidate genes. Their candidacy was substantiated by sporadic variants reported in them and their interactors, and their physical interaction with known NDD genes based on BioGrid

TABLE 2 Five positional candidate genes for syndromic NDDs identified by *in silico* CNV mapping at 1p13.3.

No.	Gene candidate & MIM	Variants in human and KO mice with NDDs phenotype	Protein interactors (references for interaction and variants in human with NDDs)
1	*VAV3* (VAV guanine nucleotide exchange factor 3) (605541)	1. Autism: *de novo* c.2305C > G (NM_006113.5); p.P769A (NP_006104.4) (Neale et al., 2012; Turner et al., 2019) 2. Autism spectrum disorder: *de novo* c.1009delC (NM_006113.5); p.L337Sfs*18 (NP_006104.4) (Iossifov et al., 2014; Li et al., 2017) 3. Autism spectrum disorder, increased risk of: *de novo* c.758A > G (NM_006113.5); p.H253R (NP_006104.4) (Lim et al., 2017) 4. Developmental disorder: *de novo* c.1897C > T (NM_006113.5); p.H633Y (NP_006104.4) (Turner et al., 2019) 5. Schizophrenia: *de novo* c.2222A > G (NM_006113.5); p.E741G (NP_006104.4) (Aleksic et al., 2013) 6. In mice, knocking out the *Vav3* gene produces broad physiological changes due to significant issues with sympathetic nervous system modulation (SNS). This is because Vav3 is involved in the formation of appropriate inhibitory GABAergic circuitry between the caudal (CVLM) and rostral (RVLM) ventrolateral medullas in the brainstem (Sauzeau et al., 2010; Rodriguez-Fdez et al., 2021) 7. In the postnatal stage, *Vav3* mice display significant motor coordination and gaiting impairments. These findings suggest that Vav3 function is important for the cerebellum's timely development (Quevedo et al., 2010)	1. *RAC1* (Movilla and Bustelo, 1999): developmental delay, brain malformation, microcephaly (Reijnders et al., 2017), intellectual disability (Lelieveld et al., 2016; Reijnders et al., 2017) 2. *EGFR* (Erdem-Eraslan et al., 2015): autism spectrum disorder (Iossifov et al., 2014; Kosmicki et al., 2017) 3. *IGF1R* (Zeng et al., 2000): short stature, intellectual disability, microcephaly, hypotonia, lack of speech (Uehara et al., 2016) 4. *ZRANB1* (Luck et al., 2020): developmental disorder (Deciphering Developmental Disorders, 2017; Kosmicki et al., 2017; Turner et al., 2019) 5. *TARDBP* (Muller et al., 2020): amyotrophic lateral sclerosis (Kabashi et al., 2008; Sreedharan et al., 2008)
2	*WDR47* (WD repeat-containing protein 47) (615734)	1. Autism spectrum disorder: *de novo* c.991_992delAT (NM_014969.6); p.I331Ffs*16 (NP_055784.3) (Callaghan et al., 2019) 2. The neuroanatomical deficits associated with *Wdr47* KO cause hyperactivity and inappropriate sensory motor gating in both male and female mice (Kannan et al., 2017). 3. The overall brain size of $Wdr47^{tm1a/tm1a}$ mice was reduced, indicating initial microcephaly that worsened postnatally (Kannan et al., 2017). 4. Mutations in 27 WDR genes (∼9 %) have been linked to brain disorders especially intellectual disability related to corpus callosum defects (Kannan et al., 2017).	1. *TCF4* (Li et al., 2015): Pitt-Hopkins syndrome with neurodevelopmental phenotypes (Amiel et al., 2007; Zweier et al., 2007), intellectual disability (Mary et al., 2018) 2. *ANGPTL4* (Huttlin et al., 2021): autism spectrum disorder (Iossifov et al., 2014), developmental disorder (Turner et al., 2019) 3. *DYRK1A* (Guard et al., 2019): autism spectrum disorder (Guo et al., 2018), microcephaly, intellectual disability, speech impairment and distinct facial features (Ji et al., 2015) 4. *RAB11FIP5* (Huttlin et al., 2021): autism spectrum disorder (Roohi et al., 2008; Matsunami et al., 2014), autism (Yuen et al., 2016) 5. *STRN* (Huttlin et al., 2021): autism spectrum disorder (Kosmicki et al., 2017; Lim et al., 2017; Satterstrom et al., 2020), bipolar disorder (Toma et al., 2020) 6. *KRAS* (Martin et al., 2017): Noonan syndrome (Schubbert et al., 2006; Zenker et al., 2007; Leventopoulos et al., 2010; Turro et al., 2020; Ando et al., 2021), intellectual disability and multiple congenital abnormalities (Vergult et al., 2014), neurodevelopmental disorder (Popp et al., 2017)
3	*ELAPOR1* (Endosome-lysosome-associated apoptosis and autophagy regulator 1) (611298)	1. Developmental disorder: *de novo* c.2482G > A (NM_001267048.2); p.A828T (NP_001253977.2) / *de novo* c.2653G > T (NM_001267048.2); p.D885Y (NP_001253977.2) (Turner et al., 2019) 2. Autism spectrum disorder: *de novo* c.2341G > A (NM_001267048.2); p.V781I (NP_001253977.2) (Iossifov et al., 2014) 3. Autism: *de novo* c.2341G > A (NM_001267048.2); p.V781I (NP_001253977.2) (Turner et al., 2019) 4. KO mouse phenotypes associated with decreased exploration in new environment: http://www.informatics.jax.org/diseasePortal/popup?isPhenotype=true&markerID=MGI:1923930&header=behavior/neurological	1. *OSBPL3* (Huttlin et al., 2021): autism (Turner et al., 2019) 2. *DDX58* (Wu et al., 2020): autism spectrum disorder (Iossifov et al., 2014; Lim et al., 2017), autism (Turner et al., 2019) 3. *ADAM15* (Huttlin et al., 2021): autism spectrum disorder (Lim et al., 2017) 4. *ATP13A1* (Huttlin et al., 2021): developmental disorder (Tran Mau-Them et al., 2020), intellectual disability (Anazi et al., 2017; Kahrizi et al., 2019) 5. *ATP6AP2* (Huttlin et al., 2021): mental retardation and epilepsy (Ramser et al., 2005; Al-Nabhani et al., 2018), developmental disorder (Turner et al., 2019), intellectual disability, epilepsy and parkinsonism (Gupta et al., 2015), mental retardation (Buysse et al., 2009), neurodevelopmental disorder (Zhang et al., 2021) 6. *CNTNAP3* (Huttlin et al., 2021): autism spectrum disorder (An et al., 2014; Le et al., 2019), simplex autism (Turner et al., 2017)

(Continued)

TABLE 2 (Continued)

No.	Gene candidate & MIM	Variants in human and KO mice with NDDs phenotype	Protein interactors (references for interaction and variants in human with NDDs)
4	*GSTM5* (Glutathione S-Transferase Mu 5) (138385)	1. GSTM5 belongs to the glutathione S-transferase enzyme family. GSTM5 is located in the brain and metabolizes a wide range of substances, both exogenous and endogenous (Eaton and Bammler, 1999) 2. GSTs (Glutathione S-transferases), which are involved in the glutathione metabolism pathway and include GstA3, Gstm1, Gstm5, Gstm3, Gstk1, and Gstp1, have been identified as risk factors for Alzheimer's disease (Lin et al., 2017) 3. Polymorphisms in *GSTM5* predicted microRNA binding sites were associated with Parkinson's disease diagnosis age (Searles Nielsen et al., 2013) 4. KO mouse phenotypes associated with decreased exploration in new environment: http://www.informatics.jax.org/diseasePortal/genoCluster/view/44861	1. *ERLIN2* (Huttlin et al., 2021): spastic paraplegia (Morais et al., 2017; D'Amore et al., 2018; Rydning et al., 2018; Travaglini et al., 2018; Wright et al., 2018; Park et al., 2020), intellectual disability(Najmabadi et al., 2011; Hu et al., 2019), motor dysfunction and joint contractures (Yildirim et al., 2011) 2. *ARFGAP1* (Huttlin et al., 2021) : autism spectrum disorder (Satterstrom et al., 2020) 3. *AGPAT1* (Huttlin et al., 2021) : autism spectrum disorder (Callaghan et al., 2019) 4. *CDC42* (Silva et al., 2019): intellectual disability, brain malformations, and facial dysmorphism (Martinelli et al., 2018), Noonan-like syndrome (Martinelli et al., 2018), epileptic encephalopathy with infantile spasms (Helbig et al., 2016; Martinelli et al., 2018), intellectual disability, brain malformations, and platelet anomalies (Martinelli et al., 2018), facial dysmorphism, neurodevelopmental delay (Szczawinska-Poplonyk et al., 2020), schizophrenia (Gilks et al., 2012) 5. *GPKOW* (Luck et al., 2020): autism spectrum disorder (Al-Mubarak et al., 2017), microcephaly and intrauterine growth restriction (Carroll et al., 2017)
5	*LRIF1* (Ligand-dependent nuclear receptor-interacting factor 1) (1615354)	1. Developmental disorder: *de novo* c.1151_1152delCT (NM_018372.4); p.S384Cfs*4 (NP_060842.3) (Turner et al., 2019) 2. LRIF1 is required for accurate chromosome segregation in mitosis (Akram et al., 2018) and genes encoding mitotic regulators are growingly linked to neurodevelopmental diseases (Degrassi et al., 2019).	1. *PLEKHA4* (Shami Shah et al., 2019): autism spectrum disorder (Iossifov et al., 2014; Lim et al., 2017), autism (Hashimoto et al., 2016; Turner et al., 2019) 2. *CBX5* (Luck et al., 2020): autism spectrum disorder (Satterstrom et al., 2020), developmental disorder (Deciphering Developmental Disorders, 2017), schizophrenia (Gulsuner et al., 2013) 3. *RARA* (Li et al., 2007): autism spectrum disorder (Iossifov et al., 2014) 4. *AHDC1* (Marcon et al., 2014): syndromic expressive language delay, hypotonia & sleep apnoea (Xia et al., 2014), Xia-Gibbs syndrome (Garcia-Acero and Acosta, 2017; Jiang et al., 2018; Wang et al., 2020; Faergeman et al., 2021), neurodevelopmental disorder (Wang et al., 2020), intellectual disability and developmental delay (Yang et al., 2015; Pekeles et al., 2019), autism spectrum disorder (Iossifov et al., 2014; Kosmicki et al., 2017; Lim et al., 2017), moderate intellectual disability, speech delay, macrocephaly, facial dysmorphism, cleft palate, hypertelorism & macrocrania (Bowling et al., 2017; Jiang et al., 2018) 5. *PQBP1* (Stelzl et al., 2005): mental retardation (Kalscheuer et al., 2003; Lenski et al., 2004; Jensen et al., 2011; Rahman et al., 2019), intellectual disability (Redin et al., 2014; Grozeva et al., 2015; Hu et al., 2016; Abdel-Salam et al., 2018), microcephaly (Shaheen et al., 2019) 6. *SETD1B* (Goehler et al., 2004): intellectual disability and seizures (Brunet et al., 2021; Roston et al., 2021), Intellectual disability, developmental delay, epilepsy, language disorder, autism, facial dysmorphism (Palumbo et al., 2015; Faundes et al., 2018; Hiraide et al., 2018, 2019, 2021), autism spectrum disorder (Iossifov et al., 2014; Satterstrom et al., 2020), Developmental and epileptic encephalopathy (Takata et al., 2019), schizophrenia (Wang et al., 2015) 7. *CDC42* (Stelzl et al., 2005): intellectual disability, brain malformations, and facial dysmorphism (Martinelli et al., 2018), Noonan-like syndrome (Martinelli et al., 2018), epileptic encephalopathy with infantile spasms (Helbig et al., 2016; Martinelli et al., 2018), intellectual disability, brain malformations, and platelet anomalies (Martinelli et al., 2018), facial dysmorphism, neurodevelopmental delay (Szczawinska-Poplonyk et al., 2020), schizophrenia (Gilks et al., 2012)

(Continued)

TABLE 2 (Continued)

No.	Gene candidate & MIM	Variants in human and KO mice with NDDs phenotype	Protein interactors (references for interaction and variants in human with NDDs)
			8. *ATP1B1* (Stelzl et al., 2005): intellectual disability & self-mutilation (Liu et al., 2015), autism(Iossifov et al., 2012; Iossifov et al., 2014; Uddin et al., 2014), autism spectrum disorder (Lim et al., 2017; Turner et al., 2019), intellectual disability (Liu et al., 2015), schizophrenia (Purcell et al., 2014) 9. *CHD3* (Goehler et al., 2004): neurodevelopmental syndrome with macrocephaly, impaired speech and language (Snijders Blok et al., 2019), developmental disorder (Deciphering Developmental Disorders, 2017; Kosmicki et al., 2017; Snijders Blok et al., 2019; Turner et al., 2019), autism (Iossifov et al., 2014; Yuen et al., 2016; Kosmicki et al., 2017; Turner et al., 2019), autism spectrum disorder (Wang et al., 2016; Lim et al., 2017; Cappi et al., 2020; Satterstrom et al., 2020) 10. *CHD4* (Marcon et al., 2014): Sifrim-Hitz-Weiss syndrome (Weiss et al., 2020), neurodevelopmental disorder (Trinh et al., 2019), intellectual disability (Weiss et al., 2016, 2020), developmental disorder (Deciphering Developmental Disorders, 2017; Turner et al., 2019; Weiss et al., 2020), autism spectrum disorder (Iossifov et al., 2014; Wang et al., 2016; Kosmicki et al., 2017), intellectual disability, macrocephaly, hyperlaxity of finger joints and hearing loss (Monroe et al., 2016; Weiss et al., 2016), schizophrenia (Girard et al., 2011; Li et al., 2016)

The candidacy of these genes was justified by their genomic positions in CNV mapping, sporadic variants reported in them and their interactors in NDDs, their physical interaction with known neurodevelopmental genes, and KO mice phenotype based on HGMD, BioGrid, STRING, and MGI. Due to a large number of interacting genes, only a limited number of them in NDD were described. KO mice data with neurobehavioral phenotype are also mentioned wherever available.

and STRING, as well as KO mice phenotype. (**Supplementary Table 1**). Disease Gene Network Analysis (DisGeNET[6], version 7.0) and HPO (Human Phenotype Ontology[7], version 1.7.16) provided additional substantiation of the candidacy of our candidate genes in NDDs.

Results

Microarray

Microarray analysis carried out on genomic DNA from Subject 1 revealed a 3.4 Mb heterozygous deletion at 1p13.3 (chr1: 107,240,429-110,671,860, [hg19]) and its inheritance was not determined. Additional microarray performed on Subject 2, Subject 3, and Subject 4 revealed a 130 kb del(1)(p13.3) arr[hg19](chr1: 108,726,456-108,853,796)x1*dn*, 120 kb del(1)(p13.3) arr[hg19](chr1; 108,729,365-108,853,796)x1*dn*, and 322 kb del(1)(p13.3) arr[hg19](chr1: 109,878,638-110,200,728)x1*mat*, respectively (**Table 1** and **Figure 1A**). Subject 4 has inherited the deletion from her mother with the same phenotype.

Identification of five positional candidate genes by *in silico* comparative genomic mapping

We compared the clinical phenotypes and flanking genomic boundaries displayed in our four subjects (Subjects 1–4) with three previously reported CNV cases encompassing 1p13.3 (Cases 1–3) (Bisgaard et al., 2007; van Kuilenburg et al., 2009; Piccione et al., 2010) (**Table 1** and **Figure 1A**) as well as 22 CNVs with NDDs from a total of 82 cases in the DECIPHER database, based on the criteria of less than 1 Mb in size (**Supplementary Table 3**). *In silico* comparative CNV mapping resulted in four refined candidate gene loci, where the maximal number of CNVs are overlapped (**Figure 1A**), and identified five positional candidate genes (**Table 2**). Loci one, three, and four have a single candidate gene, *VAV3, GSTM5*, and *LRIF1,* respectively, whereas locus two has two positional candidate genes, *WDR47* and *ELAPOR1*.

VAV3 (VAV guanine nucleotide exchange factor 3, MIM 605541) from locus 1 is a member of the VAV family

6 https://www.disgenet.org/

7 https://hpo.jax.org/app

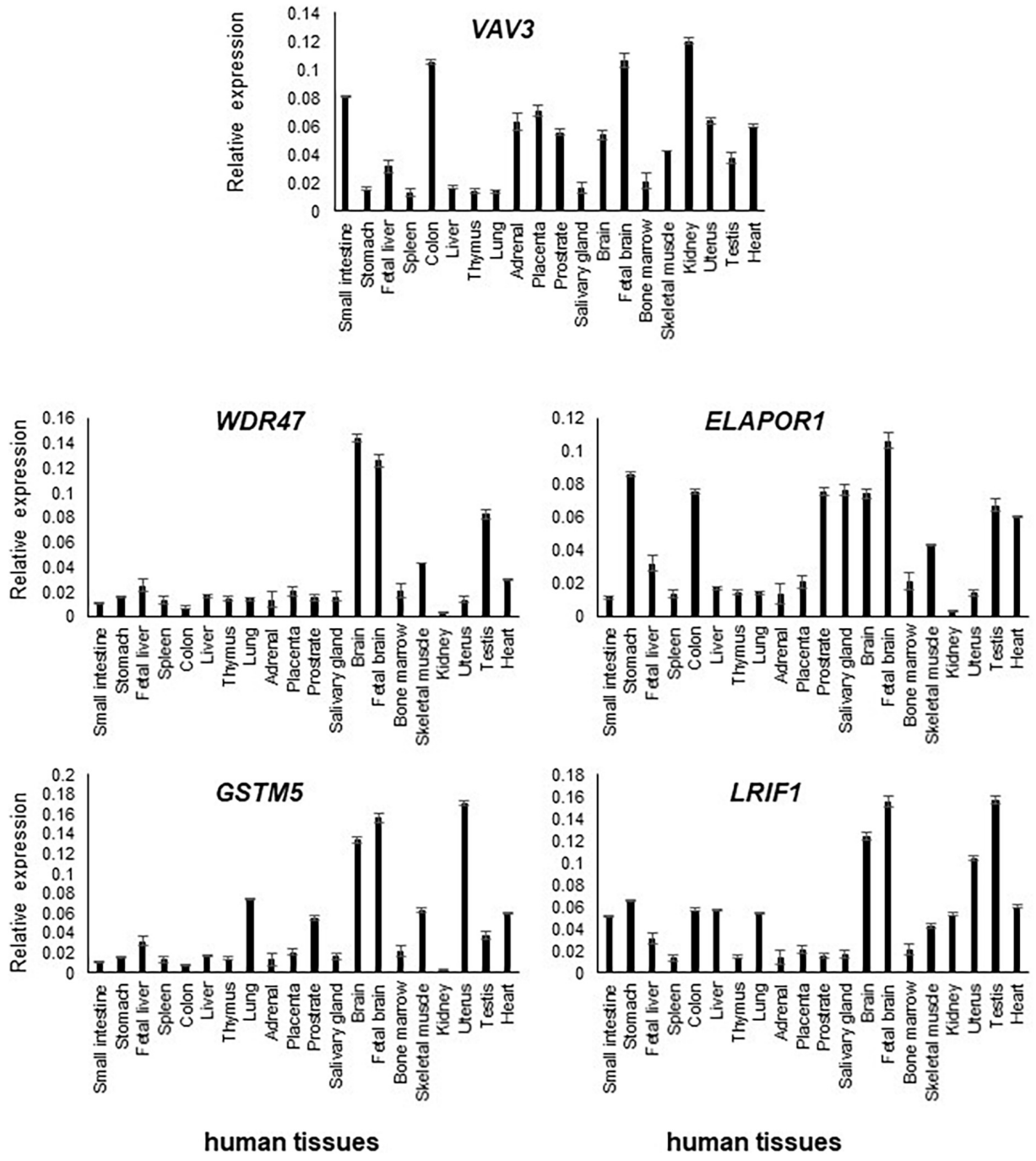

FIGURE 2
Transcript levels of *VAV3, ELAPOR1, WDR47, GSTM5,* and *LRIF1* in various human tissues were determined by RT-qPCR. Relative high expression of them was detected in the adult and fetal brain compared to other tissues.

of guanine nucleotide exchange factors for Rho and Rac GTPases. The VAV family is a group of signal transduction molecules that are regulated by tyrosine phosphorylation and positioned downstream of protein tyrosine kinases. In the ventral medulla, *VAV3* is involved in cerebellum development and axon wiring processes. In the cerebellum, it is involved in Purkinje cell dendritogenesis and the migration and survival of granule cells (Quevedo et al., 2010). In the early postnatal stages of KO mice, the loss of *VAV3* causes motor coordination defects and abnormal gait (Quevedo et al., 2010). Haploinsufficiency of *VAV3* and other four genes (*NTNG1*, *LPPR4*, *GPSM2*, and *COL11A1*) was

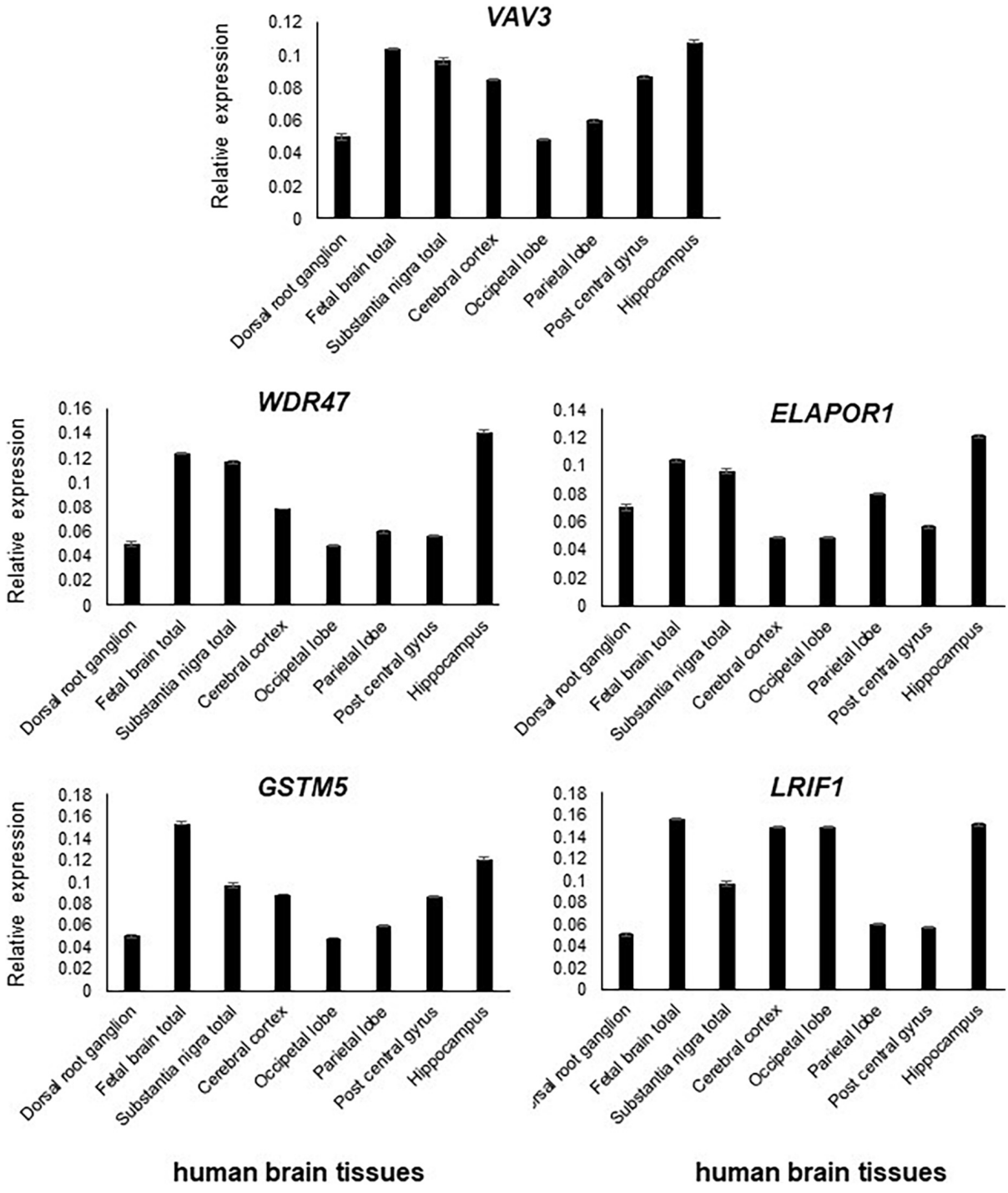

FIGURE 3
All five genes, namely, *VAV3, WDR47, ELAPOR1, GSTM5,* and *LRIF1,* are expressed in the various parts of the brain with varying levels.

postulated to be contributing factors toward the psychomotor impairment and abnormal craniofacial features reported in a subject with a 14 Mb interstitial deletion encompassing 1p13.3 (van Kuilenburg et al., 2009). Interestingly, three *de novo* variants in *VAV3* were found in individuals with autism spectrum disorder (ASD) (Neale et al., 2012; Iossifov et al., 2014; Li et al., 2017; Lim et al., 2017; Turner et al., 2019), one with neurodevelopmental disorder (Turner et al., 2019), and one with schizophrenia (Aleksic et al., 2013; **Table 2**).

SLC25A24 (solute carrier family 25 member 24, MIM 608744) is within candidate locus one, which also includes *NBPF4* (**Figure 1A**). Two recurrent missense mutations in *SLC25A24* have been reported in Gorlin-Chaudhry-Moss syndrome (GCMS) (Ehmke et al., 2017) and Fontaine syndrome (Writzl et al., 2017), which are progeroid syndromes associated with accelerated aging. Due to the extreme aging facial phenotype caused by reported heterozygous mutations, the low level of expression in the human brain, and the absence of sporadic variants in the subjects with DD or ASD from the literature, this gene was excluded from the positional candidate gene list.

NBPF4 (neuroblastoma breakpoint family, member 4, MIM 613994) is a member of the neuroblastoma breakpoint family (NBPF) and contains the DUF1220 protein domain of approximately 65 amino acids in length. This domain has undergone unusually rapid and extensive duplications due to its repetitive structure during recent primate evolution. Chromosome 1 has 20 *NBPF* genes containing highly conserved DUF1220 domains and 13 of them are dispersed at 1q21 (Vandepoele et al., 2005; Diskin et al., 2009). Although DUF1220 sequences appear to exhibit a significant direct correlation with brain-size phenotypes in humans (Dumas et al., 2012), it was excluded due to no expression in the human brain and the absence of any reported genetic variants in NDDs.

Among the five genes, namely, *WDR47, TAF13, TMEM167B, CFAP276,* and *ELAPOR1,* located in the second locus, we found two positional candidate genes.

WDR47 (WD repeat-containing protein 47, MIM 615734), sharing structural homology with lissencephaly gene *LIS1* (*PAFAH1B1*), participates in core microtubule-mediated processes, including neural stem cell proliferation, radial migration, and growth cone dynamics. KO mice lacking Wdr47 exhibited partial lethality, extensive fiber defects, microcephaly, thinner cortices, and abnormal sensory motor gait (Kannan et al., 2017). Kannan et al. speculated that mutations in this gene, particularly, truncating ones, would cause an embryonic lethal phenotype in humans, which would explain why no human mutations were identified. However, 2 years later, one frameshift variant in this gene was reported in a patient with ASD (Callaghan et al., 2019).

TAF13 (TATA-box-binding-protein-associated factor 13, MIM 600774), associated with ID combined with microcephaly, was excluded due to its autosomal recessive pattern (Tawamie et al., 2017).

TMEM167B (transmembrane protein 167B, aka *C1orf119*) was not considered as a candidate because no genetic variants in this gene were reported in NDD subjects and it is not expressed at high levels in the human brain.

CFAP276 (cilia and flagella-associated protein 276, aka *C1orf194*, MIM 618682) was excluded because two missense mutations cause dominant Charcott-Marie-Tooth disease (Sun et al., 2019); it is expressed at very low levels in the human brain, and no genetic variant was reported in NDD subjects.

Four genetic variants in *ELAPOR1* (endosome-lysosome associated apoptosis and autophagy regulator 1, aka *KIAA1324*, MIM 611298) in DD and ASD have been reported (Iossifov et al., 2014; Turner et al., 2019), and at least six of its interacting genes at the protein levels are strongly involved in diverse NDDs. Moreover, KO mice exhibit decreased exploration in a new environment (**Table 2**), suggesting *ELAPOR1* is likely a candidate gene (**Figure 1A** and **Table 2**).

The third candidate locus refined to 86 kb as depicted in **Figure 1A** implies *GSTM5* (glutathione S-transferase mu 5, MIM 138385), a member of the glutathione S-transferase (GST) family possibly involved in NDDs, because of variants found in interacting genes at the protein levels and KO mice showing decreased exploration in a new environment (**Figure 1A** and **Table 2**). Its paralog *GSTM1* null genotype in human carriers is more likely to develop ASD (Mandic-Maravic et al., 2021). GSTs are a group of enzymes that play a major role in the antioxidant defense mechanism by performing the inactivation of a large number of endogenous oxidative stress products. So far, a number of studies have suggested a link between oxidative stress and ASD (Mandic-Maravic et al., 2021). *GSTM5* has at least five interacting genes at the protein level, variants of which were reported in various NDD subjects (**Table 2**).

Finally, the fifth positional candidate gene *LRIF1* (ligand-dependent nuclear receptor-interacting factor 1, MIM 615354) is aligned near the centromeric region of 1p13.3. It overlaps with a 62 kb DECIPHER microdeletion case 290849 who presented with ID and behavioral abnormalities (**Figure 1A** and **Supplementary Table 3**). This variant was inherited from the father, whose phenotype is unknown. Importantly, however, *LRIF1* interacts with two genes among others at the protein level, namely, *PQBP1* (polyglutamine-binding protein 1, MIM 300463) and *CHD4* (chromodomain helicase DNA-binding protein 4, MIM 603277). Mutations in *PQBP1* are the cause of X-linked ID (Kalscheuer et al., 2003), while missense mutations in *CHD4* are linked to ID syndrome with distinctive dysmorphisms (Weiss et al., 2016). Furthermore, another interactor *ADHC1* (AT-hook DNA-binding motif-containing protein 1, MIM 615790) is involved in Xia-Gibbs syndrome with symptoms of ID, speech/motor delay, and facial dysmorphism (Xia et al., 2014), whereas interactor *CHD3* is associated with Snijders Blok-Campeau syndrome, an NDD exhibiting macrocephaly and speech/language delay (Snijders Blok et al., 2018). Missense variants of the interactor *CDC42* cause a diverse neurodevelopmental phenotype resembling Noonan syndrome (Martinelli et al., 2018), and the interactor *SETD1B* (aka *KMT2G*) is associated with the syndromic ID (Hiraide et al., 2018; Roston et al., 2021; Weerts et al., 2021; **Table 2**). We, therefore, suggest that *LRIF1* could be considered a strong candidate for NDD, and this single DECIPHER case

underscores the possibility of finding a neurodevelopmental disease gene (**Figure 1A**).

We also checked the interacting proteins of these five positional candidate genes using STRING (Functional Protein Association Networks, string-db.org, version 11.5) and BIOGRID (Database of Protein, Chemical, and Genetic Interactions, thebiogrid.org, version 4.4) protein–protein interaction databases and found that all of them interact with proteins already known to be associated with various NDDs. This outlines the potential role played by the proteins encoded from these five positional candidate genes and their interacting protein partners (**Table 2**).

Identification of 11 additional functional candidate genes possibly dysregulated by position effect

We have interrogated the remaining 54 genes at 1p13.3, some of which might be dysregulated by position effect even if they are not contained in the four candidate gene loci. The criteria for selecting additional candidate genes are 3-fold: (1) sporadic *de novo* genetic variants in them were reported in subjects with NDDs, (2) animal models substantiated their pathological roles in NDDs, and (3) sporadic *de novo* genetic variants in NDD subjects were reported in their interacting genes at the protein level. This approach has identified additional 11 candidate genes which might be dysregulated by position effect (**Supplementary Table 1**).

Quantitative reverse transcription PCR (RT-qPCR)

Transcript levels of the five positional candidate genes were determined by RT-qPCR in various human tissues to assess their functional importance in phenotype-relevant tissues. The spatio-temporal regulation of gene expression leads to disparate expression patterns dependent on a variety of factors including the detection methods, which may not properly define the expression patterns. Differential expression patterns in multiple publicly available resources including GTEx Portal[8] (version 8) and NCBI prompted us to use commercially available human RNA samples to measure the expression patterns through RT-qPCR experiment so that we would have a reference of expression of the genes of interest.

In comparison to other tissues, *VAV3, WDR47, ELAPOR1, GSTM5,* and *LRIF1* expressions were found relatively high in the adult brain and/or fetal brain (**Figure 2**). The high expression of these five genes in the human fetal brain suggests that they might be involved in an early neurodevelopmental phenotype such as DD when mutated. The variable expression pattern in tissues at different developmental stages underscores the significance of analyzing the fetal brain along with the adult brain.

All five genes (*VAV3, WDR47, ELAPOR1, GSTM5*, and *LRIF1)* were highly expressed in various subsections of the brain with differing levels (**Figure 3**).

Disease-gene network analysis provides additional corroboration for NDD phenotype from candidate genes

To obtain additional evidence for our candidate genes being functionally involved in the clinical phenotype observed in our subjects, we consulted DisGeNET, one of the largest publicly available collections of genes and variants associated with human diseases (Pinero et al., 2020). After combining the lists of the five positional candidates (**Table 2**) and the 11 functional candidates (**Supplementary Table 1**), we focused on two specific disorders relevant to the phenotype studied here: "mental disorders" and "nervous system diseases." Out of our 16 candidates, *FNDC7* is not present in DisGeNET, and seven are connected to at least one mental disorder confirming their involvement in the phenotype studied here (**Figure 4**). Among the 11 functional candidate genes, *STXBP3* and *KCNA2* seem to be particularly strong candidates since they are connected to disease terms like "impaired cognition" and "mental deterioration" among other relevant terms. The network for nervous system diseases is given in **Supplementary Figure 1**.

As DisGeNET was last updated in June 2020, we also consulted Human Phenotype Ontology (HPO), another resource for gene–disease relationships, which was last updated in June 2022. As in the results from DisGeNET, *KCNA2* is again linked to relevant terms like HP:0001268 (mental deterioration), HP:0001249 (intellectual disability), as well as HP:0000750 (delayed speech and language development), HP:0001263 (global developmental delay), and HP:0002317 (unsteady gait), additional relevant terms to the phenotype described in this article. *KCNA4* is also linked to HP:0000750 (delayed speech and language development) and HP:0002064 (spastic gait). Unfortunately, *STXBP3* could not be found in the HPO database nor any other genes given in **Figure 4**.

Discussion

The CNVs represent a rich source of structural chromosomal variations that can result in severe phenotypic consequences as a result of gene dosage alteration, disruptions in coding sequences, and long-range gene regulators (Stranger et al., 2007). With the advancement of detection technology,

8 https://gtexportal.org/home/

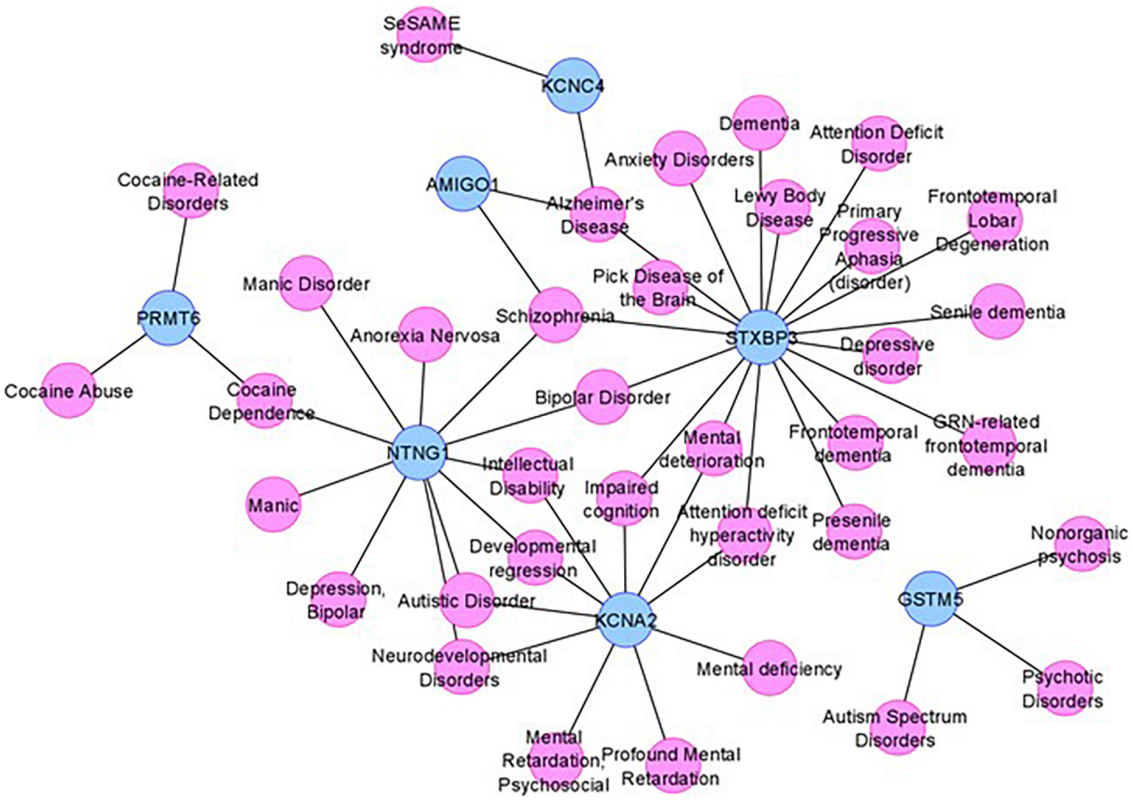

FIGURE 4
The mental disorder network. The candidate genes are depicted by blue nodes, and the disease terms are depicted by pink nodes. Edges correspond to disease associations.

it has become apparent that the collective involvement of CNVs underlies neurodevelopmental syndromes (Lee et al., 2015). Clinical features of seven heterozygous CNVs located at 1p13.3 have been described through karyotype–phenotype correlations (Tabata et al., 1991; Mattia et al., 1992; Lo et al., 1998; Utkus et al., 1999; Bisgaard et al., 2007; van Kuilenburg et al., 2009; Piccione et al., 2010) (Cases 1–7 in **Table 1**). Four of these published cases (Cases 4–7 in **Table 1**) are from the pre-microarray era, so the exact sizes, as well as the distal and proximal genomic breakpoints, of these large 1p13.3 deletions (9–21 Mb) are unknown.

Causative disease gene identification has been aided by refinement of critical regions through comparison of patients with overlapping large deletions like in Kallmann syndrome (Dode et al., 2003) and CHARGE syndrome (Vissers et al., 2004). However, understanding the genetic etiology of large pathogenic CNVs still remains a major challenge, because they frequently contain multiple genes (Rice and McLysaght, 2017).

By contrast, small CNVs containing a couple of genes provide a great potential in the identification of disease genes through comparative genomic mapping by aligning the genomic boundaries of CNVs with varying sizes and overlapping phenotypes. This was evidenced by an NDD candidate gene *SETD1B* identified from a critical 445 kb genomic region encompassing seven genes at 12q24.31 (Labonne et al., 2016). In the ensuing years, a large number of mutations in this gene were identified from next-generation sequencing (NGS) databases, verifying it as an NDD disease gene (Hiraide et al., 2018; Roston et al., 2021; Weerts et al., 2021).

Recently, we have recruited four new subjects having heterozygous microdeletions at 1p13.3 with common features of NDDs. To find out the candidate genes responsible for disease phenotypes, we aligned our cases with the aforementioned three published CNVs along with 22 informative DECIPHER cases on 1p13.3 as described in the "Results" section.

DECIPHER cases at 1p13.3 comprise 13 duplications, seven deletions, and two triplications (**Supplementary Table 3**). Nonetheless, most cases displayed neurodevelopmental phenotypes with various comorbidities. NDDs are linked to dosage alterations of several genes in both deletions and duplications (Rice and McLysaght, 2017). In addition, the majority of CNV cases are inherited from one parent with an unknown phenotype, while the inheritance of the remainders is unknown. This suggests that some CNVs at 1p13.3 might be inherited from an affected parent, have varying penetrance, or are imprinted epigenetically.

Our four subjects and seven patients reported in the literature share an overlapping phenotype of DD, ID, and facial dysmorphism (**Table 1**). This offered an opportunity for the identification of NDD genes that are responsible for a common set of phenotypes and features among all subjects with 1p13.3 interstitial deletions and duplications, regardless of whether they are inherited or *de novo*.

Based on our comparative *in silico* genomic mapping, we narrowed down the 4.6 Mb genomic region of 1p13.3 to four individual candidate gene loci and identified five positional candidate genes (*VAV3, WDR47, ELAPOR1, GSTM5,* and *LRIF1)* out of 59 genes in total (**Figure 1A** and **Table 2**). It is likely that the neurodevelopmental features in the majority of our CNV cases encompassing one or more of the five potential candidate genes are caused either by a single gene or by a combination of multiple genes among them.

Each gene has been interrogated in order to identify sporadic *de novo* variants in them or their interacting genes at the protein level in NDD subjects from the literature. Furthermore, their KO mice phenotype has been investigated to obtain supporting evidence (**Table 2** and **Supplementary Table 1**), which has substantiated the candidacy of these positional candidate genes. We also confirmed the high expression of these genes in the brain and subsequently specific brain regions, suggesting their pathogenicity in NDDs (**Figures 2**, **3**). The collective effort of *in silico* genome mapping informed by various disease gene databases, the role of interacting protein partners, and confirmation of gene expression in brain tissues strongly indicate the functional candidacy of these five positional genes in causing various NDDs.

Among the candidate genes we found, *VAV3* plays an important role in bone mass and remodeling, axon wiring in the ventrolateral medulla, and cerebellar development (Faccio et al., 2005). The cerebellum is known to be involved in motor learning and coordination. Consequentially, impairment of this region leads to dysfunctions in movement (Mapelli et al., 2022). This suggests a reason for the short stature, bone anomalies, and jerky gait pertaining to Subject 1 in this study (**Table 1**). VAV proteins have key signaling roles in the immune, cardiovascular, and nervous systems (Bustelo, 2014).

WDR47 belongs to the family of WD40-repeat (WDR) proteins. So far, mutations in 27 genes (9.4%) among 286 WDR genes have been linked to brain disorders, most notably ID associated with corpus callosum defects (Kannan et al., 2017). A smaller corpus callosum has been linked to an increased risk of autism (Paul et al., 2007), bipolar disorder (Li et al., 2014), and schizophrenia (Balevich et al., 2015). WDR47 is necessary for proper radial migration of projection neurons, and Wdr47 depletion compromises growth cone morphology and microtubule. The neuroanatomical defects found in Wdr47 KO result in hyperactivity and sensory motor gating abnormalities both in male and female mice (Kannan et al., 2017), suggesting a link between WDR47 and neurological disorder.

LRIF1 is required for accurate chromosome segregation in mitosis (Akram et al., 2018). A growing number of genes that regulate mitotic division are involved in neurodevelopmental diseases. Mitotic gene mutations give rise to insufficient cell proliferation and/or failure to replenish the neuronal stem cells in early development. The reduced number of neurons results in the underdevelopment of the central nervous system (CNS) and causes microcephaly and neuronal migration disorders (Degrassi et al., 2019). LRIF1 also interacts with many known genes involved in NDDs, which justifies its status as an NDD candidate gene (**Table 2**).

Another observation in the subjects and cases was that the severity of the phenotypes increases with the CNV size (**Table 1** and **Figure 1A**). Three of the published cases (Cases 1–3 in **Table 1**) and Subject 1 with CNVs ranging from 3 to 14 Mb displayed severe cranial anomalies including microcephaly, macrocephaly, and asymmetry of the skull. However, among the remaining subjects with small CNVs, only Subject 4 displayed cranial anomalies that were considerably less pronounced than larger CNVs. Although Case 4 with the largest deletion did not show any apparent cranial anomalies, it remains to be seen whether she will develop secondary cranial anomalies after her infancy (**Table 1**). Larger deletions (Subject 1, Case 1, Case 2, Case 5, and Case 7) exhibited a distinct muscle disorder (mild fiber atrophy, diplegia, hypertonia, areflexia, and hypotonia) in comparison to Subjects 2–4 with small deletions, who did not show any muscle disorders (**Table 1**). Additionally, in contrast to Subjects 2–4 with small deletions, epilepsy was more pronounced in published cases with larger CNVs, including Subject 1, Case 4, and Case 6 (**Table 1** and **Figure 1A**). Similarly, multiple hand, finger, feet, and toe anomalies were observed in all the published Cases 1–7 and Subject 1 that had significant large CNVs.

Furthermore, we also propose 11 additional genes, not encompassed within the demarcated loci, yet, pose as NDD candidate genes due to genetic variants in NDD subjects and KO mice with neurological phenotype. To support their candidacy, we also analyzed and compiled a list of interacting protein partners known to play a role in NDDs (**Supplementary Table 1**). These genes included in large CNVs (Subject 1 and Cases 1–3, **Figure 1A** and **Table 1**) were not contained in small CNVs, which were aligned to refine the candidate gene loci in *in silico* comparative genomic mapping. Hence, the clinical symptoms seen in these small CNVs might be caused by the position effect leading to altered expression of these 11 genes adjacent to them (Redon et al., 2005). Or these 11 genes might contribute to the phenotypes in the individuals with larger deletions and be irrelevant for cases with smaller CNVs.

Being the largest chromosome (249 Mb and representing 9% of the total human genome) containing a maximum number of 2,000 genes, chromosome 1 harbors the highest number of disease genes (Murphy et al., 2003).

We hypothesized that a total of 16 novel autosomal dominant candidate genes identified at 1p13.3 in this study are dosage sensitive in either direction and thus might not tolerate copy number change. These candidate genes will help zero in on NDD disease genes from NGS databases containing a large number of loss-of-function VUSs (variants of unknown significance) and autosomal dominant GUSs (genes of unknown significance).

Clinical reports

Subject 1 [46,XX,del(1)(p13.3), arr[hg19](chr1:107,240,429-110,671,860)x1]

Subject 1 (DGDP030) is a 44-year-old Asian woman, exhibiting a severe clinical phenotype as a result of a 3.4 Mb interstitial heterozygous deletion at 1p13.3. Her records indicate a normal birth, and her examination was within normal limits. She was adopted at 4 months of age; healthy appearing and quiet. She did not make eye contact or smile much; she would only cry when hungry and was unable to lie on her stomach. Yet, she was able to roam around the room on her back and she had a forceful grip. Her teeth did not appear until 20 months of age, after which, all grew within 3 months. Her mouth was too small for all her teeth and five had to be extracted. She then started to display mild hypotonia and suffered febrile seizures at 18 months of age.

At 3 years of age, she was diagnosed with the following symptoms: asymmetrical skull, mild anemia, febrile seizures, possible myoclonic seizures, hypotonia, hearing loss, and a recurring petechial rash. She was having seizures once a month. She also had strange night terror episodes and childhood schizophrenia. She was obsessive–compulsive and had wide mood swings that lasted 2–3 weeks each. The biopsy of her skeletal muscle from both gluteus and maximus at 18 years of age showed mild fiber atrophy and random variation in muscle fiber size. Her motor milestones were of poor quality and out of the usual order. She had a learning disability but could be directed to play; however, she preferred not to. She liked being in a room with people but did not make much of an effort to interact.

At the age of 31 years, she remained severely developmentally delayed and autistic. She had a jerky gait and would walk with arched feet. She constantly suffered from cramps in her legs and arms. She had an asymmetrical head with a smaller right parietal area, ptosis, astigmatism, low-set ears, unfolded ears, kyphosis, lordosis, and a high arched palate (**Figure 1B**). She held her hands at odd angles and held objects with her fingertips. At the age of 31 years, she had a complete emotional breakdown and increased violent behavior. At the same time, her tegretol levels were in the toxic range, and her thyroid levels were in the hypothyroid range.

At this age, she has had several bouts of myoglobinuria, unexplained fevers, recurrent infections, paradoxic and toxic reactions to medications, allergies to insect bites, hypothyroidism likely related to her seizure medication, thrombocytopenia due to medication, malignant hyperthermia, easily developed bruises, petechial rash, anemia, intermittent diarrhea, severe constipation, and both external canals intermittently plugged with cerumen. An auditory brainstem response evaluation was suggestive of a moderate peripheral deficit, potentially sensorineural, more so in the right ear than in the left ear. She was usually remarkably healthy with a normal echocardiogram and normal eye examination.

Subject 2 [46,XY,del(1)(p13.3), arr[hg19](chr1:108,726,456-108,853,796)x1*dn*]

Subject 2 is an 11-year 6-month-old Caucasian boy with a history of global developmental delay, ID, and dysmorphic features. The child was born full term at 38 weeks of pregnancy and delivered by elective cesarean section from non-consanguineous parents. At birth, he weighed 2.650 kg (10^{th} percentile) and his crown-heel length was 51 cm (50^{th} percentile). Global developmental delay was observed at an early age. Up until the age of 11 years, no morphological phenotypic data were available for the child until specific genetic physicals revealed a bulbous nasal tip, epicanthal folds, downslanted palpebral fissure, low anterior hairline, long philtrum, wide nasal bridge, thin upper lip vermilion, long ears, micrognathia, and hypertelorism. At the age of 11 years, he weighed 32.5 kg (25^{th} percentile) and measured 139 cm in height (25^{th} percentile). He sat independently at around 12 months, walked at 24 months, spoke his first words at 36 months, and was not communicating in full sentences until 11 years of age. Now, at the age of 18 years, his speech has improved but he is not yet able to speak fluently. The MRI of the head showed no remarkable findings and remained likewise subsequently. Despite being recognized as an inattentive patient, psychological assessments revealed no attention deficit hyperactivity disorder (ADHD). However, he has shown severe learning difficulties, requiring individualized educational assistance to date. He has no significant anxiety disorder and shows continued progress; nevertheless, his deficits in attention and executive functions persist. Additional clinical laboratory tests have been carried out for this patient, including an extensive metabolic workup, chromosome analysis, and chromosomal microarray analysis. Except for the microarray result, all of the tests were uneventful. However, microarray indicated a *de novo* 130 kb heterozygous genomic loss at 1p13.3.

Subject 3 [46,XX,del(1)(p13.3), arr[hg19](chr1:108,729,365-108,853,796)x1*dn*]

Subject 3 is a 6-year-old Caucasian girl with a history of neurodevelopmental delay, ID, epilepsy, and dysmorphic features. The child was born full term at 36 weeks of pregnancy and delivered by elective cesarean section. The biological parents stated that they could not rule out consanguinity; nonetheless, the child's chromosomal microarray analysis did not show long continuous stretches of homozygosity. At birth, the newborn weighed 2.415 kg (5^{th} percentile), and her crown-heel length was 50 cm (50^{th} percentile). The Apgar scores were 07/09. As a newborn, the child showed no sucking reflex, requiring assistance to nursing. Moreover, at the age of 3 days old, she displayed jaundice. Up until the age of 6 years, no morphological phenotypic data were available for the child, when specific genetic physicals revealed epicanthal folds, downslanted palpebral fissure, long philtrum, wide nasal bridge, hypertelorism, and micrognathia. At the age of 6 years, the child had one seizure episode, and her MRI indicated a small arachnoid cyst in the posterior fossa. Global developmental delay was observed at an early age. She sat independently at around 10 months and walked at 16 months. Since birth, the child has shown loose skin. Additional clinical laboratory tests were performed including an extensive metabolic workup, chromosome analysis, and microarray analysis, which indicated a *de novo* 120 kb heterozygous genomic loss at 1p13.3.

Subject 4 [46,XX,del(1)(p13.3), arr[hg19](chr1:109,878,638-110,200,728)x1*mat*]

Subject 4 is the first of four children of an unrelated Caucasian couple. The mother with the same microdeletion presents with global DD, behavioral disorders, and ID. Otherwise, the medical history of the father's family was non-contributory. Vaginal delivery occurred at 39 weeks. At birth, growth parameters were within the normal range except for OFC < –2DS (birth weight 20^{th} percentile/birth height 30^{th} percentile). She walked at 18 months of age. She suffered from anxiety and intellectual disability, the reason why she was referred to a medical geneticist at the age of 15 years. On examination, she had a long face, epicanthus, prominent nose, posteriorly rotated ears, and short fingers. Her microcephaly was persistent. She had an array-CGH that revealed a maternally inherited 322 kb heterozygous deletion at 1p13.3 arr[hg19](chr1:109,878,638-110,200,728). Her oldest brother presents with global developmental delay, speech delay, and intellectual disability. Unfortunately, this family was lost to follow-up, and the segregation including the brother within the family could not get done. We were not able to get updated information regarding her development now that she is 22 years.

Materials and methods

Karyotype

For high-resolution karyotypes, peripheral blood lymphocytes from subjects were cultured with phytohematoagglutinin and harvested for cytogenetic analysis using standard techniques. Chromosome analysis was performed on GTL-banded chromosomes at an approximately 550 band level.

For Subjects 2 and 3, conventional cell cultures, harvesting, and GTG banding with a > 550 band resolution were performed following standard procedures. Chromosome analyses were done using Zeiss Axioscope® (Göttingen, Germany) and the software IKAROS® (Metasystems Corporation, Altlussheim, Germany).

For Subject 4, array-comparative genomic hybridization analysis (CGH) was performed using 180K Agilent microarray (Agilent Technologies, Santa Clara, CA, USA). Image analysis, normalization, and annotation were done with Feature Extraction 10.5.1.1 (Agilent, Santa Clara, USA) using the default settings. Data visualization and further analysis were performed with Cytogenomics 2.7.6.0 (Agilent, Santa Clara, USA). The array-CGH also detected a duplication of 17p11.2 of 194 kb (chr17:21307889-21502083), considered as benign.

Genomic DNA extraction and microarray

The extraction of genomic DNA from Subject 1 was carried out using a standard phenol-chloroform protocol. To analyze submicroscopic copy number alterations in subjects, DNA samples from the subject's blood and pooled normal controls (PROMEGA) were differentially labeled and cohybridized using a 44K whole-genome oligonucleotide array employing the protocols for array CGH provided by the manufacturer (Agilent, Santa Clara, USA). No deletion or duplication of other chromosomes was observed using the laboratory standard cutoff values (0.0Log2 ratio at a resolution of 0.3 Mb). Image analysis, normalization, and annotation were done with Feature Extraction 10.5.1.1 (Agilent, Santa Clara, USA) using the default settings. Data visualization and further analysis were performed with GenomeCAT[9]. CNVs were determined by circular binary segmentation.

9 https://www.molgen.mpg.de/~abt_rop/molecular_cytogenetics/CGHPRO.html

Genomic DNAs from Subjects 2 and 3 as well as their parents were isolated from whole blood samples using the Illustra Blood Genomic Prep Mini Spin Kit (GE Healthcare Life Sciences, USA), following the manufacturer's instructions. Chromosomal microarray analysis (CMA) was carried out on probands and their biological parents using the GeneChip® CytoScanHD™ (ThermoFisher, USA) with 2.7 million polymorphic and non-polymorphic markers. Array analyses were done using the Chromosome Analysis Suite (ChAS®) software. The CNVs found in probands were analyzed in comparison with public databases, including the Database of Genomic Variants[10] (DGV, version 107), the Database of Chromosomal Imbalance and Phenotype in Humans using Ensemble Resources (DECIPHER), and the CytoScan™ HD (High Density) Array Database.

Fluorescence *in situ* hybridization

For Subject 1, BACs for probing genomic regions of interest were selected from the RPCI-11 (Roswell Park Cancer Institute) library *via* the UCSC genome browser[11]. Human genomic DNA inserts were extracted, fluorescently labeled using nick translation, and hybridized to a metaphase spread of the subject's lymphocytes using standard procedures (Lichter et al., 1990).

Comparative CNV mapping

The phenotypes and genomic coordinates from our four subjects (Subjects 1–4) were compared with three previously reported literature cases (Cases 1–3) (Bisgaard et al., 2007; van Kuilenburg et al., 2009; Piccione et al., 2010) and 22 unpublished DECIPHER CNVs with NDDs and less than 1 Mb in size (**Figure 1A**, **Table 1**, and **Supplementary Table 3**). Genomic coordinates from Case 1 were converted from hg17 to hg19 before the comparison was carried out. Furthermore, for the case from van Kuilenburg et al. (2009), the flanking distal and proximal genomic boundaries were between *TLCD4* and *WDR47* with the approximate genomic coordinates 95,558,073-109,584,850 (A.B.P. van Kuilenburg, personal communication, 19 May 2022) as reported in Figure 5 of their study.

Quantitative reverse transcription PCR (RT-qPCR)

RT-qPCR was performed from the total RNA of the human brain and other tissues (Human Total RNA Master Panel II, Cat# 636643, Clontech). The catalog numbers of eight brain tissues from Clontech were as follows: dorsal root ganglion-636150, fetal brain total-636526, substantia nigra total-636560, cerebral cortex-636561, occipital lobe-636570, parietal lobe-636571, postcentral gyrus-636573, and hippocampus-636565. The cDNA synthesis was performed using 1–2 μg of total RNA using high-capacity cDNA reverse transcription kit and analyzed by RT-PCR on QuantStudio 6 Flex system using SYBR Green (ThermoFisher, Waltham, MA). We used ΔCt method to calculate the relative expression of each gene. In summary, relative gene expression was calculated by the difference between the Ct value (ΔCt) of the gene of interest and reference gene, GAPDH. After determining ΔCt, the fold change ($2^{-\Delta Ct}$) was measured, and the relative expression was plotted as excel graphs.

Disease-gene network analysis

We performed disease-gene network analysis with DisGeNET (v7.0) (1) which contains 1,134,942 gene-disease associations between 21,671 genes and 30,170 diseases, disorders, traits, and clinical or abnormal human phenotypes. We used the DisGeNET Cytoscape app (Pinero et al., 2021) to browse and visualize the networks around the candidate genes. We used all sources, any association type and evidence level, and two specific disease classes of interest, namely, "mental disorders" and "nervous system diseases."

Data availability statement

The original contributions presented in this study are included in the article/**Supplementary material**, further inquiries can be directed to the corresponding author/s.

Ethics statement

The studies involving human participants were reviewed and approved by Augusta University, Georgia, USA. Written informed consent to participate in this study was provided by the participants' legal guardian/next of kin. Written informed consent was obtained from the minor(s)' legal guardian/next of kin for the publication of any potentially identifiable images or data included in this article.

Author contributions

AB-M and KJ contributed to the manuscript preparation including figure design and phenotypic data analysis. VG and PS performed the RT-qPCR and clinical examination of the

10 http://dgv.tcag.ca/dgv/app/home

11 http://genome.ucsc.edu

patient data, respectively. ADLF performed the bioinformatics analysis. YP and KS collected and analyzed the data. CK, ADDC, ASDC, IP, LM, AS, LF, PC, and CR recruited the subjects and/or performed the clinical follow-up. LL, I-KK, C-HK, and W-YK edited the subsequent manuscript drafts and analyzed the data. H-GK conceived and designed the study, analyzed the data, and drafted the first manuscript. All authors read and approved the final manuscript.

Funding

This work was supported by an internal grant QB17 of Qatar Biomedical Research Institute (H-GK), a grant from the National Research Foundation of Korea (2018M3A9B8021980 to C-HK), an NICHD grant (R01HD092505 to LL), and a grant from the National Research Foundation of Korea (2020R1A2C2006614 to I-KK). We also thank the support of funding provided by Caroline Jones-Carrick and Collin Carrick.

Acknowledgments

We thank Jill A Rosenfeld, Jade Deborah D Mello, and Shahad Sabaawi Ibrahim AlHassan for their assistance in proofreading the final version of the manuscript.

Conflict of interest

The authors declare that the research was conducted in the absence of any commercial or financial relationships that could be construed as a potential conflict of interest.

Publisher's note

All claims expressed in this article are solely those of the authors and do not necessarily represent those of their affiliated organizations, or those of the publisher, the editors and the reviewers. Any product that may be evaluated in this article, or claim that may be made by its manufacturer, is not guaranteed or endorsed by the publisher.

Supplementary material

The Supplementary Material for this article can be found online at: https://www.frontiersin.org/articles/10.3389/fnmol.2022.979061/full#supplementary-material

SUPPLEMENTARY FIGURE 1
The nervous system diseases network. The candidate genes are depicted by blue nodes and the disease terms by pink nodes. Edges correspond to disease associations. Out of our 16 candidates, 10 are connected to at least one nervous system disease providing more evidence for their involvement in the phenotype studied here.

References

Abdel-Salam, G. M. H., Miyake, N., Abdel-Hamid, M. S., Sayed, I. S. M., Gadelhak, M. I., Ismail, S. I., et al. (2018). Phenotypic and molecular insights into PQBP1-related intellectual disability. *Am. J. Med. Genet. A* 176, 2446–2450. doi: 10.1002/ajmg.a.40479

Akram, S., Yang, F., Li, J., Adams, G., Liu, Y., Zhuang, X., et al. (2018). LRIF1 interacts with HP1alpha to coordinate accurate chromosome segregation during mitosis. *J. Mol. Cell Biol.* 10, 527–538. doi: 10.1093/jmcb/mjy040

Aleksic, B., Kushima, I., Hashimoto, R., Ohi, K., Ikeda, M., Yoshimi, A., et al. (2013). Analysis of the VAV3 as candidate gene for schizophrenia: Evidences from voxel-based morphometry and mutation screening. *Schizophr. Bull.* 39, 720–728. doi: 10.1093/schbul/sbs038

Al-Mubarak, B., Abouelhoda, M., Omar, A., Aldhalaan, H., Aldosari, M., Nester, M., et al. (2017). Whole exome sequencing reveals inherited and de novo variants in autism spectrum disorder: A trio study from Saudi families. *Sci. Rep.* 7:5679.

Al-Nabhani, M., Al-Rashdi, S., Al-Murshedi, F., Al-Kindi, A., Al-Thihli, K., Al-Saegh, A., et al. (2018). Reanalysis of exome sequencing data of intellectual disability samples: Yields and benefits. *Clin. Genet.* 94, 495–501. doi: 10.1111/cge.13438

Amiel, J., Rio, M., De Pontual, L., Redon, R., Malan, V., Boddaert, N., et al. (2007). Mutations in TCF4, encoding a class I basic helix-loop-helix transcription factor, are responsible for Pitt-Hopkins syndrome, a severe epileptic encephalopathy associated with autonomic dysfunction. *Am. J. Hum. Genet.* 80, 988–993. doi: 10.1086/515582

An, J. Y., Cristino, A. S., Zhao, Q., Edson, J., Williams, S. M., Ravine, D., et al. (2014). Towards a molecular characterization of autism spectrum disorders: An exome sequencing and systems approach. *Transl. Psychiatry* 4:e394.

Anazi, S., Maddirevula, S., Salpietro, V., Asi, Y. T., Alsahli, S., Alhashem, A., et al. (2017). Expanding the genetic heterogeneity of intellectual disability. *Hum. Genet.* 136, 1419–1429.

Ando, Y., Sawada, M., Kawakami, T., Morita, M., and Aoki, Y. (2021). A patient with noonan syndrome with a KRAS mutation who presented severe nerve root hypertrophy. *Case Rep. Neurol.* 13, 108–118. doi: 10.1159/000512265

Balevich, E. C., Haznedar, M. M., Wang, E., Newmark, R. E., Bloom, R., Schneiderman, J. S., et al. (2015). Corpus callosum size and diffusion tensor anisotropy in adolescents and adults with schizophrenia. *Psychiatry Res.* 231, 244–251. doi: 10.1016/j.pscychresns.2014.12.005

Bisgaard, A. M., Rasmussen, L. N., Moller, H. U., Kirchhoff, M., and Bryndorf, T. (2007). Interstitial deletion of the short arm of chromosome 1 (1p13.1p21.1) in a girl with mental retardation, short stature and colobomata. *Clin. Dysmorphol.* 16, 109–112. doi: 10.1097/01.mcd.0000228425.89660.bf

Bowling, K. M., Thompson, M. L., Amaral, M. D., Finnila, C. R., Hiatt, S. M., Engel, K. L., et al. (2017). Genomic diagnosis for children with intellectual disability and/or developmental delay. *Genome Med.* 9:43.

Brunet, T., Jech, R., Brugger, M., Kovacs, R., Alhaddad, B., Leszinski, G., et al. (2021). De novo variants in neurodevelopmental disorders-experiences from a tertiary care center. *Clin. Genet.* 100, 14–28. doi: 10.1111/cge.13946

Bustelo, X. R. (2014). Vav family exchange factors: An integrated regulatory and functional view. *Small GTPases* 5:9. doi: 10.4161/21541248.2014.973757

Buysse, K., Delle Chiaie, B., Van Coster, R., Loeys, B., De Paepe, A., Mortier, G., et al. (2009). Challenges for CNV interpretation in clinical molecular karyotyping:

Lessons learned from a 1001 sample experience. *Eur. J. Med. Genet.* 52, 398–403. doi: 10.1016/j.ejmg.2009.09.002

Callaghan, D. B., Rogic, S., Tan, P. P. C., Calli, K., Qiao, Y., Baldwin, R., et al. (2019). Whole genome sequencing and variant discovery in the ASPIRE autism spectrum disorder cohort. *Clin. Genet.* 96, 199–206. doi: 10.1111/cge.13556

Cappi, C., Oliphant, M. E., Peter, Z., Zai, G., Conceicao Do Rosario, M., Sullivan, C. A. W., et al. (2020). De novo damaging DNA coding mutations are associated with obsessive-compulsive disorder and overlap with Tourette's disorder and autism. *Biol. Psychiatry* 87, 1035–1044. doi: 10.1016/j.biopsych.2019.09.029

Carroll, R., Kumar, R., Shaw, M., Slee, J., Kalscheuer, V. M., Corbett, M. A., et al. (2017). Variant in the X-chromosome spliceosomal gene GPKOW causes male-lethal microcephaly with intrauterine growth restriction. *Eur. J. Hum. Genet.* 25, 1078–1082. doi: 10.1038/ejhg.2017.97

Chen, Y., Bartanus, J., Liang, D., Zhu, H., Breman, A. M., Smith, J. L., et al. (2017). Characterization of chromosomal abnormalities in pregnancy losses reveals critical genes and loci for human early development. *Hum. Mutat.* 38, 669–677. doi: 10.1002/humu.23207

D'Amore, A., Tessa, A., Casali, C., Dotti, M. T., Filla, A., Silvestri, G., et al. (2018). Next generation molecular diagnosis of hereditary spastic paraplegias: An Italian Cross-Sectional Study. *Front. Neurol.* 9:981. doi: 10.3389/fneur.2018.00981

Deciphering Developmental Disorders, S. (2017). Prevalence and architecture of de novo mutations in developmental disorders. *Nature* 542, 433–438.

Degrassi, F., Damizia, M., and Lavia, P. (2019). The mitotic apparatus and kinetochores in microcephaly and neurodevelopmental diseases. *Cells* 9:49. doi: 10.3390/cells9010049

Diskin, S. J., Hou, C., Glessner, J. T., Attiyeh, E. F., Laudenslager, M., Bosse, K., et al. (2009). Copy number variation at 1q21.1 associated with neuroblastoma. *Nature* 459, 987–991. doi: 10.1038/nature08035

Dode, C., Levilliers, J., Dupont, J. M., De Paepe, A., Le Du, N., Soussi-Yanicostas, N., et al. (2003). Loss-of-function mutations in FGFR1 cause autosomal dominant Kallmann syndrome. *Nat. Genet.* 33, 463–465. doi: 10.1038/ng1122

Dumas, L. J., O'Bleness, M. S., Davis, J. M., Dickens, C. M., Anderson, N., Keeney, J. G., et al. (2012). DUF1220-domain copy number implicated in human brain-size pathology and evolution. *Am. J. Hum. Genet.* 91, 444–454. doi: 10.1016/j.ajhg.2012.07.016

Eaton, D. L., and Bammler, T. K. (1999). Concise review of the glutathione S-transferases and their significance to toxicology. *Toxicol. Sci.* 49, 156–164.

Ehmke, N., Graul-Neumann, L., Smorag, L., Koenig, R., Segebrecht, L., Magoulas, P., et al. (2017). De novo mutations in SLC25A24 cause a craniosynostosis syndrome with hypertrichosis, progeroid appearance, and mitochondrial dysfunction. *Am. J. Hum. Genet.* 101, 833–843. doi: 10.1016/j.ajhg.2017.09.016

Erdem-Eraslan, L., Gao, Y., Kloosterhof, N. K., Atlasi, Y., Demmers, J., Sacchetti, A., et al. (2015). Mutation specific functions of EGFR result in a mutation-specific downstream pathway activation. *Eur. J. Cancer* 51, 893–903. doi: 10.1016/j.ejca.2015.02.006

Faccio, R., Teitelbaum, S. L., Fujikawa, K., Chappel, J., Zallone, A., Tybulewicz, V. L., et al. (2005). Vav3 regulates osteoclast function and bone mass. *Nat. Med.* 11, 284–290. doi: 10.1038/nm1194

Faergeman, S. L., Bojesen, A. B., Rasmussen, M., Becher, N., Andreasen, L., Andersen, B. N., et al. (2021). Phenotypic heterogeneity and mosaicism in Xia-Gibbs syndrome: Five Danish patients with novel variants in AHDC1. *Eur. J. Med. Genet.* 64:104280. doi: 10.1016/j.ejmg.2021.104280

Faundes, V., Newman, W. G., Bernardini, L., Canham, N., Clayton-Smith, J., Dallapiccola, B., et al. (2018). Histone lysine methylases and demethylases in the landscape of human developmental disorders. *Am. J. Hum. Genet.* 102, 175–187. doi: 10.1016/j.ajhg.2017.11.013

Firth, H. V., Richards, S. M., Bevan, A. P., Clayton, S., Corpas, M., Rajan, D., et al. (2009). DECIPHER: Database of chromosomal imbalance and phenotype in humans using ensembl resources. *Am. J. Hum. Genet.* 84, 524–533. doi: 10.1016/j.ajhg.2009.03.010

Garcia-Acero, M., and Acosta, J. (2017). Whole-exome sequencing identifies a de novo AHDC1 mutation in a colombian patient with Xia-Gibbs Syndrome. *Mol. Syndromol.* 8, 308–312. doi: 10.1159/000479357

Gilks, W. P., Hill, M., Gill, M., Donohoe, G., Corvin, A. P., and Morris, D. W. (2012). Functional investigation of a schizophrenia GWAS signal at the CDC42 gene. *World J. Biol. Psychiatry* 13, 550–554. doi: 10.3109/15622975.2012.666359

Girard, S. L., Gauthier, J., Noreau, A., Xiong, L., Zhou, S., Jouan, L., et al. (2011). Increased exonic de novo mutation rate in individuals with schizophrenia. *Nat. Genet.* 43, 860–863. doi: 10.1038/ng.886

Goehler, H., Lalowski, M., Stelzl, U., Waelter, S., Stroedicke, M., Worm, U., et al. (2004). A protein interaction network links GIT1, an enhancer of huntingtin aggregation, to Huntington's disease. *Mol. Cell* 15, 853–865. doi: 10.1016/j.molcel.2004.09.016

Grozeva, D., Carss, K., Spasic-Boskovic, O., Tejada, M. I., Gecz, J., Shaw, M., et al. (2015). Targeted next-generation sequencing analysis of 1,000 individuals with intellectual disability. *Hum. Mutat.* 36, 1197–1204.

Guard, S. E., Poss, Z. C., Ebmeier, C. C., Pagratis, M., Simpson, H., Taatjes, D. J., et al. (2019). The nuclear interactome of DYRK1A reveals a functional role in DNA damage repair. *Sci. Rep.* 9:6539. doi: 10.1038/s41598-019-42990-5

Gulsuner, S., Walsh, T., Watts, A. C., Lee, M. K., Thornton, A. M., Casadei, S., et al. (2013). Spatial and temporal mapping of de novo mutations in schizophrenia to a fetal prefrontal cortical network. *Cell* 154, 518–529. doi: 10.1016/j.cell.2013.06.049

Guo, H., Wang, T., Wu, H., Long, M., Coe, B. P., Li, H., et al. (2018). Inherited and multiple de novo mutations in autism/developmental delay risk genes suggest a multifactorial model. *Mol. Autism* 9:64. doi: 10.1186/s13229-018-0247-z

Gupta, H. V., Vengoechea, J., Sahaya, K., and Virmani, T. (2015). A splice site mutation in ATP6AP2 causes X-linked intellectual disability, epilepsy, and parkinsonism. *Parkinsonism Relat. Disord.* 21, 1473–1475. doi: 10.1016/j.parkreldis.2015.10.001

Hashimoto, R., Nakazawa, T., Tsurusaki, Y., Yasuda, Y., Nagayasu, K., Matsumura, K., et al. (2016). Whole-exome sequencing and neurite outgrowth analysis in autism spectrum disorder. *J. Hum. Genet.* 61, 199–206. doi: 10.1038/jhg.2015.141

Helbig, K. L., Farwell Hagman, K. D., Shinde, D. N., Mroske, C., Powis, Z., Li, S., et al. (2016). Diagnostic exome sequencing provides a molecular diagnosis for a significant proportion of patients with epilepsy. *Genet. Med.* 18, 898–905.

Hiraide, T., Hattori, A., Ieda, D., Hori, I., Saitoh, S., Nakashima, M., et al. (2019). De novo variants in SETD1B cause intellectual disability, autism spectrum disorder, and epilepsy with myoclonic absences. *Epilepsia Open* 4, 476–481. doi: 10.1002/epi4.12339

Hiraide, T., Nakashima, M., Yamoto, K., Fukuda, T., Kato, M., Ikeda, H., et al. (2018). De novo variants in SETD1B are associated with intellectual disability, epilepsy and autism. *Hum. Genet.* 137, 95–104.

Hiraide, T., Yamoto, K., Masunaga, Y., Asahina, M., Endoh, Y., Ohkubo, Y., et al. (2021). Genetic and phenotypic analysis of 101 patients with developmental delay or intellectual disability using whole-exome sequencing. *Clin. Genet.* 100, 40–50.

Hu, H., Haas, S. A., Chelly, J., Van Esch, H., Raynaud, M., De Brouwer, A. P., et al. (2016). X-exome sequencing of 405 unresolved families identifies seven novel intellectual disability genes. *Mol. Psychiatry* 21, 133–148. doi: 10.1038/mp.2014.193

Hu, H., Kahrizi, K., Musante, L., Fattahi, Z., Herwig, R., Hosseini, M., et al. (2019). Genetics of intellectual disability in consanguineous families. *Mol. Psychiatry* 24, 1027–1039.

Huttlin, E. L., Bruckner, R. J., Navarrete-Perea, J., Cannon, J. R., Baltier, K., Gebreab, F., et al. (2021). Dual proteome-scale networks reveal cell-specific remodeling of the human interactome. *Cell* 184, 3022–3040 e3028. doi: 10.1016/j.cell.2021.04.011

Iossifov, I., O'Roak, B. J., Sanders, S. J., Ronemus, M., Krumm, N., Levy, D., et al. (2014). The contribution of de novo coding mutations to autism spectrum disorder. *Nature* 515, 216–221. doi: 10.1038/nature13908

Iossifov, I., Ronemus, M., Levy, D., Wang, Z., Hakker, I., Rosenbaum, J., et al. (2012). De novo gene disruptions in children on the autistic spectrum. *Neuron* 74, 285–299.

Jensen, L. R., Chen, W., Moser, B., Lipkowitz, B., Schroeder, C., Musante, L., et al. (2011). Hybridisation-based resequencing of 17 X-linked intellectual disability genes in 135 patients reveals novel mutations in ATRX, SLC6A8 and PQBP1. *Eur. J. Hum. Genet.* 19, 717–720. doi: 10.1038/ejhg.2010.244

Ji, J., Lee, H., Argiropoulos, B., Dorrani, N., Mann, J., Martinez-Agosto, J. A., et al. (2015). DYRK1A haploinsufficiency causes a new recognizable syndrome with microcephaly, intellectual disability, speech impairment, and distinct facies. *Eur. J. Hum. Genet.* 23, 1473–1481. doi: 10.1038/ejhg.2015.71

Jiang, Y., Wangler, M. F., Mcguire, A. L., Lupski, J. R., Posey, J. E., Khayat, M. M., et al. (2018). The phenotypic spectrum of Xia-Gibbs syndrome. *Am. J. Med. Genet. A* 176, 1315–1326.

Kabashi, E., Valdmanis, P. N., Dion, P., Spiegelman, D., Mcconkey, B. J., Vande Velde, C., et al. (2008). TARDBP mutations in individuals with sporadic and familial amyotrophic lateral sclerosis. *Nat. Genet.* 40, 572–574.

Kahrizi, K., Hu, H., Hosseini, M., Kalscheuer, V. M., Fattahi, Z., Beheshtian, M., et al. (2019). Effect of inbreeding on intellectual disability revisited by trio sequencing. *Clin. Genet.* 95, 151–159. doi: 10.1111/cge.13463

Kalscheuer, V. M., Freude, K., Musante, L., Jensen, L. R., Yntema, H. G., Gecz, J., et al. (2003). Mutations in the polyglutamine binding protein 1 gene cause X-linked mental retardation. *Nat. Genet.* 35, 313–315. doi: 10.1038/ng1264

Kannan, M., Bayam, E., Wagner, C., Rinaldi, B., Kretz, P. F., Tilly, P., et al. (2017). WD40-repeat 47, a microtubule-associated protein, is essential for brain development and autophagy. *Proc. Natl. Acad. Sci. U.S.A.* 114, E9308–E9317. doi: 10.1073/pnas.1713625114

Kosmicki, J. A., Samocha, K. E., Howrigan, D. P., Sanders, S. J., Slowikowski, K., Lek, M., et al. (2017). Refining the role of de novo protein-truncating variants in neurodevelopmental disorders by using population reference samples. *Nat. Genet.* 49, 504–510. doi: 10.1038/ng.3789

Labonne, J. D., Lee, K. H., Iwase, S., Kong, I. K., Diamond, M. P., Layman, L. C., et al. (2016). An atypical 12q24.31 microdeletion implicates six genes including a histone demethylase KDM2B and a histone methyltransferase SETD1B in syndromic intellectual disability. *Hum. Genet.* 135, 757–771. doi: 10.1007/s00439-016-1668-4

Le, V. S., Tran, K. T., Bui, H. T. P., Le, H. T. T., Nguyen, C. D., Do, D. H., et al. (2019). A Vietnamese human genetic variation database. *Hum. Mutat.* 40, 1664–1675.

Lee, C. T., Freed, W. J., and Mash, D. C. (2015). CNVs in neurodevelopmental disorders. *Oncotarget* 6, 18238–18239. doi: 10.18632/oncotarget.4853

Lelieveld, S. H., Reijnders, M. R., Pfundt, R., Yntema, H. G., Kamsteeg, E. J., De Vries, P., et al. (2016). Meta-analysis of 2,104 trios provides support for 10 new genes for intellectual disability. *Nat. Neurosci.* 19, 1194–1196. doi: 10.1038/nn.4352

Lenski, C., Abidi, F., Meindl, A., Gibson, A., Platzer, M., Frank Kooy, R., et al. (2004). Novel truncating mutations in the polyglutamine tract binding protein 1 gene (PQBP1) cause Renpenning syndrome and X-linked mental retardation in another family with microcephaly. *Am. J. Hum. Genet.* 74, 777–780. doi: 10.1086/383205

Leventopoulos, G., Denayer, E., Makrythanasis, P., Papapolychroniou, C., and Fryssira, H. (2010). Noonan syndrome and systemic lupus erythematosus in a patient with a novel KRAS mutation. *Clin. Exp. Rheumatol.* 28, 556–557.

Li, H. J., Haque, Z. K., Chen, A., and Mendelsohn, M. (2007). RIF-1, a novel nuclear receptor corepressor that associates with the nuclear matrix. *J. Cell Biochem.* 102, 1021–1035. doi: 10.1002/jcb.21340

Li, J., Cai, T., Jiang, Y., Chen, H., He, X., Chen, C., et al. (2016). Genes with de novo mutations are shared by four neuropsychiatric disorders discovered from NPdenovo database. *Mol. Psychiatry* 21:298.

Li, J., Kale Edmiston, E., Chen, K., Tang, Y., Ouyang, X., Jiang, Y., et al. (2014). A comparative diffusion tensor imaging study of corpus callosum subregion integrity in bipolar disorder and schizophrenia. *Psychiatry Res.* 221, 58–62. doi: 10.1016/j.pscychresns.2013.10.007

Li, J., Wang, L., Yu, P., Shi, L., Zhang, K., Sun, Z. S., et al. (2017). Vitamin D-related genes are subjected to significant de novo mutation burdens in autism spectrum disorder. *Am. J. Med. Genet. B Neuropsychiatr. Genet.* 174, 568–577. doi: 10.1002/ajmg.b.32543

Li, X., Wang, W., Wang, J., Malovannaya, A., Xi, Y., Li, W., et al. (2015). Proteomic analyses reveal distinct chromatin-associated and soluble transcription factor complexes. *Mol. Syst. Biol.* 11:775. doi: 10.15252/msb.20145504

Lichter, P., Tang, C. J., Call, K., Hermanson, G., Evans, G. A., Housman, D., et al. (1990). High-resolution mapping of human chromosome 11 by in situ hybridization with cosmid clones. *Science* 247, 64–69. doi: 10.1126/science.2294592

Lim, E. T., Uddin, M., De Rubeis, S., Chan, Y., Kamumbu, A. S., Zhang, X., et al. (2017). Rates, distribution and implications of postzygotic mosaic mutations in autism spectrum disorder. *Nat. Neurosci.* 20, 1217–1224. doi: 10.1038/nn.4598

Lin, W., Zhang, J., Liu, Y., Wu, R., Yang, H., Hu, X., et al. (2017). Studies on diagnostic biomarkers and therapeutic mechanism of Alzheimer's disease through metabolomics and hippocampal proteomics. *Eur. J. Pharm. Sci.* 105, 119–126. doi: 10.1016/j.ejps.2017.05.003

Liu, Y. F., Sowell, S. M., Luo, Y., Chaubey, A., Cameron, R. S., Kim, H. G., et al. (2015). Autism and intellectual disability-associated KIRREL3 interacts with neuronal proteins MAP1B and MYO16 with potential roles in neurodevelopment. *PLoS One* 10:e0123106. doi: 10.1371/journal.pone.0123106

Lo, I. F., Cheung, L. Y., Ng, A. Y., and Lam, S. T. (1998). Interstitial Dup(1p) with findings of Kabuki make-up syndrome. *Am. J. Med. Genet.* 78, 55–57.

Luck, K., Kim, D. K., Lambourne, L., Spirohn, K., Begg, B. E., Bian, W., et al. (2020). A reference map of the human binary protein interactome. *Nature* 580, 402–408.

Mandic-Maravic, V., Mitkovic-Voncina, M., Pljesa-Ercegovac, M., Savic-Radojevic, A., Djordjevic, M., Ercegovac, M., et al. (2021). Glutathione S-transferase polymorphisms and clinical characteristics in autism spectrum disorders. *Front. Psychiatry* 12:672389. doi: 10.3389/fpsyt.2021.672389

Mapelli, L., Soda, T., D'Angelo, E., and Prestori, F. (2022). The Cerebellar involvement in autism spectrum disorders: From the social brain to mouse models. *Int. J. Mol. Sci.* 23:3894. doi: 10.3390/ijms23073894

Marcon, E., Ni, Z., Pu, S., Turinsky, A. L., Trimble, S. S., Olsen, J. B., et al. (2014). Human-chromatin-related protein interactions identify a demethylase complex required for chromosome segregation. *Cell Rep.* 8, 297–310. doi: 10.1016/j.celrep.2014.05.050

Martin, T. D., Cook, D. R., Choi, M. Y., Li, M. Z., Haigis, K. M., and Elledge, S. J. (2017). A role for mitochondrial translation in promotion of viability in K-Ras mutant cells. *Cell Rep.* 20, 427–438. doi: 10.1016/j.celrep.2017.06.061

Martinelli, S., Krumbach, O. H. F., Pantaleoni, F., Coppola, S., Amin, E., Pannone, L., et al. (2018). Functional dysregulation of CDC42 causes diverse developmental phenotypes. *Am. J. Hum. Genet.* 102, 309–320. doi: 10.1016/j.ajhg.2017.12.015

Mary, L., Piton, A., Schaefer, E., Mattioli, F., Nourisson, E., Feger, C., et al. (2018). Disease-causing variants in TCF4 are a frequent cause of intellectual disability: Lessons from large-scale sequencing approaches in diagnosis. *Eur. J. Hum. Genet.* 26, 996–1006. doi: 10.1038/s41431-018-0096-4

Matsunami, N., Hensel, C. H., Baird, L., Stevens, J., Otterud, B., Leppert, T., et al. (2014). Identification of rare DNA sequence variants in high-risk autism families and their prevalence in a large case/control population. *Mol. Autism* 5:5. doi: 10.1186/2040-2392-5-5

Mattia, F. R., Wardinsky, T. D., Tuttle, D. J., Grix, A. Jr., Smith, K. A., and Walling, P. (1992). Interstitial deletion of the short arm of chromosome 1 (46XY, del(1)(p13p22.3)). *Am. J. Med. Genet.* 44, 551–554. doi: 10.1002/ajmg.1320440503

Monroe, G. R., Frederix, G. W., Savelberg, S. M., De Vries, T. I., Duran, K. J., Van Der Smagt, J. J., et al. (2016). Effectiveness of whole-exome sequencing and costs of the traditional diagnostic trajectory in children with intellectual disability. *Genet. Med.* 18, 949–956. doi: 10.1038/gim.2015.200

Morais, S., Raymond, L., Mairey, M., Coutinho, P., Brandao, E., Ribeiro, P., et al. (2017). Massive sequencing of 70 genes reveals a myriad of missing genes or mechanisms to be uncovered in hereditary spastic paraplegias. *Eur. J. Hum. Genet.* 25, 1217–1228.

Movilla, N., and Bustelo, X. R. (1999). Biological and regulatory properties of Vav-3, a new member of the Vav family of oncoproteins. *Mol. Cell Biol.* 19, 7870–7885. doi: 10.1128/MCB.19.11.7870

Muller, P. M., Rademacher, J., Bagshaw, R. D., Wortmann, C., Barth, C., Van Unen, J., et al. (2020). Systems analysis of RhoGEF and RhoGAP regulatory proteins reveals spatially organized RAC1 signalling from integrin adhesions. *Nat. Cell Biol.* 22, 498–511. doi: 10.1038/s41556-020-0488-x

Murphy, W. J., Fronicke, L., O'Brien, S. J., and Stanyon, R. (2003). The origin of human chromosome 1 and its homologs in placental mammals. *Genome Res.* 13, 1880–1888. doi: 10.1101/gr.1022303

Najmabadi, H., Hu, H., Garshasbi, M., Zemojtel, T., Abedini, S. S., Chen, W., et al. (2011). Deep sequencing reveals 50 novel genes for recessive cognitive disorders. *Nature* 478, 57–63. doi: 10.1038/nature10423

Neale, B. M., Kou, Y., Liu, L., Ma'ayan, A., Samocha, K. E., Sabo, A., et al. (2012). Patterns and rates of exonic de novo mutations in autism spectrum disorders. *Nature* 485, 242–245. doi: 10.1038/nature11011

Palumbo, O., Palumbo, P., Delvecchio, M., Palladino, T., Stallone, R., Crisetti, M., et al. (2015). Microdeletion of 12q24.31: Report of a girl with intellectual disability, stereotypies, seizures and facial dysmorphisms. *Am. J. Med. Genet. A* 167A, 438–444. doi: 10.1002/ajmg.a.36872

Park, J. M., Lee, B., Kim, J. H., Park, S. Y., Yu, J., Kim, U. K., et al. (2020). An autosomal dominant ERLIN2 mutation leads to a pure HSP phenotype distinct from the autosomal recessive ERLIN2 mutations (SPG18). *Sci. Rep.* 10:3295. doi: 10.1038/s41598-020-60374-y

Paul, L. K., Brown, W. S., Adolphs, R., Tyszka, J. M., Richards, L. J., Mukherjee, P., et al. (2007). Agenesis of the corpus callosum: Genetic, developmental and functional aspects of connectivity. *Nat. Rev. Neurosci.* 8, 287–299. doi: 10.1038/nrn2107

Pekeles, H., Accogli, A., Boudrahem-Addour, N., Russell, L., Parente, F., and Srour, M. (2019). Diagnostic yield of intellectual disability gene panels. *Pediatr. Neurol.* 92, 32–36.

Piccione, M., Antona, V., Antona, R., Gambino, G., Pierluigi, M., Malacarne, M., et al. (2010). Array-CGH defined chromosome 1p duplication in a patient

with autism spectrum disorder, mild mental deficiency, and minor dysmorphic features. *Am. J. Med. Genet. A* 152A, 486–489. doi: 10.1002/ajmg.a.33212

Pinero, J., Ramirez-Anguita, J. M., Sauch-Pitarch, J., Ronzano, F., Centeno, E., Sanz, F., et al. (2020). The DisGeNET knowledge platform for disease genomics: 2019 update. *Nucleic Acids Res.* 48, D845–D855. doi: 10.1093/nar/gkz1021

Pinero, J., Sauch, J., Sanz, F., and Furlong, L. I. (2021). The DisGeNET cytoscape app: Exploring and visualizing disease genomics data. *Comput. Struct. Biotechnol. J.* 19, 2960–2967. doi: 10.1016/j.csbj.2021.05.015

Popp, B., Ekici, A. B., Thiel, C. T., Hoyer, J., Wiesener, A., Kraus, C., et al. (2017). Exome Pool-Seq in neurodevelopmental disorders. *Eur. J. Hum. Genet.* 25, 1364–1376. doi: 10.1038/s41431-017-0022-1

Purcell, S. M., Moran, J. L., Fromer, M., Ruderfer, D., Solovieff, N., Roussos, P., et al. (2014). A polygenic burden of rare disruptive mutations in schizophrenia. *Nature* 506, 185–190. doi: 10.1038/nature12975

Quevedo, C., Sauzeau, V., Menacho-Marquez, M., Castro-Castro, A., and Bustelo, X. R. (2010). Vav3-deficient mice exhibit a transient delay in cerebellar development. *Mol. Biol. Cell* 21, 1125–1139. doi: 10.1091/mbc.E09-04-0292

Rahman, S. K., Okazawa, H., and Chen, Y. W. (2019). Frameshift PQBP-1 mutants K192S(fs*7) and R153S(fs*41) implicated in X-linked intellectual disability form stable dimers. *J. Struct. Biol.* 206, 305–313. doi: 10.1016/j.jsb.2019.04.003

Ramser, J., Abidi, F. E., Burckle, C. A., Lenski, C., Toriello, H., Wen, G., et al. (2005). A unique exonic splice enhancer mutation in a family with X-linked mental retardation and epilepsy points to a novel role of the renin receptor. *Hum. Mol. Genet.* 14, 1019–1027. doi: 10.1093/hmg/ddi094

Redin, C., Gerard, B., Lauer, J., Herenger, Y., Muller, J., Quartier, A., et al. (2014). Efficient strategy for the molecular diagnosis of intellectual disability using targeted high-throughput sequencing. *J. Med. Genet.* 51, 724–736.

Redon, R., Rio, M., Gregory, S. G., Cooper, R. A., Fiegler, H., Sanlaville, D., et al. (2005). Tiling path resolution mapping of constitutional 1p36 deletions by array-CGH: Contiguous gene deletion or "deletion with positional effect" syndrome? *J. Med. Genet.* 42, 166–171. doi: 10.1136/jmg.2004.023861

Reijnders, M. R. F., Ansor, N. M., Kousi, M., Yue, W. W., Tan, P. L., Clarkson, K., et al. (2017). RAC1 missense mutations in developmental disorders with diverse phenotypes. *Am. J. Hum. Genet.* 101, 466–477. doi: 10.1016/j.ajhg.2017.08.007

Rice, A. M., and McLysaght, A. (2017). Dosage sensitivity is a major determinant of human copy number variant pathogenicity. *Nat. Commun.* 8:14366. doi: 10.1038/ncomms14366

Rodriguez-Fdez, S., Lorenzo-Martin, L. F., Fabbiano, S., Menacho-Marquez, M., Sauzeau, V., Dosil, M., et al. (2021). New functions of vav family proteins in cardiovascular biology, skeletal muscle, and the nervous system. *Biology* 10:857. doi: 10.3390/biology10090857

Roohi, J., Tegay, D. H., Pomeroy, J. C., Burkett, S., Stone, G., Stanyon, R., et al. (2008). A de novo apparently balanced translocation [46,XY,t(2;9)(p13;p24)] interrupting RAB11FIP5 identifies a potential candidate gene for autism spectrum disorder. *Am. J. Med. Genet. B Neuropsychiatr. Genet.* 147B, 411–417.

Roston, A., Evans, D., Gill, H., McKinnon, M., Isidor, B., Cogne, B., et al. (2021). SETD1B-associated neurodevelopmental disorder. *J. Med. Genet.* 58, 196–204. doi: 10.1136/jmedgenet-2019-106756

Rydning, S. L., Dudesek, A., Rimmele, F., Funke, C., Kruger, S., Biskup, S., et al. (2018). A novel heterozygous variant in ERLIN2 causes autosomal dominant pure hereditary spastic paraplegia. *Eur. J. Neurol.* 25, 943–e971. doi: 10.1111/ene.13625

Satterstrom, F. K., Kosmicki, J. A., Wang, J., Breen, M. S., De Rubeis, S., An, J. Y., et al. (2020). Large-scale exome sequencing study implicates both developmental and functional changes in the neurobiology of Autism. *Cell* 180, 568–584 e523. doi: 10.1016/j.cell.2019.12.036

Sauzeau, V., Horta-Junior, J. A., Riolobos, A. S., Fernandez, G., Sevilla, M. A., Lopez, D. E., et al. (2010). Vav3 is involved in GABAergic axon guidance events important for the proper function of brainstem neurons controlling cardiovascular, respiratory, and renal parameters. *Mol. Biol. Cell* 21, 4251–4263. doi: 10.1091/mbc.E10-07-0639

Schubbert, S., Zenker, M., Rowe, S. L., Boll, S., Klein, C., Bollag, G., et al. (2006). Germline KRAS mutations cause Noonan syndrome. *Nat. Genet.* 38, 331–336.

Searles Nielsen, S., Bammler, T. K., Gallagher, L. G., Farin, F. M., Longstreth, W. Jr., Franklin, G. M., et al. (2013). Genotype and age at Parkinson disease diagnosis. *Int. J. Mol. Epidemiol. Genet.* 4, 61–69.

Shaheen, R., Maddirevula, S., Ewida, N., Alsahli, S., Abdel-Salam, G. M. H., Zaki, M. S., et al. (2019). Genomic and phenotypic delineation of congenital microcephaly. *Genet. Med.* 21, 545–552.

Shami Shah, A., Batrouni, A. G., Kim, D., Punyala, A., Cao, W., Han, C., et al. (2019). PLEKHA4/kramer attenuates dishevelled ubiquitination to modulate Wnt and planar cell polarity signaling. *Cell Rep.* 27, 2157–2170 e2158. doi: 10.1016/j.celrep.2019.04.060

Silva, L. E., Souza, R. C., Kitano, E. S., Monteiro, L. F., Iwai, L. K., and Forti, F. L. (2019). Proteomic and interactome approaches reveal PAK4, PHB-2, and 14-3-3eta as targets of overactivated Cdc42 in cellular responses to genomic instability. *J. Proteome Res.* 18, 3597–3614. doi: 10.1021/acs.jproteome.9b00260

Snijders Blok, L., Rousseau, J., Twist, J., Ehresmann, S., Takaku, M., Venselaar, H., et al. (2018). CHD3 helicase domain mutations cause a neurodevelopmental syndrome with macrocephaly and impaired speech and language. *Nat. Commun.* 9:4619. doi: 10.1038/s41467-018-06014-6

Snijders Blok, L., Rousseau, J., Twist, J., Ehresmann, S., Takaku, M., Venselaar, H., et al. (2019). Author correction: CHD3 helicase domain mutations cause a neurodevelopmental syndrome with macrocephaly and impaired speech and language. *Nat. Commun.* 10:2079.

Sreedharan, J., Blair, I. P., Tripathi, V. B., Hu, X., Vance, C., Rogelj, B., et al. (2008). TDP-43 mutations in familial and sporadic amyotrophic lateral sclerosis. *Science* 319, 1668–1672.

Stelzl, U., Worm, U., Lalowski, M., Haenig, C., Brembeck, F. H., Goehler, H., et al. (2005). A human protein-protein interaction network: A resource for annotating the proteome. *Cell* 122, 957–968.

Stranger, B. E., Forrest, M. S., Dunning, M., Ingle, C. E., Beazley, C., Thorne, N., et al. (2007). Relative impact of nucleotide and copy number variation on gene expression phenotypes. *Science* 315, 848–853. doi: 10.1126/science.1136678

Sun, S. C., Ma, D., Li, M. Y., Zhang, R. X., Huang, C., Huang, H. J., et al. (2019). Mutations in C1orf194, encoding a calcium regulator, cause dominant Charcot-Marie-Tooth disease. *Brain* 142, 2215–2229. doi: 10.1093/brain/awz151

Szczawinska-Poplonyk, A., Ploski, R., Bernatowska, E., and Pac, M. (2020). A Novel CDC42 mutation in an 11-year old child manifesting as syndromic immunodeficiency, autoinflammation, hemophagocytic lymphohistiocytosis, and malignancy: A case report. *Front. Immunol.* 11:318. doi: 10.3389/fimmu.2020.00318

Tabata, H., Sone, K., Kobayashi, T., Yanagisawa, T., Tamura, T., Shimizu, N., et al. (1991). Short arm deletion of chromosome 1: Del(1)(p13.3 p22.3) in a female infant with an extreme tetralogy of Fallot. *Clin. Genet.* 39, 132–135. doi: 10.1111/j.1399-0004.1991.tb02999.x

Takata, A., Nakashima, M., Saitsu, H., Mizuguchi, T., Mitsuhashi, S., Takahashi, Y., et al. (2019). Comprehensive analysis of coding variants highlights genetic complexity in developmental and epileptic encephalopathy. *Nat. Commun.* 10:2506. doi: 10.1038/s41467-019-10482-9

Tawamie, H., Martianov, I., Wohlfahrt, N., Buchert, R., Mengus, G., Uebe, S., et al. (2017). Hypomorphic pathogenic variants in TAF13 are associated with autosomal-recessive intellectual disability and microcephaly. *Am. J. Hum. Genet.* 100, 555–561. doi: 10.1016/j.ajhg.2017.01.032

Toma, C., Shaw, A. D., Overs, B. J., Mitchell, P. B., Schofield, P. R., Cooper, A. A., et al. (2020). De novo gene variants and familial bipolar disorder. *JAMA Netw. Open* 3:e203382.

Tran Mau-Them, F., Moutton, S., Racine, C., Vitobello, A., Bruel, A. L., Nambot, S., et al. (2020). Second-tier trio exome sequencing after negative solo clinical exome sequencing: An efficient strategy to increase diagnostic yield and decipher molecular bases in undiagnosed developmental disorders. *Hum. Genet.* 139, 1381–1390. doi: 10.1007/s00439-020-02178-8

Travaglini, L., Aiello, C., Stregapede, F., D'amico, A., Alesi, V., Ciolfi, A., et al. (2018). The impact of next-generation sequencing on the diagnosis of pediatric-onset hereditary spastic paraplegias: New genotype-phenotype correlations for rare HSP-related genes. *Neurogenetics* 19, 111–121. doi: 10.1007/s10048-018-0545-9

Trinh, J., Kandaswamy, K. K., Werber, M., Weiss, M. E. R., Oprea, G., Kishore, S., et al. (2019). Novel pathogenic variants and multiple molecular diagnoses in neurodevelopmental disorders. *J. Neurodev. Disord.* 11:11.

Turner, T. N., Coe, B. P., Dickel, D. E., Hoekzema, K., Nelson, B. J., Zody, M. C., et al. (2017). Genomic patterns of de novo mutation in simplex autism. *Cell* 171, 710–722.e712.

Turner, T. N., Wilfert, A. B., Bakken, T. E., Bernier, R. A., Pepper, M. R., Zhang, Z., et al. (2019). Sex-based analysis of de novo variants in neurodevelopmental disorders. *Am. J. Hum. Genet.* 105, 1274–1285. doi: 10.1016/j.ajhg.2019.11.003

Turro, E., Astle, W. J., Megy, K., Graf, S., Greene, D., Shamardina, O., et al. (2020). Whole-genome sequencing of patients with rare diseases in a national health system. *Nature* 583, 96–102. doi: 10.1038/s41586-020-2434-2

Uddin, M., Tammimies, K., Pellecchia, G., Alipanahi, B., Hu, P., Wang, Z., et al. (2014). Brain-expressed exons under purifying selection are enriched for de novo mutations in autism spectrum disorder. *Nat. Genet.* 46, 742–747. doi: 10.1038/ng.2980

Uehara, D. T., Hayashi, S., Okamoto, N., Mizuno, S., Chinen, Y., Kosaki, R., et al. (2016). SNP array screening of cryptic genomic imbalances in 450 Japanese subjects with intellectual disability and multiple congenital anomalies previously negative for large rearrangements. *J. Hum. Genet.* 61, 335–343. doi: 10.1038/jhg.2015.154

Utkus, A., Sorokina, I., Kucinskas, V., Rothlisberger, B., Balmer, D., Brecevic, L., et al. (1999). Duplication of segment 1p21 following paternal insertional translocation, ins(6;1)(q25;p13.3p22.1). *J. Med. Genet.* 36, 73–76.

van Kuilenburg, A. B., Meijer, J., Mul, A. N., Hennekam, R. C., Hoovers, J. M., de Die-Smulders, C. E., et al. (2009). Analysis of severely affected patients with dihydropyrimidine dehydrogenase deficiency reveals large intragenic rearrangements of DPYD and a de novo interstitial deletion del(1)(p13.3p21.3). *Hum. Genet.* 125, 581–590. doi: 10.1007/s00439-009-0653-6

Vandepoele, K., Van Roy, N., Staes, K., Speleman, F., and van Roy, F. (2005). A novel gene family NBPF: Intricate structure generated by gene duplications during primate evolution. *Mol. Biol. Evol.* 22, 2265–2274. doi: 10.1093/molbev/msi222

Vergult, S., Van Binsbergen, E., Sante, T., Nowak, S., Vanakker, O., Claes, K., et al. (2014). Mate pair sequencing for the detection of chromosomal aberrations in patients with intellectual disability and congenital malformations. *Eur. J. Hum. Genet.* 22, 652–659. doi: 10.1038/ejhg.2013.220

Vissers, L. E., van Ravenswaaij, C. M., Admiraal, R., Hurst, J. A., de Vries, B. B., Janssen, I. M., et al. (2004). Mutations in a new member of the chromodomain gene family cause CHARGE syndrome. *Nat. Genet.* 36, 955–957. doi: 10.1038/ng1407

Wang, Q., Li, M., Yang, Z., Hu, X., Wu, H. M., Ni, P., et al. (2015). Increased co-expression of genes harboring the damaging de novo mutations in Chinese schizophrenic patients during prenatal development. *Sci. Rep.* 5:18209. doi: 10.1038/srep18209

Wang, T., Guo, H., Xiong, B., Stessman, H. A., Wu, H., Coe, B. P., et al. (2016). De novo genic mutations among a Chinese autism spectrum disorder cohort. *Nat. Commun.* 7:13316. doi: 10.1038/ncomms13316

Wang, T., Hoekzema, K., Vecchio, D., Wu, H., Sulovari, A., Coe, B. P., et al. (2020). Author correction: Large-scale targeted sequencing identifies risk genes for neurodevelopmental disorders. *Nat. Commun.* 11:. doi: 10.1038/s41467-020-19289-5

Weerts, M. J. A., Lanko, K., Guzman-Vega, F. J., Jackson, A., Ramakrishnan, R., Cardona-Londono, K. J., et al. (2021). Delineating the molecular and phenotypic spectrum of the SETD1B-related syndrome. *Genet. Med.* 23, 2122–2137. doi: 10.1038/s41436-021-01246-2

Weiss, K., Lazar, H. P., Kurolap, A., Martinez, A. F., Paperna, T., Cohen, L., et al. (2020). Correction: The CHD4-related syndrome: A comprehensive investigation of the clinical spectrum, genotype-phenotype correlations, and molecular basis. *Genet. Med.* 22:669. doi: 10.1038/s41436-019-0727-3

Weiss, K., Terhal, P. A., Cohen, L., Bruccoleri, M., Irving, M., Martinez, A. F., et al. (2016). De novo mutations in CHD4, an ATP-dependent chromatin remodeler gene, cause an intellectual disability syndrome with distinctive dysmorphisms. *Am. J. Hum. Genet.* 99, 934–941. doi: 10.1016/j.ajhg.2016.08.001

Wright, F. A., Bonzerato, C. G., Sliter, D. A., and Wojcikiewicz, R. J. H. (2018). The erlin2 T65I mutation inhibits erlin1/2 complex-mediated inositol 1,4,5-trisphosphate receptor ubiquitination and phosphatidylinositol 3-phosphate binding. *J. Biol. Chem.* 293, 15706–15714. doi: 10.1074/jbc.RA118.004547

Writzl, K., Maver, A., Kovacic, L., Martinez-Valero, P., Contreras, L., Satrustegui, J., et al. (2017). De novo mutations in slc25a24 cause a disorder characterized by early aging, bone dysplasia, characteristic face, and early demise. *Am. J. Hum. Genet.* 101, 844–855. doi: 10.1016/j.ajhg.2017.09.017

Wu, S. F., Xia, L., Shi, X. D., Dai, Y. J., Zhang, W. N., Zhao, J. M., et al. (2020). RIG-I regulates myeloid differentiation by promoting TRIM25-mediated ISGylation. *Proc. Natl. Acad. Sci. U.S.A.* 117, 14395–14404. doi: 10.1073/pnas.1918596117

Xia, F., Bainbridge, M. N., Tan, T. Y., Wangler, M. F., Scheuerle, A. E., Zackai, E. H., et al. (2014). De novo truncating mutations in AHDC1 in individuals with syndromic expressive language delay, hypotonia, and sleep apnea. *Am. J. Hum. Genet.* 94, 784–789. doi: 10.1016/j.ajhg.2014.04.006

Yang, H., Douglas, G., Monaghan, K. G., Retterer, K., Cho, M. T., Escobar, L. F., et al. (2015). De novo truncating variants in the AHDC1 gene encoding the AT-hook DNA-binding motif-containing protein 1 are associated with intellectual disability and developmental delay. *Cold Spring Harb. Mol. Case Stud.* 1: a000562.

Yildirim, Y., Orhan, E.K., Iseri, S.A., Serdaroglu-Oflazer, P., Kara, B., Solakoglu, S., et al. (2011). A frameshift mutation of ERLIN2 in recessive intellectual disability, motor dysfunction and multiple joint contractures. Hum Mol Genet 20, 1886-1892

Yuen, R.K., Merico, D., Cao, H., Pellecchia, G., Alipanahi, B., Thiruvahindrapuram, B., et al. (2016). Genome-wide characteristics of de novo mutations in autism. *NPJ Genom Med* 1:, 160271–1602710.

Zeng, L., Sachdev, P., Yan, L., Chan, J.L., Trenkle, T., Mcclelland, M., et al. (2000). Vav3 mediates receptor protein tyrosine kinase signaling, regulates GTPase activity, modulates cell morphology, and induces cell transformation. *Mol Cell Biol* 20:, 9212-9224.

Zenker, M., Lehmann, K., Schulz, A.L., Barth, H., Hansmann, D., Koenig, R., et al. (2007). Expansion of the genotypic and phenotypic spectrum in patients with KRAS germline mutations. *J Med Genet* 44:, 131-135.

Zhang, Y., Wang, T., Wang, Y., Xia, K., Li, J., and Sun, Z. (2021). Targeted sequencing and integrative analysis to prioritize candidate genes in neurodevelopmental disorders. *Mol Neurobiol* 58, 3863-3873.

Zweier, C., Peippo, M.M., Hoyer, J., Sousa, S., Bottani, A., Clayton-Smith, J., et al. (2007). Haploinsufficiency of TCF4 causes syndromal mental retardation with intermittent hyperventilation (Pitt-Hopkins syndrome). *Am J Hum Genet* 80:, 994-1001.

frontiers | Frontiers in Molecular Neuroscience

TYPE Original Research
PUBLISHED 12 October 2022
DOI 10.3389/fnmol.2022.1017512

Check for updates

OPEN ACCESS

EDITED BY
Markus Wöhr,
KU Leuven, Belgium

REVIEWED BY
Michael J. Schmeisser,
Johannes Gutenberg University Mainz, Germany
Gerhard Schratt,
ETH Zürich, Switzerland

*CORRESPONDENCE
Eunjoon Kim
kime@kaist.ac.kr

†These authors have contributed equally to this work

SPECIALTY SECTION
This article was submitted to Brain Disease Mechanisms, a section of the journal Frontiers in Molecular Neuroscience

RECEIVED 12 August 2022
ACCEPTED 15 September 2022
PUBLISHED 12 October 2022

CITATION
Yoo T, Yoo Y-E, Kang H and Kim E (2022) Age, brain region, and gene dosage-differential transcriptomic changes in *Shank3*-mutant mice. *Front. Mol. Neurosci.* 15:1017512. doi: 10.3389/fnmol.2022.1017512

COPYRIGHT
© 2022 Yoo, Yoo, Kang and Kim. This is an open-access article distributed under the terms of the Creative Commons Attribution License (CC BY). The use, distribution or reproduction in other forums is permitted, provided the original author(s) and the copyright owner(s) are credited and that the original publication in this journal is cited, in accordance with accepted academic practice. No use, distribution or reproduction is permitted which does not comply with these terms.

Age, brain region, and gene dosage-differential transcriptomic changes in *Shank3*-mutant mice

Taesun Yoo[1†], Ye-Eun Yoo[1†], Hyojin Kang[2] and Eunjoon Kim[1,3*]

[1]Center for Synaptic Brain Dysfunctions, Institute for Basic Science (IBS), Daejeon, South Korea, [2]Division of National Supercomputing, Korea Institute of Science and Technology Information (KISTI), Daejeon, South Korea, [3]Department of Biological Sciences, Korea Advanced Institute of Science and Technology (KAIST), Daejeon, South Korea

Shank3 is an abundant excitatory postsynaptic scaffolding protein implicated in various neurodevelopmental disorders, including autism spectrum disorder (ASD), Phelan-McDermid syndrome, intellectual disability, and schizophrenia. *Shank3*-mutant mice show various molecular, synaptic, and behavioral deficits, but little is known about how transcriptomic phenotypes vary across different ages, brain regions, and gene dosages. Here, we report transcriptomic patterns in the forebrains of juvenile and adult homozygous *Shank3*-mutant mice that lack exons 14–16 and also the prefrontal, hippocampal, and striatal transcriptomes in adult heterozygous and homozygous *Shank3*-mutant mice. The juvenile and adult mutant transcriptomes show patterns opposite from and similar to those observed in ASD (termed reverse-ASD and ASD-like patterns), respectively. The juvenile transcriptomic changes accompany synaptic upregulations and ribosomal and mitochondrial downregulations, whereas the adult transcriptome show opposite changes. The prefrontal, hippocampal, and striatal transcriptomes show differential changes in ASD-related gene expressions and biological functions associated with synapse, ribosome, mitochondria, and spliceosome. These patterns also differ across heterozygous and homozygous *Shank3*-mutant mice. These results suggest age, brain region, and gene dosage-differential transcriptomic changes in *Shank3*-mutant mice.

KEYWORDS

autism spectrum disorder, *Shank3*, age, cortex, hippocampus, striatum, gene dosage, RNA-seq

Introduction

The Shank family proteins are postsynaptic scaffolding proteins that regulate excitatory synaptic development and function (Boeckers et al., 1999; Naisbitt et al., 1999; Sheng and Sala, 2001; Kim and Sheng, 2004; Sheng and Kim, 2011). Among the three known Shank family proteins, Shank2 and Shank3 have been associated with various brain disorders, including autism spectrum disorder (ASD), Phelan-McDermid syndrome, intellectual disability, and schizophrenia (Durand et al., 2007; Moessner et al., 2007; Gauthier et al., 2009; Berkel et al., 2010; Leblond et al., 2014; Phelan et al., 2022). Numerous studies on the functions of Shank2 and Shank3, including those using mouse genetic approaches, have provided substantial insights into the mechanisms underlying Shank2- or Shank3-related brain disorders (Bozdagi et al., 2010; Peca et al., 2011; Schmeisser et al., 2012; Won et al., 2012; reviewed in Sheng and Kim, 2000, 2011; Boeckers et al., 2002; Bourgeron, 2009; Grabrucker et al., 2011; Sala et al., 2015; Schmeisser, 2015; Monteiro and Feng, 2017; Mossa et al., 2017, 2018; De Rubeis et al., 2018; Eltokhi et al., 2018; Ey et al., 2020; Jung and Park, 2022). However, it remains unclear how the mechanistic deviations observed in *Shank3*-mutant mice differ by age or brain region under different gene-dosage conditions. Investigating gene-dosage effects is important, considering that there have been debates regarding whether heterozygous or homozygous *Shank3*-mutant mice provide a better model for human ASD conditions.

Here we compared transcriptomes of the forebrain regions of juvenile (P25) and adult (P60) Shank3-homozygous (HM) mice. In addition, we analyzed transcriptomic patterns in the prefrontal cortex (termed cortex hereafter), hippocampus, and striatum regions of adult (~postnatal day 90 or P90) *Shank3* heterozygous (HT)- and homozygous (HM)-mutant mice lacking exons 14–16 (Shank3-HT/HM mice). We also compared these results with those previously reported from *Shank2*-mutant mice (Lee et al., 2021; Yoo et al., 2022). Our findings collectively indicate that there are age, brain region, and gene dosage-differential transcriptomes within and between *Shank2*- and *Shank3*-mutant mice, which may provide insight into altered biological functions and ASD-related/risk gene expression patterns.

Materials and methods

Animals

Shank3-mutant mice lacking exons 14–16 have been reported previously (Yoo et al., 2018, 2019) and were generated by Biocytogen. Mice were maintained at the mouse facility of the Korea Advanced Institute of Science and Technology (KAIST); they were fed *ad libitum* and maintained according to the Animal Research Requirements of KAIST.

RNA-seq analysis

The abundance of the transcripts was quantified using Salmon (v1.1.0) (Patro et al., 2017) via a quasi-mapping approach with GC bias correction (–gcBias). The results were imported to R (v.4.1.3) using Tximport (Soneson et al., 2015) package, which was followed by the analysis of differential gene expression using R/Bioconductor DEseq2 (v1.30.1) (Love et al., 2014). Raw read counts were normalized to gene size and fitted to a negative binomial distribution. The p values were adjusted through multiple comparisons using Benjamini–Hochberg correction to obtain adjusted p values. Genes with adjusted p values less than 0.05 were considered as differentially expressed genes (DEGs). Volcano plots were generated using R ggplot2 (v.3.3.3) package.

Gene Set Enrichment Analysis (GSEA)[1] (Subramanian et al., 2005) was used to determine whether WT and *Shank3*-mutant transcripts show significant enrichments for priori-defined gene sets. GSEA was performed using GSEAPreranked (gsea-3.0.jar) module on gene set collections downloaded from Molecular Signature Database (MSigDB) v7.4.[2] GSEAPreranked was performed using the list of all genes expressed, ranked by the fold changes multiplied by the inverse of the p values with recommended default settings (1,000 permutations and a classic scoring scheme). The False Discovery Rate (FDR) was calculated to control for false positive outcomes by comparing the tails of the observed and null distributions derived from the 1,000 gene set permutations for a given Normalized Enrichment Score (NES). The gene sets with an FDR of less than 0.05 were considered as significant enrichment. Integration and visualization of the GSEA results were performed using the EnrichmentMap Cytoscape App (version 3.9.0) (Merico et al., 2010; Isserlin et al., 2014).

Results

DEG analysis and GSEA of P25-Shank3 and P60-Shank3 transcripts

To explore age-dependent transcriptomic changes in juvenile and adult *Shank3*-homozygous mutant mice lacking exons 14–16 (Yoo et al., 2018, 2019) at P25 and P60, respectively, we set out to perform RNA-Seq analysis of transcripts from mouse forebrain lacking the olfactory bulb (**Figure 1A** and **Supplementary Table 1**). The analysis

1 http://software.broadinstitute.org/gsea
2 http://software.broadinstitute.org/gsea/msigdb

A *Shank3-mutant*

Age	Brain region	Genotype	DEG numbers		
			All	Up	Down
Juvenile (P25)	Forebrain	HM/WT (3 pairs)	23	9	14
Adult (P60)		HM/WT (3 pairs)	34	13	21

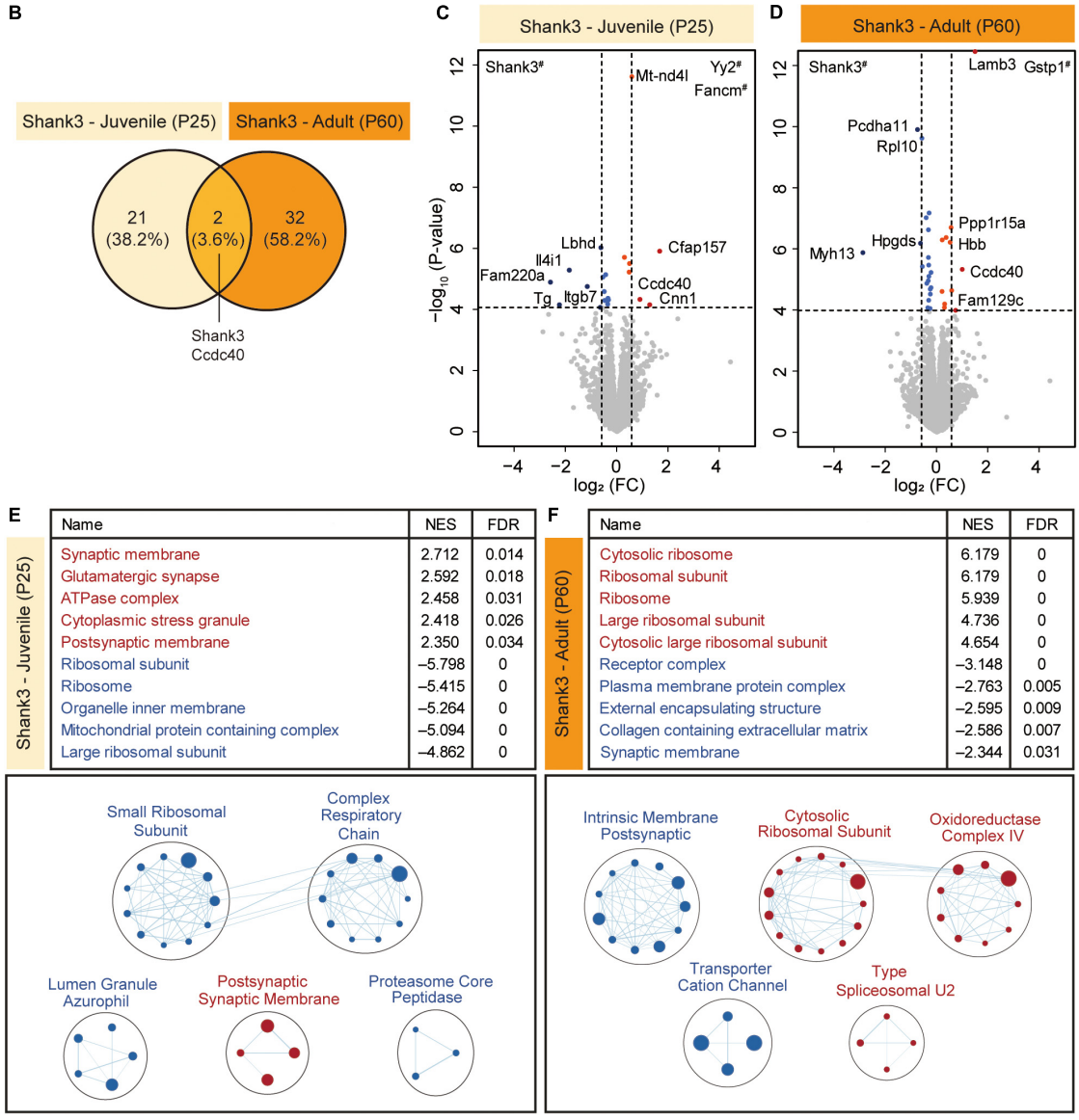

E

Shank3 - Juvenile (P25)	NES	FDR
Synaptic membrane	2.712	0.014
Glutamatergic synapse	2.592	0.018
ATPase complex	2.458	0.031
Cytoplasmic stress granule	2.418	0.026
Postsynaptic membrane	2.350	0.034
Ribosomal subunit	−5.798	0
Ribosome	−5.415	0
Organelle inner membrane	−5.264	0
Mitochondrial protein containing complex	−5.094	0
Large ribosomal subunit	−4.862	0

F

Shank3 - Adult (P60)	NES	FDR
Cytosolic ribosome	6.179	0
Ribosomal subunit	6.179	0
Ribosome	5.939	0
Large ribosomal subunit	4.736	0
Cytosolic large ribosomal subunit	4.654	0
Receptor complex	−3.148	0
Plasma membrane protein complex	−2.763	0.005
External encapsulating structure	−2.595	0.009
Collagen containing extracellular matrix	−2.586	0.007
Synaptic membrane	−2.344	0.031

FIGURE 1
Differentially expressed gene (DEG) analysis and gene set enrichment analysis (GSEA) of P25-Shank3 and P60-Shank3 transcripts. **(A)** Summary of the DEGs from the forebrain of homozygous *Shank3*-mutant mice at P25 and P60 (P25-Shank3 and P60-Shank3 mice), compared with wild-type/WT mice at P25 and P60. DEGs were defined by transcript changes with adjusted p value < 0.05 ($n = 3$ mice for P25-WT, P25-Shank3, P60-WT, and P60-Shank3). **(B)** Venn diagrams showing DEGs that overlap between P25-Shank3 and P60-Shank3 mice. **(C,D)** Volcano plots showing DEGs from P25-Shank3 and P60-Shank3 mice. The DEGs (adjusted p value < 0.05) were further color-coded to indicate those with stronger fold changes (>1.5) (see **Supplementary Table 2** for full results). Genes with # labels indicate those with p values beyond the indicated p-value ranges ($n = 3$ mice for P25-WT, P25-Shank3, P60-WT, and P60-Shank3). **(E,F)** GSEA of P25-Shank3 and P60-Shank3 transcripts were performed using the gene sets of the cellular component (CC) domain. The results are shown as lists of the top-five positively/negatively enriched gene sets (top; see **Supplementary Table 3** for full results) and functional clustering of enriched gene sets, which was performed using the EnrichmentMap Cytoscape App (bottom). The sizes and colors of the circles in the EnrichmentMap results indicate the sizes of gene sets and the extents of positive/negative (red/blue) enrichments, respectively ($n = 3$ mice for P25-WT, P25-Shank3, P60-WT, and P60-Shank3).

of DEGs revealed relatively small sets of DEGs that were up- or downregulated in P25-Shank3 or P60-Shank3 mice (**Figure 1A** and **Supplementary Table 2**), and even smaller sets that overlapped between P25-Shank3 and P60-Shank3 mice (*Shank3* and *Ccdc40*) (**Figure 1B**). In the P25-Shank3 transcripts, the strongly upregulated DEGs included *Yy2* and *Fancm* and the strongly downregulated DEGs included *Shank3*, as shown by the volcano plot (**Figure 1C**). In the P60-Shank3 transcripts, the strongly upregulated DEGs included *Gstp1* and *Lamb3* and the strongly downregulated DEGs included *Shank3*, *Pcdha11*, and *Rpl10* (**Figure 1D**). CCDC40, a coiled-coil protein whose transcript levels are increased in both P25-Shank3 and P60-Shank3 transcripts, is known to regulate motile cilia function and left-right axis formation with implications in the primary ciliary dyskinesia (Becker-Heck et al., 2011). These results indicate that *Shank3* deletion in juvenile and adult mice is associated with relatively small sets of DEGs.

The scarcity of DEGs from P25-Shank3 and P60-Shank3 mice prompted us to apply GSEA. The results of GSEA performed using genes in the cellular component (CC) domain of the C5 gene sets indicated that P25-Shank3 transcripts were positively and moderately enriched for gene sets associated with synaptic functions (synaptic membrane, glutamatergic synapse, and postsynaptic membrane), as indicated by top-five most strongly enriched gene sets (**Figure 1E**, top and **Supplementary Table 3**). A similar conclusion was drawn from our functional clustering of positively enriched gene sets (postsynaptic membrane), which was performed using EnrichmentMap Cytoscape App (**Figure 1E**, bottom). P25-Shank3 transcripts were negatively and strongly enriched for gene sets associated with ribosomes (ribosomal subunit, ribosome, and large ribosomal subunit) and mitochondria (organelle inner membrane, mitochondrial protein-containing complex), as supported by the top-five gene sets and the EnrichmentMap results (**Figure 1E**). GSEA performed using the gene sets in the BP and MF domains of the C5 database yielded partly similar results; positive enrichments for synapse-related gene sets and negative enrichments for ribosome (translation)/mitochondria (electron transport, oxidative phosphorylation, and ATP synthesis)-related gene sets in the BP domain, and negative enrichments of P25-Shank3 transcripts for ribosome/mitochondria-related gene sets in the MF domain (**Supplementary Figure 1** and **Supplementary Table 3**).

Gene set enrichment analysis of P60-Shank3 transcripts revealed strong positive enrichments for gene sets associated with ribosomes and mitochondria, as shown by the top-five gene sets and EnrichmentMap results (**Figure 1F** and **Supplementary Table 3**). In addition, P60-Shank3 transcripts were negatively but moderately enriched for synapse-related gene sets (receptor complex and synaptic membrane), as shown by the top-five gene sets and EnrichmentMap results (**Figure 1F**). GSEA using the gene sets in the BP and MF domains of the C5 database also yielded similar results; positive enrichments for ribosome/mitochondria-related gene sets in the BP domain, and positive enrichments for ribosome/mitochondria-related gene sets in the MF domain (**Supplementary Figure 2** and **Supplementary Table 3**).

These findings indicate that Shank3 mice show age-dependent and nearly opposite transcriptomic patterns at juvenile and adult stages: Synaptic and ribosomal/mitochondrial genes are up- and downregulated, respectively, at P25, whereas opposite changes are observed at P60.

ASD-related patterns in P25-Shank3 and P60-Shank3 transcripts

We next tested if P25-Shank3 and P60-Shank3 transcripts are enriched for ASD-related/risk gene sets. P25-Shank3 transcripts were negatively enriched for a gene set containing genes that are upregulated in ASD (Co-Exp Up M16 Voineagu) and positively enriched for gene sets containing genes that are downregulated in ASD (DEG Down Voineagu, and Co-Exp Down M12 Voineagu) (Voineagu et al., 2011; Werling et al., 2016; **Figure 2A**, **Supplementary Figure 3**, and **Supplementary Table 4**). In addition, P25-Shank3 transcripts were positively enriched for the SFARI gene set, which is usually downregulated in ASD, and other gene sets, such as FMRP Targets, DeNovoMissense, DeNovoVariants, and AutismKB (**Figure 2A**). These results suggest that P25-Shank3 transcripts display a transcriptomic pattern that is largely opposite to those observed in ASD. In contrast, P60-Shank3 transcripts were negatively enriched for ASD-risk gene sets (**Figure 2A**), and thus conformed to the pattern observed in ASD. The opposite enrichments of P25-Shank3 and P60-Shank3 transcripts for two gene sets (SFARI Genes [All] and FMRP Targets) involved ∼50% of the genes in each gene set and small correlative fold changes of co-up/down regulations (**Supplementary Figure 4**). These results suggest that P25- and P60-Shank3 transcripts show transcriptomic patterns that are largely opposite to each other, with a reverse-ASD pattern in juvenile stages converting to an ASD-like pattern in adult stages.

In GSEA performed using cell type-specific gene sets (Albright and Gonzalez-Scarano, 2004; Cahoy et al., 2008; Kang et al., 2011; Zeisel et al., 2015; Werling et al., 2016; Velmeshev et al., 2019, 2020; **Supplementary Table 4**), P25-Shank3 transcripts were positively enriched for neuron-related gene sets and negatively enriched for glia-related gene sets (**Figures 2B,C**). This pattern is largely opposite to that observed in ASD, which typically exhibits decreased neuronal/oligodendrocytic gene expression and increased

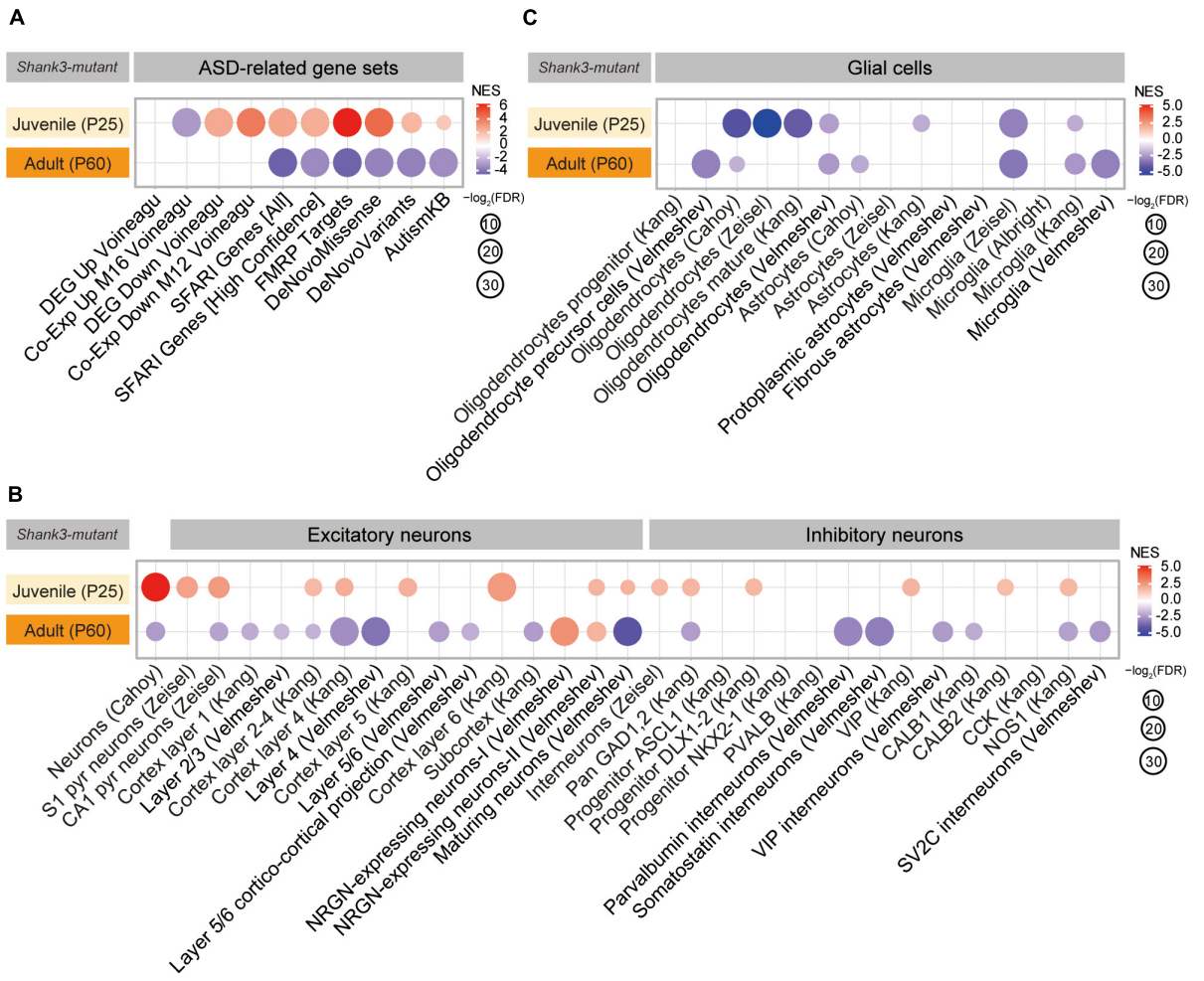

FIGURE 2
Autism spectrum disorder (ASD)-related patterns in P25-Shank3 and P60-Shank3 transcripts. **(A)** Gene set enrichment analysis (GSEA) results for P25- and P60-Shank3 transcripts relative to ASD-related gene sets that are upregulated (DEG Up Voineagu and Co-Exp Up M16 Voineagu) and downregulated (DEG Down Voineagu and Co-Exp Down M12 Voineagu) in ASD, as well as ASD-risk gene sets (SFARI Genes [All], SFARI Genes [High Confidence], FMRP Targets, DeNovoMissense, DeNovoVariants, and AutismKB) (n = 3 mice [P25-Shank3 and P60-Shank3]) (n = 3 mice [P25-Shank3 and P60-Shank3]). **(B)** GSEA results for P25- and P60-Shank3 transcripts for cell-type-specific gene sets (glutamate and GABA neurons) (n = 3 mice [P25-Shank3 and P60-Shank3]). **(C)** GSEA results for P25- and P60-Shank3 transcripts for cell-type-specific gene sets (glial cells) (n = 3 mice [P25-Shank3 and P60-Shank3]).

astrocytic/microglial gene expression (Voineagu et al., 2011; Werling et al., 2016). The pattern in P60-Shank3 transcripts contrasted with that in P25-Shank3 transcripts by being negatively enriched for neuron-related gene sets, but resembled that in P25-Shank3 transcripts by being negatively enriched for oligodendrocyte/microglia-related gene sets (**Figures 2B,C**).

These GSEA results collectively suggest that P25- and P60-Shank3 transcripts display reverse-ASD and ASD-like transcriptomic patterns, respectively, based their enrichment patterns for gene sets that are up/downregulated in ASD, as well as those belonging to ASD-risk and cell type-specific gene sets.

DEG analysis and GSEA of transcripts from the cortex, hippocampus, and striatum of Shank3-HT and Shank3-HM mice

We next tested if different brain regions and gene deletion dosages affect the transcriptomic patterns in adult (P90) heterozygous and homozygous *Shank3*-mutant mice (Shank3-HT and Shank3-HM mice, respectively; 5 mice per group) by performing RNA-Seq analyses of transcripts from the prefrontal cortex (termed cortex hereafter), hippocampus, and striatum (**Figure 3A** and **Supplementary Table 5**). These brain regional

A

Shank3-mutant

Age	Brain region	Genotype	DEG numbers		
			All	Up	Down
Adult stage (13-weeks)	Cortex	HT/WT (5 pairs)	4	1	3
		HM/WT (5 pairs)	2	1	1
	Hippocampus	HT/WT (5 pairs)	7	6	1
		HM/WT (5 pairs)	7	4	3
	Striatum	HT/WT (5 pairs)	4	2	2
		HM/WT (5 pairs)	101	67	34

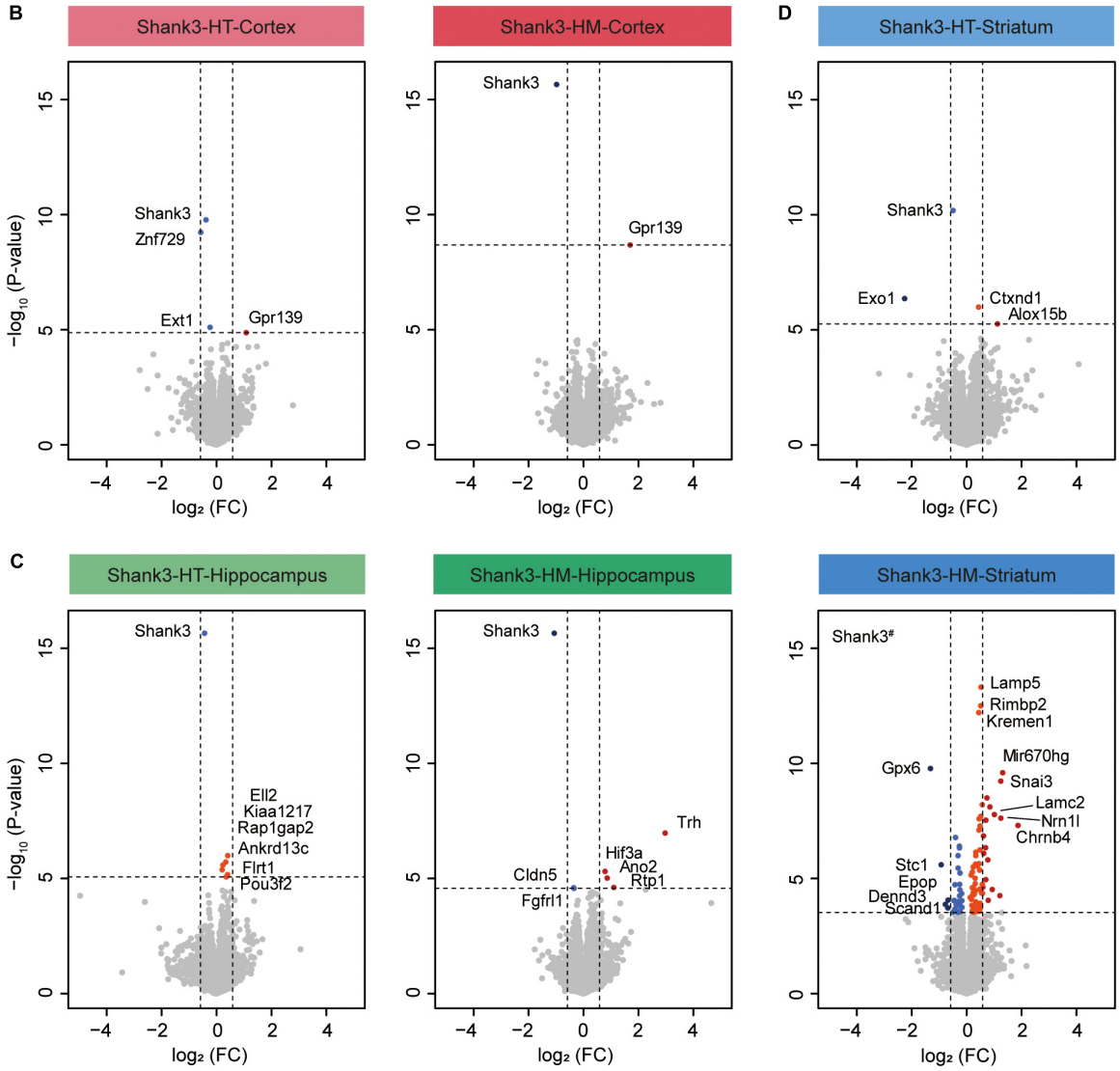

FIGURE 3
Differentially expressed gene (DEG) analysis of transcripts from the cortex, hippocampus, and striatum of Shank3-HT and Shank3-HM mice. **(A)** Outline of the DEGs from the cortex, hippocampus, and striatum of adult *Shank3*-heterozygous (HT) and *Shank3*-homozygous (HM) mutant mice, compared with WT mice. DEGs were defined by transcriptional changes with adjusted *p* value < 0.05 ($n = 5$ mice for cortex/hippocampus/striatum regions in WT, Shank3-HT, and Shank3-HM mice). **(B–D)** Volcano plots showing DEGs from the cortex, hippocampus, and striatum of adult *Shank3*-heterozygous (HT) and *Shank3*-homozygous (HM) mutant mice. The DEGs (adjusted *p* value < 0.05) were further color-coded to indicate those with stronger fold changes (>1.5). Shank3$^{\#}$ in the Shank3-HM volcano plot indicates a *p* value beyond the indicated *p*-value ranges ($n = 5$ mice for cortex/hippocampus/striatum regions in WT, Shank3-HT, and Shank3-HM mice).

transcriptomes were well separated in a clustering analysis (**Supplementary Figure 5**).

All three brain regions of the Shank3-HT and Shank3-HM mice displayed small numbers of DEGs, except for the striatal region of Shank3-HM mice (**Figure 3A**). In volcano plots and the list of top DEGs, *Shank3* was identified in all six groups of downregulated DEGs (cortex/hippocampus/striatum of Shank3-HT/HM mice) (**Figures 3B–D** and **Supplementary Table 6**), indicating that the RNA-Seq results were generally reliable. The most prominent identified DEGs included *Znf729* (Shank3-HT cortical, downregulated), *Trh* (Shank3-HM hippocampal, upregulated), *Mir670hg* (Shank3-HM striatal, upregulated), and *Gpx6* (Shank3-HM striatal, downregulated). DAVID analysis of the striatal DEGs (n = 101) did not yield any significant biological GO term.

We next performed GSEA to examine whether the cortical/hippocampal/striatal Shank3-HT and Shank3-HM transcripts were associated with specific biological functions. The cortical Shank3-HT transcripts were positively enriched for gene sets associated with ribosome/mitochondrial functions, as supported by the top-five gene sets and EnrichmentMap gene set clustering (**Figure 4A** and **Supplementary Table 7**). The cortical Shank3-HT transcripts were negatively enriched for gene sets associated with synaptic functions (**Figure 4A**). The cortical Shank3-HM transcripts were positively enriched for gene sets associated with spliceosomes and ribosomes, as supported by the top-five gene sets and EnrichmentMap gene set clustering, and negatively enriched for gene sets associated with synapses (neuronal synapse, presynapse, active zone) (**Figure 4B**). These results indicate that Shank3-HT and Shank3-HM cortical transcripts show similar upregulations of ribosome-related genes and downregulations of synapse-related genes.

The hippocampal Shank3-HT transcripts were positively enriched for synapse (pre/postsynaptic membrane)-related gene sets and negatively enriched for ribosome/mitochondria/spliceosome-related gene sets (**Figure 4C**). The hippocampal Shank3-HM transcripts were positively and weakly enriched for synapse-related gene sets and negatively enriched for ribosome/mitochondria, and spliceosome-related gene sets (**Figure 4D**). These results indicate that hippocampal Shank3-HT and Shank3-HM show similar patterns of synapse-related gene upregulation and ribosome/mitochondria- and spliceosome-related gene downregulation. Interestingly, these patterns are largely opposite those observed in the cortical Shank3-HT/HM transcripts (**Figures 4A,B**).

The striatal Shank3-HT transcripts were positively enriched for ribosome/mitochondria/ECM-related gene sets and negatively enriched for chromosome/spliceosome/cilia-related gene sets (**Figure 4E**). The striatal Shank3-HM transcripts were positively enriched for ribosome-related gene sets and did not exhibit any significant negative enrichment (**Figure 4F**). These results indicate that the striatal Shank3-HT and Shank3-HM transcript patterns are dissimilar to each other, except for the ribosome-related gene upregulation, and also dissimilar to the cortical and hippocampal patterns.

ASD-related patterns in cortical, hippocampal, and striatal Shank3-HT and Shank3-HM transcripts

We next tested whether the cortical, hippocampal, and striatal transcripts from Shank3-HT and Shank3-HM mice were enriched for ASD-related/risk gene sets. The cortical Shank3-HT transcripts were negatively enriched for the gene set downregulated in ASD (Co-Exp Down M12 Voineagu) (Voineagu et al., 2011; Werling et al., 2016) and negatively enriched for ASD-risk gene sets (SFARI Genes [All] and FMRP Targets) (**Figure 5A**, **Supplementary Figure 6**, and **Supplementary Table 4**). The cortical Shank3-HM transcripts showed similar ASD-like patterns.

In contrast, the hippocampal Shank3-HT and Shank3-HM transcripts displayed strong reverse-ASD patterns, as the transcripts were positively enriched for all six ASD-risk gene sets (SFARI Genes [All and High Confidence], FMRP Targets, DeNovoMissense, DeNovoVariants, and AutismKB) (**Figure 5A**). In contrast, the striatal Shank3-HT and Shank3-HM transcripts displayed ASD-like patterns: The transcripts were positively enriched for gene sets that are upregulated in ASD (DEG Up Voineagu, and Co-Exp Up M16 Voineagu), but no enrichment was observed for the ASD-risk gene sets (**Figure 5A**).

When GSEA was performed using cell type-specific gene sets, the results revealed that cortical Shank3-HT transcripts were negatively enriched for neuron-related gene sets, indicative of an ASD-like pattern. However, they were positively enriched for oligodendrocyte-related gene sets, which weakened the ASD-like pattern (**Figures 5B,C**). The cortical Shank3-HM transcripts were negatively enriched for neuron-related gene sets, which was similar to the ASD-like pattern seen in the cortical Shank3-HT transcripts. However, they were positively enriched for oligodendrocyte-related gene sets and negatively enriched for astrocyte/microglia-related gene sets, which weakened the ASD-like pattern.

The hippocampal Shank3-HT and Shank3-HM transcripts were positively enriched for neuron/oligodendrocyte-related gene sets, indicative of a reverse-ASD pattern. However, they were positively enriched for astrocyte/microglia-related gene sets, which weakened the reverse-ASD pattern (**Figures 5B,C**). The striatal Shank3-HT and Shank3-HM transcripts were negatively enriched for neuron-related gene sets and positively enriched for astrocyte/microglia-related gene sets, albeit to lesser extents in Shank3-HM transcripts, indicative of an ASD-like pattern. However, they were positively enriched for oligodendrocyte-related gene sets, which weakened the ASD-like pattern (**Figures 5B,C**).

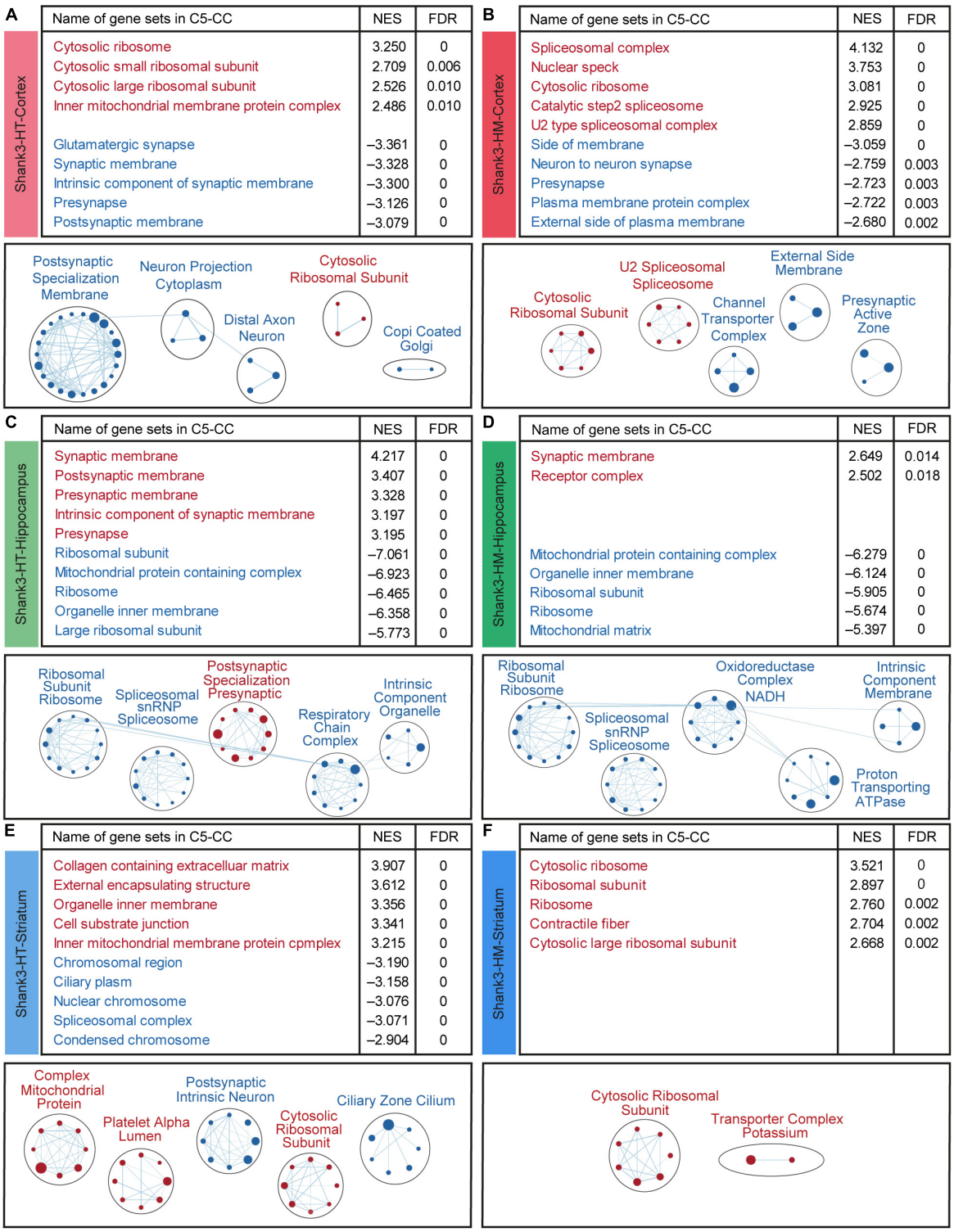

FIGURE 4
Gene set enrichment analysis (GSEA) of transcripts from the cortex, hippocampus, and striatum of Shank3-HT and Shank3-HM mice. **(A–F)** GSEA results obtained for cortical, hippocampal, and striatal Shank3-HT and Shank3-HM transcripts using the gene sets in the cellular component (CC) domain, as represented by the list of top-five positively/negatively enriched gene sets (top; see **Supplementary Table 7** for full results) and functional clustering of enriched gene sets performed using the EnrichmentMap Cytoscape App (bottom). The sizes and colors of the circles in the EnrichmentMap results indicate the extents and directions (positive/negative; red/blue) of the enrichments, respectively (n = 5 mice for cortex/hippocampus/striatum regions in WT, Shank3-HT, and Shank3-HM mice).

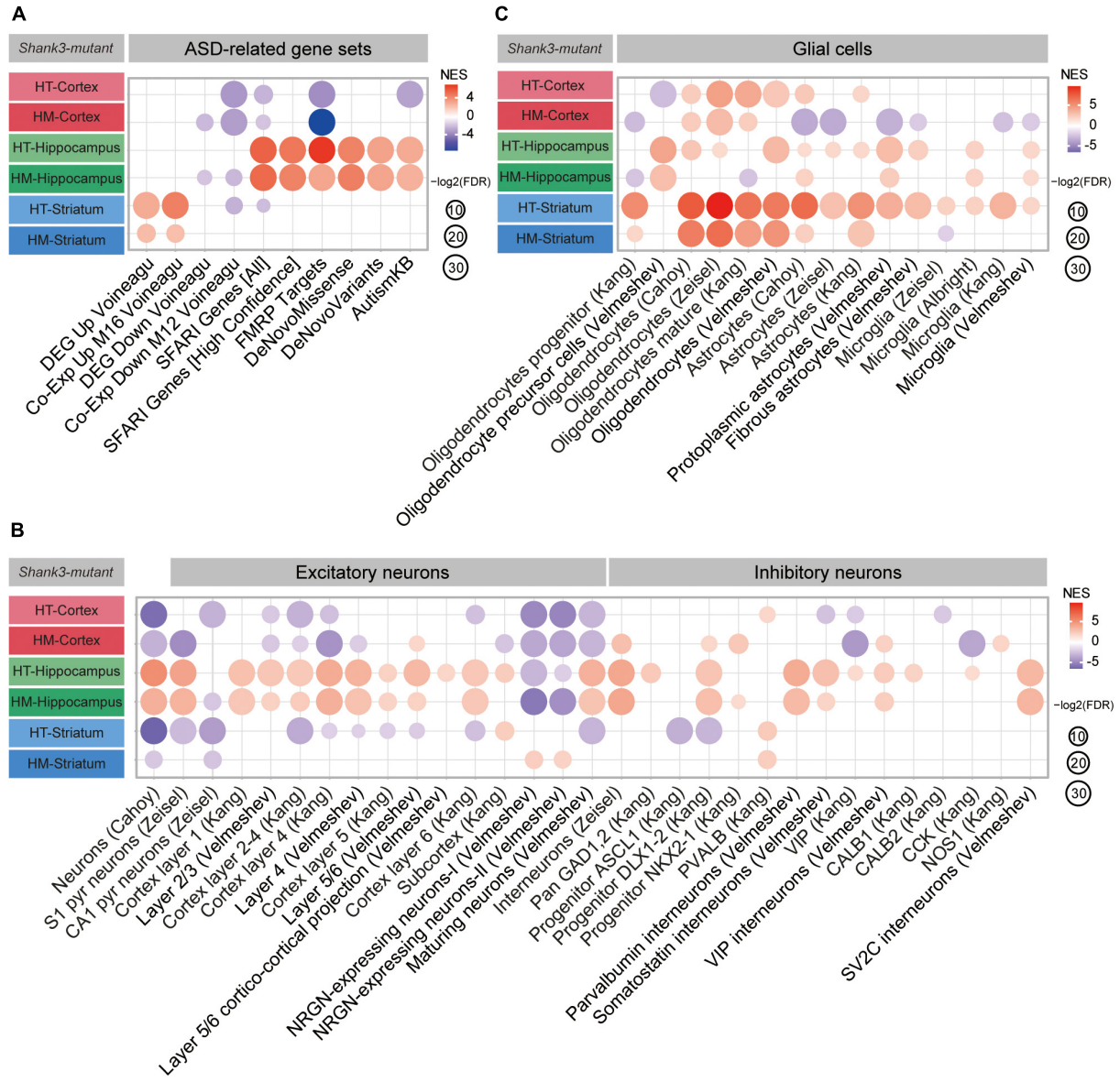

FIGURE 5
Autism spectrum disorder (ASD)-related patterns in the transcripts from the cortex, hippocampus, and striatum of Shank3-HT and Shank3-HM mice. **(A)** Gene set enrichment analysis (GSEA) results for the cortical, hippocampal, and striatal Shank3-HT and Shank3-HM transcripts: Enrichment patterns for ASD-related gene sets that are upregulated (DEG Up Voineagu and Co-Exp Up M16 Voineagu) or downregulated (DEG Down Voineagu and Co-Exp Down M12 Voineagu) in ASD, as well as for ASD-risk gene sets (SRARI Genes [All], SFARI Genes [High Confidence], FMRP Targets, DeNovoMissense, DeNovoVariants, and AutismKB) (n = 5 mice for cortex/hippocampus/striatum regions in WT, Shank3-HT, and Shank3-HM mice). **(B)** GSEA results for the cortical, hippocampal, and striatal Shank3-HT and Shank3-HM transcripts, indicating enrichment patterns for cell type-specific gene sets (glutamate and GABA neurons) (n = 5 mice for cortex/hippocampus/striatum regions in WT, Shank3-HT, and Shank3-HM mice). **(C)** GSEA results for the cortical, hippocampal, and striatal Shank3-HT and Shank3-HM transcripts, indicating enrichment patterns for cell type-specific gene sets (glial cells) (n = 5 mice for cortex/hippocampus/striatum regions in WT, Shank3-HT, and Shank3-HM mice).

These results from GSEA performed using ASD-related/risk and cell type-specific gene sets collectively suggest that cortical, hippocampal, and striatal Shank3-HT and Shank3-HM transcripts show both shared and distinct patterns wherein: (1) Shank3-HT and Shank3-HM show similar ASD-like patterns (limited gene dosage effects). (2) The cortex and striatum show ASD-like patterns, whereas the hippocampus shows a reverse-ASD pattern. (3) The ASD-like patterns in the cortex and striatum involve differential gene sets (the ASD-risk vs. ASD-related gene sets, respectively).

Discussion

Here we investigated transcriptomic changes in the prefrontal cortex, hippocampus, and striatum regions of adult Shank3-HT and Shank3-HM mice. In addition, we compared the transcriptomes from juvenile and adult Shank3-HM mice. The results point to age, brain region, and gene dosage-differential transcriptomic changes involving altered biological functions and expressions of ASD-related/risk genes in *Shank3*-mutant mice, which also differ from the overall patterns observed in *Shank2*-mutant mice (comparisons summarized in **Figures 6**, **7** and discussed below).

Transcriptomic changes in *Shank3*-mutant mice

Juvenile (P25) and adult (P60) Shank3-HM mice showed largely contrasting transcriptomic changes in the forebrain. GSEA of P25 Shank3-HM transcripts revealed upregulation of synapse-related genes and downregulation of ribosome/mitochondria-related genes, corresponding to reverse ASD-like transcriptomic changes (**Figures 1**, **2**). In contrast, P60 Shank3-HM transcripts showed downregulated synapse-related genes and upregulated ribosome/mitochondria-related genes, representing ASD-like transcriptomic patterns. These results suggest that these mice undergo a strong age-dependent transcriptomic change from a reverse-ASD pattern to an ASD-like pattern through the alteration of synaptic gene expression. A similar age-dependent change from a reverse-ASD to ASD-like pattern was previously reported in the mPFC region of Shank2-HM mice (exons 6–7), although the altered biological functions and ASD-related/risk genes were different (Lee et al., 2021). Despite this difference, the results from Shank2 and Shank3 mice collectively indicate at the minimum age-dependent transcriptomic inversion with respect to ASD-related/risk gene expressions.

Whether this age-dependent change in Shank3 forebrain transcriptomes correlates with altered neuronal and synaptic functions remains to be determined. Notably, however, the synaptic gene upregulations in the P25 *Shank3*-mutant forebrain correlate with the increased frequency of excitatory synaptic transmission in the juvenile *Shank3*-mutant mPFC (Yoo et al., 2019), although it remains unclear whether the adult *Shank3*-mutant mPFC would display suppressed excitatory transmission at P60 in line with the transcriptomic changes. It is possible that the early postnatal increase in excitatory synaptic function in *Shank3*-mutant mice may lead to an opposite change (excitatory synaptic depression) at adult stages. In support of this possibility, early and excessive excitatory synaptic functions have been shown to cause deleterious long-lasting effects in other mouse models of ASD, including Shank3B mice (exons 13–16 deletion) (Peixoto et al., 2016), Shank2 mice (Chung et al., 2019), and SynGAP1 mice (Clement et al., 2012, 2013; Aceti et al., 2015; reviewed in Chung et al., 2021).

Gene Set Enrichment Analysis of transcripts from the different brain regions of adult Shank3-HT and Shank3-HM mice revealed the following notable patterns (**Figures 3–5**): (1) The cortical, hippocampal, and striatal transcripts show distinctly altered biological functions and ASD-related/risk gene expression patterns. (2) Shank3-HT and Shank3-HM transcripts in a given brain region display largely similar patterns in biological functions and ASD-related/risk gene expression, suggesting that the gene dosage effect is small. (3) Synapse- and ribosome/mitochondria-related gene expression patterns frequently change in opposite directions consistently across all three brain regions. (4) Upregulated synapse-related genes and downregulated ribosome/mitochondria-related genes are frequently associated with reverse-ASD transcriptomic changes, and vice versa. (5) The hippocampal HT/HM transcripts display a reverse-ASD pattern, whereas the cortical and striatal HT/HM transcripts display ASD-like patterns. These patterns are partly similar to and distinct from those observed in *Shank2*-mutant mice (see below).

Whether these brain region-differential transcriptomic changes are associated with parallel changes in proteomes remains to be determined. However, a previous proteomic study on hippocampal and striatal postsynaptic density fractions from *Shank3*$\Delta 11^{-/-}$ mice reported enrichments of the differentially expressed proteins for actin- and synapse-related GO functions, respectively (Reim et al., 2017). This differs from our results in that hippocampal and striatal transcripts from Shank3-HM mice show enrichments for ribosome/mitochondria- and ribosome-related functions, respectively. The reason for the discrepancy could be that different *Shank3* exons were deleted in the two mouse lines.

Comparison of *Shank2*- and *Shank3*-mutant transcriptomes

Differentially expressed gene analyses revealed an interesting difference between *Shank2*- and *Shank3*-mutant transcriptomes: More DEGs were identified in Shank2-HT/HM transcriptomes than in Shank3-HT/HM transcriptomes (**Figure 3**; Yoo et al., 2022). However, GSEA revealed strong enrichments of both *Shank2*- and *Shank3*-mutant transcriptomes for biological functions and ASD-related/risk gene sets (**Figures 4**, **5**; Yoo et al., 2022). Therefore, *Shank2* deletion seems to induce two distinct types of transcriptomic changes: large changes in a small number of top genes that are readily detectable by DEG analyses, and small changes in a large number of genes that are readily detectable by GSEA. Meanwhile, *Shank3* deletion appears to induce mainly small changes in a large number of genes.

For *Shank2*- and *Shank3*-mutant transcriptomes, the GSEA results for biological functions and ASD-related/risk gene

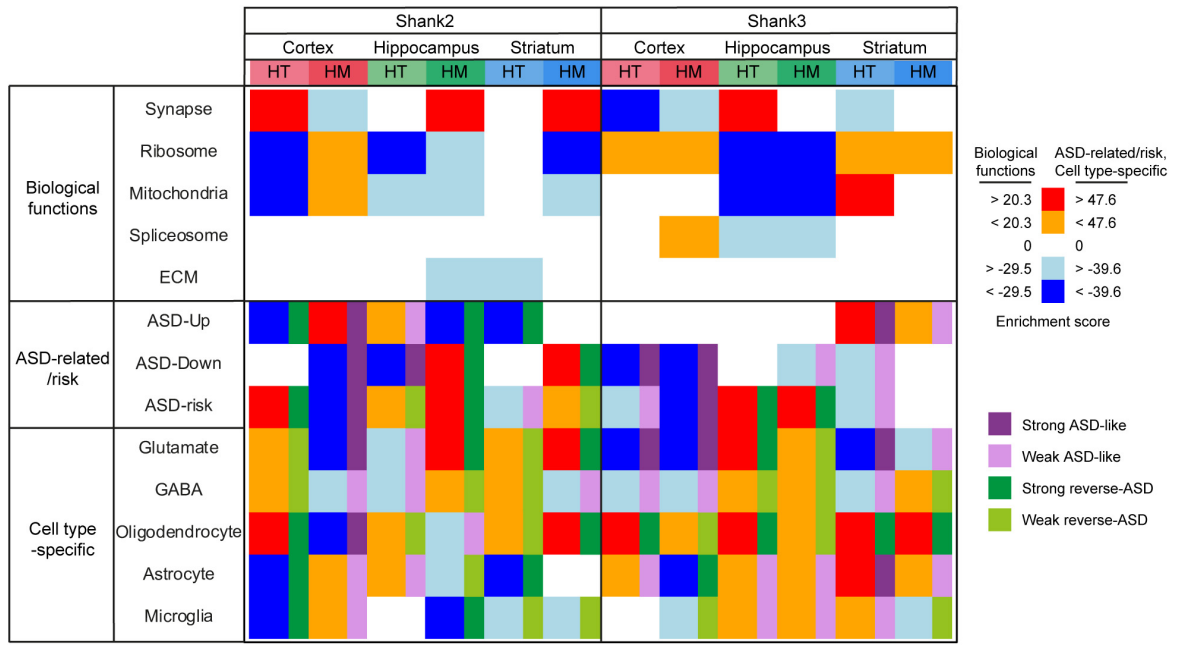

FIGURE 6
Summary of all gene set enrichment analysis (GSEA) results for Shank2-HT/HM and Shank3-HT/HM transcripts. To summarize the GSEA results for Shank2-HT/HM and Shank3-HT/HM transcripts in a single table, we selected the strongest gene-set cluster in the Cytoscape EnrichmentMap results (for gene sets associated with biological functions) or combined relevant gene sets [for autism spectrum disorder (ASD)-related/risk and single cell-type gene sets], and calculated comparative scores by summing the NES values of the gene sets in the indicated gene-set clusters (for biological functions) and by averaging the NES × p values of gene sets in the indicated gene-set groups (for ASD-related/risk and single-cell-specific gene sets) (see **Supplementary Table 8** for the details).

expressions reveal notable similarities and differences (see **Figure 6** and **Supplementary Table 8**). Regarding similarities, we note that: (1) The three brain regions show distinct transcriptomic changes in both *Shank2*- and *Shank3*-mutant mice. (2) Synapse- and ribosome/mitochondria-related genes are frequently changed toward opposite directions in all three brain regions. (3) Upregulated synapse-related genes and downregulated ribosome/mitochondria-related genes are frequently associated with reverse ASD-like transcriptomic changes, and vice versa.

Regarding dissimilarities, we find that: (1) Shank2-HT/HM and Shank3-HT/HM transcripts show different gene dosage effects, in that Shank2-HT and Shank2-HM transcripts show largely opposite patterns with regard to altered biological functions and ASD-related/risk gene expressions, whereas Shank3-HT and Shank3-HM transcripts are largely similar in these aspects. (2) Stronger similarities across Shank2 and Shank3 mice are observed in HM conditions mice, whereas stronger dissimilarities are observed in HT conditions; i.e., Shank2-HM and Shank3-HM cortical transcripts show similar ASD-like patterns, and Shank2-HM and Shank3-HM hippocampal transcripts show similar reverse-ASD patterns, whereas Shank2-HT and Shank3-HT cortical transcripts, or Shank2-HT and Shank3-HT hippocampal transcripts, show opposite ASD-like patterns. (3) Opposite ASD-like patterns are observed in the striatal regions of Shank2-HT and Shank3-HT mice (reverse-ASD and ASD-like, respectively), similar to cortical and hippocampal regions, although the difference becomes less clear in Shank2/3-HM striatal transcripts, unlike cortical and hippocampal regions in which Shank2/3-HM transcripts become similar.

Additional similarities and differences between *Shank2*- and *Shank3*-mutant mice were also evident in detailed comparisons of ASD-related/risk GSEA patterns (**Figure 7**), as follows: (1) The changes observed in the ASD-related/risk gene expression patterns of Shank2-HT/HM transcripts involved both ASD-related and ASD-risk changes, whereas those in Shank3-HT/HM transcriptomes involved largely either ASD-related or ASD-risk changes. (2) The changes observed in neuronal gene expression patterns involved both excitatory and inhibitory neurons in both Shank2-HT/HM and Shank3-HT/HM transcripts. (3) Although ASD usually induces opposite changes in two groups of glial cell transcripts that are frequently observed in ASD (oligodendrocytic downregulations and astrocytic/microglial upregulations), we frequently observed exceptions to this (i.e., similar oligodendrocytic/astrocytic/microglial upregulations or downregulations) in both Shank2-HT/HM and Shank3-HT/HM transcriptomes (i.e., in that of Shank3-HT striatum).

Interpretations of the largely opposite changes in the expression patterns of synaptic genes and

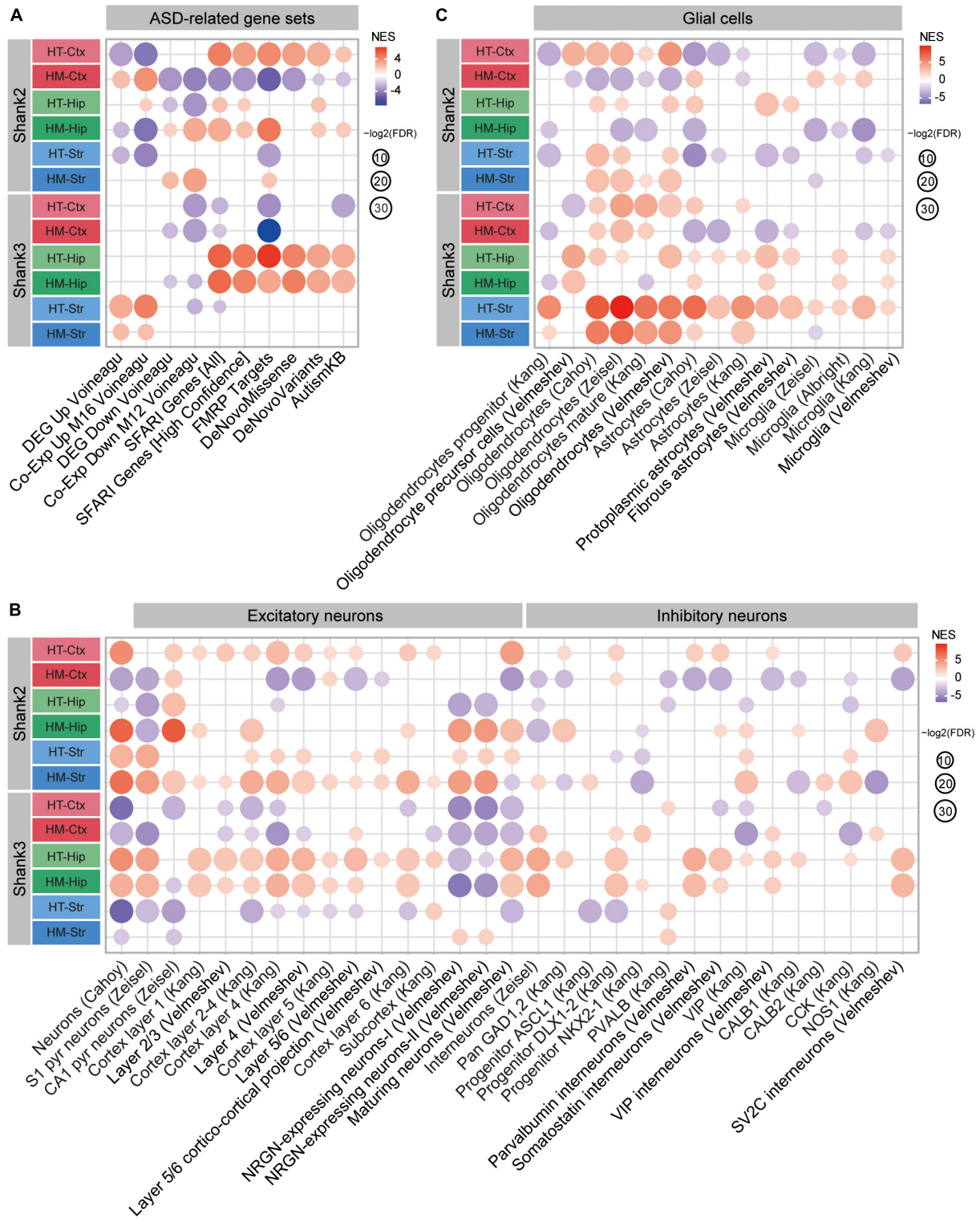

FIGURE 7
Summary of the gene set enrichment analysis (GSEA) results obtained using autism spectrum disorder (ASD)-related/risk and cell type-specific gene sets for Shank2-HT/HM and Shank3-HT/HM transcripts. **(A–C)** GSEA results for Shank2-HT/HM and Shank3-HT/HM transcripts obtained using ASD-related/risk and cell type-specific gene sets (Yoo et al., 2022; **Figure 5**) are combined here to enable better visualization of the similarities and differences.

ribosomal/mitochondrial genes could differ in different brain regions and gene dosage conditions. For instance, the upregulation of synaptic genes in the Shank2-HM hippocampal transcriptome (Yoo et al., 2022), which coincides with the decreased synaptic transmission in the mutant hippocampus (Won et al., 2012), might reflect compensatory increases in synaptic gene expression. Meanwhile, the decreased synaptic transmission in *Shank2*-mutant mice might have suppressed ribosomal/mitochondrial gene expression to minimize energy production and expenditure (for protein synthesis) (Morita et al., 2015) in the absence of synaptic activity. In support of this possibility, synaptic activity has been functionally coupled with mitochondrial activity (Li et al., 2004; Vos et al., 2010; Sheng and Cai, 2012; Santini and Klann, 2014; Lee et al., 2018). In addition, ASD has been associated with mitochondrial deficits (Hollis et al., 2017; Frye, 2020; Rojas-Charry et al., 2021) and altered levels of ribosomal proteins in post-mortem brains and human neural progenitor cells (Lombardo, 2021).

Our observation that strong gene dosage differences are seen in Shank2 transcriptomes but not in Shank3 transcriptomes could reflect that *Shank2* heterozygous and homozygous deletions fall in a range where they could induce quantitively different disruptions of biological functions. The lack of dosage responses in the Shank3 transcriptomes could indicate that *Shank3* heterozygous deletion is sufficient to yield the full spectrum of phenotypic deficits. This might suggest the stronger impacts of *Shank3* mutations relative to *Shank2* mutations in animal models of ASD, and might be in line with the greater prevalence of *Shank3* mutations in ASD, relative to *Shank2* mutations (Leblond et al., 2014).

The current RNA-Seq results do not give clear answers on whether the observed transcriptomic changes represent molecular pathophysiology or responses that arise to compensate for the gene deletion. In addition, it would be difficult to functionally validate the identified biological functions and pathways, given the known and expected complexity of synaptic, ribosomal, and mitochondrial systems in different brain cell types. However, RNA-Seq analyses can provide unbiased clues on altered biological functions and hints on whether the overall transcriptomic changes in our systems mimic those observed in ASD (ASD-like vs. reverse-ASD). For instance, regardless of whether certain transcriptomic changes represent pathophysiology or responses, the absence of ASD-like transcriptomic changes indicate the absence or normalization of ASD-related phenotypes, i.e., at neuronal, synaptic, circuit, or behavioral levels. In addition, RNA-Seq analyses are useful in that they can be attempted in various *in vivo* contexts, including in different mouse ages, brain regions, gene dosages (heterozygous and homozygous), and pathological/rescue environments. The results may facilitate the design and data interpretation of future experiments. For instance, the results obtained in our setting suggest that *Shank3*- and *Shank2*-mutant mice may exhibit distinct gene dosage-related shifts in phenotypes (heterozygous vs. homozygous). In addition, other studies showed that RNA-Seq can be used to monitor ASD-related transcriptomic phenotypes when *Shank2*-mutant mice were treated with memantine at early postnatal stages, which corrected the synaptic and behavioral phenotypes at adult stages (Chung et al., 2019, 2021; Yoo et al., 2021).

The RNA-Seq results in the present study were obtained specifically from *Shank2*- and *Shank3*-mutant mouse lines lacking exons 6–7 and 14–16, respectively (Won et al., 2012; Yoo et al., 2018, 2019, 2021; Chung et al., 2019). Given that different mutations in the same Shank genes can lead to different mouse phenotypes (Sheng and Kim, 2000, 2011; Boeckers et al., 2002; Bourgeron, 2009; Grabrucker et al., 2011; Jiang and Ehlers, 2013; Sala et al., 2015; Schmeisser, 2015; Monteiro and Feng, 2017; Mossa et al., 2017, 2018; De Rubeis et al., 2018; Eltokhi et al., 2018; Ey et al., 2020), further work is warranted to examine whether convergent transcriptomic changes are be observed in additional *Shank2*- and *Shank3*-mutant mouse lines.

In summary, our results, together with the previous transcriptomic results from Shank2 mice, indicate that *Shank2* and *Shank3* deletions lead to age-, brain region-, and gene dosage-differential transcriptomic changes associated with altered biological functions and ASD-related/risk gene expression patterns. These results provide unbiased clues on the mechanisms underlying the ASD-related phenotypes in *Shank2/3*-mutant mice and will be useful in designing future experiments using these mice and interpreting the results.

Data availability statement

The datasets presented in this study can be found in online repositories. The raw RNA-Seq results are available as GSE201621 (Shank3 brain regions), GSE201853 (Shank3 juvenile and adult forebrains), and GSE201854 (GSE201621 + GSE201853) at GEO (Gene Expression Omnibus), NCBI (National Center for Biotechnology Information).

Ethics statement

The animal study was reviewed and approved by the Committee of Animal Research at KAIST (KA2020-93).

Author contributions

TY, Y-EY, and EK designed the experiments. TY, Y-EY, and HK performed RNA-Seq analyses. HK and EK wrote the manuscript. All authors contributed to the article and approved the submitted version.

Funding

This work was supported by the Korea Institute of Science and Technology Information (K-19-L02-C07-S01 to HK) and the Institute for Basic Science (IBS-R002-D1 to EK).

Conflict of interest

The authors declare that the research was conducted in the absence of any commercial or financial relationships that could be construed as a potential conflict of interest.

Publisher's note

All claims expressed in this article are solely those of the authors and do not necessarily represent those of their affiliated organizations, or those of the publisher, the editors and the reviewers. Any product that may be evaluated in this article, or claim that may be made by its manufacturer, is not guaranteed or endorsed by the publisher.

Supplementary material

The Supplementary Material for this article can be found online at: https://www.frontiersin.org/articles/10.3389/fnmol.2022.1017512/full#supplementary-material

SUPPLEMENTARY FIGURE 1
Gene set enrichment analysis (GSEA) of P25-Shank3 transcripts using the gene sets in the biological process (BP) and molecular function (MF) domains. **(A,B)** Results of GSEA performed for P25-Shank3 forebrain transcripts using gene sets in the BP and MF domains, represented by the list of top-five positively/negatively enriched gene sets (top; see **Supplementary Table 3** for full results) and functional clustering of enriched gene sets performed using the EnrichmentMap Cytoscape App (bottom) (n = 3 mice [P25-Shank3]).

SUPPLEMENTARY FIGURE 2
Gene set enrichment analysis (GSEA) for P60-Shank3 transcripts using the gene sets in the biological process (BP) and molecular function (MF) domains. **(A,B)** Results of GSEA for P60-Shank3 forebrain transcripts performed using gene sets in the BP and MF domains, represented by the list of top-five positively/negatively enriched gene sets (top; see **Supplementary Table 3** for full results) and functional clustering of enriched gene sets performed using the EnrichmentMap Cytoscape App (bottom) (n = 3 mice [P60-Shank3]).

SUPPLEMENTARY FIGURE 3
Autism spectrum disorder (ASD)-related patterns in P25-Shank3 and P60-Shank3 transcripts. **(A–C)** The GSEA results in **Figure 2** are shown here again with the insignificantly enriched gene sets indicated by square dots, together with the significant enrichments indicated by circular dots, to show that the insignificant enrichments have generally smaller NES scores compared with those of significant enrichments.

SUPPLEMENTARY FIGURE 4
Individual gene expression patterns for the opposite enrichments of P25-Shank3 and P60-Shank3 forebrain transcripts for two select autism spectrum disorder (ASD)-risk gene sets. **(A,B)** The opposite enrichments of P25-Shank3 and P60-Shank3 forebrain transcripts for two select ASD-risk gene sets (SFARI Genes [All] and FMRP Targets) were mediated by ∼50% of the genes in the gene sets **(A)** and are further supported by correlative fold changes for co-up/down regulations **(B)** [n = 3 mice (P25-Shank3 and P60-Shank3), Pearson test].

SUPPLEMENTARY FIGURE 5
Distinct clustering of three brain regional transcriptomes from Shank3-HT/HM mice. Clustering of cortical, hippocampal, and striatal transcriptomes from Shank3-WT, Shank3-HT, and Shank3-HM mice shown by heatmaps (13 weeks; male; n = 5 mice [WT], 5 [HT], and 5 [HM]).

SUPPLEMENTARY FIGURE 6
ASD-related patterns in the transcripts from the cortex, hippocampus, and striatum of Shank3-HT and Shank3-HM mice. **(A–C)** The GSEA results in **Figure 5** are shown here again with the insignificantly enriched gene sets indicated by square dots, together with the significant enrichments indicated by circular dots, to show that the insignificant enrichments have generally smaller NES scores compared with those of significant enrichments.

References

Aceti, M., Creson, T. K., Vaissiere, T., Rojas, C., Huang, W. C., Wang, Y. X., et al. (2015). Syngap1 haploinsufficiency damages a postnatal critical period of pyramidal cell structural maturation linked to cortical circuit assembly. *Biol. Psychiatry* 77, 805–815. doi: 10.1016/j.biopsych.2014.08.001

Albright, A. V., and Gonzalez-Scarano, F. (2004). Microarray analysis of activated mixed glial (microglia) and monocyte-derived macrophage gene expression. *J. Neuroimmunol.* 157, 27–38. doi: 10.1016/j.jneuroim.2004.09.007

Becker-Heck, A., Zohn, I. E., Okabe, N., Pollock, A., Lenhart, K. B., Sullivan-Brown, J., et al. (2011). The coiled-coil domain containing protein CCDC40 is essential for motile cilia function and left-right axis formation. *Nat. Genet.* 43, 79–84. doi: 10.1038/ng.727

Berkel, S., Marshall, C. R., Weiss, B., Howe, J., Roeth, R., Moog, U., et al. (2010). Mutations in the SHANK2 synaptic scaffolding gene in autism spectrum disorder and mental retardation. *Nat. Genet.* 42, 489–491. doi: 10.1038/ng.589

Boeckers, T. M., Bockmann, J., Kreutz, M. R., and Gundelfinger, E. D. (2002). ProSAP/Shank proteins - a family of higher order organizing molecules of the postsynaptic density with an emerging role in human neurological disease. *J. Neurochem.* 81, 903–910. doi: 10.1046/j.1471-4159.2002.00931.x

Boeckers, T. M., Winter, C., Smalla, K. H., Kreutz, M. R., Bockmann, J., Seidenbecher, C., et al. (1999). Proline-rich synapse-associated proteins ProSAP1 and ProSAP2 interact with synaptic proteins of the SAPAP/GKAP family. *Biochem. Biophys. Res. Commun.* 264, 247–252. doi: 10.1006/bbrc.1999.1489

Bourgeron, T. (2009). A synaptic trek to autism. *Curr. Opin. Neurobiol.* 19, 231–234. doi: 10.1016/j.conb.2009.06.003

Bozdagi, O., Sakurai, T., Papapetrou, D., Wang, X., Dickstein, D. L., Takahashi, N., et al. (2010). Haploinsufficiency of the autism-associated Shank3 gene leads to deficits in synaptic function, social interaction, and social communication. *Mol. Autism* 1:15. doi: 10.1186/2040-2392-1-15

Cahoy, J. D., Emery, B., Kaushal, A., Foo, L. C., Zamanian, J. L., Christopherson, K. S., et al. (2008). A transcriptome database for astrocytes, neurons, and oligodendrocytes: A new resource for understanding brain development and function. *J. Neurosci.* 28, 264–278. doi: 10.1523/JNEUROSCI.4178-07.2008

Chung, C., Ha, S., Kang, H., Lee, J., Um, S. M., Yan, H., et al. (2019). Early correction of N-Methyl-D-aspartate receptor function improves autistic-like social behaviors in Adult Shank2(-/-) Mice. *Biol. Psychiatry* 85, 534–543. doi: 10.1016/j.biopsych.2018.09.025

Chung, C., Shin, W., and Kim, E. (2021). Early and late corrections in mouse models of autism spectrum disorder. *Biol. Psychiatry* 91, 934–944. doi: 10.1016/j.biopsych.2021.07.021

Clement, J. P., Aceti, M., Creson, T. K., Ozkan, E. D., Shi, Y., Reish, N. J., et al. (2012). Pathogenic SYNGAP1 mutations impair cognitive development by disrupting maturation of dendritic spine synapses. *Cell* 151, 709–723. doi: 10.1016/j.cell.2012.08.045

Clement, J. P., Ozkan, E. D., Aceti, M., Miller, C. A., and Rumbaugh, G. (2013). SYNGAP1 links the maturation rate of excitatory synapses to the duration of critical-period synaptic plasticity. *J. Neurosci.* 33, 10447–10452. doi: 10.1523/JNEUROSCI.0765-13.2013

De Rubeis, S., Siper, P. M., Durkin, A., Weissman, J., Muratet, F., Halpern, D., et al. (2018). Delineation of the genetic and clinical spectrum of Phelan-McDermid syndrome caused by SHANK3 point mutations. *Mol. Autism* 9:31. doi: 10.1186/s13229-018-0205-9

Durand, C. M., Betancur, C., Boeckers, T. M., Bockmann, J., Chaste, P., Fauchereau, F., et al. (2007). Mutations in the gene encoding the synaptic scaffolding protein SHANK3 are associated with autism spectrum disorders. *Nat. Genet.* 39, 25–27. doi: 10.1038/ng1933

Eltokhi, A., Rappold, G., and Sprengel, R. (2018). Distinct phenotypes of Shank2 mouse models reflect neuropsychiatric spectrum disorders of human patients with SHANK2 variants. *Front. Mol. Neurosci.* 11:240. doi: 10.3389/fnmol.2018.00240

Ey, E., Bourgeron, T., Boeckers, T. M., Kim, E., and Han, K. (2020). Editorial: Shankopathies: Shank protein deficiency-induced synaptic diseases. *Front. Mol. Neurosci.* 13:11. doi: 10.3389/fnmol.2020.00011

Frye, R. E. (2020). Mitochondrial dysfunction in autism spectrum disorder: Unique abnormalities and targeted treatments. *Semin. Pediatr. Neurol.* 35:100829. doi: 10.1016/j.spen.2020.100829

Gauthier, J., Spiegelman, D., Piton, A., Lafreniere, R. G., Laurent, S., St-Onge, J., et al. (2009). Novel de novo SHANK3 mutation in autistic patients. *Am. J. Med. Genet. B Neuropsychiatr. Genet.* 150B, 421–424. doi: 10.1002/ajmg.b.30822

Grabrucker, A. M., Schmeisser, M. J., Schoen, M., and Boeckers, T. M. (2011). Postsynaptic ProSAP/Shank scaffolds in the cross-hair of synaptopathies. *Trends Cell Biol.* 21, 594–603. doi: 10.1016/j.tcb.2011.07.003

Hollis, F., Kanellopoulos, A. K., and Bagni, C. (2017). Mitochondrial dysfunction in autism spectrum disorder: Clinical features and perspectives. *Curr. Opin. Neurobiol.* 45, 178–187. doi: 10.1016/j.conb.2017.05.018

Isserlin, R., Merico, D., Voisin, V., and Bader, G. D. (2014). Enrichment Map - a Cytoscape app to visualize and explore OMICs pathway enrichment results. *F1000Res* 3:141. doi: 10.12688/f1000research.4536.1

Jiang, Y. H., and Ehlers, M. D. (2013). Modeling autism by SHANK gene mutations in mice. *Neuron* 78, 8–27. doi: 10.1016/j.neuron.2013.03.016

Jung, S., and Park, M. (2022). Shank postsynaptic scaffolding proteins in autism spectrum disorder: Mouse models and their dysfunctions in behaviors, synapses, and molecules. *Pharmacol. Res.* 182:106340. doi: 10.1016/j.phrs.2022.106340

Kang, H. J., Kawasawa, Y. I., Cheng, F., Zhu, Y., Xu, X., Li, M., et al. (2011). Spatio-temporal transcriptome of the human brain. *Nature* 478, 483–489. doi: 10.1038/nature10523

Kim, E., and Sheng, M. (2004). PDZ domain proteins of synapses. *Nat. Rev. Neurosci.* 5, 771–781.

Leblond, C. S., Nava, C., Polge, A., Gauthier, J., Huguet, G., Lumbroso, S., et al. (2014). Meta-analysis of SHANK mutations in autism spectrum disorders: A gradient of severity in cognitive impairments. *PLoS Genet.* 10:e1004580. doi: 10.1371/journal.pgen.1004580

Lee, A., Hirabayashi, Y., Kwon, S. K., Lewis, T. L. Jr., and Polleux, F. (2018). Emerging roles of mitochondria in synaptic transmission and neurodegeneration. *Curr. Opin. Physiol.* 3, 82–93. doi: 10.1016/j.cophys.2018.03.009

Lee, S., Kang, H., Jung, H., Kim, E., and Lee, E. (2021). Gene dosage- and age-dependent differential transcriptomic changes in the prefrontal cortex of Shank2-mutant mice. *Front. Mol. Neurosci.* 14:683196. doi: 10.3389/fnmol.2021.683196

Li, Z., Okamoto, K., Hayashi, Y., and Sheng, M. (2004). The importance of dendritic mitochondria in the morphogenesis and plasticity of spines and synapses. *Cell* 119, 873–887. doi: 10.1016/j.cell.2004.11.003

Lombardo, M. V. (2021). Ribosomal protein genes in post-mortem cortical tissue and iPSC-derived neural progenitor cells are commonly upregulated in expression in autism. *Mol. Psychiatry* 26, 1432–1435. doi: 10.1038/s41380-020-0773-x

Love, M. I., Huber, W., and Anders, S. (2014). Moderated estimation of fold change and dispersion for RNA-seq data with DESeq2. *Genome Biol.* 15:550. doi: 10.1186/s13059-014-0550-8

Merico, D., Isserlin, R., Stueker, O., Emili, A., and Bader, G. D. (2010). Enrichment map: A network-based method for gene-set enrichment visualization and interpretation. *PLoS One* 5:e13984. doi: 10.1371/journal.pone.0013984

Moessner, R., Marshall, C. R., Sutcliffe, J. S., Skaug, J., Pinto, D., Vincent, J., et al. (2007). Contribution of SHANK3 mutations to autism spectrum disorder. *Am. J. Hum. Genet.* 81, 1289–1297. doi: 10.1086/522590

Monteiro, P., and Feng, G. (2017). SHANK proteins: Roles at the synapse and in autism spectrum disorder. *Nat. Rev. Neurosci.* 18, 147–157. doi: 10.1038/nrn.2016.183

Morita, M., Gravel, S. P., Hulea, L., Larsson, O., Pollak, M., St-Pierre, J., et al. (2015). mTOR coordinates protein synthesis, mitochondrial activity and proliferation. *Cell Cycle* 14, 473–480. doi: 10.4161/15384101.2014.991572

Mossa, A., Giona, F., Pagano, J., Sala, C., and Verpelli, C. (2017). SHANK genes in autism: Defining therapeutic targets. *Prog. Neuropsychopharmacol. Biol. Psychiatry* 84(Pt B), 416–423.

Mossa, A., Giona, F., Pagano, J., Sala, C., and Verpelli, C. (2018). SHANK genes in autism: Defining therapeutic targets. *Prog. Neuropsychopharmacol. Biol. Psychiatry* 84, 416–423. doi: 10.1016/j.pnpbp.2017.11.019

Naisbitt, S., Kim, E., Tu, J. C., Xiao, B., Sala, C., Valtschanoff, J., et al. (1999). Shank, a novel family of postsynaptic density proteins that binds to the NMDA receptor/PSD-95/GKAP complex and cortactin. *Neuron* 23, 569–582. doi: 10.1016/s0896-6273(00)80809-0

Patro, R., Duggal, G., Love, M. I., Irizarry, R. A., and Kingsford, C. (2017). Salmon provides fast and bias-aware quantification of transcript expression. *Nat. Methods* 14, 417–419. doi: 10.1038/nmeth.4197

Peca, J., Feliciano, C., Ting, J. T., Wang, W., Wells, M. F., Venkatraman, T. N., et al. (2011). Shank3 mutant mice display autistic-like behaviours and striatal dysfunction. *Nature* 472, 437–442. doi: 10.1038/nature09965

Peixoto, R. T., Wang, W., Croney, D. M., Kozorovitskiy, Y., and Sabatini, B. L. (2016). Early hyperactivity and precocious maturation of corticostriatal circuits in Shank3B(-/-) mice. *Nat. Neurosci.* 19, 716–724. doi: 10.1038/nn.4260

Phelan, K., Boccuto, L., Powell, C. M., Boeckers, T. M., van Ravenswaaij-Arts, C., Rogers, R. C., et al. (2022). Phelan-McDermid syndrome: A classification system after 30 years of experience. *Orphanet. J. Rare Dis.* 17:27. doi: 10.1186/s13023-022-02180-5

Reim, D., Distler, U., Halbedl, S., Verpelli, C., Sala, C., Bockmann, J., et al. (2017). Proteomic analysis of post-synaptic density fractions from Shank3 mutant mice reveals brain region specific changes relevant to autism spectrum disorder. *Front. Mol. Neurosci.* 10:26. doi: 10.3389/fnmol.2017.00026

Rojas-Charry, L., Nardi, L., Methner, A., and Schmeisser, M. J. (2021). Abnormalities of synaptic mitochondria in autism spectrum disorder and related neurodevelopmental disorders. *J. Mol. Med (Berl)* 99, 161–178. doi: 10.1007/s00109-020-02018-2

Sala, C., Vicidomini, C., Bigi, I., Mossa, A., and Verpelli, C. (2015). Shank synaptic scaffold proteins: Keys to understanding the pathogenesis of autism and other synaptic disorders. *J. Neurochem.* 135, 849–858. doi: 10.1111/jnc.13232

Santini, E., and Klann, E. (2014). Reciprocal signaling between translational control pathways and synaptic proteins in autism spectrum disorders. *Sci. Signal* 7:re10. doi: 10.1126/scisignal.2005832

Schmeisser, M. J. (2015). Translational neurobiology in Shank mutant mice–model systems for neuropsychiatric disorders. *Ann. Anat.* 200, 115–117. doi: 10.1016/j.aanat.2015.03.006

Schmeisser, M. J., Ey, E., Wegener, S., Bockmann, J., Stempel, V., Kuebler, A., et al. (2012). Autistic-like behaviours and hyperactivity in mice lacking ProSAP1/Shank2. *Nature* 486, 256–260. doi: 10.1038/nature11015

Sheng, M., and Kim, E. (2000). The shank family of scaffold proteins. *J. Cell Sci.* 113 (Pt 11), 1851–1856.

Sheng, M., and Kim, E. (2011). The postsynaptic organization of synapses. *Cold Spring Harb. Perspect. Biol.* 3:a005678. doi: 10.1101/cshperspect.a005678

Sheng, M., and Sala, C. (2001). PDZ domains and the organization of supramolecular complexes. *Annu. Rev. Neurosci.* 24, 1–29.

Sheng, Z. H., and Cai, Q. (2012). Mitochondrial transport in neurons: Impact on synaptic homeostasis and neurodegeneration. *Nat. Rev. Neurosci.* 13, 77–93. doi: 10.1038/nrn3156

Soneson, C., Love, M. I., and Robinson, M. D. (2015). Differential analyses for RNA-seq: Transcript-level estimates improve gene-level inferences. *F1000Res* 4:1521. doi: 10.12688/f1000research.7563.2

Subramanian, A., Tamayo, P., Mootha, V. K., Mukherjee, S., Ebert, B. L., Gillette, M. A., et al. (2005). Gene set enrichment analysis: A knowledge-based approach for interpreting genome-wide expression profiles. *Proc. Natl. Acad. Sci. U.S.A.* 102, 15545–15550. doi: 10.1073/pnas.0506580102

Velmeshev, D., Magistri, M., Mazza, E. M. C., Lally, P., Khoury, N., D'Elia, E. R., et al. (2020). Cell-type-specific analysis of molecular pathology in autism identifies common genes and pathways affected across neocortical regions. *Mol. Neurobiol.* 57, 2279–2289. doi: 10.1007/s12035-020-01879-5

Velmeshev, D., Schirmer, L., Jung, D., Haeussler, M., Perez, Y., Mayer, S., et al. (2019). Single-cell genomics identifies cell type-specific molecular changes in autism. *Science* 364, 685–689. doi: 10.1126/science.aav8130

Voineagu, I., Wang, X., Johnston, P., Lowe, J. K., Tian, Y., Horvath, S., et al. (2011). Transcriptomic analysis of autistic brain reveals convergent molecular pathology. *Nature* 474, 380–384. doi: 10.1038/nature10110

Vos, M., Lauwers, E., and Verstreken, P. (2010). Synaptic mitochondria in synaptic transmission and organization of vesicle pools in health and disease. *Front. Synaptic Neurosci.* 2:139. doi: 10.3389/fnsyn.2010.00139

Werling, D. M., Parikshak, N. N., and Geschwind, D. H. (2016). Gene expression in human brain implicates sexually dimorphic pathways in autism spectrum disorders. *Nat. Commun.* 7:10717. doi: 10.1038/ncomms10717

Won, H., Lee, H. R., Gee, H. Y., Mah, W., Kim, J. I., Lee, J., et al. (2012). Autistic-like social behaviour in Shank2-mutant mice improved by restoring NMDA receptor function. *Nature* 486, 261–265. doi: 10.1038/nature11208

Yoo, T., Cho, H., Lee, J., Park, H., Yoo, Y. E., Yang, E., et al. (2018). GABA neuronal deletion of Shank3 Exons 14-16 in mice suppresses striatal excitatory synaptic input and induces social and locomotor abnormalities. *Front. Cell Neurosci.* 12:341. doi: 10.3389/fncel.2018.00341

Yoo, T., Cho, H., Park, H., Lee, J., and Kim, E. (2019). Shank3 Exons 14-16 deletion in glutamatergic neurons leads to social and repetitive behavioral deficits associated with increased cortical Layer 2/3 neuronal excitability. *Front. Cell Neurosci.* 13:458. doi: 10.3389/fncel.2019.00458

Yoo, Y. E., Lee, S., Kim, W., Kim, H., Chung, C., Ha, S., et al. (2021). Early chronic memantine treatment-induced transcriptomic changes in Wild-Type and Shank2-mutant mice. *Front. Mol. Neurosci.* 14:712576. doi: 10.3389/fnmol.2021.712576

Yoo, Y. E., Yoo, T., Kang, H., and Kim, E. (2022). Brain region and gene dosage-differential transcriptomic changes in Shank2-mutant mice. *Front. Mol. Neurosci.* doi: 10.3389/fnmol.2022.977305

Zeisel, A., Munoz-Manchado, A. B., Codeluppi, S., Lonnerberg, P., La Manno, G., Jureus, A., et al. (2015). Brain structure. Cell types in the mouse cortex and hippocampus revealed by single-cell RNA-seq. *Science* 347, 1138–1142. doi: 10.1126/science.aaa1934

frontiers | Frontiers in Molecular Neuroscience

TYPE Review
PUBLISHED 13 October 2022
DOI 10.3389/fnmol.2022.1021207

Check for updates

OPEN ACCESS

EDITED BY
Jay S. Schneider,
Thomas Jefferson University,
United States

REVIEWED BY
Olivia Engmann,
University Hospital Jena, Germany
Guoqian He,
Sichuan University, China

*CORRESPONDENCE
Bin Liu
lbliubinlb@163.com
Yan-bin Li
13864006933@163.com

†These authors have contributed equally to this work and share first authorship

SPECIALTY SECTION
This article was submitted to Brain Disease Mechanisms, a section of the journal Frontiers in Molecular Neuroscience

RECEIVED 17 August 2022
ACCEPTED 21 September 2022
PUBLISHED 13 October 2022

CITATION
Shen X-y, Shi S-h, Li H, Wang C-c, Zhang Y, Yu H, Li Y-b and Liu B (2022) The role of Gadd45b in neurologic and neuropsychiatric disorders: An overview.
Front. Mol. Neurosci. 15:1021207.
doi: 10.3389/fnmol.2022.1021207

COPYRIGHT
© 2022 Shen, Shi, Li, Wang, Zhang, Yu, Li and Liu. This is an open-access article distributed under the terms of the Creative Commons Attribution License (CC BY). The use, distribution or reproduction in other forums is permitted, provided the original author(s) and the copyright owner(s) are credited and that the original publication in this journal is cited, in accordance with accepted academic practice. No use, distribution or reproduction is permitted which does not comply with these terms.

The role of Gadd45b in neurologic and neuropsychiatric disorders: An overview

Xiao-yue Shen[1,2†], Shu-han Shi[3†], Heng Li[1], Cong-cong Wang[1], Yao Zhang[1], Hui Yu[1], Yan-bin Li[1*] and Bin Liu[1*]

[1]Department of Neurology, The First Affiliated Hospital of Shandong First Medical University and Shandong Provincial Qianfoshan Hospital, Jinan, China, [2]The First Clinical Medical College, Shandong University of Traditional Chinese Medicine, Jinan, China, [3]College of Traditional Chinese Medicine, Shandong University of Traditional Chinese Medicine, Jinan, China, [4]School of Clinical Medicine, Weifang Medical University, Weifang, China

Growth arrest and DNA damage-inducible beta (Gadd45b) is directly intertwined with stress-induced DNA repair, cell cycle arrest, survival, and apoptosis. Previous research on Gadd45b has focused chiefly on non-neuronal cells. Gadd45b is extensively expressed in the nervous system and plays a critical role in epigenetic DNA demethylation, neuroplasticity, and neuroprotection, according to accumulating evidence. This article provided an overview of the preclinical and clinical effects of Gadd45b, as well as its hypothesized mechanisms of action, focusing on major psychosis, depression, autism, stroke, seizure, dementia, Parkinson's disease, and autoimmune diseases of the nervous system.

KEYWORDS

neuropsychiatric disorders, cerebral ischemia, mental illness, neurologic disorders, BDNF, Gadd45b

Introduction

The growth arrest DNA damage-inducible gene (Gadd45) family consists of Gadd45a, Gadd45b, and Gadd45g. All of them are nuclear proteins with a molecular weight of 18 KD. These molecules are widely expressed in the nervous system. And it is required for the stress response, apoptosis, and mitosis of neuronal and glial cells (Kearsey et al., 1995; Hildesheim et al., 2002). The Gadd45 protein is mainly involved in regulating the cell cycle, cell apoptosis, proliferation, and DNA damage repair and may be interested in DNA demethylation (Barreto et al., 2007; Liebermann and Hoffman, 2007; Ma et al., 2009). DNA methylation is a major epigenetic factor, the specific temporal control of which is critical for the growth and differentiation of the mammalian central nervous system (CNS) (Fan et al., 2001, 2005; Feng et al., 2005; Golshani et al., 2005). DNA methylation is a crucial regulatory process involved in brain formation, learning, memory, and disorder (Rizzardi et al., 2019), and it is known to be modified in individuals with neuropsychiatric disorders such as schizophrenia, addiction, and

Alzheimer's disease (Jeong et al., 2021). Writers, erasers, and readers are the three main types of enzymes that create, identify, and remove DNA methylation. DNA methylation is the mechanism by which methyl groups can be covalently attached to the 50 positions on cytosine nucleotides, resulting in the formation of 5-methylcytosine (5mC). Demethylation remains incompletely understood but includes DNA damage repair enzymes and various intermediates, such as 5-hydroxymethylcytosine (5-hmC) (Tahiliani et al., 2009). Specifically, the conversion of 5mC to 5hmC may be mediated by base-excision and repair (BER) or after the transformation of 5hmC to 5-hydroxymethyluracil (5hmU) by the activation-induced deaminase (AID). As a member of the Gadd45 family, Gadd45b, is a demethylase, participating in the BER of mutated cytosines and may perform a similar function in neurons. Besides, Gadd45b has been proven to have a crucial function in the nervous system and immunity, epigenetic DNA demethylation, neuroplasticity, and neuroprotection. Conclusively, Gadd45b is commonly implicated in neurologic and neuropsychiatric diseases because of its critical involvement in brain plasticity (**Figure 1**).

Neurological diseases are a group of disorders or abnormalities in the nervous system, commonly including stroke, seizure, dementia, Parkinson's disease and multiple sclerosis. Meanwhile, brain diseases often result in psychological symptoms, including schizophrenia, depression, autism, etc. Neuropsychiatric diseases mainly affect cognitive, emotional, and behavioral disorders. Although neurological and neuropsychiatric illnesses are two distinct disease categories, their etiology and pathophysiology often overlap Gadd45b-dependent molecular signaling pathways.

The role of Gadd45b in neuropsychiatric disorders

Major psychosis

Major psychosis, which refers chiefly to schizophrenia and bipolar disorder, is a severe, recurrent, and chronic mental condition. These disorders are not only a cause of morbidity but also increased mortality, which results from a relatively high rate of suicide and a shorter life span, due mainly to the medical complications of these illnesses.

Multiple investigations over the last decade have identified Gadd45b in the pathogenesis of psychosis of the major psychosis. Patients with psychiatric disorders were shown to have increased Gadd45b-stained cells in prefrontal cortex layers II, III, and V. This research demonstrated that individuals with psychiatric disorders bind less Gadd45b to the BDNF promoter (Gavin et al., 2012). In addition, the scientists showed a decrease in BDNF mRNA expression and an increase in 5-methylcytosine and 5-hydroxymethylcytosine at its promoter. Similarly, the Gadd45 protein is also engaged in regulating histone modifications in the pathological process and therapy of schizophrenia (Guidotti et al., 2009; Labrie et al., 2012). Altered metabotropic glutamate receptor (mGlu) activity is followed by DNA methylation dynamics, as activation of subclass II (composed of mGlu2 and mGlu3 types) attenuates presynaptic glutamate activity, which is linked with antipsychotic effects, according to prior studies (Conn et al., 2009; Kurita et al., 2012). In the mouse frontal cortex and hippocampus, intraperitoneal injection of LY379268 (a brain-permeable mGlu2/3 activator) increases the expression of the Gadd45b mRNA and restores social function. LY379268 also enhances the specific binding of Gadd45b to BDNF and glutamate decarboxylase 67 (GAD67) promoter regions (Matrisciano et al., 2011). Thus, evidence suggests Gadd45b as a viable target for treating schizophrenia. Additionally, Gadd45b is sometimes considered DNA demethylase. Gadd45b binds differentially to the BDNF and GAD67 promoters, altering the demethylation of the BDNF and GAD67 promoters. Notably, Gadd45b levels are increased in mice administered antipsychotic drugs (Guidotti et al., 2011; Matrisciano et al., 2011). Gadd45b appears to control methylation and upregulate reelin, GAD67, and BDNF expression in the brains of individuals with psychosis. These findings imply that Gadd45b is involved in altering brain circuits in patients with major psychosis and modulates antipsychotic treatment (**Figure 2**).

Chronic stress and depression

Depression is a prevalent mental illness. According to estimates, 5% of individuals worldwide experience depression (Evans-Lacko et al., 2018). Nevertheless, mechanisms involved in depression pathophysiology are not yet fully understood, and current therapies are inadequate for a substantial proportion of patients with depression (Evans-Lacko et al., 2018; Hasin et al., 2018). Depression severely affects the incidence and prognosis of many common general medical comorbidities, such as stroke. Nevertheless, mechanisms involved in depression pathophysiology are not yet fully understood, and current therapies are inadequate for a substantial proportion of patients with depression. Multiple mechanisms contribute to the

Abbreviations: Gadd45b, growth arrest and DNA damage-inducible beta; BDNF, brain-derived neurotrophic factor; mGlu2, metabotropic glutamate receptor 2; GAD67, glutamate decarboxylase 67; TGF-β, transforming growth factor β; ECT, electroconvulsive therapy; Ntrk2, neurotrophic tyrosine kinase receptor type 2; Dlx5, distal-less homeobox 5; MeCP2, methyl-CpG-binding protein 2; Adra2a, A2-adrenoceptor; SVZ, subventricular zone; ALK5, activin receptor-like kinase 5; MMP-9, matrix metallopeptidase 9; p53, protein 53; NF-κB, nuclear factor kappa-B; HA, Hirsein A; IFN-γ, interferon γ; AD, Alzheimer's disease; Aβ, amyloid β-protein; EAE, experimental allergic encephalitis; MG, myasthenia gravis.

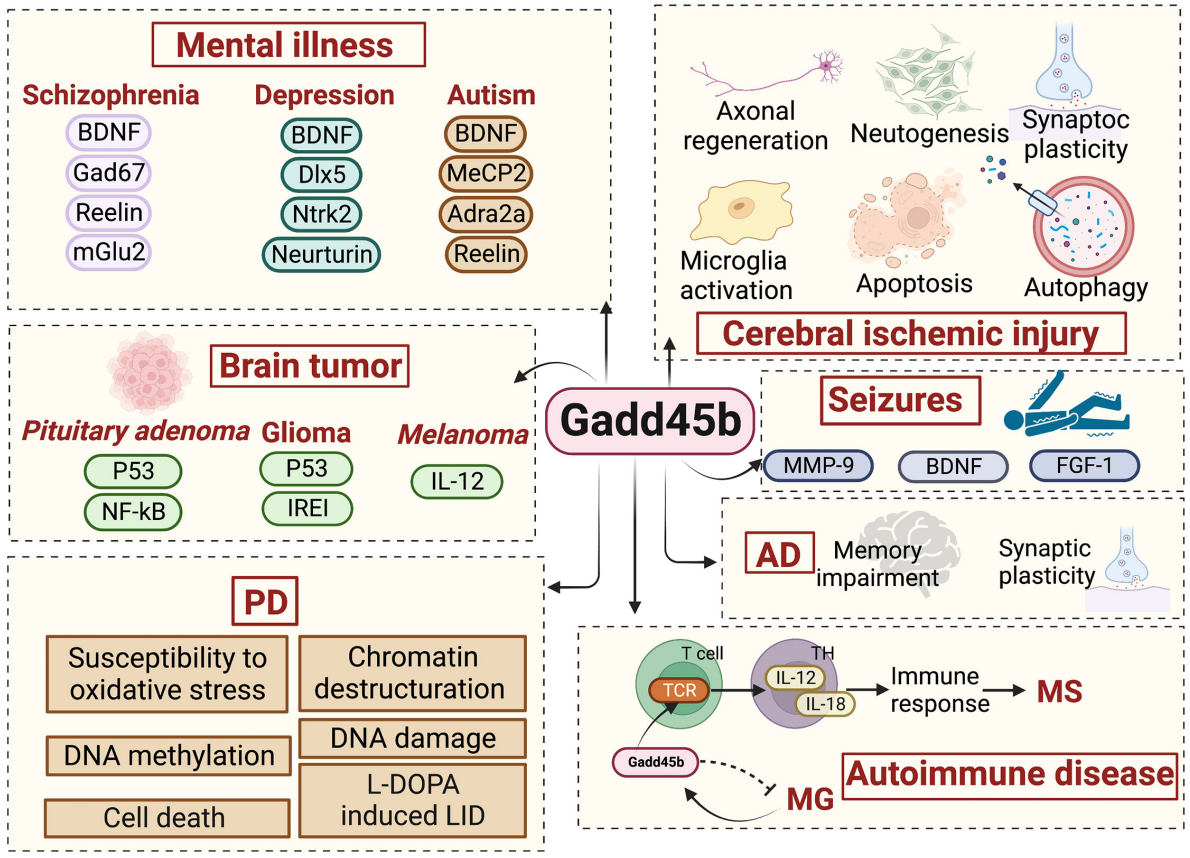

FIGURE 1
The role of growth arrest and DNA damage-inducible beta (Gadd45b) in neurologic and neuropsychiatric disorders.

pathophysiology and etiology of depression, such as microglia activation, neuroinflammation, and reduced neurogenesis in the hippocampus (Ménard et al., 2016).

Restricted hippocampus neurogenesis elicits depressive-like effects (Kraus et al., 2017). Neurogenesis is governed by substances like BDNF, which is absent in patients with major depression. Anti-depressant treatments, whether pharmacological or psychosocial, restore BDNF levels in individuals with depression (Molendijk et al., 2014; Gururajan et al., 2016). In particular, Gadd45b contributes to BDNF promoter demethylation by enabling the elimination of 5HMC (Gavin et al., 2015).

Likewise, in the Flinders Sensitive Line (FSL) genetic rodent model of depression, an observed trend of decreased Gadd45b mRNA levels in these hypermethylated untreated rats is consistent with the demethylating function of Gadd45b in the adult brain (Melas et al., 2012). In unpredictable chronic mild stress (UCMS) mice, a model for depression, the expression of Gadd45b was down-regulated in the hippocampus by the growth factor β (TGF-β) signaling pathway. This process was involved in the transcriptional regulation of genes (Grassi et al., 2017).

Furtherly, Yin et al. identified a substantial correlation between Gadd45b knockdown and depressive-like behaviors following ischemic stroke. They determined that Gadd45b could play a role in neuronal remodeling activity-related neurogenesis in the hippocampus of adult rats, alleviating poststroke depression through the BDNF signaling pathway (Yin et al., 2021). These findings suggest that Gadd45b is involved in antidepressant-like activity induction.

Electroconvulsive therapy (ECT) was claimed to be an effective treatment for depression (Rasmussen, 2011; Azis et al., 2019). Likewise, ECT has been discovered to trigger the gene Gadd45b, which plays a part in BDNF demethylation in the dentate gyrus of the hippocampus formation (Ma et al., 2009). After ECT treatment, an analysis of the gene expression profiles of hippocampal dentate gyrus granulosa cells revealed that BDNF, neuropeptide Y, and Gadd45b were up-regulated (Ploski et al., 2006). Accordingly, Gadd45b, generated by ECT, at least in part mediates the therapeutic benefits of ECT on depression.

On the contrary, a recent study showed the pro-depressant role of Gadd45b on social behaviors through chronic social defeat stress (Labonté et al., 2019). Gadd45b intervenes in depression by modifying the DNA methylation levels of GAD67,

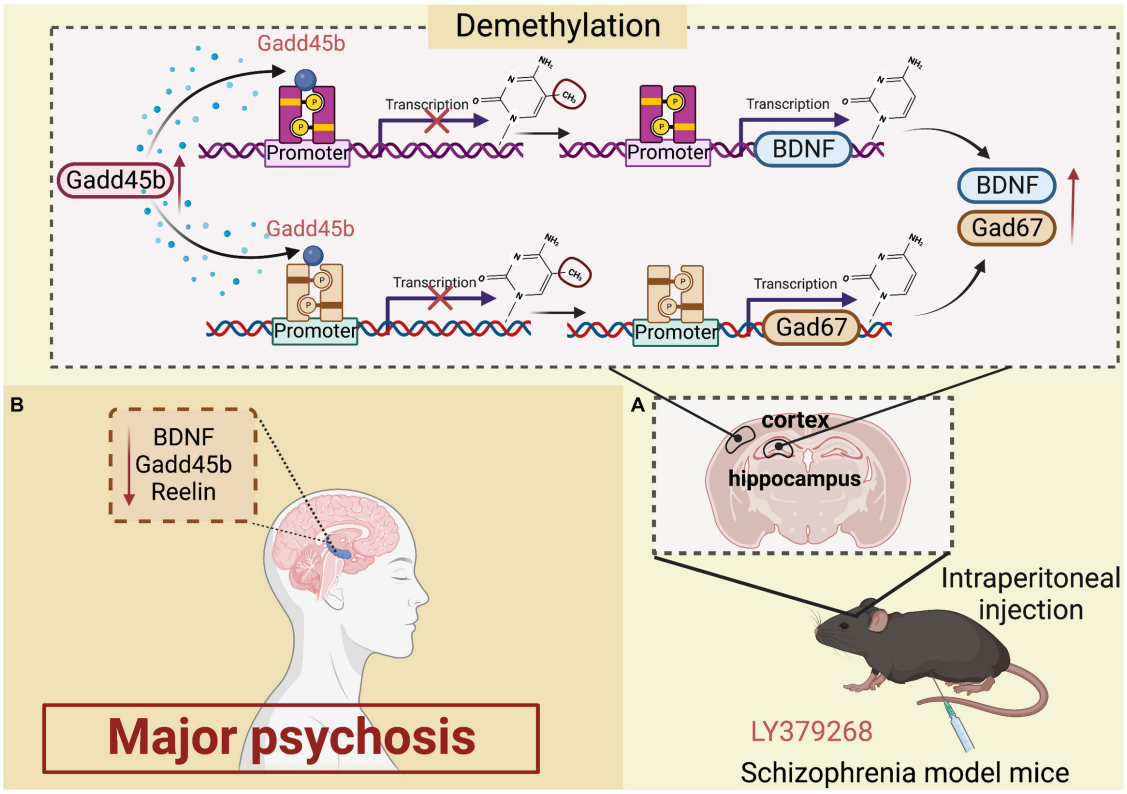

FIGURE 2
Roles of growth arrest and DNA damage-inducible beta (Gadd45b) in major psychosis. **(A)** Increased expression of gadd45b in the hippocampal region is detected in schizophrenic mice after intraperitoneal injection of ly379268, which alters the Demethylation of BDNF and Gad67, increasing BDNF and Gad67 activation in large amounts. **(B)** Decreased Gadd45b, BDNF and Reelin expression in the brain of patients with major psychosis (Figure was created with BioRender.com).

recombinant neurotrophic tyrosine kinase receptor type 2 (Ntrk2), neurturin, and distal-less homeobox 5 (Dlx5). Gadd45b expression was considerably elevated in the nucleus accumbens of susceptible mice in response to persistent social defeat stress. Also, the over-activation of Gadd45b promoted depressed behavior in mice. Moreover, this study revealed that Gadd45b is a novel downstream molecular target of BDNF in the nucleus accumbens.

Collectively, these findings indicate that Gadd45b could be a novel mediator of depression-like behaviors (**Figure 3**). Presently, the clinical effect of Gadd45b in the treatment of depression remains contentious and requires additional investigation in future trials.

Autism

Autism is a neurodevelopmental condition characterized by language and social interaction deficits and is generally accompanied by seizures, cognitive deficits, or other brain disorders (Kidd, 2002). This condition is considered to be caused by hereditary factors and cerebral inflammation (Ratajczak, 2011). Some studies have revealed the abnormal DNA and histone methylation regulation in the prefrontal cortex of patients with autism (Nguyen et al., 2010; Shulha et al., 2012). Furthermore, A microarray analysis has detected elevated Gadd45b expression in the superior temporal gyrus of autism (Garbett et al., 2008).

Noteworthily, Gadd45b deletion in neonatal rats reduces the expression of numerous genes linked to psychiatric illnesses, including MeCP2, Reelin, and BDNF (Kigar et al., 2015). Similarly, Serum BDNF levels are decreased in patients with autism (Hashimoto et al., 2006; Abdallah et al., 2013). Also, Methyl-CpG-binding protein 2 (MeCP2) deletion in the developing amygdala limits social interaction in adolescent rats (Kurian et al., 2008). A2-adrenoceptor (Adra2a) is required to regulate social behavior in adolescent rats. Furthermore, Gadd45b siRNA therapy considerably reduced Adra2a expression in the juvenile rat amygdala (Siviy and Baliko, 2000). In addition, multiple ankyrin repeat domains protein 3 (SHANK3) is a potential autism-related gene. And it has been shown to be involved in the action of Gadd45b on DNA demethylation (Monteiro and Feng, 2017). Collectively, these findings suggest that Gadd45b has a vital role in the epigenetic

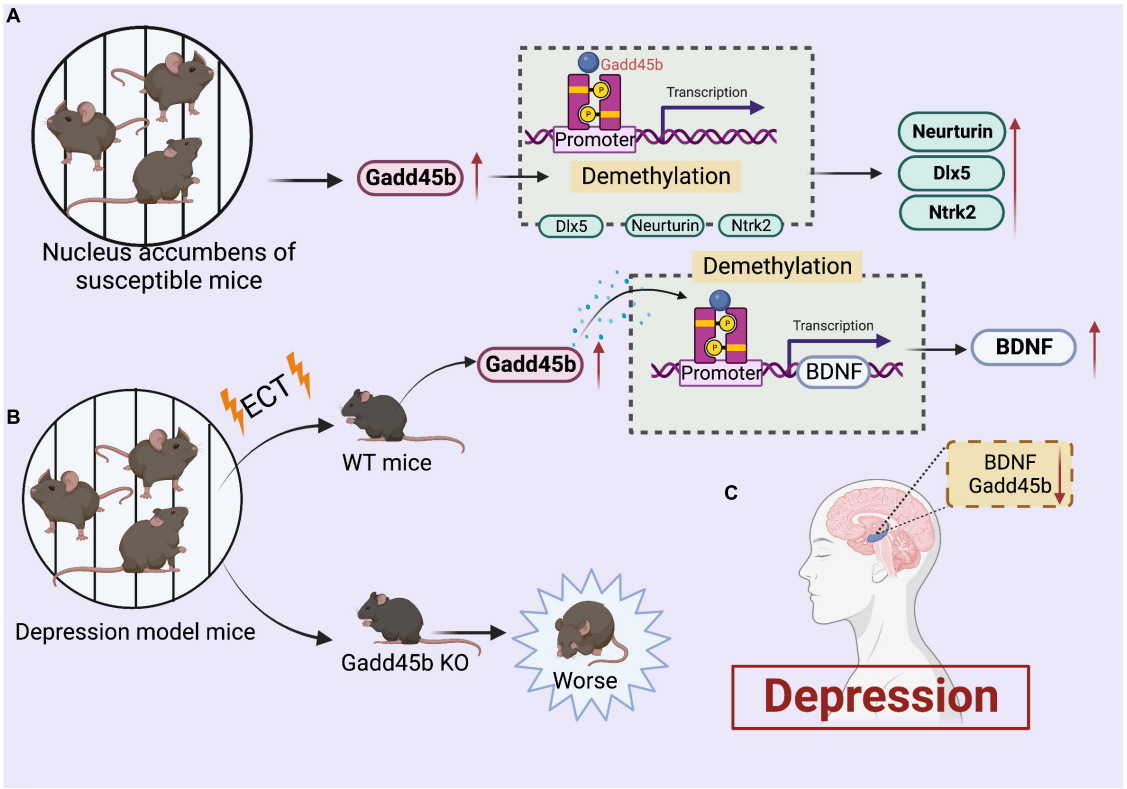

FIGURE 3
Roles of growth arrest and DNA damage-inducible beta (Gadd45b) in depression. **(A)** Increased gadd45b expression in the brain of nucleus accumbens of susceptible mice alters the demethylation of Neurturin, Dlx5, and Ntrk2, resulting in increased Neurturin, Dlx5, and Ntrk2 performance. **(B)** Increased gadd45b expression in the brains of depressed mice after ect therapy boosts BDNF function by modifying BDNF demethylation. **(C)** Decreased Gadd45b, BDNF expression in the brain of patients with depression (Figure was created with BioRender.com).

process of autism (Figure 4). Still, its precise mechanism must be proven by conducting a large number of studies.

The role of Gadd45b in neurologic disorders

Stroke

Stroke is the leading cause of permanent severe disability. More than half of older than 65-year-old stroke survivors have reduced mobility. Approximately 87% of all strokes are ischemic stroke. Due to the time limits of surgical therapy and the danger of recombinant tissue-type plasminogen activator therapy, neuroprotectants that inhibit the inflammatory response to combat ischemic injury have recently emerged as a new direction in stroke treatment (Paul and Candelario-Jalil, 2021). In the past several decades, Gadd45b has been demonstrated as an inherent neuroprotective factor protecting retinal ganglion cells from injury (Liu et al., 2009, 2013). Therefore, Gadd45b may be a new target for stroke treatment.

Researchers reported the continuous detection of Gadd45 immunoreactivity in neurons within the infarct from 4 to 24 h and in sublethally injured neurons within the penumbra from 24 to 48 h (Charriaut-Marlangue et al., 1999). From this investigation, we reached the conclusion that the expression of the Gadd45 family changes after cerebral ischemia. Specifically, the term of the Gadd45 mRNA in the ischemic hemisphere increases 3 h after reperfusion and approximately three-fold after 24 h compared to the contralateral or sham-operated group (Hou et al., 1997). In addition, Jin et al. (1996) discovered that Gadd45 protein is continuously expressed only in the ischemic penumbra from 4 to 24 h after cerebral ischemia. Meanwhile, the evidence revealed that Gadd45 protein could promote injury repair and expressed at higher levels in surviving neurons after cerebral ischemia. Consequently, the Gadd45 protein may protect against neuronal injury caused by cerebral ischemia.

In addition, several newly published preclinical studies demonstrate that Gadd45b protects against cerebral ischemia damage in both transitory localized and global models of cerebral ischemia. Chen et al. (1998) discovered meaningful increases in the expression of the Gadd45 mRNA and protein in the brain after transient global cerebral ischemia.

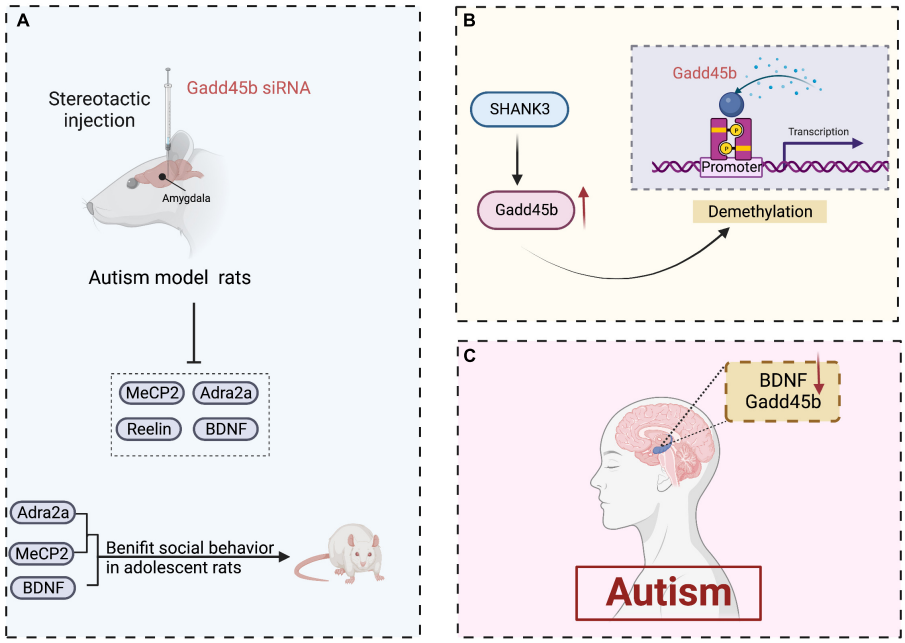

FIGURE 4
Roles of growth arrest and DNA damage-inducible beta (Gadd45b) in autism. **(A)** Stereotactic injection of gadd45b siRNA decreases the production of MeCP2, BDNF, Adra2a, and Reelin in autistic rats, where MeCP2, BDNF, and Adra2a contribute to adolescent rats' social competence. **(B)** SHANK3 enhances gadd45b expression, which may be related to gadd45b demethylation. **(C)** Decreased Gadd45b and BDNF expression in the brain of patients with autism (Figure was created with BioRender.com).

Liu and coworkers showed that cerebellar fastigial nucleus stimulation induces Gadd45b expression in the cerebral cortex after cerebral ischemia. Over-activation of Gadd45b promotes functional recovery after focal cerebral ischemia, implying that Gadd45b may be related to motor function after cerebral ischemia (Liu et al., 2012).

The recovery process after a stroke involves neurogenesis and axonal remodeling within the ischemic brain. Neurogenesis occurs following ischemic brain injury. Stroke generates a considerable increase in cell proliferation in the lateral ventricle's subventricular zone (SVZ) in the ischemic penumbra. However, the intrinsic neurogenesis abilities are generally insufficient to improve functional recovery (Arvidsson et al., 2002). A recent study showed that Gadd45b is related to SVZ neurogenesis following middle cerebral artery occlusion (MCAO), and Gadd45b mediates neurogenesis in the SVZ *via* BDNF (Tan et al., 2021). Gadd45b has been shown to alter the methylation of BDNF following cerebral ischemia-reperfusion injury (He et al., 2015). Both activin receptor-like kinase 5 (ALK5) signaling and DNA demethylation are crucial in adult neurogenesis. ALK5 regulates the protein level and demethylation of BDNF through controlling the production of Gadd45b, consequently encouraging the recovery of brain function (Zhang et al., 2019). Axonal remodeling is also induced by cerebral ischemia. Liu et al. (2015) discovered that Gadd45b leads to axonal regeneration and promotes functional recovery following MCAO in rats. Gadd45b regulated axon regeneration by BDNF and its downstream cAMP/PKA/CREB pathway after transient cerebral ischemia. In summary, Gadd45b could play a role in promoting axonal plasticity and neurogenesis. This procedure may enhance stroke recovery, which is important for brain recovery.

Neuronal apoptosis in ischemic brain penumbra is one of the major factors of neurological diseases. To investigate the role of Gadd45b in cerebral ischemia, lentiviral vector-associated RNA interference was injected stereotaxically into the ipsilateral lateral ventricle to inhibit Gadd45b expression. In this study, Gadd45b was shown to protect against rat brain ischemia injury by inhibiting apoptosis. The investigation suggested Gadd45b as a neuroprotective effector against apoptosis by regulating Bcl-2 and Bax (Liu et al., 2015b). In addition, Gadd45b expression is dramatically increased in hippocampal CA1 neurons from rats with transient global cerebral ischemia. Gadd45b protects neurons from ischemic injury by activating the DNA demethylation of the BDNF regulatory region in global ischemia-induced neuronal death (Cho et al., 2019). Equally, in an *in vitro* model of hypoxia and ischemia, Gadd45b was also shown to inhibit autophagy and alleviate neuron cell apoptosis (He et al., 2016).

Of note, microglia activation is critical for attenuating neuronal apoptosis, enhancing neurogenesis, and facilitating functional recovery after cerebral ischemia. In a mouse model

of transient focal cerebral ischemia, Guo et al. used unbiased single-cell sequencing in conjunction with bulk RNA-seq analysis to study microglia diversity at an early stage of ischemic stroke. They discovered that Gadd45b is overexpressed in microglia cells in the ischemic brain (Guo et al., 2021). Mitogen-activated protein kinase kinase-7 (MKK-7) is an upstream activator of the c-Jun-N-terminal kinase (JNK) signaling pathway, which is related to brain damage after acute cerebral ischemia. Fortunately, researchers have discovered Gadd45b-I, an effector peptide based on the Gadd45b domain (Vercelli et al., 2015). Gadd45-I was capable of binding to MKK7 and, by coupling it to the TAT peptide sequence, enabling membrane penetration. Studies *in vitro* reveal that Gadd45-I significantly lowers neuronal mortality generated by *N*-methyl-D-aspartate exposure or oxygen-glucose deprivation-induced excitotoxicity. In addition, Gadd45-I exhibited long-lasting neuroprotection against ischemia *in vivo*. Taken together, Gadd45b is a new putative target for ischemic stroke (**Figure 5** and **Table 1**).

Seizure

A seizure is an abrupt, uncontrolled electrical disruption in the brain. Seizures are associated with several alterations in the neuroplasticity of hippocampal circuits, including neurogenesis and dendritic development in the dentate gyrus (Naegele, 2009). Seizures are among the most potent stimulators of neurogenesis, hastening the differentiation of adult-born neurons (Tongiorgi et al., 2004; McNamara et al., 2006). Similarly, electroconvulsive therapy-induced epileptic episodes have increased dentate granulosa cell neurogenesis (Madsen et al., 2000; Scott et al., 2000). Coincidentally, recent research has linked neurogenesis to Gadd45b (Ma et al., 2009). Seizures have also been shown to stimulate the transcription of the Gadd45 gene (Henshall et al., 1999).

It is well-established that matrix metallopeptidase 9 (MMP-9) is a critical protein inducing the development of epilepsy in humans and rodents, and excess MMP-9 enhances the incidence of seizures (Wilczynski et al., 2008; Konopka et al., 2013). The increased MMP-9 expression in the hippocampus induced by epileptogenesis results from a complex epigenetic mechanism. Further research revealed that Gadd45b accumulation *in vivo* is one of the mechanisms of MMP-9 demethylation (Zybura-Broda et al., 2016). The study also implied that Gadd45b production induced by status epilepticus is mainly limited to postmitotic granule cells in the dentate gyrus.

In addition, Gadd45b-induced demethylation of BDNF has been hypothesized as a potential mechanism for the SE-induced enhancement of neurogenesis in the dentate gyrus (Xiao et al., 2020). The authors elegantly noted that following the elimination of Gadd45b, the degree of SE-induced demethylations of BDNF effectively was increased bout 5-fold. The mechanism of SE-induced BDNF demethylation by Gadd45b involves binding to the BDNF-specific Oct4 promoter, which drives region-specific demethylation through DNA nucleotide and base excision repair pathways, similar to the known role of Gadd45b in 5-hmC excision.

Ma et al. found that electroconvulsive treatment (ECT) in adult mice induced Gadd45b expression in granule cells of the hippocampal dentate gyrus with endogenous neural stem cell proliferation, new neuron formation, and temporal hippocampal dendrite growth. Gadd45b functions as an immediate-early gene by promoting endogenous gene (BDNF and FGF-1) demethylation. Knockdown of the Gadd45b gene in rats reduced ECT-induced proliferation of endogenous neural stem cells, neurite production, and dendritic growth in the hippocampus. The Gadd45b-induced increases in BDNF and FGF-1 expression are virtually eliminated in Gadd45b knockout rats. Based on these observations, Gadd45b could play a role in enhancing long-term neuroplasticity in the post-epileptic brain. This procedure, to some extent, facilitates structural repair of brain tissue and promotes functional recovery after epilepsy (**Figure 6**).

Dementia

Dementia is a disorder defined by a deterioration in cognition relative to a prior level, impairing occupational, household, or social functioning (Gale et al., 2018). Memory loss is a crucial and early indication of dementia and occurs in conjunction with it.

Interestingly, a new modified porcine placenta extract improves age-related memory loss in mice by upregulating Gadd45b (Yamauchi et al., 2019). Meanwhile, Gadd45b knockout mice exhibit a hippocampus-dependent long-term memory impairment (Leach et al., 2012). Furthermore, Gadd45b deletion increases fear in a hippocampus-dependent manner and promotes memory and synaptic plasticity (Sultan et al., 2012). These studies implicate Gadd45b as a regulator of memory formation and may be a viable therapeutic target in cognitive disease.

The most widespread type of dementia is Alzheimer's disease (AD). It is a progressive neurodegenerative disease of the brain that disrupts memory and other basic cognitive functions, leading to persistent mental decline and behavioral abnormalities that severely affect the daily life of patients. Deposing extracellular amyloid β-peptide (Aβ) plaques in the brain is a hallmark pathological feature of AD (Lambert et al., 1998). According to previous studies, Gadd45 is expressed in hippocampal CA1 pyramidal cells, which are susceptible to AD (Torp et al., 1998).

Alzheimer's disease is characterized by the pathological combination of Aβ, tau, and α-synuclein. Mutations in the genes encoding Aβ, tau, and α-synuclein are common. Overexpression of these mutant proteins may result in

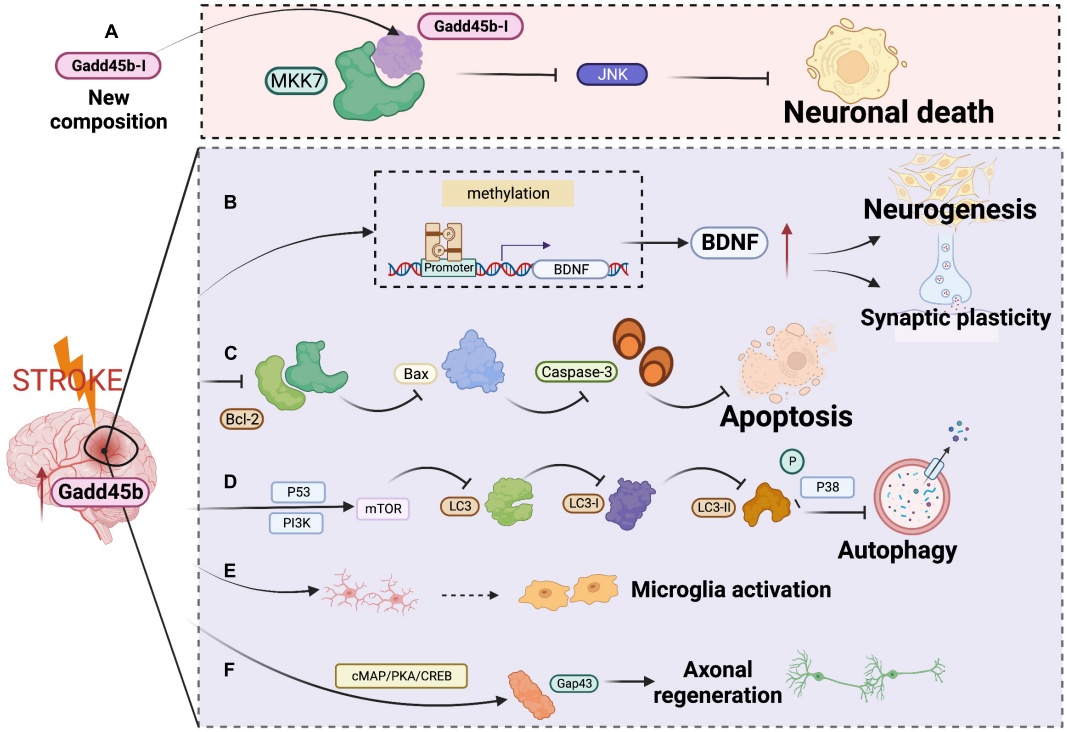

FIGURE 5
Roles of growth arrest and DNA damage-inducible beta (Gadd45b) in cerebral ischemic disease. **(A)** Gadd45b-I specifically binds to MKK-7 and inhibits JNK-mediated neural death. **(B)** Gadd45b promotes neurogenesis and synaptic remodeling by altering the demethylation of BDNF. **(C)** Gadd45b decreases the release of Bcl-2 and Bax to inhibit apoptosis. **(D)** Gadd45b inhibits cellular autophagy by stimulating PI3K/P53 signaling pathway and suppressing the P38 signaling pathway. **(E)** Gadd45b may be associated with microglia polarization. **(F)** Gadd45b promotes axonal regeneration through the camp/PKA/CREB signaling pathway (Figure was created with BioRender.com).

TABLE 1 Studies of growth arrest and DNA damage-inducible beta (Gadd45b) in cerebral ischemia.

Study type	Study (year)/references	Study findings
Rat global cerebral ischemia	Cho et al. (2019)	(1) Ischemic insults increase the abundance of Gadd45b and BDNF
		(2) Gadd45b blocks caspase activation and neuronal death
Rat tMCAO	Liu et al. (2012)	The expression of Gadd45b increased after transient focal cerebral ischemic injury
	Tan et al. (2021)	(1) Gadd45b increases neurogenesis in subventricular zone
		(2) Treatment with EE following ischemic stroke increases Gadd45b expression and neurogenesis in subventricular zone
		(3) Inhibition of Gadd45b ameliorates the increased neurogenesis induced by EE
	Zhang et al. (2019)	(1) ALK5 mediates Gadd45b protein levels by regulating Smad2/3 phosphorylation
		(2) ALK5 mediates neurogenesis and functional recovery *via* Gadd45b
	Liu et al. (2015)	(1) Gadd45b promotes axonal plasticity after MCAO
		(2) Gadd45b mediates axonal regeneration through BDNF and cAMP/PKA/pCREB pathway
	Liu et al. (2015) and Vercelli et al. (2015)	(1) Gadd45b prevents apoptosis
		(2) Gadd45b affects the expression of Bax and Bcl-2
		Gadd45b-I inhibits cell death by binding specifically to MKK7
OGD	He et al. (2016)	Gadd45b prevents autophagy and apoptosis
	He et al. (2015)	Gadd45b increases the BDNF and methylation level of the forth CpG islands

tMCAO, transient middle cerebral artery occlusion; EE, environmental enrichment; OGD, oxygen-glucose deprivation; BDNF, brain-derived neurotrophic factor; cAMP, cyclic adenosine monophosphate; PKA, protein kinase A; CREB, cAMP-responsive element binding protein.

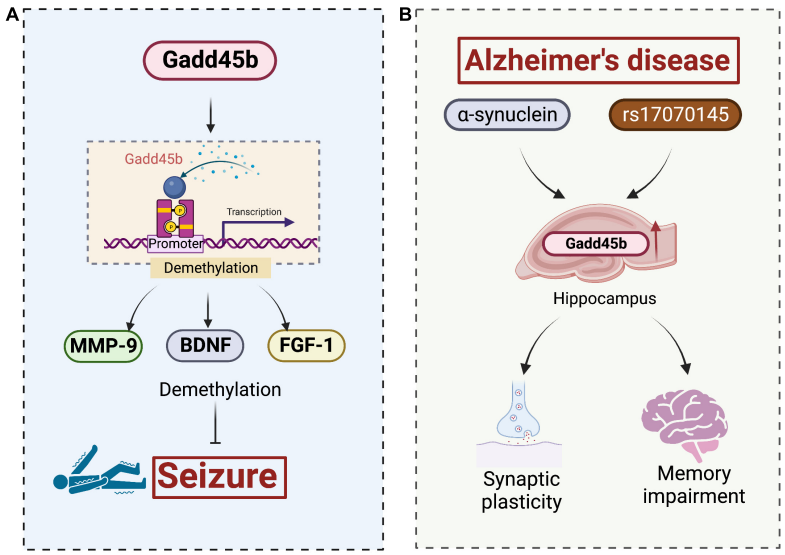

FIGURE 6
Roles of growth arrest and DNA damage-inducible beta (Gadd45b) in the seizures and Alzheimer's disease. **(A)** Gadd45b suppresses seizures by altering the demethylation of MMP-9, BDNF, and FGF-1. **(B)** α-synuclein and rs17070145, recognized pathological features in AD, promote Gadd45b expression in hippocampal, facilitating synaptic remodeling and memory repairment (Figure was created with BioRender.com).

a disease-associated phenotype (Goedert, 2015). Of note, extracellular α-synuclein induces the activation of Gadd45b (Motyl et al., 2018). The rs17070145-T variant of the WWC1 gene, which encodes the KIBRA protein, has a connection to improved episodic memory performance and a lower risk of late-onset AD, whereas rs17070145 increases Gadd45b expression (Piras et al., 2017). Thus, we infer that Gadd45b represents a potential target for AD treatment, but the exact mechanism remains to be investigated (**Figure 6**).

Parkinson's disease

Parkinson's disease (PD) is a neurodegenerative disorder characterized by a significant loss of dopamine (DA) neurons in substantia nigra pars compacta (SNpc) (Benayoun et al., 2015). Studies showed that Gadd45b expression rose dramatically both in SNpc of patients with PD and mouse brains with age. Therefore, Gadd45b, a known DNA demethylation enzyme, may play a significant role in PD (**Figure 7**).

Recent research (Ravel-Godreuil et al., 2021) revealed that Gadd45b overexpression led to a variety of alterations in the striatum of PD model mice, including loss of Chromatin structure, altered DNA methylation, and increased vulnerability of mDA neurons to oxidative stress, and neuronal death. Clearly, they hypothesized that the Gadd45b activates methylation changes of LINE-1, a prospective DNA damage factor (Blaudin de Thé et al., 2018), altering the heterochromatic structure and causing neurological disease.

Dopamine is prone to oxidation when discharged into the cytoplasm or extracellular space. Both oxidized DA and excessive Zn2+ may contribute to neuronal death and cause Parkinson's disease (Blum et al., 2001; Jenner, 2003). Yang indicated that Gadd45b could be the mediator of this route. It was found that the expression of Gadd45b was considerably boosted in PC12 cells induced by oxidized DA and excessive Zn2+. They hypothesized that Gadd45b induces PC12 death by blocking the P38/JNK signaling pathway and increasing the cell death process.

However, Gadd45b could be a potential target in countering dopamine precursor 3,4-dihydroxyphenyl-L-alanine (L-DOPA)-induced dyskinesia (LID) Parkinson's disease (Park et al., 2016). Researchers developed a 6-OHDA animal model of hemi-parkinsonism. In the striatum of the model animals, prolonged overstimulation with L-DOPA raised Gadd45b mRNA levels through the R1D pathway (Heiman et al., 2014). Park et al. (2016) demonstrated that overexpression of Gadd45b inhibited the L-DOPA-induced elevation in c-Fos and FosB/FosB mRNA levels, which inhibited LID.

Brain tumor

Gadd45 is associated with the development of several oncological diseases. Numerous studies have shown that the Gadd45 protein is aberrantly expressed in pancreatic cancer, hepatocellular carcinoma, lung cancer, gastrointestinal tumors, and lymphoma. Upregulation of Gadd45 induces tumor cell cycle arrest and apoptosis. Coincidentally, the anticancer

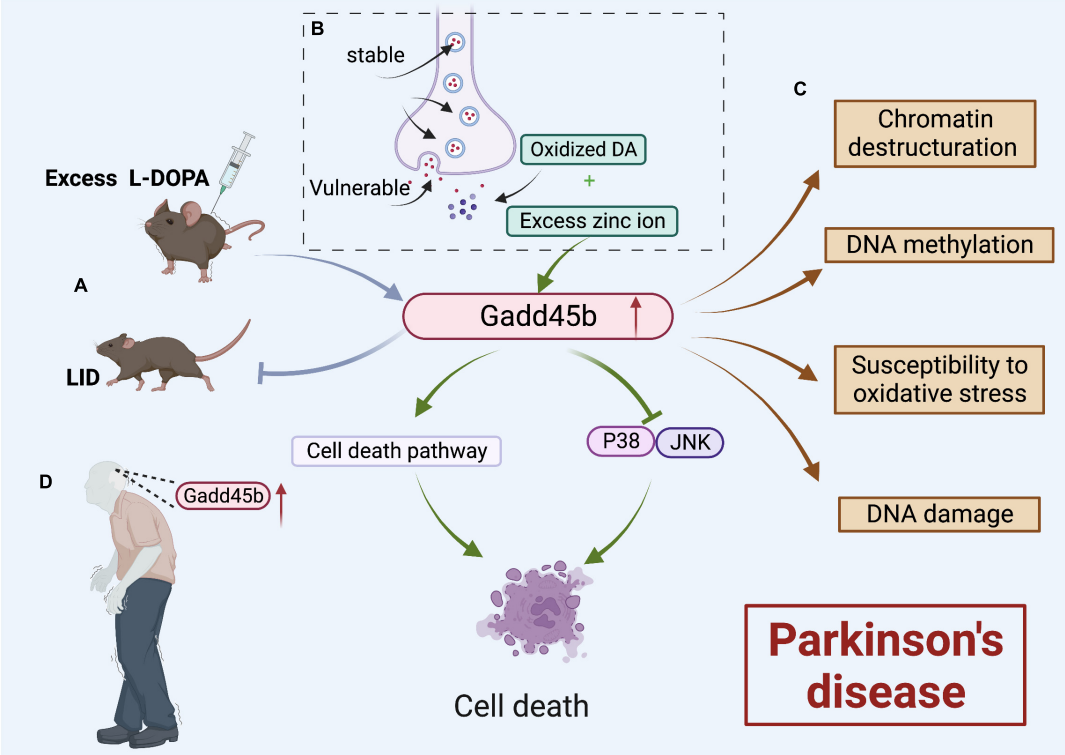

FIGURE 7
Roles of growth arrest and DNA damage-inducible beta (Gadd45b) in Parkinson's disease. **(A)** Gadd45b could prevent LID caused by excessive L-DOPA. **(B)** Oxidized DA and Excess Zn2+ could increase Gadd45b, which induced cell death by inhibiting the JNK/P38 signaling pathway and promoting the cell death process. **(C)** Gadd45b may be related to chromatin destructuration, DNA methylation, susceptibility to oxidative stress and DNA damage. **(D)** Increased Gadd45b expression in the brain of patients with PD (Figure was created with BioRender.com).

activity of chemotherapeutic agents (Rishi et al., 1999) and non-steroidal anti-inflammatory drugs depends on this effect (Zerbini et al., 2006). Therefore, Gadd45 has been identified as a potential target for antitumor drug therapy. The Gadd45b protein has been studied in neurological tumors, mainly in pituitary tumors, fibrillary astrocytoma, and adult neural tube cell tumors (**Figure 8**).

Human pituitary adenoma is a common intracranial tumor caused by hormone-secreting cells in the anterior pituitary (Ezzat et al., 2004). According to microarray studies, Gadd45b was downregulated 68-fold in pituitary tumors, and its loss may contribute to tumorigenesis or progression (Michaelis et al., 2011). Thus, this study identified Gadd45b as a novel pituitary tumor suppressor whose re-expression blocks proliferation, survival, and tumorigenesis. In addition, Gadd45b is a putative downstream target of protein 53 (p53) (Michaelis et al., 2011). Daptomycin has been shown to inhibit cell proliferation in AtT 20 corticotropic tumor cells *via* the p53-Gadd45b pathway, exerting anticancer effects (Kageyama et al., 2015). Furthermore, inhibiting the Gadd45 gene family through promoter methylation or nuclear factor kappa-B (NF-κB) activation is a critical step in cancer development (Tamura et al., 2012). In addition, p53 regulates Gadd45b expression through the NF-κB pathway (Zhai et al., 2019). Conversely, Gadd45b protein and mRNA expression are significantly reduced in human patients with gonadotrophic tumors. Gadd45b promotes gonadotrophic tumor apoptosis, primarily by arresting cells in G1/S and G2/M phases, but its upstream regulatory pathways are unknown (Zhang et al., 2002).

Gliomas are the most common primary tumors of the brain and spinal cord. The primary gliomas include astrocytic, oligodendrocyte, ependymal, neuronal, and mixed glial tumors (such as ganglioglioma) (Chen et al., 2017). Inhibition of the inositol requiring enzyme-1 (IRE1) pathway has been shown to substantially slow glioma growth in previous investigations (Drogat et al., 2007; Auf et al., 2010). Hypoxia is also related to the development of gliomas, and both hypoxia and IRE1 inhibition have been shown to promote Gadd45b gene expression in U87 glioma cells (Minchenko et al., 2016). Galectin-1 is an effective regulator of glioblastoma cell growth. Reduced production of the proangiogenic molecule Galectin-1 abolishes the level of the Gadd45b mRNA (Le Mercier et al., 2008). Gourabine E retards mitosis in human glioblastoma cell tumor cells by upregulating the expression of Gadd45b, thereby inhibiting tumor growth (Cheng et al., 2019). In addition, Tricyclodecan-9-yl-xanthogenate also blocks

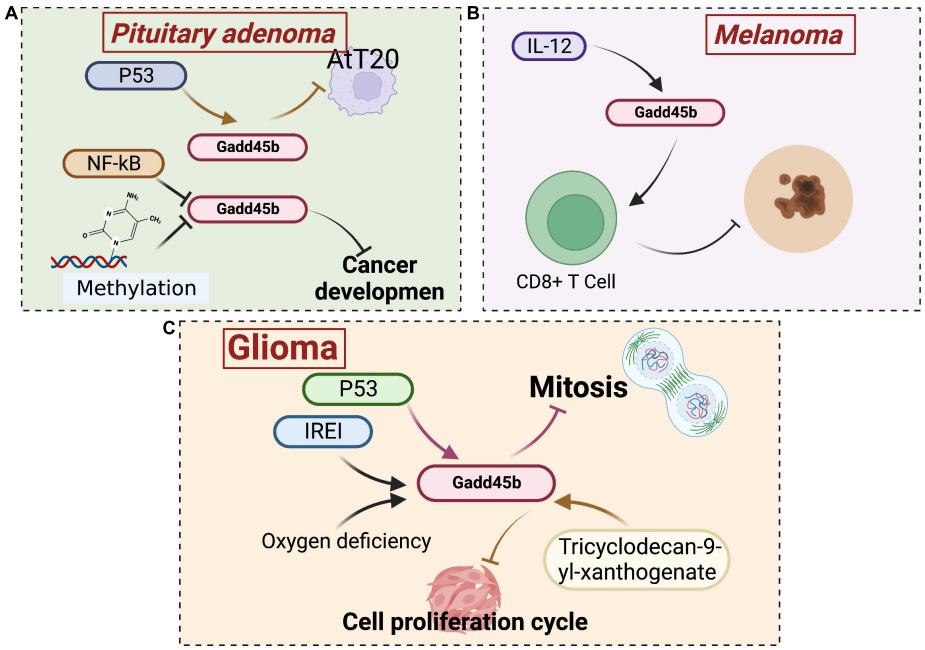

FIGURE 8
Roles of growth arrest and DNA damage-inducible beta (Gadd45b) in brain tumor. **(A)** Gadd45b is associated with NF-kB and P53 signaling pathways inhibiting pituitary adenoma cell growth. **(B)** The inhibitory effect of Gadd45b on melanoma growth is associated with IL-12. **(C)** The inhibitory effect of Gadd45b on glioma growth may be related to P53, IREI, and Tricyclodecan-9-yl-xanthogenate (Figure was created with BioRender.com).

cell cycle progression and inhibits tumor cell growth by decreasing Gadd45b expression in glioma stem cell-like cells (Kalluri et al., 2017).

Primary intracranial melanoma is sporadic, accounting for only 0.07% of all intracranial tumors (Arai et al., 2018). Hiring A (HA) inhibits melanin production. Coincidentally, the expression of Gadd45b is increased drastically in B16 melanoma cells treated with HA. The dendritic morphology observed after HA treatment is most likely attributed to increased expression of Gadd45b. In general, the melanocyte dendritic morphology is directly related to melanogenic activity (Villareal et al., 2012). Gadd45b specifically stimulates p38 activation, increasing interferon γ (IFN-γ) levels in CD8+ T cells. Gadd45b expression is upregulated by interleukin-12 (IL-12), which increases TCR-triggered activation of p38 MAP kinase and thus encodes a key signaling protein required for effective anti-melanoma immune responses (Ju et al., 2009).

Autoimmune diseases of the nervous system

Autoimmune diseases are disorders of the autoimmune system that cause the body to attack its organs, cells, and tissues. Because the specific biological pathogenesis of autoimmune diseases is unknown, the condition cannot be cured but only managed. In particular, the potential importance of epigenetic phenomena in autoimmune diseases has been highlighted (Wang et al., 2015). Interestingly, *in vivo* and *in vitro* studies have shown that immunization increases Gadd45b expression (Wang et al., 2006). Experimental studies have indicated that some autoimmune diseases are closely related to Gadd45b. For example, the Gadd45b mRNA is expressed at lower levels in patients with rheumatoid arthritis (RA) than in healthy people (Li et al., 2019). In particular, increased Gadd45b expression or inhibition of the activity of JNK or its upstream regulator MKK-7 alleviates the clinical symptoms of patients with RA (Svensson et al., 2009).

Neurological autoimmune diseases are diseases in which autoimmune cells and molecules are the main pathogenic factors attacking the nervous system. Multiple sclerosis (MS) is an immune-mediated inflammatory demyelinating disease of the central nervous system driven by autoreactive Th cells. Experimental allergic encephalitis (EAE) is an animal model of induced demyelinating disease with major symptoms that are very similar to those of humans with MS. Gadd45b deletion exacerbates EAE (Liu et al., 2005; Lu, 2006). Gadd45b is important for initiating TH1 cell responses by mediating pathogen-associated molecular pattern (PAMP) signaling in innate immune cells, enhancing and prolonging TCR signaling in T cells, and prolonging IL-12/IL-18 signaling in TH1 cells, which are important for initiating the TH1 response. TH1

cells are important components of chronic inflammation and are involved in the pathogenesis of autoimmune diseases (Svensson et al., 2009).

Additionally, myasthenia gravis (MG) is an autoimmune disease caused by dysfunctional neuromuscular junction transmission, and Gadd45b expression is downregulated in patients with thymoma presenting with myasthenia gravis (Yu et al., 2019). Thus, Gadd45b is involved in the regulation of several neurological autoimmune diseases. However, the specific mechanisms and functions of Gadd45b in these diseases have not been thoroughly established due to the lack of sufficient evidence.

Conclusion

In summary, Gadd45b is widely expressed in the central nervous system, plays a vital role in various nervous system diseases, and is a potential target for the treatment of various nervous system diseases. Gadd45b could enhance the long-term neuroplasticity of the brain and exert a neuroprotective effect. Consistent with their discovery, knockdown or overexpression of Gadd45b could cause a range of neurodevelopmental outcomes. For instance, the phenotypes of Gadd45b in mice include aberrant dendritic cell physiology, inappropriate production of IL-4, IL-6, and IFN-γ, as well as enhanced T cell proliferation (McMurry et al., 2016; Shefchek et al., 2020). Gadd45b knockdown or knockout inhibited the activity-driven proliferation of neural progenitors and the dendritic formation of newborn neurons (Kaufmann et al., 2011). Still, we are unaware of any observed human phenotypes associated with the Gadd45 family. In addition, no PWAS research linking Gadd45 to human disorders has been discovered by the authors. GWAS have effectively revealed risk loci for a multitude of neuropsychiatric disorders and traits, such as anorexia nervosa, major depressive disorder, schizophrenia, insomnia, and Alzheimer's disease, among others (Brandes et al., 2020). Therefore, future research is required to connect genes and phenotypes *via* functional changes in proteins, revealing insights into the architecture of the discovery of novel disease-causing genes and pathways as well as the identification of new therapeutic targets and disease biomarkers.

Noteworthy, multiple intriguing studies have displayed Gadd45b's contribution to the growing subject of cognitive neuro-epigenetics. The most notable distinction between these processes and those previously addressed is their operation in normal, senescent adult neurons, as opposed to those undergoing intentional cell death or growth (Sultan and Sawaya, 2022). Also, disruptions in DNA methylation patterns have been linked to the development of neurologic and neuropsychiatric illnesses (Shirvani-Farsani et al., 2021). Drug addiction is a chronic psychiatric disorder in which global and site-specific changes in DNA methylation can be observed (Wang et al., 2012). In addition, there is a substantial correlation between BDNF promoter methylation and the likelihood of drug abuse (Wang et al., 2012). However, only a single study has shown that striatal Gadd45b operates as a dopamine-induced gene that is required for cocaine reward memory through modulating DRD1 transcriptional activity (Zipperly et al., 2021). Therefore, the exploration of Gadd45 in its field holds great promise.

In addition, the breadth of loci targeted by Gadd45b for epigenetic regulation is largely unknown and a subject for future investigation. Fortunately, certain therapies, such as electroconvulsive treatment, have enhanced Gadd45b expression. Of note, researchers have discovered Gadd45b-I, an effector peptide based on the Gadd45b domain. Therefore, we conclude that using Gadd45b as a target for the therapy of neurologic and neuropsychiatric diseases may have far-reaching implications.

Author contributions

X-YS and S-HS were responsible for literature review, investigation, and draft preparation. BL was responsible for literature review and editing. Y-BL was responsible for drawing and editing. All authors contributed to the article and approved the submitted version.

Funding

This work was supported by National Natural Science Foundation of China (grant no. 81601018), Natural Science Foundation of Shandong Province, China (ZR2021MH043), and Academic Promotion Programme of Shandong First Medical University (2019QL013).

Conflict of interest

The authors declare that the research was conducted in the absence of any commercial or financial relationships that could be construed as a potential conflict of interest.

Publisher's note

All claims expressed in this article are solely those of the authors and do not necessarily represent those of their affiliated organizations, or those of the publisher, the editors and the reviewers. Any product that may be evaluated in this article, or claim that may be made by its manufacturer, is not guaranteed or endorsed by the publisher.

References

Abdallah, M. W., Mortensen, E. L., Greaves-Lord, K., Larsen, N., Bonefeld-Jørgensen, E. C., Nørgaard-Pedersen, B., et al. (2013). Neonatal levels of neurotrophic factors and risk of autism spectrum disorders. *Acta Psychiatr. Scand.* 128, 61–69. doi: 10.1111/acps.12020

Arai, N., Kagami, H., Mine, Y., Ishii, T., and Inaba, M. (2018). Primary solitary intracranial malignant melanoma: A systematic review of literature. *World Neurosurg.* 117, 386–393. doi: 10.1016/j.wneu.2018.06.138

Arvidsson, A., Collin, T., Kirik, D., Kokaia, Z., and Lindvall, O. (2002). Neuronal replacement from endogenous precursors in the adult brain after stroke. *Nat. Med.* 8, 963–970. doi: 10.1038/nm747

Auf, G., Jabouille, A., Guérit, S., Pineau, R., Delugin, M., Bouchecareilh, M., et al. (2010). Inositol-requiring enzyme 1alpha is a key regulator of angiogenesis and invasion in malignant glioma. *Proc. Natl. Acad. Sci. U.S.A.* 107, 15553–15558. doi: 10.1073/pnas.0914072107

Azis, I. A., Hashioka, S., Tsuchie, K., Miyaoka, T., Abdullah, R. A., Limoa, E., et al. (2019). Electroconvulsive shock restores the decreased coverage of brain blood vessels by astrocytic endfeet and ameliorates depressive-like behavior. *J. Affect. Disord* 257, 331–339. doi: 10.1016/j.jad.2019.07.008

Barreto, G., Schäfer, A., Marhold, J., Stach, D., Swaminathan, S. K., Handa, V., et al. (2007). Gadd45a promotes epigenetic gene activation by repair-mediated DNA demethylation. *Nature* 445, 671–675. doi: 10.1038/nature05515

Benayoun, B. A., Pollina, E. A., and Brunet, A. (2015). Epigenetic regulation of ageing: Linking environmental inputs to genomic stability. *Nat. Rev. Mol. Cell Biol.* 16, 593–610. doi: 10.1038/nrm4048

Blaudin de Thé, F. X., Rekaik, H., Peze-Heidsieck, E., Massiani-Beaudoin, O., Joshi, R. L., Fuchs, J., et al. (2018). Engrailed homeoprotein blocks degeneration in adult dopaminergic neurons through LINE-1 repression. *EMBO J.* 37:e97374. doi: 10.15252/embj.201797374

Blum, D., Torch, S., Lambeng, N., Nissou, M., Benabid, A. L., Sadoul, R., et al. (2001). Molecular pathways involved in the neurotoxicity of 6-OHDA, dopamine and MPTP: Contribution to the apoptotic theory in Parkinson's disease. *Prog. Neurobiol.* 65, 135–172. doi: 10.1016/s0301-0082(01)00003-x

Brandes, N., Linial, N., and Linial, M. (2020). PWAS: Proteome-wide association study-linking genes and phenotypes by functional variation in proteins. *Genome Biol.* 21:173. doi: 10.1186/s13059-020-02089-x

Charriaut-Marlangue, C., Richard, E., and Ben-Ari, Y. (1999). DNA damage and DNA damage-inducible protein Gadd45 following ischemia in the P7 neonatal rat. *Brain Res. Dev. Brain Res.* 116, 133–140. doi: 10.1016/s0165-3806(99)00084-x

Chen, J., Uchimura, K., Stetler, R. A., Zhu, R. L., Nakayama, M., Jin, K., et al. (1998). Transient global ischemia triggers expression of the DNA damage-inducible gene GADD45 in the rat brain. *J. Cereb Blood Flow Metab.* 18, 646–657. doi: 10.1097/00004647-199806000-00007

Chen, R., Smith-Cohn, M., Cohen, A. L., and Colman, H. (2017). Glioma subclassifications and their clinical significance. *Neurotherapeutics* 14, 284–297. doi: 10.1007/s13311-017-0519-x

Cheng, A. C., Hsu, Y. C., and Tsai, C. C. (2019). The effects of cucurbitacin E on GADD45β-trigger G2/M arrest and JNK-independent pathway in brain cancer cells. *J. Cell Mol. Med.* 23, 3512–3519. doi: 10.1111/jcmm.14250

Cho, C. H., Byun, H. R., Jover-Mengual, T., Pontarelli, F., Dejesus, C., Cho, A. R., et al. (2019). Gadd45b Acts as neuroprotective effector in global ischemia-induced neuronal death. *Int. Neurourol. J.* 23(Suppl 1), S11–S21. doi: 10.5213/inj.1938040.020

Conn, P. J., Lindsley, C. W., and Jones, C. K. (2009). Activation of metabotropic glutamate receptors as a novel approach for the treatment of schizophrenia. *Trends Pharmacol. Sci.* 30, 25–31. doi: 10.1016/j.tips.2008.10.006

Drogat, B., Auguste, P., Nguyen, D. T., Bouchecareilh, M., Pineau, R., Nalbantoglu, J., et al. (2007). IRE1 signaling is essential for ischemia-induced vascular endothelial growth factor-A expression and contributes to angiogenesis and tumor growth *in vivo*. *Cancer Res.* 67, 6700–6707. doi: 10.1158/0008-5472.Can-06-3235

Evans-Lacko, S., Aguilar-Gaxiola, S., Al-Hamzawi, A., Alonso, J., Benjet, C., Bruffaerts, R., et al. (2018). Socio-economic variations in the mental health treatment gap for people with anxiety, mood, and substance use disorders: Results from the WHO World Mental Health (WMH) surveys. *Psychol. Med.* 48, 1560–1571. doi: 10.1017/s0033291717003336

Ezzat, S., Asa, S. L., Couldwell, W. T., Barr, C. E., Dodge, W. E., Vance, M. L., et al. (2004). The prevalence of pituitary adenomas: A systematic review. *Cancer* 101, 613–619. doi: 10.1002/cncr.20412

Fan, G., Beard, C., Chen, R. Z., Csankovszki, G., Sun, Y., Siniaia, M., et al. (2001). DNA hypomethylation perturbs the function and survival of CNS neurons in postnatal animals. *J. Neurosci.* 21, 788–797. doi: 10.1523/jneurosci.21-03-00788.2001

Fan, G., Martinowich, K., Chin, M. H., He, F., Fouse, S. D., Hutnick, L., et al. (2005). DNA methylation controls the timing of astrogliogenesis through regulation of JAK-STAT signaling. *Development* 132, 3345–3356. doi: 10.1242/dev.01912

Feng, J., Chang, H., Li, E., and Fan, G. (2005). Dynamic expression of de novo DNA methyltransferases Dnmt3a and Dnmt3b in the central nervous system. *J. Neurosci. Res.* 79, 734–746. doi: 10.1002/jnr.20404

Gale, S. A., Acar, D., and Daffner, K. R. (2018). Dementia. *Am. J. Med.* 131, 1161–1169. doi: 10.1016/j.amjmed.2018.01.022

Garbett, K., Ebert, P. J., Mitchell, A., Lintas, C., Manzi, B., Mirnics, K., et al. (2008). Immune transcriptome alterations in the temporal cortex of subjects with autism. *Neurobiol. Dis.* 30, 303–311. doi: 10.1016/j.nbd.2008.01.012

Gavin, D. P., Kusumo, H., Sharma, R. P., Guizzetti, M., Guidotti, A., and Pandey, S. C. (2015). Gadd45b and N-methyl-D-aspartate induced DNA demethylation in postmitotic neurons. *Epigenomics* 7, 567–579. doi: 10.2217/epi.15.12

Gavin, D. P., Sharma, R. P., Chase, K. A., Matrisciano, F., Dong, E., and Guidotti, A. (2012). Growth arrest and DNA-damage-inducible, beta (GADD45b)-mediated DNA demethylation in major psychosis. *Neuropsychopharmacology* 37, 531–542. doi: 10.1038/npp.2011.221

Goedert, M. (2015). NEURODEGENERATION. Alzheimer's and Parkinson's diseases: The prion concept in relation to assembled Aβ, tau, and α-synuclein. *Science* 349:1255555. doi: 10.1126/science.1255555

Golshani, P., Hutnick, L., Schweizer, F., and Fan, G. (2005). Conditional Dnmt1 deletion in dorsal forebrain disrupts development of somatosensory barrel cortex and thalamocortical long-term potentiation. *Thalamus Relat. Syst.* 3, 227–233. doi: 10.1017/s1472928807000222

Grassi, D., Franz, H., Vezzali, R., Bovio, P., Heidrich, S., Dehghanian, F., et al. (2017). Neuronal Activity, TGFβ-Signaling and unpredictable chronic stress modulate transcription of Gadd45 Family Members and DNA methylation in the hippocampus. *Cereb. Cortex* 27, 4166–4181. doi: 10.1093/cercor/bhx095

Guidotti, A., Auta, J., Chen, Y., Davis, J. M., Dong, E., Gavin, D. P., et al. (2011). Epigenetic GABAergic targets in schizophrenia and bipolar disorder. *Neuropharmacology* 60, 1007–1016. doi: 10.1016/j.neuropharm.2010.10.021

Guidotti, A., Dong, E., Kundakovic, M., Satta, R., Grayson, D. R., and Costa, E. (2009). Characterization of the action of antipsychotic subtypes on valproate-induced chromatin remodeling. *Trends Pharmacol. Sci.* 30, 55–60. doi: 10.1016/j.tips.2008.10.010

Guo, K., Luo, J., Feng, D., Wu, L., Wang, X., Xia, L., et al. (2021). Single-Cell RNA sequencing with combined use of bulk RNA sequencing to reveal cell heterogeneity and molecular changes at acute stage of ischemic stroke in mouse cortex penumbra area. *Front. Cell Dev. Biol.* 9:624711. doi: 10.3389/fcell.2021.624711

Gururajan, A., Clarke, G., Dinan, T. G., and Cryan, J. F. (2016). Molecular biomarkers of depression. *Neurosci. Biobehav. Rev.* 64, 101–133. doi: 10.1016/j.neubiorev.2016.02.011

Hashimoto, K., Iwata, Y., Nakamura, K., Tsujii, M., Tsuchiya, K. J., Sekine, Y., et al. (2006). Reduced serum levels of brain-derived neurotrophic factor in adult male patients with autism. *Prog. Neuropsychopharmacol. Biol. Psychiatry* 30, 1529–1531. doi: 10.1016/j.pnpbp.2006.06.018

Hasin, D. S., Sarvet, A. L., Meyers, J. L., Saha, T. D., Ruan, W. J., Stohl, M., et al. (2018). Epidemiology of Adult DSM-5 Major Depressive Disorder and Its Specifiers in the United States. *JAMA Psychiatry* 75, 336–346. doi: 10.1001/jamapsychiatry.2017.4602

He, G. Q., Xu, W. M., Li, J. F., Li, S. S., Liu, B., Tan, X. D., et al. (2015). Huwe1 interacts with Gadd45b under oxygen-glucose deprivation and reperfusion injury in primary Rat cortical neuronal cells. *Mol. Brain* 8:88. doi: 10.1186/s13041-015-0178-y

He, G., Xu, W., Tong, L., Li, S., Su, S., Tan, X., et al. (2016). Gadd45b prevents autophagy and apoptosis against rat cerebral neuron oxygen-glucose deprivation/reperfusion injury. *Apoptosis* 21, 390–403. doi: 10.1007/s10495-016-1213-x

Heiman, M., Heilbut, A., Francardo, V., Kulicke, R., Fenster, R. J., Kolaczyk, E. D., et al. (2014). Molecular adaptations of striatal spiny projection neurons during levodopa-induced dyskinesia. *Proc. Natl. Acad. Sci. U.S.A.* 111, 4578–4583. doi: 10.1073/pnas.1401819111

Henshall, D. C., Sinclair, J., and Simon, R. P. (1999). Relationship between seizure-induced transcription of the DNA damage-inducible gene GADD45. DNA fragmentation, and neuronal death in focally evoked limbic epilepsy. *J. Neurochem.* 73, 1573–1583. doi: 10.1046/j.1471-4159.1999.0731573.x

Hildesheim, J., Bulavin, D. V., Anver, M. R., Alvord, W. G., Hollander, M. C., Vardanian, L., et al. (2002). Gadd45a protects against UV irradiation-induced skin tumors, and promotes apoptosis and stress signaling *via* MAPK and p53. *Cancer Res.* 62, 7305–7315.

Hou, S. T., Tu, Y., Buchan, A. M., Huang, Z., Preston, E., Rasquinha, I., et al. (1997). Increases in DNA lesions and the DNA damage indicator Gadd45 following transient cerebral ischemia. *Biochem. Cell Biol.* 75, 383–392.

Jenner, P. (2003). Oxidative stress in Parkinson's disease. *Ann. Neurol.* 53 Suppl 3, S26–S36. doi: 10.1002/ana.10483

Jeong, H., Mendizabal, I., Berto, S., Chatterjee, P., Layman, T., Usui, N., et al. (2021). Evolution of DNA methylation in the human brain. *Nat. Commun.* 12:2021. doi: 10.1038/s41467-021-21917-7

Jin, K., Chen, J., Kawaguchi, K., Zhu, R. L., Stetler, R. A., Simon, R. P., et al. (1996). Focal ischemia induces expression of the DNA damage-inducible gene GADD45 in the rat brain. *Neuroreport* 7, 1797–1802. doi: 10.1097/00001756-199607290-00022

Ju, S., Zhu, Y., Liu, L., Dai, S., Li, C., Chen, E., et al. (2009). Gadd45b and Gadd45g are important for anti-tumor immune responses. *Eur. J. Immunol.* 39, 3010–3018. doi: 10.1002/eji.200839154

Kageyama, K., Sugiyama, A., Murasawa, S., Asari, Y., Niioka, K., Oki, Y., et al. (2015). Aphidicolin inhibits cell proliferation *via* the p53-GADD45β pathway in AtT-20 cells. *Endocr. J.* 62, 645–654. doi: 10.1507/endocrj.EJ15-0084

Kalluri, H. S. G., Kuo, J. S., and Dempsey, R. J. (2017). Chronic D609 treatment interferes with cell cycle and targets the expression of Olig2 in Glioma Stem like Cells. *Eur J Pharmacol* 814, 81–86. doi: 10.1016/j.ejphar.2017.08.001

Kaufmann, L. T., Gierl, M. S., and Niehrs, C. (2011). Gadd45a, Gadd45b and Gadd45g expression during mouse embryonic development. *Gene Expr. Patterns* 11, 465–470. doi: 10.1016/j.gep.2011.07.005

Kearsey, J. M., Coates, P. J., Prescott, A. R., Warbrick, E., and Hall, P. A. (1995). Gadd45 is a nuclear cell cycle regulated protein which interacts with p21Cip1. *Oncogene* 11, 1675–1683.

Kidd, P. M. (2002). Autism, an extreme challenge to integrative medicine. Part: 1: The knowledge base. *Altern. Med. Rev.* 7, 292–316.

Kigar, S. L., Chang, L., and Auger, A. P. (2015). Gadd45b is an epigenetic regulator of juvenile social behavior and alters local pro-inflammatory cytokine production in the rodent amygdala. *Brain Behav. Immun.* 46, 60–69. doi: 10.1016/j.bbi.2015.02.018

Konopka, A., Grajkowska, W., Ziemiańska, K., Roszkowski, M., Daszkiewicz, P., Rysz, A., et al. (2013). Matrix metalloproteinase-9 (MMP-9) in human intractable epilepsy caused by focal cortical dysplasia. *Epilepsy Res.* 104, 45–58. doi: 10.1016/j.eplepsyres.2012.09.018

Kraus, C., Castrén, E., Kasper, S., and Lanzenberger, R. (2017). Serotonin and neuroplasticity - Links between molecular, functional and structural pathophysiology in depression. *Neurosci. Biobehav. Rev.* 77, 317–326. doi: 10.1016/j.neubiorev.2017.03.007

Kurian, J. R., Bychowski, M. E., Forbes-Lorman, R. M., Auger, C. J., and Auger, A. P. (2008). Mecp2 organizes juvenile social behavior in a sex-specific manner. *J. Neurosci.* 28, 7137–7142. doi: 10.1523/jneurosci.1345-08.2008

Kurita, M., Holloway, T., García-Bea, A., Kozlenkov, A., Friedman, A. K., Moreno, J. L., et al. (2012). HDAC2 regulates atypical antipsychotic responses through the modulation of mGlu2 promoter activity. *Nat. Neurosci.* 15, 1245–1254. doi: 10.1038/nn.3181

Labonté, B., Jeong, Y. H., Parise, E., Issler, O., Fatma, M., Engmann, O., et al. (2019). Gadd45b mediates depressive-like role through DNA demethylation. *Sci. Rep.* 9:4615. doi: 10.1038/s41598-019-40844-8

Labrie, V., Pai, S., and Petronis, A. (2012). Epigenetics of major psychosis: Progress, problems and perspectives. *Trends Genet.* 28, 427–435. doi: 10.1016/j.tig.2012.04.002

Lambert, M. P., Barlow, A. K., Chromy, B. A., Edwards, C., Freed, R., Liosatos, M., et al. (1998). Diffusible, nonfibrillar ligands derived from Abeta1-42 are potent central nervous system neurotoxins. *Proc. Natl. Acad. Sci. U.S.A.* 95, 6448–6453. doi: 10.1073/pnas.95.11.6448

Le Mercier, M., Lefranc, F., Mijatovic, T., Debeir, O., Haibe-Kains, B., Bontempi, G., et al. (2008). Evidence of galectin-1 involvement in glioma chemoresistance. *Toxicol. Appl. Pharmacol.* 229, 172–183. doi: 10.1016/j.taap.2008.01.009

Leach, P. T., Poplawski, S. G., Kenney, J. W., Hoffman, B., Liebermann, D. A., Abel, T., et al. (2012). Gadd45b knockout mice exhibit selective deficits in hippocampus-dependent long-term memory. *Learn. Mem.* 19, 319–324. doi: 10.1101/lm.024984.111

Li, R. N., Lin, Y. Z., Pan, Y. C., Lin, C. H., Tseng, C. C., Sung, W. Y., et al. (2019). GADD45a and GADD45b Genes in Rheumatoid arthritis and systemic lupus erythematosus patients. *J. Clin. Med.* 8:801. doi: 10.3390/jcm8060801

Liebermann, D. A., and Hoffman, B. (2007). Gadd45 in the response of hematopoietic cells to genotoxic stress. *Blood Cells Mol. Dis.* 39, 329–335. doi: 10.1016/j.bcmd.2007.06.006

Liu, B., Li, J., Li, L., Yu, L., and Li, C. (2012). Electrical stimulation of cerebellar fastigial nucleus promotes the expression of growth arrest and DNA damage inducible gene β and motor function recovery in cerebral ischemia/reperfusion rats. *Neurosci. Lett.* 520, 110–114. doi: 10.1016/j.neulet.2012.05.044

Liu, B., Li, L. L., Tan, X. D., Zhang, Y. H., Jiang, Y., He, G. Q., et al. (2015a). Gadd45b mediates axonal plasticity and subsequent functional recovery after experimental stroke in rats. *Mol. Neurobiol.* 52, 1245–1256. doi: 10.1007/s12035-014-8909-0

Liu, B., Sun, X., Suyeoka, G., Garcia, J. G., and Leiderman, Y. I. (2013). TGFβ signaling induces expression of Gadd45b in retinal ganglion cells. *Invest. Ophthalmol. Vis. Sci.* 54, 1061–1069. doi: 10.1167/iovs.12-10142

Liu, B., Suyeoka, G., Papa, S., Franzoso, G., and Neufeld, A. H. (2009). Growth arrest and DNA damage protein 45b (Gadd45b) protects retinal ganglion cells from injuries. *Neurobiol. Dis.* 33, 104–110. doi: 10.1016/j.nbd.2008.09.020

Liu, B., Zhang, Y. H., Jiang, Y., Li, L. L., Chen, Q., He, G. Q., et al. (2015b). Gadd45b is a novel mediator of neuronal apoptosis in ischemic stroke. *Int. J. Biol. Sci.* 11, 353–360. doi: 10.7150/ijbs.9813

Liu, L., Tran, E., Zhao, Y., Huang, Y., Flavell, R., and Lu, B. (2005). Gadd45 beta and Gadd45 gamma are critical for regulating autoimmunity. *J. Exp. Med.* 202, 1341–1347. doi: 10.1084/jem.20051359

Lu, B. (2006). The molecular mechanisms that control function and death of effector CD4+ T cells. *Immunol. Res.* 36, 275–282. 36, 275. doi: 10.1385/ir

Ma, D. K., Jang, M. H., Guo, J. U., Kitabatake, Y., Chang, M. L., Pow-Anpongkul, N., et al. (2009). Neuronal activity-induced Gadd45b promotes epigenetic DNA demethylation and adult neurogenesis. *Science* 323, 1074–1077. doi: 10.1126/science.1166859

Madsen, T. M., Treschow, A., Bengzon, J., Bolwig, T. G., Lindvall, O., and Tingström, A. (2000). Increased neurogenesis in a model of electroconvulsive therapy. *Biol. Psychiatry* 47, 1043–1049. doi: 10.1016/s0006-3223(00)00228-6

Matrisciano, F., Dong, E., Gavin, D. P., Nicoletti, F., and Guidotti, A. (2011). Activation of group II metabotropic glutamate receptors promotes DNA demethylation in the mouse brain. *Mol. Pharmacol.* 80, 174–182. doi: 10.1124/mol.110.070896

McMurry, J. A., Köhler, S., Washington, N. L., Balhoff, J. P., Borromeo, C., Brush, M., et al. (2016). Navigating the phenotype frontier: The monarch initiative. *Genetics* 203, 1491–1495. doi: 10.1534/genetics.116.188870

McNamara, J. O., Huang, Y. Z., and Leonard, A. S. (2006). Molecular signaling mechanisms underlying epileptogenesis. *Sci. STKE* 2006:re12. doi: 10.1126/stke.3562006re12

Melas, P. A., Rogdaki, M., Lennartsson, A., Björk, K., Qi, H., Witasp, A., et al. (2012). Antidepressant treatment is associated with epigenetic alterations in the promoter of P11 in a genetic model of depression. *Int. J. Neuropsychopharmacol.* 15, 669–679. doi: 10.1017/s1461145711000940

Ménard, C., Hodes, G. E., and Russo, S. J. (2016). Pathogenesis of depression: Insights from human and rodent studies. *Neuroscience* 321, 138–162. doi: 10.1016/j.neuroscience.2015.05.053

Michaelis, K. A., Knox, A. J., Xu, M., Kiseljak-Vassiliades, K., Edwards, M. G., Geraci, M., et al. (2011). Identification of growth arrest and DNA-damage-inducible gene beta (GADD45beta) as a novel tumor suppressor in pituitary gonadotrope tumors. *Endocrinology* 152, 3603–3613. doi: 10.1210/en.2011-0109

Minchenko, O. H., Kryvdiuk, I. V., Riabovol, O. O., Minchenko, D. O., Danilovskyi, S. V., and Ratushna, O. O. (2016). Inhibition of IRE1 modifies the hypoxic regulation of GADD family gene expressions in U87 glioma cells. *Ukr. Biochem. J.* 88, 25–34. doi: 10.15407/ubj88.02.025

Molendijk, M. L., Spinhoven, P., Polak, M., Bus, B. A., Penninx, B. W., and Elzinga, B. M. (2014). Serum BDNF concentrations as peripheral manifestations of depression: Evidence from a systematic review and meta-analyses on 179 associations (N=9484). *Mol. Psychiatry* 19, 791–800. doi: 10.1038/mp.2013.105

Monteiro, P., and Feng, G. (2017). SHANK proteins: Roles at the synapse and in autism spectrum disorder. *Nat. Rev. Neurosci.* 18, 147–157. doi: 10.1038/nrn.2016.183

Motyl, J., Wencel, P. L., Cieślik, M., Strosznajder, R. P., and Strosznajder, J. B. (2018). Alpha-synuclein alters differently gene expression of Sirts, PARPs and

other stress response proteins: Implications for neurodegenerative disorders. *Mol. Neurobiol.* 55, 727–740. doi: 10.1007/s12035-016-0317-1

Naegele, J. (2009). Epilepsy and the plastic mind. *Epilepsy Curr.* 9, 166–169. doi: 10.1111/j.1535-7511.2009.01331.x

Nguyen, A., Rauch, T. A., Pfeifer, G. P., and Hu, V. W. (2010). Global methylation profiling of lymphoblastoid cell lines reveals epigenetic contributions to autism spectrum disorders and a novel autism candidate gene, RORA, whose protein product is reduced in autistic brain. *FASEB J.* 24, 3036–3051. doi: 10.1096/fj.10-154484

Park, H. Y., Ryu, Y. K., Kim, Y. H., Park, T. S., Go, J., Hwang, J. H., et al. (2016). Gadd45β ameliorates L-DOPA-induced dyskinesia in a Parkinson's disease mouse model. *Neurobiol. Dis.* 89, 169–179. doi: 10.1016/j.nbd.2016.02.013

Paul, S., and Candelario-Jalil, E. (2021). Emerging neuroprotective strategies for the treatment of ischemic stroke: An overview of clinical and preclinical studies. *Exp. Neurol.* 335:113518. doi: 10.1016/j.expneurol.2020.113518

Piras, I. S., Krate, J., Schrauwen, I., Corneveaux, J. J., Serrano, G. E., Sue, L., et al. (2017). Whole transcriptome profiling of the human hippocampus suggests an involvement of the KIBRA rs17070145 polymorphism in differential activation of the MAPK signaling pathway. *Hippocampus* 27, 784–793. doi: 10.1002/hipo.22731

Ploski, J. E., Newton, S. S., and Duman, R. S. (2006). Electroconvulsive seizure-induced gene expression profile of the hippocampus dentate gyrus granule cell layer. *J. Neurochem.* 99, 1122–1132. doi: 10.1111/j.1471-4159.2006.04156.x

Rasmussen, K. G. (2011). Electroconvulsive therapy and melancholia: Review of the literature and suggestions for further study. *J. ECT* 27, 315–322. doi: 10.1097/YCT.0b013e31820a9482

Ratajczak, H. V. (2011). Theoretical aspects of autism: Causes–a review. *J. Immunotoxicol.* 8, 68–79. doi: 10.3109/1547691x.2010.545086

Ravel-Godreuil, C., Massiani-Beaudoin, O., Mailly, P., Prochiantz, A., Joshi, R. L., and Fuchs, J. (2021). Perturbed DNA methylation by Gadd45b induces chromatin disorganization, DNA strand breaks and dopaminergic neuron death. *iScience* 24,:102756. doi: 10.1016/j.isci.2021.102756

Rishi, A. K., Sun, R. J., Gao, Y., Hsu, C. K., Gerald, T. M., Sheikh, M. S., et al. (1999). Post-transcriptional regulation of the DNA damage-inducible gadd45 gene in human breast carcinoma cells exposed to a novel retinoid CD437. *Nucleic Acids Res.* 27, 3111–3119. doi: 10.1093/nar/27.15.3111

Rizzardi, L. F., Hickey, P. F., Rodriguez DiBlasi, V., Tryggvadóttir, R., Callahan, C. M., Idrizi, A., et al. (2019). Neuronal brain-region-specific DNA methylation and chromatin accessibility are associated with neuropsychiatric trait heritability. *Nat. Neurosci.* 22, 307–316. doi: 10.1038/s41593-018-0297-8

Scott, B. W., Wojtowicz, J. M., and Burnham, W. M. (2000). Neurogenesis in the dentate gyrus of the rat following electroconvulsive shock seizures. *Exp. Neurol.* 165, 231–236. doi: 10.1006/exnr.2000.7458

Shefchek, K. A., Harris, N. L., Gargano, M., Matentzoglu, N., Unni, D., Brush, M., et al. (2020). The Monarch Initiative in 2019: An integrative data and analytic platform connecting phenotypes to genotypes across species. *Nucleic Acids Res.* 48, D704–D715. doi: 10.1093/nar/gkz997

Shirvani-Farsani, Z., Maloum, Z., Bagheri-Hosseinabadi, Z., Vilor-Tejedor, N., and Sadeghi, I. (2021). DNA methylation signature as a biomarker of major neuropsychiatric disorders. *J. Psychiatr. Res.* 141, 34–49. doi: 10.1016/j.jpsychires.2021.06.013

Shulha, H. P., Cheung, I., Whittle, C., Wang, J., Virgil, D., Lin, C. L., et al. (2012). Epigenetic signatures of autism: Trimethylated H3K4 landscapes in prefrontal neurons. *Arch. Gen.Psychiatry* 69, 314–324. doi: 10.1001/archgenpsychiatry.2011.151

Siviy, S. M., and Baliko, C. N. (2000). A further characterization of alpha-2 adrenoceptor involvement in the rough-and-tumble play of juvenile rats. *Dev. Psychobiol.* 37, 25–34. doi: 10.1002/1098-2302(200007)37:1<25::aid-dev4<3.0.co;2-c

Sultan, F. A., and Sawaya, B. E. (2022). Gadd45 in neuronal development. Function, and Injury. *Adv. Exp. Med. Biol.* 1360, 117–148. doi: 10.1007/978-3-030-94804-7_9

Sultan, F. A., Wang, J., Tront, J., Liebermann, D. A., and Sweatt, J. D. (2012). Genetic deletion of Gadd45b, a regulator of active DNA demethylation, enhances long-term memory and synaptic plasticity. *J. Neurosci.* 32, 17059–17066. doi: 10.1523/jneurosci.1747-12.2012

Svensson, C. I., Inoue, T., Hammaker, D., Fukushima, A., Papa, S., Franzoso, G., et al. (2009). Gadd45beta deficiency in rheumatoid arthritis: Enhanced synovitis through JNK signaling. *Arth. Rheum* 60, 3229–3240. doi: 10.1002/art.24887

Tahiliani, M., Koh, K. P., Shen, Y., Pastor, W. A., Bandukwala, H., Brudno, Y., et al. (2009). Conversion of 5-methylcytosine to 5-hydroxymethylcytosine in mammalian DNA by MLL partner TET1. *Science* 324, 930–935. doi: 10.1126/science.1170116

Tamura, R. E., de Vasconcellos, J. F., Sarkar, D., Libermann, T. A., Fisher, P. B., and Zerbini, L. F. (2012). GADD45 proteins: Central players in tumorigenesis. *Curr. Mol. Med.* 12, 634–651. doi: 10.2174/156652412800619978

Tan, X. D., Liu, B., Jiang, Y., Yu, H. J., and Li, C. Q. (2021). Gadd45b mediates environmental enrichment-induced neurogenesis in the SVZ of rats following ischemia stroke *via* BDNF. *Neurosci. Let.* 745:135616. doi: 10.1016/j.neulet.2020.135616

Tongiorgi, E., Armellin, M., Giulianini, P. G., Bregola, G., Zucchini, S., Paradiso, B., et al. (2004). Brain-derived neurotrophic factor mRNA and protein are targeted to discrete dendritic laminas by events that trigger epileptogenesis. *J. Neurosci.* 24, 6842–6852. doi: 10.1523/jneurosci.5471-03.2004

Torp, R., Su, J. H., Deng, G., and Cotman, C. W. (1998). GADD45 is induced in Alzheimer's disease, and protects against apoptosis in vitro. *Neurobiol. Dis.* 5, 245–252. doi: 10.1006/nbdi.1998.0201

Vercelli, A., Biggi, S., Sclip, A., Repetto, I. E., Cimini, S., Falleroni, F., et al. (2015). Exploring the role of MKK7 in excitotoxicity and cerebral ischemia: A novel pharmacological strategy against brain injury. *Cell Death Dis.* 6:e1854. doi: 10.1038/cddis.2015.226

Villareal, M. O., Han, J., Ikuta, K., and Isoda, H. (2012). Mechanism of Mitf inhibition and morphological differentiation effects of hirsein A on B16 melanoma cells revealed by DNA microarray. *J. Dermatol. Sci.* 67, 26–36. doi: 10.1016/j.jdermsci.2012.04.005

Wang, J. C., Kapoor, M., and Goate, A. M. (2012). The genetics of substance dependence. *Annu. Rev. Genom. Hum. Genet.* 13, 241–261. doi: 10.1146/annurev-genom-090711-163844

Wang, L., Du, F., Cao, Q., Sheng, H., Shen, B., Zhang, Y., et al. (2006). Immunization with autologous T cells enhances *in vivo* anti-tumor immune responses accompanied by up-regulation of GADD45beta. *Cell Res.* 16, 702–712. doi: 10.1038/sj.cr.7310083

Wang, L., Wang, F. S., and Gershwin, M. E. (2015). Human autoimmune diseases: A comprehensive update. *J. Intern. Med.* 278, 369–395. doi: 10.1111/joim.12395

Wilczynski, G. M., Konopacki, F. A., Wilczek, E., Lasiecka, Z., Gorlewicz, A., Michaluk, P., et al. (2008). Important role of matrix metalloproteinase 9 in epileptogenesis. *J. Cell Biol.* 180, 1021–1035. doi: 10.1083/jcb.200708213

Xiao, X. L., Wu, X. L., Yang, P. B., Hu, H. B., Chen, Y., Min, L., et al. (2020). Status epilepticus induced Gadd45b is required for augmented dentate neurogenesis. *Stem Cell Res.* 49:102102. doi: 10.1016/j.scr.2020.102102

Yamauchi, A., Tone, T., Sugimoto, K., Seok Lim, H., Kaku, T., Tohda, C., et al. (2019). Porcine placental extract facilitates memory and learning in aged mice. *Food Sci. Nutr.* 7, 2995–3005. doi: 10.1002/fsn3.1156

Yin, Q., Du, T., Yang, C., Li, X., Zhao, Z., Liu, R., et al. (2021). Gadd45b is a novel mediator of depression-like behaviors and neuroinflammation after cerebral ischemia. *Biochem. Biophys. Res. Commun.* 554, 107–113. doi: 10.1016/j.bbrc.2021.03.104

Yu, L., Ke, J., Du, X., Yu, Z., and Gao, D. (2019). Genetic characterization of thymoma. *Sci. Rep.* 9:2369. doi: 10.1038/s41598-019-38878-z

Zerbini, L. F., Czibere, A., Wang, Y., Correa, R. G., Otu, H., Joseph, M., et al. (2006). A novel pathway involving melanoma differentiation associated gene-7/interleukin-24 mediates nonsteroidal anti-inflammatory drug-induced apoptosis and growth arrest of cancer cells. *Cancer Res.* 66, 11922–11931. doi: 10.1158/0008-5472.Can-06-2068

Zhai, X., Wang, L., Xu, C., Hou, Q., Zhang, L., Li, Z., et al. (2019). Triptolide preserves glomerular barrier function *via* the inhibition of p53-mediated increase of GADD45B. *Arch. Biochem. Biophys.* 671, 210–217. doi: 10.1016/j.abb.2019.07.012

Zhang, K., Zhang, Q., Deng, J., Li, J., Li, J., Wen, L., et al. (2019). ALK5 signaling pathway mediates neurogenesis and functional recovery after cerebral ischemia/reperfusion in rats *via* Gadd45b. *Cell Death Dis.* 10:360. doi: 10.1038/s41419-019-1596-z

Zhang, X., Sun, H., Danila, D. C., Johnson, S. R., Zhou, Y., Swearingen, B., et al. (2002). Loss of expression of GADD45 gamma, a growth inhibitory gene, in human pituitary adenomas: Implications for tumorigenesis. *J. Clin. Endocrinol. Metab.* 87, 1262–1267. doi: 10.1210/jcem.87.3.8315

Zipperly, M. E., Sultan, F. A., Graham, G. E., Brane, A. C., Simpkins, N. A., Carullo, N. V. N., et al. (2021). Regulation of dopamine-dependent transcription and cocaine action by Gadd45b. *Neuropsychopharmacology* 46, 709–720. doi: 10.1038/s41386-020-00828-z

Zybura-Broda, K., Amborska, R., Ambrozek-Latecka, M., Wilemska, J., Bogusz, A., Bucko, J., et al. (2016). Epigenetics of Epileptogenesis-Evoked Upregulation of Matrix Metalloproteinase-9 in Hippocampus. *PLoS One* 11:e0159745. doi: 10.1371/journal.pone.0159745

frontiers | Frontiers in Molecular Neuroscience

TYPE Original Research
PUBLISHED 13 October 2022
DOI 10.3389/fnmol.2022.977305

Check for updates

OPEN ACCESS

EDITED BY
Markus Wöhr,
KU Leuven, Belgium

REVIEWED BY
Michael J. Schmeisser,
Johannes Gutenberg University Mainz, Germany
Gerhard Schratt,
ETH Zürich, Switzerland

*CORRESPONDENCE
Eunjoon Kim
kime@kaist.ac.kr

†These authors have contributed equally to this work

SPECIALTY SECTION
This article was submitted to Brain Disease Mechanisms, a section of the journal Frontiers in Molecular Neuroscience

RECEIVED 24 June 2022
ACCEPTED 16 September 2022
PUBLISHED 13 October 2022

CITATION
Yoo Y-E, Yoo T, Kang H and Kim E (2022) Brain region and gene dosage-differential transcriptomic changes in *Shank2*-mutant mice. *Front. Mol. Neurosci.* 15:977305. doi: 10.3389/fnmol.2022.977305

COPYRIGHT
© 2022 Yoo, Yoo, Kang and Kim. This is an open-access article distributed under the terms of the Creative Commons Attribution License (CC BY). The use, distribution or reproduction in other forums is permitted, provided the original author(s) and the copyright owner(s) are credited and that the original publication in this journal is cited, in accordance with accepted academic practice. No use, distribution or reproduction is permitted which does not comply with these terms.

Brain region and gene dosage-differential transcriptomic changes in *Shank2*-mutant mice

Ye-Eun Yoo[1†], Taesun Yoo[1†], Hyojin Kang[2] and Eunjoon Kim[1,3*]

[1]Center for Synaptic Brain Dysfunctions, Institute for Basic Science (IBS), Daejeon, South Korea, [2]Division of National Supercomputing, Korea Institute of Science and Technology Information (KISTI), Daejeon, South Korea, [3]Department of Biological Sciences, Korea Advanced Institute of Science and Technology (KAIST), Daejeon, South Korea

Shank2 is an abundant excitatory postsynaptic scaffolding protein that has been implicated in various neurodevelopmental and psychiatric disorders, including autism spectrum disorder (ASD), intellectual disability, attention-deficit/hyperactivity disorder, and schizophrenia. *Shank2*-mutant mice show ASD-like behavioral deficits and altered synaptic and neuronal functions, but little is known about how different brain regions and gene dosages affect the transcriptomic phenotypes of these mice. Here, we performed RNA-Seq-based transcriptomic analyses of the prefrontal cortex, hippocampus, and striatum in adult *Shank2* heterozygous (HT)- and homozygous (HM)-mutant mice lacking exons 6–7. The prefrontal cortical, hippocampal, and striatal regions showed distinct transcriptomic patterns associated with synapse, ribosome, mitochondria, spliceosome, and extracellular matrix (ECM). The three brain regions were also distinct in the expression of ASD-related and ASD-risk genes. These differential patterns were stronger in the prefrontal cortex where the HT transcriptome displayed increased synaptic gene expression and reverse-ASD patterns whereas the HM transcriptome showed decreased synaptic gene expression and ASD-like patterns. These results suggest brain region- and gene dosage-differential transcriptomic changes in *Shank2*-mutant mice.

KEYWORDS

autism spectrum disorder, *Shank2*, cortex, hippocampus, striatum, gene dosage, transcriptome, RNA-seq

Introduction

Transcriptomic analyses of brain samples from individuals with autism spectrum disorder (ASD) have provided substantial insights into the convergent biological functions and pathways that are dysregulated in ASD, which include chromatin regulation, transcription, translation, synapse function, neuronal and glial development, and immune function (Garbett et al., 2008; Voineagu et al., 2011; Parikshak et al., 2013, 2016; Gupta et al., 2014; Krishnan et al., 2016; Velmeshev et al., 2019). Studies on mouse models of ASD have also revealed altered transcriptomic patterns that are associated with dysregulated biological functions and pathways (Jiang and Ehlers, 2013; Barnard et al., 2015; Bourgeron, 2015; Lee et al., 2015a, 2017; Nelson and Valakh, 2015; Sahin and Sur, 2015; Hulbert and Jiang, 2016; Monteiro and Feng, 2017; Varghese et al., 2017; Mossa et al., 2018; Winden et al., 2018; Bagni and Zukin, 2019; Basilico et al., 2020; Rein and Yan, 2020; Takumi et al., 2020; Moffat et al., 2021; Yan and Rein, 2021) However, relatively little is known about how controllable parameters in mouse models of ASD, such as age, brain region, and dosage, can affect brain transcriptomic patterns. Such knowledge would be expected to facilitate the appropriate design and data interpretation of future experiments.

Shank2, also known as ProSAP1, is an abundant scaffolding protein that is enriched in the postsynaptic density of an excitatory synapse (Du et al., 1998; Boeckers et al., 1999; Lim et al., 1999; Naisbitt et al., 1999; reviewed in Sheng and Kim, 2000, 2011; Boeckers et al., 2002; Grabrucker et al., 2011; Sala et al., 2015; Mossa et al., 2017; Eltokhi et al., 2018). Shank2 has been implicated in various brain disorders, including ASD, intellectual disability, developmental delay, attention deficit/hyperactivity disorder, schizophrenia, epilepsy, and obsessive compulsive disorder (Berkel et al., 2010, 2011; Pinto et al., 2010; Leblond et al., 2012, 2014; Rauch et al., 2012; Sanders et al., 2012; Chilian et al., 2013; Liu et al., 2013; Guilmatre et al., 2014; Costas, 2015; Peykov et al., 2015a,b; Homann et al., 2016; Bowling et al., 2017; Mossa et al., 2017; Yuen et al., 2017; Bai et al., 2018; Guo et al., 2018; Lu et al., 2018; Callaghan et al., 2019; Satterstrom et al., 2020; Trost et al., 2020; Wang et al., 2020; Ma et al., 2021; Ohashi et al., 2021; Chenbhanich and So, 2022). Previous studies in mouse/rat models of ASD and human neurons deficient of Shank2 have suggested various molecular, synaptic, neuronal, and circuit mechanisms underlying Shank2-related phenotypes (Schmeisser et al., 2012; Won et al., 2012; Ey et al., 2013, 2018; Lee et al., 2015b, 2018, 2020, 2021a,b; Ferhat et al., 2016; Ha et al., 2016; Ko et al., 2016; Peter et al., 2016; Lim et al., 2017; Pappas et al., 2017; Sato et al., 2017, 2020; Yoon et al., 2017; Heise et al., 2018; Kim et al., 2018; Modi et al., 2018; Wegener et al., 2018; Chung et al., 2019; de Chaumont et al., 2019; Zaslavsky et al., 2019; Chen et al., 2020; Han et al., 2020; Daini et al., 2021; Grabrucker et al., 2021; Horner et al., 2021; Lutz et al., 2021; Yoo et al., 2021; Wahl et al., 2022) [reviewed in (Boeckers et al., 2002; Grabrucker et al., 2011; Jiang and Ehlers, 2013; Guilmatre et al., 2014; Yoo et al., 2014; Sala et al., 2015; Schmeisser, 2015; Monteiro and Feng, 2017; Mossa et al., 2017; Eltokhi et al., 2018; Ey et al., 2020; Jung and Park, 2022)]. However, it remains unclear whether and how different brain regions distinctly contribute to the observed Shank2-related mouse phenotypes. In addition, heterozygous Shank2 deletion in mice has been shown to induce much weaker changes in behavioral phenotypes relative to a homozygous gene deletion (Schmeisser et al., 2012; Won et al., 2012; Pappas et al., 2017). However, because autistic human individuals usually carry heterozygous SHANK2 mutations, it is important to test if heterozygous Shank2 deletion in mice leads to detectable changes in molecular, neuronal, and/or synaptic phenotypes. In addition, we previously performed transcriptomic analyses of the medial prefrontal brain regions from heterozygous and homozygous Shank2-mutant mice lacking exons 6 and 7. We observed stronger reverse-ASD-like transcriptomic changes in heterozygous mutant mice than in homozygous mutant mice, which were more prominent at juvenile stages relative to adult stages (Lee et al., 2021b). This led us to question whether such changes are conserved across a larger prefrontal area and/or in other brain regions.

In the present study, we set out to perform transcriptomic analyses of the prefrontal cortex (termed cortex hereafter), hippocampus, and striatum regions of adult (~postnatal day 90 or P90) *Shank2* HT- and HM-mutant mice lacking exons 6–7. Our findings collectively indicate brain region and gene dosage-differential transcriptomic patterns in *Shank2*-mutant mice.

Materials and methods

Animals

Shank2-mutant mice lacking exons 6–7 have been reported previously (Won et al., 2012) and have been deposited at the Jackson Laboratory (B6N.129S4-*Shank2*^{TM1Mgle}/CsbdJ; Jackson 033667). Mice were maintained at the mouse facility of the Korea Advanced Institute of Science and Technology (KAIST); they were fed *ad libitum* and maintained according to the Animal Research Requirements of KAIST.

RNA-seq analysis

Transcript abundance was estimated with Salmon (v1.1.0) (Patro et al., 2017) in Quasi-mapping-based mode onto the *Mus musculus* (mouse) genome (GRCm38) with GC bias correction (–gcBias). Quantified gene-level abundance data was imported to R (v.4.1.3) with the tximport (Soneson et al., 2015) package and differential gene

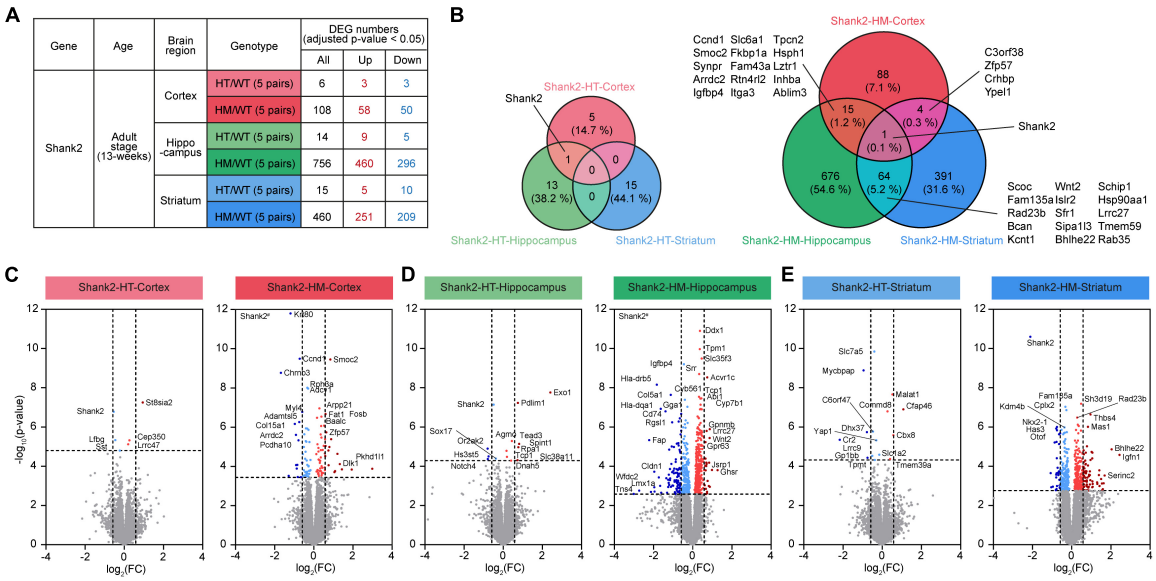

FIGURE 1
Differentially expressed genes (DEGs) among Shank2-heterozygous (HT) and Shank2-homozygous (HM) transcripts in the cortex, hippocampus, and striatum. **(A)** Numbers of DEGs from cortical, hippocampal, and striatal regions in Shank2-HT and Shank2-HM mice relative to wild-type (WT) [13 weeks; male; *n* = 5 mice (WT), 5 (HT/heterozygote), and 5 (HM/homozygote)]. DEGs were defined as genes showing transcript changes above the cutoff (adjusted *p*-value < 0.05). **(B)** Venn diagrams showing the overlaps of DEGs between cortical, hippocampal, and striatal regions in Shank2-HT and Shank2-HM mice [13 weeks; male; *n* = 5 mice (WT), 5 (HT), and 5 (HM)]. **(C–E)** Volcano plot representations of DEGs from cortical, hippocampal, and striatal transcripts in Shank2-HT and Shank2-HM mice. The DEGs (*p*-value < 0.05) were further color-coded to indicate those with strong fold changes (>1.5). Note that *Shank2* was not indicated as a DEG in some volcano plots (HT-Striatum) because of the low adjusted *p*-values ($p = 0.2850$), although their *p*-values were below 0.05 ($p = 0.0019$). Shank2$^{\#}$ in HM-Cortex and HM-Hippocampus volcano plots indicate very small *p*-values [$-\log_{10}$ (adjusted *p*-value) = 26 and 28 for HM-Cortex and HM-Hippocampus, respectively].

expression analysis was carried out using R/Bioconductor DEseq2 (v1.30.1) (Love et al., 2014). Normalized read counts were computed by dividing the raw read counts by size factors and fitted to a negative binomial distribution. The *P*-values were adjusted for multiple testing with the Benjamini–Hochberg correction. Genes with an adjusted *P*-value of less than 0.05 were considered as differentially expressed. Volcano plots were generated using the R ggplot2 (v.3.3.3) package. The gene ontology (GO) enrichment analyses were performed using database for annotation, visualization, and integrated discovery (DAVID) (version 6.8) (Huang et al., 2009) using *Mus musculus* (mouse) as a background.[1]

Synaptic gene ontologies (SynGO) analysis[2] was performed to associate synapse functions to the identified DEGs. Comparison to all brain-expressed genes was used to determine the extent of enrichments for SynGO terms. The gene count indicates the number of unique genes from the input gene list against SynGO, or child, terms and was used to build the sunburst plot color-coded by gene counts. STRING analysis was used to obtain and visualize protein-protein interaction (PPI) plots for SynGO-DEGs.[3]

Gene set enrichment analysis (GSEA)[4] (Subramanian et al., 2005) was used to determine whether priori-defined gene sets would show statistically significant differences in expression between wild-type (WT) and *Shank2*-mutant mice. Enrichment analysis was performed using GSEAPreranked (gsea-3.0.jar) module on gene set collections downloaded from the Molecular Signature Database (MSigDB) v7.4.[5] GSEA Preranked was applied using the list of all genes expressed, ranked by the fold change, and multiplied by the inverse of the *P*-value with recommended default settings (1,000 permutations and a classic scoring scheme). The false discovery rate (FDR) was estimated to control the false positive finding of a given normalized enrichment score (NES) by comparing the tails of the observed and null distributions derived from 1,000 gene set permutations. The gene sets with an FDR of less than 0.05 were considered as significantly enriched. Integration and visualization of the GSEA results were performed using the EnrichmentMap Cytoscape App (version 3.8.1) (Merico et al., 2010; Isserlin et al., 2014).

1 https://david.ncifcrf.gov/
2 https://www.syngoportal.org/
3 https://string-db.org/
4 http://software.broadinstitute.org/gsea
5 http://software.broadinstitute.org/gsea/msigdb

Results

Differentially expressed genes (DEGs) in Shank2-HT and Shank2-HM transcripts

To explore whether different brain regions distinctly contribute to the various phenotypes observed in *Shank2*-mutant mice, we performed RNA-seq analysis of the prefrontal cortex (termed cortex hereafter), hippocampus, and striatum in Shank2-HT and Shank2-HM mice lacking exons 6–7 (n = 5 mice) at an adult stage (∼postnatal day 90 or P90) (**Figure 1A** and **Supplementary Table 1**). These three groups of transcripts were well separated in a heatmap analysis (**Supplementary Figure 1**).

The RNA-seq results were first analyzed for genes that were differentially expressed (DEGs) between WT mice and Shank2-HT or Shank2-HM mice. In the cortex, the Shank2-HT and Shank2-HM transcripts contained a total of 6 and 108 DEGs (adjusted $p < 0.05$), respectively, relative to WT (**Figure 1A** and **Supplementary Table 2**). Hippocampal Shank2-HT and Shank2-HM transcripts contained 14 and 756 DEGs, respectively, while striatal Shank2-HT and Shank2-HM transcripts contained 15 and 460 DEGs, respectively (**Figure 1A**). These results suggest that HM *Shank2* deletion is associated with more DEGs in all three brain regions compared to HT *Shank2* deletion.

The overlaps of the DEGs between different brain regions were small, ranging from ∼6 to 20% between Shank2-HT/HM cortical, hippocampal, and striatal transcripts (**Figure 1B**). The small overlaps between different brain regions were also supported by small correlations of fold changes (FC) between two groups of transcripts (**Supplementary Figure 2**). The hippocampus and striatum tended to share more DEGs than did the hippocampus/striatum and the cortex. *Shank2* was the only DEG shared by all three brain regions.

Volcano plots of the DEGs further highlighted the stronger transcriptomic impacts of HM *Shank2* deletion relative to HT *Shank2* deletion (**Figures 1C–E**).

Database for annotation, visualization, and integrated discovery (DAVID) analysis of Shank2-HT and Shank2-HM DEGs

Database for annotation, visualization, and integrated discovery analyses were performed using the Shank2-HM cortical, hippocampal, and striatal DEGs. Our DAVID analysis of the cortical Shank2-HM transcripts revealed only minimal enrichments in the GO terms (**Figure 2A**). In contrast, the hippocampal Shank2-HM transcripts were strongly enriched for GO terms associated with neuronal synapses, such as "postsynaptic density," "synapse," and "postsynaptic membrane," as well as with subneuronal regions/structures, such as "dendrite," "neuronal cell body," and "neuronal projection" in the cellular component domain (**Figure 2B**). Another strong association was "protein binding" in the molecular function (MF) domain, suggesting that there may be alterations in multi-molecular synaptic interactions.

The results from the striatum indicated enhancement for GO terms associated with neuronal synapses, such as "synapse," "postsynaptic membrane," and "postsynaptic density," along with subneuronal regions/structures, such as "neuronal cell body," "axon," and "dendrite" in the cellular component domain (**Figure 2C**). Another strong association was "protein binding" in the molecular function domain.

These results suggest that the Shank2-HM hippocampal and striatal DEGs are functionally similar to one another.

Synaptic gene ontologies (SynGO) and protein-protein interaction (PPI) analyses of Shank2-HT and Shank2-HM DEGs

Given that our DAVID analyses of DEGs in Shank2-HM hippocampal/striatal transcripts yielded numerous synapse-associated GO terms, we further analyzed the Shank2-HT/HM DEGs using SynGO, which is an evidence-based and expertly curated resource for synaptic function and gene enrichment analyses (Koopmans et al., 2019).

Substantial proportions of the Shank2-HT/HM cortical/hippocampal/striatal DEGs belonged to SynGO genes (SynGO-DEGs), including 33/19% of Shank2-HT/HM cortical DEGs, 7/18% of Shank2-HT/HM hippocampal DEGs, and 7/19% of Shank2-HT/HM striatal DEGs (**Supplementary Table 2**). Notably, the enrichment levels of the differentially expressed SynGO genes were similar in the three brain regions for Shank2-HM (but not Shank2-HT) DEGs with sufficient numbers.

Functional analysis of SynGO-DEGs using sunburst plotting revealed distinct synaptic functions. These were more evident in large SynGO-DEG datasets, such as those for Shank2-HM SynGO-DEGs versus Shank2-HT SynGO-DEGs and hippocampal/striatal SynGO-DEGs versus cortical SynGO-DEGs (**Figures 3A–C**). Specifically, the upregulated hippocampal Shank2-HM SynGO-DEGs were enriched for pre- and postsynaptic functions, whereas the downregulated hippocampal Shank2-HM SynGO-DEGs were more strongly enriched for postsynaptic functions compared to presynaptic functions.

The upregulated striatal Shank2-HM DEGs were more strongly enriched for presynaptic functions. The downregulated striatal Shank2-HM SynGO-DEGs were more strongly enriched

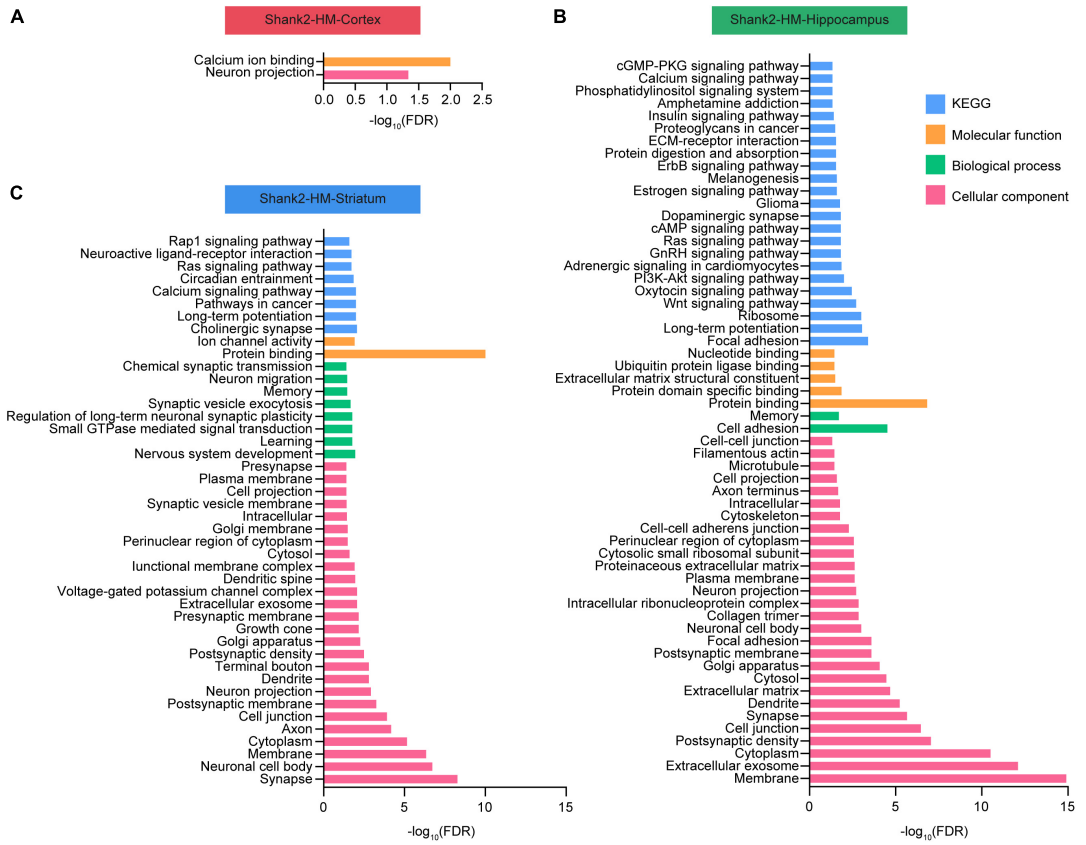

FIGURE 2
Database for annotation, visualization, and integrated discovery (DAVID) analysis of Shank2-heterozygous (HT) and Shank2-homozygous (HM) differentially expressed genes (DEGs). **(A–C)** DEGs in the cortical, hippocampal, and striatal transcripts from Shank2-HT and Shank2-HM mice [13 weeks; male; *n* = 5 mice wild-type (WT), 5 (HT), and 5 (HM)] were subjected to DAVID analysis for associations with gene ontology (GO) terms in the molecular function (MF), biological process (BP), cellular component, and KEGG domains. The low GO scores for the cortical DEGs may reflect the small number of these DEGs. FDR, false discovery rate.

for postsynaptic functions, similar to the hippocampus. The up- and downregulated cortical Shank2-HM SynGO-DEGs were also distinctly enriched for pre- and postsynaptic functions, although this conclusion is less reliable given that the dataset was relatively small (20 genes in the cortex relative to 135 genes in the hippocampus and 89 genes in the striatum).

Protein–protein interaction analysis of the hippocampal and striatal SynGO-DEGs revealed distinct PPI patterns (Figures 3D–F). The hippocampal Shank2-HM SynGO-DEGs formed a cluster of postsynaptic scaffolding/receptor genes, including *Shank2*, *Dlgap1* (SAPAP1/GKAP), *Dlg3* (encoding SAP102), *Gria1* (GluA1 subunit of AMPA receptors), *Camk2a/b* (calcium/calmodulin-dependent protein kinase IIα/β), and *Shisa6* (encoding an AMPA receptor auxiliary protein) (Figure 3E). With the exception of *Shank2*, these genes tended to be upregulated. Another notable cluster that is linked to the abovementioned cluster contained many genes encoding signaling proteins such as *Src* (Src proto-oncogene, non-receptor tyrosine), *Fyn* (Fyn proto-oncogene, Src family tyrosine kinase), *Mapk1* (mitogen-activated protein kinase 1), *Ppp2ca* (protein phosphatase 2 catalytic subunit alpha) as well as actin-related genes (*Abi1*, *Cyfip2*, *Actr2*, and *Arpc2*), which are mostly upregulated. A downregulated cluster that is largely independent from the abovementioned clusters contained genes encoding ribosomal subunit proteins (*Rpl* and *Rps*).

Protein–protein interaction analysis of the striatal Shank2-HM SynGO-DEGs revealed a cluster of genes, including *Shank2*, *Shank3*, *Dlgap3* (SAPAP3), *Nrxn3* (Neurexin 3), *Grin1* (GluN1 subunit of NMDARs), and *Grm5* (metabotropic glutamate receptor 5), which are downregulated. Unlike our findings in the hippocampus, there was no independent cluster of *Rpl* or *Rps* genes.

The results of our SynGO and PPI analyses of hippocampal and striatal Shank2-HM DEGs collectively suggest that hippocampal and striatal Shank2-HM DEGs are: (1) strongly enriched for SynGO genes, (2) differentially associated with distinct sets of synaptic genes.

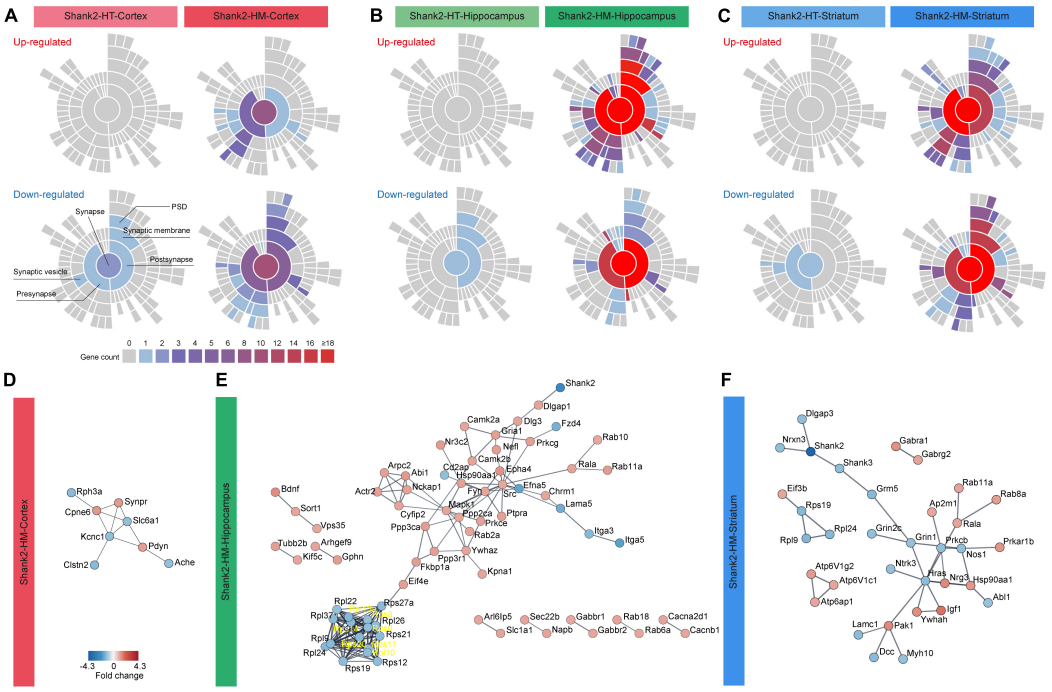

FIGURE 3
Synaptic gene ontologies (SynGO) and protein-protein interaction (PPI) analyses of Shank2-heterozygous (HT) and Shank2-homozygous (HM) differentially expressed genes (DEGs). **(A–C)** Sunburst plot visualization of the SynGO results, highlighting the extents of pre/postsynaptic functions in the up/downregulated DEGs belonging to SynGO genes (SynGO-DEGs) of cortical, hippocampal, and striatal regions of Shank2-HT and Shank2-HM mice [13 weeks; male; n = 5 mice wild-type (WT), 5 (HT), and 5 (HM)]. **(D–F)** PPI analysis of cortical, hippocampal, and striatal Shank2-HM SynGO-DEGs. Differential cutoff values were used for different brain regions to increase the visibility of the PPI clusters [medium confidence (0.400) for HM-Cortex and high confidence (0.900) for HM-hippocampus and HM-striatum]. Red and blue colors indicate up and down fold changes, respectively.

Biological functions derived from gene set enrichment analysis of Shank2-HT and Shank2-HM cortical transcripts

We next performed GSEA, wherein the whole set of transcripts is ranked by p-value and fold change with the goal of identifying biological functions that are influenced by many genes with moderate but coordinated transcriptional changes see footnote 4 (Mootha et al., 2003; Subramanian et al., 2005). This method avoids using an artificial and biased cutoff to identify a subset of transcripts for analysis, such as in DEG-based methods.

Our GSEA results indicated that the Shank2-HT cortical transcripts are positively enriched for gene sets associated with neuronal synapses, as indicated by the top five gene sets enriched among those in the cellular component (CC) domain of the C5 gene sets (currently, ∼15,000 gene sets) (**Figure 4A**, top and **Supplementary Table 3**). This synaptic upregulation was further supported when we clustered the enriched gene sets using EnrichmentMap Cytoscape App (**Figure 4A**, bottom), a program that visualizes the functional clustering of the enriched gene sets (Merico et al., 2010; Isserlin et al., 2014). The Shank2-HT cortical transcripts were negatively enriched for gene sets associated with ribosomal and mitochondrial functions, as supported by the top five enriched gene sets and gene-set clustering by EnrichmentMap Cytoscape App (**Figure 4A**).

The Shank2-HM cortical transcripts were positively enriched for gene sets associated with ribosomes and mitochondria (**Figure 4B**), which contrasts with the negative enrichments of Shank2-HT transcripts for ribosome/mitochondria functions. In addition, the Shank2-HM cortical transcripts were negatively enriched for gene sets associated with neuronal synapses (**Figure 4B**). GSEA against the gene sets in the biological process (BP) and molecular function (MF) domains of the C5 database yielded partly similar results for Shank2-HT/HM cortical transcripts; negative enrichments of Shank2-HT cortical transcripts for ribosome/mitochondria-related gene sets in the BP domain, and negative enrichments of Shank2-HM cortical transcripts for potassium channel-related gene sets in the MF domain (**Supplementary Figure 3**).

These results suggest that Shank2-HT and Shank2-HM cortical transcripts show gene dosage-dependent distinct transcriptomic patterns that are associated with synaptic

FIGURE 4
Biological functions derived from gene set enrichment analysis (GSEA) of Shank2-heterozygous (HT) and Shank2-homozygous (HM) cortical, hippocampal, and striatal transcripts. **(A–F)** GSEA results for Shank2-HT/HM cortical/hippocampal/striatal transcripts showing a list of the top five positively (red) and negatively (blue) enriched gene sets (top), and their integrated visualization generated using the Cytoscape App, EnrichmentMap (bottom). Only the results for C5-cellular component (CC) are shown here; those for C5-biological process (BP) and C5-molecular function (MF) are shown in **Supplementary Figures 3–5**. Note that only the top five gene sets are shown here (see **Supplementary Table 3** for full results). In the EnrichmentMap results, each circle in a cluster indicates a significantly [false discovery rate (FDR) < 0.05] enriched gene set; the circle sizes and colors (red/blue) indicate the gene-set size and positive/negative enrichment based on NES scores, respectively [$n = 5$ mice (Shank2-HT/HM cortex, hippocampus, and striatum)].

and ribosomal/mitochondrial functions and are largely opposite to each other.

Biological functions derived from GSEA of Shank2-HT and Shank2-HM hippocampal transcripts

Surprisingly, our GSEA results for the Shank2-HT hippocampal transcripts did not identify any significant positive enrichment, as indicated by the top five enriched gene sets and EnrichmentMap Cytoscape results (**Figure 4C** and **Supplementary Table 3**). However, the negative enrichments of Shank2-HT hippocampal transcripts were significant for gene sets associated with ribosomes and mitochondria, as supported by the top five enriched gene sets and EnrichmentMap Cytoscape results (**Figure 4C**).

The Shank2-HM hippocampal transcripts were positively enriched for gene sets associated with neuronal synapses and negatively enriched for gene sets associated with the neuronal extracellular matrix (ECM), ribosomes, and mitochondria (**Figure 4D**). GSEA against the gene sets in the BP and MF domains of the C5 database yielded partly similar results for Shank2-HT/HM hippocampal transcripts; negative enrichments of Shank2-HT hippocampal transcripts for ribosome/mitochondria-related gene sets in the BP domain, and positive enrichments of the Shank2-HM hippocampal transcripts for synapse-related gene sets in the BP domain (**Supplementary Figure 4**).

These results suggest that Shank2-HT and Shank2-HM hippocampal transcripts show transcriptomic changes that are different from each other and also distinct from those observed in the cortex. For example, the synaptic gene upregulation observed in the Shank2-HT cortex was absent from the Shank2-HT hippocampus but present in the Shank2-HM hippocampus.

Biological functions derived from GSEA analysis of Shank2-HT and Shank2-HM striatal transcripts

The GSEA results for the Shank2-HT striatal transcripts did not indicate any significant positive enrichment based on the top five enriched gene sets and EnrichmentMap Cytoscape results (**Figure 4E** and **Supplementary Table 3**). This was similar to the results obtained for Shank2-HT hippocampal transcripts. However, the Shank2-HT striatal transcripts were negatively and modestly enriched for gene sets associated with the ECM (**Figure 4E**).

The Shank2-HM striatal transcripts were positively enriched for gene sets associated with presynaptic genes (**Figure 4F**). In addition, the Shank2-HM striatal transcripts were negatively enriched for gene sets associated with neuronal ribosomes and mitochondria (**Figure 4F**). GSEA against the gene sets in the BP and MF domains of the C5 database yielded partly similar results for Shank2-HT/HM striatal transcripts; positive enrichments of Shank2-HM striatal transcripts for synapse-related gene sets and negative enrichments of the Shank2-HM striatal transcripts for ribosome/mitochondria-related gene sets in the BP domain (**Supplementary Figure 5**).

These results suggest that Shank2-HT and Shank2-HM striatal transcripts show transcriptomic changes that are distinct from each other and those observed in the cortex, but similar to those observed in the hippocampus. Notably, the enrichment patterns of the Shank2-HM striatal transcripts most closely resemble those of Shank2-HM hippocampal transcripts and Shank2-HT (not Shank2-HM) cortical transcripts.

ASD-related patterns in Shank2-HT and Shank2-HM transcripts

Previous reports described transcriptomic changes associated with ASD (Garbett et al., 2008; Voineagu et al., 2011; Gupta et al., 2014; Parikshak et al., 2016; Velmeshev et al., 2019) and identified ASD-related gene sets that are up- or downregulated in ASD. These include DEG Up Voineagu, Co-Exp Up M16 Voineagu, DEG Down Voineagu, and Co-Exp Down M12 Voineagu (from cortical samples of individuals ranging in age from 2 to 560 years) (Voineagu et al., 2011; Werling et al., 2016). The genes in these gene sets are summarized in **Supplementary Table 4**.

Human genetic studies on ASD have also yielded various ASD-risk gene sets, including SFARI genes (Abrahams et al., 2013),[6] FMRP targets (Darnell et al., 2011; Werling et al., 2016), DeNovoMissense (protein-disrupting or missense rare *de novo* variants) (Iossifov et al., 2014; Werling et al., 2016), DeNovoVariants (protein-disrupting rare *de novo* variants) (Iossifov et al., 2014; Werling et al., 2016), and AutismKB (Autism KnowledgeBase) (Xu et al., 2012; Yang et al., 2018; **Supplementary Table 4**). These genes are thought to be downregulated in ASD through mutations, including missense, nonsense, splice-site, frame-shift, and deletion mutations.

Here, we used GSEA to test whether these ASD-related and ASD-risk gene sets were enriched in the Shank2-HT and Shank2-HM transcripts. In our GSEA for the cortex, the Shank2-HT transcripts were negatively enriched for ASD-related gene sets that are upregulated in ASD, such as DEG Up Voineagu and Co-Exp Up M16 Voineagu and positively enriched for ASD-risk gene sets, including SFARI genes (all and high confidence), FMRP targets, DeNovoMissense, DeNovoVariants, and AutismKB (**Figure 5A** and **Supplementary Figure 6**). These

6 https://gene.sfari.org/

enrichment patterns are opposite to those observed in ASD (termed reverse-ASD patterns hereafter), and are likely to represent changes that arise to compensate for HT *Shank2* deletion.

In sharp contrast, Shank2-HM cortical transcripts were positively enriched for gene sets that are upregulated in ASD (DEG Up Voineagu and Co-Exp Up M16 Voineagu) and negatively enriched for gene sets that are downregulated in ASD (DEG Down Voineagu and Co-Exp Down M12 Voineagu) and for ASD-risk gene sets (SFARI genes, FMRP targets, DeNovoMissense, DeNovoVariants, and AutismKB) (**Figure 5A**). These patterns are similar to the transcriptomic changes occurring in ASD (termed ASD-like patterns hereafter).

The opposite changes in the enrichments of Shank2-HT and Shank2-HM cortical transcripts in two select gene sets [SFARI genes (all) and FMRP targets] were mediated by ∼50% of the genes in the two gene sets and were further supported by the small correlations of FC for co-up/down regulations (**Supplementary Figure 7**). The opposite changes in the SFARI genes, however, were weaker than those in FMRP target genes, as supported by the greater correlation coefficient (r^2 = 0.1899 vs. 0.0425) involving frequent co-up/down regulations of more strongly changed transcripts. Collectively, these results indicate that HT and HM *Shank2* deletions in the cortex lead to largely opposite ASD-related/risk transcriptomic changes.

In the hippocampus, Shank2-HT transcripts showed both ASD-like and reverse-ASD patterns: They were positively enriched for the Co-Exp Up M16 Voineagu gene set, negatively enriched for the DEG Down Voineagu and Co-Exp Down M12 Voineagu gene sets (ASD-like patterns), and positively enriched for some of the ASD-risk gene sets (reverse-ASD patterns) (**Figure 5A**). In contrast, Shank2-HM hippocampal transcripts showed strong reverse-ASD patterns: They were negatively enriched for DEG Up Voineagu and Co-Exp Up M16 Voineagu and positively enriched for DEG Down Voineagu, Co-Exp Down M12 Voineagu, and all of the ASD-risk gene sets. Therefore, the hippocampal Shank2-HT and Shank2-HM patterns were distinct and the Shank2-HM hippocampal pattern (reverse-ASD) was similar to the Shank2-HT cortical pattern but largely opposite the Shank2-HM cortical pattern.

In the striatum, Shank2-HT and Shank2-HM transcripts showed patterns similar to those observed in the hippocampus, in that the Shank2-HT striatal transcripts showed a mixed pattern and the Shank2-HM striatal transcripts showed a reverse-ASD pattern. However, the overall extents of these changes were weaker than those observed in the hippocampus (**Figure 5A**). These results collectively suggest that the hippocampal and striatal transcriptomic patterns are more similar to each other than they are to the cortical patterns in *Shank2*-mutant mice.

Cell-type-specific patterns in Shank2-HT and Shank2-HM transcripts

Cell-type-specific transcriptomic changes have been observed in ASD, including downregulation of neuron- and oligodendrocyte-related genes and upregulation of astrocyte- and microglia-related genes (Voineagu et al., 2011; Werling et al., 2016). We thus tested Shank2-HT and Shank2-HM transcripts for the cell-type-specific gene sets reported in previous studies (Albright and Gonzalez-Scarano, 2004; Cahoy et al., 2008; Kang et al., 2011; Zeisel et al., 2015; Werling et al., 2016; Velmeshev et al., 2019, 2020; **Supplementary Table 4**).

In the cortex, Shank2-HT transcripts were positively enriched for excitatory and inhibitory neuron-related gene sets as well as oligodendrocyte-related gene sets, as shown by enrichment patterns for single-cell-type gene sets (**Figures 5B,C**). In addition, Shank2-HT transcripts were negatively enriched for astrocyte- and microglia-related gene sets. These patterns were largely opposite those observed in ASD (reverse-ASD), and are in line with the abovementioned reverse-ASD patterns observed in our GSEA for ASD-related/risk gene sets (**Figure 5A**). In contrast, Shank2-HM cortical transcripts were overall negatively enriched for neuron (excitatory and inhibitory)- and oligodendrocyte-related gene sets and positively enriched for astrocyte- and microglia-related gene sets (**Figures 5B,C**), yielding a generally ASD-like pattern. These results from cell-type-specific gene set analyses suggest that an increase in the *Shank2* deletional dosage converts a reverse-ASD pattern to an ASD-like pattern, as seen for our GSEA results on ASD-related/risk gene sets (**Figure 5A**).

In the hippocampus, Shank2-HT transcripts displayed a mixed pattern (both ASD-like and reverse-ASD), as supported by largely negative enrichments for neuron-related gene sets, positive enrichments for oligodendrocyte-related gene sets, and moderate positive enrichments for astrocyte/microglia-related gene sets (**Figures 5B,C**). Shank2-HM transcripts showed a reverse-ASD pattern, but it was still mixed, displaying largely positive enrichments for neuron-related gene sets, negative enrichments for oligodendrocyte-related gene sets, and negative enrichments for astrocyte/microglia-related gene sets (**Figures 5B,C**). Therefore, unlike our observation in the cortex, an increase in the *Shank2* deletional dosage intensified the reverse-ASD pattern in the hippocampus.

In the striatum, Shank2-HT transcripts showed a reverse-ASD pattern with largely positive enrichments for neuron/oligodendrocyte-related gene sets and negative enrichments for astrocyte/microglia-related gene sets (**Figures 5B,C**). Shank2-HM transcripts showed a similar reverse-ASD pattern with positive enrichments for neuron/oligodendrocyte-related gene sets and a moderately negative enrichment for microglia-related genes (**Figures 5B,C**).

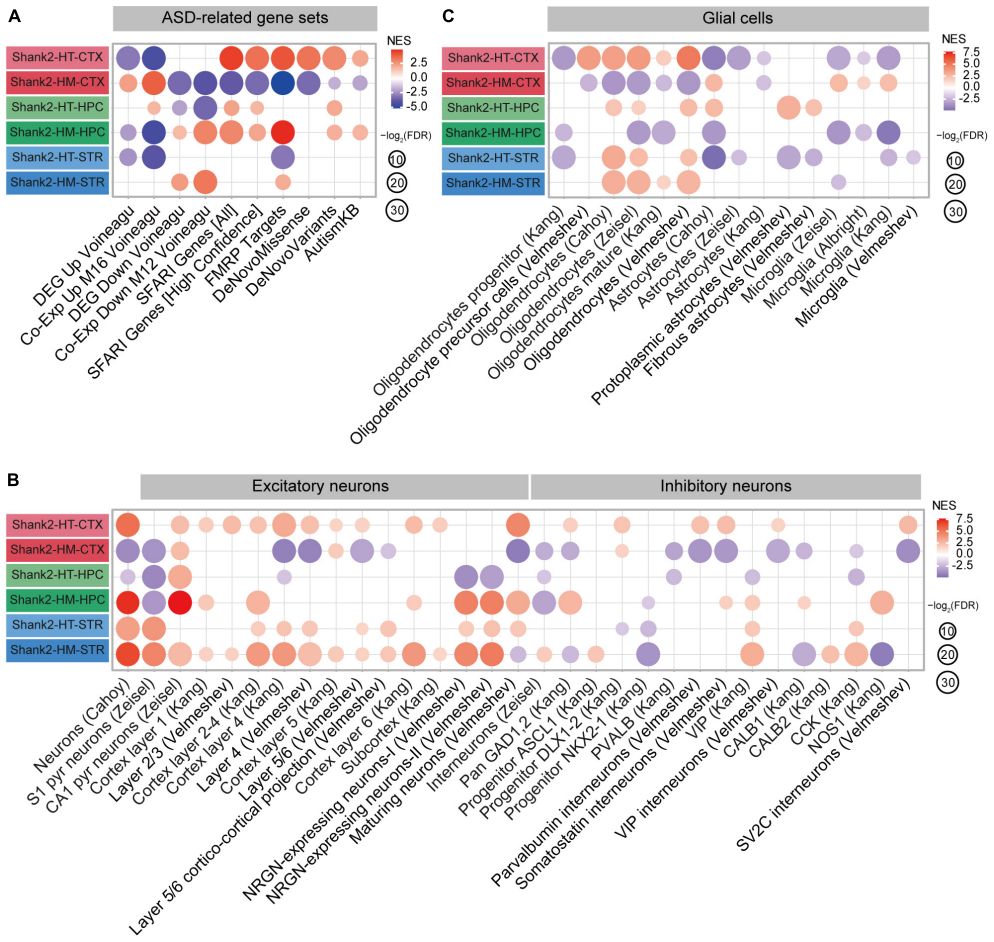

FIGURE 5
Autism spectrum disorder (ASD)-related patterns revealed by gene set enrichment analysis (GSEA) of Shank2-heterozygous (HT) and Shank2-homozygous (HM) cortical/hippocampal/striatal transcripts. **(A)** GSEA results for Shank2-HT/HM cortical/hippocampal/striatal transcripts, as shown by enrichment patterns for ASD-related gene sets that are upregulated in ASD (DEG Up Voineagu and Co-Exp Up M16 Voineagu) and downregulated in ASD (DEG Down Voineagu and Co-Exp Down M12 Voineagu) and ASD-risk gene sets [SFARI genes (all), SFARI genes (high confidence), FMRP targets, *DeNovo* Missense, *DeNovo* Variants, and AutismKB; n = 5 mice (Shank2-HT/HM cortex, hippocampus, and striatum)]. **(B)** GSEA results for Shank2-HT/HM cortical/hippocampal/striatal transcripts, as shown by enrichment patterns for cell-type-specific gene sets (glutamate and GABA neurons; n = 5 mice for Shank2-HT/HM cortex/hippocampus/striatum). **(C)** GSEA results for Shank2-HT/HM cortical/hippocampal/striatal transcripts, as shown by enrichment patterns for cell-type-specific gene sets (glial cells) [n = 5 mice (Shank2-HT/HM cortex, hippocampus, and striatum)].

Therefore, HT and HM *Shank2* deletion in the striatum lead to similar reverse-ASD patterns.

These results collectively suggest that HT and HM *Shank2* deletions lead to distinct gene dosage effects on ASD-related/risk gene expressions in the cortex and hippocampus but not in the striatum; increased *Shank2* deletional dosage intensifies the ASD-like pattern in the cortex, weakens it in the hippocampus, and has no effect on it in the striatum.

Discussion

Inthe current study, we investigated transcriptomic changes occurring in three different brain regions (prefrontal cortex, hippocampus, and striatum) of adult Shank2-HT/HM mice. The results indicate that there are brain region and gene dosage-differential transcriptomic changes associated with altered biological functions and ASD-related/risk gene expression patterns.

Transcriptomic changes in *Shank2*-mutant mice

The results of our DEG and DAVID analyses indicated that the hippocampal and striatal Shank2-HM DEGs are differentially associated with synapse- and neuronal

subregion/substructure-related functions (**Figures 1**, **2**). In addition, our SynGO and PPI analyses indicated that hippocampal and striatal Shank2-HM DEGs belonging to SynGO genes are differentially enriched for pre- and postsynaptic functions and form differential PPI networks (**Figure 3**). For instance, the hippocampal SynGO-DEGs formed a PPI cluster of mainly upregulated synaptic genes (with the exception of ribosome-related genes), whereas the striatal SynGO-DEGs formed a cluster of synaptic genes with mixed up and downregulations. Although additional details remain to be determined, these results suggest that different *Shank2*-mutant brain regions (hippocampus and striatum) respond to *Shank2* deletion by distinct up/downregulations and *via* different PPI networks of synaptic genes.

The DEG results also indicate that there are more DEGs in Shank2-HM transcripts compared to Shank2-HT transcripts, regardless of the brain region examined (**Figure 1**). Our previous study showed that Shank2-HT mice display largely normal behaviors, whereas Shank2-HM mice show strong autistic-like behaviors (Won et al., 2012). We therefore speculate that the greater numbers of DEGs in these three brain regions of Shank2-HM mice relative to Shank2-HT mice may collectively contribute to the mechanistic deviations that underlie the observed abnormal behaviors. An alternative and not mutually exclusive explanation could be that the greater numbers of DEGs in Shank2-HM transcripts relative to Shank2-HT transcripts may reflect that stronger compensatory transcriptomic responses are induced by a stronger mutation.

Gene set enrichment analysis of the cortical Shank2-HT transcripts showed a reverse-ASD pattern associated with increased synapse-related gene expression (**Figures 4**, **5**). In contrast, the Shank2-HM transcripts showed an ASD-like pattern associated with decreased synaptic gene expression. It is possible that the increased synaptic gene expression in Shank2-HT mice may be compensatory in nature and may underlie the largely normal behaviors seen in these mice, whereas the decreased synaptic gene expression in Shank2-HM mice associated with the ASD-like transcriptomic pattern may promote the behavioral abnormalities seen in these mice. In line with this hypothesis, Shank2-HM mice show impaired neuronal responses to social contexts in the medial prefrontal cortex (mPFC), which has been strongly implicated in ASD (Yizhar et al., 2011; Yan and Rein, 2021); this impairment involves decreased inhibition of target pyramidal neurons by parvalbumin-positive interneurons (Lee et al., 2021a).

When the current GSEA results for Shank2-HT and Shank2-HM cortical/prefrontal transcripts, covering wider areas of the prefrontal cortex including more caudal regions, are compared with the previous results for Shank2-HT and Shank2-HM mPFC transcripts (Lee et al., 2021b) for ASD-related/risk patterns, the reverse-ASD pattern of the current Shank2-HT (but not Shank2-HM showing ASD-like pattern) prefrontal transcripts are more similar to the previous results (reverse-ASD for both Shank2-HT and Shank2-HM mPFC transcripts). It might be possible that the mPFC region may be more resilient in inducing compensatory and reverse-ASD transcriptomic changes even in the presence of a strong HM *Shank2* deletion.

Gene set enrichment analysis of the hippocampal Shank2-HT transcripts revealed mixed ASD-like and reverse-ASD patterns associated with largely normal synapse-related gene expression levels. In contrast, the Shank2-HM transcripts showed a strong reverse-ASD pattern associated with increased synaptic and FMRP target gene expression levels, as well as increased excitatory neuronal gene expression and decreased glial (astrocytic and microglial) gene expression (**Figures 4**, **5**). Previous studies on adult Shank2-HM mice revealed the presence of impaired hippocampal synaptic functions that have been causally associated with behavioral deficits (Won et al., 2012; Lee et al., 2015b) and early postnatal NMDAR hyperfunction (Chung et al., 2019; Yoo et al., 2021). In addition, reduced hippocampal inhibitory synaptic transmission has been causally associated with impaired spatial memory in *Shank2*-mutant mice that lack exons 6–7 (Lim et al., 2017). It is therefore possible that the strong reverse-ASD pattern observed in Shank2-HM hippocampal transcripts, which was absent from Shank2-HT hippocampal transcripts, may represent compensatory changes that occur in response to a stronger *Shank2* deletion and but fail to fully rescue the hippocampal synaptic deficits. This sharply contrasts with the abovementioned hypothesis that the reverse-ASD patterns seen in the Shank2-HT cortex may represent transcriptomic changes that successfully contribute to normalizing behavioral phenotypes.

In the striatum, the Shank2-HT transcripts also showed mixed ASD-like and reverse-ASD patterns associated with largely normal synaptic gene expression levels. The Shank2-HM transcripts, however, showed a strong reverse-ASD pattern associated with increased synaptic and excitatory neuronal (both excitatory and inhibitory) gene expression levels (**Figures 4**, **5**). A notable difference between the Shank2-HM hippocampal and striatal transcripts is that the same reverse-ASD patterns seem to more strongly involve ASD-related/risk gene sets in the hippocampus but cell type-specific gene sets in the striatum, suggesting that there are distinct molecular/cellular and neuronal mechanisms.

In summary, our results indicate that *Shank2* deletion leads to brain region and gene dosage-differential transcriptomic changes associated with altered biological functions and ASD-related/risk gene expression patterns. These results provide unbiased clues on the mechanisms underlying the ASD-related phenotypes in *Shank2*-mutant mice and will be useful in designing future experiments using these mice and interpreting the results.

Data availability statement

The datasets presented in this study can be found in online repositories. The raw RNA-Seq results are available as GSE200439 (*Shank2* brain regions) at GEO (Gene Expression Omnibus), NCBI (National Center for Biotechnology Information).

Ethics statement

The animal study was reviewed and approved by the Committee of Animal Research at KAIST (KA2020-99).

Author contributions

Y-EY, TY, and EK designed the experiments. Y-EY, TY, and HK performed the RNA-seq analyses. HK and EK wrote the manuscript. All authors contributed to the article and approved the submitted version.

Funding

This work was supported by the Korea Institute of Science and Technology Information (K-19-L02-C07-S01 to HK) and the Institute for Basic Science (IBS-R002-D1 to EK).

Conflict of interest

The authors declare that the research was conducted in the absence of any commercial or financial relationships that could be construed as a potential conflict of interest.

Publisher's note

All claims expressed in this article are solely those of the authors and do not necessarily represent those of their affiliated organizations, or those of the publisher, the editors and the reviewers. Any product that may be evaluated in this article, or claim that may be made by its manufacturer, is not guaranteed or endorsed by the publisher.

Supplementary material

The Supplementary Material for this article can be found online at: https://www.frontiersin.org/articles/10.3389/fnmol.2022.977305/full#supplementary-material

SUPPLEMENTARY FIGURE 1
Clustering of three brain regional transcripts from Shank2-heterozygous (HT)/homozygous (HM) mice by heatmap analysis. Transcript groups from the three brain regions (cortex, hippocampus, and striatum) of Shank2-wild-type (WT), Shank2-HT, and Shank2-HM mice were analyzed by a heatmap analysis [13 weeks; male; n = 5 mice (WT), 5 (HT), and 5 (HM)].

SUPPLEMENTARY FIGURE 2
Small correlations of fold changes (FC) between the transcript groups from two different brain regions. **(A–C)** Correlograms of the FC of the transcripts from two brain regions, in which one group contains transcripts that are differentially expressed genes (DEGs) in one brain region but not in another brain region, indicate small correlation coefficients, except for the transcripts that are DEGs in both brain regions [n = 5 mice wild-type (WT), 5 heterozygous (HT), and 5 homozygous (HM), Pearson test].

SUPPLEMENTARY FIGURE 3
Biological functions derived from gene set enrichment analysis (GSEA) of Shank2-heterozygous (HT) and Shank2-homozygous (HM) cortical transcripts using gene sets in the C5-biological process (BP) and C5-molecular function (MF) domains. **(A–D)** GSEA results for Shank2-HT/HM cortical transcripts showing a list of the top five positively (red) and negatively (blue) enriched gene sets (top), and their integrated visualization generated using the Cytoscape App, EnrichmentMap (bottom). Note that only the top five gene sets are shown here (see **Supplementary Table 3** for full results). Circles in the EnrichmentMap results indicate significantly [false discovery rate (FDR) < 0.05] enriched individual gene sets, with circle sizes and colors (red/blue) indicating gene-set size and positive/negative enrichment based on normalized enrichment score (NES) scores, respectively [n = 5 mice (Shank2-HT/HM cortex)].

SUPPLEMENTARY FIGURE 4
Biological functions derived from gene set enrichment analysis (GSEA) of Shank2-heterozygous (HT) and Shank2-homozygous (HM) hippocampal transcripts using gene sets in the C5-biological process (BP) and C5-molecular function (MF) domains. **(A–D)** GSEA results for Shank2-HT/HM hippocampal transcripts showing a list of the top five positively (red) and negatively (blue) enriched gene sets (top), and their integrated visualization generated using the Cytoscape App, EnrichmentMap (bottom) [n = 5 mice (Shank2-HT/HM hippocampus)].

SUPPLEMENTARY FIGURE 5
Biological functions derived from gene set enrichment analysis (GSEA) of Shank2-heterozygous (HT) and Shank2-homozygous (HM) striatal transcripts using gene sets in the C5-biological process (BP) and C5-molecular function (MF) domains. **(A–D)** GSEA results for Shank2-HT/HM striatal transcripts showing a list of the top five positively (red) and negatively (blue) enriched gene sets (top), and their integrated visualization generated using the Cytoscape App, EnrichmentMap (bottom) [n = 5 mice (Shank2-HT/HM striatum)].

SUPPLEMENTARY FIGURE 6
Autism spectrum disorder (ASD)-related patterns revealed by gene set enrichment analysis (GSEA) of Shank2-heterozygous (HT) and Shank2-homozygous (HM) cortical/hippocampal/striatal transcripts. **(A–C)** GSEA results shown in **Figure 5** are shown here again with the indication of color-coded NES scores for insignificantly enriched gene sets in square dots, together with circular dots (significant enrichments). Note that the normalized enrichment score (NES) scores in the insignificant enrichments are smaller than those for significant enrichments [n = 5 mice (Shank2-HT/HM cortex, hippocampus, and striatum)].

SUPPLEMENTARY FIGURE 7
Analysis of individual gene expression patterns for opposite enrichments of Shank2-heterozygous (HT) and Shank2-homozygous (HM) cortical transcripts for two select autism spectrum disorder (ASD)-risk gene sets. **(A,B)** The opposite enrichments of Shank2-HT and Shank2-HM cortical transcripts for two select ASD-risk gene sets [SFARI genes (all) and FMRP targets] were mediated by a large portion (~50%) of the genes in the gene sets **(A)** and were further supported by the small correlations of the fold changes for co-up/down regulations **(B)** [n = 5 mice (Shank2-HT/HM cortex), Pearson test].

References

Abrahams, B. S., Arking, D. E., Campbell, D. B., Mefford, H. C., Morrow, E. M., Weiss, L. A., et al. (2013). SFARI Gene 2.0: a community-driven knowledgebase for the autism spectrum disorders (ASDs). *Mol. Autism* 4:36. doi: 10.1186/2040-2392-4-36

Albright, A. V., and Gonzalez-Scarano, F. (2004). Microarray analysis of activated mixed glial (microglia) and monocyte-derived macrophage gene expression. *J. Neuroimmunol.* 157, 27–38. doi: 10.1016/j.jneuroim.2004.09.007

Bagni, C., and Zukin, R. S. (2019). A synaptic perspective of fragile x syndrome and autism spectrum disorders. *Neuron* 101, 1070–1088. doi: 10.1016/j.neuron.2019.02.041

Bai, Y., Qiu, S., Li, Y., Li, Y., Zhong, W., Shi, M., et al. (2018). Genetic association between SHANK2 polymorphisms and susceptibility to autism spectrum disorder. *IUBMB Life* 70, 763–776. doi: 10.1002/iub.1876

Barnard, R. A., Pomaville, M. B., and O'Roak, B. J. (2015). Mutations and modeling of the chromatin remodeler CHD8 define an emerging autism etiology. *Front. Neurosci.* 9:477. doi: 10.3389/fnins.2015.00477

Basilico, B., Morandell, J., and Novarino, G. (2020). Molecular mechanisms for targeted ASD treatments. *Curr. Opin. Genet. Dev.* 65, 126–137. doi: 10.1016/j.gde.2020.06.004

Berkel, S., Marshall, C. R., Weiss, B., Howe, J., Roeth, R., Moog, U., et al. (2010). Mutations in the SHANK2 synaptic scaffolding gene in autism spectrum disorder and mental retardation. *Nat. Genet.* 42, 489–491.

Berkel, S., Tang, W., Trevino, M., Vogt, M., Obenhaus, H. A., Gass, P., et al. (2011). Inherited and de novo SHANK2 variants associated with autism spectrum disorder impair neuronal morphogenesis and physiology. *Hum. Mol. Genet.* 21, 344–357.

Boeckers, T. M., Bockmann, J., Kreutz, M. R., and Gundelfinger, E. D. (2002). ProSAP/Shank proteins - a family of higher order organizing molecules of the postsynaptic density with an emerging role in human neurological disease. *J. Neurochem.* 81, 903–910. doi: 10.1046/j.1471-4159.2002.00931.x

Boeckers, T. M., Kreutz, M. R., Winter, C., Zuschratter, W., Smalla, K. H., Sanmarti-Vila, L., et al. (1999). Proline-rich synapse-associated protein-1/cortactin binding protein 1 (ProSAP1/CortBP1) is a PDZ-domain protein highly enriched in the postsynaptic density. *J. Neurosci.* 19, 6506–6518.

Bourgeron, T. (2015). From the genetic architecture to synaptic plasticity in autism spectrum disorder. *Nat. Rev. Neurosci.* 16, 551–563. doi: 10.1038/nrn3992

Bowling, K. M., Thompson, M. L., Amaral, M. D., Finnila, C. R., Hiatt, S. M., Engel, K. L., et al. (2017). Genomic diagnosis for children with intellectual disability and/or developmental delay. *Genome Med.* 9:43. doi: 10.1186/s13073-017-0433-431

Cahoy, J. D., Emery, B., Kaushal, A., Foo, L. C., Zamanian, J. L., Christopherson, K. S., et al. (2008). A transcriptome database for astrocytes, neurons, and oligodendrocytes: a new resource for understanding brain development and function. *J. Neurosci.* 28, 264–278.

Callaghan, D. B., Rogic, S., Tan, P. P. C., Calli, K., Qiao, Y., Baldwin, R., et al. (2019). Whole genome sequencing and variant discovery in the ASPIRE autism spectrum disorder cohort. *Clin. Genet.* 96, 199–206. doi: 10.1111/cge.13556

Chen, S. T., Lai, W. J., Zhang, W. J., Chen, Q. P., Zhou, L. B., So, K. F., et al. (2020). Insulin-like growth factor 1 partially rescues early developmental defects caused by SHANK2 knockdown in human neurons. *Neural Regen. Res.* 15, 2335–2343. doi: 10.4103/1673-5374.285002

Chenbhanich, J., and So, J. (2022). An adult male with SHANK2 variant with epilepsy and obsessive-compulsive disorder: expanding the shankopathy phenotypic spectrum. *Clin. Genet.* 101, 472–473. doi: 10.1111/cge.14109

Chilian, B., Abdollahpour, H., Bierhals, T., Haltrich, I., Fekete, G., Nagel, I., et al. (2013). Dysfunction of SHANK2 and CHRNA7 in a patient with intellectual disability and language impairment supports genetic epistasis of the two loci. *Clin. Genet.* 84, 560–565. doi: 10.1111/cge.12105

Chung, C., Ha, S., Kang, H., Lee, J., Um, S. M., Yan, H., et al. (2019). Early Correction of N-Methyl-D-Aspartate receptor function improves autistic-like social behaviors in adult Shank2(-/-) mice. *Biol. Psychiatry* 85, 534–543.

Costas, J. (2015). The role of SHANK2 rare variants in schizophrenia susceptibility. *Mol. Psychiatry* 20:1486. doi: 10.1038/mp.2015.119

Daini, E., Hagmeyer, S., De Benedictis, C. A., Cristovao, J. S., Bodria, M., Ross, A. M., et al. (2021). S100B dysregulation during brain development affects synaptic SHANK protein networks via alteration of zinc homeostasis. *Transl. Psychiatry* 11:562. doi: 10.1038/s41398-021-01694-z

Darnell, J. C., Van Driesche, S. J., Zhang, C., Hung, K. Y., Mele, A., Fraser, C. E., et al. (2011). FMRP stalls ribosomal translocation on mRNAs linked to synaptic function and autism. *Cell* 146, 247–261. doi: 10.1016/j.cell.2011.06.013

de Chaumont, F., Ey, E., Torquet, N., Lagache, T., Dallongeville, S., Imbert, A., et al. (2019). Real-time analysis of the behaviour of groups of mice via a depth-sensing camera and machine learning. *Nat. Biomed. Eng.* 3, 930–942. doi: 10.1038/s41551-019-0396-1

Du, Y., Weed, S. A., Xiong, W. C., Marshall, T. D., and Parsons, J. T. (1998). Identification of a novel cortactin SH3 domain-binding protein and its localization to growth cones of cultured neurons. *Mol. Cell. Biol.* 18, 5838–5851. doi: 10.1128/MCB.18.10.5838

Eltokhi, A., Rappold, G., and Sprengel, R. (2018). Distinct phenotypes of Shank2 mouse models reflect neuropsychiatric spectrum disorders of human patients with SHANK2 variants. *Front. Mol. Neurosci.* 11:240. doi: 10.3389/fnmol.2018.00240

Ey, E., Bourgeron, T., Boeckers, T. M., Kim, E., and Han, K. (2020). Editorial: shankopathies: shank protein deficiency-induced synaptic diseases. *Front. Mol. Neurosci.* 13:11. doi: 10.3389/fnmol.2020.00011

Ey, E., Torquet, N., de Chaumont, F., Levi-Strauss, J., Ferhat, A. T., Le Sourd, A. M., et al. (2018). Shank2 mutant mice display hyperactivity insensitive to methylphenidate and reduced flexibility in social motivation, but normal social recognition. *Front. Mol. Neurosci.* 11:365. doi: 10.3389/fnmol.2018.00365

Ey, E., Torquet, N., Le Sourd, A. M., Leblond, C. S., Boeckers, T. M., Faure, P., et al. (2013). The Autism ProSAP1/Shank2 mouse model displays quantitative and structural abnormalities in ultrasonic vocalisations. *Behav. Brain Res.* 256, 677–689. doi: 10.1016/j.bbr.2013.08.031

Ferhat, A. T., Torquet, N., Le Sourd, A. M., de Chaumont, F., Olivo-Marin, J. C., Faure, P., et al. (2016). Recording mouse ultrasonic vocalizations to evaluate social communication. *J. Vis. Exp.* 53871. doi: 10.3791/53871

Garbett, K., Ebert, P. J., Mitchell, A., Lintas, C., Manzi, B., Mirnics, K., et al. (2008). Immune transcriptome alterations in the temporal cortex of subjects with autism. *Neurobiol. Dis.* 30, 303–311. doi: 10.1016/j.nbd.2008.01.012

Grabrucker, A. M., Schmeisser, M. J., Schoen, M., and Boeckers, T. M. (2011). Postsynaptic ProSAP/Shank scaffolds in the cross-hair of synaptopathies. *Trends Cell Biol.* 21, 594–603. doi: 10.1016/j.tcb.2011.07.003

Grabrucker, S., Pagano, J., Schweizer, J., Urrutia-Ruiz, C., Schon, M., Thome, K., et al. (2021). Activation of the medial preoptic area (MPOA) ameliorates loss of maternal behavior in a Shank2 mouse model for autism. *EMBO J.* 40:e104267. doi: 10.15252/embj.2019104267

Guilmatre, A., Huguet, G., Delorme, R., and Bourgeron, T. (2014). The emerging role of SHANK genes in neuropsychiatric disorders. *Dev. Neurobiol.* 74, 113–122. doi: 10.1002/dneu.22128

Guo, H., Wang, T., Wu, H., Long, M., Coe, B. P., Li, H., et al. (2018). Inherited and multiple de novo mutations in autism/developmental delay risk genes suggest a multifactorial model. *Mol. Autism* 9:64. doi: 10.1186/s13229-018-0247-z

Gupta, S., Ellis, S. E., Ashar, F. N., Moes, A., Bader, J. S., Zhan, J., et al. (2014). Transcriptome analysis reveals dysregulation of innate immune response genes and neuronal activity-dependent genes in autism. *Nat. Commun.* 5:5748. doi: 10.1038/ncomms6748

Ha, S., Lee, D., Cho, Y. S., Chung, C., Yoo, Y. E., Kim, J., et al. (2016). Cerebellar Shank2 regulates excitatory synapse density, motor coordination, and specific repetitive and anxiety-like behaviors. *J. Neurosci.* 36, 12129–12143. doi: 10.1523/JNEUROSCI.1849-16.2016

Han, K. A., Yoon, T. H., Shin, J., Um, J. W., and Ko, J. (2020). Differentially altered social dominance- and cooperative-like behaviors in Shank2- and Shank3-mutant mice. *Mol. Autism* 11:87. doi: 10.1186/s13229-020-00392-399

Heise, C., Preuss, J. M., Schroeder, J. C., Battaglia, C. R., Kolibius, J., Schmid, R., et al. (2018). Heterogeneity of cell surface glutamate and GABA receptor expression in shank and CNTN4 autism mouse models. *Front. Mol. Neurosci.* 11:212. doi: 10.3389/fnmol.2018.00212

Homann, O. R., Misura, K., Lamas, E., Sandrock, R. W., Nelson, P., McDonough, S. I., et al. (2016). Whole-genome sequencing in multiplex families with psychoses reveals mutations in the SHANK2 and SMARCA1 genes segregating with illness. *Mol. Psychiatry* 21, 1690–1695. doi: 10.1038/mp.2016.24

Horner, A. E., Norris, R. H., McLaren-Jones, R., Alexander, L., Komiyama, N. H., Grant, S. G. N., et al. (2021). Learning and reaction times in mouse touchscreen tests are differentially impacted by mutations in genes encoding postsynaptic interacting proteins SYNGAP1, NLGN3, DLGAP1, DLGAP2 and SHANK2. *Genes Brain Behav.* 20:e12723. doi: 10.1111/gbb.12723

Huang, D. W., Sherman, B. T., and Lempicki, R. A. (2009). Systematic and integrative analysis of large gene lists using DAVID bioinformatics resources. *Nat. Protoc.* 4, 44–57. doi: 10.1038/nprot.2008.211

Hulbert, S. W., and Jiang, Y. H. (2016). Monogenic mouse models of autism spectrum disorders: common mechanisms and missing links. *Neuroscience* 321, 3–23. doi: 10.1016/j.neuroscience.2015.12.040

Iossifov, I., O'Roak, B. J., Sanders, S. J., Ronemus, M., Krumm, N., Levy, D., et al. (2014). The contribution of de novo coding mutations to autism spectrum disorder. *Nature* 515, 216–221. doi: 10.1038/nature13908

Isserlin, R., Merico, D., Voisin, V., and Bader, G. D. (2014). Enrichment Map - a cytoscape app to visualize and explore OMICs pathway enrichment results. *F1000Research* 3:141. doi: 10.12688/f1000research.4536.1

Jiang, Y. H., and Ehlers, M. D. (2013). Modeling autism by SHANK gene mutations in mice. *Neuron* 78, 8–27. doi: 10.1016/j.neuron.2013.03.016

Jung, S., and Park, M. (2022). Shank postsynaptic scaffolding proteins in autism spectrum disorder: mouse models and their dysfunctions in behaviors, synapses, and molecules. *Pharmacol. Res.* 182:106340. doi: 10.1016/j.phrs.2022.106340

Kang, H. J., Kawasawa, Y. I., Cheng, F., Zhu, Y., Xu, X., Li, M., et al. (2011). Spatio-temporal transcriptome of the human brain. *Nature* 478, 483–489.

Kim, R., Kim, J., Chung, C., Ha, S., Lee, S., Lee, E., et al. (2018). Cell-Type-Specific Shank2 deletion in mice leads to differential synaptic and behavioral phenotypes. *J. Neurosci.* 38, 4076–4092. doi: 10.1523/JNEUROSCI.2684-17.2018

Ko, H. G., Oh, S. B., Zhuo, M., and Kaang, B. K. (2016). Reduced acute nociception and chronic pain in Shank2-/- mice. *Mol. Pain* 12:1744806916647056. doi: 10.1177/1744806916647056

Koopmans, F., van Nierop, P., Andres-Alonso, M., Byrnes, A., Cijsouw, T., Coba, M. P., et al. (2019). SynGO: an evidence-based, expert-curated knowledge base for the synapse. *Neuron* 103, 217–234.e4. doi: 10.1016/j.neuron.2019.05.002.

Krishnan, A., Zhang, R., Yao, V., Theesfeld, C. L., Wong, A. K., Tadych, A., et al. (2016). Genome-wide prediction and functional characterization of the genetic basis of autism spectrum disorder. *Nat. Neurosci.* 19, 1454–1462. doi: 10.1038/nn.4353

Leblond, C. S., Heinrich, J., Delorme, R., Proepper, C., Betancur, C., Huguet, G., et al. (2012). Genetic and functional analyses of SHANK2 mutations suggest a multiple hit model of autism spectrum disorders. *PLoS Genet.* 8:e1002521. doi: 10.1371/journal.pgen.1002521

Leblond, C. S., Nava, C., Polge, A., Gauthier, J., Huguet, G., Lumbroso, S., et al. (2014). Meta-analysis of SHANK mutations in autism spectrum disorders: a gradient of severity in cognitive impairments. *PLoS Genet.* 10:e1004580. doi: 10.1371/journal.pgen.1004580

Lee, E., Lee, J., and Kim, E. (2017). Excitation/Inhibition imbalance in animal models of autism spectrum disorders. *Biol. Psychiatry* 81, 838–847. doi: 10.1016/j.biopsych.2016.05.011

Lee, E., Lee, S., Shin, J. J., Choi, W., Chung, C., Lee, S., et al. (2021a). Excitatory synapses and gap junctions cooperate to improve Pv neuronal burst firing and cortical social cognition in Shank2-mutant mice. *Nat. Commun.* 12:5116. doi: 10.1038/s41467-021-25356-25352

Lee, S., Kang, H., Jung, H., Kim, E., and Lee, E. (2021b). Gene dosage- and age-dependent differential transcriptomic changes in the prefrontal cortex of Shank2-mutant mice. *Front. Mol. Neurosci.* 14:683196. doi: 10.3389/fnmol.2021.683196

Lee, E. J., Choi, S. Y., and Kim, E. (2015a). NMDA receptor dysfunction in autism spectrum disorders. *Curr. Opin. Pharmacol.* 20C, 8–13. doi: 10.1016/j.coph.2014.10.007

Lee, E. J., Lee, H., Huang, T. N., Chung, C., Shin, W., Kim, K., et al. (2015b). Trans-synaptic zinc mobilization improves social interaction in two mouse models of autism through NMDAR activation. *Nat. Commun.* 6:7168. doi: 10.1038/ncomms8168

Lee, S., Lee, E., Kim, R., Kim, J., Lee, S., Park, H., et al. (2018). Shank2 deletion in parvalbumin neurons leads to moderate hyperactivity, enhanced self-grooming and suppressed seizure susceptibility in mice. *Front. Mol. Neurosci.* 11:209. doi: 10.3389/fnmol.2018.00209

Lee, Y. S., Yu, N. K., Chun, J., Yang, J. E., Lim, C. S., Kim, H., et al. (2020). Identification of a novel Shank2 transcriptional variant in Shank2 knockout mouse model of autism spectrum disorder. *Mol. Brain* 13:54. doi: 10.1186/s13041-020-00595-594

Lim, C. S., Kim, H., Yu, N. K., Kang, S. J., Kim, T., Ko, H. G., et al. (2017). Enhancing inhibitory synaptic function reverses spatial memory deficits in Shank2 mutant mice. *Neuropharmacology* 112, 104–112. doi: 10.1016/j.neuropharm.2016.08.016

Lim, S., Naisbitt, S., Yoon, J., Hwang, J. I., Suh, P. G., Sheng, M., et al. (1999). Characterization of the shank family of synaptic proteins. multiple genes, alternative splicing, and differential expression in brain and development. *J. Biol. Chem.* 274, 29510–29518. doi: 10.1074/jbc.274.41.29510

Liu, Y., Du, Y., Liu, W., Yang, C., Liu, Y., Wang, H., et al. (2013). Lack of association between NLGN3, NLGN4, SHANK2 and SHANK3 gene variants and autism spectrum disorder in a Chinese population. *PLoS One* 8:e56639. doi: 10.1371/journal.pone.0056639

Love, M. I., Huber, W., and Anders, S. (2014). Moderated estimation of fold change and dispersion for RNA-seq data with DESeq2. *Genome Biol.* 15:550. doi: 10.1186/s13059-014-0550-558

Lu, Z. A., Mu, W., Osborne, L. M., and Cordner, Z. A. (2018). Eighteen-year-old man with autism, obsessive compulsive disorder and a SHANK2 variant presents with severe anorexia that responds to high-dose fluoxetine. *BMJ Case Rep.* 2018:bcr2018225119. doi: 10.1136/bcr-2018-225119

Lutz, A. K., Perez Arevalo, A., Ioannidis, V., Stirmlinger, N., Demestre, M., Delorme, R., et al. (2021). SHANK2 mutations result in dysregulation of the ERK1/2 pathway in human induced pluripotent stem cells-derived neurons and shank2(-/-) mice. *Front. Mol. Neurosci.* 14:773571. doi: 10.3389/fnmol.2021.773571

Ma, S. L., Chen, L. H., Lee, C. C., Lai, K. Y. C., Hung, S. F., Tang, C. P., et al. (2021). Genetic overlap between attention deficit/hyperactivity disorder and autism spectrum disorder in SHANK2 Gene. *Front. Neurosci.* 15:649588. doi: 10.3389/fnins.2021.649588

Merico, D., Isserlin, R., Stueker, O., Emili, A., and Bader, G. D. (2010). Enrichment map: a network-based method for gene-set enrichment visualization and interpretation. *PLoS One* 5:e13984. doi: 10.1371/journal.pone.0013984

Modi, M. E., Brooks, J. M., Guilmette, E. R., Beyna, M., Graf, R., Reim, D., et al. (2018). Hyperactivity and hypermotivation associated with increased striatal mGluR1 signaling in a Shank2 rat model of autism. *Front. Mol. Neurosci.* 11:107. doi: 10.3389/fnmol.2018.00107

Moffat, J. J., Smith, A. L., Jung, E. M., Ka, M., and Kim, W. Y. (2021). Neurobiology of ARID1B haploinsufficiency related to neurodevelopmental and psychiatric disorders. *Mol. Psychiatry* 27, 476–489. doi: 10.1038/s41380-021-01060-x

Monteiro, P., and Feng, G. (2017). SHANK proteins: roles at the synapse and in autism spectrum disorder. *Nat. Rev. Neurosci.* 18, 147–157. doi: 10.1038/nrn.2016.183

Mootha, V. K., Lindgren, C. M., Eriksson, K. F., Subramanian, A., Sihag, S., Lehar, J., et al. (2003). PGC-1alpha-responsive genes involved in oxidative phosphorylation are coordinately downregulated in human diabetes. *Nat. Genet.* 34, 267–273. doi: 10.1038/ng1180

Mossa, A., Giona, F., Pagano, J., Sala, C., and Verpelli, C. (2017). SHANK genes in autism: defining therapeutic targets. *Prog. Neuropsychopharmacol. Biol. Psychiatry* 84, 416–423. doi: 10.1016/j.pnpbp.2017.11.019

Mossa, A., Giona, F., Pagano, J., Sala, C., and Verpelli, C. (2018). SHANK genes in autism: defining therapeutic targets. *Prog. Neuropsychopharmacol. Biol. Psychiatry* 84, 416–423.

Naisbitt, S., Kim, E., Tu, J. C., Xiao, B., Sala, C., Valtschanoff, J., et al. (1999). Shank, a novel family of postsynaptic density proteins that binds to the NMDA receptor/PSD-95/GKAP complex and cortactin. *Neuron* 23, 569–582. doi: 10.1016/s0896-6273(00)80809-0

Nelson, S. B., and Valakh, V. (2015). Excitatory/Inhibitory balance and circuit homeostasis in autism spectrum disorders. *Neuron* 87, 684–698. doi: 10.1016/j.neuron.2015.07.033

Ohashi, K., Fukuhara, S., Miyachi, T., Asai, T., Imaeda, M., Goto, M., et al. (2021). Comprehensive genetic analysis of non-syndromic autism spectrum disorder in clinical settings. *J. Autism. Dev. Disord.* 51, 4655–4662. doi: 10.1007/s10803-021-04910-4913

Pappas, A. L., Bey, A. L., Wang, X., Rossi, M., Kim, Y. H., Yan, H., et al. (2017). Deficiency of Shank2 causes mania-like behavior that responds to mood stabilizers. *JCI Insight* 2:e92052. doi: 10.1172/jci.insight.92052

Parikshak, N. N., Luo, R., Zhang, A., Won, H., Lowe, J. K., Chandran, V., et al. (2013). Integrative functional genomic analyses implicate specific molecular pathways and circuits in autism. *Cell* 155, 1008–1021. doi: 10.1016/j.cell.2013.10.031

Parikshak, N. N., Swarup, V., Belgard, T. G., Irimia, M., Ramaswami, G., Gandal, M. J., et al. (2016). Genome-wide changes in lncRNA, splicing, and regional gene expression patterns in autism. *Nature* 540, 423–427. doi: 10.1038/nature20612

Patro, R., Duggal, G., Love, M. I., Irizarry, R. A., and Kingsford, C. (2017). Salmon provides fast and bias-aware quantification of transcript expression. *Nat. Methods* 14, 417–419. doi: 10.1038/nmeth.4197

Peter, S., Ten Brinke, M. M., Stedehouder, J., Reinelt, C. M., Wu, B., Zhou, H., et al. (2016). Dysfunctional cerebellar purkinje cells contribute to autism-like behaviour in Shank2-deficient mice. *Nat. Commun.* 7:12627. doi: 10.1038/ncomms12627

Peykov, S., Berkel, S., Degenhardt, F., Rietschel, M., Nothen, M. M., and Rappold, G. A. (2015a). Rare SHANK2 variants in schizophrenia. *Mol. Psychiatry* 20, 1487–1488. doi: 10.1038/mp.2015.122

Peykov, S., Berkel, S., Schoen, M., Weiss, K., Degenhardt, F., Strohmaier, J., et al. (2015b). Identification and functional characterization of rare SHANK2 variants in schizophrenia. *Mol. Psychiatry* 20, 1489–1498. doi: 10.1038/mp.2014.172

Pinto, D., Pagnamenta, A. T., Klei, L., Anney, R., Merico, D., Regan, R., et al. (2010). Functional impact of global rare copy number variation in autism spectrum disorders. *Nature* 466, 368–372.

Rauch, A., Wieczorek, D., Graf, E., Wieland, T., Endele, S., Schwarzmayr, T., et al. (2012). Range of genetic mutations associated with severe non-syndromic sporadic intellectual disability: an exome sequencing study. *Lancet* 380, 1674–1682. doi: 10.1016/S0140-6736(12)61480-9

Rein, B., and Yan, Z. (2020). 16p11.2 copy number variations and neurodevelopmental disorders. *Trends Neurosci.* 43, 886–901. doi: 10.1016/j.tins.2020.09.001

Sahin, M., and Sur, M. (2015). Genes, circuits, and precision therapies for autism and related neurodevelopmental disorders. *Science* 350:10.1126/science.aab3897 aab3897.

Sala, C., Vicidomini, C., Bigi, I., Mossa, A., and Verpelli, C. (2015). Shank synaptic scaffold proteins: keys to understanding the pathogenesis of autism and other synaptic disorders. *J. Neurochem.* 135, 849–858. doi: 10.1111/jnc.13232

Sanders, S. J., Murtha, M. T., Gupta, A. R., Murdoch, J. D., Raubeson, M. J., Willsey, A. J., et al. (2012). De novo mutations revealed by whole-exome sequencing are strongly associated with autism. *Nature* 485, 237–241.

Sato, M., Kawano, M., Mizuta, K., Islam, T., Lee, M. G., and Hayashi, Y. (2017). Hippocampus-Dependent goal localization by head-fixed mice in virtual reality. *eNeuro* 4:ENEURO.0369-16.2017. doi: 10.1523/ENEURO.0369-16.2017

Sato, M., Mizuta, K., Islam, T., Kawano, M., Sekine, Y., Takekawa, T., et al. (2020). Distinct mechanisms of over-representation of landmarks and rewards in the hippocampus. *Cell Rep.* 32:107864. doi: 10.1016/j.celrep.2020.107864

Satterstrom, F. K., Kosmicki, J. A., Wang, J., Breen, M. S., De Rubeis, S., An, J. Y., et al. (2020). Large-Scale exome sequencing study implicates both developmental and functional changes in the neurobiology of autism. *Cell* 180:568–584.e3. doi: 10.1016/j.cell.2019.12.036.

Schmeisser, M. J. (2015). Translational neurobiology in Shank mutant mice–model systems for neuropsychiatric disorders. *Ann. Anat.* 200, 115–117. doi: 10.1016/j.aanat.2015.03.006

Schmeisser, M. J., Ey, E., Wegener, S., Bockmann, J., Stempel, V., Kuebler, A., et al. (2012). Autistic-like behaviours and hyperactivity in mice lacking ProSAP1/Shank2. *Nature* 486, 256–260. doi: 10.1038/nature11015

Sheng, M., and Kim, E. (2000). The Shank family of scaffold proteins. *J. Cell Sci.* 113(Pt 11), 1851–1856.

Sheng, M., and Kim, E. (2011). The postsynaptic organization of synapses. *Cold Spring Harb. Perspect. Biol.* 3:a005678.

Soneson, C., Love, M. I., and Robinson, M. D. (2015). Differential analyses for RNA-seq: transcript-level estimates improve gene-level inferences. *F1000Research* 4:1521. doi: 10.12688/f1000research.7563.2

Subramanian, A., Tamayo, P., Mootha, V. K., Mukherjee, S., Ebert, B. L., Gillette, M. A., et al. (2005). Gene set enrichment analysis: a knowledge-based approach for interpreting genome-wide expression profiles. *Proc. Natl. Acad. Sci. U S A.* 102, 15545–15550. doi: 10.1073/pnas.0506580102

Takumi, T., Tamada, K., Hatanaka, F., Nakai, N., and Bolton, P. F. (2020). Behavioral neuroscience of autism. *Neurosci. Biobehav. Rev.* 110, 60–76. doi: 10.1016/j.neubiorev.2019.04.012

Trost, B., Engchuan, W., Nguyen, C. M., Thiruvahindrapuram, B., Dolzhenko, E., Backstrom, I., et al. (2020). Genome-wide detection of tandem DNA repeats that are expanded in autism. *Nature* 586, 80–86. doi: 10.1038/s41586-020-2579-z

Varghese, M., Keshav, N., Jacot-Descombes, S., Warda, T., Wicinski, B., Dickstein, D. L., et al. (2017). Autism spectrum disorder: neuropathology and animal models. *Acta Neuropathol.* 134, 537–566. doi: 10.1007/s00401-017-1736-1734

Velmeshev, D., Magistri, M., Mazza, E. M. C., Lally, P., Khoury, N., D'Elia, E. R., et al. (2020). Cell-Type-Specific analysis of molecular pathology in autism identifies common genes and pathways affected across neocortical regions. *Mol. Neurobiol.* 57, 2279–2289. doi: 10.1007/s12035-020-01879-1875

Velmeshev, D., Schirmer, L., Jung, D., Haeussler, M., Perez, Y., Mayer, S., et al. (2019). Single-cell genomics identifies cell type-specific molecular changes in autism. *Science* 364, 685–689. doi: 10.1126/science.aav8130

Voineagu, I., Wang, X., Johnston, P., Lowe, J. K., Tian, Y., Horvath, S., et al. (2011). Transcriptomic analysis of autistic brain reveals convergent molecular pathology. *Nature* 474, 380–384. doi: 10.1038/nature10110

Wahl, L., Punt, A. M., Arbab, T., Willuhn, I., Elgersma, Y., and Badura, A. (2022). A novel automated approach for improving standardization of the marble burying test enables quantification of burying bouts and activity characteristics. *eNeuro* 9:ENEURO.0446-21.2022. doi: 10.1523/ENEURO.0446-21.2022

Wang, T., Hoekzema, K., Vecchio, D., Wu, H., Sulovari, A., Coe, B. P., et al. (2020). Large-scale targeted sequencing identifies risk genes for neurodevelopmental disorders. *Nat. Commun.* 11:4932. doi: 10.1038/s41467-020-18723-y

Wegener, S., Buschler, A., Stempel, A. V., Kang, S. J., Lim, C. S., Kaang, B. K., et al. (2018). Defective synapse maturation and enhanced synaptic plasticity in Shank2 Deltaex7(-/-) mice. *eNeuro* 5:ENEURO.0398-17.2018. doi: 10.1523/ENEURO.0398-17.2018

Werling, D. M., Parikshak, N. N., and Geschwind, D. H. (2016). Gene expression in human brain implicates sexually dimorphic pathways in autism spectrum disorders. *Nat. Commun.* 7:10717. doi: 10.1038/ncomms10717

Winden, K. D., Ebrahimi-Fakhari, D., and Sahin, M. (2018). Abnormal mTOR activation in autism. *Annu. Rev. Neurosci.* 41, 1–23. doi: 10.1146/annurev-neuro-080317-61747

Won, H., Lee, H. R., Gee, H. Y., Mah, W., Kim, J. I., Lee, J., et al. (2012). Autistic-like social behaviour in Shank2-mutant mice improved by restoring NMDA receptor function. *Nature* 486, 261–265. doi: 10.1038/nature11208

Xu, L. M., Li, J. R., Huang, Y., Zhao, M., Tang, X., and Wei, L. (2012). AutismKB: an evidence-based knowledgebase of autism genetics. *Nucleic Acids Res.* 40, D1016–D1022. doi: 10.1093/nar/gkr1145

Yan, Z., and Rein, B. (2021). Mechanisms of synaptic transmission dysregulation in the prefrontal cortex: pathophysiological implications. *Mol. Psychiatry* 27, 445–465. doi: 10.1038/s41380-021-01092-3

Yang, C., Li, J., Wu, Q., Yang, X., Huang, A. Y., Zhang, J., et al. (2018). AutismKB 2.0: a knowledgebase for the genetic evidence of autism spectrum disorder. *Database (Oxford)* 2018:bay106. doi: 10.1093/database/bay106

Yizhar, O., Fenno, L. E., Prigge, M., Schneider, F., Davidson, T. J., O'Shea, D. J., et al. (2011). Neocortical excitation/inhibition balance in information processing and social dysfunction. *Nature* 477, 171–178. doi: 10.1038/nature10360

Yoo, J., Bakes, J., Bradley, C., Collingridge, G. L., and Kaang, B. K. (2014). Shank mutant mice as an animal model of autism. *Philos. Trans. R. Soc. Lond. B Biol. Sci.* 369:20130143. doi: 10.1098/rstb.2013.0143

Yoo, Y. E., Lee, S., Kim, W., Kim, H., Chung, C., Ha, S., et al. (2021). Early chronic memantine treatment-induced transcriptomic changes in wild-type and Shank2-Mutant mice. *Front. Mol. Neurosci.* 14:712576. doi: 10.3389/fnmol.2021.712576

Yoon, S. Y., Kwon, S. G., Kim, Y. H., Yeo, J. H., Ko, H. G., Roh, D. H., et al. (2017). A critical role of spinal Shank2 proteins in NMDA-induced pain hypersensitivity. *Mol. Pain* 13:1744806916688902. doi: 10.1177/1744806916688902

Yuen, R. K. C., Merico, D., Bookman, M., Howe, L. J., Thiruvahindrapuram, B., Patel, R. V., et al. (2017). Whole genome sequencing resource identifies 18 new candidate genes for autism spectrum disorder. *Nat. Neurosci.* 20, 602–611. doi: 10.1038/nn.4524

Zaslavsky, K., Zhang, W. B., McCready, F. P., Rodrigues, D. C., Deneault, E., Loo, C., et al. (2019). SHANK2 mutations associated with autism spectrum disorder cause hyperconnectivity of human neurons. *Nat. Neurosci.* 22, 556–564. doi: 10.1038/s41593-019-0365-368

Zeisel, A., Munoz-Manchado, A. B., Codeluppi, S., Lonnerberg, P., La Manno, G., Jureus, A., et al. (2015). Brain structure. cell types in the mouse cortex and hippocampus revealed by single-cell RNA-seq. *Science* 347, 1138–1142. doi: 10.1126/science.aaa1934

frontiers | Frontiers in Molecular Neuroscience

TYPE Review
PUBLISHED 20 October 2022
DOI 10.3389/fnmol.2022.1017144

Check for updates

OPEN ACCESS

EDITED BY
Michel J. Simonneau,
École Normale Supérieure
Paris-Saclay, France

REVIEWED BY
J. Peter H. Burbach,
University Medical Center Utrecht,
Netherlands
Davide Comoletti,
Victoria University of Wellington,
New Zealand

*CORRESPONDENCE
Frances St. George-Hyslop
f.stgeorge.hyslop@mail.utoronto.ca

SPECIALTY SECTION
This article was submitted to
Brain Disease Mechanisms,
a section of the journal
Frontiers in Molecular Neuroscience

RECEIVED 11 August 2022
ACCEPTED 20 September 2022
PUBLISHED 20 October 2022

CITATION
St. George-Hyslop F, Kivisild T and
Livesey FJ (2022) The role
of contactin-associated protein-like 2
in neurodevelopmental disease
and human cerebral cortex evolution.
Front. Mol. Neurosci. 15:1017144.
doi: 10.3389/fnmol.2022.1017144

COPYRIGHT
© 2022 St. George-Hyslop, Kivisild and
Livesey. This is an open-access article
distributed under the terms of the
Creative Commons Attribution License
(CC BY). The use, distribution or
reproduction in other forums is
permitted, provided the original
author(s) and the copyright owner(s)
are credited and that the original
publication in this journal is cited, in
accordance with accepted academic
practice. No use, distribution or
reproduction is permitted which does
not comply with these terms.

The role of contactin-associated protein-like 2 in neurodevelopmental disease and human cerebral cortex evolution

Frances St. George-Hyslop[1,2]*, Toomas Kivisild[3,4] and Frederick J. Livesey[1]

[1]Zayed Centre for Research Into Rare Disease in Children, UCL Great Ormond Street Institute of Child Health, University College London, London, United Kingdom, [2]Temerty Faculty of Medicine, University of Toronto, Toronto, ON, Canada, [3]Estonian Biocentre, Institute of Genomics, University of Tartu, Tartu, Estonia, [4]Department of Human Genetics, KU Leuven, Leuven, Belgium

The contactin-associated protein-like 2 *(CNTNAP2)* gene is associated with multiple neurodevelopmental disorders, including autism spectrum disorder (ASD), intellectual disability (ID), and specific language impairment (SLI). Experimental work has shown that *CNTNAP2* is important for neuronal development and synapse formation. There is also accumulating evidence for the differential use of *CNTNAP2* in the human cerebral cortex compared with other primates. Here, we review the current literature on *CNTNAP2*, including what is known about its expression, disease associations, and molecular/cellular functions. We also review the evidence for its role in human brain evolution, such as the presence of eight human accelerated regions (HARs) within the introns of the gene. While progress has been made in understanding the function(s) of *CNTNAP2*, more work is needed to clarify the precise mechanisms through which *CNTNAP2* acts. Such information will be crucial for developing effective treatments for *CNTNAP2* patients. It may also shed light on the longstanding question of what makes us human.

KEYWORDS

autism (ASD), neurodevelopmental disorders, cerebral cortex, genetics, *CNTNAP2*

Introduction

The contactin-associated protein-like 2 gene *(CNTNAP2)* is located at chromosome 7q35. *CNTNAP2* spans 2.3 Mb across 24 exons and is the one of the largest genes in the genome (**Figures 1A,B**; Rodenas-Cuadrado et al., 2014). Mutations in *CNTNAP2* have been linked to neurodevelopmental disorders like autism spectrum disorder (ASD), intellectual disability (ID), and specific language impairment (SLI). There is also growing evidence that the temporal and spatial expression of *CNTNAP2* during brain development in humans is different from other primates. The potential evolutionary

significance of *CNTNAP2* is further highlighted by the presence of eight human accelerated regions (HARs) in its introns. HARs are DNA sequences that are highly conserved across primates or mammals, but have an unexpectedly large number of human-specific nucleotide changes (see section "*What are HARs?*" for a full description) (Pollard et al., 2006; Prabhakar et al., 2006; Bird et al., 2007; Bush and Lahn, 2008; Lindblad-Toh et al., 2011). Given the association between *CNTNAP2* and human cognitive disorders, and the evidence for its potential role in human evolution, this review aims to synthesize clinical, experimental, and evolutionary data to understand *CNTNAP2* function and the biological consequences of its disruption.

The contactin-associated protein-like 2 protein

Contactin-associated protein-like 2 encodes the contactin-associated protein-like 2 (CASPR2) protein. CASPR2 is a single-pass transmembrane protein composed of 1,331 residues and with a mass of 138 kDa (Rodenas-Cuadrado et al., 2014). The protein contains eight extracellular, one transmembrane, and two intracellular subdomains (**Figure 1C**). CASPR2 belongs to the neurexin superfamily of transmembrane proteins, which are cell adhesion molecules involved in synapse formation and function. Several other CASPR proteins exist (CASPR1 – 5), however, these proteins have fewer disease associations than CASPR2 and there is less evidence for their involvement in human evolution. They also all share less than 50% sequence identity to CASPR2, implying that CASPR2 serves differing functions.

CASPR2 is highly conserved amongst mammals – for example, human and mouse amino acid sequences are 94% identical (Rodenas-Cuadrado et al., 2014). This conservation is even greater between humans and chimpanzees, with only 6/1,331 residues differing (99.5% identity). Comparisons with archaic humans show yet further conservation. Between both Denisovans and Neanderthals, only one amino acid difference is noted with modern humans. Residue 345 is a valine in *Homo sapiens* but isoleucine in the two other species. One other noteworthy difference exists: position 215 is an asparagine in humans and Denisovans, but in all other species (including Neanderthals) it is a Lysine. It is currently unclear whether either of these amino acid changes have had functional consequences. However, PolyPhen-2 predicts both 345-I and 215-N to be functionally neutral (Adzhubei et al., 2010).

Although the molecular function(s) of CASPR2 are not completely understood, it was first characterized in the axon initial segment (AIS) and juxtaparanodal regions of myelinated neurons in the peripheral nervous system (Poliak et al., 1999). At juxtaparanodes, CASPR2 forms a complex with the contactin-2 protein (CNTN2). CASPR2 also binds to contactin-1 (CNTN1), an interaction which may play a role in nerve myelination, but this is currently not well characterized (Rubio-Marrero et al., 2016). Conversely, the CASPR2-CNTN2 complex has been robustly demonstrated to be required for the clustering of voltage-gated K^+ channels, which function in the conduction of nerve impulses (Strauss et al., 2006). Several studies have reported that *Cntnap2* knockout mice have a significant reduction in the density of Kv1.2 potassium channels in cortical myelinated axons (Poliak et al., 2003; Scott et al., 2019). Scott et al. (2019) observed these changes correlated with an increase in excitatory transmission and increased probability of neurotransmitter release. However, given that *CNTNAP2* expression is high in development - at timepoints prior to nerve myelination - other developmental functions are also likely to exist. These include proposed roles in neurite outgrowth and in the formation of synaptic connections (both discussed later in this review).

Lastly, recent work has identified that synaptic potentiation triggers the N-terminal region of CASPR2 to be cleaved (Martín-de-Saavedra et al., 2022). This ecto-domain localizes extracellularly near synapses, and binds and activates the PMCA calcium extrusion pump. In other words, synaptic activity causes CASPR2 to promote calcium export from neurons, thereby suppressing excitability and network activity. A loss of CASPR2 could therefore lead to hyperexcitability by increasing intracellular calcium. This finding is especially noteworthy in light of the neuronal over-excitation frequently reported in the brains of autistic individuals (Rodenas-Cuadrado et al., 2016), and could relate to the seizures that commonly occur in individuals with *CNTNAP2* loss-of-function mutations. Accordingly, the levels of the cleaved CASPR2 N-terminus are reduced in the cerebral spinal fluid of individuals with ASD, which further supports this hypothesis (Martín-de-Saavedra et al., 2022).

Other proteins that interact with CASPR2 include the scaffolding protein PAR3 (Gao et al., 2020) and the serine protein kinase CASK (Gao et al., 2019). These interactions may be required for the correct localization of CASPR2 within developing neurons – either intracellularly or on the plasma membrane, respectively – as mis-localization of CASPR2 occurs with a loss of their binding (Gao et al., 2019, 2020). Immunoprecipitation experiments have also suggested CASPR2 binds intracellularly to ADAM22, LGI1, GPR37, and subunits of the Kv1.1 channel (KCNA1) (Poot, 2017). Extracellularly, CASPR2 binds to the scaffolding proteins DLG1 and DLG4. However, the precise functions of these interactions are not currently known.

Contactin-associated protein-like 2 expression in the human, primate, and rodent cortex

Although *CNTNAP2* was first described in the peripheral nervous system (Poliak et al., 1999), it is primarily expressed in the cerebral cortex (Bakkaloglu et al., 2008; Vernes et al., 2008).

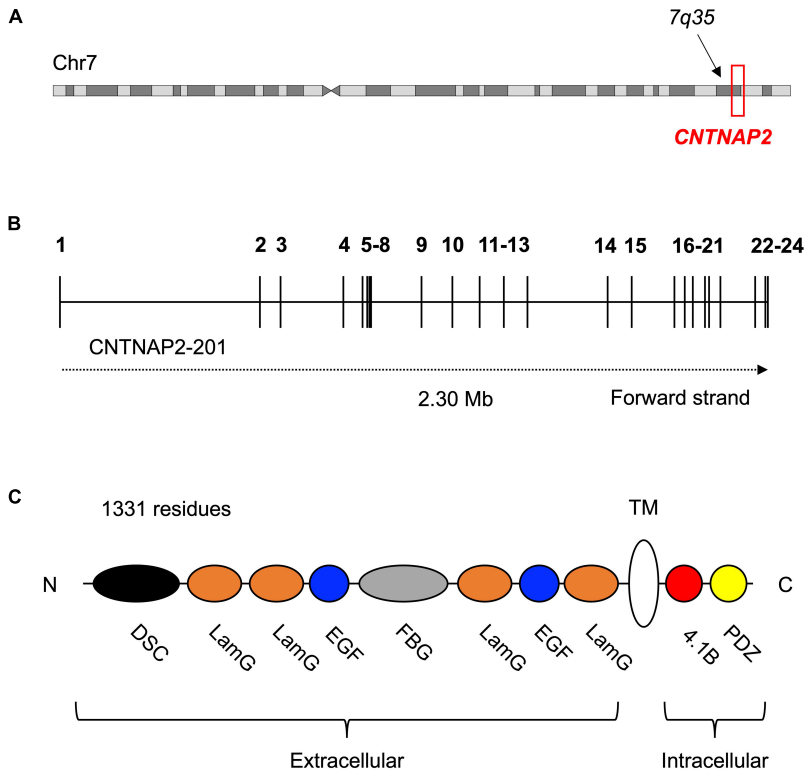

FIGURE 1
Location and structure of the contactin-associated protein-like 2 (*CNTNAP2*) gene and protein. **(A)** Contactin-associated protein-like 2 is located at the distal end of the long arm (q) of chromosome 7 (GRCh38 chr7: 146,116,002–148,420,998). **(B)** Schematic of the 24 exons (numbered) and 23 introns of the *CNTNAP2* gene. Transcript CNTNAP2-201 is the canonical transcript. **(C)** Structure of the contactin-associated protein-like 2 (CASPR2) protein and its eight extracellular, one transmembrane, and two intracellular subdomains. The extracellular subdomains include a discoidin domain (DSC) and a fibrinogen-like domain (FBG), both of which are known to facilitate cell-cell adhesion and interactions with the extracellular matrix. The remaining extracellular subdomains are four laminin-G domains (LamG) and two epidermal growth factor-like domains (EGF). These are predicted to mediate receptor-ligand interactions and cell adhesion, migration, and differentiation. The intracellular region of CASPR2 is mostly involved in protein-protein interactions, as it contains a type II PDZ domain (PDZ) and a protein 4.1B binding site (4.1B). N-terminus (N); C-terminus (C).

In adult humans, the highest expression is observed in layers II–V of the frontal and temporal cortices. Sub-cortically, *CNTNAP2* is also present in the thalamus, amygdala, and striatum. Interestingly, this pattern of expression is dramatically restricted to the cortico-striato-thalamic circuitry that mediates higher cognitive functions (Abrahams et al., 2007).

In the human fetal brain, *CNTNAP2* is expressed in the frontal and anterior temporal lobes, medial ganglionic eminence, striatum, and dorsal thalamus (Alarcon et al., 2008). This anterior cortical enrichment is not observed in rodents. In the developing mouse and rat cortex, *Cntnap2* is broadly expressed throughout the brain and is low or absent in the cortical plate (with highest expression – when present – located posteriorly) (Abrahams et al., 2007). Even in adulthood, *Cntnap2* is never enriched in the rodent frontal cortex, unlike in humans.

In addition to the differences in *CNTNAP2* expression between humans and rodents, differential expression has also been observed between humans and non-human primates. Recent single cell RNA-Seq (scRNA-Seq) data revealed *CNTNAP2* is significantly increased in the excitatory neurons of 2 month old cortical organoids derived from humans versus chimpanzees (Kanton et al., 2019). Increased expression in human organoids was also identified relative to macaque for both excitatory neurons and interneurons. *CNTNAP2* expression was also significantly higher in chimpanzee excitatory neurons than in macaque. These findings suggest that cortical *CNTNAP2* expression has increased along the lineage leading to humans.

Due to the limits on accessing primate fetal cortex, only one scRNA-Seq dataset of primary human and non-human primate developing brain currently exists (Pollen et al., 2019). This study includes matched samples from macaque (post-conception weeks 8–24) and human (post-conception weeks 4–40). In both deep and upper layer excitatory neurons, *CNTNAP2* is increased in human relative to macaque. However, neither remain significant after correction for multiple testing. As additional transcriptomic studies of human and non-human

primate fetal brain become available, this relationship can be tested further.

In primary adult cortex, scRNA-Seq of human, chimpanzee, and macaque does not show evidence of increased expression in humans. Indeed, in a study by Kanton et al. (2019) the only significant differences identified were decreases in human *CNTNAP2* expression. In chimpanzees, excitatory layer 6a neurons showed significantly increased *CNTNAP2* compared to human. In macaques, excitatory layers 1, 3e, and 6b as well as inhibitory layers 4b and 6b all had increased expression relative to human. The lack of increased human *CNTNAP2* expression in adulthood reinforces that a human-specific role for *CNTNAP2* is most likely occurring during cortical development.

It is important to note, however, that *CNTNAP2* has multiple protein-coding isoforms that cluster at the 3' end of the locus. As most scRNA-Seq technology only detects the 3' end of a transcript, the different isoforms cannot be distinguished. Thus, the above scRNA-seq expression data of *CNTNAP2* should be interpreted with this in mind.

Contactin-associated protein-like 2 mutations are linked to human neurodevelopmental disorders

Individuals with *CNTNAP2* loss-of-function mutations typically display four core phenotypes: (1) ID (Lu et al., 2021), (2) ASD (O'Roak et al., 2011), (3) SLI (Centanni et al., 2015), and (4) epilepsy (Friedman et al., 2008). Other disorders associated with *CNTNAP2* include schizophrenia (Lee et al., 2015), attention deficit hyperactivity disorder (ADHD) (Elia et al., 2010), Tourette syndrome (Verkerk et al., 2003), dyslexia (Veerappa et al., 2013), and major depression (Rodenas-Cuadrado et al., 2014). These illnesses have been identified in individuals with microdeletions or point mutations affecting only the *CNTNAP2* locus.

Homozygous loss-of-function mutations usually lead to a diagnosis of either cortical dysplasia focal epilepsy (CDFE) or Pitt-Hopkins syndrome (PTHS) (Zweier et al., 2009; Freri et al., 2021). Both disorders are characterized by uncontrollable seizures, language regression, social/behavioral disturbances, and intellectual disability (**Figure 2** and **Table 1**). Most *CNTNAP2* mutations are heterozygous, suggesting two functional copies of the gene are required for normal cognitive function (**Figure 3**). Homozygous mutations cause the most severe phenotypes and are often found in children of unaffected carrier parents (Strauss et al., 2006). This implies certain *CNTNAP2* mutations are fully penetrant while others are not.

In addition to the association between mutation homozygosity and disease severity, there are other lines of evidence suggesting *CNTNAP2* dosage is important for determining phenotype. Specifically, Nord et al. (2011) identified an autism patient with a 62 kb deletion in the *CNTNAP2* promoter region. This deletion was confirmed to reduce *CNTNAP2* gene expression in patient-derived lymphoblasts (versus those from healthy controls). A separate study from Chiocchetti et al. (2015) found a novel variant, g.-215G > A, associated with ASD and delayed age of first word. The variant also lies within the *CNTNAP2* promoter and was predicted to disrupt transcription factor binding sites. In a luciferase assay, the g.-215G > A variant was shown to significantly decrease enhancer potential in SH-SY5Y cells.

Intronic disease-causing mutations in *CNTNAP2* have also been discovered. Three unrelated patients with deletions in intron 1, which contains a regulatory element that binds with the FOXP2 transcription factor, displayed dysarthric language, autism, intellectual disability, bipolar disorder and/or ADHD (Rodenas-Cuadrado et al., 2014; Scala et al., 2021). Thus, changes in the expression level of the gene itself are sufficient to cause disorder and may explain the emergence of specific brain phenotypes.

Contactin-associated protein-like 2 may promote neurite development

Dendritic abnormalities have been noted in humans harboring *CNTNAP2* mutations. Post-mortem brain analyses of *CNTNAP2* patients with CDFE have identified neurons in the temporal cortex with irregularly oriented dendritic processes (Strauss et al., 2006). While no additional studies in human patients are available, there is strong evidence in mice to suggest *Cntnap2* is involved in neurite development and/or synaptic transmission.

Anderson et al. (2012) showed shRNA-mediated knockdown of CASPR2 in mouse cortical cultures decreased the length and branching of neurites in excitatory neurons. These effects caused a reduction in the amplitude and frequency of excitatory and inhibitory mini post-synaptic currents. Delivery of the CASPR2 shRNA with either lentivirus or calcium phosphate transfection – targeting all neurons or individual neurons, respectively – both produced the same results, suggesting the observed effects were cell-autonomous. No changes to dendritic spine density or synapse density were observed, however, the width of spine heads was significantly reduced.

A subsequent study by Canali et al. (2018) examined neuronal cultures from both homozygous and heterozygous knockout mice. Homozygous knockout neurons had significantly reduced axon lengths, while heterozygous neurons were intermediate to wild type and homozygous. Recent work by Elia et al. (2010) came to similar findings. They over-expressed *CNTNAP2* p.R777G, a mutation associated with intellectual disability and epilepsy, in mouse cortical neurons. Both neurite branching and neurite outgrowth were decreased

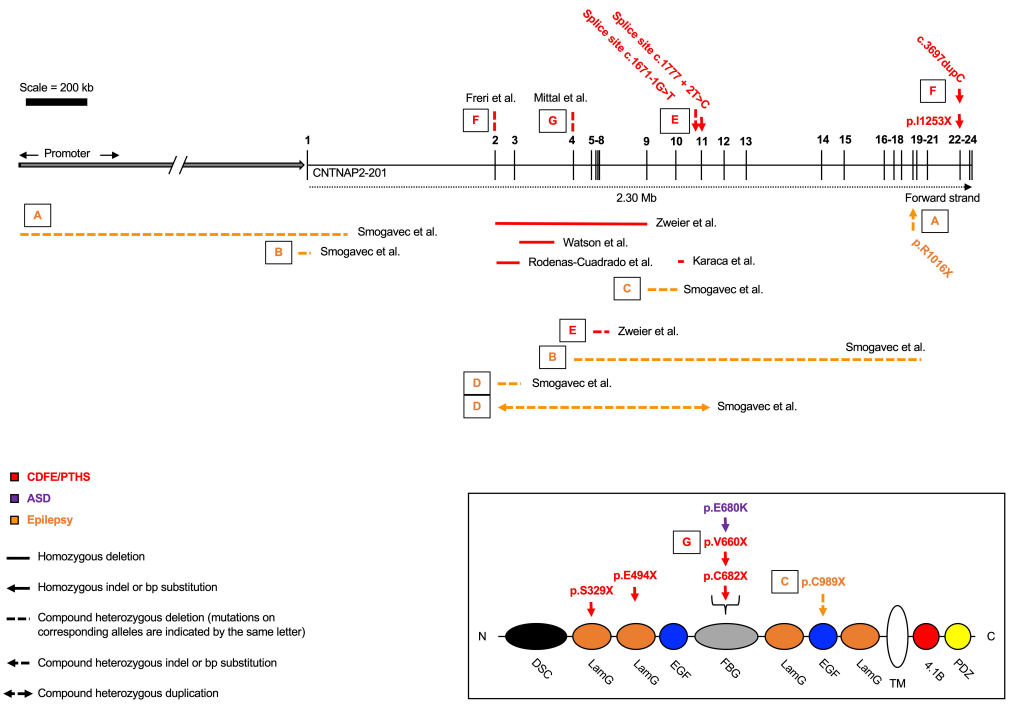

FIGURE 2
Homozygous and compound heterozygous contactin-associated protein-like 2 (*CNTNAP2*) mutations. Mutations affecting the *CNTNAP2* locus are shown with their associated disorders. Mutations are commonly found in the middle of the gene, between exons 2 – 13. Cortical dysplasia focal epilepsy/Pitt-Hopkins syndrome (CDFE/PTHS) are the most common diagnoses, though patients typically fall into multiple categories. Mutations that map to a subdomain of the contactin-associated protein-like 2 (CASPR2) protein are shown separately. Diagram not perfectly to scale. Works cited are listed in **Supplementary Material 1**. ASD, autism spectrum disorder.

in the mutant cultures. These neurons had reduced amplitude of spontaneous excitatory post-synaptic currents (EPSCs), in addition to decreased action potential firing. Such reductions in EPSC amplitude have also been reported by other groups (Fernandes et al., 2019; Kim et al., 2019; Lazaro et al., 2019; Sacai et al., 2020).

Finally, Gao et al. (2018) reported that *Cntnap2* is involved in neurite outgrowth, but only in cortical interneurons. The authors showed mature interneurons from *Cntnap2* knockout mice (*in vitro* and *in vivo*) had reduced dendritic branching and dendritic length. No phenotype was observed in excitatory neurons from the same knockout mice or cell cultures. Moreover, as no difference in branching or length was observed in immature neurons (in either inhibitory or excitatory cells), the authors concluded the reduction in branching was due to decreased neurite stabilization and not impaired outgrowth.

Contactin-associated protein-like 2 may modulate dendritic spine density

As well as the proposed role for *Cntnap2* in neurite branching and stabilization, several studies have suggested the gene may regulate dendritic spine dynamics. Gdalyahu et al. (2015) were the first to report a reduction in dendritic spine density in an *in vivo* study of Thy1-GFP/*Cntnap2* null mice. Using 2-photon microscopy, the authors showed knockout mice had significantly decreased spine density in cortical layer Vb. The reduction was caused by decreased stability of newly formed spines (i.e., loss of spines shortly after they form). No reduction in the formation of new spines was observed, nor was any effect on the maintenance or pruning of already-formed/stable spines. This suggests *CNTNAP2* may be required for the stabilization of new synaptic contacts, a process thought to be critical for brain plasticity (Gdalyahu et al., 2015).

Lazaro et al. (2019) added further evidence that loss of *Cntnap2* reduces dendritic spine density *in vivo*. The authors reported knockout mice had significantly decreased spine densities and synaptic inputs in layer II–III excitatory neurons. This resulted in a 2-fold decrease in the frequency and amplitude of mEPSCs. No differences in intrinsic neuronal excitability, neurotransmitter release probability, or synapse maturity were observed between genotypes. The knockout neurons did, however, have reduced network synchrony and less precise firing patterns.

Lastly, Varea et al. (2015) have also reported reductions in dendritic spine density in *in vitro* knockout cultures. The

TABLE 1 Homozygous contactin-associated protein-like 2 (*CNTNAP2*) mutations.

Mutation	L39X	del33-500	A156X	S329X	E494X	del1498-1671	c.1777 + 2T > C	C682X	I1253X
Mutation location and size	Exon 2–3; 203 kb	Exons 2–9; 1.15 Mb	Exon 3–intron 3; 76.8 kb	Exon 7; 1 bp (c.985delA)	Exon 9; 1 bp (c.1480G > T)	Exon 10; 173 bp	Exon 11–intron 11; 1 bp	Exon 13; 1 bp (c.2046C > A)	Exon 22; 1 bp (c.3709delG)
Mutation effect	Frameshift, premature stop	Loss of functional domains	Frameshift, premature stop	Frameshift, premature stop	Premature stop	Loss of exon 10	Splice site disruption	Premature stop	Frameshift, premature stop
No. of patients	2	2	2	1	1	2	1	2	9
Diagnosis	–	PTHS	–	–	–	–	–	–	CDFE
Patient sex	F, F	M, F	M, F	M	F	M, M	M	M, M	–
Parents	Healthy carriers	Healthy carriers	Healthy carriers	Healthy carriers	Healthy carriers	–	–	Healthy carriers	–
ID	Severe	Severe	Severe	Moderate	Severe	Severe	Severe	Severe	Severe
Speech	No	No	Simple (F), no (M)	No	No	–	–	No	Yes, with regression
Walking	–	Normal	Delayed (4 yrs.)	Delayed (30 mo.)	Delayed (2 yrs.)	–	–	No	Delayed (16–30 mo.)
Age of seizure onset	20–36 mo.	22–30 mo.	2 yrs.	14 mo.	2 yrs.	–	16 mo.	2 yrs.	14–20 mo.
Autistic features	Yes	No	–	Yes	Yes	–	–	Yes	Yes (67%)

Reported homozygous mutations affecting the *CNTNAP2* locus. All patients develop severe seizures in infancy, language impairment, and intellectual disability (ID). Double dashes indicate data was not reported. Source publications as follows: L39X = Rodenas-Cuadrado et al. (2016); del33-500 = Zweier et al. (2009); A156X = Watson et al. (2014); S329X = Riccardi et al. (2019); E494X = Smogavec et al. (2016); del1498-1671 = Karaca et al. (2015); c.1777 + 2T > C = Parrini et al. (2017); C682X = Smogavec et al. (2016); I1253X = Strauss et al. (2006), Jackman et al. (2009).

authors additionally observed reduced GluA1 AMPA receptor subunit expression in spines, and GluA1 cytoplasmic aggregates in cell bodies. These aggregates were found to contain trafficking proteins (e.g., clathrin and rab5), suggesting loss of *Cntnap2* could affect intracellular GluA1 transport. Two other papers reported similar reductions in glutamate receptor expression (Fernandes et al., 2019; Kim et al., 2019). More recent work identified that CASPR2 binds GluA1 through complexing with the protein CASK (Gao et al., 2019). Mutations in the gene encoding CASK have been linked to intellectual disability and ASD, which implies the pathway downstream of the CASPR2-CASK complex is important for disease pathophysiology (Becker et al., 2020).

Contactin-associated protein-like 2 and cortical interneurons

Contactin-associated protein-like 2 is robustly expressed in interneurons, and in the ganglionic eminence where interneurons derive from Peñagarikano et al. (2011); Gordon et al. (2016). Peñagarikano et al. (2011) described a loss of GABAergic interneurons in *Cntnap2* null mice. The authors noted a significant reduction in all cortical layers. Parvalbumin positive (PV^+) interneurons were the most affected (20% loss), while calretinin- (CALB2) and neuropeptide Y- (NPY) positive neurons were also significantly reduced. The loss of interneurons was hypothesized to underly the frequent seizures observed in *Cntnap2* null mice (as reported by others, see Hoffman et al., 2016; Thomas et al., 2017). *In vivo* 2-photon calcium imaging of layer II–III neurons revealed firing was highly asynchronous relative to wild type. The authors did not detect any changes to firing amplitude or frequency, suggesting the asynchronicity was not due to abnormal neuronal activity/conduction, but to defects in synaptic networks.

These findings were followed up by a study from Selimbeyoglu et al. (2017), who found that the PV^+ interneurons of *Cntnap2* knockout mice had significantly decreased activity *in vivo*. Activating PV^+ interneurons or inhibiting excitatory neurons rescued the observed excitation: inhibition imbalance. Finally, a recent study by Hali et al. (2020) reported significant reductions in the number of interneurons in cortical organoids derived from *Cntnap2* knockout mice. No differences in glutamatergic neurons were observed. The authors also noted knockout organoids had dramatically reduced expression of transcription factors expressed in ventral telencephalic (interneuron) progenitor cells (e.g., *Dlx2*, *Nkx2.1*, and *Ascl1*). Similar results have also been observed in a zebrafish *Cntnap2* knockout model (Hoffman et al., 2016) and in *Cntnap2* knockout mouse hippocampal neurons (Paterno et al., 2021).

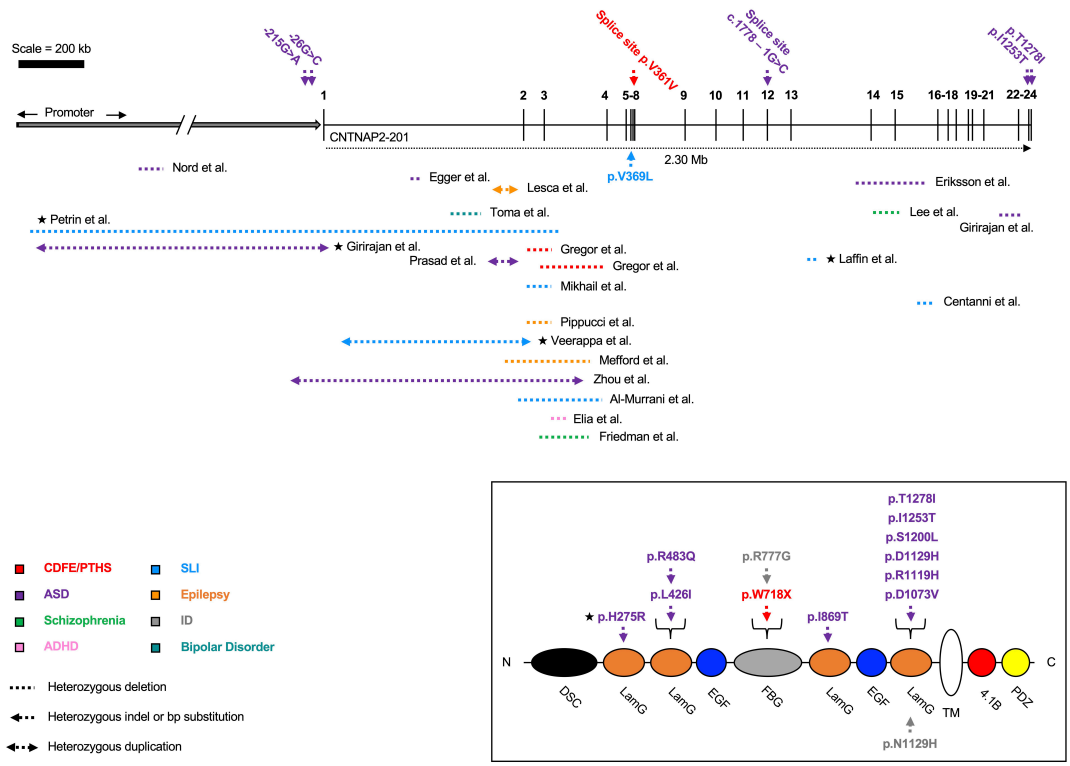

FIGURE 3
Heterozygous contactin-associated protein-like 2 (*CNTNAP2*) mutations. Mutations affecting the *CNTNAP2* locus are shown with their associated disorders. Mutations in patients with multiple affected genes are marked by a star (★). Autism spectrum disorder (ASD) is the most common diagnosis, though patients typically fall into multiple categories. The majority of deletions are found before exon 8. Mutations that map to a subdomain of the contactin-associated protein-like 2 (CASPR2) protein are shown separately. Diagram not perfectly to scale. Works cited are listed in **Supplementary Material 2**. CDFE/PTHS (cortical dysplasia focal epilepsy); ADHD (attention deficit hyperactivity disorder); SLI (specific language impairment); ID (intellectual disability).

Nucleotides 1-59

```
homo_sapiens              GAAGCTTATCCGCCAATTCACAATTCTGAAGCACAGCAAAGCTGTTTCTGTATTG-GTGT
pan_troglodytes           AAAGCTTATCTGCCAATTCACAATTCTCAAGCACAGCAAAGCTGTTTCTATATTG-GTGT
gorilla_gorilla           AAAGCTTATCCGCCAATTCACAATTCTCAAGCACAGCAAAGCTGTTTCTATATTG-GTGT
macaca_fascicularis       AAAGCTTATCTGCCAATTCACAATTCTCTAGCACAGCAAAGCTGTTTCTATATTG-GTGT
                           ********* ****************  ******************** ***** ****
```

Nucleotides 60-109

```
homo_sapiens              TAATTATTTATTAA--TGCAGTGAAAACACTTTAAATTCCTATTAAATTGTC
pan_troglodytes           TAATTATTTATTAA--TGCAGTGAAAACACTTTAAATTCCAATTAAATTGTC
gorilla_gorilla           TAATTATTTATTAA--TGCAGTGAAAACACTTTAAATTCCAATTAAATTGTC
macaca_fascicularis       TAATTATTTATTAA--TGCAGTGAAAACACTTTAAATACCAATTAAATTGTC
                          ************** ********************** ** ***********
```

FIGURE 4
Multiple species alignment of human accelerated conserved non-coding sequence 97 (HACNS_97) [109 bp HAR located within intron 1 of contactin-associated protein-like 2 (*CNTNAP2*)]. Human accelerated regions (HARs) are sequences of DNA that are highly conserved in non-human primates but have an unexpected number of unique nucleotide substitutions in humans. On average, a 100 bp-long HAR will contain ∼1.7 human-specific substitutions (HARs have a mean length of 266 bp). In contrast, chimpanzees (who carry the highly conserved ortholog), will have ∼0.2 unique substitutions. Even if a HAR gains only a small number of human-specific changes, this rate is significantly higher than observed in other conserved elements. Moreover, the regions surrounding HARs are usually still conserved, suggesting HARs may be part of a larger functional structure. Human Accelerated Conserved Non-coding Sequence 97 (HACNS_97) is shown as an example. HACNS_97 contains four nucleotides that are fixed in all humans but are absent in other primates (nucleotides highlighted in red and blue, respectively). *Pan troglodytes* = chimpanzee; *Gorilla gorilla* = western gorilla; *Macaca fascicularis* = crab-eating macaque.

Contactin-associated protein-like 2 and human evolution

What are human accelerated regions?

The sheer size of the human genome (approximately 3 billion nucleotides) poses a major challenge for identifying the genomic regions important for human evolution. In order to prioritize sequences for further study, Pollard et al. (2006) published a statistical test to find "HARs." As mentioned in the introduction of this paper, HARs are DNA sequences that fulfill two key criteria (see **Figure 4**; Pollard et al., 2006; Prabhakar et al., 2006; Bird et al., 2007; Bush and Lahn, 2008; Lindblad-Toh et al., 2011):

(i) They are highly conserved across a wider clade (e.g., primates, mammals, or vertebrates) – this suggests the region may be functional;
(ii) They have an unexpectedly large number of human-specific nucleotide changes – this suggests the sequence may be important for human evolution.

Approximately 4,000 HARs have been identified to date – ∼97% of them in non-coding portions of the genome (Capra et al., 2013; Uebbing et al., 2021). This distribution has made it difficult to assign HARs a function, because most of the non-coding genome is uncharacterized. Even so, there is growing evidence that many HARs are gene enhancers. For example, Capra et al. (2013) used existing functional genomics data, in combination with machine learning algorithms, to show that 60% of non-coding HARs overlap epigenetic enhancer marks like H3K4me1, H3K27ac, or p300. Half of these HARs were predicted to target genes active during development, and one third to act in the brain.

These predictions were supported by the finding that HARs are highly enriched in transcription factor binding motifs (Capra et al., 2013; Doan et al., 2016). ∼60% of HARs are also located within 1 Mb of a gene that is differentially expressed between humans and chimpanzees (Levchenko et al., 2018). While only a few HARs have been experimentally characterized (most using mouse enhancer assays), these studies have generally validated the predictions made by Capra et al. (2013) (Ryu et al., 2018; Girskis et al., 2021; Uebbing et al., 2021).

Contactin-associated protein-like 2 contains eight human accelerated regions

Contactin-associated protein-like 2 is unusual for containing eight HARs in its introns (**Table 2**):

1. HACNS_116[1] (Prabhakar et al., 2006);
2. HACNS_97 (Prabhakar et al., 2006);
3. 2xHAR.395 (Lindblad-Toh et al., 2011);
4. HACNS_884 (Prabhakar et al., 2006);
5. ANC1208[2] (Bird et al., 2007);
6. HACNS_590 (Prabhakar et al., 2006);
7. ANC1209 (Bird et al., 2007);
8. HACNS_954 (Prabhakar et al., 2006).

While this is likely related to the sheer size of the gene, the density of HARs is still higher than expected. Since *CNTNAP2* is 2.3 Mb long, one would expect only two to three HARs to fall within the gene (using the 4,000 HARs identified, and assuming that HARs are evenly distributed across the genome). From this perspective, eight HARs would be unexpectedly high.

Half of the *CNTNAP2* HARs are located in intron 1 – a common location for gene regulatory elements (Chorev and Carmel, 2012). The HARs range in length from 24 bp (2xHAR.395) to 510 bp (HACNS_954), and from 3 to 6 human-specific substitutions. Most of these human-specific changes are shared with Neanderthals and Denisovans, indicating they arose before the emergence of *Homo sapiens*. However, HACNS_97, ANC1209, ANC1209, and HACNS_954 each contain one substitution that is unique to modern humans alone (Burbano et al., 2012). Multiple species alignments for each *CNTNAP2* HAR can be found in **Figure 4** and **Supplementary Figures 1–7**.

Although HARs are a highly powerful tool, a number of caveats apply to their interpretation. These include the low reproducibility between studies that have used different methods to detect HARs, and the dependence on the size of human reference panels in defining which mutations are likely to be fixed in humans species-wide. Each of the *CNTNAP2* HARs was identified by only one of the six major HAR publications [excluding HACNS_884, which was identified by both Gittelman et al. (2015) and Prabhakar et al. (2006)]. Secondly, one of the HARs, HACNS_116, has a human-specific substitution that was subsequently found to be polymorphic (Hubisz and Pollard, 2014). All remaining HAR substitutions appear – according to currently available evidence – to be fixed in humans.

That said, there is some indication that one or more of the *CNTNAP2* HARs could be enhancers. HACNS_884 was shown by Gittelman et al. (2015) to overlap a human-specific DNase I hypersensitive site (DHS). DNase I selectively cleaves regions of open/active DNA, which is the expected chromatin state of regulatory elements (Dorschner et al., 2004). Won et al. (2019) further identified six of the eight HARs as overlapping DHSs in fetal brain (all except 2xHAR.395 and ANC1208). Similarly, Capra et al. (2013) detected HACNS_884 and HACNS_954 as putative enhancers using their enhancer finding pipeline. They were also able to bioinformatically predict

1 HACNS: human accelerated conserved non-coding sequence.

2 ANC: accelerated conserved non-coding sequence.

TABLE 2 Contactin-associated protein-like 2 (*CNTNAP2*) human accelerated regions (HARs).

HAR	Intron	Coordinates	Length (bp)	No. of human substitutions	No. polymorphic	No. shared with archaic humans	No. A/T to G/C
HACNS_116 (Prabhakar)	1	chr7: 146,214,973–146,215,168	196	5	1	5	2
HACNS_97 (Prabhakar)	1	chr7: 146,290,445–146,290,553	109	4	0	4	2
2xHAR.395 (Linblad-Toh)	1	chr7: 146,420,329–146,420,351	24	3	0	3	2
HACNS_884 (Prabhakar)	1	chr7: 146,654,063–146,654,409	347	5	0	5	3
ANC1208 (Bird)	11	chr7: 147,516,200–147,516,488	289	4	0	3	1
HACNS_590 (Prabhakar)	13	chr7: 147,859,118–147,859,418	301	4	0	4	1
ANC1209 (Bird)	13	chr7: 147,878,720–147,878,918	199	4	0	2	1
HACNS_954 (Prabhakar)	18	chr7: 148,173,396–148,173,905	510	6	0	6	3

Eight HARs lie within the *CNTNAP2* locus. Of these, four are located within intron 1 and two are located in intron 13. The number of human-specific nucleotide substitutions is shown in column 5, followed by the number of these substitutions that are polymorphic in humans (column 6), the number shared in Neanderthals/Denisovans (column 7), and the number of substitutions that are *G*/*C* in humans from *A*/*T* in other primates (i.e., weak to strong). The majority of *CNTNAP2* HARs appear to be composed of fixed substitutions that are shared with archaic humans. Between 1/4 and 1/2 are weak to strong transitions. Coordinates map to human genome GRCh38; original sources describing each HAR are shown in brackets. Data adapted from Hubisz and Pollard (2014).

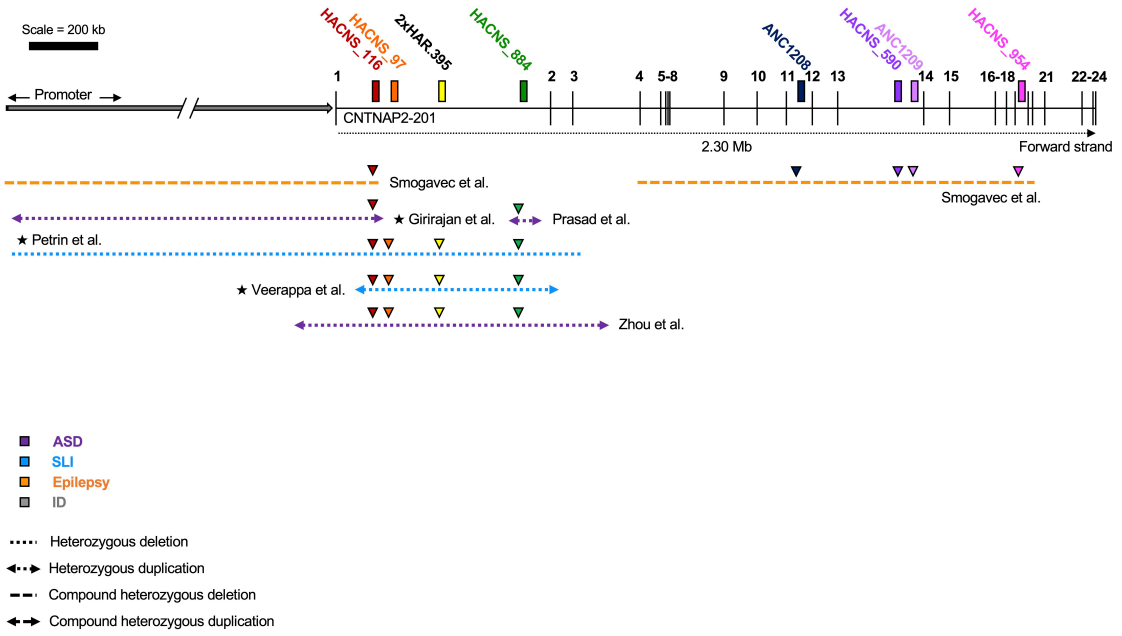

FIGURE 5
Overlap of human accelerated regions (HARs) and contactin-associated protein-like 2 (*CNTNAP2*) mutations. Disease-associated mutations that overlap one or more human accelerated region. Colored triangles indicate overlap: the color represents the specific HAR involved. Mutations in patients with multiple affected genes are marked by a star (★). HACNS_116 in intron 1 intersects the most mutations (five), while ANC1208, HACNS_590, ANC1209, and HACNS_954 all intersect the fewest (one mutation). ASD (autism spectrum disorder); SLI (specific language impairment); ID (intellectual disability). Diagram not perfectly to scale.

that HACNS_884 is active in fetal brain but could not provide a prediction for HACNS_954. More recently, Girskis et al. (2021) identified HACNS_116, HACNS_590, and ANC1209 as potential enhancers using a massively parallel reporter assay. Interestingly, HACNS_116 was found to have over 2x the enhancer activity as its chimpanzee ortholog.

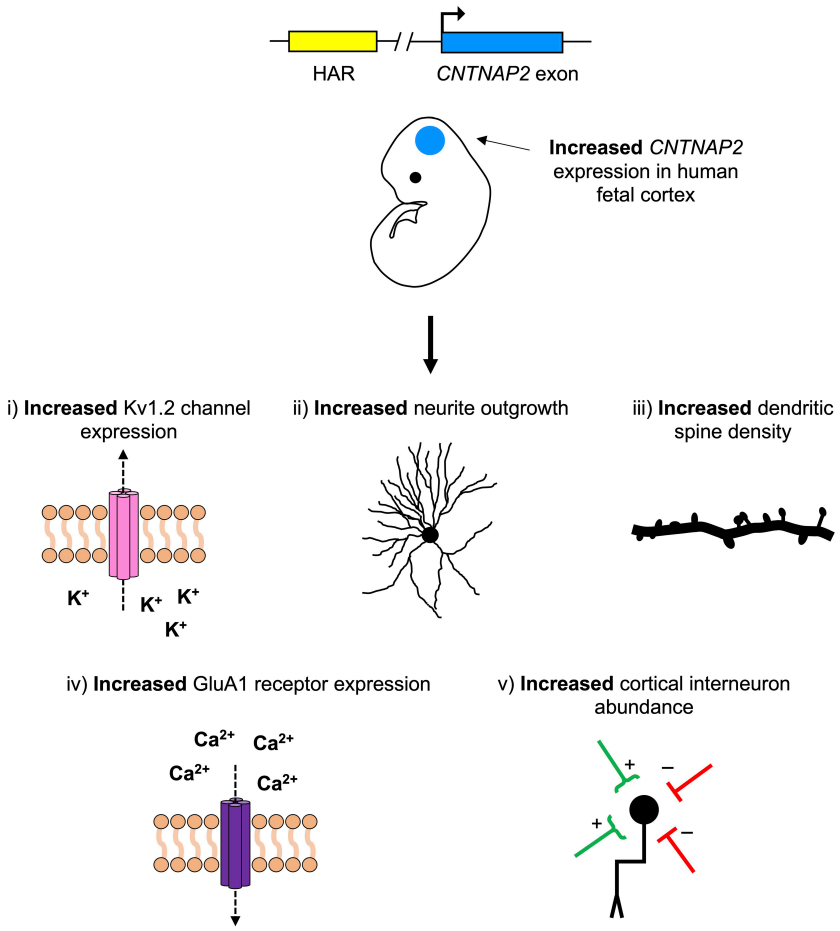

FIGURE 6
A hypothetical model for the role of contactin-associated protein-like 2 (*CNTNAP2*) in human neurodevelopmental disease and cerebral cortex evolution. Mutations that decrease *CNTNAP2* expression [e.g., nonsense mutations or those disrupting a human accelerated region (HAR)] cause reductions in (1) potassium channel (Kv1.2) expression, (2) neurite branching, (3) dendritic spine density, (4) glutamate receptor (GluA1) expression, and (5) cortical interneuron abundance. Since *CNTNAP2* has higher expression in the cortex of humans than in non-human primates, the opposite (i.e., increases in these features) may have contributed to differences in human versus non-human primate brain function. One (or more) of the *CNTNAP2* HARs may be driving this increase in expression by functioning as an enhancer with human-specific properties.

Also suggestive of their functional role is the fact that the *CNTNAP2* HARs overlap deletions associated with neurodevelopmental disorders, including ASD, SLI, ID, and epilepsy (**Figure 5**). Curiously, all of these disease-linked mutations are heterozygous (or compound heterozygous), which suggests that the loss of even a single copy of a HAR may be enough to affect brain function. However, there is no evidence to suggest directly that these mutations are pathogenic due to the loss of the HAR. This cannot be assumed, particularly because many of the mutations are large, and therefore not specific. Moreover, most of the mutations encompass multiple HARs, suggesting it could be a combinatorial loss of HAR function(s) that leads to disease. HACNS_116 overlaps the most pathogenic mutations (five in number), followed by HACNS_884 (four in number), and then HACNS_97 and 2xHAR.395 each with three.

Contactin-associated protein-like 2 contains signatures of positive selection in human populations

A "selective sweep" occurs when a positively selected variant rapidly increases in frequency, and nearby linked variants rise in frequency along with it (Jobling, 2014). This occurs as there is no time for recombination to break down the linkage between the selected and non-selected loci. In other words, sweeps cause genetic diversity in the region around the selected variant to decrease (Sabeti et al., 2006).

Evidence for selective sweeps have been identified at the *CNTNAP2* locus in humans (Ayub et al., 2013; Mozzi et al., 2016). Specifically, Ayub et al. (2013) detected sweep signatures in *CNTNAP2* introns 1 and 13. Since Neanderthals and Denisovans carry the ancestral sequences at these loci, this

suggests selection began after the split of modern humans from archaic hominins. The sweep signatures were identified in some but not all human populations, implying that selection occurred after the Out-of-Africa (OOA) dispersals. Introns 1 and 13 each contain several HARs: HACNS_116, HACNS_97, 2xHAR.395, and HACNS_884 in intron 1, and HACNS_590 and ANC1208 in intron 13. Notably, HACNS_97 coincides directly with one of the sweeps and may therefore be a target for further study.

Conclusion

Taken altogether, there are initial grounds to suggest *CNTNAP2* has played a role in the evolution of the human brain. There is also a strong body of literature linking mutations in *CNTNAP2* to neurodevelopmental disorders. Despite these advances, a number of unanswered questions remain about *CNTNAP2* function, and in particular, the mechanism(s) through which *CNTNAP2* acts.

One attractive hypothesis is that one or more of the *CNTNAP2* HARs are gene enhancers. These may be driving human-specific patterns of *CNTNAP2* expression in the developing cortex. In turn, this human-specific increase in *CNTNAP2* expression may have contributed to human brain function and increased human susceptibility to cognitive disorders. The studies summarized in this review suggest five mechanisms by which this may have occurred: increases in (1) potassium channel expression, (2) neurite development, (3) dendritic spine formation, (4) glutamate receptor expression, and/or (5) cortical interneuron abundance (**Figure 6**). Further experimentation is needed to clarify which of these mechanisms (if any) are at play, and which genes/pathways they involve.

Additionally, little experimental work has been conducted in human models, with most studies limited to either rodents or zebrafish. Human systems should be adopted for investigations into *CNTNAP2* function, including the use of stem cell-derived neurons and primary patient samples, where possible. Such studies will be invaluable for understanding the role of *CNTNAP2* in human-specific neurobiology, and in deciphering the downstream molecular events caused by human *CNTNAP2* mutations.

Author contributions

FS researched and wrote the manuscript under the supervision of FL and TK. All authors contributed to the article and approved the submitted version.

Funding

FL's group was supported by a Wellcome Trust Senior Investigator Award WT101052MA, Great Ormond Street Children's Charity (Stem Cell Professorship) and Alzheimer's Research UK (Stem Cell Research Center). FS was funded by the Canadian Centennial Scholarship Fund. This work was supported by the NIHR Great Ormond Street Biomedical Research Center.

Conflict of interest

The authors declare that the research was conducted in the absence of any commercial or financial relationships that could be construed as a potential conflict of interest.

Publisher's note

All claims expressed in this article are solely those of the authors and do not necessarily represent those of their affiliated organizations, or those of the publisher, the editors and the reviewers. Any product that may be evaluated in this article, or claim that may be made by its manufacturer, is not guaranteed or endorsed by the publisher.

Supplementary material

The Supplementary Material for this article can be found online at: https://www.frontiersin.org/articles/10.3389/fnmol.2022.1017144/full#supplementary-material

References

Abrahams, B. S., Tentler, D., Perederiy, J. V., Oldham, M. C., Coppola, G., and Geschwind, D. H. (2007). Genome-wide analyses of human perisylvian cerebral cortical patterning. *Proc. Natl. Acad. Sci. U.S.A.* 104, 17849–17854. doi: 10.1073/pnas.0706128104

Adzhubei, I. A., Schmidt, S., Peshkin, L., Ramensky, V. E., Gerasimova, A., Bork, P., et al. (2010). A method and server for predicting damaging missense mutations. *Nat. Methods* 7, 248–249.

Alarcon, M., Abrahams, B. S., Stone, J. L., Duvall, J. A., Perederiy, J. V., Bomar, J. M., et al. (2008). Linkage, association, and gene-expression analyses identify CNTNAP2 as an autism-susceptibility gene. *Am. J. Hum. Genet.* 82, 150–159. doi: 10.1016/j.ajhg.2007.09.005

Anderson, G. R., Galfin, T., Xu, W., Aoto, J., Malenka, R. C., and Sudhof, T. C. (2012). Candidate autism gene screen identifies critical role for cell-adhesion molecule CASPR2 in dendritic arborization and spine development. *Proc. Natl. Acad. Sci. U.S.A.* 109, 18120–18125. doi: 10.1073/pnas.1216398109

Ayub, Q., Yngvadottir, B., Chen, Y., Xue, Y., Hu, M., Vernes, S. C., et al. (2013). FOXP2 targets show evidence of positive selection in European populations. *Am. J. Hum. Genet.* 92, 696–706. doi: 10.1016/j.ajhg.2013.03.019

Bakkaloglu, B., O'Roak, B. J., Louvi, A., Gupta, A. R., Abelson, J. F., Morgan, T. M., et al. (2008). Molecular cytogenetic analysis and resequencing of contactin associated protein-like 2 in autism spectrum disorders. *Am. J. Hum. Genet.* 82, 165–173. doi: 10.1016/j.ajhg.2007.09.017

Becker, M., Mastropasqua, F., Reising, J. P., Maier, S., Ho, M. L., Rabkina, I., et al. (2020). Presynaptic dysfunction in CASK-related neurodevelopmental disorders. *Transl. Psychiatry* 10:312. doi: 10.1038/s41398-020-00994-0

Bird, C. P., Stranger, B. E., Liu, M., Thomas, D. J., Ingle, C. E., Beazley, C., et al. (2007). Fast-evolving noncoding sequences in the human genome. *Genome Biol.* 8:R118.

Burbano, H. A., Green, R. E., Maricic, T., Lalueza-Fox, C., de la Rasilla, M., Rosas, A., et al. (2012). Analysis of human accelerated DNA regions using archaic hominin genomes. *PLoS One* 7:e32877. doi: 10.1371/journal.pone.0032877

Bush, E. C., and Lahn, B. T. (2008). A genome-wide screen for noncoding elements important in primate evolution. *BMC Evol. Biol.* 8:17. doi: 10.1186/1471-2148-8-17

Canali, G., Garcia, M., Hivert, B., Pinatel, D., Goullancourt, A., Oguievetskaia, K., et al. (2018). Genetic variants in autism-related CNTNAP2 impair axonal growth of cortical neurons. *Hum. Mol. Genet.* 27, 1941–1954. doi: 10.1093/hmg/ddy102

Capra, J. A., Erwin, G. D., McKinsey, G., Rubenstein, J. L., and Pollard, K. S. (2013). Many human accelerated regions are developmental enhancers. *Philos. Trans. R Soc. Lond. B Biol. Sci.* 368:20130025.

Centanni, T. M., Sanmann, J. N., Green, J. R., Iuzzini-Seigel, J., Bartlett, C., Sanger, W. G., et al. (2015). The role of candidate-gene CNTNAP2 in childhood apraxia of speech and specific language impairment. *Am. J. Med. Genet. B Neuropsychiatr. Genet.* 168, 536–543. doi: 10.1002/ajmg.b.32325

Chiocchetti, A. G., Kopp, M., Waltes, R., Haslinger, D., Duketis, E., Jarczok, T. A., et al. (2015). Variants of the CNTNAP2 5' promoter as risk factors for autism spectrum disorders: A genetic and functional approach. *Mol. Psychiatry* 20, 839–849. doi: 10.1038/mp.2014.103

Chorev, M., and Carmel, L. (2012). The function of introns. *Front. Genet.* 3:55. doi: 10.3389/fgene.2012.00055

Doan, R. N., Bae, B. I., Cubelos, B., Chang, C., Hossain, A. A., Al-Saad, S., et al. (2016). Mutations in human accelerated regions disrupt cognition and social behavior. *Cell* 167, 341.e–354.e. doi: 10.1016/j.cell.2016.08.071

Dorschner, M. O., Hawrylycz, M., Humbert, R., Wallace, J. C., Shafer, A., Kawamoto, J., et al. (2004). High-throughput localization of functional elements by quantitative chromatin profiling. *Nat. Methods* 1, 219–225.

Elia, J., Gai, X., Xie, H. M., Perin, J. C., Geiger, E., Glessner, J. T., et al. (2010). Rare structural variants found in attention-deficit hyperactivity disorder are preferentially associated with neurodevelopmental genes. *Mol. Psychiatry* 15, 637–646. doi: 10.1038/mp.2009.57

Fernandes, D., Santos, S. D., Coutinho, E., Whitt, J. L., Beltrao, N., Rondao, T., et al. (2019). Disrupted AMPA receptor function upon genetic- or antibody-mediated loss of autism-associated CASPR2. *Cereb. Cortex* 29, 4919–4931.

Freri, E., Castellotti, B., Canafoglia, L., Ragona, F., Solazzi, R., Vannicola, C., et al. (2021). Severe epilepsy in CNTNAP2-related Pitt-Hopkins-like syndrome successfully treated with stiripentol. *Seizure* 88, 143–145. doi: 10.1016/j.seizure.2021.04.012

Friedman, J. I., Vrijenhoek, T., Markx, S., Janssen, I. M., van der Vliet, W. A., Faas, B. H., et al. (2008). CNTNAP2 gene dosage variation is associated with schizophrenia and epilepsy. *Mol. Psychiatry* 13, 261–266.

Gao, R., Piguel, N. H., Melendez-Zaidi, A. E., Martin-de-Saavedra, M. D., Yoon, S., Forrest, M. P., et al. (2018). CNTNAP2 stabilizes interneuron dendritic arbors through CASK. *Mol. Psychiatry* 23, 1832–1850.

Gao, R., Pratt, C. P., Yoon, S., Martin-de-Saavedra, M. D., Forrest, M. P., and Penzes, P. (2020). CNTNAP2 is targeted to endosomes by the polarity protein PAR3. *Eur. J. Neurosci.* 51, 1074–1086. doi: 10.1111/ejn.14620

Gao, R., Zaccard, C. R., Shapiro, L. P., Dionisio, L. E., Martin-de-Saavedra, M. D., Piguel, N. H., et al. (2019). The CNTNAP2-CASK complex modulates GluA1 subcellular distribution in interneurons. *Neurosci. Lett.* 701, 92–99. doi: 10.1016/j.neulet.2019.02.025

Gdalyahu, A., Lazaro, M., Penagarikano, O., Golshani, P., Trachtenberg, J. T., and Geschwind, D. H. (2015). The autism related protein contactin-associated protein-like 2 (CNTNAP2) stabilizes new spines: An in vivo mouse study. *PLoS One* 10:e0125633. doi: 10.1371/journal.pone.0125633

Girskis, K. M., Stergachis, A. B., DeGennaro, E. M., Doan, R. N., Qian, X., Johnson, M. B., et al. (2021). Rewiring of human neurodevelopmental gene regulatory programs by human accelerated regions. *Neuron* 109, 3239.e–3251.e. doi: 10.1016/j.neuron.2021.08.005

Gittelman, R. M., Hun, E., Ay, F., Madeoy, J., Pennacchio, L., Noble, W. S., et al. (2015). Comprehensive identification and analysis of human accelerated regulatory DNA. *Genome Res.* 25, 1245–1255.

Gordon, A., Salomon, D., Barak, N., Pen, Y., Tsoory, M., Kimchi, T., et al. (2016). Expression of Cntnap2 (Caspr2) in multiple levels of sensory systems. *Mol. Cell. Neurosci.* 70, 42–53. doi: 10.1016/j.mcn.2015.11.012

Hali, S., Kim, J., Kwak, T. H., Lee, H., Shin, C. Y., and Han, D. W. (2020). Modelling monogenic autism spectrum disorder using mouse cortical organoids. *Biochem. Biophys. Res. Commun.* 521, 164–171. doi: 10.1016/j.bbrc.2019.10.097

Hoffman, E. J., Turner, K. J., Fernandez, J. M., Cifuentes, D., Ghosh, M., Ijaz, S., et al. (2016). Estrogens suppress a behavioral phenotype in zebrafish mutants of the autism risk gene. CNTNAP2. *Neuron* 89, 725–733. doi: 10.1016/j.neuron.2015.12.039

Hubisz, M. J., and Pollard, K. S. (2014). Exploring the genesis and functions of human accelerated regions sheds light on their role in human evolution. *Curr. Opin. Genet. Dev.* 29, 15–21. doi: 10.1016/j.gde.2014.07.005

Jackman, C., Horn, N. D., Molleston, J. P., and Sokol, D. K. (2009). Gene associated with seizures, autism, and hepatomegaly in an Amish girl. *Pediatr. Neurol.* 40, 310–313.

Jobling, M. A. (2014). *Human evolutionary genetics*. New York, NY: Garland Science.

Kanton, S., Boyle, M. J., He, Z., Santel, M., Weigert, A., Sanchís-Calleja, F., et al. (2019). Organoid single-cell genomic atlas uncovers human-specific features of brain development. *Nature* 574, 418–422. doi: 10.1038/s41586-019-1654-9

Karaca, E., Harel, T., Pehlivan, D., Jhangiani, S. N., Gambin, T., Coban Akdemir, Z., et al. (2015). Genes that affect brain structure and function identified by rare variant analyses of mendelian neurologic disease. *Neuron* 88, 499–513.

Kim, J. W., Park, K., Kang, R. J., Gonzales, E. L. T., Kim, D. G., Oh, H. A., et al. (2019). Pharmacological modulation of AMPA receptor rescues social impairments in animal models of autism. *Neuropsychopharmacology* 44, 314–323.

Lazaro, M. T., Taxidis, J., Shuman, T., Bachmutsky, I., Ikrar, T., Santos, R., et al. (2019). Reduced prefrontal synaptic connectivity and disturbed oscillatory population dynamics in the CNTNAP2 model of autism. *Cell Rep.* 27, 2567.e–2578.e. doi: 10.1016/j.celrep.2019.05.006

Lee, I. S., Carvalho, C. M., Douvaras, P., Ho, S. M., Hartley, B. J., Zuccherato, L. W., et al. (2015). Characterization of molecular and cellular phenotypes associated with a heterozygous CNTNAP2 deletion using patient-derived hiPSC neural cells. *NPJ Schizophr.* 1:15019. doi: 10.1038/npjschz.2015.19

Levchenko, A., Kanapin, A., Samsonova, A., and Gainetdinov, R. R. (2018). Human accelerated regions and other human-specific sequence variations in the context of evolution and their relevance for brain development. *Genome Biol. Evol.* 10, 166–188. doi: 10.1093/gbe/evx240

Lindblad-Toh, K., Garber, M., Zuk, O., Lin, M. F., Parker, B. J., Washietl, S., et al. (2011). A high-resolution map of human evolutionary constraint using 29 mammals. *Nature* 478, 476–482. doi: 10.1038/nature10530

Lu, P., Wang, F., Zhou, S., Huang, X., Sun, H., Zhang, Y. W., et al. (2021). A Novel CNTNAP2 mutation results in abnormal neuronal E/I balance. *Front. Neurol.* 12:712773. doi: 10.3389/fneur.2021.712773

Martín-de-Saavedra, M. D., Dos Santos, M., Culotta, L., Varea, O., Spielman, B. P., Parnell, E., et al. (2022). Shed CNTNAP2 ectodomain is detectable in CSF and regulates Ca(2+) homeostasis and network synchrony via PMCA2/ATP2B2. *Neuron* 110, 627.e–643.e. doi: 10.1016/j.neuron.2021.11.025

Mozzi, A., Forni, D., Clerici, M., Pozzoli, U., Mascheretti, S., Guerini, F. R., et al. (2016). The evolutionary history of genes involved in spoken and written language: Beyond FOXP2. *Sci Rep.* 6:22157. doi: 10.1038/srep22157

Nord, A. S., Roeb, W., Dickel, D. E., Walsh, T., Kusenda, M., O'Connor, K. L., et al. (2011). Reduced transcript expression of genes affected by inherited and de novo CNVs in autism. *Eur. J. Hum. Genet.* 19, 727–731. doi: 10.1038/ejhg.2011.24

O'Roak, B. J., Deriziotis, P., Lee, C., Vives, L., Schwartz, J. J., Girirajan, S., et al. (2011). Exome sequencing in sporadic autism spectrum disorders identifies severe de novo mutations. *Nat Genet.* 43, 585–589.

Parrini, E., Marini, C., Mei, D., Galuppi, A., Cellini, E., Pucatti, D., et al. (2017). Diagnostic targeted resequencing in 349 patients with drug-resistant pediatric epilepsies identifies causative mutations in 30 different genes. *Hum. Mutat.* 38, 216–225.

Paterno, R., Marafiga, J. R., Ramsay, H., Li, T., Salvati, K. A., and Baraban, S. C. (2021). Hippocampal gamma and sharp-wave ripple oscillations are altered in a Cntnap2 mouse model of autism spectrum disorder. *Cell Rep.* 37:109970. doi: 10.1016/j.celrep.2021.109970

Peñagarikano, O., Abrahams, B. S., Herman, E. I., Winden, K. D., Gdalyahu, A., Dong, H., et al. (2011). Absence of CNTNAP2 leads to epilepsy, neuronal

migration abnormalities, and core autism-related deficits. *Cell* 147, 235–246. doi: 10.1016/j.cell.2011.08.040

Poliak, S., Gollan, L., Martinez, R., Custer, A., Einheber, S., Salzer, J. L., et al. (1999). Caspr2, a new member of the neurexin superfamily, is localized at the juxtaparanodes of myelinated axons and associates with K+ channels. *Neuron* 24, 1037–1047. doi: 10.1016/s0896-6273(00)81049-1

Poliak, S., Salomon, D., Elhanany, H., Sabanay, H., Kiernan, B., Pevny, L., et al. (2003). Juxtaparanodal clustering of Shaker-like K+ channels in myelinated axons depends on Caspr2 and TAG-1. *J Cell Biol.* 162, 1149–1160. doi: 10.1083/jcb.200305018

Pollard, K. S., Salama, S. R., King, B., Kern, A. D., Dreszer, T., Katzman, S., et al. (2006). Forces shaping the fastest evolving regions in the human genome. *PLoS Genet.* 2:e168. doi: 10.1371/journal.pgen.0020168

Pollen, A. A., Bhaduri, A., Andrews, M. G., Nowakowski, T. J., Meyerson, O. S., Mostajo-Radji, M. A., et al. (2019). Establishing cerebral organoids as models of human-specific brain evolution. *Cell* 176, 743.e–756.e.

Poot, M. (2017). Intragenic CNTNAP2 deletions: A bridge too far? *Mol. Syndromol.* 8, 118–130. doi: 10.1159/000456021

Prabhakar, S., Noonan, J. P., Paabo, S., and Rubin, E. M. (2006). Accelerated evolution of conserved noncoding sequences in humans. *Science* 314:786.

Riccardi, F., Urquhart, J., McCullagh, G., Lawrence, P., and Douzgou, S. A. (2019). patient with a novel CNTNAP2 homozygous variant: Further delineation of the CASPR2 deficiency syndrome and review of the literature. *Clin. Dysmorphol.* 28, 66–70.

Rodenas-Cuadrado, P., Ho, J., and Vernes, S. C. (2014). Shining a light on CNTNAP2: Complex functions to complex disorders. *Eur. J. Hum. Genet.* 22, 171–178. doi: 10.1038/ejhg.2013.100

Rodenas-Cuadrado, P., Pietrafusa, N., Francavilla, T., La Neve, A., Striano, P., and Vernes, S. C. (2016). Characterisation of CASPR2 deficiency disorder–a syndrome involving autism, epilepsy and language impairment. *BMC Med. Genet.* 17:8. doi: 10.1186/s12881-016-0272-8

Rubio-Marrero, E. N., Vincelli, G., Jeffries, C. M., Shaikh, T. R., Pakos, I. S., Ranaivoson, F. M., et al. (2016). Structural characterization of the extracellular domain of CASPR2 and insights into its association with the novel ligand contactin1. *J. Biol. Chem.* 291, 5788–5802. doi: 10.1074/jbc.M115.705681

Ryu, H., Inoue, F., Whalen, S., Williams, A., Kircher, M., Martin, B., et al. (2018). Massively parallel dissection of human accelerated regions in human and chimpanzee neural progenitors. *bioRxiv* [Preprint]. doi: 10.1101/256313

Sabeti, P. C., Schaffner, S. F., Fry, B., Lohmueller, J., Varilly, P., Shamovsky, O., et al. (2006). Positive natural selection in the human lineage. *Science* 312, 1614–1620.

Sacai, H., Sakoori, K., Konno, K., Nagahama, K., Suzuki, H., Watanabe, T., et al. (2020). Autism spectrum disorder-like behavior caused by reduced excitatory synaptic transmission in pyramidal neurons of mouse prefrontal cortex. *Nat. Commun.* 11:5140. doi: 10.1038/s41467-020-18861-3

Scala, M., Anijs, M., Battini, R., Madia, F., Capra, V., Scudieri, P., et al. (2021). Hyperkinetic stereotyped movements in a boy with biallelic CNTNAP2 variants. *Ital. J. Pediatr.* 47:208. doi: 10.1186/s13052-021-01162-w

Scott, R., Sanchez-Aguilera, A., van Elst, K., Lim, L., Dehorter, N., Bae, S. E., et al. (2019). Loss of Cntnap2 causes axonal excitability deficits. Developmental Delay in cortical myelination, and abnormal stereotyped motor behavior. *Cereb Cortex* 29, 586–597. doi: 10.1093/cercor/bhx341

Selimbeyoglu, A., Kim, C. K., Inoue, M., Lee, S. Y., Hong, A. S. O., Kauvar, I., et al. (2017). Modulation of prefrontal cortex excitation/inhibition balance rescues social behavior in CNTNAP2-deficient mice. *Sci. Transl. Med.* 9:eaah6733. doi: 10.1126/scitranslmed.aah6733

Smogavec, M., Cleall, A., Hoyer, J., Lederer, D., Nassogne, M. C., Palmer, E. E., et al. (2016). Eight further individuals with intellectual disability and epilepsy carrying bi-allelic CNTNAP2 aberrations allow delineation of the mutational and phenotypic spectrum. *J. Med. Genet.* 53, 820–827.

Strauss, K. A., Puffenberger, E. G., Huentelman, M. J., Gottlieb, S., Dobrin, S. E., Parod, J. M., et al. (2006). Recessive symptomatic focal epilepsy and mutant contactin-associated protein-like 2. *N. Engl. J. Med.* 354, 1370–1377. doi: 10.1056/NEJMoa052773

Thomas, A. M., Schwartz, M. D., Saxe, M. D., and Kilduff, T. S. (2017). Cntnap2 knockout rats and mice exhibit epileptiform activity and abnormal sleep-wake physiology. *Sleep* 40. *P. doi: 10.1093/sleep/zsw026

Uebbing, S., Gockley, J., Reilly, S. K., Kocher, A. A., Geller, E., Gandotra, N., et al. (2021). Massively parallel discovery of human-specific substitutions that alter enhancer activity. *Proc. Natl. Acad. Sci. U.S.A.* 118:e2007049118.

Varea, O., Martin-de-Saavedra, M. D., Kopeikina, K. J., Schurmann, B., Fleming, H. J., Fawcett-Patel, J. M., et al. (2015). Synaptic abnormalities and cytoplasmic glutamate receptor aggregates in contactin associated protein-like 2/Caspr2 knockout neurons. *Proc. Natl. Acad. Sci. U.S.A.* 112, 6176–6181. doi: 10.1073/pnas.1423205112

Veerappa, A. M., Saldanha, M., Padakannaya, P., and Ramachandra, N. B. (2013). Family-based genome-wide copy number scan identifies five new genes of dyslexia involved in dendritic spinal plasticity. *J. Hum. Genet.* 58, 539–547. doi: 10.1038/jhg.2013.47

Verkerk, A. J., Mathews, C. A., Joosse, M., Eussen, B. H., Heutink, P., and Oostra, B. A. (2003). CNTNAP2 is disrupted in a family with Gilles de la Tourette syndrome and obsessive compulsive disorder. *Genomics* 82, 1–9. doi: 10.1016/s0888-7543(03)00097-1

Vernes, S. C., Newbury, D. F., Abrahams, B. S., Winchester, L., Nicod, J., Groszer, M., et al. (2008). A functional genetic link between distinct developmental language disorders. *N. Engl. J. Med.* 359, 2337–2345.

Watson, C. M., Crinnion, L. A., Tzika, A., Mills, A., Coates, A., Pendlebury, M., et al. (2014). Diagnostic whole genome sequencing and split-read mapping for nucleotide resolution breakpoint identification in CNTNAP2 deficiency syndrome. *Am. J. Med. Genet. A* 164a, 2649–2655.

Won, H., Huang, J., Opland, C. K., Hartl, C. L., and Geschwind, D. H. (2019). Human evolved regulatory elements modulate genes involved in cortical expansion and neurodevelopmental disease susceptibility. *Nat. Commun.* 10:2396. doi: 10.1038/s41467-019-10248-3

Zweier, C., de Jong, E. K., Zweier, M., Orrico, A., Ousager, L. B., Collins, A. L., et al. (2009). CNTNAP2 and NRXN1 are mutated in autosomal-recessive Pitt-Hopkins-like mental retardation and determine the level of a common synaptic protein in Drosophila. *Am. J. Hum. Genet.* 85, 655–666. doi: 10.1016/j.ajhg.2009.10.004

Frontiers in
Molecular Neuroscience

Leading research into the brain's molecular structure, design and function

Part of the most cited neuroscience series, this journal explores and identifies key molecules underlying the structure, design and function of the brain across all levels.

Discover the latest Research Topics

See more →

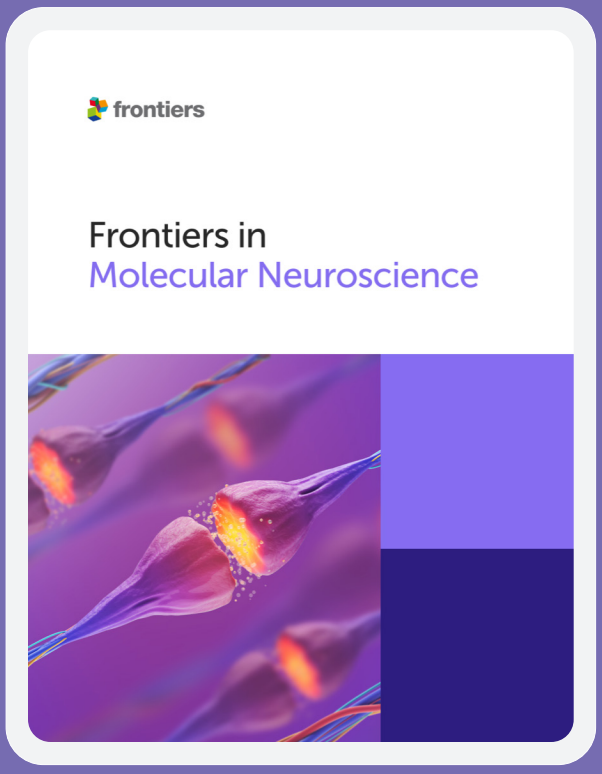

Frontiers

Avenue du Tribunal-Fédéral 34
1005 Lausanne, Switzerland
frontiersin.org

Contact us

+41 (0)21 510 17 00
frontiersin.org/about/contact